VISIBLE LIGHT MEDIATED PHOTOCATALYSIS OF *N-N* BOND BASED

COMPOUNDS

A Dissertation
Submitted to the Graduate Faculty
of the
North Dakota State University
of Agriculture and Applied Science

By

Akila Iyer

In Partial Fulfillment of the Requirements
for the Degree of
DOCTOR OF PHILOSOPHY

Major Department:
Chemistry and Biochemistry

September 2016

Fargo, North Dakota

North Dakota State University
Graduate School

Title

VISIBLE LIGHT MEDIATED PHOTOCATALYSIS OF *N-N* BOND
BASED COMPOUNDS

By

Akila Iyer

The Supervisory Committee certifies that this ***disquisition*** complies with North

Dakota State University's regulations and meets the accepted standards for the

degree of

DOCTOR OF PHILOSOPHY

SUPERVISORY COMMITTEE:

Dr. Jayaraman Sivaguru

Chair

Dr. Gregory Cook

Dr. Pinjing Zhao

Dr. Kalpana Katti

Approved:

27 September 2016	Dr. Gregory Cook
Date	Department Chair

ABSTRACT

The well-established principles of organic photochemistry, offer chemists the fundamental understanding and tools for studying light induced chemical transformations. Employing visible light for photocatalysis, one can design and develop benign routes for the synthesis of new organic materials. In our present investigation, we have developed novel *N-N* bond based compounds for visible light mediated phototransformations. We have presented synthesis for targeting achiral/chiral *N-N* bond based compounds and their study for various light driven applications. To name a few applications, these compounds have shown to react smoothly under visible light, metal-free conditions for classical photoreactions, chloromethylation, asymmetric photocyclization and photopolymerization. A diverse range of compounds has shown to react smoothly to afford products in high yields.

The scope of this methodology has been evaluated for both intermolecular and intramolecular reactions. Our work benefits from the ability of these compounds to undergo desired phototransformation in both solution and in crystalline media. We have provided photochemical and photophysical details that corroborates our experimental findings and highlights the role of excited state reactivity of the novel *N-N* bond based compounds. This thesis will be an effort to make chemists familiarize with potential of these compounds in light induced reactions.

DEDICATION

This thesis is dedicated to the living gods in my life and those in the heaven who have continued to

shower their choicest blessings on me.

Ever supporting and loving husband -Vinoth Kumar

Utmost caring, encouraging and doting parents -Subhashini and Prabhakar

Their love, confidence and continuing prayers have made it possible for me to reach new heights and for

fulfilling my dreams.

TABLE OF CONTENTS

x

xv

LIST OF TABLES

LIST OF FIGURES

xxix

LIST OF SCHEMES

xl

LIST OF CHARTS

LIST OF ABBREVIATIONS

Å .... Angstrom

AcOH ....…Acetic acid

MeCN.. …..Acetonitrile

Ac .... …..Acetyl

anhyd ....…....…….Anhydrous

AFM .... Atomic force microscopy

ATRA ....Atom transfer radical addition

atm .... …..Atmosphere(s)

BeT ....….…... Back electron transfer

k_B...….…..Boltzmann's constant

BuLi...……...…….Butyllithium

$CHCl_3$ .... …...Chloroform

CRIP ……………………………………………..………..Contact radical ion pair

CCT..Correlated Color Temperature

COSY……………...Correlation spectroscopy

CRI..Color Rendering Index

CIF .... Crystallographic information file

CV .... Cyclic voltammetry

DP ....Degree of polymerization

$CDCl_3$... …..Deuterated chloroform

DAQs ....(Diacylamino)quinazolinones

de ....…...…..Diastereomeric excess

dr...…...…..Diastereomeric ratio

DCM..…...…..Dichloromethane

TX ....Thioxanthone

Et$_3$N.. …...Triethylamine

TFA ....…....……..Trifluoroacetic acid

TPM .... …...Triphenyl methane

E$_T$ ....…........……..Triplet energy of the excited state species

TBR... Triplet biradical

UV-VIS .... …...Ultra-Violet/Visible light

VLP…………………………………………………………………...Visible light photocatalysis

v/v .... …...Volume by volume (percentage)

w/w... …...Weight by weight (percentage)

XRD ....…....……..X-ray diffraction

ZW ....Zwitterionic intermediate

CHAPTER 1. FUNDAMENTALS OF ORGANIC PHOTOCHEMISTRY AND AN OVERVIEW ON VISIBLE LIGHT MEDIATED CHEMICAL PHOTOCATALYSIS

1.1. Introduction

Organic photochemistry is the branch of science that deals with study of interaction of ultraviolet or visible light with organic materials, leading to desired chemical transformations.[1-3] The operating paradigm for organic photochemical transformations includes irradiation of reactant(s) (**R**) with the appropriate source of light resulting in the excited reactant (**R***) molecule which leads to a reactive intermediate (**I**) that eventually leads to the formation of photoproduct(s) (**P**) (Scheme 1.1). In contrast to thermal reactions where all the participating molecules exist in ground states and are initiated by a continuous variation of the energy along the reaction coordinate, the photochemical process occur directly with the quantum/discrete nature of the light-matter interaction (Scheme 1.1).[4]
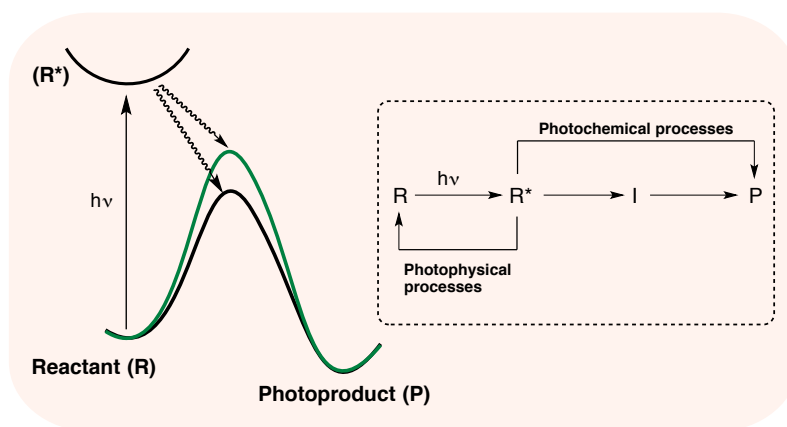
Scheme 1.1: Working paradigm for organic photochemical reactions.[5]

On irradiation of light, the absorbing chromophore interacts with the incident photon and gets photoexcited to higher energy state that has a different reactivity when compared to the ground state compound. The photoexcited compound in the higher energy state then returns to the ground state by releasing energy in the form of heat (photophysical process) or light (photophysical process) or by reacting with a ground state molecule (photochemical process). Both photophysical and photochemical processes deal with the impact of energy in the form of photons on materials.

The only difference being the former process deals with physical changes that result from the impact of photons, while the latter process focuses on the chemistry involved resulting from the impact of incident photons.

Table 1.1: Wavelength in vacuum and energy distribution of electromagnetic radiation.[2]

Classification of electromagnetic spectrum	Wavelength (Å)	Energy (*kcal/mol*)
Far infrared	10^5 (10 µm)	2.86
Near infrared	10^4 (1 µm)	28.6
Red	7.0×10^3 (700 nm)	40.8
Orange	6.2×10^3 (620 nm)	46.1
Yellow	5.8×10^3 (580 nm)	49.3
Green	5.3×10^3 (500 nm)	53.9
Blue	4.7×10^3 (470 nm)	60.8
Violet	4.2×10^3 (420 nm)	68.1
Near ultraviolet	3.0×10^3 (300 nm)	95.3
Medium ultraviolet	2.0×10^3 (500 nm)	142.9
Far and Schumann	1.5×10^3 (150 nm)	190.6
X-ray	3.0×10^2 - 1.0×10^0 (30 – 0.1 nm)	953 - 2.86×10^5
γ-ray	1.0×10^{-2} (1 pm)	2.86×10^8

All chemical transformations require energy that is stored either in the reagents or reactants. In organic photochemistry the chemical transformation occurs from the interaction of radiation that belongs to visible or UV regions of the electromagnetic spectrum (Table 1.1). This energy is sufficient to promote electrons (σ, π or n electrons) to excited states of atoms/molecules to stimulate the desired photochemical processes. Photochemistry in general applies to all chemical modifications that result from interaction of light with matter. Electromagnetic radiation belonging to near-IR to far UV region is of prime importance for studies dealing

with photochemistry and photobiology adjacent to this range are of interest for other applications. Recently, the extensive studies on multi photon absorption has resulted in the frequent use of IR radiations among photochemists.[6]

1.2. Interaction of light with matter

Quantum mechanics forms the basis of understanding interaction of light with matter.[7] Light is considered as electromagnetic radiation constituting electric (E) and magnetic field (M) vector components oscillating in perpendicular directions. The E and M vectors sets the electrons in oscillating motion with a force (F) that is proportional to the intensity of these two components:

$$F \propto (eE) + eMv / c$$

Where e is the charge on electron, v is the speed of moving electron and c is the speed of light in vacuum. Since the speed of light is larger than speed of moving electrons (the latter being of at least two orders of magnitude lower), the contribution of magnetic field component to the total force is negligible (Figure 1.1).
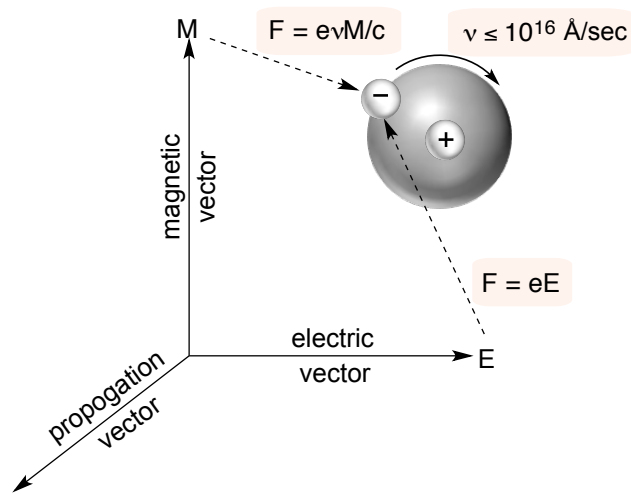
Figure 1.1: Interaction of electric field E and magnetic field M of an electromagnetic wave with an electron in an orbital. [8]

3

Two possible situations arising from interaction of light with matter are listed as follows:

a)   When the energy of incident light does not match with the difference in energy between occupied and unoccupied atomic/molecular orbitals or occupied bonding and unoccupied antibonding orbitals, the light is reflected or refracted by the matter and these phenomena are governed by the laws of classical optical physics.[4]

b)   In case when the energy of incident light matches with the energy gap between bonding and antibonding atomic/molecular orbitals, the energy is said to be in resonance with the frequencies at which electrons oscillate in bonds and around nuclei.

In case of atoms this resonance frequency lies in the range of 10^{15} - 10^{16} which translates to $\lambda \sim$ 200 - 700 nm resulting in a motion that describes an orbital of higher energy. For example in case of molecular hydrogen, when the electric field of the incident light is along the molecular axis, a π like orbital (Figure 1.2) is produced (transition caused by $\lambda \sim$ 121.2 nm), while for direction of light when perpendicular to the molecular axis results in a σ^* antibonding orbital (transition caused by $\lambda \sim$ 110.9 nm).
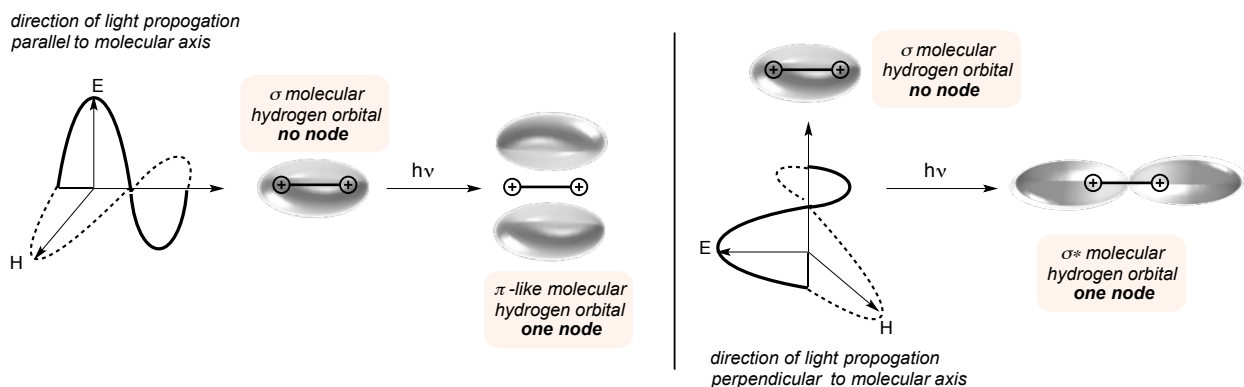
Figure 1.2: Schematic representation of light absorption by molecular hydrogen. [8]

4

1.2.1. Photophysical processes

Organic compounds have paired electron spins (↑↓) in the bonding molecular orbitals (singlet state, S_0). On photoexcitation the electron from a low energy occupied molecular orbital gets promoted to higher energy unoccupied molecular orbital resulting in an electronic excited singlet state "S_n" or triplet state "T_n". Quantum mechanics selection rules suggest the electronic transitions between electronic excited singlet to triplet states are forbidden. Photophysical processes include transitions that involve transfer of excited energy with another excited state molecule or with a ground state molecule. These photophysical processes that are plausible after absorption of light by an organic molecule can be conveniently summarized in terms of state energy diagram (Figure 1.3).[2,9] Photochemical processes are possible when the rate constants for singlet reaction or triplet reaction ($k_R{}^S$ or $k_R{}^T$) are higher than *radiative* (fluorescence lifetime k_F – 10^{-15} - 10^{-6} sec or phosphorescence lifetime k_P – 10^{-6} - 30 sec) or *radiationless* photophysical processes (internal conversion k_{IC}).
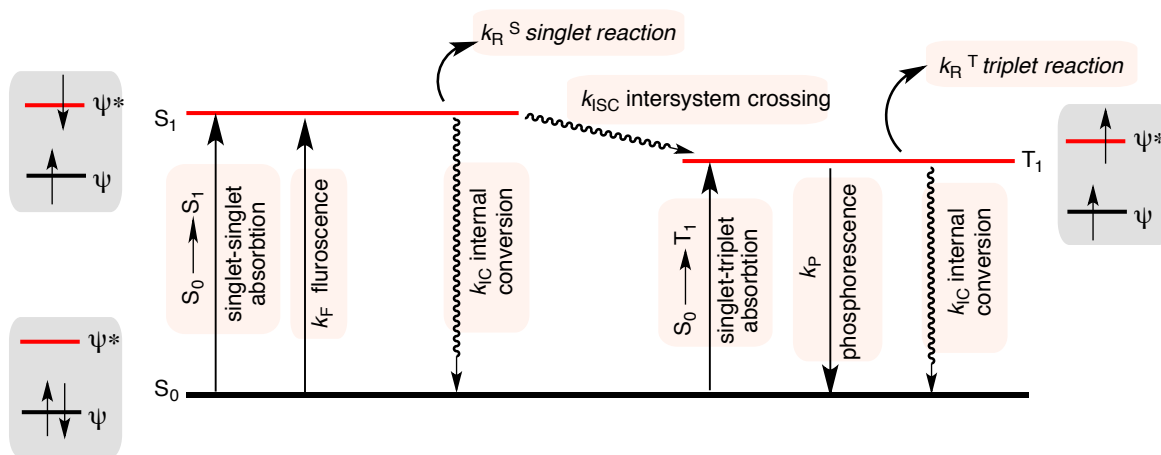
Figure 1.3: State energy diagram representing various photophysical processes possible after absorption of light by a system.[2,8]

In the latter photophysical process, the absorbed energy is dissipated over all allowed vibrational or rotational states. The probability of these transitions are regulated by the Frank-Condon factor which states that transitions are allowed between vibrational levels for a positive overlap of the vibrational wave function of the ground with the excited state. The Frank-Condon principle relates to these transitions and requires the electrons to be reorganized while the heavier nuclei to remain unaffected during the allowed transition. In many of the organic compounds, for the *radiative* processes the transitions are governed by

Kasha's rule. The rule states that the emission occurs from the lowest vibrational and rotational level of the excited state. As a consequence, the emission occurs at a lower energy compared to the absorbance. Unlike spectral features of atoms at low pressure vapor phase, (Figure 1.4, case A) the typical absorption and emission spectra for organic compounds are not distinctly sharp. In the latter case, the system lacks rotations or vibrations that can lead to the broadening of spectrum. However in molecules even in vapor phase there exist some coupling of electron and vibrations that results in "vibronic" transitions possessing a range of energies.[2] In relation to density of vibrational states, the absorption or the emission spectrum of such a rigid molecule in vapor phase appears as a structured band with visible vibrational structure (Figure 1.4, case B). For organic compounds where the molecules are surrounded by solvent, the coupling extends to solvent molecules. Such transitions effect the molecular vibrational structure by broadening, blurring or completely erasing the vibrational structure (featureless band, Figure 1.4, case C).
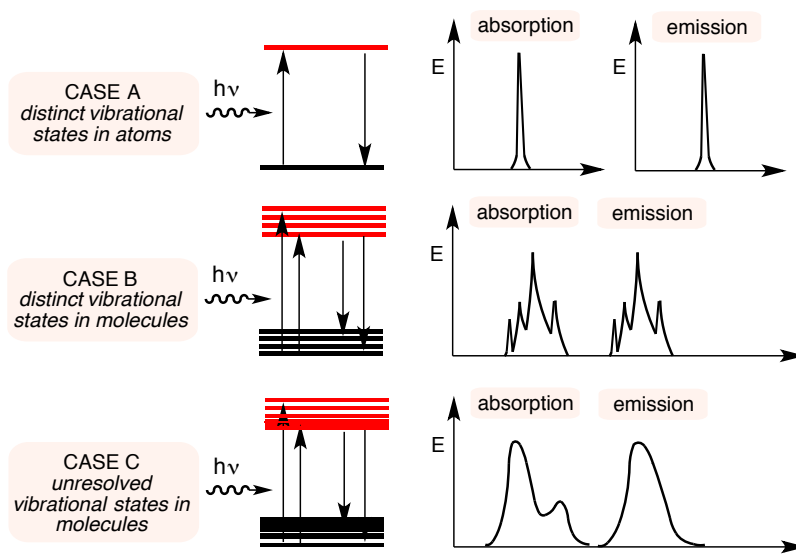
Figure 1.4: Density of vibrational states in atoms at low pressure vapor phase, rigid molecules and molecules in solution.[2]

1.3.   Photochemical processes

The photoexcited molecule in excited singlet or triplet state has energy much higher when compared to energy of chemical bonds. The photoexcited singlet or triplet molecule can adopt any of the possible photochemical pathways that includes elimination, cleavage, rearrangement, isomerization, cyclization, addition, electron or energy transfer (Scheme 1.2).[10]
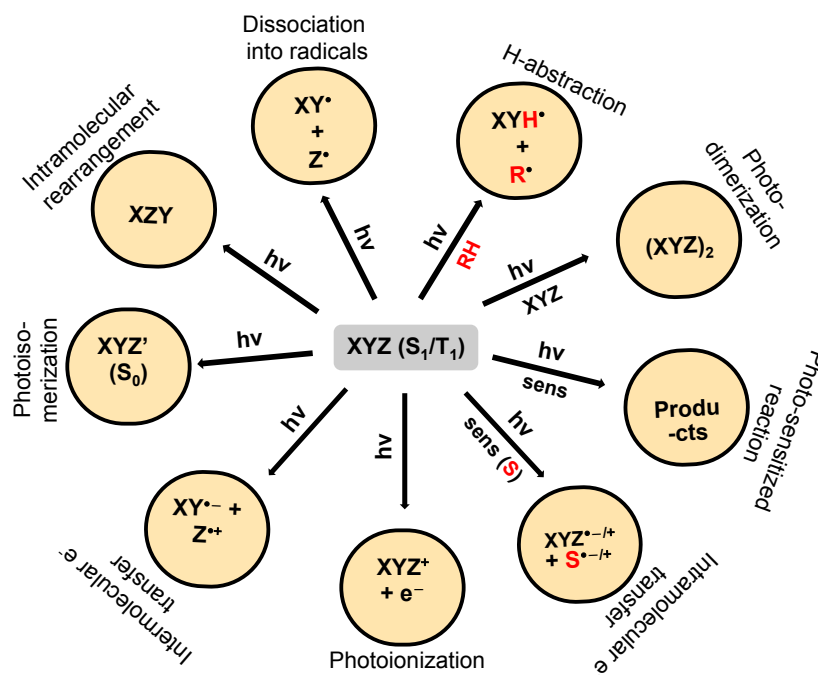
Scheme 1.2: Primary photochemical processes.[4]

The photochemical processes are governed by two fundamental principles formulated by Grotthuss (1817) and Draper (1843)[11], who postulated that "*Only the light which is absorbed by a molecule can be effective in producing photo-chemical change in the molecule.*" The law put forward by them was later reformulated by Stark (1908-1912) and Einstein (1912-1913) who suggested that "*The absorption of light is a one-quantum process so that sum of all primary process quantum yields Φ must be unity*" i.e. $\sum \Phi_i = 1$ where Φ_i is the quantum yield of ith primary process.[4,11] The law was again revised by Stark and Bodenstain (1913) who postulated the rule to be applied to only primary photochemical process. The law states that "*One quantum of light is absorbed per molecule of absorbing and reacting substance that disappears.*" The law holds valid for systems with short-lived excited states and when intensity of irradiation is low.

The quantum yield Φ defines the efficiency of a photochemical reaction and is described as the ratio of number of molecules that are consumed during a photochemical process to the number of photons absorbed by the molecules undergoing the transformation (Equation 1.1).

$$\text{Quantum Yield } (\phi) = \frac{\text{Number of molecules of reactants consumed}}{\text{Number of photons absorbed}}$$

(Equation 1.1)

1.4. Ground and excited state molecular interactions

In some organic molecules where ground state intermolecular interactions exist, it is required to have knowledge of the binding constants. The outcome of these interactions is observed in the spectral changes of the absorption spectra. Another possibility presented by organic molecules is the inter- or intramolecular excited state interactions that are often referred to as excimers or exciplexes.[12] For understanding the photo-induced energy or electron transfer possible in the excited dimers or complexes requires the measurement of rates for the corresponding processes. These processes are described in detail in the following section.

1.4.1. Energy transfer (ET)

In organic systems where two like or unlike molecules can undergo photo-induced energy transfer in the excited state, the energy acceptor (A) is required to be in proximity of the excited energy donor (D). This energy transfer process results in a ground state donor molecule and excited state acceptor molecule (Figure 1.5). Another requisite for energy transfer to occur is the energy level of the excited state of D* needs be higher than that of A* and the time window required for energy transfer process to occur must be faster than the lifetime of D*.
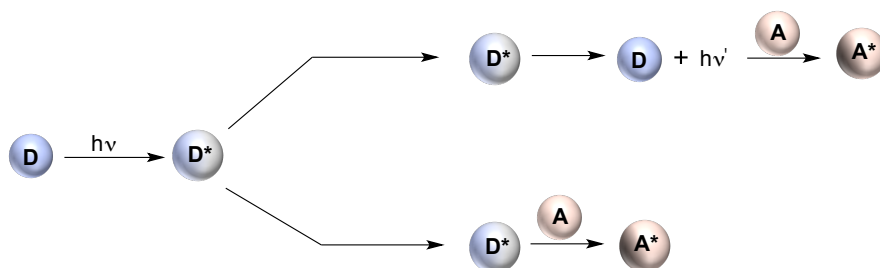
Figure 1.5: Energy transfer from donor organic molecule (D) to acceptor organic molecule (A).

Energy transfer from a donor molecule to an acceptor molecule can occur *via a trivial*, *Förster* or *Dexter* mechanism. In the *trivial* energy transfer the energy from the D* is emitted in form of luminescence (hv'), that is absorbed by the acceptor (A). For the *trivial* energy transfer to occur, the emission integral of D* needs to have an effective overlap with absorption integral of A. In addition a large distance (~100 Å) between D* and A is required for the energy transfer to operate.[12] This mechanism of energy transfer where there is a through space energy transfer, is considered to be an inefficient process because only a small fraction of the emitted light (hv') of D* can be transferred to the acceptor.

The two commonly encountered energy transfer processes are *Förster* and *Dexter* ET that are discussed below.

1.4.2. Förster energy transfer

The Förster energy transfer process was proposed by Theodor Förster and is also popularly referred to as *Coulombic mechanism* or *Dipole-induced dipole interaction*.[13-14] For the energy transfer process to operate the emission band of D* must overlaps with the absorption band of A. The transfer of energy occurs by the coupling of electrical dipoles of D* with that of A (Figure 1.6).
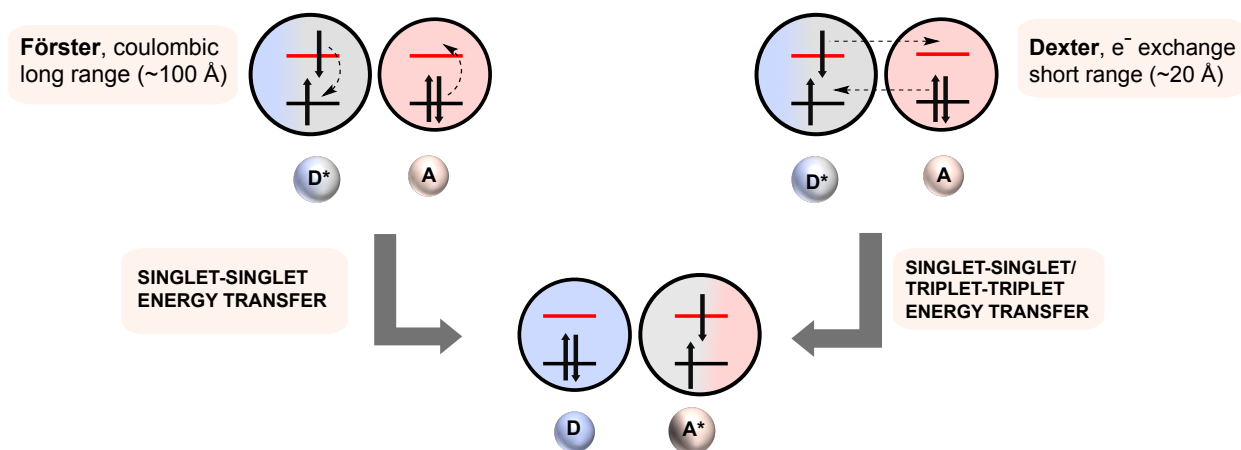
Figure 1.6: Energy transfer mechanisms.

Depending on the solvent and nature of interactions between D* and A, the Förster energy transfer can occur over long distances (~100 Å). On photoexcitation of the organic molecule, the electron in the LUMO of D* relaxes to the HOMO and the energy released in this process is transferred to A through coulombic interactions between the D* and A. As a result, an electron initially in the HOMO of the acceptor is promoted to the LUMO (Figure 1.6). This kind of interactions occurs when the participating photoexcited states of D* and A are of singlet in nature. This can be understood in regards to large dipole moment singlet-singlet transitions. The rate of energy transfer k_{ET} for Förster mechanism is provided in Equation 1.2.

$$k_{ET} = k_D R_F{}^6 \left(\frac{1}{R}\right)^6$$

(Equation 1.2)

R is distance between the absorbing chromophores in D* and A, k_D is the emission rate constant for the donor; R_F is the Förster radius and is calculated by the overlap of the emission spectrum of D* and absorption spectrum of A.

1.4.3. Dexter energy transfer

In Dexter energy transfer mechanism, a double electron exchange occurs between D* and A (Figure 1.6). This mechanism operates with no formal separation of charges while the two electrons are changing their position in the electronic states (Figure 1.6). Unlike the Förster energy transfer, which operates only when the involved excited states are singlets, the Dexter mechanism occurs when the involved photoexcited states are either singlets or triplets. The Dexter energy transfer operates when there is an effective molecular orbital overlap between D* and A. In addition, for the intermolecular photoreactions to proceed *via* this mechanism it is required to have effective intermolecular collisions. The energy transfer operates through short distances (~20 Å) and the rate of Dexter energy transfer ($k_{ET'}$) is directly proportional to the intermolecular distance between D* and A (Equation 1.3).

$$k_{ET'} = \left(\frac{2\pi}{h}\right) V_0{}^2 J_D \exp\left(-\frac{2R_{DA}}{L}\right)$$

(Equation 1.3)

Where, R_{DA} is distance between D* and A. J_D is the overlap integral of the emission spectrum of D* and absorption spectrum of A.

L is the Bohr radius of the orbitals between which the electron is transferred, h is Planck's constant, V_0 is the electronic coupling constant between D* and A at the distance of the energy transfer.

1.4.4. Electron transfer (eT) – Marcus equation

Photoinduced electron transfer in organic systems takes place between photoexcited donor and acceptor molecule that leads to charge transfer states (contact radical ion pair - CRIP), consisting of donor radical cation ($D^{+\cdot}$) and acceptor radical anion ($A^{-\cdot}$) (Figure 1.7). Depending on the interaction with the solvent, the radical ion pair can undergo solvation to become a solvent separated radical ion pair (SSRIP). The SSRIP can then return to their respective ground states by a process of back electron transfer (BeT)/charge recombination process.
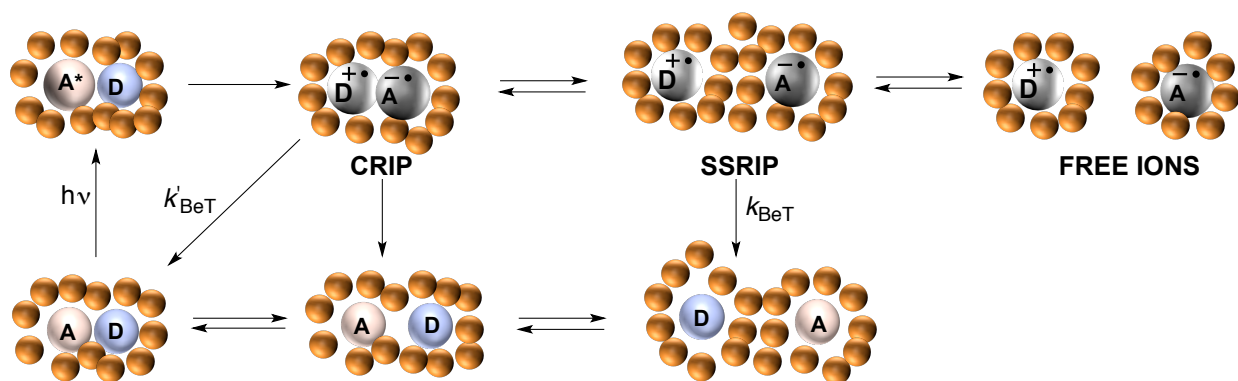
Figure 1.7: Pictorial representations of the process of photoinduced electron transfer in non-viscous solvents.

The SSRIP can then return to their respective ground states by a process of back electron transfer (BeT)/charge recombination process. On escaping the solvent cage the donor and acceptor can move freely leading to desired chemical transformation. The charges can recombine by a *non-radiative* process or a *radiative* process. In the latter case the luminescence is often referred to as charge transfer fluorescence. The Nobel laureate R. A. Marcus has proposed a detailed theory to explain the phenomenon of photoinduced electron transfer in solution, which has been widely accepted by community of experimental and theoretical photochemists.[15-17] Based on his seminal work on electron transfer theory, one can comprehend electron transfer reaction by a simple model (Figure 1.8) where the reactant state is the excited donor/acceptor and the product state is the charge-separated donor/ acceptor states.
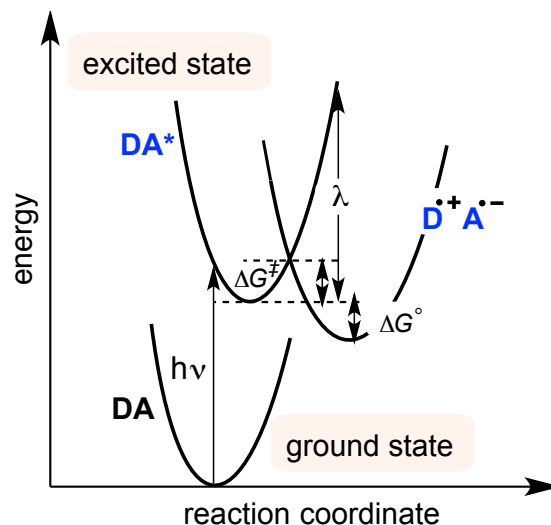
Figure 1.8: Reaction profile from Marcus theory for the ground state (DA), the excited state (DA*) and the charge-separated state.[12]

Frank-Condon excitation describes that the vertical transitions occurs much faster to the excited state giving no time for nuclear coordinates to undergo rearrangement. The photoexcitation of donor/acceptor (reactant) system results in electron transfer to occur at the crossing of the equilibrated excited state surface and the charge-separated donor/acceptor (product) surface (Figure 1.8).[12] The activation energy ($\Delta G^{\ddagger}$) for this process (Equation 1.4) is inversely related to the reorganization energy (λ). The latter describes the total energy required for the reactant molecules to reorganize themselves in a given solvent to afford the product without undergoing any electron transfer.

$$\Delta G^{\ddagger} = \frac{\left(\lambda + \Delta G^{\circ}\right)^2}{4\lambda}$$

(Equation 1.4)

Where, ΔG° is the reaction free energy and equals the difference in free energy between the equilibrium configuration of the reactant and product states.

The rate of electron transfer k_{eT} (based on classical Marcus theory) is directly related to activation energy ($\Delta G^{\ddagger}$) and is shown in Equation 1.5.

$$k_{eT} = \kappa_{eT}\, \nu_n \exp\left(\frac{-\Delta G^{\ddagger}}{k_B T}\right)$$

(Equation 1.5)

Where, ν_n is the frequency factor for nuclear motions and κ_{eT} is the electronic transmission coefficient.
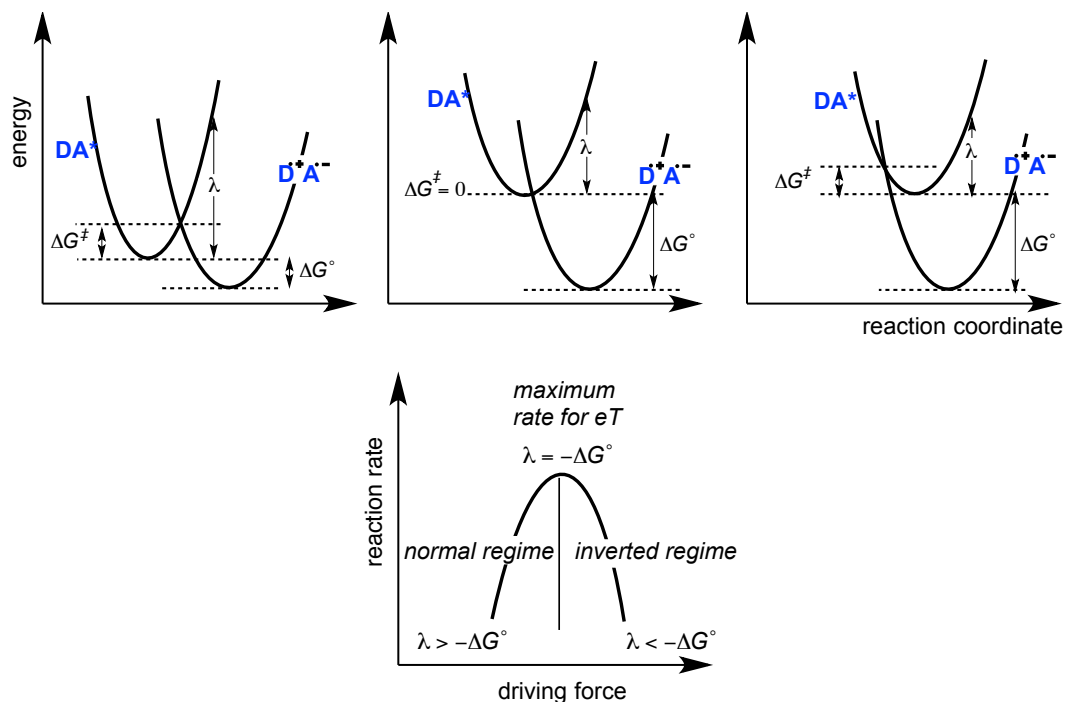
Figure 1.9: Free energy regimes for electron transfer predicted by Marcus theory.[12]

This useful relation between k_{eT} and $\Delta G^{\ddagger}$ is helpful in predicting the driving force for electron transfer as a function of reaction rate (Figure 1.9). In addition it provides an estimate of rate of electron transfer where the free reaction energy $\Delta G°$ decreases with an increase in the rate of electron transfer (*Marcus normal regime*). In case where there is an activationless surface crossing ($\Delta G^{\ddagger} = 0$, $-\Delta G° = \lambda$,) the driving force for electron transfer becomes equal to reorganization energy (*Marcus optimal regime* where the rate of eT is maximum). For $-\Delta G° > \lambda$, the rate of electron transfer decreases as the $\Delta G°$ increases (*Marcus inverted regime*). Closs and Miller were the first (1984) to verify the inverted regime postulated by Marcus theory form their detailed intermolecular PET experiments.[18]

1.4.5. Electron transfer- Rehm and Weller equation

For photoinduced electron transfer in bimolecular reactions where $\Delta G°$ becomes increasingly negative, results in increasing rate constant for electron transfer. The rate constant reaches the maximum value (diffusion controlled) and then remains pegged to maximum with decrease in free energy, this is referred to as *Rehm-Weller behavior* (Figure 1.10).
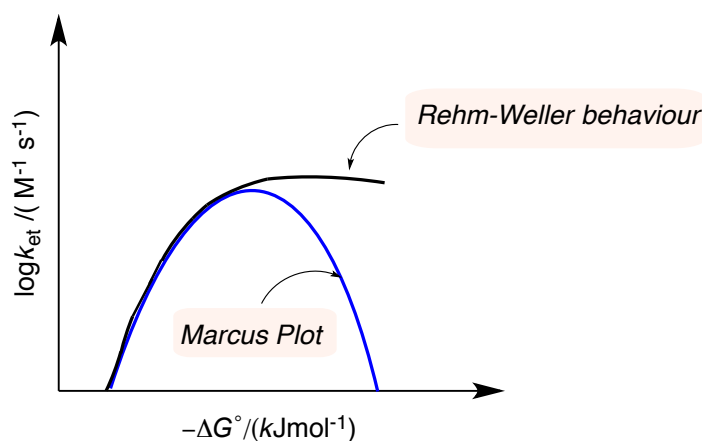
Figure 1.10: Plot for photoinduced electron transfer in a non-viscous media for bimolecular photoreactions (the *Rehm-Weller behavior)*. The predicted Marcus plot is included to visualize the deviation.[19]

The Rehm-Weller equation (Equation 1.6) predicts the driving force (Gibbs free energy change) for photo-induced electron transfer between a donor and acceptor molecule.[20]

$$\Delta G° = E(D^+/D) - E(A/A^-) - E_{00}^* - \left(\frac{e^2}{4\pi\varepsilon\varepsilon_0 r} \right)$$

(Equation 1.6)

Where, $E(D^+/D)$ and $E(A/A^-)$ are the oxidation and reduction potentials of the donor and acceptor respectively. The fourth term in the equation 1.6 is the Coulombic term and $E_{00}*$ is the energy of the photoexcited reactant molecule. Coulombic term compensates for the separation between the donor and acceptor molecules participating in energy transfer process. Rehm and Weller investigated over 60 donor-acceptor pairs for bimolecular quenching studies but did not observe the Marcus inverted region, as the process was limited by rates of diffusion. Therefore for bimolecular electron transfer reactions that occur in a diffusion-controlled rate, it is assumed that *Marcus inverted regime* will not be observed.

1.5.   Beginnings of organic photochemistry

Light mediated organic synthesis provides an easy access to structurally complex scaffolds; therefore it has been employed for key transformations in the synthesis of many natural products.[21-24] In 1834 a German pharmacist, Hermann Trommsdorff (1811-1884) is referred to have first reported an organic photochemical reaction in the literature.[24-26] The work highlights the effects of sunlight on crystals of santonin **1**. His initial observations were based from visual inspection of color change, which occurred when the crystals were subjected to irradiation. Based on his observations from light irradiation on santonin, he was able to predict the presence of "*two isomeric modifications*". His statement was later verified by other scientists who observed a photochemical rearrangement of santonin on irradiation, followed by a Diels-Alder reaction and [2+2] photocycloaddition to afford the "*isomeric*" photoproduct (Scheme 1.3).
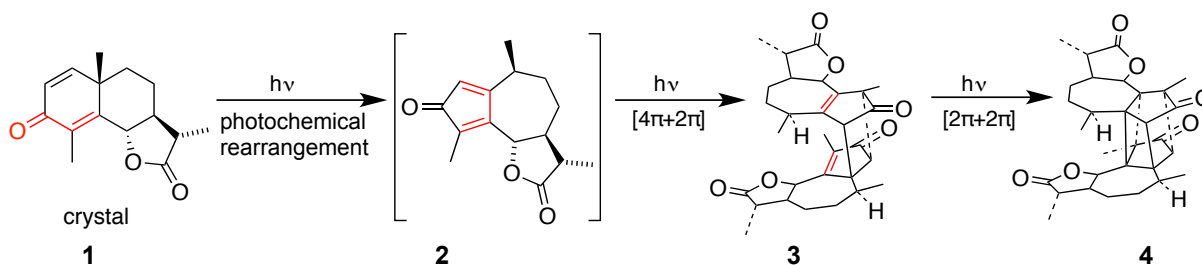
Scheme 1.3: Photoreaction of santonin in solid state.[27]

With the initial studies documented by Trommsdorff on solid state photoirradiation of santonin paved the path for Stanislao Cannizzaro (1826-1910), Fausto Allessandro Sestini (1839-1904), Carl Julius Fritzsche (1808-1871), William Henry Perkin (1838-1907), Johannes Wislicenus (1835-1902), Carl Theodor Liebermann (1842-1914) and Heinrich Klinger (1853-1954) who continued investigating photochemistry of organic small molecules. Cannizzaro marked the dawn of organic photochemistry by introducing exceptionally skilled and visionary chemists Giacomo Ciamician (1857-1922) and Paul Silber (1851-1932).[25,28] They performed systematic investigations on the photochemistry of keto-compounds (α and β-cleavage/photopinacolization) and intramolecular photocycloaddition reactions.[29-30]

Their work provided the fundamental understanding of molecular photochemistry and therefore their efforts are regarded with utmost respect among chemists across various disciplines who employ light for various functional group transformations.[30]

1.6. Visible light mediated chemical photocatalysis of organic compounds

The term photocatalysis is defined as "*Change in the rate of a chemical reaction or its initiation under the action of ultraviolet, visible or infrared radiation in the presence of a substance—the photocatalyst—that absorbs light and is involved in the chemical transformation of the reaction partners.*"[31] In addition, IUPAC defines a photocatalyst as a "*Catalyst able to produce, upon absorption of light, chemical transformations of the reaction partners. The excited state of the photocatalyst repeatedly interacts with the reaction partners forming reaction intermediates and regenerates itself after each cycle of such interactions.*"[31-32] Photocatalysis provides mild operating conditions and avoids the need of light absorbing chromophore in the molecule undergoing transformation. Photocatalysis meets some of the principles set by green chemistry and thus is regarded to be an ideal candidate for 'green chemical synthesis'. [33-34] Some of the utilities that justify this title are listed below:

a. For the photoreactions where the absorption of light is localized within the absorbing chromophore can be controlled by wavelength of irradiation.

b. The organic compound can be photoexcited either by direct or sensitized (catalyzed) pathways.

c. The light itself does not produce any chemical waste that eliminates the issue of disposal problems that are associated with reagents utilized in thermal reactions.

d. Most of the photochemical processes can be safely stopped by turning off the light source.

Despite of several advantages offered by photochemical reactions, some of the serious challenges set by them relates to the issue of unsustainability. Some of the most common shortcomings associated with photoreactions are listed below:

a. Most organic compounds absorb in the ultraviolet (UV) region and the high energy UV irradiations often lead to significant decomposition/side reactions, particularly when weak bonds are present in the molecule.[35]

b. High intense light radiations are harmful to humans and require specialized housing equipments for safe operation protocols.[3,10,36] In addition, conversion of electrical power into intense light radiations comes with substantial heat generation that requires continuous water-intensive cooling making the use of photoreaction set-up very expensive.

c. One of the other limitations associated with the use of artificial light sources is the requirement of constant maintenance and short lifetimes.[10]

Visible light photocatalysis (VLP) offers the best solution to the above listed issues. It utilizes visible light as the clean and renewable source of energy to drive the chemical transformation in presence of a suitable photocatalyst. Another terminology that is often used for a photocatalyst is a photosensitizer. The latter is defined as "*the molecular entity that absorbs the incident radiation and initiates a photophysical or photochemical alteration; in mechanistic organic photochemistry the term is limited to use for the cases where it is regenerated after desired chemical transformation*".[32] Therefore in organic photochemistry the term photosensitizer is used interchangeably for a photocatalyst.

A judicious choice of photocatalyst/photosensitizer is crucial for the successful outcome of VLP in organic synthesis.[37] The early efforts in employing photocatalyst/photosensitizer for wielding visible light in constructing new bonds and providing fundamental understanding of operating mechanism was put forward by David Whitten.[38-39] His seminal work on photo-induced electron transfer by utilizing metal complexes as the photocatalysts/photosensitizer has been extensively employed in the recent times for various useful chemical transformations under the title of "*Photoredox catalysis*".

Based on the chemical framework and photophysical properties, the photocatalysts/photosensitizers for VLP can be broadly classified into 4 categories viz, organic dyes, metal complexes, organic materials, and semiconducting materials. Each of these categories has been described briefly in the following section with a focus on their use in the recent times.

1.6.1. Organic dyes

In the lines of making VLP a completely sustainable process, organic dyes (ODs) can be a judicial choice for photocatalysts.[40] To name a few advantages, ODs have low toxicity, low price and can efficiently work in aqueous media.[41] Depending on the redox potential and triplet energy, these can operate by a process of photo-induced electron transfer (PET) or a triplet energy transfer. Some of the well-evaluated systems towards VLP along with their respective electrochemical and photophysical data have been summarized in Chart 1.1. One of the important drawbacks associated with the use of dyes relates to their ineffective degradation by acids/bases. Therefore in order to make the use of ODs sustainable, one needs to design routes to access them from biomass and subject them to an easy degradation protocol after use.

1.6.2. Metal complexes

Metal complexes that are effective photocatalysts/photosensitizers for VLP include co-ordination complexes and metal organic frameworks (MOF). [42-46] In the 20-th century, under visible light irradiation Ir and Ru based metal complexes have been extensively evaluated for various useful bond forming reactions. The first report on the use of Ru metal based complex for light induced chemical transformation was documented in the year 1978. [47] The reaction utilized Ru (II) complex for accelerated reduction of phenacyl onium salt under visible light irradiation (Scheme 1.4).
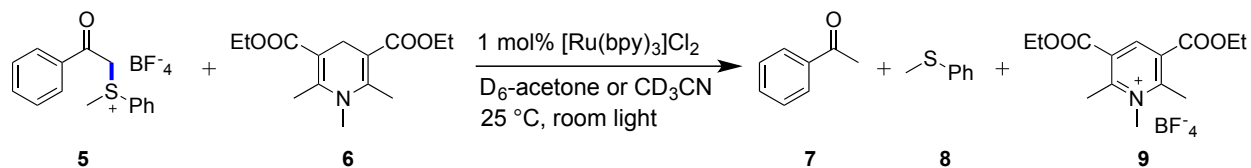
Scheme 1.4: Ru (II) complex catalyzed accelerated reduction of phenacyl onium salt under visible light irradiation.[47]

Later with the development of techniques to study time resolved spectroscopy it became possible to design and develop novel metal complexes. The ease of manipulating the ligands/metal center(s) (Chart 1.1) in these complexes provides a handle to modulate the redox potential making them applicable to wide variety of substrates. In the 20th century David Macmillan, Tehshik Yoon and Corey R. J. Stephenson by their independent investigation on photoredox catalysis marked the beginning of the use of visible light as a powerful tool for chemical reactions.[48-51] Some of the drawbacks associated with the use of metal complexes, includes expenses incurred from synthesis, toxicity of rare earth metals, photobleaching and long-term usage. The recent efforts to address some of these issues include the recyclability of the photocatalyst. Many groups have showcased the metal-complex when immobilized on a polymer backbone behave as an effective recyclable photocatalyst.[52-55] Kappe and coworkers have appended the metal-complex on to a dendrimer and have shown recovery of this novel macromolecular system after the desired functional group transformation.[56]

1.6.3. Organic materials

Design and development of organic materials as photocatalysts has provided room for tunable electronic and optical properties. Given the low toxicity and long term sustainability associated with organic materials, these have attracted the interest of many researchers. The pool of organic materials that have been evaluated for VLP and are found to be effective photocatalysts/photosensitizers include organic compounds that are efficient triplet sensitizers[2], porous organic frameworks[57-59], supramolecular systems[60], conjugated microporous polymers, graphitic carbon nitride polymers[61], conducting macromolecules[62-65] and flavin derivatives[66-67] (Chart 1.1). Owing to their robust synthesis and easy electronic manipulations, organic materials hold promising applications in metal-free, visible light driven chemical transformations.[68]

1.6.4. Semiconducting materials

Semiconducting materials like quantum dots-inorganic nanocrystals[69], CdS quantum dots-TiO_2 nanotubes and other doped-TiO_2 materials[70-71] have shown to have adjustable band gap that can be custom tailored for absorption in desired optical window. Another advantage offered by these materials includes the possibility of multiple exciton generation that can lead to high quantum efficiencies.

Metal nanoparticles (M-NP's) have shown to facilitate functional group modification in organic compounds under visible-light irradiation.[72] With TiO_2 as the support, the metals that form the bimetallic core of M-NP's can be Au, Ag or Cu.[73-76] These nanostructures show different efficiencies based on temperature at which the light induced chemical reaction is carried out. These M-NP's can also be employed as mixed metal alloys' forming Plasmonic M-NP's that can render them new properties in regards to absorption characteristics and photocatalytic activity.[77]

Unlike the operating mechanism in VLP that employs metal complexes/organic materials/organic dyes as photocatalysts, light absorption and activation of reactants by these plasmonic M-NP's is different. The M-NP's visible light absorption occurs due to localized surface plasmon resonance effect (LSPR) or by another mechanism that depends on which M-NP absorbs light (based off the Photoelectric effect). In the LSPR absorption mechanism, a localized surface plasmon ("*The quantization of the collective longitudinal excitation of a conductive electron gas in a metal is known as Plasmon*"[78]) results in a strong interaction between the incident electric field and the conduction electrons of M-NP's (Figure 1.11).
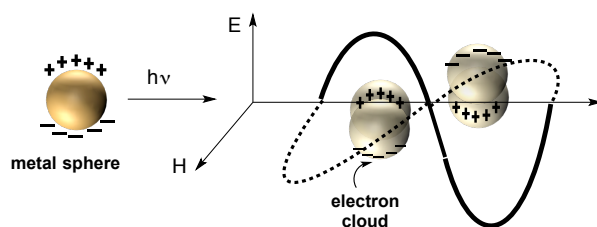
Figure 1.11: Interaction of light with a metal in a localized surface plasmon resonance effect.[75]

The transfer/activation of reactants by these M-NP's can occur by either: (1) Elastic radiative re-emission of photons (2) non-radiative Landau damping – conversion of photon energy into charge-carriers excitation in the M-NP's and (3) Chemical interface damping - interaction of excited surface plasmons with unpopulated states of the acceptor molecule (Figure 1.12). The future efforts required to develop semiconductor mediated VLP is to design and study novel M-NP's materials for chemical synthesis that possess high density of conduction electrons on the surface and exhibit easy ejection of conduction electrons after excitation.
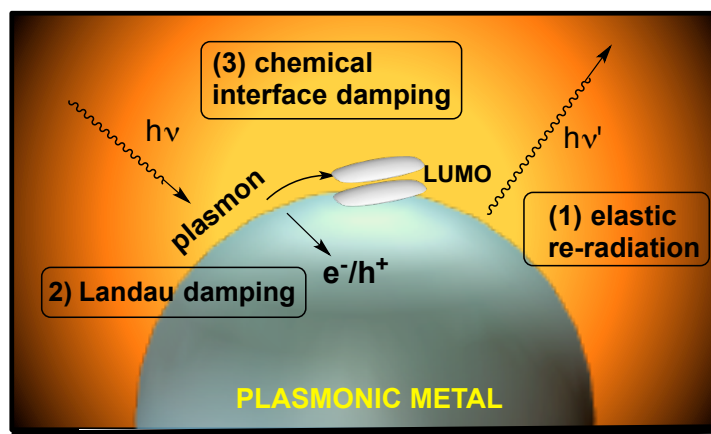
Figure 1.12: Schematic representation of three operating mechanisms for transfer of light energy in direct-metal photocatalysis. [79]

Methylene blue (10)
$E_{1/2}(MB^+/MB\bullet) = -0.47$ V vs SCE

Methylene green (11)
$EPC(MG^+/MG\bullet) = -0.22$ V vs SCE

Nile blue (12)
$EPC(MG^+/MG\bullet) = -1.05$ V vs SCE

Rhodamine B (13)
$E_{1/2}(RhB^+/MG\bullet) = -0.55$ V vs SCE

9-Mesityl-10-methylacridinium (14)
$EPC(Mes-Acr^+/Mes-Acr\bullet) = -0.47$ V vs SCE

Eosin Y (15)
$E_{1/2}(EY^+/EY) = 0.78$ V vs SCE

Tris(2,2'-bipyridyl)dichlororuthenium(II) (16)
$E_{1/2}(Ru_2^+/Ru^+) = -1.28$ V vs SCE
$E_{1/2}(Ru_3^+/Ru_2^+) = 1.25$ V vs SCE

fac-Tris(2'-phenylpyridinato-C_2,N)iridium (III) (17)
$E_{1/2}(Ir_3^+/Ir_2^+) = -2.19$ V vs SCE
$E_{1/2}(Ir_4^+/Ir_3^+) = 0.77$ V vs SCE

benzoselenadiazole containing Zr-MOF with terphenyl dicarboxylate as linker: UiO-68Se (18)

UiO-68Se

Thioxanthen-9-one (19)
$E_{1/2}(TX^+/TX) = 1.7$ V vs SCE

Carbazolic porous organic framework (Cz-POF) (20)
$E_{1/2}(Cz-POF^+/Cz-POF) = 1.38$ V vs SCE

Cz-POF

Plasmonic metal nanoparticles (21)

Ag Au Cu

Chart 1.1: Summarized group of few photocatalysts that have been well documented in the literature for visible light photocatalysis, along with their optical and/ redox potential(s). ■ Organic dyes (**10**[41,80-81], **11**[41,81], **12**[41,82-84], **13**[41,85-86], **14**[41,87-89], **15**[41,82,90-92]), ■ Metal complexes (**16**[41,93-99], **17**[41,100-101], **18**[45]), ■ Organic materials (**19**[102-104], **20**[57]), ■ Plasmonic metal nanoparticle (**21**[74,105]).

1.7.   Visible light and color

Color is a function of the human visual system and does not constitute an intrinsic property.[106] It is determined first by frequency.[106-107] When we look at any object the color we observe is the light that it gives "off". Certain objects like stained glass (or a filter) transmit light, the operating principle being, only certain wavelengths passes through the object while others are absorbed.[107] The wavelengths that pass through are the ones that we can perceive. A judicious adjustment of filter's intensity can be a useful handle to control the amount of light passing through it. Filtration is also useful for controlling the color of light during exposure.[107]

Visible light corresponds to the wavelength range of 400 – 700 nm in the electromagnetic spectrum (Figure 1.13).[108] A radiation of single frequency is called as monochromatic light.[109] Thus visible spectrum shows all the colors that can be made out of monochromatic light.[110] The main colors constituting the visible spectrum (Figure 1.13) that a human eye can perceive range from violet color (low wavelength) to red color (high wavelength). A mixture of all these colors of the visible spectrum result in white light.[111] An absence of light results in black color.
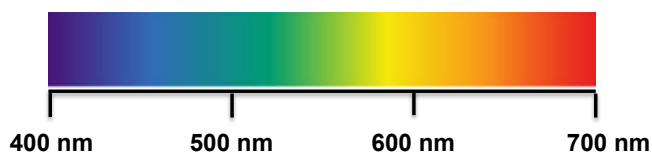
Figure 1.13: Visible light spectrum.[112]

1.8. Characteristics of light sources

A light source is an object that emits light with energy that is not described and varies.[113] Therefore a "light source" is not described mathematically and can not be reproduced.[113] Light sources that emit light with energy that can be described and are reproducible are referred to as "illuminants". Light sources, whether an actual source or an illuminant, are characterized by its color temperature, spectral power distribution, Photometry, efficacy and timing.

Color Temperature[114-115] –The heat generated by a light source is a reflection of its color temperature (measured in *kelvins*). It describes how bright the light source looks when turned on. As the color temperature of the light source varies it effects the relative power of its constituent wavelengths. The quality of the emitted light by a light source/illuminant is determined by two measurement techniques namely Correlated Color Temperature (CCT) and Color Rendering Index (CRI). The former (CCT) describes the color temperature of light sources while the latter (CRI) relates to the reproduction system of the various colors observed from the light sources. CRI is universally recognized by the lighting industry.

Spectral power distribution[115-117] – Spectral power distribution/spectral distribution of a light source/illuminant refers to the energy radiated at different wavelengths at a given color temperature. It provides a visual representation of the colors emitted by the light source/illuminant. It is essentially a graph that describes the relative intensities of the light source/illuminant at various wavelengths. Analysis of spectral distribution of various light sources/illuminants provides a complete description of the color properties of the light source.

Photometry[118-119] – Photometry is the science of measurement of light intensity/flux perceived by the human eye. The science is based on a statistical model of the visual response to light under controlled conditions.[120] All the important parameters that are considered in the study are discussed below.

a. Luminous intensity I, (measured in candela) refers to the amount of energy emitted by a light source/illuminant and describes the efficiency of the source. The unit candela originates from the brightness of a "standard candle". It measures the amount of light emitted in the range of an angular span. The angular span is expressed in terms of a unit-less quantity termed steradian.

b. Luminance L (measured in cd/m^2) is an indication the brightness of an illuminated surface as perceived by the human eye. It is given by the luminous intensity (I) emitted by a light source/illuminant per unit area.

c. Luminous flux Φ (measured in lumens), that describes the amount of light radiating from a source and is given by the quantity of the energy of the emitted light per second in all directions. Measurement of luminous flux of a light source/illuminant is referred to as photometry. Luminous flux is measured by using a light meter possessing a photoelectric cell. Equation1.5 represent the relation of lumens to candela.

$$\text{lumens} = \text{candela} \times \text{steradian}$$

(Equation 1.5)

The relationship between radiometric and photometric units are summarized below in Table 1.2.

Table 1.2: Correspondence between radiometric and photometric quantities.[120]

Physical quantity	Radiometric units	Photometric units
Power	watt (W)	lumens (lm)
Power per unit area	W/m^2	lm/m^2
Power per unit solid angle	W/sr	lm/sr (= cd)
Power per unit per unit solid angle	W/m^2 sr	lm/m^2 sr = cd/m^2

Efficacy [115]– Efficacy (measured in *lumens per watt*) of a light source/illuminant is given by the ratio of light output to the consumed electric power.

Timing[115] – The time of illumination another important characteristic of light sources/illuminants. The time required to flicker (flicker refers to the event where the light turns off when the AC line passes through 0 volts) or for glowing when the light source/illuminant is turned on determines the efficiency and lifetime of the light sources/illuminants.

Shape and size of light sources/illuminants[118] – Commonly employed artificial light sources/illuminants are housed in regular/soda lime glass and borosilicate heat-resisting glass. The borosilicate glasses are capable of withstanding high temperatures. Some light sources use materials that are capable of withstanding still higher temperatures These use glass envelope that are made of fused silica (quartz) or aluminosilicate glass.

Knowledge of these properties of a given light source/illuminant is essential for determining the efficiency of a visible light mediated photoreaction.

1.9. Visible light sources

Within the wide spectrum of electromagnetic radiation encountered in our everyday life only a portion of it constitutes the visible light. Sunlight is the major source of visible light readily available for use. The spectral distribution of sunlight is shown in Figure 1.14.[112] The profile represents the spectrum of sunlight emitted during noon. Sunlight is the greatest source of white light.
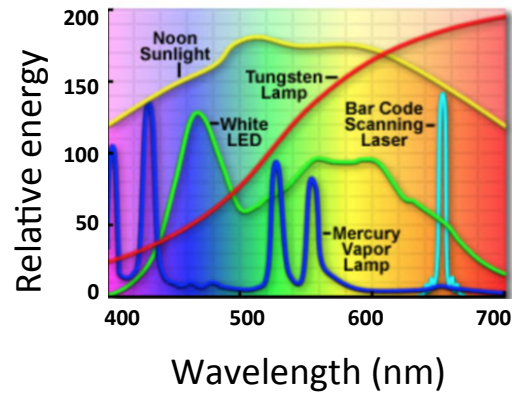
Figure 1.14: Spectral distribution of light emitted by various visible light sources.[112]

The other natural sources of visible light include lightning, moon, planets, stars, volcanoes and forest fires. In addition, there are certain species capable of emitting visible light (the phenomenon being referred to as bioluminescence). These include lightning bugs, jellyfish, certain bacteria and fishes. With advancing technology, there are a number of commercially available artificial sources that emit visible light. These artificial visible light sources can be classified on the basis of the light intensity characteristics *viz* light sources that emit the same amount of light over a fixed period of time and light sources that emit light that vary over time. A combination of one or more lamps, optical devices, socket/bases and connection to electric power is required for the operation of any artificial visible light source. These are sometimes utilized in conjunction to a luminaire, which is a device that is capable of controlling the distribution of light.

These artificial light sources can also be classified into two main categories namely fluorescent and incandescent light sources. These light sources are discussed in the following section below.

1.9.1.   Incandescent light sources[112,121]

When a fire burns, the chemical energy stored in the combustible material is released in the form of heat and light. With this knowledge, humans have successfully mastered the art of utilizing various combustible materials for emitting gases thus making atoms in the gas incandesce. During combustion the electrons within the atoms get promoted to higher energy levels. When these relax back to their ground state the process is accompanied by release of heat and light. The color of the flame indicates the temperature and the energy of heat that is released during the process of combustion. Sun and candle flame(s) are the natural source of incandescent light.

Artificial light sources that radiate light when heated by electrical energy are referred to as incandescent light sources. The primary source of incandescent light includes high-intensity tungsten lamps. The filament (tungsten) in an incandescent lamp heats up when supplied with electrical energy. The efficacy of light source depends on the temperature of the filament. Higher the temperature of the filament, higher is the radiated energy that falls in the visible region. The filament possesses a high electrical resistance that causes it to glow. The spectral distribution of tungsten-based lamp is shown in Figure 1.14. The energy of tungsten light increases as the wavelength increases, that affects the average color temperature. Tungsten based incandescent lamps emit a continuous spectrum of light that extends from 300 nm - 1400 nm.

These lamps are operationally straightforward and are composed of sealed glass envelope, evacuated or filled with an inert gas and containing the filament (tungsten). The average values for color temperature range for tungsten based incandescent lamps varies from about 2200 K to 3400 K. The efficacy of these lamps is typically 15 lm/W.[122-123] One of the drawbacks of tungsten-based incandescent lamps is the decrease in light intensity with use. With aging the filament in the lamp evaporate thus increasing the resistance.

In addition the glass cover of the lamp usually blackens with time due to deposition of tungsten particles on the lamp. This event results in decrease in the light output. In order to address this issue halogen-tungsten (efficacy being ~ 20 lm/W) based incandescent lamps have been developed.[123] These have longer life spans (~10 years) and have comparable intensity. The operating mechanism of halogen-tungsten lamps is similar to that of incandescent lamps, the only difference being the halogen utilized is regenerated.

One of the challenges associated with halogen-tungsten based incandescent lamps relates to the high operating temperatures that require fully ventilated conditions for operation. The incandescent lamps are associated with dimming issues. The CCT levels for these lamps drop with dimming. Typical incandescent lamps emit light of 15 lumens per watt and with CCT of ~ 2700 K.

1.9.2. Fluorescent light sources[112,121]

Fluorescent light sources are the most commonly encountered form of artificial visible light source. The operating mechanism in these light sources is based on electric discharge through a gas such as neon, krypton, argon, and xenon. These artificial visible light sources require the atoms and ions in the gas to collide when electrical current is passed across the electrodes. The general make-up of a fluorescent lamp constitutes a glass covered by a coating of fluorescent powder commonly referred to as phosphors. The lamp is filled with mercury vapor at very low pressure. On applying the voltage, electric current that flows in the electrodes causes the filaments to heat and emit electrons. The emitted electrons then flow towards the positive electrode producing the UV light. The UV light excites the phosphor coating, resulting in white light (visible light). The luminous flux, efficacy and color of the light from a fluorescent light source depend on the pressure of mercury vapor that in turn depends on the operating temperature.

Some of the major components of fluorescent lamps that affect the output of the lamps are discussed below:

Electrodes – The electrodes are mounted at the two ends of the fluorescent lamp and are capable of operating as either cold or hot cathodes. When the electrodes operate as cold cathode it is referred to as glow mode. While for the hot cathode mode of operation is termed as arc mode.

Gas Fill – The operating mechanism of the fluorescent light sources depends on the generation of the electric discharge between the electrodes. Apart from mercury vapor a rare gas or a combination of gases is added to facilitate the discharge.

Phosphors – The color of the fluorescent light sources largely depends on the nature of phosphors coated on the inner wall of glass lamp. Based on the blend of the phosphors coated, the spectra power distribution ranges from narrow to a combination of continuous and line spectra.

Bases – For high output efficiency, the fluorescent light sources is required to be mounted on to electrical circuit with proper voltage. Among the various possible designs for bases, a single-pin based system is known to have advantages. These provide rapid start times and avoid the pre-heating of the lamp.

The advantages associated with fluorescent light sources relate to their lower costs, efficiency and long lifetimes when compared to incandescent light sources. In addition, the fluorescent light sources are capable of generating narrow spectral bands. These can generate visible light with desired wavelength. Compact fluorescent lamps are known to emit light of 50 lumens per watt and with CCT of ~ 2700-3000 K.[122] The drawback of the fluorescent light sources that utilize mercury is associated to the toxicity of the metal. Since in an event of lamp breakage an alarming concern of cleaning ensues, therefore these lamps require additional safety for operation.

Also, these lamps require longer start times when turned on that effects their efficacy. These lamps "turn on" by a two-step protocol. In the first step, the electrodes get heated, which is followed by the ionization of gas.

1.9.3. Other artificial visible light sources[19,112,118]

Arc Discharge lamps – These lamps operate through ionization of xenon gas (or mercury vapor in some cases) housed inside a glass container. The ionization of gas allows the capacitor to discharge, resulting in a sudden burst of light. The gas then returns to its non-conductive state, which is followed by the recharging of the capacitor. These lamps are brighter than their tungsten-based incandescent counterparts and can often generate monochromatic light when coated with filters. For the mercury arc lamps much of the spectral distribution is centered in near-ultraviolet and blue spectrum. On the other hand the xenon arc lamps have a broader spectral distribution. These lamps require long time to turn on. However, an advantage associated with arc discharge lamps relates to the lack of filament in these lamps. An absence of filament results in no observable flickers during operation. Compact-arc lamps can provide light of very high luminance. These are utilized in searchlights, projectors and in optical instruments.

Flashtubes – Flashtubes also known as flash lamps produce flashes of high intensity and incoherent light of short duration. These find application mainly in photography, emergency lights, medical and for entertainment applications. Flashtubes operate at high voltages and require a lot of precaution for operation.

Electroluminescent lamps – Electroluminescent lamp or EL lamps are light emitting capacitors. In the EL lamps, a dielectric material (phosphor) is sandwiched between two parallel conductors. The dielectric material gets energized by a pulsating electric field, which emits light. Since the conductor utilized in the EL lamps is transparent it allows for the illuminated phosphor to be visible. The properties being these EL lamps are thin, flat, with flexible light sources. The flexibility of these light sources allows them to take various shapes and find useful application in LCD displays, aircraft instrument panels and mobile phones.

Light Emitting Diodes (LEDs) – These are semiconductor devices that produce visible light when an electrical current passed through them. The semiconducting material opted in LED is selected such that the wavelength of the released photons falls within the visible spectrum. Different materials emit photons at different wavelengths that appear as different light color. The typical efficacy of LEDs range from 23-43 lumens per watt at a CCT of ~ 2600-3500 K.[122]

These light sources do not radiate heat as in the case of incandescent lamps. This is because LEDs possess a heat sink, that absorbs the heat produced during lighting and keeps LEDs from overheating. LEDs possessing high luminous intensity have a narrow apex angle and like-wise LEDs with low luminous intensity have wide apex angle.

There are number of advantages associated with use of LEDs as an artificial visible light source that are listed below.[124]

a. LEDs produce high lumen output resulting in bright white light.

b. Tunable color LEDs provides a narrow spectral distribution.

c. LEDs are more energy-efficient thus requiring very low operational costs.

d. LED set up is flexible and can be custom built according to the operational requirements,

e. LEDs do not emit infrared radiation or possess toxic gases/metals. In addition these do not possess filaments that can break and are therefore very safe to operate.

f. These operate over a wide range of temperature and can easily withstand vibrations.

g. LEDs have longer life span than the conventional light sources.

h. LEDs can be digitally controlled for better efficiency and flexibility.

i. LEDs when dimmed to as low as 10%, still produce even luminous intensity across the LED matrix.

Light Amplification by the Stimulated Emission of Radiation (LASER)[125-127] – LASERs are artificial light sources that concentrate light waves into a low divergence beam. These devices emit continuous beam of light composed of a single discrete wavelength that exits the device as a coherent light. The material (laser crystal, diode, or gas) utilized in the LASER is responsible for the wavelength of the emitted light. One can classify them as semiconductor, solid-state, gas or as a liquid LASERs. In the recent times the use of semiconductor material based laser diodes have reduced the size and power requirements for light sources. LASER diodes require less power and are often faster in response than LEDs. The important characteristics of LASERs are these light sources emit monochromatic light and produce high energy density radiation. Recently Ning and co-workers have reported a monolithic white laser that is capable of emitting one or all the colors of the visible spectrum at once.[134]

Continued research in the development of efficient and user-friendly visible light emitting LASERs has a strong potential for application in photocatalysis. The serious limitation to the use of LASERs include expenses incurred for the light source (material used in the LASERs), the risk of damaging the optics, expensive lens, mirrors and other equipments, risk in damaging the retina while operating. Use of LASERs, as the artificial light sources require careful handling conditions. Another drawback associated with LASERs relate to its inefficiency in converting applied electric energy into light energy.

1.10. Choice of solvent

In addition to a photocatalyst and visible light source an additional parameter that plays a crucial role in photocatalysis is the choice of solvent.[128] A poor choice of solvent can often lead to undesired side products, decomposition of the starting material or the photoproduct(s). For visible light mediated photocatalysis it is imperative that the solvent employed should have no optical density in the irradiation window/wavelength. Some of the important considerations required while performing photocatalysis are described below:

a. Solvent should be free of impurities/additives.

b. For an efficient outcome, the solvent should be capable of dissolving the reactant(s) to afford a homogenous solution thus avoiding any issues from scattering/reflection of the light.

c. As mentioned earlier, the solvent must be optically transparent at the wavelength of excitation where the photocatalyst/photosensitizer absorbs exclusively.

d. The concentration of the reaction mixture for photocatalysis needs to be optimized for to avoiding internal filter effects from the solvent.

e. It is desirable to choose a green solvent/solvent mixtures whenever possible. The idea of "green solvents" describes the goal of green chemistry to minimize the environmental impact resulting from the use of solvents during chemical production.[129]

Table 1.3 summarizes some of the commonly employed organic solvents, their approximate cut off wavelength and the score (from 1-10, with a score of 10 being of most concern and a score of 1 suggesting few issue) for environmental waste and health concerns arising during a chemical transformation (adopted from ACS Green Chemistry Institute).[129-133]

Table 1.3: Common organic solvents with their respective dielectric constants, UV-Cut off values and the corresponding score for impact on health and environmental waste.

Entry	Solvent	Dielectric constant	UV Cut-off (nm)	Environmental waste	Health
1	*n*-hexanes	1.9	195	1 🟩	7
2	Cyclohexane	2.0	215	2 🟩	5
3	Carbon tetrachloride	2.2	265	7	8 🟥
4	Benzene	2.3	280	2 🟩	10 🟥
5	Toluene	2.4	285	7	2 🟩
6	1,4-Dioxane	2.2	230	7	6
7	Chloroform	4.8	245	9 🟥	6
8	Diethyl ether	4.3	215	5	4
9	Dichloromethane	9.1	230	7	7
10	Tetrahydrofuran	7.5	245	6	5
11	Ethyl acetate	6.0	255	4	4
12	Isobutyl acetate	20.0	255	3 🟩	2 🟩
12	Acetone	21.0	330	4	5
13	Acetonitrile	36.6	190	5	6
14	Dimethylsulfoxide	47.0	277	4	8 🟥
15	Ethanol	24.6	204	3 🟩	6
16	Methanol	32.6	205	5	6
17	Acetic acid	6.2	250	6	6
18	Water	78.5	185	-[a]	-[a]

[a] Information not available. Solvents with scores 1 - 3 are accompanied by 🟩 and solvents with score between 8 -10 are shown by 🟥 indicating possible concerns).

1.11. Summary and outlook

The well-established principles of organic photochemistry have opened avenues for chemists to study/employ light induced chemical transformations for targeting complex architectures. With visible light mediated photocatalysis, one can design and develop new organic materials for various applications. Even though there's been a plethora of reports on visible light induced organic reactions, there is still room for developing new methodologies. With an aim to contribute and expand the library of photochemical strategies, this thesis focuses on utilizing visible light with catalytic loading of photocatalyst/photosensitizer for performing traditional photoreactions. In this document we are also presenting studies to understand operating mechanisms for various visible-light mediated photochemical reactions.

Chapter-1 provides necessary background information to gain a basic understanding of organic photochemistry. It summarizes the recent efforts in the area of developing visible light induced organic reactions that proceeds *via* redox/redox-neutral intermediates. In addition, the chapter provides compilation of various visible light sources that can be utilized for visible light photocatalysis.

Chapter-2 highlights the role of *N-N* bond in performing visible light mediated traditional photoreactions. We have demonstrated classical photoreactions that require high-energy UV light, can be driven by visible light irradiation by incorporating hydrazide functionality as a "photoauxiliary". To demonstrate the applicability of this novel strategy, we have shown a diverse range of compounds have reacted smoothly to afford desired photoproducts under environmentally benign conditions. The work is equipped by detailed photophysical experiments that corroborate the experimental findings and showcases the role of excited state reactivity in hydrazide photochemistry. To the best of our knowledge this is the first account on *visible light mediated photocatalysis of traditional photoreactions*.

Chapter-3 extends the detailed photochemical investigations on hydrazides discussed in chapter-2. This work highlights the studies on developing *N-N* bond based chiral acrylanilides and their role in asymmetric photochemistry under visible light illumination. In addition, we have utilized *N-N* bond as a photoauxiliary for performing photocyclization, affording *N*-aminodihydroquinolinone derivatives, which are known to have significant biological activity.

We have also demonstrated the *role of N-N bond featuring restricted bond rotation leading to axial chirality influences the process of photocyclization in both isotropic and in crystalline media*.

Chapter-4 adds to the potential of hydrazides in visible light induced C-C bond formation under the conditions of sensitization. This chapter presents work that addresses one of the challenges in organic chemistry of increasing reaction efficiency by performing reactions with complete atom economy. We have provided detailed photochemical investigation on *visible light mediated chloromethylation of hydrazides,* under mild reaction conditions. The hydrazides were found to undergo intermolecular photoreactions smoothly to afford anilide based products.

Chapter-5 reflects the ability of the novel *hydrazides for catalyzing reactions under visible light sensitization* for useful applications viz synthesis of synthetic polymers with narrow molecular weight distribution. The chapter also compiles miscellaneous work that I have performed for developing strategies for visible light mediated sensitized photoreactions.

The work performed in the chapter-2, chapter-3, chapter-4 and a portion of chapter-5 has been documented in the provisional patent US 62/305,044. Reference: Sivaguru, J.; Iyer, A. Hydrazide Based Molecular Templates for Applications in Material Chemistry, Synthesis and Biological Systems. US 62/305, March 22, 2016. A part of work documented in the chapter-5 has been published. Reference: Iyer, A. Jockusch, S. Sivaguru, J. *J. Phys. Chem. A.* **2014**, *118*, 10596-10602.

1.12.   References

(1)   Klán, P.; Šolomek, T.; Bochet, C. G.; Blanc, A.; Givens, R.; Rubina, M.; Popik, V.; Kostikov, A.; Wirz, J. *Chem. Rev.* **2013**, *113*, 119-91.

(2)   Turro, N. J. R., V.; Scaiano, J. C. *Modern Molecular Photochemistry of Organic Molecules*; University Science Books: Sausalito, CA, 2010.

(3)   Albini, A.; Germani, L. *Photochemical Methods*; Wiley-VCH Verlag GmbH & Co. KGaA, 2009, 10.1002/9783527628193.ch1.

(4)   *Organic and Bio-molecular Chemistry - Volume II*; EOLSS Publications, 2009.

(5)   Turro, N. J.; Ramamurthy, V.; Scaiano, J. C. *Modern Molecular Photochemistry of Organic Molecules*; University Science Books: Sausalito, CA, 2010.

(6)   Danen, W. C.; Rio, V. C.; Setser, D. W. *J. Am. Chem. Soc.* **1982**, *104*, 5431-40.

(7)   Chang, W. S. C. *Principles of Lasers and Optics*; Cambridge University Press, 2005.

(8)   Papagni, A. In *Encyclopedia of Life Support Systems EOLSS*.

(9)   Frackowiak, D. *Journal of Photochemistry and Photobiology B: Biology* **1988**, *2*, 399.

(10)   Oelgemöller, M. *Chem. Rev.* **2016**, 10.1021/acs.chemrev.5b00720.

(11)   Albini, A. *Photochem. Photobiol. Sci.* **2016**, *15*, 319-24.

(12)   Aly, S. M.; Carraher, C. E.; Harvey, P. D. *Introduction to Photophysics and Photochemistry*; John Wiley & Sons, Inc., 2010.

(13)   Förster, T. *Annalen der Physik* **1948**, *437*, 55-75.

(14)   Forster, T. *Discussions of the Faraday Society* **1959**, *27*, 7-17.

(15)   Marcus, R. A.; Sutin, N. *Biochimica et Biophysica Acta (BBA) - Reviews on Bioenergetics* **1985**, *811*, 265-322.

(16)   Marcus, R. A. *Annu. Rev. Phys. Chem.* **1964**, *15*, 155-96.

(17)   Marcus, R. A. *Can. J. Chem.* **1959**, *37*, 155-63.

(18)   Closs, G. L.; Calcaterra, L. T.; Green, N. J.; Penfield, K. W.; Miller, J. R. *J. Phys. Chem.* **1986**, *90*, 3673-83.

(19)   Klán, P.; Wirz, J. *Photochemistry of Organic Compounds: From Concepts to Practice*; Wiley-Blackwell, 2009.

(20)   Rosspeintner, A.; Angulo, G.; Vauthey, E. *J. Am. Chem. Soc.* **2014**, *136*, 2026-32.

(21)   Kärkäs, M. D.; Porco, J. A.; Stephenson, C. R. J. *Chem. Rev.* **2016**, 10.1021/acs.chemrev.5b00760.

(22)   Bach, T.; Hehn, J. P. *Angew. Chem. Int. Ed.* **2011**, *50*, 1000-45.

(23)   Demuth, M. *Pure Appl. Chem.* **2009**, *58*, 1233-38.

(24)   Trommsdorff, H. *Annalen der Pharmacie* **1834**, *11*, 190-207.

(25)   Roth, H. D. *Angew. Chem. Int. Ed.* **1989**, *28*, 1193-207.

(26)   Roth, H. D. *Photochem. Photobiol. Sci.* **2011**, *10*, 1849-53.

(27)   Albini, A. *Photochemistry: Past, Present and Future*; 1st ed. ed.; Springer, 2016.

(28)   *Chemical photocatalysis*; Berlin: Walter de Gruyter GmbH & Co. KG., 2013.

(29)   Ciamician, G.; Silber, P. *Berichte der deutschen chemischen Gesellschaft* **1902**, *35*, 4128-31.

(30)   Ciamician, G. *Science* **1912**, *36*, 385-94.

(31)   McNaught, A. D.; Wilkinson, A.; Blackwell Scientific Publications: Oxford, 2014.

(32)   McNaught, A. D.; Wilkinson, A.; BlaBlackwell Scientific Publications: Oxford 1997.

(33)   Yoon, T. P.; Ischay, M. A.; Du, J. *Nat. Chem.* **2010**, *2*, 527-32.

(34)   Albini, A. PhotoGreen Lab. http://www-2.unipv.it/photochem/ricerca_en.php - sezione1 (accessed 23 July 2016).

(35)   Schultz, D. M.; Yoon, T. P. *Science* **2014**, *343*.

(36)   Hazards of Ultraviolet Radiation. http://www.uvm.edu/safety/lab/hazards-of-ultraviolet-radiation (accessed 19 July 2016).

(37)   Romero, N. A.; Nicewicz, D. A. *Chem. Rev.* **2016**, 10.1021/acs.chemrev.6b00057.

(38)   Whitten, D. G.; Zarnegar, P. P. *J. Am. Chem. Soc.* **1971**, *93*, 3776-77.

(39)   Whitten, D. G. *Acc. Chem. Res.* **1980**, *13*, 83-90.

(40)   Nicewicz, D. A.; Nguyen, T. M. *ACS Catal.* **2014**, *4*, 355-60.

(41)   Pitre, S. P.; McTiernan, C. D.; Scaiano, J. C. *ACS Omega* **2016**, *1*, 66-76.

(42)   Li, X.; Chen, D.; Liu, Y.; Yu, Z.; Xia, Q.; Xing, H.; Sun, W. *CrystEngComm* **2016**, *18*, 3696-702.

(43)   Toyao, T.; Ueno, N.; Miyahara, K.; Matsui, Y.; Kim, T.-H.; Horiuchi, Y.; Ikeda, H.; Matsuoka, M. *Chem. Commun.* **2015**, *51*, 16103-06.

(44)   Johnson, J. A.; Luo, J.; Zhang, X.; Chen, Y.-S.; Morton, M. D.; Echeverra, E.; Torres, F. E.; Zhang, J. *ACS Catal.* **2015**, *5*, 5283-91.

(45)   Zhang, W.-Q.; Li, Q.-Y.; Zhang, Q.; Lu, Y.; Lu, H.; Wang, W.; Zhao, X.; Wang, X.-J. *Inorg. Chem.* **2016**, *55*, 1005-07.

(46)   Wang, S.; Wang, X. *Small* **2015**, *11*, 3097-112.

(47)   Hedstrand, D. M.; Kruizinga, W. H.; Kellogg, R. M. *Tetrahedron Lett.* **1978**, *19*, 1255-58.

(48)   Yoon, T. P. *ACS Catal.* **2013**, *3*, 895-902.

(49)   Narayanam, J. M. R.; Stephenson, C. R. J. *Chem. Soc. Rev.* **2011**, *40*, 102-13.

(50)   Prier, C. K.; Rankic, D. A.; MacMillan, D. W. C. *Chem. Rev.* **2013**, *113*, 5322-63.

(51)   Zeitler, K. *Angew. Chem. Int. Ed.* **2009**, *48*, 9785-89.

(52)   Liang, Y.; Bergbreiter, D. E. *Catal. Sci. Techonol* **2016**, *6*, 215-21.

(53)   Pan, J.; Zhang, B.; Jiang, X.; Zhang, L.; Cheng, Z.; Zhu, X. *Macromol. Rapid Commun.* **2014**, *35*, 1615-21.

(54)   Liu, P.; Ye, Z.; Wang, W.-J.; Li, B.-G. *Macromolecules* **2013**, *46*, 72-82.

(55)   Bergbreiter, D. E. *ACS Macro Lett.* **2014**, *3*, 260-65.

(56)   Guerra, J.; Cantillo, D.; Kappe, C. O. *Catal. Sci. Techonol* **2016**, *6*, 4695-99.

(57)   Luo, J.; Zhang, X.; Zhang, J. *ACS Catal.* **2015**, *5*, 2250-54.

(58)   Su, C.; Tandiana, R.; Tian, B.; Sengupta, A.; Tang, W.; Su, J.; Loh, K. P. *ACS Catal.* **2016**, *6*, 3594-99.

(59)   Ghasimi, S.; Landfester, K.; Zhang, K. A. I. *ChemCatChem* **2016**, *8*, 694-98.

(60)   Liu, D.; Wang, J.; Bai, X.; Zong, R.; Zhu, Y. *Adv. Mater.* **2016**, 10.1002/adma.201601168.

(61)   Zheng, Y.; Lin, L.; Wang, B.; Wang, X. *Angew. Chem. Int. Ed.* **2015**, *54*, 12868-84.

(62)   Wang, Z. J.; Ghasimi, S.; Landfester, K.; Zhang, K. A. I. *Adv. Mater.* **2015**, *27*, 6265-70.

(63)   Wang, Z. J.; Garth, K.; Ghasimi, S.; Landfester, K.; Zhang, K. A. I. *ChemSusChem* **2015**, *8*, 3459-64.

(64)   Ma, B. C.; Ghasimi, S.; Landfester, K.; Vilela, F.; Zhang, K. A. I. *J. Mater. Chem. A* **2015**, *3*, 16064-71.

(65)   Wang, L.; Huang, W.; Li, R.; Gehrig, D.; Blom, P. W. M.; Landfester, K.; Zhang, K. A. I. *Angew. Chem. Int. Ed.* **2016**, 10.1002/anie.201603789, n/a-n/a.

(66)   Hering, T.; Mühldorf, B.; Wolf, R.; König, B. *Angew. Chem. Int. Ed.* **2016**, *55*, 5342-45.

(67)   Hartman, T.; Cibulka, R. *Org. Lett.* **2016**, 10.1021/acs.orglett.6b01743.

(68)   Boutin, C. NIST Shows Organic Solar Industry Something New Under the Sun. Published Online: 2015. http://www.nist.gov/pml/div682/201507_organic_solar.cfm (accessed 20 July 2016).

(69)   Zhao, N.; Caputo, J.; Sowers, K.; Weix, D.; Krauss, T., University of Rochester

(70)   Xiao, F.-X.; Miao, J.; Wang, H.-Y.; Liu, B. *J. Mater. Chem. A* **2013**, *1*, 12229-38.

(71)   Primo, A.; Corma, A.; Garcia, H. *Phys. Chem. Chem. Phys.* **2011**, *13*, 886-910.

(72)   Watanabe, K.; Menzel, D.; Nilius, N.; Freund, H.-J. *Chem. Rev.* **2006**, *106*, 4301-20.

(73)   Zheng, Z.; Huang, B.; Qin, X.; Zhang, X.; Dai, Y.; Whangbo, M.-H. *J. Mater. Chem.* **2011**, *21*, 9079-87.

(74)   Peiris, S.; McMurtrie, J.; Zhu, H.-Y. *Catal. Sci. Techonol* **2016**, *6*, 320-38.

(75)   Xiao, Q.; Jaatinen, E.; Zhu, H. *Chem. –An Asian J.* **2014**, *9*, 3046-64.

(76)   Banin, U.; Ben-Shahar, Y.; Vinokurov, K. *Chem. Mater.* **2014**, *26*, 97-110.

(77)   Subramanian, V.; Wolf, E.; Kamat, P. V. *J. Phys. Chem. B* **2001**, *105*, 11439-46.

(78)   Margapoti, E. Plasmonics: Fundamentals and Applications. Published Online: 2012. http://www.wsi.tum.de/portals/0/media/lectures/1e3fd2e6-eb4e-466a-b891-93fa9ee4b9d2/plasmonics_chapter_1.pdf (accessed 22 July 2016).

(79)   Kale, M. J.; Avanesian, T.; Christopher, P. *ACS Catal.* **2014**, *4*, 116-28.

(80)   Timpe, H.-J.; Neuenfeld, S. *J. Chem. Soc., Faraday Trans.* **1992**, *88*, 2329-36.

(81)   Kayser, R. H.; Young, R. H. *Photochem. Photobiol.* **1976**, *24*, 395-401.

(82)   Tajalli, H.; Gilani, A. G.; Zakerhamidi, M. S.; Tajalli, P. *Dyes Pigm.* **2008**, *78*, 15-24.

(83)   Jose, J.; Ueno, Y.; Burgess, K. *Chem. Eur. J.* **2009**, *15*, 418-23.

(84)   Spectroscopic and electrochemical studies on redox dyes http://shodhganga.inflibnet.ac.in/bitstream/10603/25632/9/09_chapter 1.pdf (accessed 23 July 2016).

(85)   Austin, J. M.; Harrison, I. R.; Quickenden, T. I. *J. Phys. Chem.* **1986**, *90*, 1839-43.

(86)   Beaumont, P. C.; Johnson, D. G.; Parsons, B. J. *J. Chem. Soc., Faraday Trans.* **1993**, *89*, 4185-91.

(87)   Benniston, A. C.; Elliott, K. J.; Harrington, R. W.; Clegg, W. *Eur. J. Org. Chem.* **2009**, *2009*, 253-58.

(88)   Fukuzumi, S.; Ohkubo, K. *Chem. Sci.* **2013**, *4*, 561-74.

(89)   Morse, P. D.; Nicewicz, D. A. *Chem. Sci.* **2015**, *6*, 270-74.

(90)   Hari, D. P.; Konig, B. *Chem. Commun.* **2014**, *50*, 6688-99.

(91)   Rao, P. S.; Hayon, E. *J. Phys. Chem.* **1973**, *77*, 2753.

(92)   Prahl, S. Eosin Y. http://omlc.org/spectra/PhotochemCAD/html/061.html (accessed 23 July 2016).

(93)   Prahl, S.; Oregon Medical Laser Center.

(94)   Kalyanasundaram, K. *Coord. Chem. Rev.* **1982**, *46*, 159-244.

(95)   Van Houten, J.; Watts, R. J. *J. Am. Chem. Soc.* **1976**, *98*, 4853-58.

(96)   Bock, C. R.; Connor, J. A.; Gutierrez, A. R.; Meyer, T. J.; Whitten, D. G.; Sullivan, B. P.; Nagle, J. K. *J. Am. Chem. Soc.* **1979**, *101*, 4815-24.

(97)   Nicewicz, D. A.; MacMillan, D. W. C. *Science* **2008**, *322*, 77-80.

(98)   Ischay, M. A.; Anzovino, M. E.; Du, J.; Yoon, T. P. *J. Am. Chem. Soc.* **2008**, *130*, 12886-87.

(99)   Narayanam, J. M. R.; Tucker, J. W.; Stephenson, C. R. J. *J. Am. Chem. Soc.* **2009**, *131*, 8756-57.

(100)   Kerr, E.; Doeven, E. H.; Barbante, G. J.; Hogan, C. F.; Hayne, D. J.; Donnelly, P. S.; Francis, P. S. *Chem. Sci.* **2016**, 10.1039/C6SC01570K.

(101)   Takayasu, S.; Suzuki, T.; Shinozaki, K. *J. Phys. Chem. B* **2013**, *117*, 9449-56.

(102)   Dadashi-Silab, S.; Aydogan, C.; Yagci, Y. *Polymer Chemistry* **2015**, *6*, 6595-615.

(103)   Dadashi-Silab, S.; Doran, S.; Yagci, Y. *Chem. Rev.* **2016**, 10.1021/acs.chemrev.5b00586.

(104)   Thioxanthone. *National Institute of Standards and Technology*. Published Online: 2011. http://webbook.nist.gov/cgi/cbook.cgi?ID=C492228&Mask=400 (accessed 23 July 2016).

(105)   Scaiano, J. C.; Stamplecoskie, K. G.; Hallett-Tapley, G. L. *Chem. Commun.* **2012**, *48*, 4798-808.

(106)   Leung, A. *Multimedia, Communication and Computing Application*; CRC Press, 2014.

(107)   The Physics Hypertextbook. http://physics.info (accessed 1 September 2016).

(108)   National Aeronautics and Space Administration. http://science-
         edu.larc.nasa.gov/EDDOCS/Wavelengths_for_Colors.html (accessed 1 September 2016).

(109)   Harris, D. C.; Bertolucci, M. D. *Symmetry and Spectroscopy*; Dover Publications, 1978.

(110)   Light and Color. http://lodev.org/cgtutor/color.html (accessed 1 September 2016).

(111)   The Nature of Light and Color. http://dba.med.sc.edu/price/irf/Adobe_tg/color/light.html (accessed
         1 September 2016).

(112)   Sources of Visible Light. http://www.olympusmicro.com/primer/lightandcolor/lightsourcesintro.html
         (accessed 1September 2016).

(113)   Light sources and illuminants. http://www.konicaminolta.eu/en/measuring-instruments/learning-
         centre/light-measurement/light/light-sources-and-illuminants.html (accessed 1 September 2016).

(114)   Bowersox, A. Understanding Light Quality: Color Temperature and Color Rendering Index.
         http://blogs.umass.edu/abowersox/files/2015/02/Understanding-Light-Quality-CT-and-CRI.pdf
         (accessed 1 September 2016).

(115)   Watson, S. Basic Characteristics of Light Sources.
         http://www.ledinside.com/knowledge/2012/9/basic_characteristics_light_sources_20120917
         (accessed 1 September 2016).

(116)   Spectral Power Distribution Curves.
         http://www.gelighting.com/LightingWeb/na/resources/tools/lamp-and-ballast/spectral-power-
         distribution-curves.jsp.

(117)   Hye Oh, J.; Ji Yang, S.; Rag Do, Y. *Light Sci Appl* **2014**, *3*, 141.

(118)   Fundamentals. http://paduaresearch.cab.unipd.it/273/1/20080128_TESI_Copia_consegnata.pdf
         (accessed 1 September 2016).

(119)   NIST Photometry-National Institue of Standards and Technology.
         https://http://www.nist.gov/programs-projects/photometry (accessed 1 September 2016).

(120)   Photometeric definitions. http://www.stanfordcomputeroptics.com/download/photometry.pdf (accessed 1 September).

(121)   Incandescent and Fluorescent Lighting. http://www.canon.com/technology/s_labo/light/002/02.html (accessed 1 September).

(122)   Color Quality of Whtie LEDs. http://www.cool.conservation-us.org/byorg/us-doe/color_quality_of_white_leds.pdf (accessed 1 September 2016).

(123)   LED Basics. http://energy.gov/eere/ssl/led-basics (accessed 1 September 2016).

(124)   Color Kinetics. http://www.colorkinetics.com/Learn/What-is-an-LED/ (accessed 1 September 2016).

(125)   Introduction to Lasers. https://http://www.sony.net/Products/SC-HP/laserdiodewld/technology/guide.html (accessed 1 September 2016).

(126)   Shimoda, K. *Introduction to Laser Physics*; Springer, 1984.

(127)   Telle, H. H.; Urena, A. G.; Donovan, J. *Laser Chemistry: Spectroscopy, Dynamics and Applications*; Wiley 2007.

(128)   Kalyanasundaram, K. *Photochemistry in Microheterogenous Systems*; Academic Press, 1987.

(129)   Capello, C.; Fischer, U.; Hungerbuhler, K. *Green Chemistry* **2007**, *9*, 927-34.

(130)   Reichardt, C.; Welton, T. *Solvent Effects on the Absorption Spectra of Organic Compounds*; Wiley-VCH Verlag GmbH & Co. KGaA, 2010, 10.1002/9783527632220.ch6.

(131)   *Handbook of Photochemistry, Third Edition*; Taylor & Francis Group, LLC, 2006.

(132)   Common Organic Solvents. https://http://www.organicdivision.org/orig/organic_solvents.html (accessed 1 September 2016).

(133)   Maryott, A. A.; Smith, E. R. Table of Dielectric Constant of Pure Liquids. Published Online: 1951. http://www.dtic.mil/dtic/tr/fulltext/u2/a278956.pdf (accessed 1 September 2016).

(134)   Fan, F.; Turkdogan, S.; Liu, Z.; Shelhammer, D.; Ning, C. Z. *Nat. Nanotechnol.* **2015**, *10*, 796-803.

CHAPTER 2. VISIBLE LIGHT MEDIATED PHOTOCATALYSIS OF CLASSICAL PHOTOREACTIONS

2.1.   Introduction

Nature uses light as a powerful tool to catalyze transformations with precision to perform life-sustaining processes.[1] This serves as an inspiration for scientists to study photoinduced processes to design and develop methodologies for the synthesis of complex structural scaffolds and for building photoresponsive materials and molecular assemblies with unique architectures.[2] Recently, the use of visible light for generating radical species has attracted the attention of chemists as it provides an environmentally friendly strategy to initiate chemical reactions.[3-4] The light induced organic reactions have been studied to access pharmaceutics, agrochemicals, macromolecules and polymers.

Organic photochemistry provides an easy and benign route to access complex scaffolds often in a single step phototransformation.[1-2,5-9] Photoreactions have been frequently employed as a key step in the synthesis of many natural products. Light induced chemical transformations provides a green route to construct C-C / C-O bonds while avoiding metal catalysts.

Scheme 2.1: Classical photoreactions - excited state photochemistry.

Classical photoreactions are well studied and documented in the literature. A few useful classical photoreactions include [2+2] photocycloaddition, Paternò-Büchi reaction, 6π photocyclization, and Norrish-Yang reaction (Scheme 2.1).[10] On absorbing light, the ground state molecule gets excited to the higher energy level and this photoexcited species finally leads to the formation of photoproduct (Figure 2.1). The classical photoreactions are known to involve intermediates that are excited state species (Scheme 2.1).[10] The excited species are often characterized by short lifetimes. These photoreactions provide a useful toolbox for constructing complex scaffolds that find utility in chemical, materials and biological applications.[1] For example, the [2+2] photocycloaddition reactions are an important class of photoreactions that lead to cyclobutane based photoproducts.
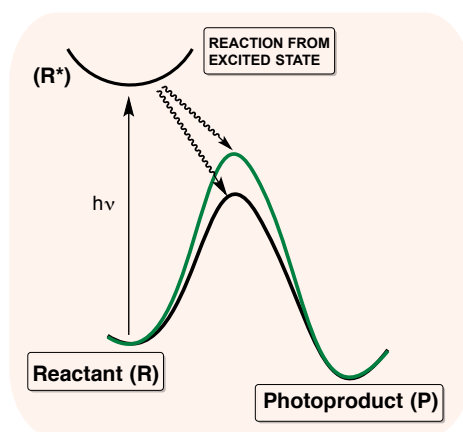
Figure 2.1: Illustration of photochemical paradigm for light induced chemical transformations.

An excited state olefin adds to another alkene (same or different) to afford a cyclobutane based photoadduct. In case of Paternò-Büchi reaction, a carbonyl group containing molecule gets excited by absorbing appropriate energy of light and adds to an alkene that leads to the formation of oxetane derivative. If the excited carbonyl group has a γ–H available for abstraction then the light induced process leads to an intramolecular photoreaction that would result in β-lactam based photoproduct. This class of photoreactions is termed as Norrish-Yang reactions. Another useful classical photoreaction is 6π photocyclization. A compound containing conjugated 6π electron system with suitable energetics, can undergo a concerted light induced conrotatory 6π ring closure to form six membered ring system on absorbing light.

In the recent times, the photoredox chemistry has emerged as a useful strategy to utilize visible light and an appropriate photocatalyst to access various compounds.[11] Due to the strong potential for classical photoreactions to access complex scaffolds we became interested in developing visible light mediated photocatalysis of classical photoreactions. In addition a chemical reaction mediated by visible light provides a green route for the synthesis of desired compounds, which made us focus our attention on utilizing visible light for organic transformations.

N-N bond based compounds are amongst the diverse range of synthetically useful organic functionalities. This particular functionality caught our attention, as it is present in many natural products and in biologically useful compounds.[12-14] Even though one can find vast literature on photochemistry of azo compounds (R-*N*=*N*-R) and on azides (R-*N*=*N$^+$*=*N$^-$*), due to the lack of reports on the synthesis of *N-N* bond based compounds their photochemistry in not well documented in the literature.[12,14-16] With photoredox chemistry emerging as a useful tool in recent times, there has been few reports on photoinduced electron transfer reactions involving *N*-centered radical generated from *N-N* bond based compounds.[17] With a focus on light induced chemical transformations, we have classified photoreactions of *N-N* bond based compounds in two main categories *viz.* (a) UV/Visible light mediated metal free photoreactions of *N-N* bond based compounds and (b) Visible light mediated photoredox catalysis involving *N-N* bond based compounds.

(a)   UV/Visible light mediated metal free photoreactions of *N-N* bond based compounds

The first communication conferred by the group of Gilchrist, Rees and Stanton on photoreactions of *N-N* bond based compounds dates back to the year 1971.[18] The group studied the photochemistry of Phthalimidoziridines and related systems. They observed that on irradiating a solution of 1- phthalimidoziridine **22** in presence of another olefin, the former underwent an addition of the olefin to yield the corresponding aziridine skeleton **24** (Scheme 2.2). The proof of concerted fragmentation of the phthalimidoziridines to give olefin and corresponding phthalimidonitrene was confirmed by trapping the nitrene with another olefin.

| **22** | **23** | **24** | **25** |
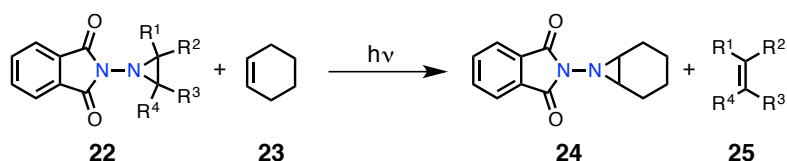
Scheme 2.2: Photoreaction of phthalimidoziridines.[18]

Early reports on electron transfer photo-oxidation of hydrazines from Nelson and co-workers[19], inspired Ferroud and coworkers to study the visible light mediated photocyanation of tertiary amine based hydrazines for obtaining α-aminonitriles.[20] The formal charge of a hydrazinium radical cation **27** distributed over two nitrogen atoms explains the observed photochemical stability of these compounds (Scheme 2.3). The measured electrochemical potential (E° value) for hydrazines (acetonitrile, vs SEC) were observed to vary between 0.2 and 0.4 V and were lower than regular tertiary amines (0.7 - 0.8 V).

| **26** | **27** |
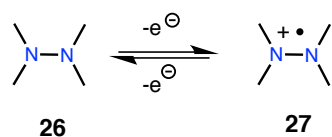
Scheme 2.3: Single electron transfer reaction in tertiary hydrazine.[21]

The electrochemical data was consistent for quenching of $^1O_2$ by easily ionizable tertiary hydrazines. The catalytic system employed involved a combination of tertiary hydrazine, organic photocatalyst (methylene blue), a source of cyanide anion and visible light to afford the corresponding α-aminonitrile (Scheme 2.4).
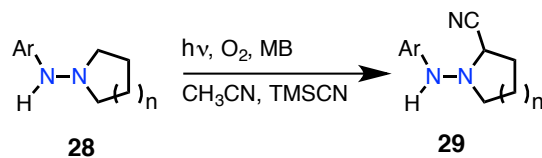
Scheme 2.4: Visible light mediated synthesis of α-hydrazinonitriles.[20]

A wide variety of α-hydrazinonitriles underwent typical SET photocatalytic reaction smoothly and efficiently in moderate to excellent yields (ca. 59 - 94%). The crude products obtained from photooxidation reaction of hydrazines were pure enough for further synthetic use. Later, the group reported that on changing the nucleophile from cyanide to hydroxide anion resulted in the photocyanation of hydrazine **31** to give corresponding amino-dialkylacetals **34** (Scheme 2.5).[21]
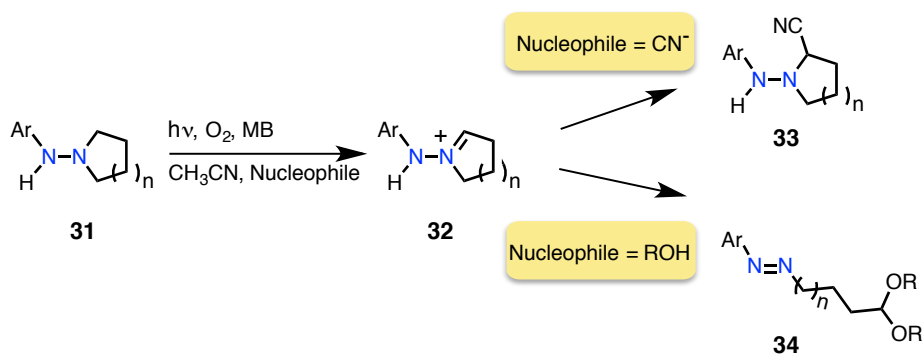
Scheme 2.5: Light mediated single electron transfer reaction in *N*-arylaminopyrrolidines with different nucleophiles.[22]

Based on these two results the group evaluated a sequential photoinduced oxidation of hydrazines under the mild and green conditions. In the study they demonstrated a successive photooxidation of *N*-arylaminopyrrolidines **35** to give the corresponding lactam based products **40** (Scheme 2.6).[23]
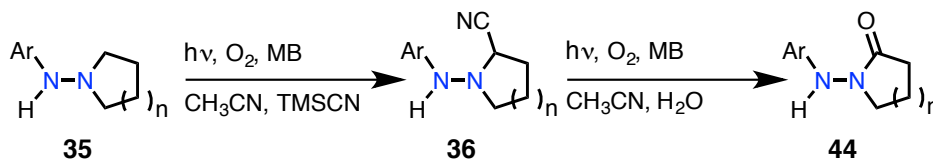
Scheme 2.6: Photoinduced sequential single electron transfer reactions of *N*-arylaminopyrrolidines.[22]

This transformation occurs by the reaction of an initial hydrazinium cation **35** with cyanide ion as nucleophile followed by reaction with water. A particularly noteworthy observation is that the second oxidation of the nitrile derivative **36** proceeds by a photocatalytic process. Direct evidence for the oxidation step of α-aminonitriles when compared to α-hydrazinonitriles was obtained by means of cyclic voltammetry measurements. These electrochemical results demonstrated the greater ease of oxidation of the α-hydrazinonitriles **35** than the corresponding α-aminonitriles **36** (*i.e.* 1.19 V (**35**) compared to 1.47 V (**36**))[23]. The results were consistent with the fact that this process involved a catalytic amount of methylene blue (MB) under oxygen atmosphere. It was proposed that the photooxygenation involved energy transfer from excited triplet of the sensitizer (MB) to the molecular oxygen.[22] The triplet sensitizer results in the conversion of ground state triplet oxygen ($^3O_2$) into a short-lived and highly reactive singlet oxygen ($^1O_2$). Another possible route for photooxygenation was possible from a SET from cyanohydrazine **36** derivative to the excited MB. The generated radical anion of MB could get re-oxidized by molecular oxygen to produce the superoxide anion. The reaction between the hydrazinium radical cation **37** and the superoxide anion could lead to oxidation products. Deprotonation of the radical cation **37** generated by either mechanism yields the α-hydrazino or the hydrazyl radical **39** that could then get oxidized to corresponding hydrazinium alkylidene ion **42** that exists in equilibrium with the 1,1-dialkyl-2-phenyldiazenium ion **41**.
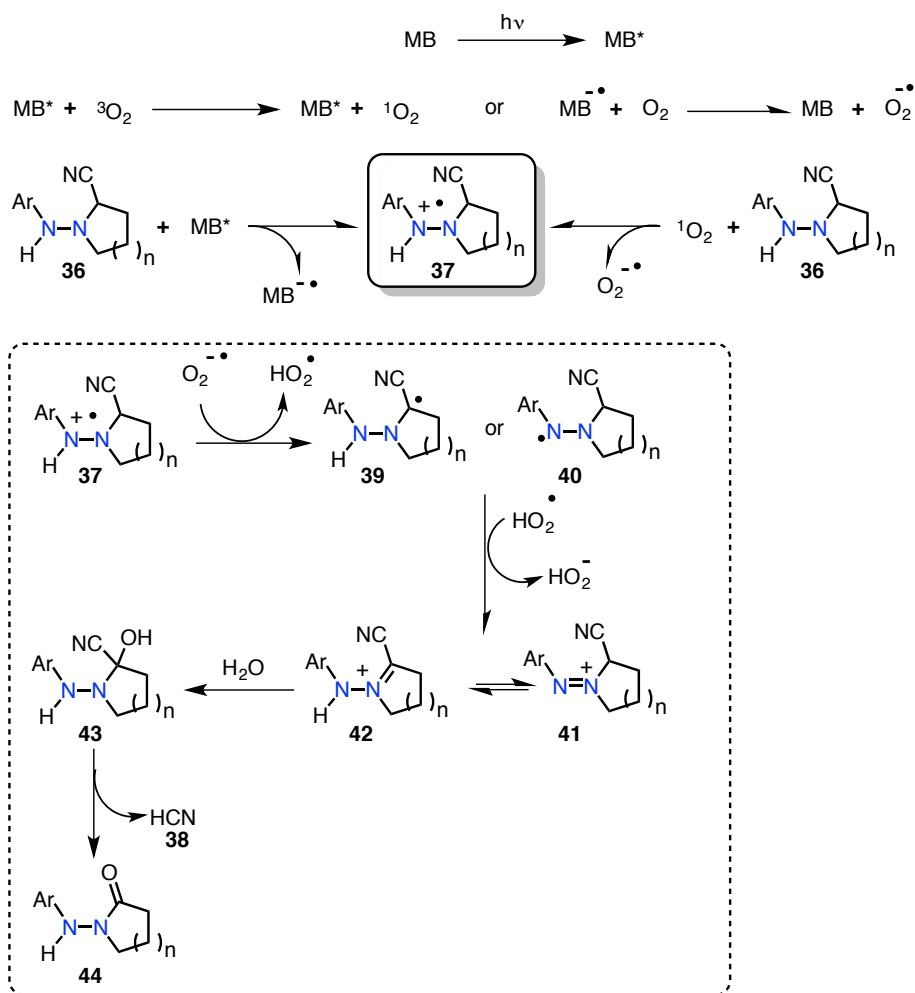
Scheme 2.7: Plausible mechanism for photoinduced sequential single electron transfer in *N*-arylaminopyrrolidines.[22-23]
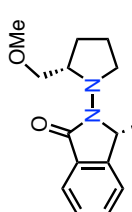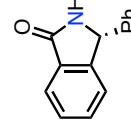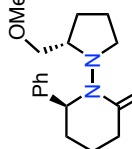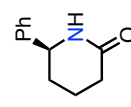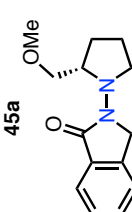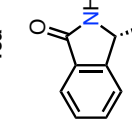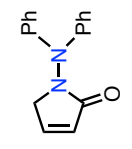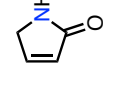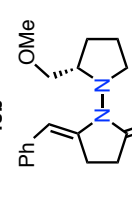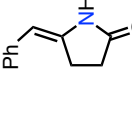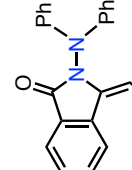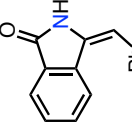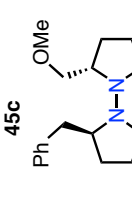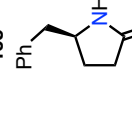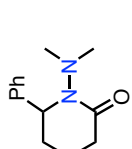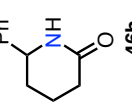
Quenching of alkylidene cation **42** by a water molecule followed by an elimination of HCN **38** leads to the observed hydrazide derivative **44**. The mechanism was bolstered by the irradiation of cyanohydrazine under the conditions of photooxygenation while avoiding water to yield only the starting material. Addition of small amounts of water initiates the photooxidation thus confirming the plausible mechanism. Couture et al. reported light mediated *N–N* bond cleavage in *N,N*-disubstituted hydrazides.[24] The work showcased a mild, efficient and greener methodology for *N–N* bond cleavage. The strategy utilizes non-oxidative, photoinduced *N–N* bond cleavage thus affording secondary amides **46 a-h** (Scheme 2.8). The benefits associated with this methodology against the traditional methods include functional group tolerance and compatibility with chiral substrates (Table 2.1).

The study provides an easy and cleaner alternative for deamination of hydrazides. The photochemical cleavage is assumed to proceed via homolytic *N–N* bond cleavage. The authors hypothesized that the cleavage was a consequence of low energy requirement for the *N–N* bond cleavage. The hydrazide on 254 nm light irradiation undergoes energy dissipation to *N–N* bond which is the least stable bond in the chromophore.

45 a-h　　　　　　　　**46 a-h**
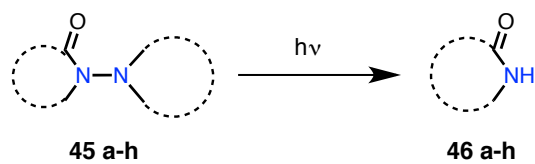
Scheme 2.8: Light mediated *N–N* bond cleavage.[24]
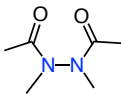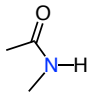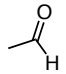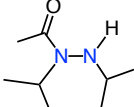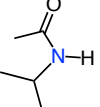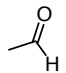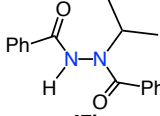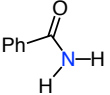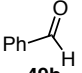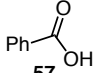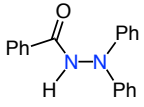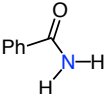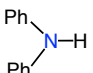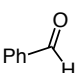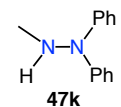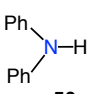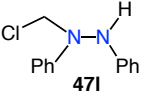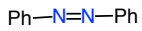
Table 2.1: Hydrazides and corresponding photoproducts from photoinduced non-oxidative *N–N* bond cleavage.[a]

Entry	Hydrazide	Photoproduct	Isolated Yield [%]	Entry	Hydrazide	Photoproduct	Isolated Yield [%]
1	45a	46a	64	5	45e	46e	71
2	45b	46b	66	6	45f	46f	63
3	45c	46c	62	7	45g	46g	61
4	45d	46d	69	8	45h	46h	76

[a]Irradiation conditions: Solution of hydrazide (0.2 mmol) in toluene (5 mL) and *n*-hexane (200 mL) was purged by bubbling argon followed by photolyses in a water-cooled quartz reactor equipped with dry argon inlet and magnetic stirrer. The solution was irradiated in a Rayonet photochemical reactor containing eight RUL 2537 Å lamps. [Data adapted from reference 24]

The other report that sheds little insights into the hydrazide photochemistry comes from Watterson and coworkers (Scheme 2.9). They observed hydrazides on UV light irradiation underwent N–N / N-C (carbonyl carbon) bond cleavage (Table 2.2).[25]

| 47 a-l | 48 a-l | 49 a-l | 50 - 57 |

Scheme 2.9: Photoinduced N–N bond cleavage in hydrazides.[25]

Table 2.2: Hydrazides and corresponding cleaved photoproducts.[a]

Entry	Hydrazide	N-N bond cleaved products			OC-N cleaved products	
1	47a	50 (14 %)	48a (4.5 %)	51 (23 %)	49a (8.1 %)	53 (19.6 %)
2	47b		48b (19 %)		49b (5.4 %)	
3	47c		48c (10 %)		49c (4.3 %)	
4	47d		48d (25 %)	52 (21 %)	49d (4.3 %)	
5	47e		48e (30 %)		49e (9.2 %)	54 (2.1 %)

[a] Irradiation conditions: Solution of hydrazide (0.1 – 0.001 M) in benzene was purged by bubbling dry nitrogen for 0.5 h followed by photolyses with Rayonet photochemical reactor containing 253.7 nm lamps in quartz tube.

Table 2.2: Hydrazides and corresponding cleaved photoproducts (continued).[a]

Entry	Hydrazide	N-N bond cleaved products		OC-N cleaved products	
6	**47f**	**48f** (27 %)		**49f** (1.2 %)	
7	**47g**	**48g** (27 %)		**49g** (10 %)	
8	**47h**	**48h** (11 %)		**49h** (8.3 %)	**57** (9.9 %)
9	**47i**	**48i** (24 %)	**55** (37 %)	**49k** (4.7 %)	
10	**47k**		**56** (23 %)		
11	**47l**			Ph—N=N—Ph **57** (52 %)	

[a] Irradiation conditions: Solution of hydrazide (0.1 – 0.001 M) in benzene was purged by bubbling dry nitrogen for 0.5 h followed by photolyses with Rayonet photochemical reactor containing 253.7 nm lamps in quartz tube.

(b) **Visible light mediated photoredox catalysis involving N-N bond based compounds.**

Few reports mentioned in the literature involving photoinduced electron transfer process in *N-N* bond based compounds include *N*-aminopyridinium salts, organic azides and imines.[17] The first report involving *N*-aminopyridinium salt (Scheme 2.10, **58** - **60**) in visible light-induced direct amidation of arenes and heteroarenes comes from Studer and coworkers.[26] Their work highlights a mild and an efficient method for converting *N–N* bond into *N*-centered radical that eventually leads to products. The pyrylium salts reported in their work were highly stable and could be stored for months at room temperature.

They utilized Ru(bpy)₃Cl₂ as the photocatalyst and blue LEDs as the light source. They showcased a diverse range of amidation products were possible for both electron-rich arenes (**61**) and heteroarenes (**65**). The reactions worked in good yields and with complete regioselectivity in the product. The proposed mechanism for the reaction involves an oxidative quenching of the photoexcited photocatalyst *Ru(II) complex by *N*-aminopyridinium salts (Scheme 2.10). The neutral *N*-centered radical intermediate (**64**) is formed from the cleavage of *N–N* bond by SET and a strongly oxidizing Ru(III) species is simultaneously generated. This is followed by the interception of the *N*- centered radical to heteroarene that finally leads to the desired amidation product **68**.
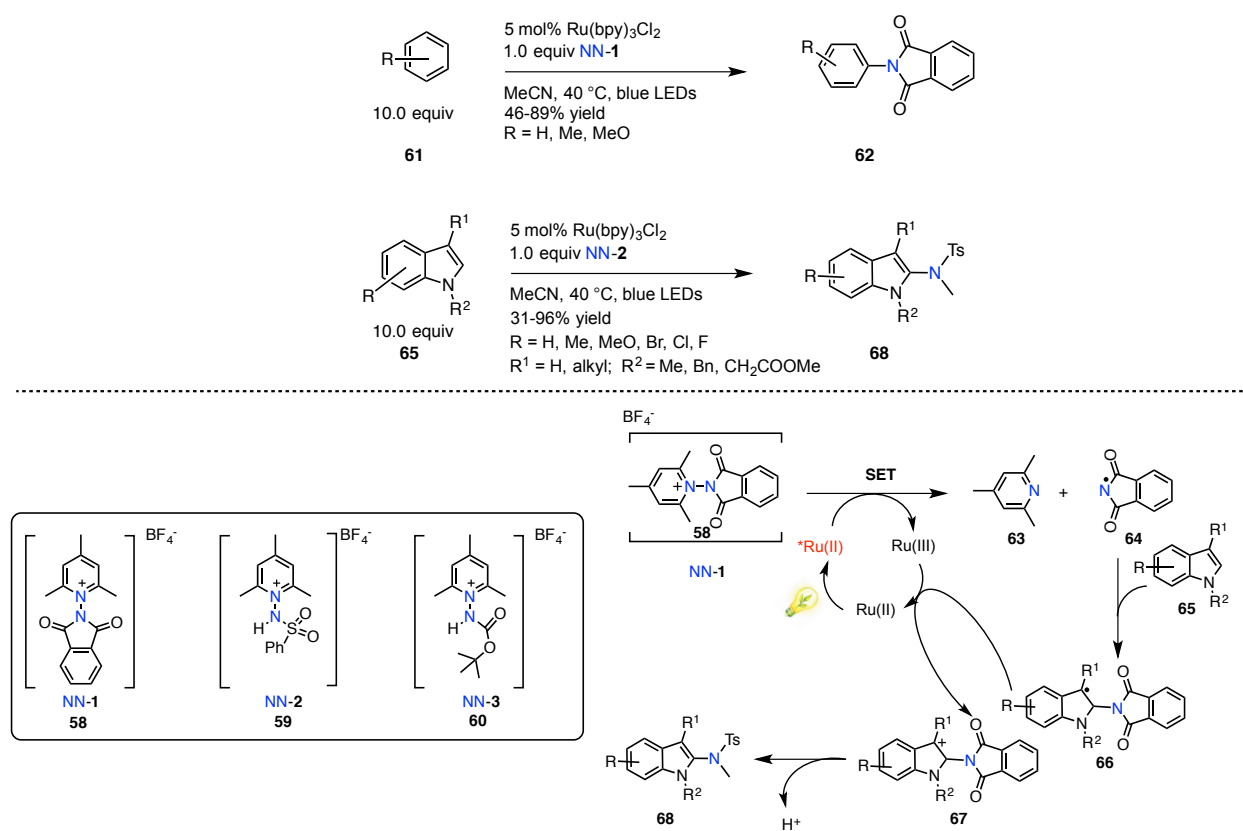
Scheme 2.10: Visible light mediated direct amidation of arenes and heteroarenes.[26]

Another report on the use of *N*-aminopyridinium salts comes from the group of Koike and Akita.[27] They developed *N*–Ts-protected 1-aminopyridinium salt **69** for aminohydroxylation of olefins (**72**) to afford vicinal aminoalcohol derivatives (**75**) (Scheme 2.11). A variety of styrene analogues bearing electron-donating / withdrawing substituents on the phenyl ring reacted smoothly in the presence of Ir(III) complex under visible light irradiation to afford the corresponding aminoalcohols in good yields. In addition they demonstrated gram scale reaction to illustrate the efficiency of their methodology. In order to substantiate their mechanism, they performed a ring-opening radical clock reaction with 1-phenyl-2-(1-phenylethenyl)cyclopropane **72a** under the standard experimental conditions (Scheme 2.11). The reaction worked efficiently to yield the expected ring-opened product in good yields. Based on their control experiment it was suggested that a single electron transfer (SET) initiated aminohydroxylation reaction (Scheme 2.11).
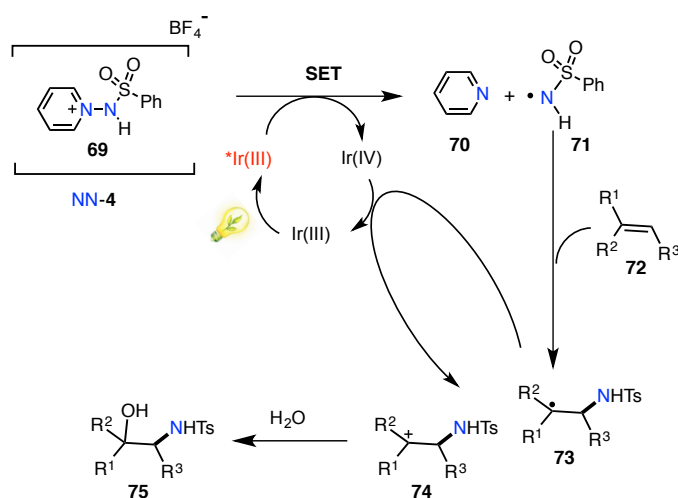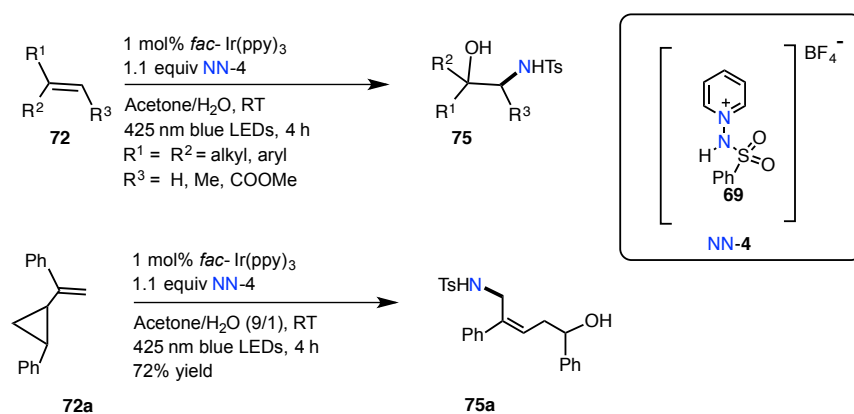
Scheme 2.11: Synthesis of aminoalcohols by visible light irradiation of alkene.[27]

The role of organic azides **76** in photoredox chemistry was illustrated by the Liu group (Scheme 2.12).[28] The catalytic system that they employed involved a combination of organic azide, inorganic photocatalyst, a tertiary ammonium salt, a visible light source and a sacrificial hydrogen donor to generate the *N*-centered radical. The catalytic system proved to be efficient for the synthesis of primary amines **79** with good chemoselectivity and yields. The work illustrated the reduction of azide-containing biomolecules, such as DNA oligonucleotide and flavanone disaccharide-derived azides. The compatibility of their reaction in aqueous media and the use of biomolecules as the azide moiety established the diversity of their work in biological applications. In their proposed mechanism (Scheme 2.12), a SET occurs from photoexcited Ru(II) complex by DIPEA to afford Ru(I) species. The organic azide **76** is then reduced by the Ru(I) species to form the azide radical anion **77** that undergoes an extrusion of N_2 molecule, followed by protonation to give the neutral aminyl radical **78**. This aminyl radical **78** then leads to formation of the corresponding amine based derivative **79**.
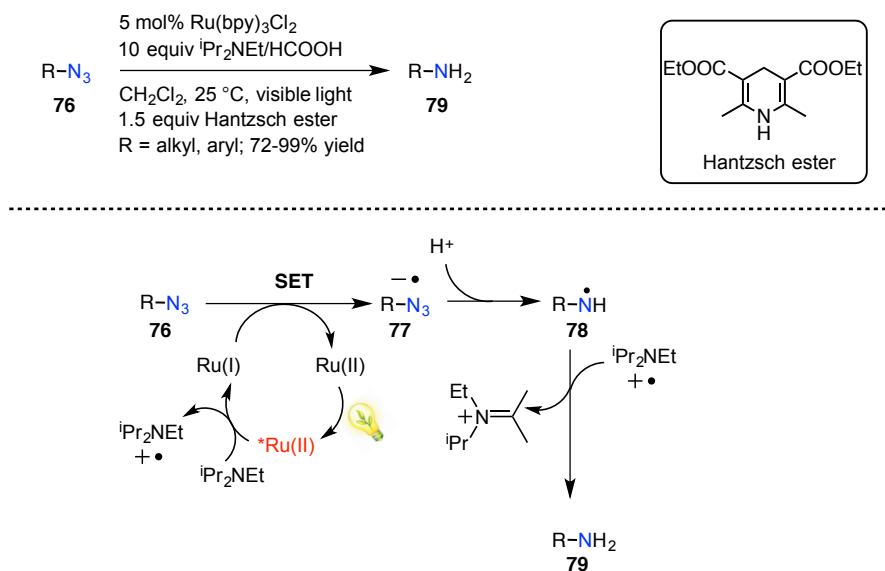
Scheme 2.12: Photoredox catalysis of organic azides generating *N*-centered radical.[28]
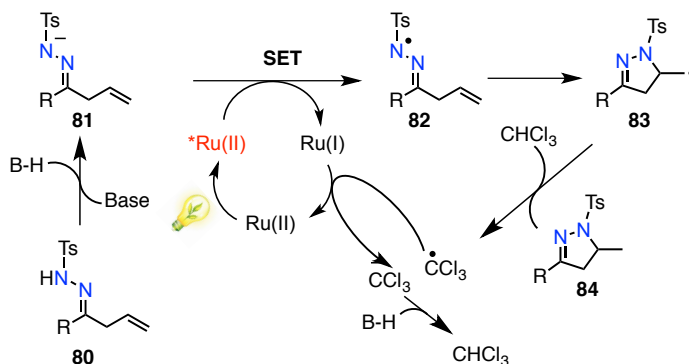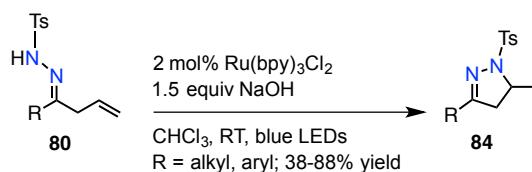
Scheme 2.13: Visible light mediated generation of *N*-hydrazonyl radical.[17,29]

For the photoredox catalysis involving *N*-centered hydrazonyl radical with an imine as the precursor was first illustrated by Xiao, Chen and co-workers.[29] The work demonstrated a mild methodology for direct conversion of strong *N*–H bonds in imines into the *N*-centered radicals using blue LEDs as the light source, Ru(II) complex, a sacrificial hydrogen donor under ambient conditions. An intramolecular addition of hydrazonyl radical **82** to a terminal alkene (Scheme 2.13) propagates the reaction followed by hydroimination leading to a heterocyclic product **84**. The wide substrate scope, large functional group tolerance and benign reaction conditions resulted in the success of their strategy. In their recent communication, they proved that they could switch the product selectivity from a 5-membered ring **86** system to a 6-membered heterocyclic product (**88/89**) on appropriately substituting the terminal alkene (Scheme 2.14).[28] Again the work illustrated a wide substrate scope with an excellent functional group tolerance for their substituted alkene.

To showcase the potential application of their strategy they converted the 6-membered heterocyclic product (**88a/88b**) to corresponding Diazinium salts (**94a/94b**). The latter was evaluated for *in vitro* antifungal activities against eight human pathogenic fungi and was compared to the commercially available fluconazole. In contrast to the antibacterial activities reported for related diazinium salts in literature, the results demonstrated that some of these compounds showed promising activities against four common clinical pathogenic fungi (*Candida albicans*, *C. parapsilosis*, *C. neoformans* and *C. glabrata*).
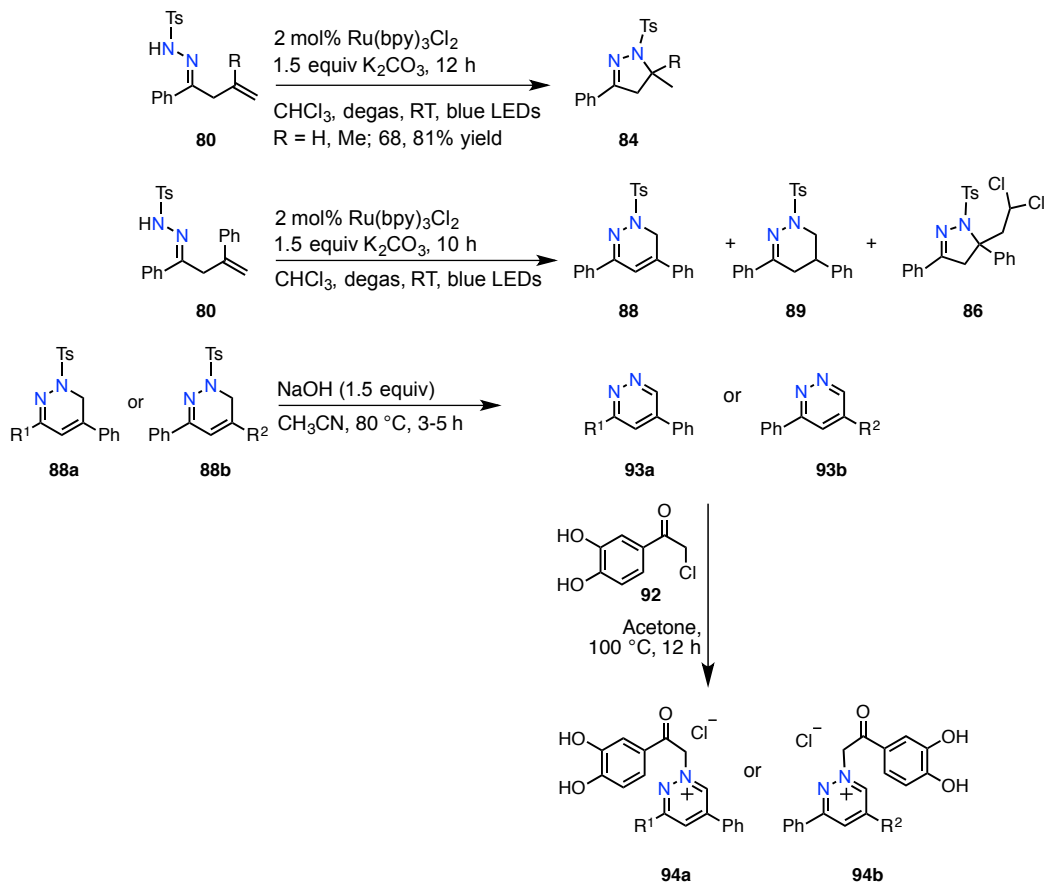
Scheme 2.14: Switching of product selectivity in visible light mediated photoredox catalysis of imines.[17,29]

Other photoredox reactions involving *N–N* bond based compounds include photoinduced *N–N* bond cleavage. Zheng and co-workers illustrated *N,N*-disubstituted hydrazine and hydrazide derivatives, including arylhydrazides **97**, *N*-alkyl- *N*-arylhydrazines, and *N,N*-diarylhydrazines **95** underwent facile *N–N* bond cleavage to afford synthetically useful secondary aromatic amines **104** and other products (**108/112**) (Scheme 2.15).[30]
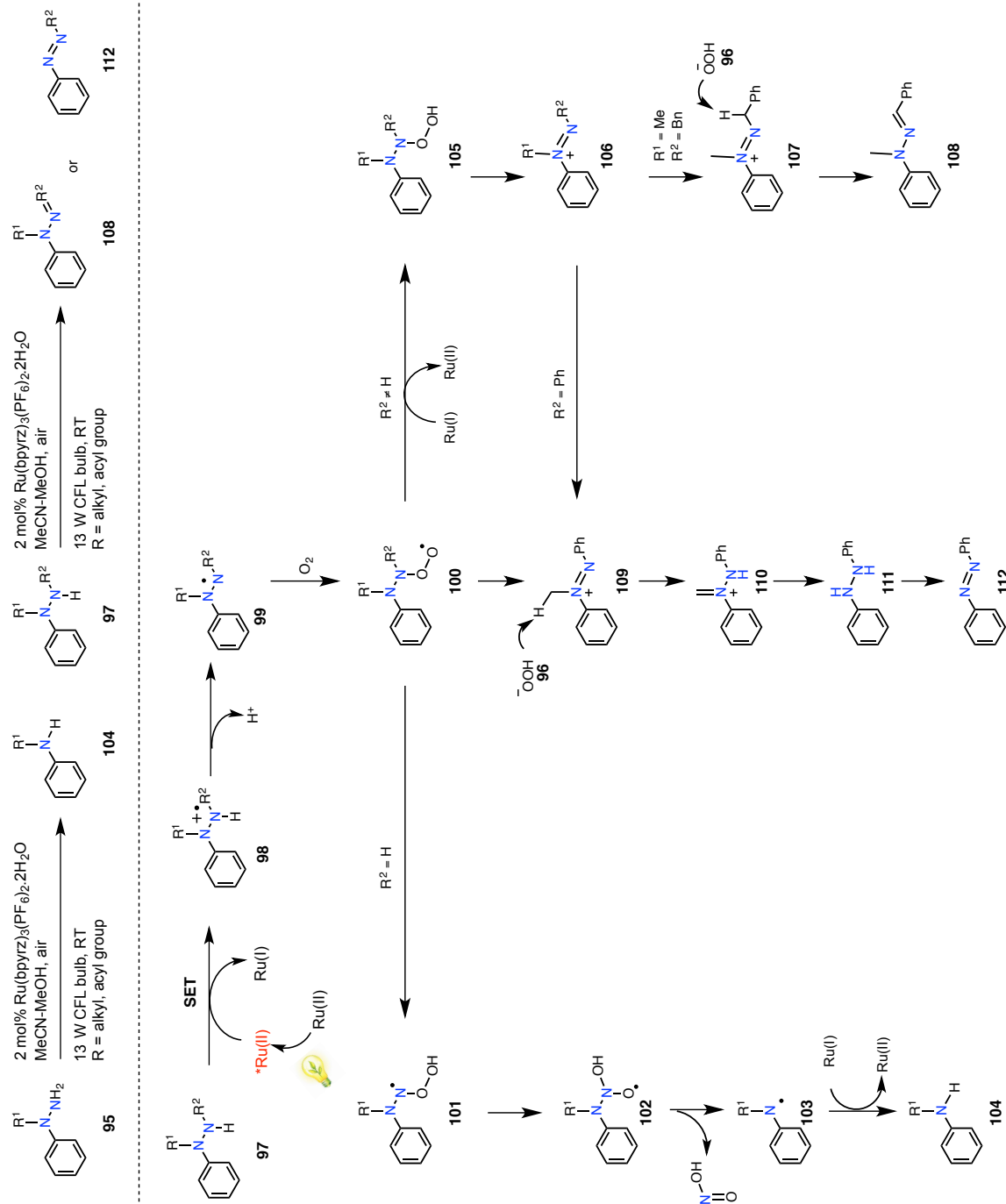
Scheme 2.15: Visible light mediated photoredox catalysis involving *N–N* bond cleavage.[30]
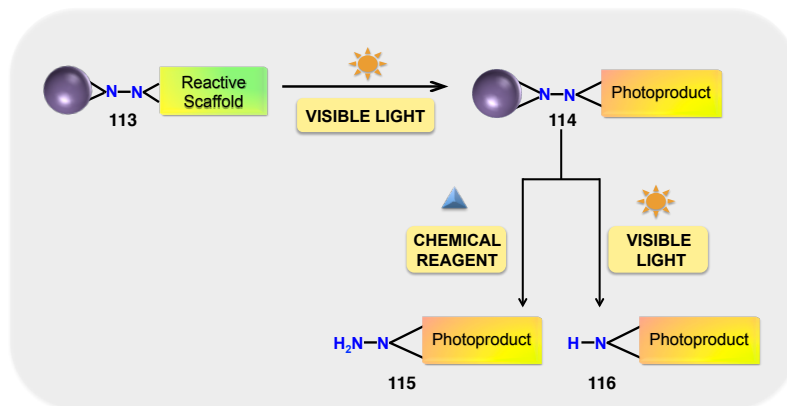
Scheme 2.16: Working paradigm of novel hydrazide based visible light mediated photocatalysis.

Though there are few reports in the literature involving *N–N* bond based compounds that undergo visible light mediated reactions, to the best of our knowledge there is no report on Visible light photocatalysis (VLP) of hydrazides. Keeping that in our mind we designed and developed hydrazide based systems **113** where one of the *N*-atom was attached to either a carbocycle or to an alkyl/aryl functionality while the other *N*-atom was functionalized with photochromophore (Scheme 2.16). Our initial hypothesis was to construct a hydrazide that is compatible with different photochromophores and thus facilitate various traditional photoreactions. Further, we aimed to develop a hydrazide that was stable towards the light irradiation without undergoing side reactions/decomposition. For visible light photocatalysis, we wanted to employ a metal-free cheap organic photocatalyst that is readily available or easy to synthesize. Our aim was to cleave/convert (Scheme 2.16) the hydrazide based photoproduct **114** to other useful compound(s) (**115**/**116**). Based on this strategy we explored many of the classic photoreactions in photochemistry under visible light irradiations *viz.* [2+2]-photocycloaddition, 6π photocyclization, Paternò-Büchi reaction and Norrish-Yang cyclization.

Based on our novel-operating paradigm, we designed substrates that featured *N-N* bond and evaluated them towards various photoreactions (Chart 2.1). The synthesized *N-N* bond based hydrazides and their precursors listed in the following Chart 2.1. The substrates **113a-d** were synthesized from the corresponding *N*-Aminophthalimide derivatives in good yields and were subjected to photochemical reactions (Scheme 2.16). The *N*-Aminophthalimide was accessible from phthalic anhydride; the latter was synthesized in a green route starting from furan, thus featuring a biomass-based synthesis of the reactants.[31-32]

The substrates and photoproducts were characterized by various spectroscopic techniques *viz.*, ^{1}H NMR spectroscopy, ^{13}C NMR spectroscopy, UV-Vis spectroscopy and high-resolution mass spectrometry. To avoid ambiguity in some cases, structural characterization was performed using single crystal XRD.

113a	**114a**	**117a**	**115a**

113b	**114b**

113c	**114c**

113d	**114d**	**115d**

113e-k	**114e-k**	**117e-k**

Imide	**Amide**	**Carbamate**	**Amine**
e) R[1] = PhCO; R[2] = CH$_3$CO	**f)** R[1] = PhCO, R[2] = CH$_3$ **g)** R[1] = PhCO, R[2] = H	**h)** R[1] = CH$_3$, R[2] = Boc	**i)** R[1] = R[2] = CH$_3$ **j)** R[1] = CH$_3$, R[2] = H **k)** R[1] = R[2] = H
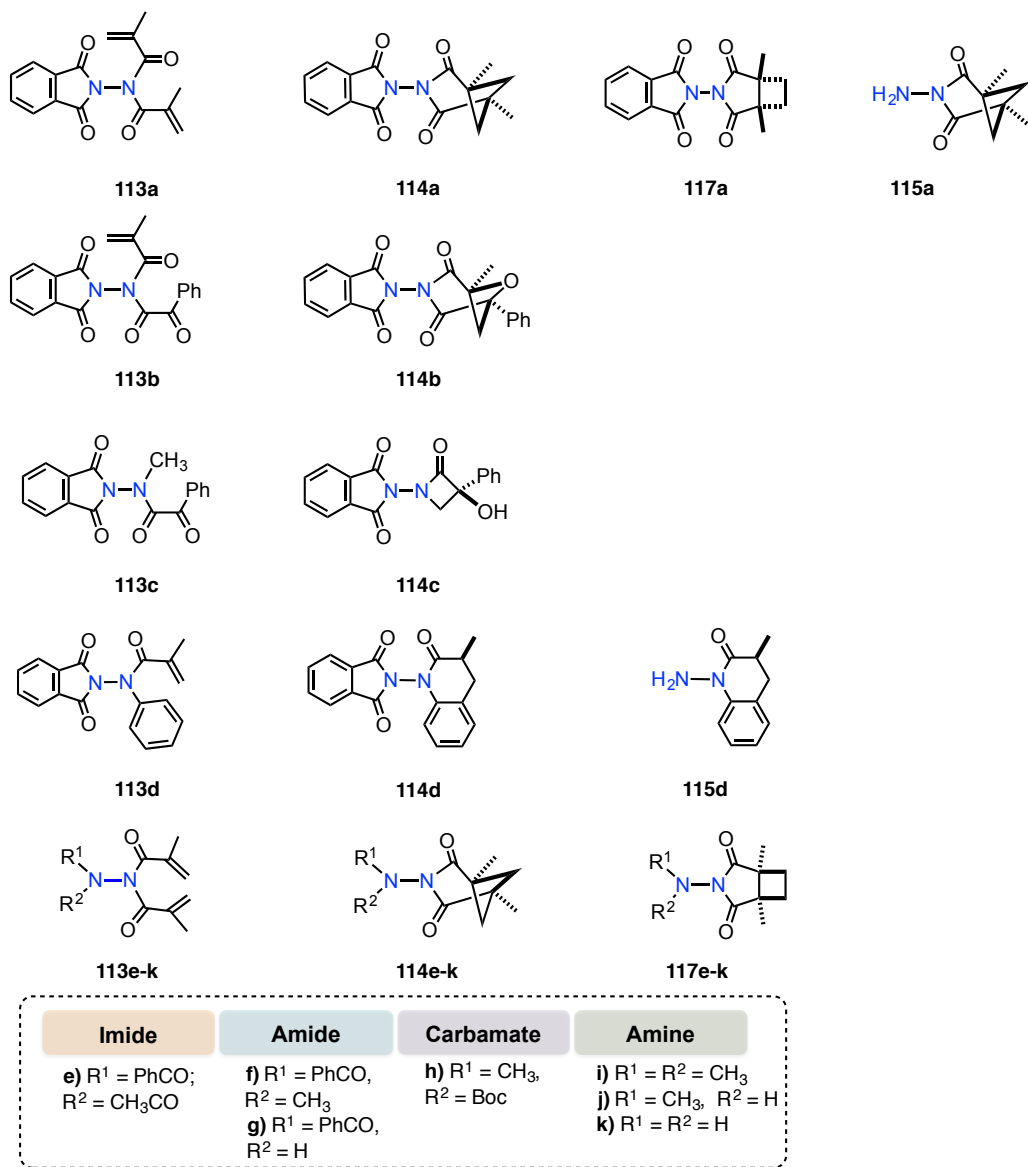
Chart 2.1: Structures of *N-N* bond based hydrazides, their precursors and their photoproducts utilized in the study.
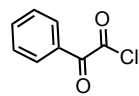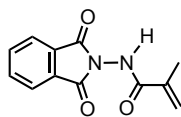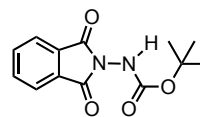
118 **119** **120**
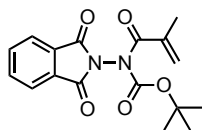
121
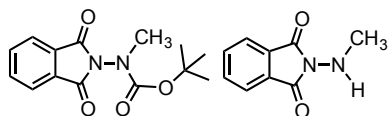
122 **123**

Chart 2.2: Structures of precursors for the study of hydrazides.

2.2. Photoreactivity of *N–N* bond based hydrazides towards classical photoreactions

To apprehend the light induced transformation of *N-N* derivatives (Scheme 2.17) for classical phototransformations we evaluated their reactivity towards direct irradiation as well as under visible light irradiation with thioxanthone acting as an organic photosensitizer. To establish the reaction conditions we first evaluated hydrazides derived from phthalimide **113a-d** towards [2+2]-photocycloaddition, Paternò-Büchi reaction, 6π photocyclization and Norrish-Yang reaction, respectively (Scheme 2.17).
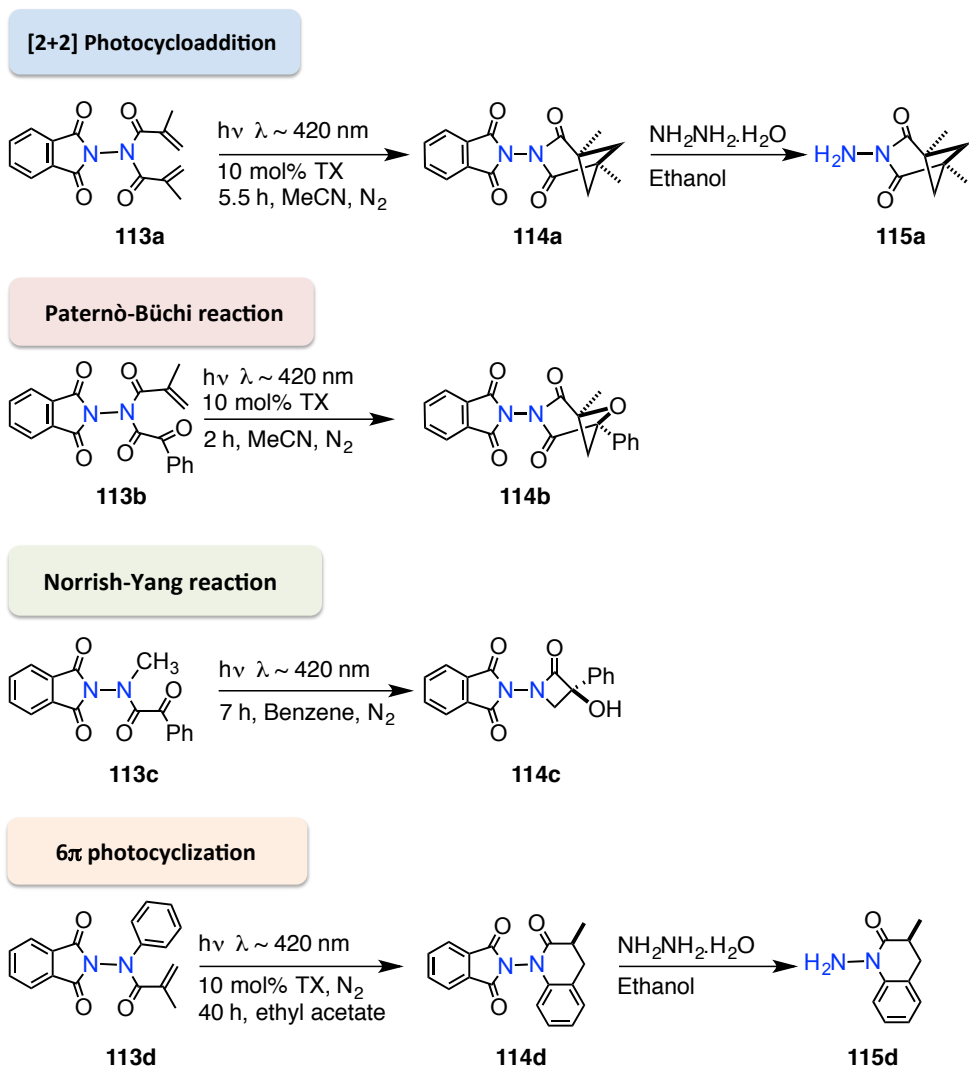
Scheme 2.17: Hydrazide derivatives as model systems for initiating traditional photoreactions with visible light.

Table 2.3: Visible-light mediated photoreactions with different loading levels of the thioxanthone (TX) [a]

Entry	TX(mol%)	% Conversion (% Isolated Yield) [b]		
		113a	**113b**	**113d**
1	0	0	19	7
2	1	8	26	88
3	5	39	100	-
4	10	100 (71)[c]	100 (88)	90 (62)

[a] All irradiations were performed at room temperature in HPLC grade acetonitrile; TX = thioxanthone; [**113a**] ≈ 3.35 mM, hv time ≈ 5.5 h; [**113b**] ≈ 3.33 mM, hv time = 2 h; [**113d**] ≈ 3.26 mM; hv time ≈ 40 h. Reported values are an average of a minimum of 3 trials (±5% error). [b] % Conversions calculated by ^{1}H NMR spectroscopy using triphenylmethane as an internal standard. Isolated yields in parenthesis. [b] Minor amounts (< 10%) of straight photocycloaddition product **117a** was observed depending on the solvent employed.

Inspection of Table 2.3 shows that employing 1-10 mol% of thioxanthone sensitizer in acetonitrile was effective for transforming phthalimide based substrates to the corresponding photoproducts. We first evaluated our strategy for the well-established and synthetically useful [2+2]-photocycloaddition. Phthalimide derived acrylimide **113a** with 1, 5 and 10 mol% of thioxanthone as the photocatalyst (~420 nm irradiation) led to cyclobutane based photoproduct in 8, 39 and 100% conversion, respectively (Table 2.3). For acrylimide **113a** (with 10 mol% of thioxanthone loading) the photoproduct **114a** was isolated with 71% yield when the photoreaction was performed in large scale. The phthalimide based hydrazides **113a-d** were subjected to chemical transformation for removing the phthalimide ring after the photoreaction **115a-d** (Scheme 2.16).

Irradiation of **113a** at ~420 nm in the absence of thioxanthone did not result in any noticeable conversion with complete recovery of the starting material. Building on the preliminary results, we evaluated Paternò-Büchi reaction of **113b** in the presence of 1, 5 and 10-mol% of thioxanthone (~420 nm irradiation) that lead to the corresponding oxetane based photoproduct in 26, 100 and 100% conversions, respectively (Table 2.4). The isolated yield for large-scale photoreaction was 88% with 10 mol% of thioxanthone. Direct irradiation of **113b** under ~420 nm in the absence of thioxanthone led to formation of photoproduct **114b** with ~19% conversion.

In case of 6π photocyclization of **113d** in the presence of 1 and 10-mol% of thioxanthone (~420 nm irradiation) led to the corresponding 3,4-dihydroquinolin-2-one based photoproduct **114d** in 88 and 90% conversions, respectively (Table 2.4) with an isolated yield of 62% (with 10 mol% of thioxanthone as the sensitizer). Direct irradiation of acrylanilide derivative **113d** at ~420 nm (Rayonet irradiation) resulted in ~7% conversion.

Table 2.4: Solvent screening for visible-light mediated photoreactions.[a]

Entry	Solvent	% conversion			
		113a	**113b**	**113c**[b]	**113d**
1	Methanol	100	-[c]	-[c]	91
2	Acetonitrile	100	100	16	90
3	Ethyl acetate	<7	78	55	100
4	Benzene	63	100	80	60
5	Methylcyclohexane	0	71	-[d]	71

[a] Irradiations at ~420 nm in a Rayonet reactor (16 tubes × 14 W each) with HPLC grade solvents with 10 mol% thioxanthone. [**113a**] = 3.35 mM, hν time = 5.5 h; [**113b**] = 3.33 mM, hν time = 2 h; [**113c**] = 5.1 mM, hν time = 7 h and [**113d**] = 3.26 mM, hν time = 40 h. Reported values are an average of a minimum of 3 trials (±5% error). % Conversions were calculated by ^{1}H-NMR spectroscopy using triphenylmethane as an internal standard. [b] Direct irradiation of **113c** without thioxanthone. [c] Decomposition observed. [d] No reaction observed.

For Norrish-Yang cyclization, due to absorptivity of **113c** in the visible region, direct irradiation in MeCN led to β-lactam based photoproduct **114c** in ~16% conversion (Table 2.4). For improving the yield of β-lactam based photoproduct **114c** during Norrish-Yang cyclization of **113c**, the reaction was performed in various solvents (Table 2.4). The observed conversions for cyclization to afford photoproduct **114c** were 80% and 55% in benzene and ethyl acetate. Similarly, the reaction of acrylimide derivative **113a** in methanol resulted in complete conversion (similar to acetonitrile) to yield the [2+2] cycloaddition product (**2**:**3** ~ 83:17). Benzene and acetonitrile were found to be the best solvent for Paternò-Büchi reaction of **113b** leading to oxetane based photoproduct **114b**. 6π-Photocyclization of **113d** was efficient in all the solvents utilized in the study; showing moderate conversions in non-polar solvents like benzene and methylcyclohexane (MCH) and close to quantitative conversions in polar solvents like methanol, acetonitrile and ethyl acetate.

After evaluating phthalimide based hydrazides (Scheme 2.18) in promoting traditional photochemical reactions to work under visible light irradiations; we shifted our attention towards the features necessary for generalizing the chromophore responsible for photochemical reactivity. Due to the established photochemistry of acrylimides in the literature, the *N-N* bond based chromophores was chosen as the model system to understand the reactivity of hydrazides by VLP.[33] Acrylimides **113e-k** were synthesized (Scheme 2.18) as the control substrates to evaluate the role of phthalimide functionality during photochemical reaction.

Imide	Amide	Carbamate	Amine
e) R^1 = PhCO; R^2 = CH_3CO	**f)** R^1 = PhCO, R^2 = CH_3 **g)** R^1 = PhCO, R^2 = H	**h)** R^1 = CH_3, R^2 = Boc	**i)** R^1 = R^2 = CH_3 **j)** R^1 = CH_3, R^2 = H **k)** R^1 = R^2 = H
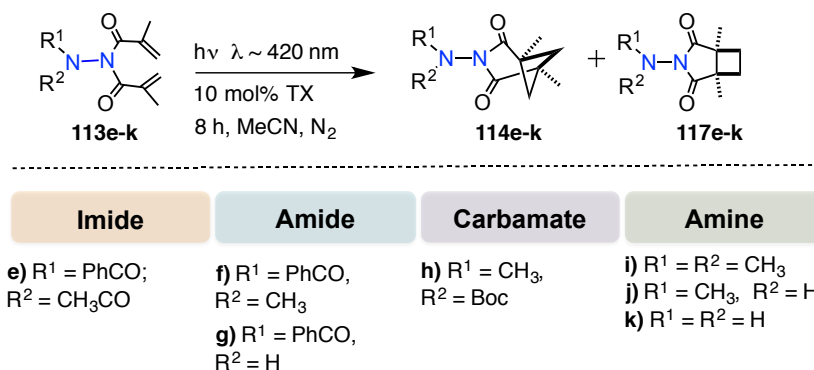
Scheme 2.18: Evaluating photochemical reactivity of acyclic imide, amide, carbamate and amine based hydrazides.

Based on the photoreactivity of acrylimide derivative **113a** that underwent facile [2+2] photocycloaddition, we kept the same di-methacryloyl functionality on the 2nd nitrogen featuring one of the following functionalities viz., imide **113e**; 3° amide **113f**; 2° amide **113g**; carbamate **113h**; 3° amine **113i**; 2° amine **113j** and 1° amine **113k**.

Table 2.5: Photocycloaddition of **113e-k** by visible-light irradiation using 10 mol% of thioxanthone (TX) in acetonitrile. [a]

Entry	Substrate [b]	% Conversion [c]	% Yield [c]	**114**: **117** [c]
1	**113e**	56	52	-[d]
2	**113f**	-[e]	-	-
3	**113g**	-[f]	-	-
4	**113h**	82	29	-[d]
5	**113i**	95	40	70:30
6	**113j**	>99	40	80:20
7	**113k**	-[f]	-	-

[a] Irradiations (8 h) at ~420 nm using a Rayonet reactor (16 bulbs × 14 W each). Values are an average of a minimum of 3 trials (±5% error). [b] [**113a**] = 3.18 mM; [**113b**] = 3.49 mM; [**113c**] = 3.67 mM; [**113d**] = 3.54 mM; [**113e**] = 5.1 mM; [**113f**] = 5.49 mM; and [**113g**] = 2.38 mM. [c] % conversions, yields and **114**:**117** ratio were calculated by ^{1}H-NMR spectroscopy using triphenylmethane as an internal standard. [d] Ratios not reported due to overlapping peaks in ^{1}H NMR spectroscopy. [e] Decomposition observed. [f] No reaction was observed.

Table 2.5 shows the results from the photoreaction of **113e-k** in acetonitrile under visible light irradiation with 10 mol% of thioxanthone. [2+2] Photocycloaddition of **113e**, which features imide functionality, underwent photoreaction with moderate isolated yield (Table 2.5; entry 1). Moving from **113e** to **113f/113g**, the change in functionality from an imide to an amide derivative resulted in either decomposition (with 3° amide **113f**) or no photoreaction (with 2° amide **113g**). In the case of carbamate based hydrazide **113h** the photocycloaddition resulted in 82% conversion of starting material with an isolated yield of 29%. We then focused our attention towards amine based hydrazide **113i-k**. Tertiary and secondary amine based hydrazide derivatives **113i** and **113j** resulted in quantitative conversions (95 and 97% respectively) with low isolated 40% yield; **114i**:**117i** = 70:30 and **114j**:**117j** = 80:20). For the 1° amine derivative **113k** no observable photoreaction was observed.

A systematic solvent screening and photocatalyst/photosensitizer loading levels for [2+2] photocycloaddition of **113i** was performed in order to probe the reactivity of amines. Changing the thioxanthone loading levels from 1, 5 to 10 resulted in 74%, 93% and 95% conversions, respectively (Table 2.6). The reaction with 10 mol% of thioxanthone was also effective in ethyl acetate and in benzene with 55% and 52% conversions, respectively. MeCN was found to be the best solvent for [2+2] photocycloaddition of **113i** with moderate isolated yields (Table 2.7).

70

Despite quantitative conversion, it was difficult to analyze the other side products from photoreaction, as the resulting crude mixture had no absorption under UV lamp illumination. In addition the crude NMR for photocycloaddition of **113i**/**113j** was not clean in comparison to that of **113e** and **113h** hinting the possibility of side reactions during phototransformation. Literature evidence for the possible side reactions observed during photocycloaddition of **113i**/**113j** comes from the report from Couture et al. who observed *N-N* and *N-CO* cleaved products during UV light irradiation of hydrazides.[24] In comparison to MeCN, the photoreactions in benzene and ethyl acetate resulted in poor yields in photoproduct (28 and 27% respectively). Further, complete decomposition was observed for photocycloaddition when MCH was utilized as solvent.

Table 2.6: Sensitizer loading for [2+2] photocycloaddition of tertiary amine based derivative.[a]

Entry	TX (x mol%)	Conversion/%
1	0	0
2	1	74
3	5	93
4	10	95

[a] [**113i**] = 5.1 mM, TX: Thioxanthone

Table 2.7: Solvent screening for [2+2] photocycloaddition of tertiary amine based derivative.[a]

Entry	Solvent	Conversion/%	NMR yield/%	114i:117i
1	Methanol	-[b]	-[b]	-[b]
2	Acetonitrile	95	40	70:30
3	Ethyl acetate	55	27	75:25
4	Benzene	52	28	75:25
6	Methylcyclohexane	Decomposition	-	-

[a] [**113i**] = 5.1 mM, TX: Thioxanthone, [b] Difficult to determine due to overlapping peaks

2.3. Mechanistic rationale for visible light photocatalysis for *N–N* bond based hydrazides

To highlight the role of hydrazide functionality in classical photoreactions under visible light conditions, it was necessary for us to understand the mechanistic aspects for rationalizing the reactivity. Based on our detailed photochemical reactions, we hypothesized hydrazides that proceeded under thioxanthone sensitization can occur either by energy transfer or electron transfer or a combination of both. To ascertain the feasibility of electron transfer from hydrazide to thioxanthone (TX) or vice versa, we performed electrochemical measurements on thioxanthone and hydrazide derivatives **113a-k** (Table 2.8).[34] The free energy ΔG_{eT} for electron transfer from excited thioxanthone to hydrazides was calculated using the Rehm-Weller equation.[3,33,35] In all cases, the free energy for electron transfer (ΔG_{eT}) was either close to zero or negative, indicating that an electron transfer mechanism was possible in the system under study (Table 2.8).[34] To determine the feasibility of energy transfer process for sensitized photoreactions of hydrazides we carried out detailed photophysical studies. UV-Vis spectra of phthalimide based substrates **113a-d** were recorded in spectrophotometric solvents like 2-methyltetrahydrofuran (MeTHF), MeCN and ethanol to ascertain the optical density at different wavelengths.

Table 2.8: Triplet energy (E_T) and free energy for electron transfer from thioxanthone for various substrates.[a]

Entry	Compd[b]	E_{red} (eV)[a]	ΔG_{eT} (kcal/mol)[b]	E_T (kcal/mol)[c]	k_q (10^7 M^{-1}s^{-1})[d]
1	**113a**	-1.25	1.2	64.5	12±1
2	**113b**	-0.99	-4.8	62.0	98±2
3	**113c**	-1.28	1.8	62.4	67±1
4	**113d**	-1.15	-1.2	62.4	31±1
5	**113e**	-1.11	-2.1	75.8	6.0±0.1
6	**113g**	-0.76	-10.1	71.8	5.9±0.1
7	**113h**	-1.33	3.0	70.4	8.8±0.2
8	**113i**	-0.99	-4.8	70.7	7.2±0.2

[a] vs. SEC. Working electrode glassy carbon. MeCN/ [**113a**] = 1.0 mM; [**113b**] = 0.83 mM; [**113c**] = 0.49 mM; [**113d**] = 0.49 mM; [**113e**] = 0.48 mM; [**113g**] = 1.06 mM; and [**113h**] = 0.76 mM, [**113i**] = 0.82 mM. [b] ΔG_{eT} calculated from E_{ox} of thioxanthone of 1.7 V using Rehm-Weller equation (reference [33,35]). We were unable to ascertain an E_{ox} for the substrates under our experimental condition using cyclic voltammetry [c] Based on phosphorescence spectra recorded in 2-Methyl THF glass at 77 K. [d] TX triplet quenching rate constants determined by laser flash photolysis in acetonitrile.

Hydrazides **113c** showed absorbance in the UV region, while **113a**, **113b** and **113d** had showed tailing absorbance in visible region at the reaction concentration. The low optical density for those hydrazides explains the slight conversion for them under direct irradiation conditions (~420 nm). No appreciable luminescence was observed for **113a-d** at room temperature; hence we recorded the steady-state luminescence at 77 K in MeTHF glass. The observed steady-state luminescence was from phosphorescence based on the luminescence lifetime which was observed to be in the range of millisecond to seconds timescale. The triplet energies were calculated from the phosphorescence spectra and are tabulated in Table 2.8 (entries 1-4).[34] Comparing the triplet energy of thioxanthone ($E_T \approx 63$ kcal/mol) with that of hydrazides, triplet energy transfer from thioxanthone to the phthalimide substrates was feasible. The phosphorescence spectra of the control substrates **113e-k** suggested higher triplet energies than thioxanthone. Despite of higher triplet energy, the control substrates **113e**, **113d** and **113i** underwent photoreaction in the presence of thioxanthone acting as a visible light absorbing catalyst/sensitizer.
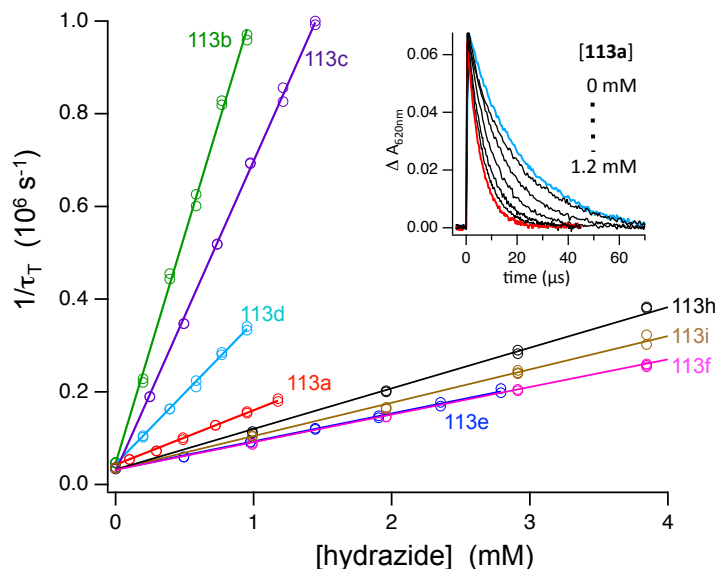
Figure 2.2: Bimolecular quenching rate constants k_q for quenching of thioxanthone triplet states by hydrazide derivatives determined by laser flash photolysis (λ_{ex} = 355 nm, 7 ns pulse width). Plot of inverse thioxanthone triplet lifetime (determined from triplet absorption decay traces monitored at 620 nm) vs. varying hydrazide concentrations in argon saturated acetonitrile solutions. Inset: Transient absorption decay traces of TX triplets measured at 625 nm at different concentrations of **113a**.

We also studied the bimolecular quenching rate constant (k_q) for quenching of TX in the presence of varying concentration of hydrazides as quencher (Figure 2.2). Values for bimolecular rate constants k_q for quenching of TX correlated well with the observed triplet energy, E_T and ΔG_{eT} values in Table 2.8. In the case of hydrazide **113b** for which both exergonic electron transfer and exothermic energy transfer values were observed, k_q (= 9.8×10^8 M^{-1} s^{-1}) was found to be close to diffusion limit (Table 2.8; entry 2). For hydrazide **113c** that showed a slightly positive ΔG_{eT} and a favorable energy transfer from excited TX quenching rate constant was found to be 6.7×10^8 M^{-1} s^{-1} (Table 2.8; entry 3). Hydrazide **113d** with a slightly endergonic ΔG_{eT} (when compared to **113c)** and exothermic energy transfer from excited TX resulted in k_q of 3.1×10^8 M^{-1} s^{-1} (Table 2.8; entry 4). Hydrazide **113a** with slightly endergonic ΔG_{eT} and endothermic energy transfer from excited TX gave k_q of 1.2×10^8 M^{-1} s^{-1} (Table 2.8; entry 1). For control substrate **113e** endergonic electron transfer was the only possibility that explains the observed photoreaction as the substrate has high triplet energy that was correlated by the k_q of 6.0×10^7 M^{-1} s^{-1} (Table 2.8; entry 5). The bimolecular quenching rate constants for various hydrazides exhibit a scenario where the photoreaction occurs either by an electron transfer or energy transfer or a combination of both from the excited thioxanthone.
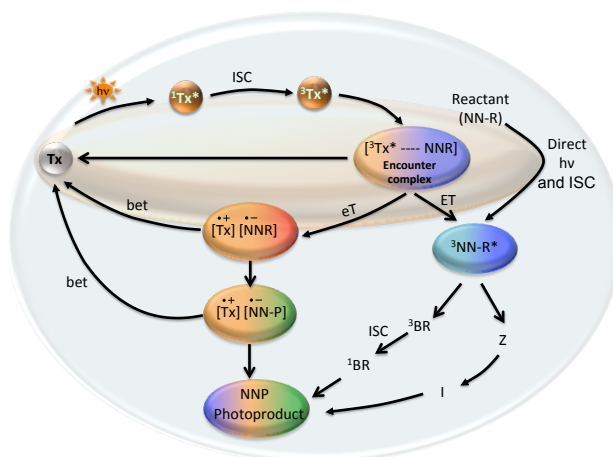
Figure 2.3: Mechanistic model for visible light mediated photochemical reactivity in hydrazides.

The detailed photophysical and ΔG_{eT} values were useful hypothesize a mechanistic model to explain the observed excited state photoreactivity of hydrazides (Figure 2.3). Photoexcitation of thioxanthone (TX) leads to triplet excited thioxanthone (^{3}TX*). Interaction of excited TX with hydrazide (NNR) leads to the formation of an encounter complex (^{3}TX*---NNR). This encounter complex can then lead to triplet energy transfer provided the triplet energy level of the substrate is lower than TX. In case of a favorable redox potential (as in case of **113b, 113d** and **113e, 113f** and **113i**), an electron transfer pathway is feasible that leads to a radical ion pair that subsequently reacts to form the photoproduct radical anion.

This product radical anion can then do a back electron transfer to regenerate TX thus making the use of TX photocatalytic. Back electron transfer is also possible to generate the triplet-excited state of the hydrazide, however such a scenario in the present case is less likely due to the energetics present in the system. The mechanistic route via an electron transfer or energy transfer pathway leading to radical ion pair or diradicaloid intermediate depends on the employed hydrazide. For instance, for **113e** an electron transfer pathway is more likely due to favorable energetics and higher triplet state energies of the hydrazide when compared to that of TX. In the case of the ketoamide derivative **113b**, the formation of a triplet-excited state (^{3}*NN*-R) is feasible (due to the ketoamide chromophore and the favorable triplet energy).[34,36-38] This triplet-excited state can then react either from a diradicaloid (^{3}DR) intermediate or through an intramolecular charge transfer pathway. In cases of hydrazides that have optical density in the visible region, the reactants in those cases could undergo direct irradiation.[34,36-38] Even though the mechanistic details for a specific substrate employed in our study requires further scrutiny our generalized model in which we form an excited state encounter complex that initiates the photochemical reactivity is quite reasonable.

2.4.   X-Ray crystal structure data of hydrazide

Structure determination: Single crystal X-ray diffraction data of the compounds **119, 113a** and **114a** were collected on a Bruker Apex Duo diffractometer with a Apex 2 CCD area detector at T = 100K. Cu radiation was used in all the cases. All structures were processed using Apex 2 v2010.9-1 software package. Direct method was used to solve the structures after multi-scan absorption corrections.
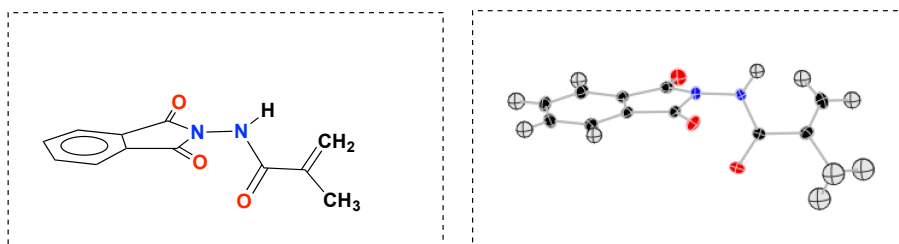
Figure 2.4: Crystal structure of **119** (Crystallized from: hexanes/chloroform).
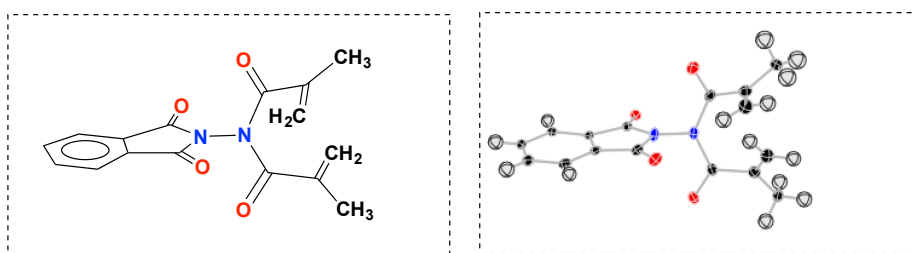
Figure 2.5: Crystal structure of **113a** (Crystallized from: hexanes/ethylacetate).
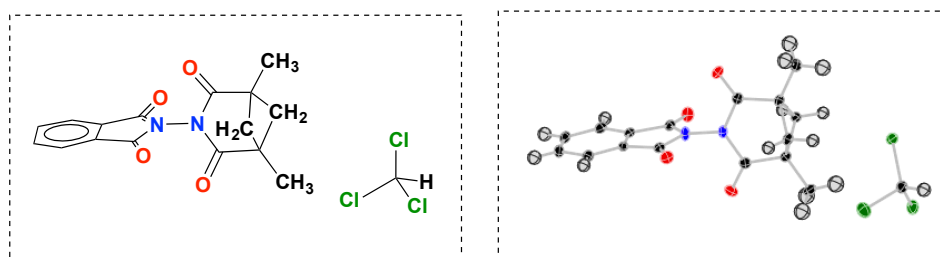
Figure 2.6: Crystal structure of **114a** (Crystallized from: hexanes/chloroform).

Table 2.9: Structural parameter table for hydrazides **119**, **113a** and **114a**.

Crystals	119	113a	114a
Formula	$C_{12}H_{10}N_2O_3$	$C_{16}H_{14}N_2O_4$	$C_{16}H_{14}N_2O_4$, $CHCl_3$
Formula Weight	230.22	298.29	417.66
Space Group, Z	P 21/c	P 21/c	P -1
a/Å	8.5484(3)	32.0290(13)	7.9595(3)
b/Å	34.4488(11)	11.6208(5)	15.2345(5)
c/Å	15.2307(4)	16.5874(7)	16.7559(6)
α /°	90	90	110.399
β/°	101.098(2)	103.875(2)	100.744
γ /°	90	90	97.410
V (Å^3)	4401.3(3)	5993.7(4)	1829.03(11)
h, k , I_{max}	10,41,18	38,13,19	9,18,19
ρ_{calc} [mg/mm^3]	1.390	1.322	1.517
μ [mm^{-1}]	0.852	0.803	4.772
Radiation type	CuKα (λ = 1.54178)	CuKα (λ = 1.54178)	CuKα (λ = 1.54178)
F(000)	1920.0	2504.35	856.0
No. of measured reflections	7716	10593	6332
No. of independent reflections	6487	9800	5905
Final R indexes (I ≥ 2 s)	R_1 = 0.0363, wR_2 = 0.0941	R_1 = 0.0612, wR_2 = 0.1768	R_1 = 0.0295, wR_2 = 0.0748
R1/wR2 (I ≥ 2 s) [%]	0.0363/0.0941	0.0612/0.1768	0.0295/0.0748

2.5.   Summary and outlook

We have performed an in depth study on visible light mediated photocatalysis of novel hydrazides. Our work has opened additional avenues to harness visible light for useful organic transformations. Our study has utilized hydrazides in promoting classical photoreactions with thioxanthone as the photocatalyst/photosensitizer. We have illustrated that hydrazides can undergo facile photoreactions without any decomposition or side products. After the phototransformation, we employed chemical reagents to perform post photochemical transformation. We also evaluated light for *N-N* bond cleavage that requires further study to highlight the role of oxygen in the cleavage mechanism. Thus the hydrazides essentially act as a "photo-auxiliary" enabling us to perform the classical photoreactions under visible light sensitization.

Our current strategy will enable chemists across various disciplines to initiate photochemical reactions under metal free visible light irradiation conditions. Using our mechanistic model we have proposed an encounter complex (EC) formed by the interaction between hydrazide and photoexcited thioxanthone. Depending on the electrochemical potential and on the triplet energy of the hydrazide derivative, the EC then leads to formation of photoproduct by adopting differing routes (*viz* electron *vs.* energy transfer pathways). Our future efforts include a detailed photophysical understanding of individual substrates presented in this study.

2.6.   General methods and materials

All commercially obtained reagents/solvents were used as received; chemicals that were purchased from Alfa Aesar, Sigma – Aldrich®, Acros®, TCI® America, Mallinckrodt®, and Oakwood Products® were used as received without further purification. Spectroscopic grade acetonitrile purchased from EMD® were used for photoreactions and for recording absorbance spectra of various substrates. Unless otherwise stated dichloromethane and acetone were freshly distilled from CaH_2 and potassium carbonate before employing in a reaction. Unless stated otherwise, reactions were conducted in oven-dried glassware under an atmosphere of nitrogen using anhydrous solvents; Photoreactions were performed under N_2 or O_2 atmosphere. ^{1}H NMR and ^{13}C NMR spectra were recorded on Varian 400 MHz (100 MHz for ^{13}C NMR) and on 500 MHz (125 MHz for ^{13}C NMR) spectrometers. The residual solvent signal was used as reference. ($CDCl_3$: δ_H = 7.26 ppm, δ_C = 77.2 ppm). Data for ^{1}H NMR spectra are reported as follows: chemical shift (δ ppm), multiplicity, coupling constant (Hz) and integration. In many instances, it was not possible to obtain a signal for the carbonyl carbon, despite long relaxation times and concentrated samples. However these signals are reported wherever possible.

High-resolution mass spectrum data was recorded in Electrospray Ionization mode on a Bruker–Daltronics® BioTof mass spectrometer in positive (ESI+) ion mode. The reactants and photoproducts were purified by flash chromatography using silica gel (by standard technique with solvents as indicated. RediSep®, silica gel standard grade: Porosity 60 Å, Particle size: 230 x 400 mesh, Average particle size: 60 to 70 micron). The Retardation Factor (R_f) values were recorded using various combination of solvent systems as mobile phase (as mentioned in the text) and on SORBENT TECHNOLOGIES® Silica Gel TLC plates (200 µm thickness w/UV$_{254}$).

2.6.1. Photophysical methods

Spectrophotometric grade solvents were used wherever necessary unless otherwise mentioned. The compounds were purified by combiflash equipped with dual wavelength. UV-Vis spectra were recorded on Cary 300 series UV-Vis spectrometer using UV quality fluorimeter cells (with range until 190 nm) purchased from Luzchem. Low temperature luminescence experiments were performed using a quartz tube (3 mm inner diameter) that fitted in a custom built quartz Dewar jacket with an optical window. Emission spectra were recorded using Horiba Scientific® Fluorolog 3 spectrophotometer (FL3-22) equipped with double-grating monochromators, dual lamp housing containing a 450-watt CW xenon lamp and a UV xenon flash lamp (FL-1040), Fluorohub/MCA/MCS electronics and R928 PMT detector. Emission spectra were corrected in all the cases for source intensity (lamp and grating) and emission spectral response (detector and grating) by standard instrument correction provided in the instrument software. Lifetime measurements were performed by time correlated single photon counting using a pulsed nano LED lamp (Horiba) with a pulse repetition rate of 40 kHz in conjunction with an OB920 spectrometer (Edinburgh Analytical Instruments).

Laser flash photolysis experiments employed the pulses from a Spectra Physics GCR-150-30 Nd:YAG laser (355 nm, *ca.* 5 mJ/pulse, 7 ns pulse length or 266 nm, ca 5 mJ/pulse, 5 ns pulse length) and a computer controlled system that has been described elsewhere.[39]

2.6.2. Electrochemistry

Cyclic voltammograms was performed using HPLC grade acetonitrile as the solvent on a CH instrument. Working electrode employed was glassy carbon, reference electrode was silver chloride and counter electrode was platinum electrode. A solution of tetrabutylammonium hexafluorophosphate (TBAP) was used as the supporting electrolyte. The experiments were performed under constant flow of nitrogen.

2.7. Synthetic route to acrylimide derivative 113a
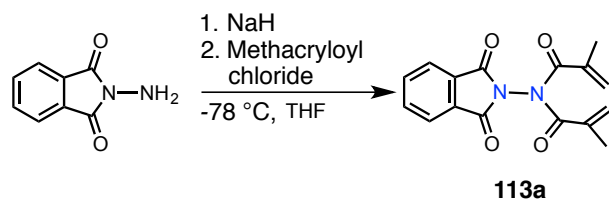
Scheme 2.19: Synthesis of acrylimide **113a**.

N-Aminophthalimide (1 equiv) was dissolved in freshly distilled THF under N_2 atmosphere. The reaction mixture was then cooled to -78 °C and this was followed by the addition of 5 equiv of NaH followed by the dropwise addition of methacryloyl chloride (2.2 equiv). After stirring for 1 h, the mixture was brought to room temperature and stirred for 2.5 h (reaction was monitored by TLC). The reaction was quenched with 5 mL of NH_4Cl, stirred and the layers were separated. The organic layer was sequentially washed with DI water (2 × 10 mL), saturated $NaHCO_3$ (2 × 10 mL) and finally with brine. The organic layer was dried over anhyd Na_2SO_4, filtered and the solvent was removed under reduced pressure to yield crude product. The crude product was purified by combiflash using hexanes and ethyl acetate mixture to get the desired acrylimide. The product was characterized by NMR spectroscopy. TLC condition - R_f = 0.8 (50% ethyl acetate:hexanes), Crystalline solid (Yield = 35%).

¹H-NMR (400 MHz, CDCl₃, δ ppm): 1.96 (s, 6H), 5.52-5.54 (m, 2H), 5.79 (bs, 2H), 7.78-7.80 (dd, *J* = 5.2 Hz, 2.8 Hz, 2H) and 7.89-7.91 (dd, *J* = 5.2 Hz, 3.2 Hz, 2H).
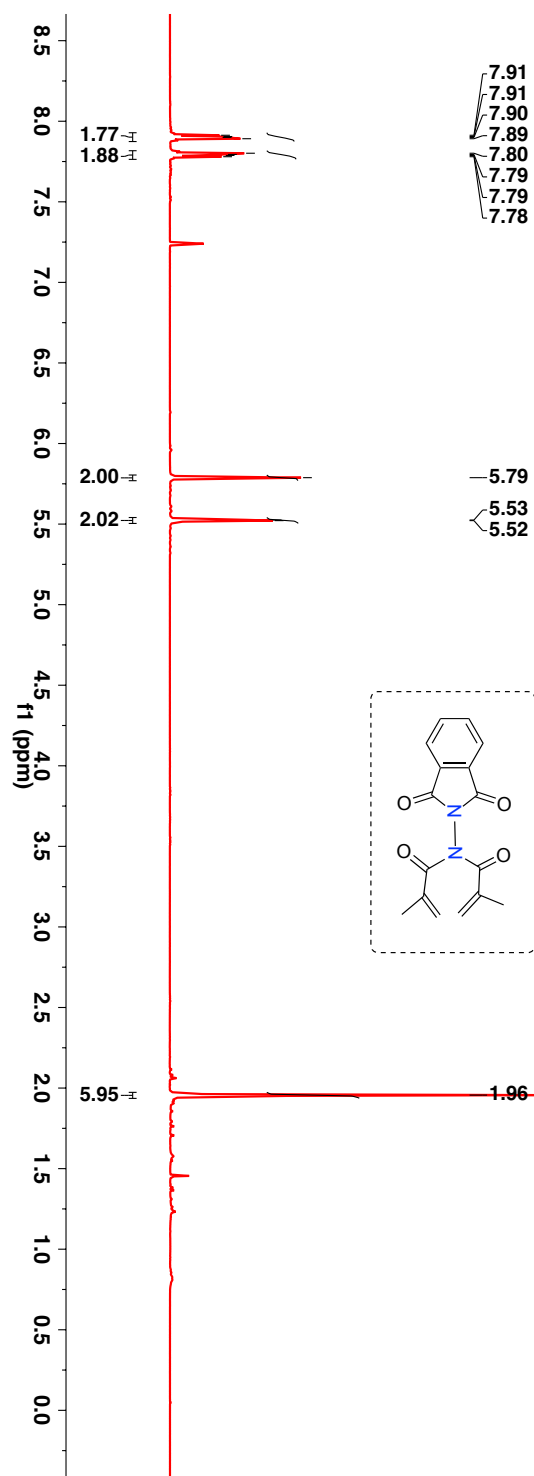
Figure 2.7: ¹H-NMR (400 MHz, CDCl₃, δ ppm) spectrum of **113a**.

^{13}C-NMR (100 MHz, CDCl$_3$, δ ppm): 18.8, 122.8, 124.4, 130.2, 135.1, 140.7, 164.4, and 171.1.
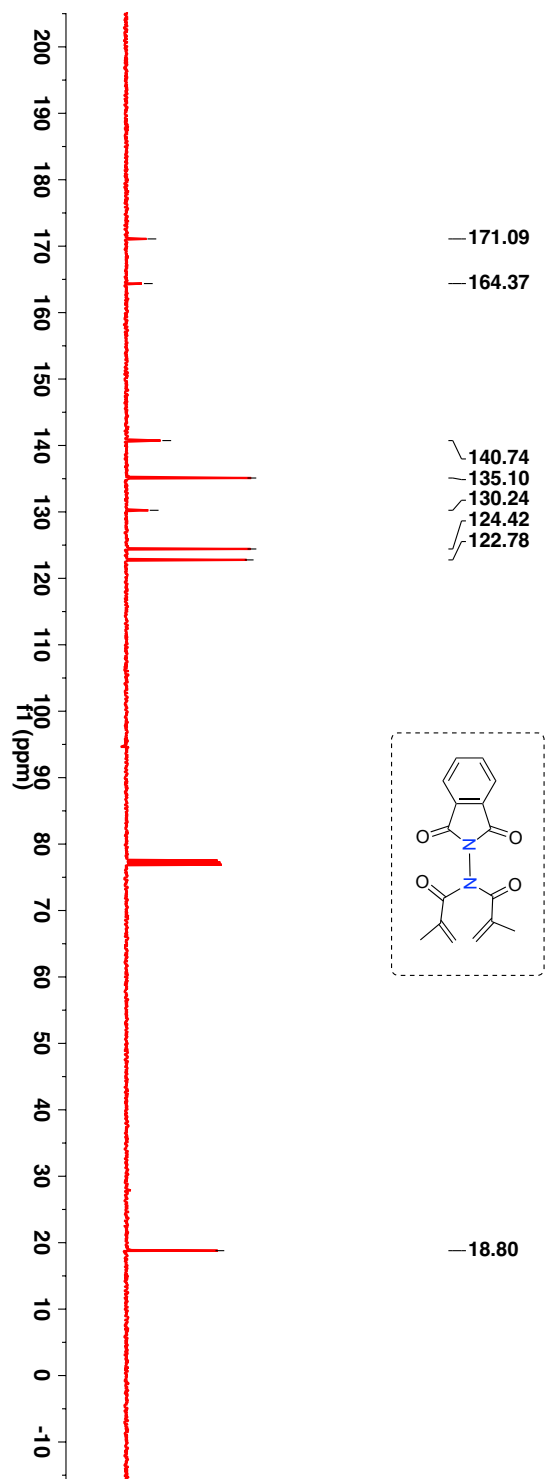
Figure 2.8: ^{13}C-NMR (100 MHz, CDCl$_3$, δ ppm) spectrum of **113a**.

HRMS-ESI (m/z) ([M + Na]$^+$):

Chemical Formula   : $C_{16}H_{14}N_2O_4$

Calculated   : 321.0851

Observed   : 321.0859

|Δm| : 2.5 ppm
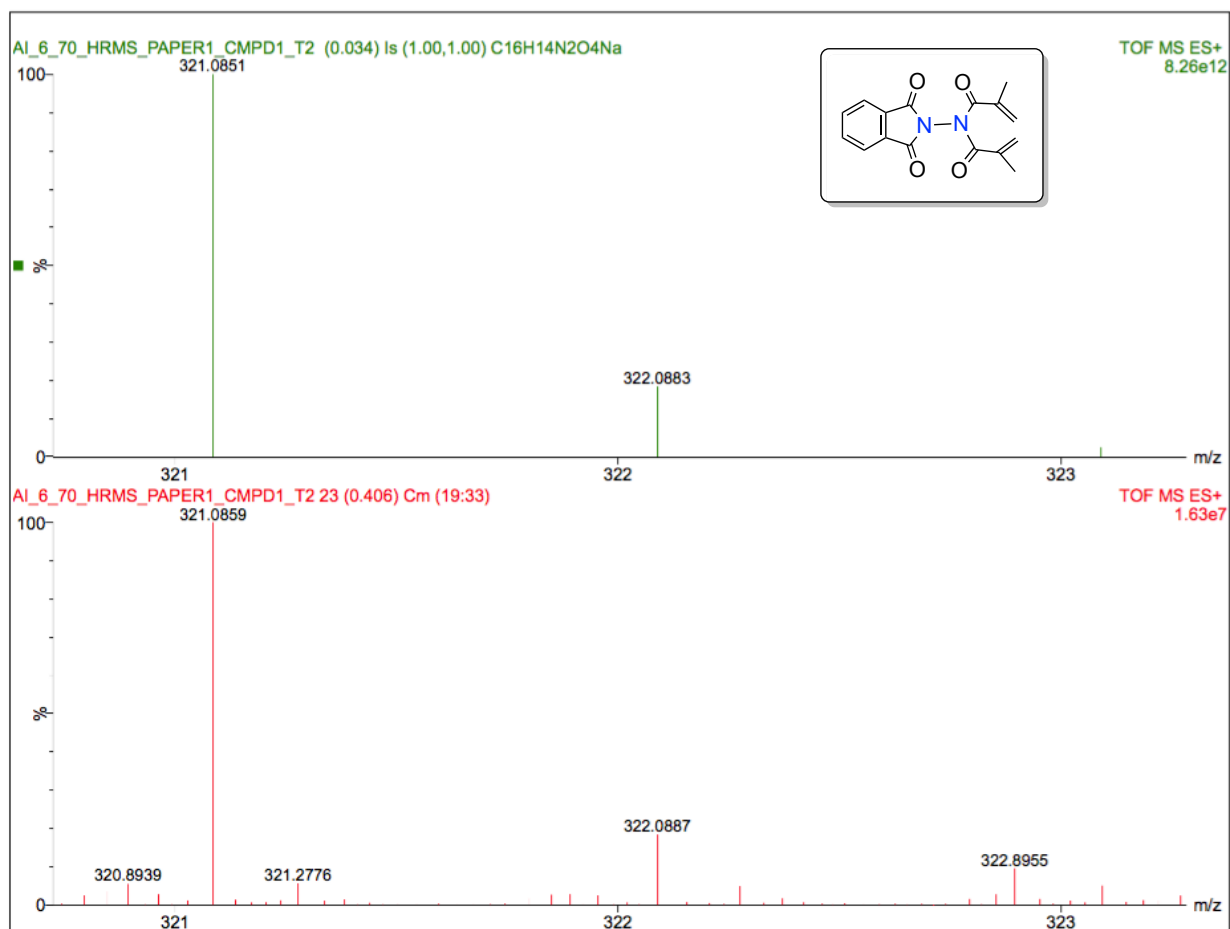
Figure 2.9: HRMS spectra of **113a**.

2.8.   Synthesis of phthalimide based amide derivative 119

The amide derivative **119** was synthesized by two different routes:

ROUTE 2.1
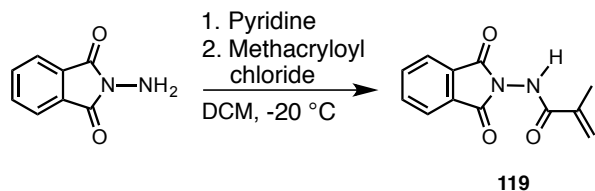
Scheme 2.20: Synthesis of amide **119**.

N-Aminophthalimide (1 equiv) was dissolved in freshly distilled DCM under N_2 atmosphere. To this solution, 1.5 equiv of pyridine was added and the reaction mixture was then cooled to -20 °C, followed by the dropwise addition of methacryloyl chloride (1.2 equiv). After stirring for 15 min, the mixture was brought to room temperature and stirred for 1 h (reaction was monitored by TLC). The reaction was quenched with 5 mL of H_2O, stirred and the organic layer was separated. The organic layer was sequentially washed with DI water (2 × 10 mL), saturated $NaHCO_3$ (2 × 10 mL) and finally with brine. The organic layer was dried over anhyd Na_2SO_4, filtered and the solvent was removed under reduced pressure to yield crude product. The crude product was purified by combiflash using hexanes and ethyl acetate mixture to get the desired acrylimide. The product was characterized by NMR spectroscopy.

TLC conditions R_f = 0.7 (50% ethyl acetate:hexanes), Crystalline solid (Yield = 65%).

^{1}H-NMR (400 MHz, CDCl$_3$, δ ppm): 2.04 (s, 3H), 5.57 (bs, 1H), 5.97 (bs, 1H), 7.74 (bs, 1H), 7.76-7.78 (dd, J = 5.6 Hz, 3.2 Hz, 2H) and 7.88-7.90 (dd, J = 5.6 Hz, 3.2 Hz, 2H).
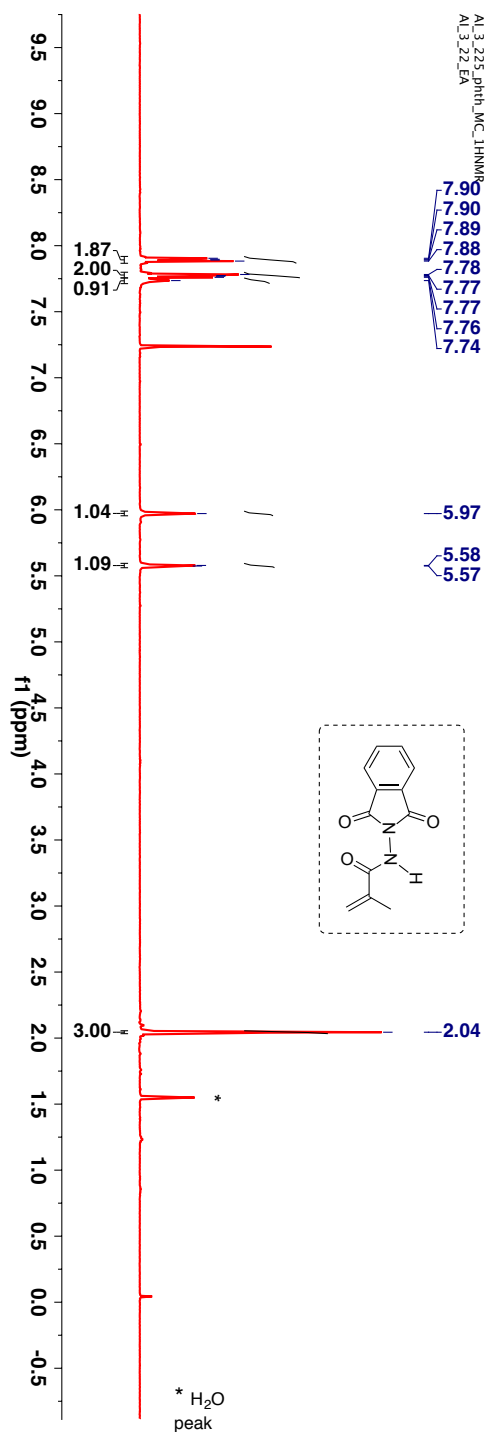
Figure 2.10: ^{1}H-NMR (400 MHz, CDCl$_3$, δ ppm) spectrum of **119**.

^{13}C-NMR (100 MHz, CDCl$_3$, δ ppm): 18.6, 123.1, 124.2, 130.3, 134.9, 137.9, 137.1, and 165.5.
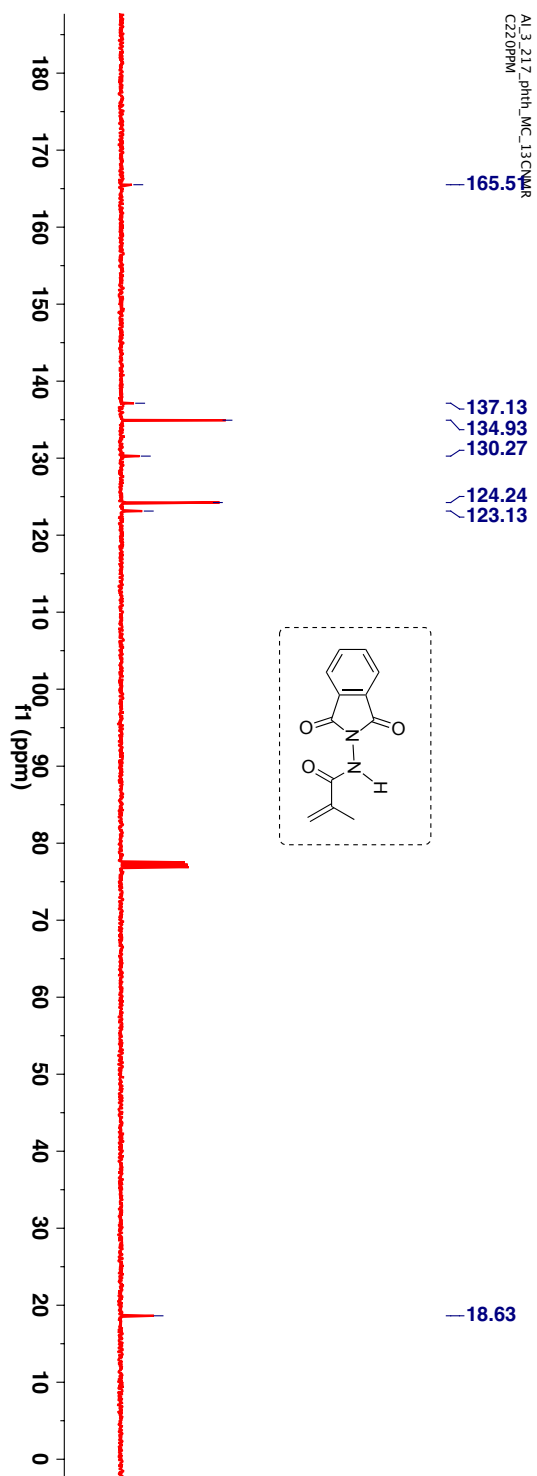
Figure 2.11: ^{13}C-NMR (100 MHz, CDCl$_3$, δ ppm) spectrum of **119**.

ROUTE 2.2

120   **121**   **119**

STEP 1

120
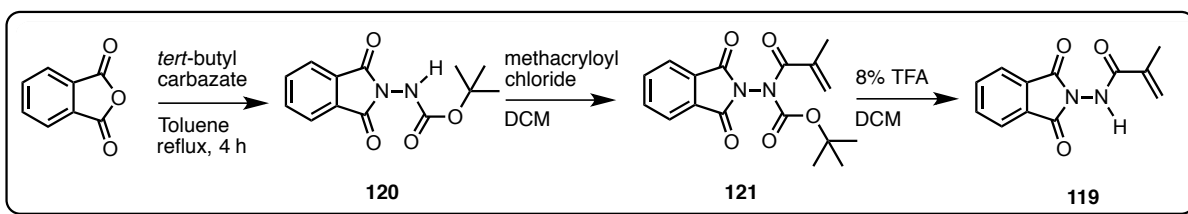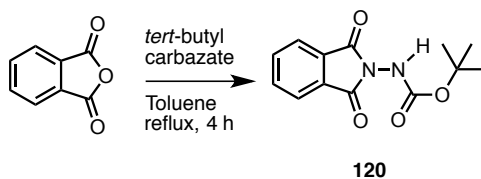
Scheme 2.21: Synthesis of amide derivative **120**.

Modifying a procedure reported by Abbas et al. to a suspension *tert*-butylcarbazate (1 equiv) in toluene, phthalic anhydride (1 equiv) was added and refluxed in a two-neck round bottom flask in a Dean-Stark trap for 4 h. The mixture was cooled and concentrated.[40] The crude product was purified by column chromatography using hexanes and ethyl acetate mixture to get the desired amide and the product was characterized by NMR spectroscopy.

TLC conditions R_f = 0.5 (20% ethyl acetate:hexanes), Crystalline solid (Yield = 94%).

^{1}H-NMR (400 MHz, CDCl$_3$, δ ppm): 1.48 (s, 9H), 6.55 (bs, 1H), 7.75-7.77 (dd, J = 5.6 Hz, 3.2 Hz, 2H) and 7.88-7.90 (dd, J = 5.6 Hz, 3.2 Hz, 2H).
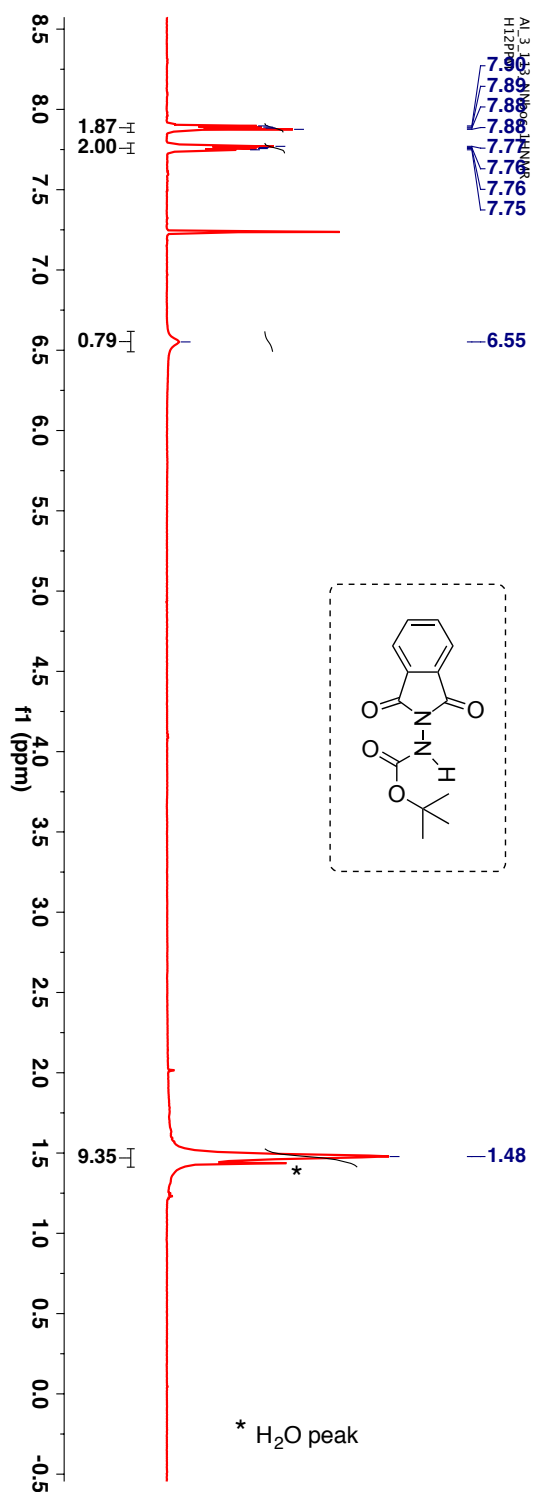
Figure 2.12: ^{1}H-NMR (400 MHz, CDCl$_3$, δ ppm) spectrum of **120**.

¹³C-NMR (100 MHz, CDCl$_3$, δ ppm): 28.2, 83.3, 124.2, 130.2, 134.9 and 153.5.
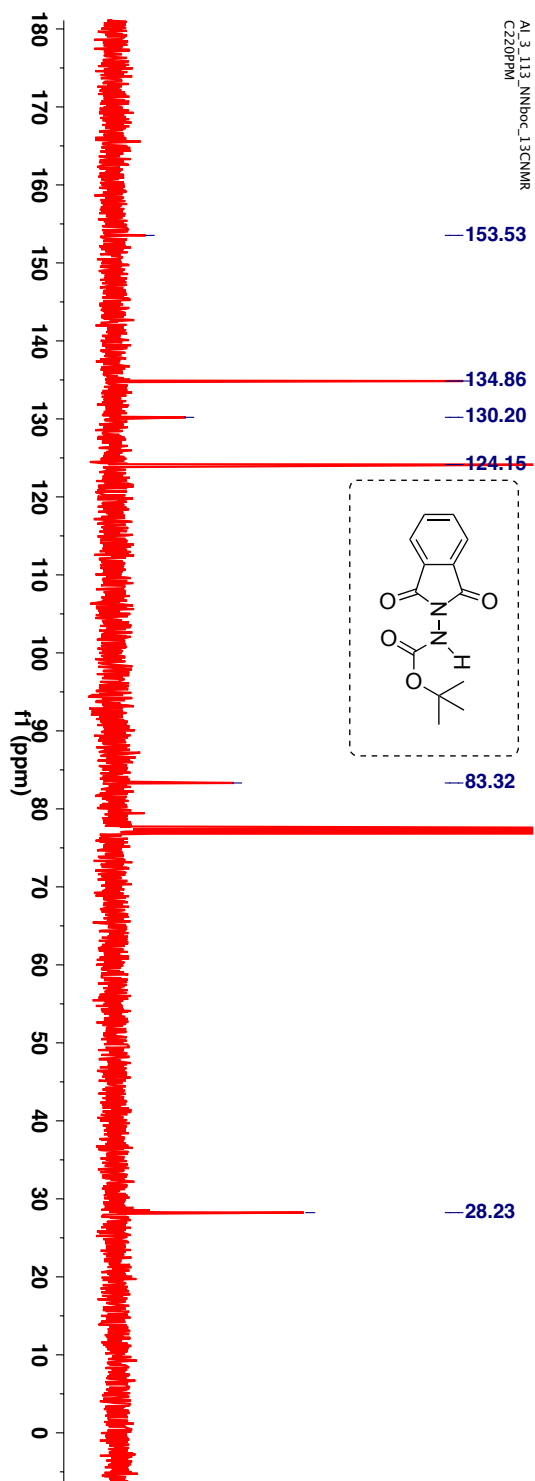
Figure 2.13: ¹³C-NMR (100 MHz, CDCl$_3$, δ ppm) spectrum of **120**.

STEP 2
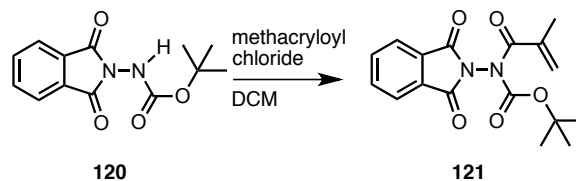
Scheme 2.22: Synthesis of imide derivative **121**.

The amide derivative **120** (1 equiv) was taken in a round bottom flask under N_2 atmosphere, followed by the addition of anhydrous CH_2Cl_2. The solution was cooled to -20 °C and to this solution Et_3N (5 equiv) was added. To this solution 2.0 equiv of methacryloyl chloride was added slowly. The solution was stirred at -20 °C for 1 h and then at room temperature for 20 h. The reaction was quenched with 5 mL of H_2O, stirred and the layers were separated. The organic layer was sequentially washed with DI water (2 × 10 mL), saturated $NaHCO_3$ (2 × 10 mL) and brine. The organic layer was dried over anhyd Na_2SO_4, filtered and the solvent was removed under reduced pressure to yield crude product. The crude product was purified by combiflash using hexanes and ethyl acetate as the eluting solvents.

TLC condition - R_f = 0.5 (20% ethyl acetate:hexanes), Crystalline solid (Yield = 65%).

^{1}H-NMR (400 MHz, CDCl$_3$, δ ppm): 1.38 (s, 9H), 2.0 (s, 3H), 5.36 (bs, 1H), 5.64 (bs, 1H), 7.70-7.72 (m, 2H) and 7.78-7.81 (m, 2H).
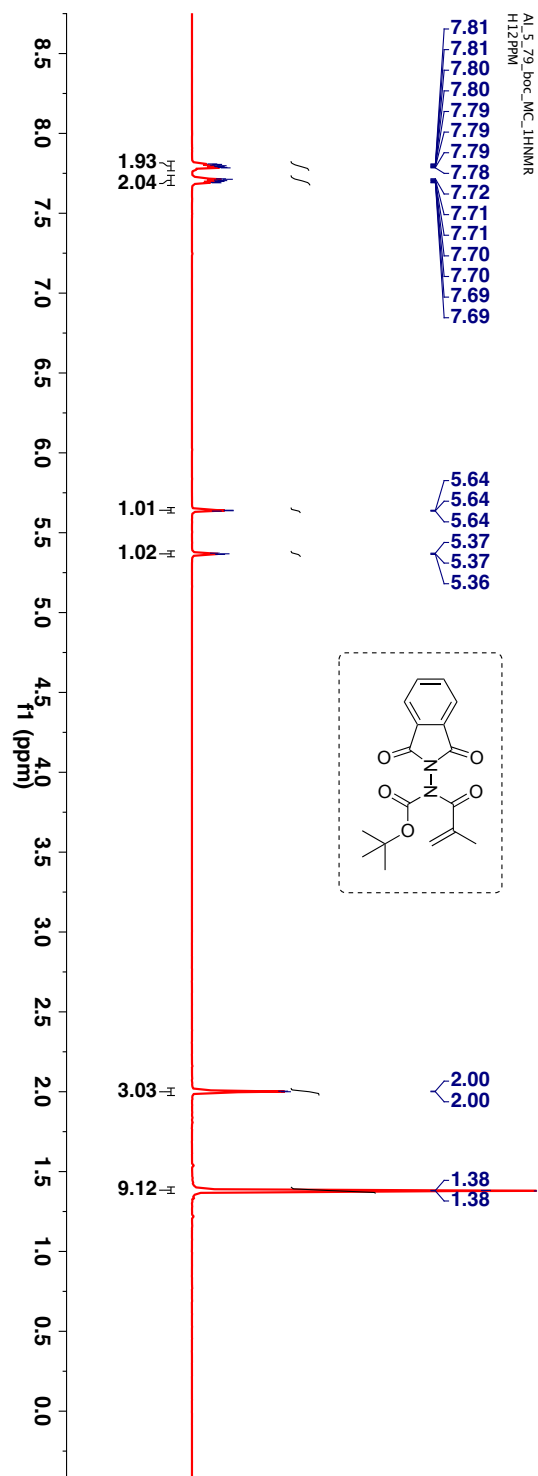
Figure 2.14: ^{1}H-NMR (400 MHz, CDCl$_3$, δ ppm) spectrum of **121**.

^{13}C-NMR (100 MHz, CDCl$_3$, δ ppm): 19.1, 27.8, 86.2, 120.5, 124.2, 130.0, 135.1, 140.4, 149.8, 164.0 and 170.1.
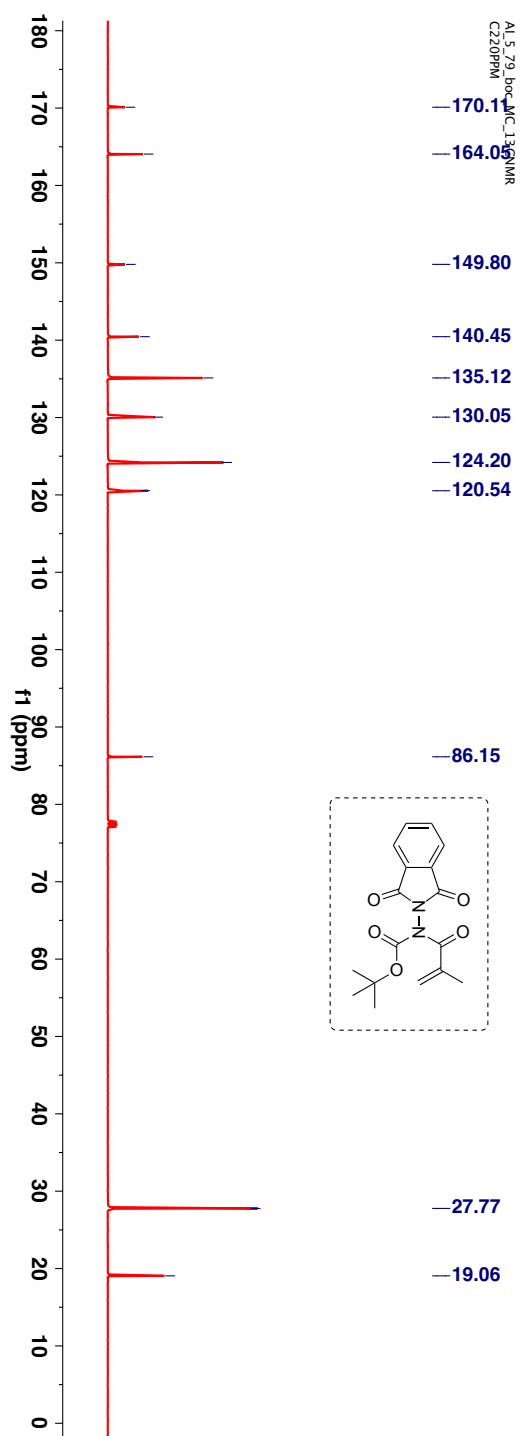
Figure 2.15: ^{13}C-NMR (100 MHz, CDCl$_3$, δ ppm) spectrum of **121**.

STEP 3
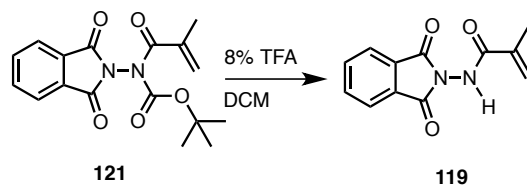
Scheme 2.23: Synthesis of amide derivative **119**.

Modifying a procedure reported by Abbas et al., to a solution of *N*-acyl-*N*-*tert*-butyloxycarbonylaminophthalimide **121** (1 equiv) in anhydrous CH_2Cl_2 was added small volumes of trifluoroacetic acid (8% TFA in CH_2Cl_2) (25 equiv) at 0 °C.[40] The mixture was stirred overnight and more TFA was added until complete consumption of starting material was observed. The solution was concentrated under vacuum. The crude was dissolved in ethyl acetate and the organic layer was sequentially washed with DI water (2 × 10 mL), saturated $NaHCO_3$ (2 × 10 mL) and brine. The organic layer was dried over anhyd Na_2SO_4, filtered and the solvent was removed under reduced pressure to yield crude product. After concentrating the organic layer, the crude product was purified by combiflash using hexanes and ethyl acetate mixture.

TLC condition - R_f = 0.4 (20% ethyl acetate:hexanes), Crystalline solid (Yield = 90%).

^{1}H-NMR (400 MHz, CDCl$_3$, δ ppm): 2.04 (s, 3H), 5.57 (bs, 1H), 5.97 (bs, 1H), 7.74 (bs, 1H), 7.76-7.78 (dd, *J* = 5.6 Hz, 3.2 Hz, 2H) and 7.88-7.90 (dd, *J* = 5.6 Hz, 3.2 Hz, 2H).
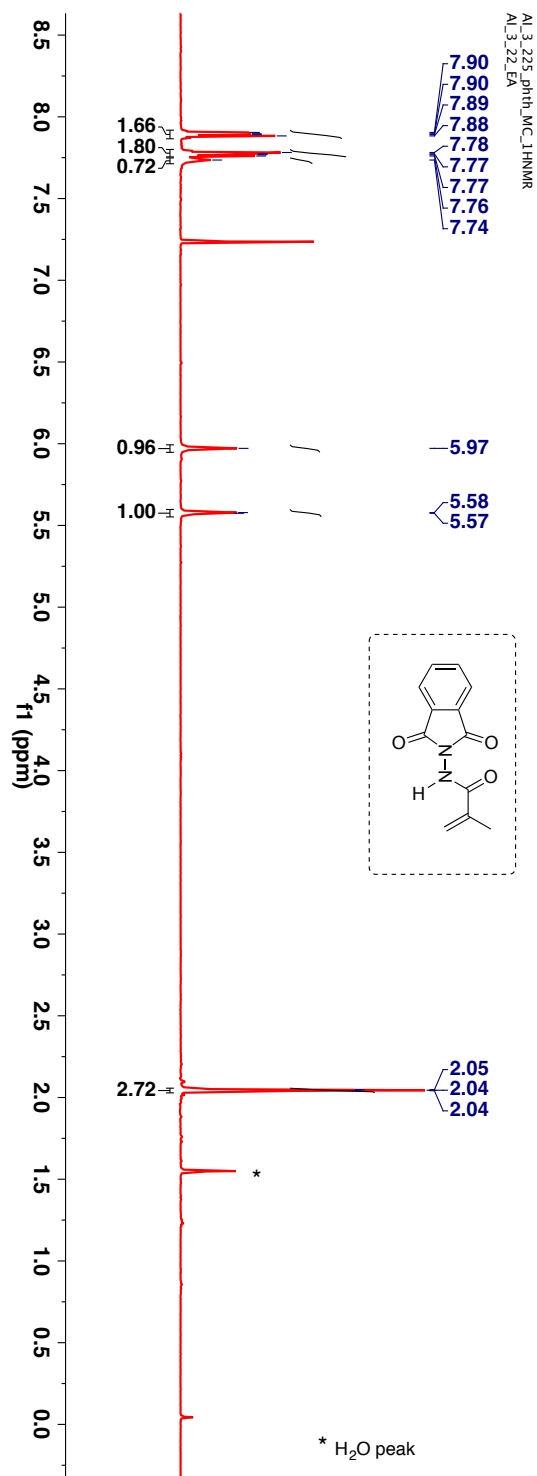
Figure 2.16: ^{1}H-NMR (400 MHz, CDCl$_3$, δ ppm) spectrum of **119**.

2.9. Synthesis of α-oxoamide derivative 113b
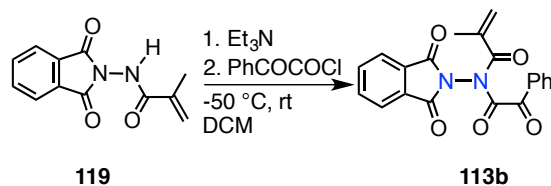
Scheme 2.24: Synthesis of α-oxoamide amide derivative **113b**.

The amide derivative **119** (1 equiv) was taken in a round bottom flask under N_2 protection. This was followed by the addition of dry CH_2Cl_2 and the solution was cooled to -50 °C. To this solution Et_3N (5 equiv) was added. To this solution was added corresponding acid chloride (2.0 equiv) of phenylglyoxylic acid. The solution was stirred at -50 °C for 1 h and then at rt for 20 h. The reaction was quenched with 5 mL of H_2O, stirred and the layers were separated. The organic layer was sequentially washed with DI water (2 × 10 mL), saturated $NaHCO_3$ (2 × 10 mL) and finally with brine. The organic layer was dried over anhyd Na_2SO_4, filtered and the solvent was removed under reduced pressure to yield crude product. After concentrating the organic layer, the crude product was purified by combiflash using hexanes and ethyl acetate as the eluting solvents.

TLC condition - R_f = 0.5 (50% ethyl acetate:hexanes), Pale yellow solid (Yield = 42%).

^{1}H-NMR (400 MHz, CDCl$_3$, δ ppm): 1.88 (s, 3H), 5.41 (s, 1H), 5.69 (s, 1H), 7.50-7.54 (m, 2H), 7.62-7.64 (m, 1H), 7.83-7.85 (m, 2H), 7.95-8.01 (m, 4H).
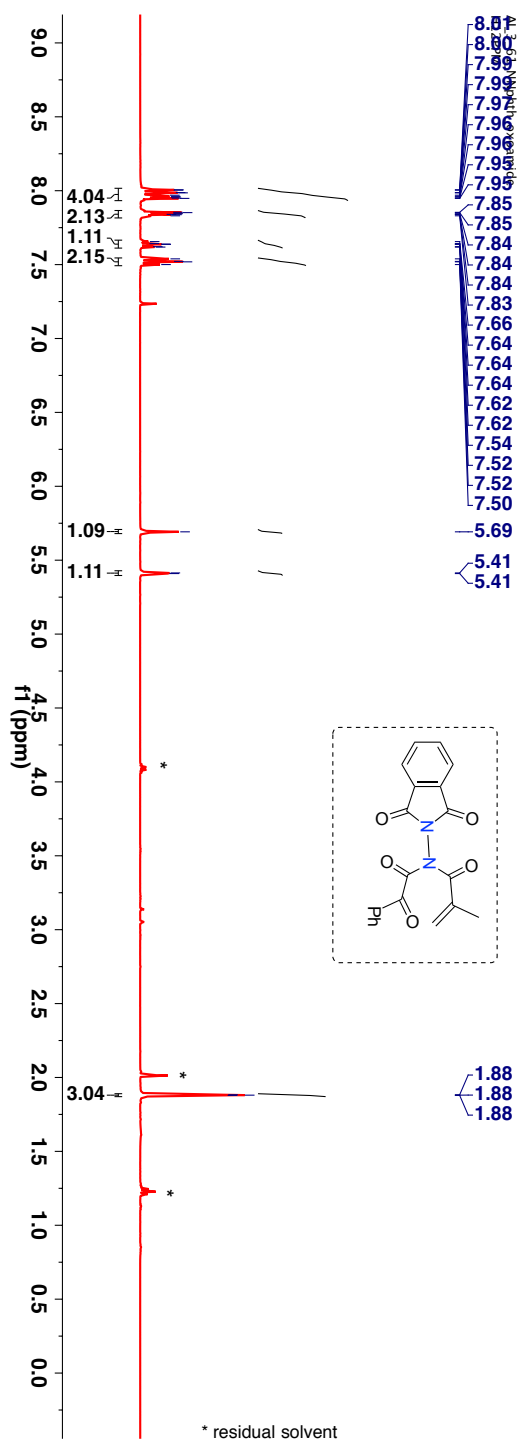
Figure 2.17: ^{1}H-NMR (400 MHz, CDCl$_3$, δ ppm) spectrum of **113b**.

^{13}C-NMR (100 MHz, CDCl$_3$, δ ppm): 18.9, 123.8, 124.8, 129.3, 129.8, 129.9, 132.5, 134.9, 135.5, 137.5, 166.0, 163.8, 170.6 and 185.0.
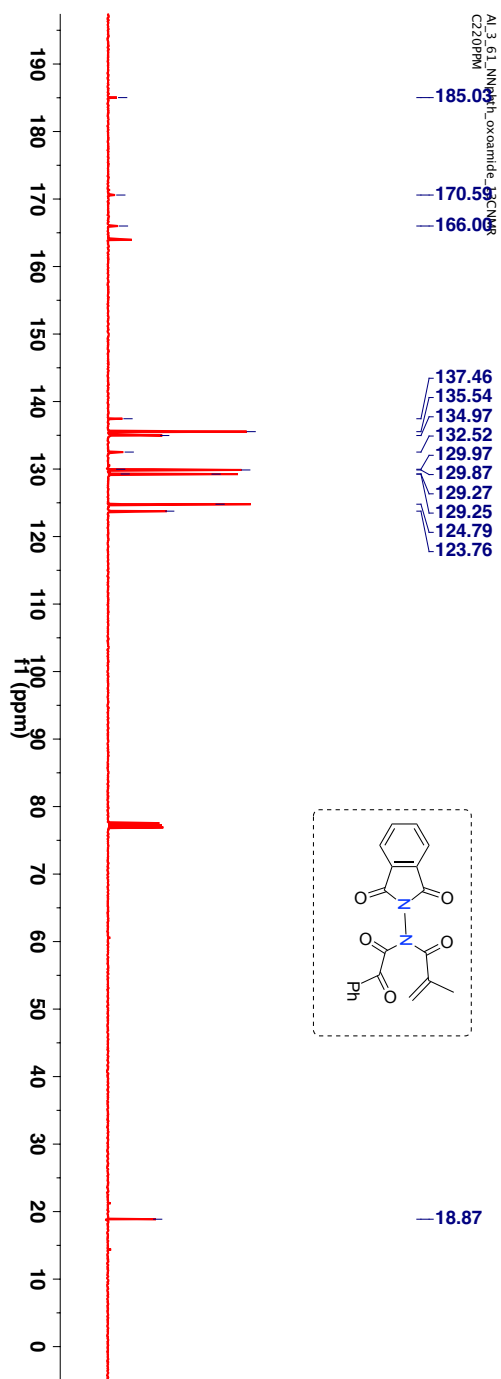
* residual solvent

Figure 2.18: ^{13}C-NMR (100 MHz, CDCl$_3$, δ ppm) spectrum of **113b**.

HRMS-ESI (m/z) ([M + Na]$^+$):

Chemical Formula	: C$_{20}$H$_{14}$N$_2$O$_5$
Calculated	: 385.0800
Observed	: 385.0817
|Δm|	: 4.4 ppm
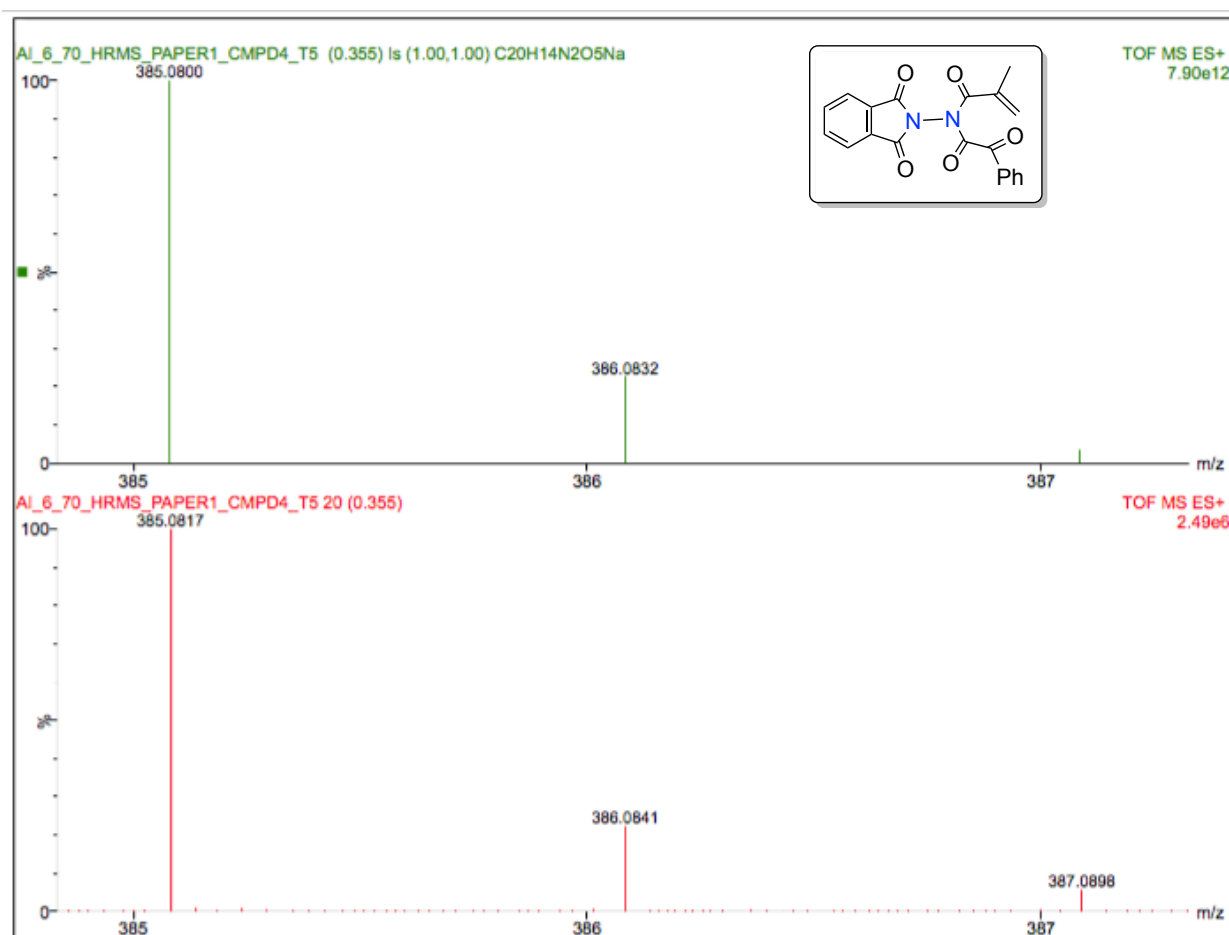
Figure 2.19: HRMS spectra of **113b**.

2.10. Synthesis of α-oxoamide derivative 113c
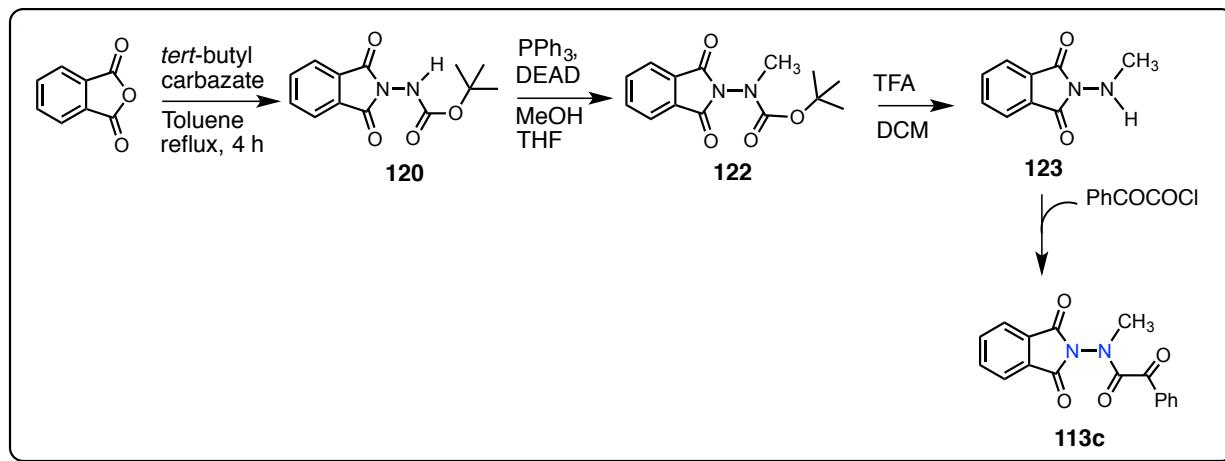
STEP 1
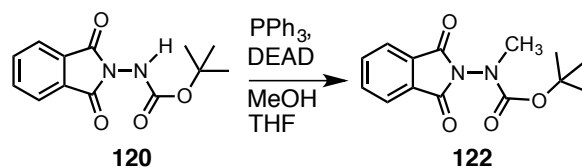
Scheme 2.25: Synthesis of α-oxoamide derivative **122**.

Modifying a procedure reported by Abbas et al., to a solution of *N-tert*-butyloxycarbonylaminophthalimide **120** (1 equiv), PPh₃ (1.5 equiv) and methanol (3 equiv) in anhydrous THF and under N_2 atmosphere was added one portion of Diethyl azodicarboxylate (DEAD) (1.5 equiv) under stirring at 0-5 °C.[40] The resulting solution was stirred overnight and concentrated under vacuum. The crude was purified by column chromatography on silica gel using hexanes and ethyl acetate. The product was characterized by NMR spectroscopy.

TLC condition - R_f = 0.6 (50% ethyl acetate:hexanes), Clear solid (Yield = 87%).

^{1}H-NMR (400 MHz, CDCl$_3$, δ ppm, mixture of rotamers): 1.35 (s, 9H), 1.54 (s), 3.30 (s, 3H), 3.33 (s), 3.92 (s), 7.54-7.56 (m), 7.73-7.78 (m), 7.77-7.78 (m), 7.80-7.82 (m, 2H) and 7.89-7.93 (m, 2H).
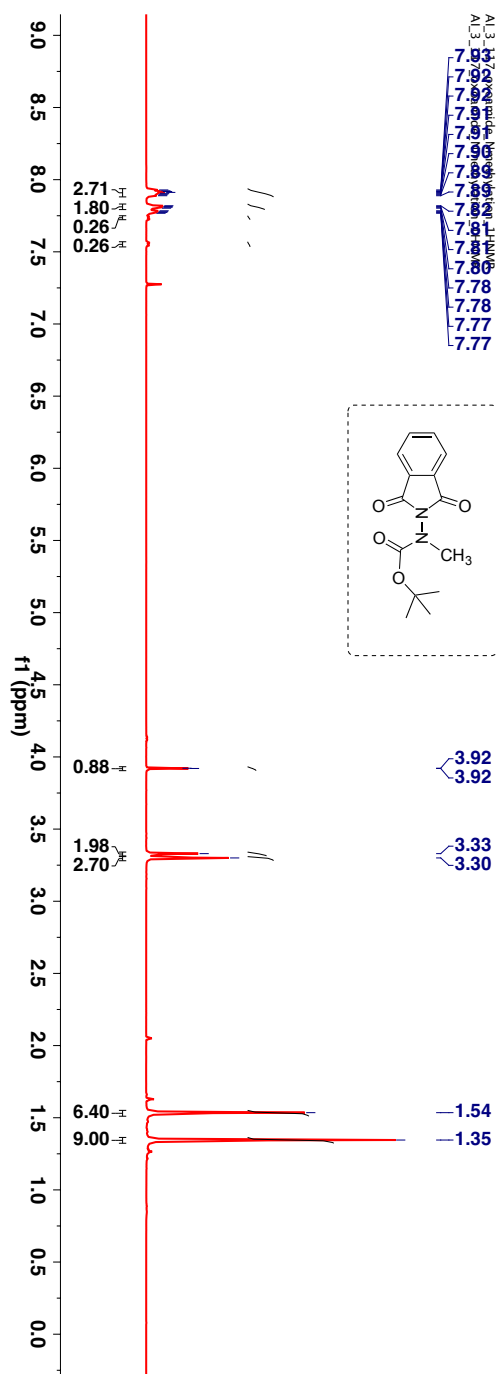
Figure 2.20: ^{1}H-NMR (400 MHz, CDCl$_3$, δ ppm) spectrum of **122**.

^{13}C-NMR (100 MHz, CDCl$_3$, δ ppm, mixture of rotamers): 28.1, 28.4, 36.8, 38.3, 52.9, 82.4, 83.1, 124.1, 124.1, 129.1, 130.3, 131.3, 132.2, 134.8, 134.9, 153.8, 153.9, 165.2 and 165.5.
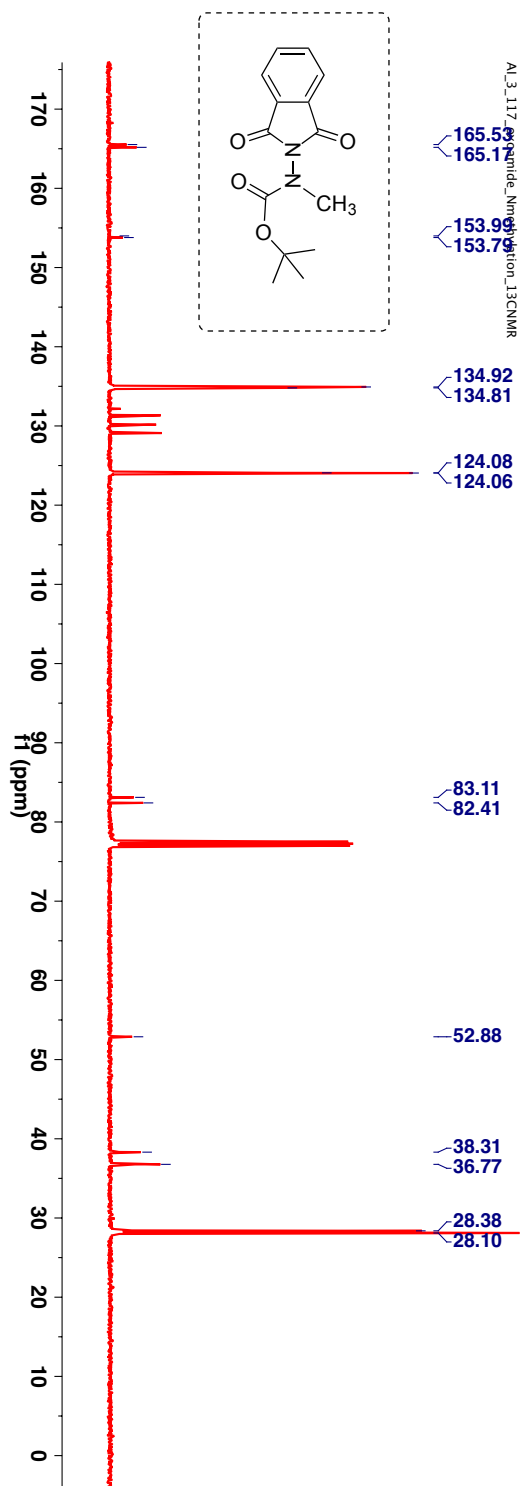
Figure 2.21: ^{13}C-NMR (100 MHz, CDCl$_3$, δ ppm) spectrum of **122**.

STEP 2
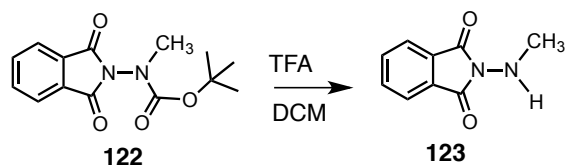
Scheme 2.26: Synthesis of hydrazide derivative **123**.

Modifying a procedure reported by Abbas et al. to a solution of *N*-alkyl-*N*-*tert*-butyloxycarbonylaminophthalimide **122** (1 equiv) in anhydrous CH_2Cl_2 was added small portions of trifluoroacetic acid (8% TFA in CH_2Cl_2) (25 equiv) at 0 °C.[40] The mixture was stirred overnight. The mixture was stirred overnight. More TFA was added until complete consumption of starting material was observed. The solution was concentrated under vacuum. The crude was dissolved in ethyl acetate and the organic layer was sequentially washed with DI water (2 × 10 mL), saturated $NaHCO_3$ (2 × 10 mL) and finally with brine. The organic layer was dried over anhyd Na_2SO_4, filtered and the solvent was removed under reduced pressure to yield crude product. After concentrating the organic layer, the crude product was purified by combiflash using hexanes and ethyl acetate mixture to get the desired compound.

TLC condition - R_f = 0.3 (50% ethyl acetate:hexanes), Colorless solid (Yield = 77%).

^{1}H-NMR (400 MHz, CDCl$_3$, δ ppm): 2.81 (s, 3H), 4.47 (bs, 1H), 7.69-7.71(m, 2H) and 7.81-7.83 (m, 2H).
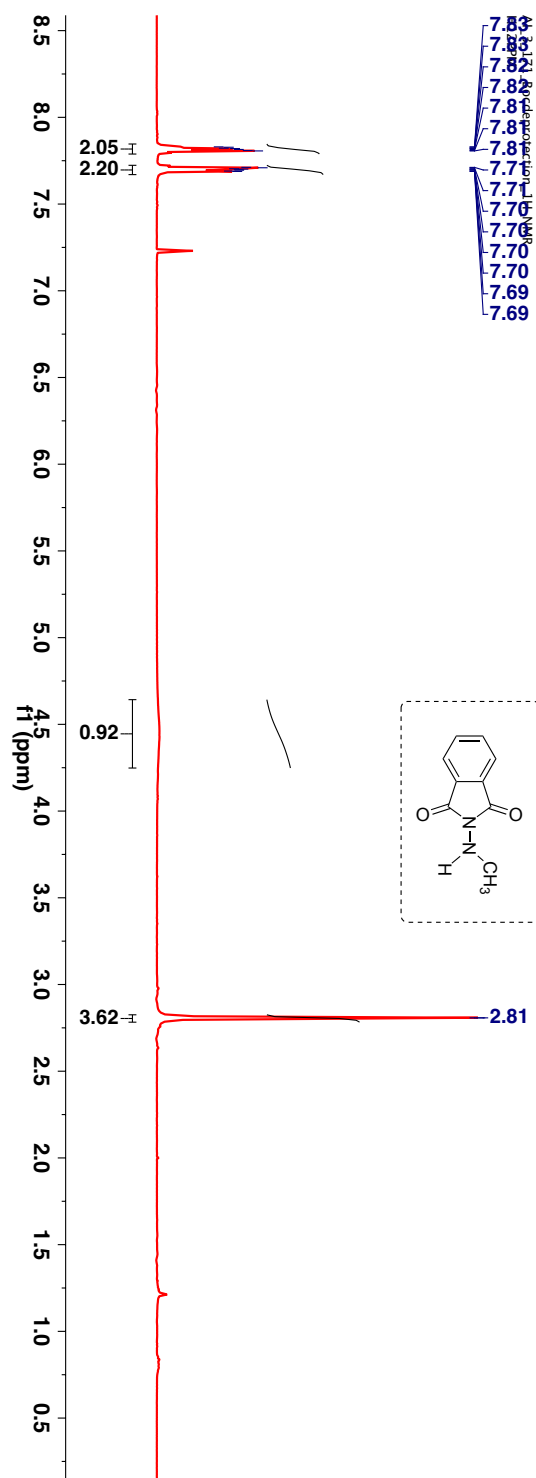
Figure 2.22: ^{1}H-NMR (400 MHz, CDCl$_3$, δ ppm) spectrum of **123**.

^{13}C-NMR (100 MHz, CDCl$_3$, δ ppm): 38.8, 123.6, 130.5, 134.4 and 166.6.
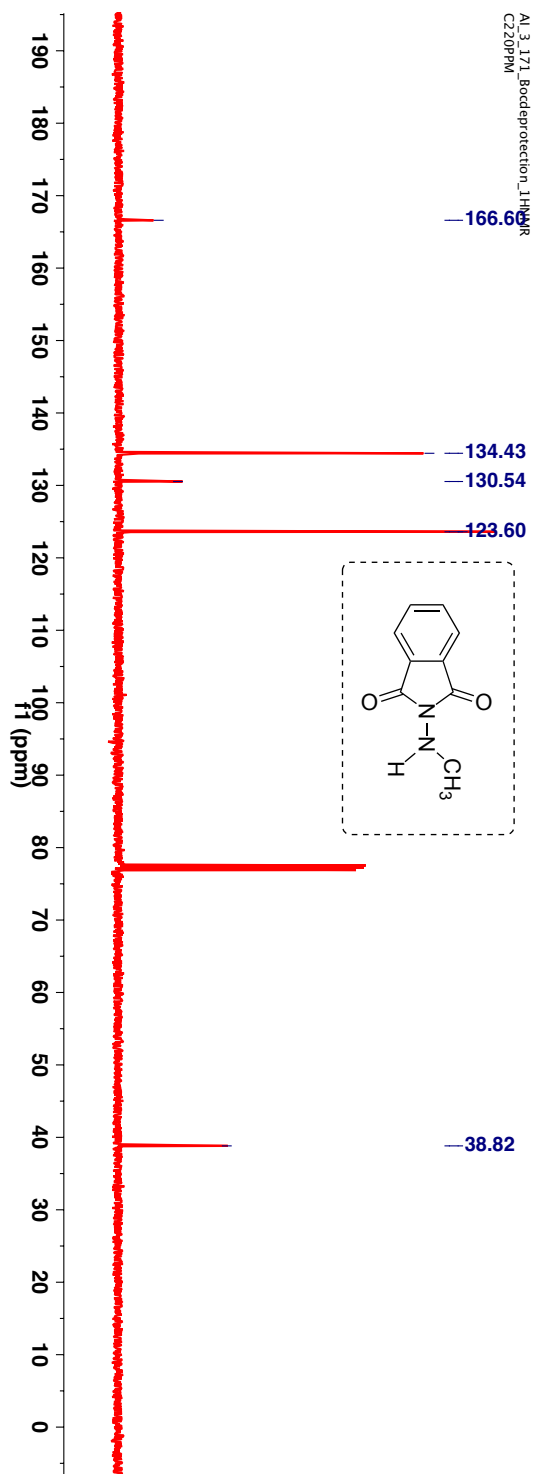
Figure 2.23: ^{13}C-NMR (100 MHz, CDCl$_3$, δ ppm) spectrum of **123**.

STEP 3
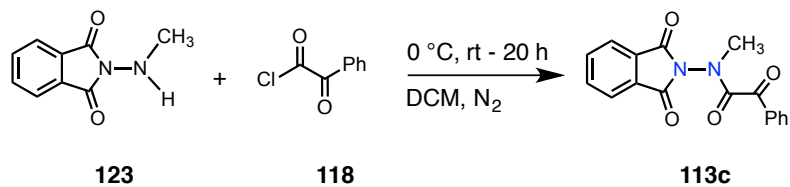
Scheme 2.27: Synthesis of oxoamide derivative **113c**.

To the hydrazide derivative **123** (1 equiv) in a round bottom flask under N_2 protection, dry CH_2Cl_2 was added and the solution was cooled to -20 °C. To this solution Et_3N (5 equiv) was added. To this solution was added freshly prepared acyl chloride **118** (2 equiv). The solution was stirred at -20 °C for 1 h and then at rt for 20 h. The reaction was quenched with 5 mL of H_2O, stirred and the layers were separated. The organic layer was sequentially washed with DI water (2 × 10 mL), saturated $NaHCO_3$ (2 × 10 mL) and finally with brine. The organic layer was dried over anhyd Na_2SO_4, filtered and the solvent was removed under reduced pressure to yield crude product.

TLC condition - R_f = 0.6 (50% ethyl acetate:hexanes), Yellow solid (Yield = 68%).

^{1}H-NMR (400 MHz, CDCl$_3$, δ ppm, 1.9 : 1.0 rotamer ratio, mixture of rotamers):): 3.37 (s), 3.44 (s, 3H), 7.40-7.44 (m, 2H), 7.53-7.59 (m, 2H), 7.65-7.69 (m), 7.72-7.74 (m, 2H), 7.79-7.81 (m, 2H), 7.89-7.93 (m, 3H) and 8.10-8.13 (m, 1H).
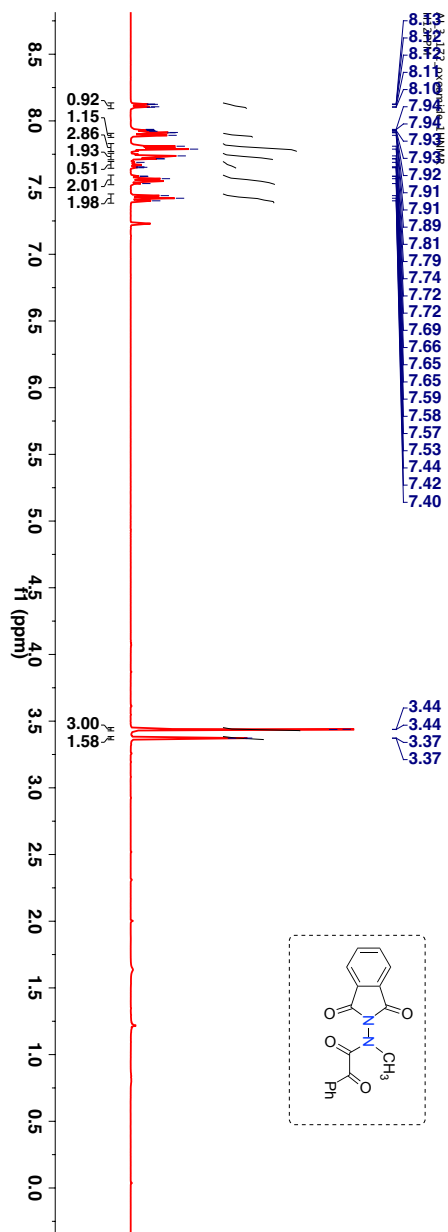
Figure 2.24: ^{1}H-NMR (400 MHz, CDCl$_3$, δ ppm) spectrum **113c**.

¹³C-NMR (100 MHz, CDCl₃, δ ppm, all peaks are reported together as it is difficult to assign certain peaks in aromatic region to minor rotamer peaks): 35.4, 38.8, 124.4, 124.6, 128.9, 129.5, 129.6, 130.1, 130.3, 130.5, 132.3, 132.7, 135.1, 135.2, 135.3, 135.6, 164.0, 164.4, 165.3, 167.1, 188.8 and 189.8.

Figure 2.25: ¹³C-NMR (100 MHz, CDCl₃, δ ppm) spectrum of **113c**.

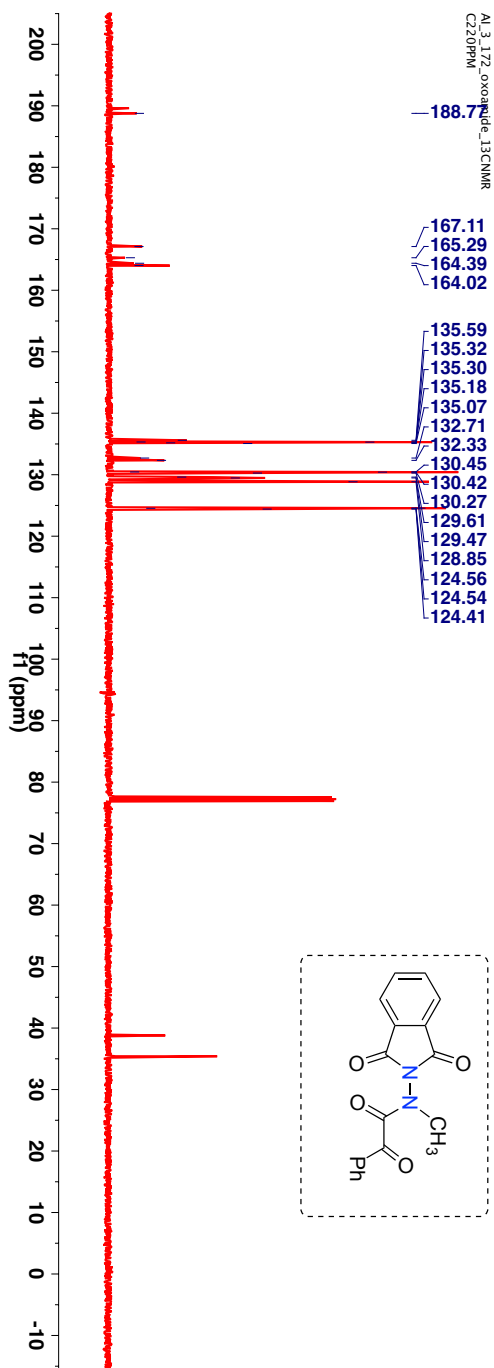
Figure 2.25: ^{13}C-NMR (100 MHz, CDCl$_3$, δ ppm) spectrum of **113c**.

HRMS-ESI (m/z) ([M + Na]$^+$):

Chemical Formula	: C$_{17}$H$_{12}$N$_2$O$_4$
Calculated	: 331.0695
Observed	: 331.0700
|Δm|	: 1.5 ppm
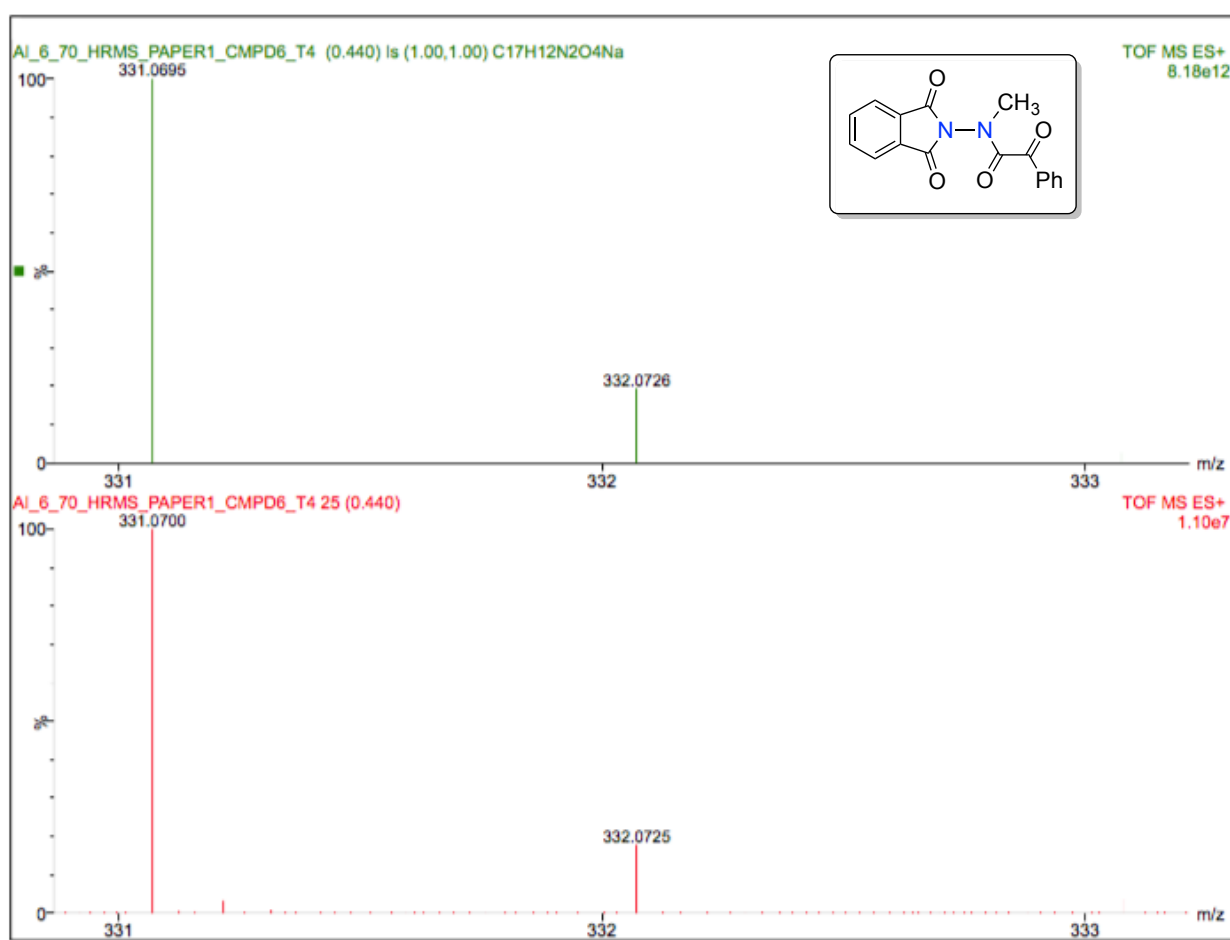
Figure 2.26: HRMS spectra of **113c**.

2.11. Synthesis of acrylanilide derivative 113d
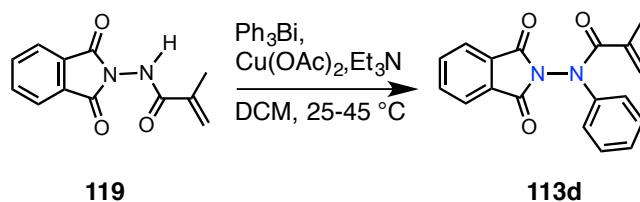
Scheme 2.28: Synthesis of acrylanilide derivative **113d**.

Following the modified procedure reported by Kikugawa et al., a mixture of amide **119** (1 equiv), triphenylbismuth (2 equiv), cupric acetate (1.5 equiv), and triethylamine (1.5 equiv) was stirred in anhydrous CH_2Cl_2 for 1.5 h at room temperature under N_2 protection and then refluxed for 20 h.[41] After completion of the reaction, the solution was diluted with ethyl acetate (20 mL) and filtered through a short celite pad. The filtrate was evaporated under reduced pressure. The crude product was chromatographed with a flash column using ethyl acetate and hexanes as the eluting solvent.

TLC condition - R_f = 0.7 (50% ethyl acetate:hexanes), Crystalline solid (Yield = 33%).

¹H-NMR (400 MHz, CDCl₃, δ ppm): 1.89 (s, 3H), 5.22 (s, 1H), 5.35 (s, 1H), 7.28-7.37 (m, 3H), 7.50-7.52 (m, 2H), 7.74-7.76 (m, 2H), and 7.86-7.88 (m, 2H).
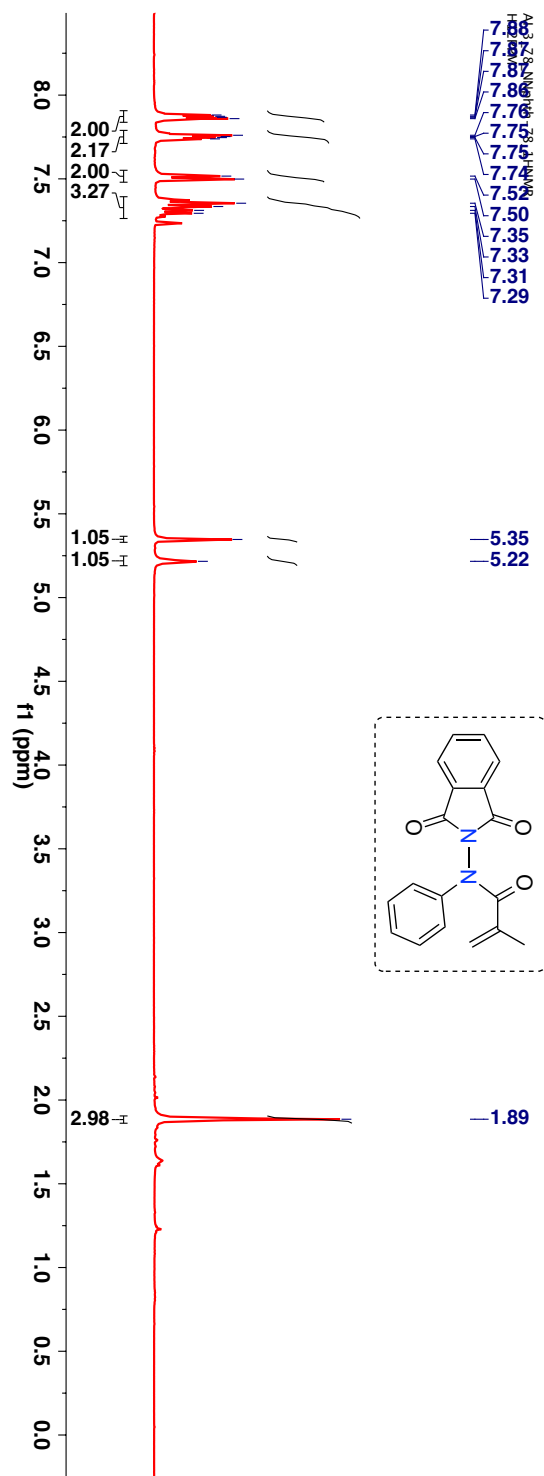
Figure 2.27: ¹H-NMR (400 MHz, CDCl₃, δ ppm) of **113d**.

^{13}C-NMR (100 MHz, CDCl$_3$, δ ppm): 20.0, 124.3, 127.7, 128.8, 129.6, 130.2, 134.9 and 165.1.
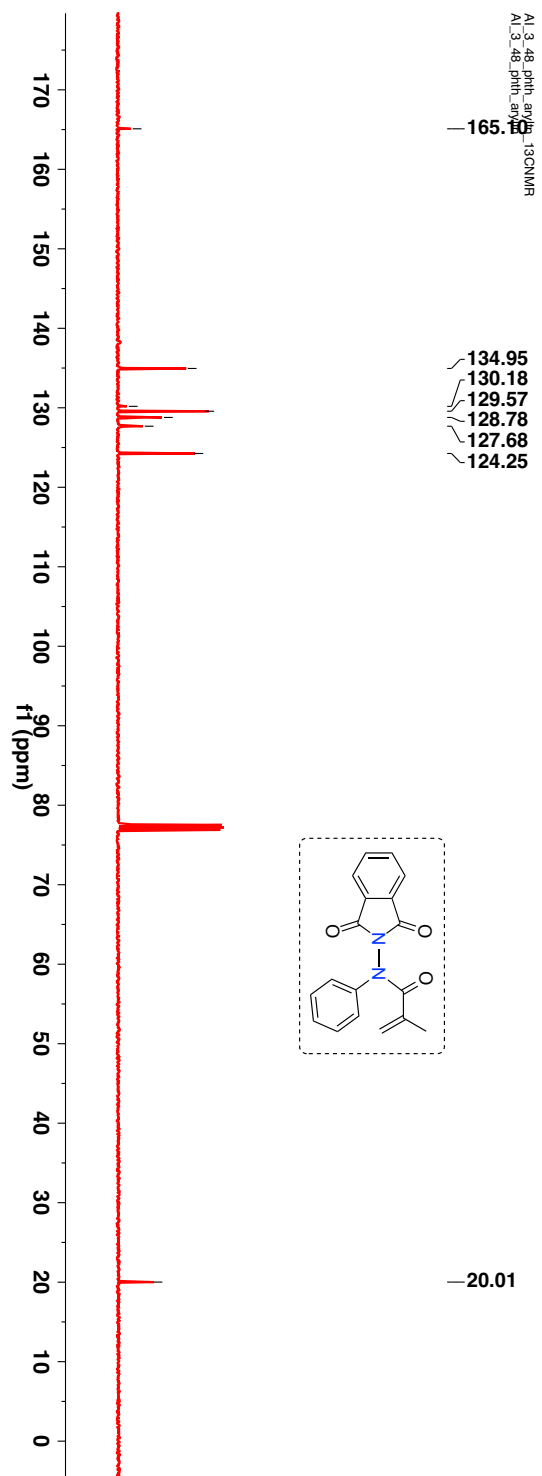
Figure 2.28: ^{13}C-NMR (100 MHz, CDCl$_3$, δ ppm) spectrum of **113d**.

HRMS-ESI (m/z) ([M + H]):

Chemical Formula   : $C_{18}H_{14}N_2O_3$

Calculated   : 329.0902

Observed   : 329.0914

|Δm| : 3.6 ppm
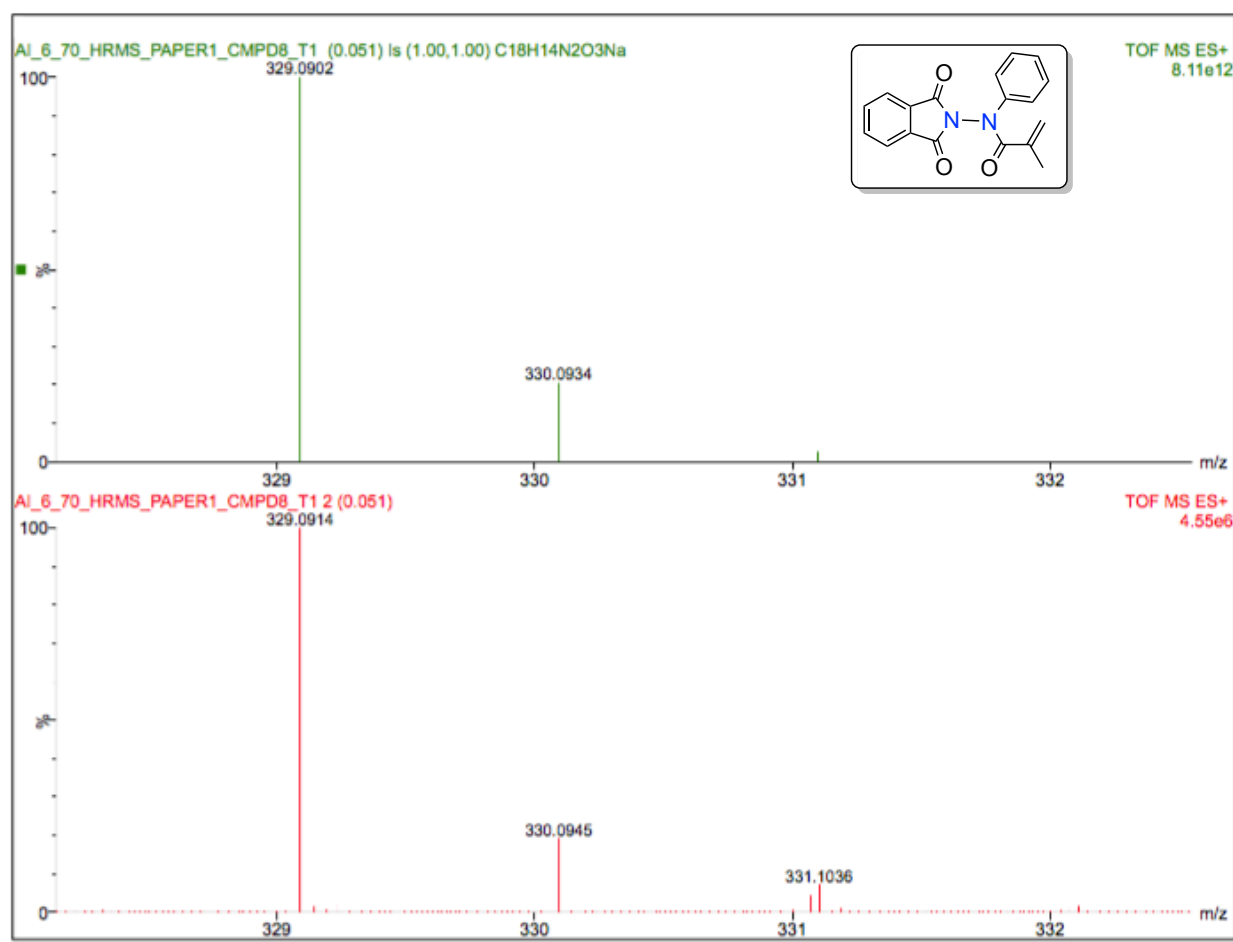
Figure 2.29: HRMS spectra of **113d**.

2.12. Synthesis of amide based hydrazide derivative 113g
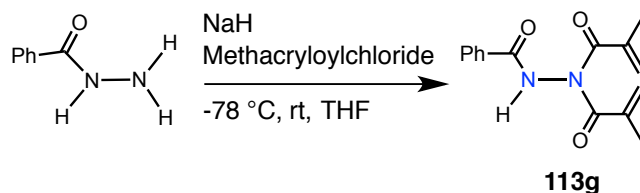
Scheme 2.29: Synthesis of imide based hydrazide derivative **113g**.

Benzhydrazine (1 equiv) was taken in a round bottom flask under N_2 protection and dissolved in in freshly distilled THF. The solution was cooled to -78 °C. To this solution, NaH (5 equiv) was added slowly in portions. To this solution was added methacryloyl chloride (2.0 equiv). The solution was stirred at -50 °C for 2 h and then at room temperature for 20 h. The reaction was quenched with 5 mL of H_2O, stirred and the layers were separated. The organic layer was sequentially washed with DI water (2 × 10 mL), saturated $NaHCO_3$ (2 × 10 mL) and finally with brine. The organic layer was dried over anhyd Na_2SO_4, filtered and the solvent was removed under reduced pressure to yield crude product. After concentrating the organic layer, the desired compound was purified by combiflash using hexanes and ethyl acetate as the eluting solvent.

TLC condition - R_f = 0.5 (50% ethyl acetate:hexanes, mixture of rotamers). Viscous clear liquid (Yield = 44%).

^{1}H-NMR (400 MHz, CDCl$_3$, δ ppm): 1.85 (s), 1.90 (s), 1.94 (s), 5.35-5.36 (m), 5.44 (s), 5.67 (s), 5.70-5.72 (m), 7.37-7.40 (m), 7.49-7.50 (m), 7.67-7.69 (m), 7.81-7.83 (m), 8.87 (bs) and 9.31 (bs).
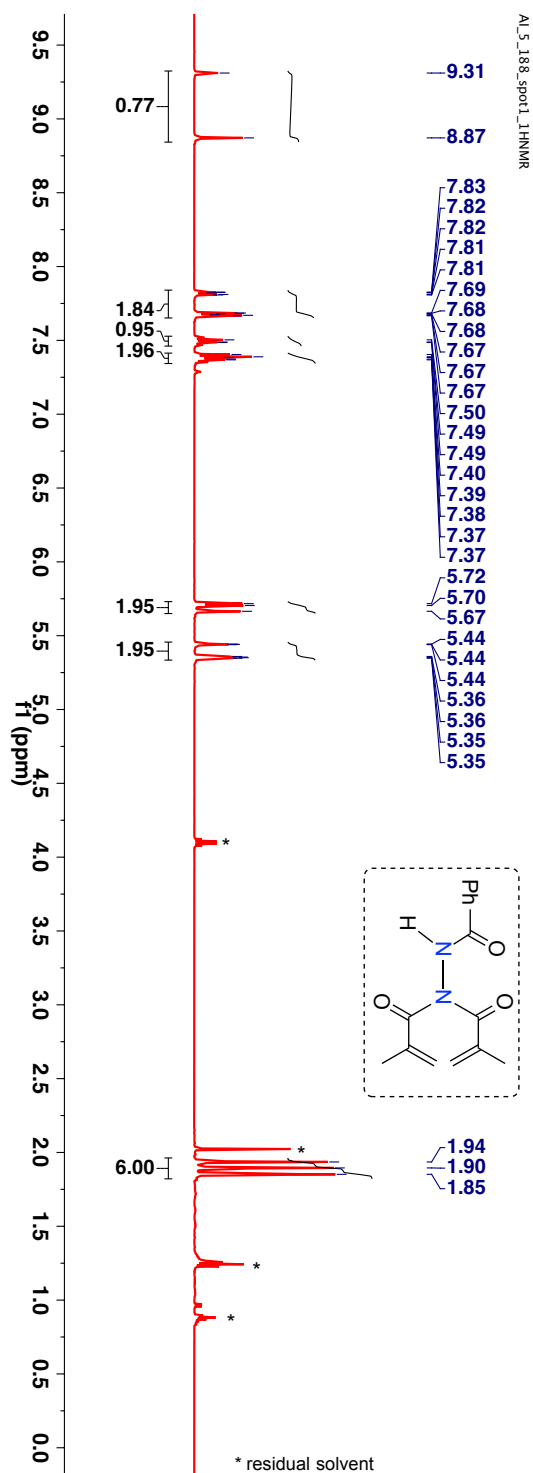
Figure 2.30: ^{1}H-NMR (400 MHz, CDCl$_3$, δ ppm) spectrum of **113g**.

^{13}C-NMR (100 MHz, CDCl$_3$, δ ppm, mixture of rotamers): 18.4, 18.6, 18.9, 122.1, 122.5, 122.7, 127.8, 128.7, 128.8, 128.8, 128.9, 131.2, 132.8, 132.8, 134.1, 137.5, 140.5, 141.3, 166.7, 167.8, 172.2, 173.2 and 173.4.
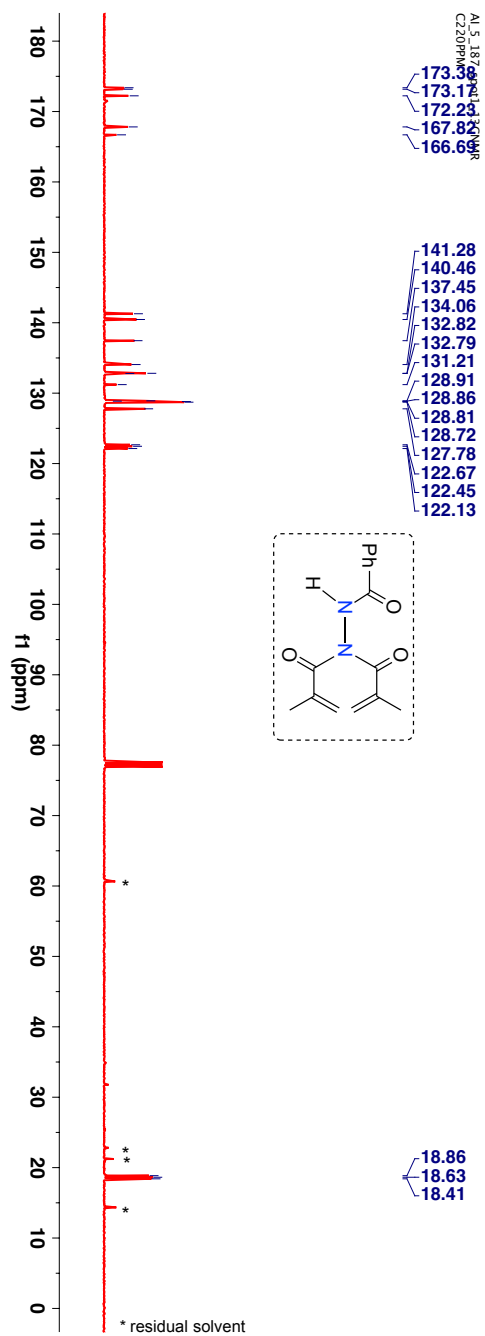
Figure 2.31: ^{13}C-NMR (100 MHz, CDCl$_3$, δ ppm) spectrum of **113g**.

HRMS-ESI (m/z) ([M + H]):

Chemical Formula   : $C_{15}H_{16}N_2O_3$

Calculated   : 295.1059

Observed   : 295.1074

|Δm| : 1.6 ppm
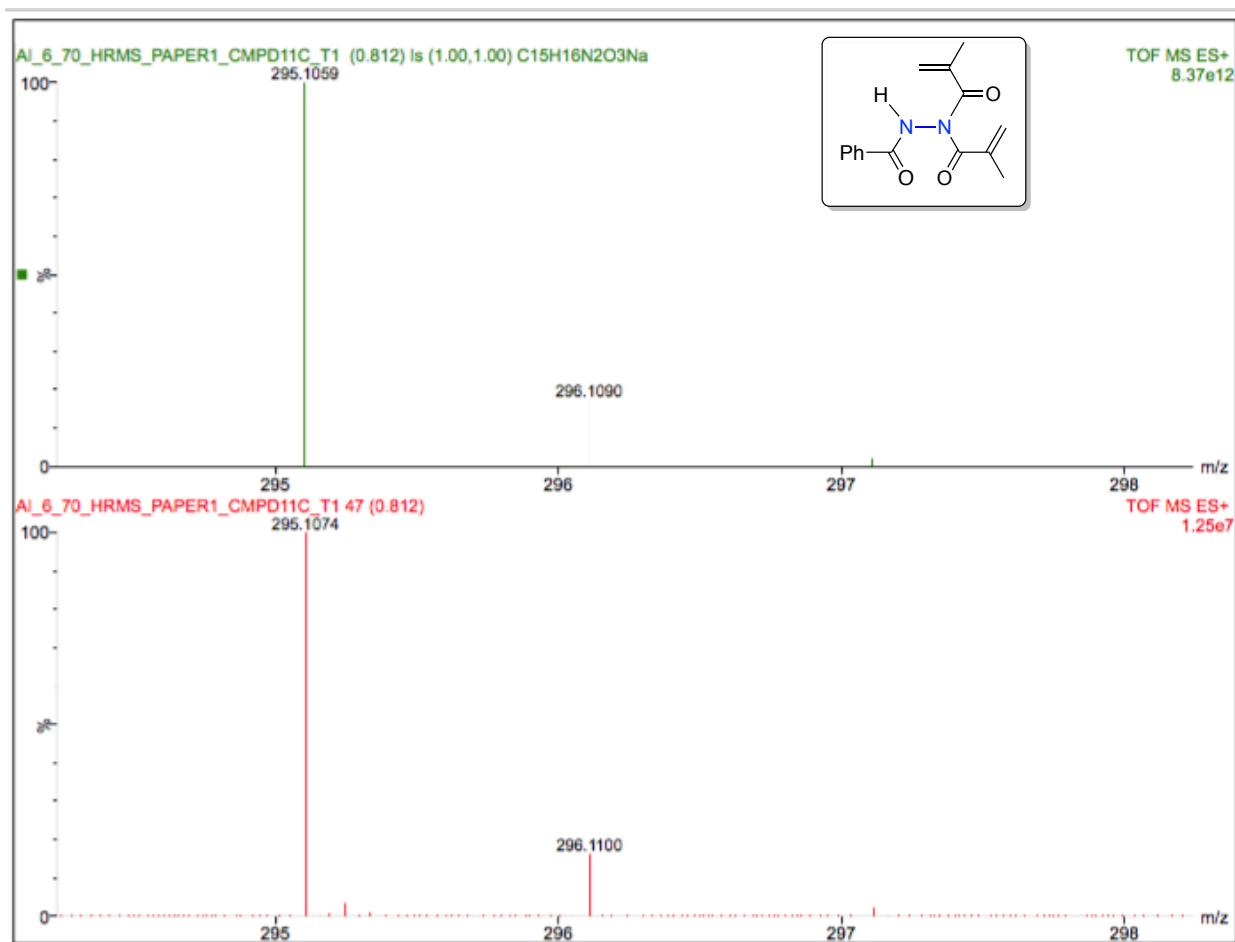
Figure 2.32: HRMS spectra of **113g**.

2.13. Synthesis of amide based hydrazide derivative 113g
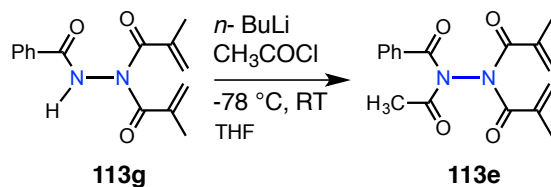
Scheme 2.30: Synthesis of imide based hydrazide derivative **113e**.

The amide based hydrazide derivative **113g** (1 equiv) was taken in a round bottom flask under N_2 protection and dissolved in freshly distilled THF. The solution was cooled to -78 °C. To this solution *n*-BuLi (1 equiv) was added dropwise over a period of 10 minutes. This was followed by addition of freshly distilled acetyl chloride (1.1 equiv). The solution was stirred at -78 °C for 2 h after which TLC showed complete consumption of starting material. The reaction was quenched with 5 mL of H_2O, stirred and the layers were separated. The organic layer was sequentially washed with DI water (2 × 10 mL), saturated $NaHCO_3$ (2 × 10 mL) and finally with brine. The organic layer was dried over anhyd Na_2SO_4, filtered and the solvent was removed under reduced pressure to yield crude product. After concentrating the organic layer, the desired compound was purified by combiflash using hexanes and ethyl acetate as the eluting solvent.

TLC condition - R_f = 0.6 (50% ethyl acetate:hexanes), Viscous liquid that became solid on standing (Yield = 71%).

^{1}H-NMR (400 MHz, CDCl$_3$, δ ppm): 1.73 (s, 3H), 2.04 (s, 3H), 2.51 (s, 3H), 5.28 (s, 1H), 5.41 (s, 1H), 5.54 (s, 1H), 5.60 (s, 1H), 7.43-7.46 (m, 2H), 7.53-7.56 (m, 1H) and 7.62-7.64 (m, 2H).
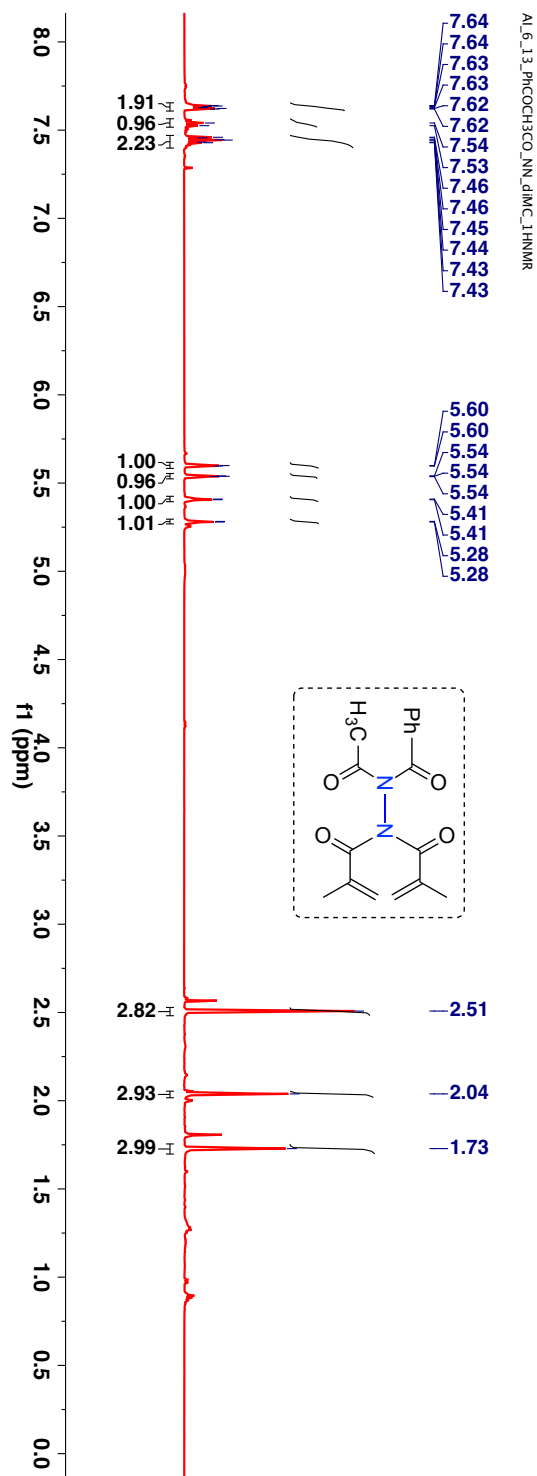
Figure 2.33: ^{1}H-NMR (400 MHz, CDCl$_3$, δ ppm) spectrum of **113e**.

^{13}C-NMR (100 MHz, CDCl$_3$, δ ppm, mixture of rotamers): 18.7, 19.2, 25.2, 120.3, 124.9, 127.3, 128.9, 133.0, 140.0, 141.1, 142.0, 170.8, 171.0, 171.1 and 172.0.

Figure 2.34: ^{13}C-NMR (100 MHz, CDCl$_3$, δ ppm) spectrum of **113e**.

HRMS-ESI (m/z) ([M + Na]$^+$):

Chemical Formula : C$_{17}$H$_{18}$N$_2$O$_4$

Calculated   : 337.1164

Observed   : 337.1184

|Δm| : 5.9 ppm
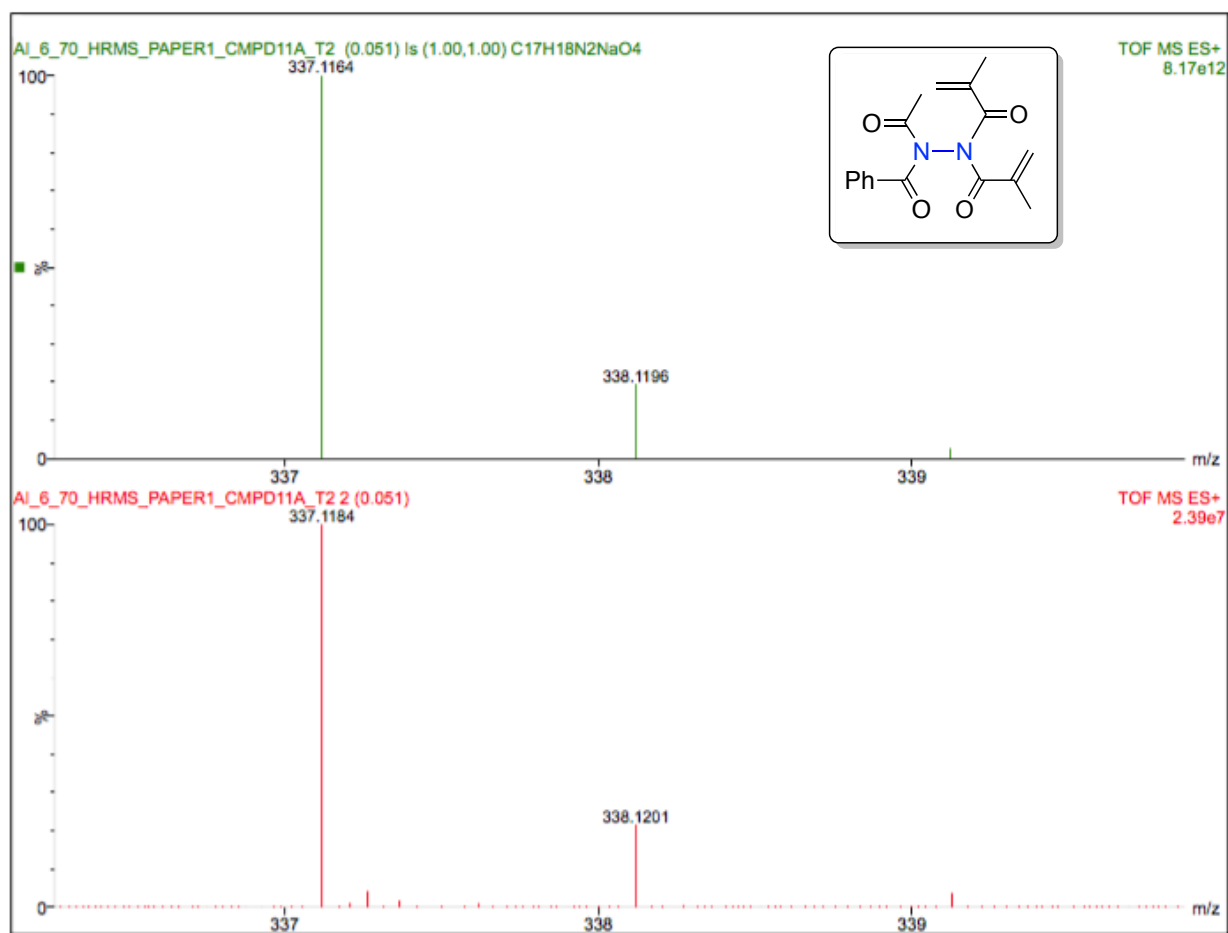
Figure 2.35: HRMS spectra of **113e**.

2.14. Synthesis of secondary carbamate based hydrazide derivative 113h
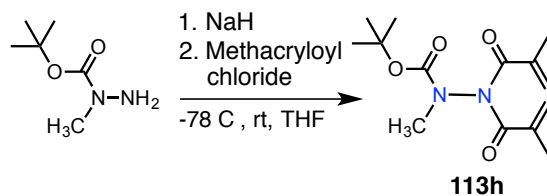
Scheme 2.31: Synthesis of carbamate based hydrazide derivative **113h**.

1-Boc-1-methylhydrazine (1 equiv) was dissolved in freshly distilled THF under N_2 atmosphere. The reaction mixture was then cooled to -78 °C and this was followed by the addition of 5 equiv of NaH followed by the dropwise addition of methacryloyl chloride (2.5 equiv). After stirring for 1 h at this temperature, the mixture was brought to room temperature and stirred for 20 h. The reaction was quenched with 5 mL of NH_4Cl, stirred and the layers were separated. The organic layer was sequentially washed with DI water (2 × 10 mL), saturated $NaHCO_3$ (2 × 10 mL) and finally with brine. The organic layer was dried over anhyd Na_2SO_4, filtered and the solvent was removed under reduced pressure to yield crude product. The crude product was purified by combiflash using hexanes and ethyl acetate mixture to get the desired acrylimide derivative **113h**.

TLC condition - R_f = 0.4 (50% ethyl acetate:hexanes), Viscous liquid (Yield = 32%).

^{1}H-NMR (400 MHz, CDCl$_3$, δ ppm, 1.9 : 1.0 rotamer ratio, mixture of rotamer): 1.30 (s, 9H), 1.37 (s), 1.82 (s, 6H), 1.81 (s), 2.99(s, 3H), 3.04 (s), 5.31 (m, 4H) and 5.42 (s).
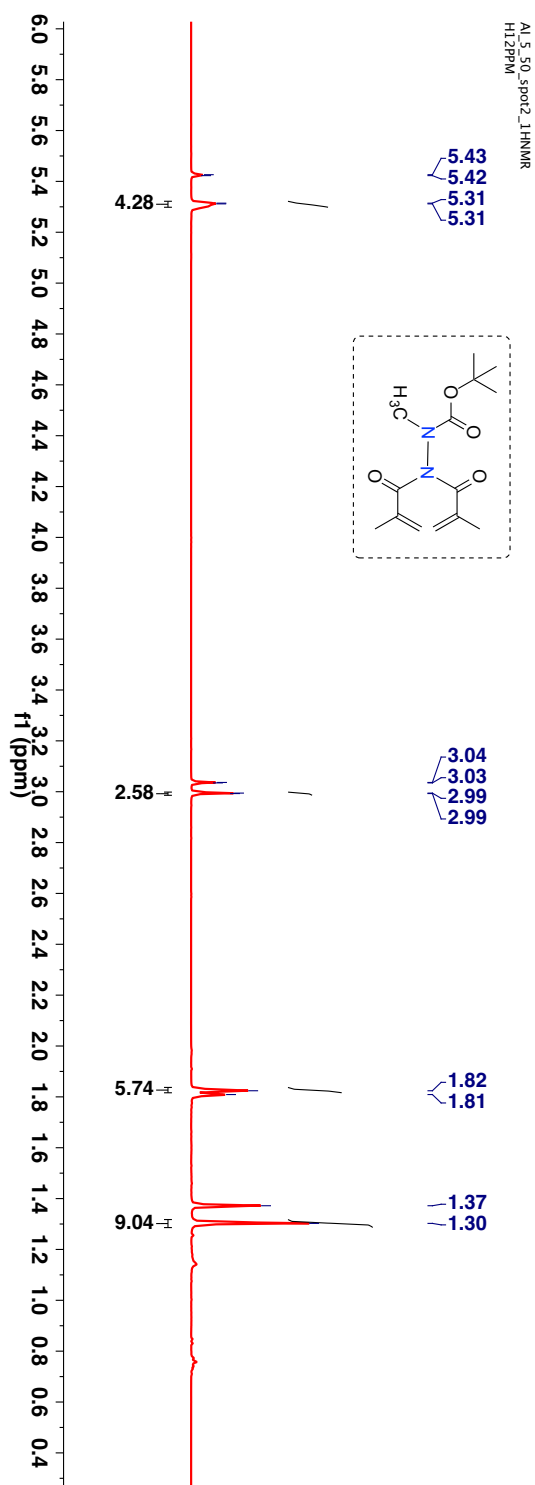
Figure 2.36: ^{1}H-NMR (400 MHz, CDCl$_3$, δ ppm) spectrum of **113h**.

^{13}C-NMR (100 MHz, CDCl$_3$, δ ppm, mixture of rotamer): 14.2, 18.6, 22.8, 28.2, 28.2, 31.7, 36.2, 37.5, 82.3, 82.3, 120.8, 120.9, 141.9, 141.9, 154.6, 154.7, 172.1 and 172.4.
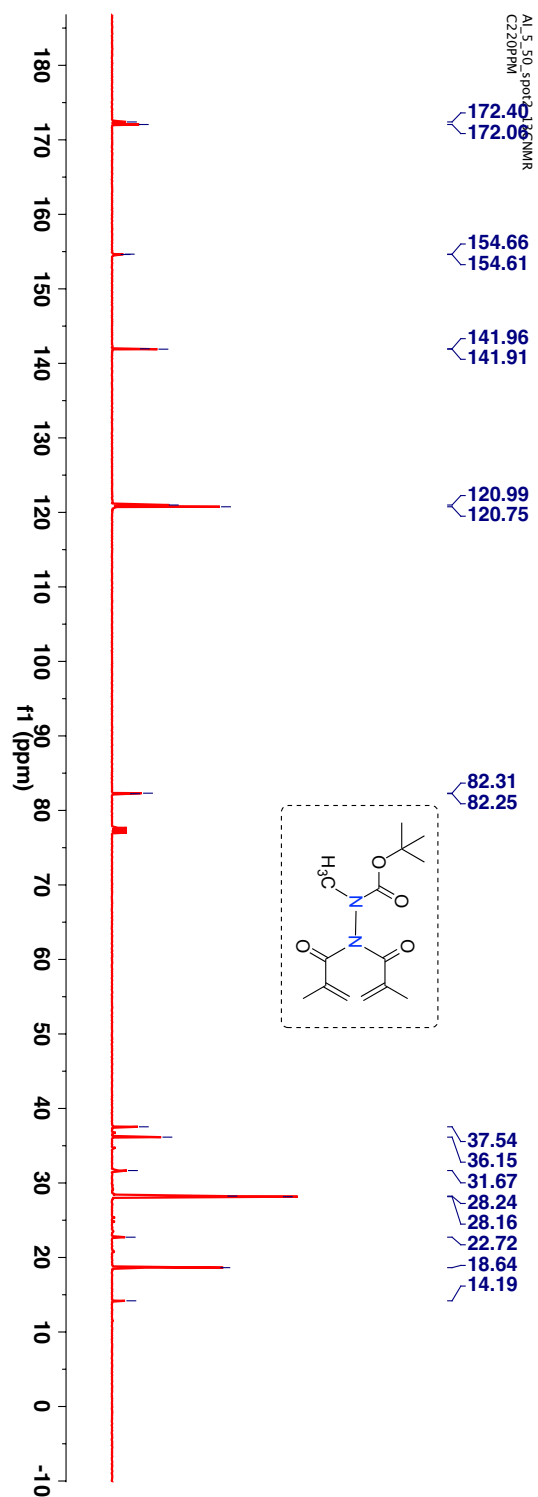
Figure 2.37: ^{13}C-NMR (100 MHz, CDCl$_3$, δ ppm) spectrum of **113h**.

HRMS-ESI (m/z) ([M + Na]$^+$):

Chemical Formula   : C$_{14}$H$_{22}$N$_2$O$_4$

Calculated   : 305.1477

Observed   : 305.1493

|Δm| : 5.2 ppm
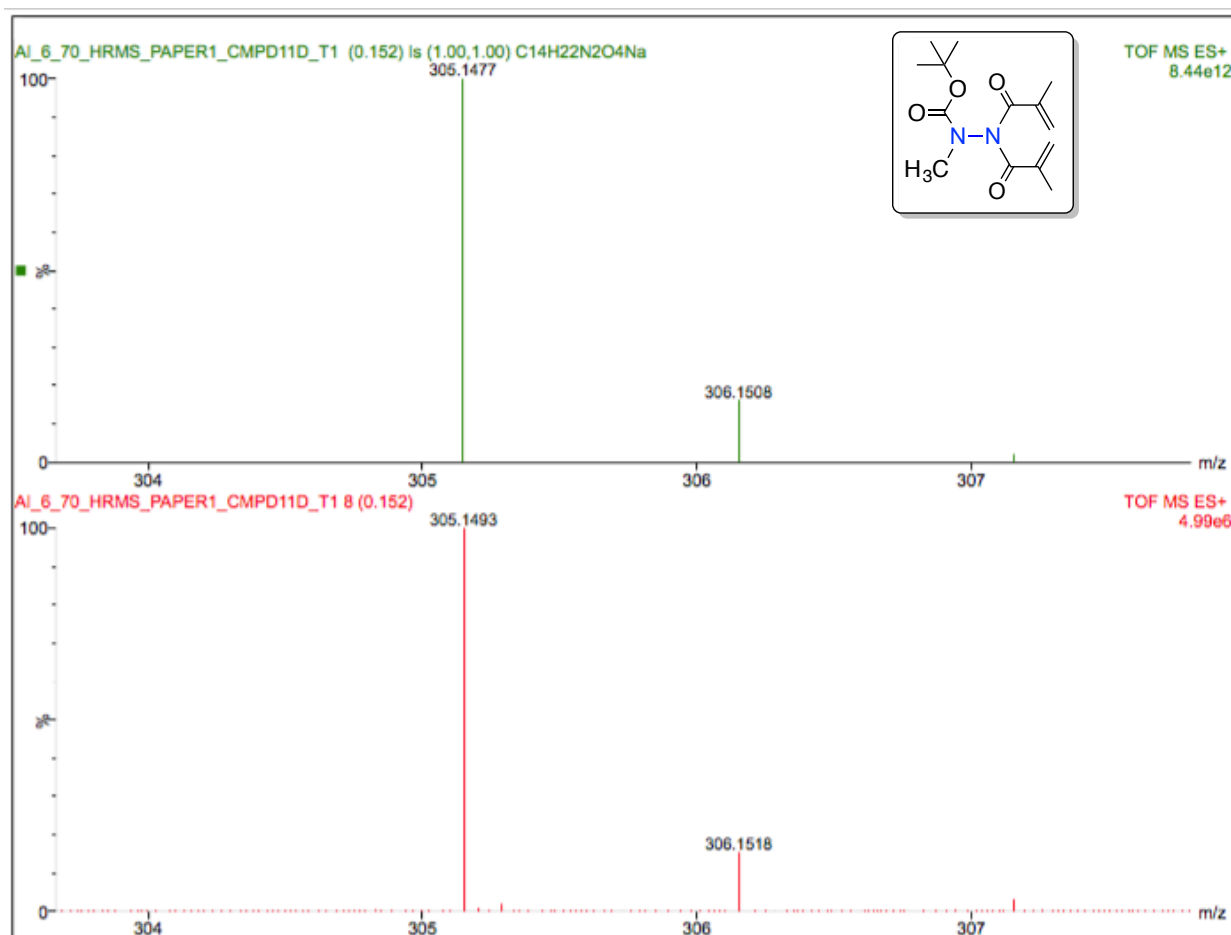
Figure 2.38: HRMS spectra of **113h**.

2.15. Synthesis of amide based hydrazide derivative 113g
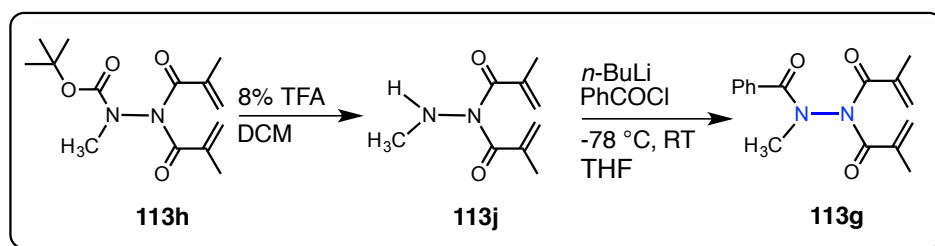
STEP1
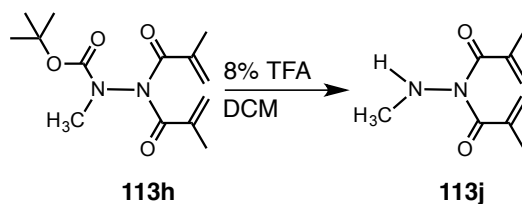
Scheme 2.32: Synthesis of amide based hydrazide derivative **113j**.

To a solution of imide derivative **113h** (1 equiv) in anhydrous CH_2Cl_2 was added small portions of trifluoroacetic acid (8% TFA in CH_2Cl_2) (25 equiv) at 0 °C. The mixture was stirred overnight. More TFA was added until complete consumption of starting material was observed. The solution was concentrated under vacuum. The crude was dissolved in ethyl acetate and the organic layer was sequentially washed with DI water (2 × 10 mL), saturated $NaHCO_3$ (2 × 10 mL) and finally with brine. The organic layer was dried over anhyd Na_2SO_4, filtered and the solvent was removed under reduced pressure to yield crude product. After concentrating the organic layer, the crude product was purified by combiflash using hexanes and ethyl acetate mixture to get the desired compound.

TLC condition -R_f = 0.4 (20% ethyl acetate:hexanes), Viscous clear liquid (Yield = 38%)

^{1}H-NMR (400 MHz, CDCl$_3$, δ ppm): 1.91 (s, 6H), 2.60 (s, 3H) and 5.28-5.31 (m, 4H).
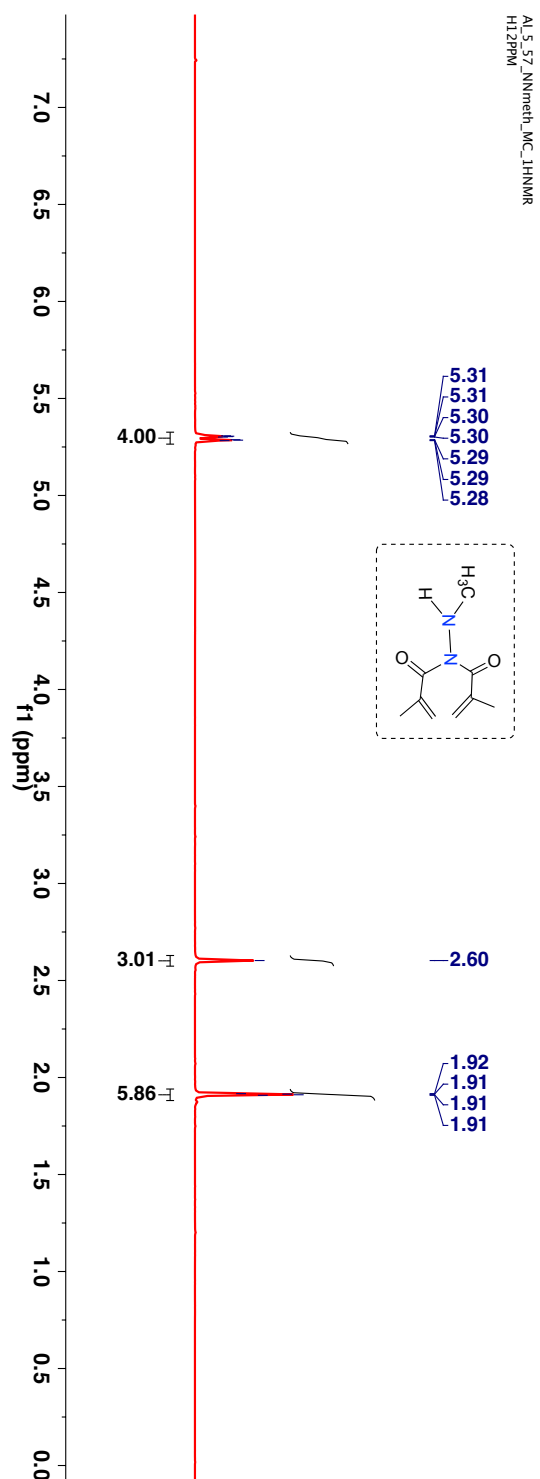
Figure 2.39: ^{1}H-NMR (400 MHz, CDCl$_3$, δ ppm) spectrum of **113j**.

^{13}C-NMR (100 MHz, CDCl$_3$, δ ppm): 19.0, 37.9, 120.3, 142.8 and 174.2.
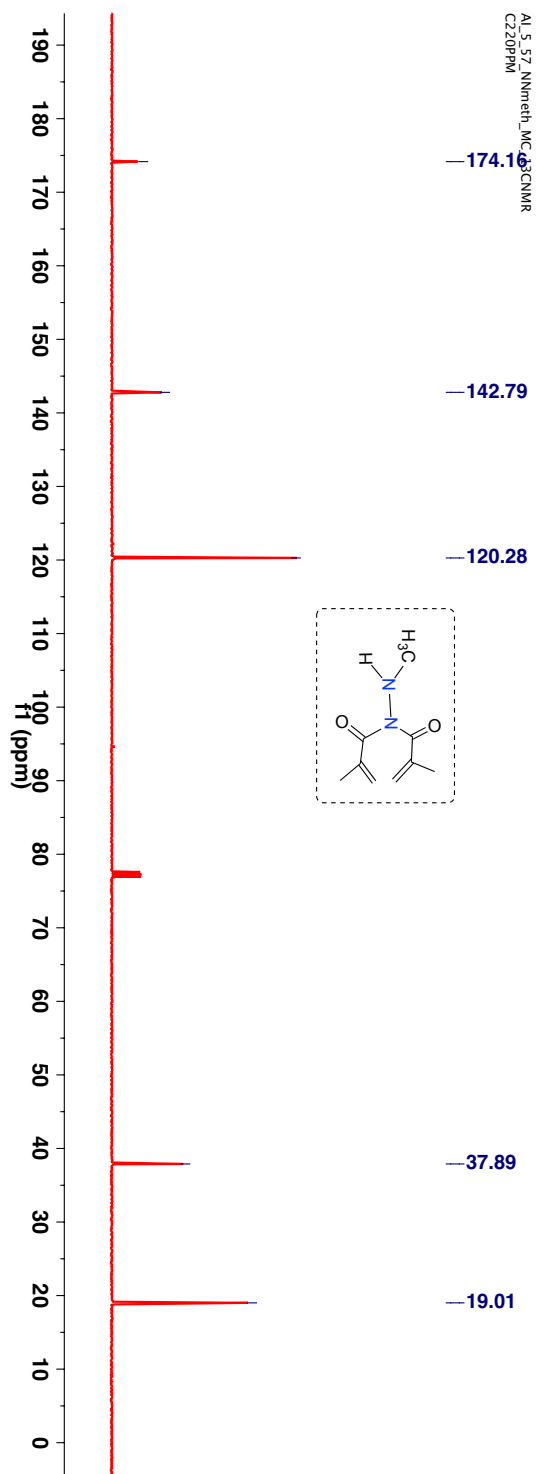
Figure 2.40: ^{13}C-NMR (100 MHz, CDCl$_3$, δ ppm) spectrum of **113j**.

HRMS-ESI (m/z) ([M + Na]$^+$):

Chemical Formula   : C$_9$H$_{14}$N$_2$O$_2$

Calculated   : 205.0953

Observed   : 205.0963

|Δm| : 4.9 ppm
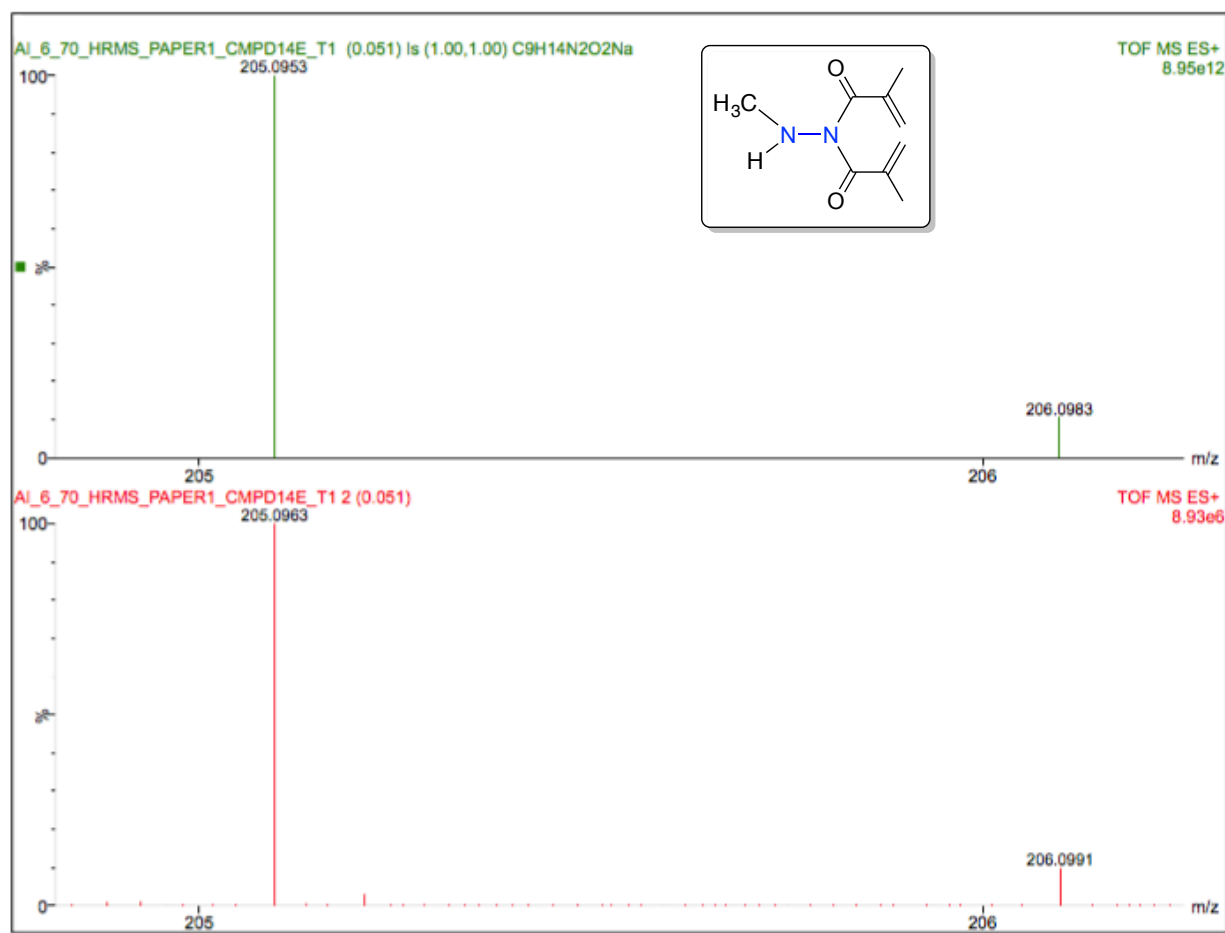
Figure 2.41: HRMS spectra of **113j**.

STEP 2
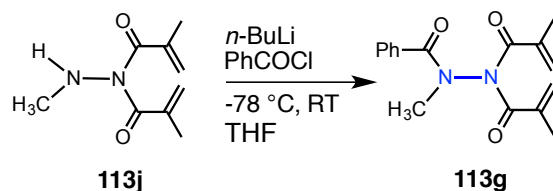
Scheme 2.33: Synthesis of amide based hydrazide derivative **113g**.

The hydrazide derivative **113j** (1 equiv) was taken in a round bottom flask under N_2 protection and dissolved in freshly distilled THF. The solution was cooled to -78 °C. To this solution *n*-BuLi (1 equiv) was added dropwise over a period of 10 minutes. This was followed by addition of freshly distilled benzoyl chloride (1.1 equiv). The solution was stirred at -78 °C for 3 h after which TLC showed complete consumption of starting material. The reaction was quenched with 5 mL of H_2O, stirred and the layers were separated. The organic layer was sequentially washed with DI water (2 × 10 mL), saturated $NaHCO_3$ (2 × 10 mL) and finally with brine. The organic layer was dried over anhyd Na_2SO_4, filtered and the solvent was removed under reduced pressure to yield crude product. After concentrating the organic layer, the crude product was purified by combiflash using hexanes and ethyl acetate and ethyl acetate as eluting solvents.

TLC condition - R_f = 0.3 (20% ethyl acetate:hexanes), Clear oil (Yield = 20%).

^{1}H-NMR (400 MHz, CDCl$_3$, δ ppm, mixture of rotamers): 1.92 (s), 1.96 (s), 3.32 (s), 3.33 (s), 5.09 (s), 5.16 (s), 5.23 (s), 5.27 (s), 5.31 (s), 5.38 (s), 5.72 (s), 7.42-7.54 (m) and 7.69-7.71 (m).
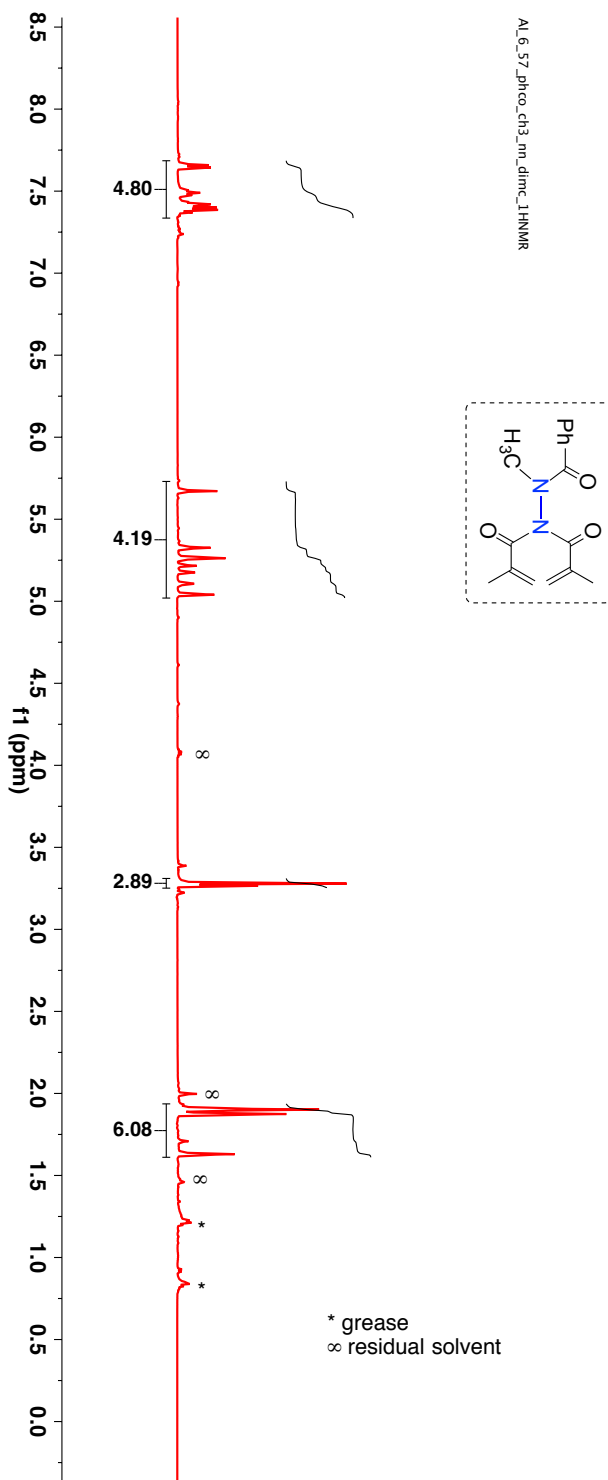
Figure 2.42: ^{1}H-NMR (400 MHz, CDCl$_3$, δ ppm) spectrum of **113g**.

^{13}C-NMR (100 MHz, CDCl$_3$, δ ppm, mixture of rotamers): 18.6, 18.7, 19.7, 20.2, 35.4, 39.7, 116.4, 118.3, 122.3, 124.1, 128.4, 128.6, 128.8, 129.3, 132.7, 133.0, 134.8, 139.0, 139.7, 141.1, 142.0, 171.1, 171.2 and 171.6.
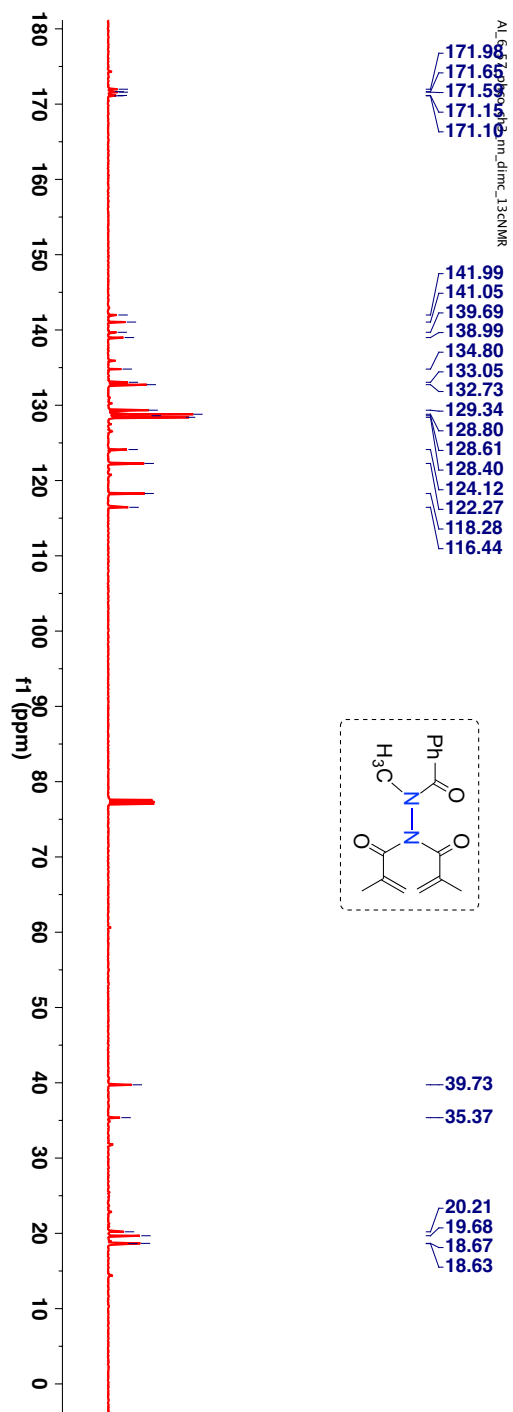
Figure 2.43: ^{13}C-NMR (100 MHz, CDCl$_3$, δ ppm) spectrum of **113g**.

HRMS-ESI (m/z) ([M + Na]$^+$):

Chemical Formula   : C$_{16}$H$_{18}$N$_2$O$_3$

Calculated   : 309.1215

Observed   : 309.1221

|Δm| : 1.9 ppm
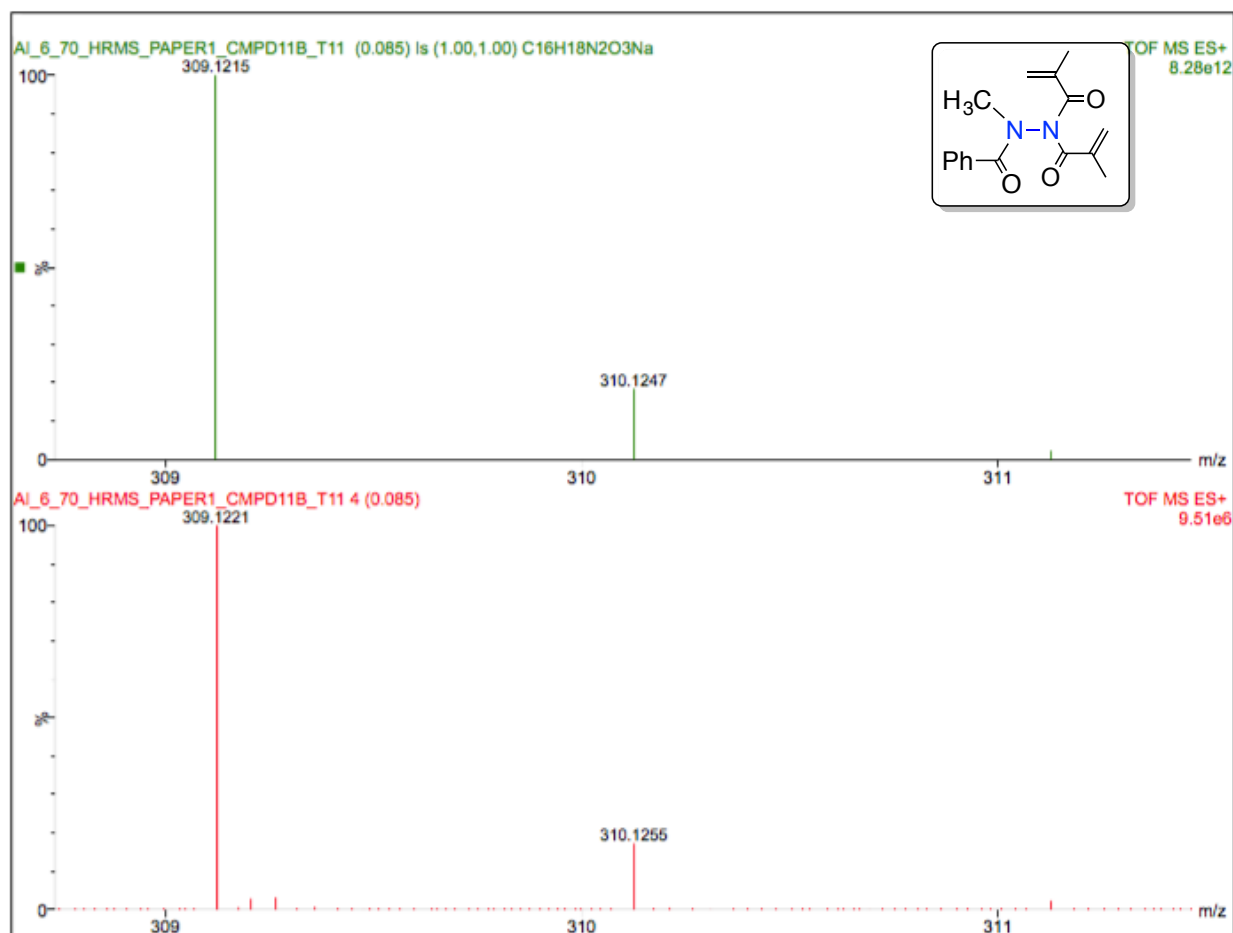
Figure 2.44: HRMS spectra of **113g**.

2.16. Synthesis of tertiary amine based hydrazide derivative 113i
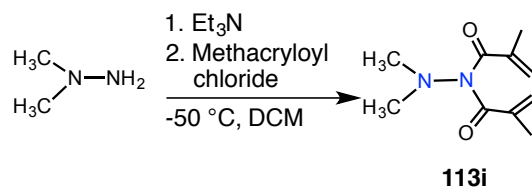
Scheme 2.34: Synthesis of acrylimide derivative **113i**.

To *N,N*-dimethylhydrazine (1 equiv) in a round bottom flask under N_2 protection, anhydrous CH_2Cl_2 was added and the solution was cooled to -50 °C. To this solution Et_3N (5 equiv) was added. To this solution was added methacryloyl chloride (2.0 equiv). The solution was stirred at -50 °C for 2 h and then at rt for 20 h. The reaction was quenched with 5 mL of H_2O, stirred and the layers were separated. The organic layer was sequentially washed with DI water (2 × 10 mL), saturated $NaHCO_3$ (2 × 10 mL) and finally with brine. The organic layer was dried over anhyd Na_2SO_4, filtered and the solvent was removed under reduced pressure to yield crude product. After concentrating the organic layer, the crude product was purified by combiflash using hexanes and ethyl acetate and ethyl acetate as eluting solvents.

TLC condition - R_f = 0.5 (20% ethyl acetate:hexanes), Viscous clear liquid (Yield = 15%).

^{1}H-NMR (400 MHz, CDCl$_3$, δ ppm): 1.87 (s, 6H), 2.78 (s, 6H) and 5.24-5.27 (m, 4H).
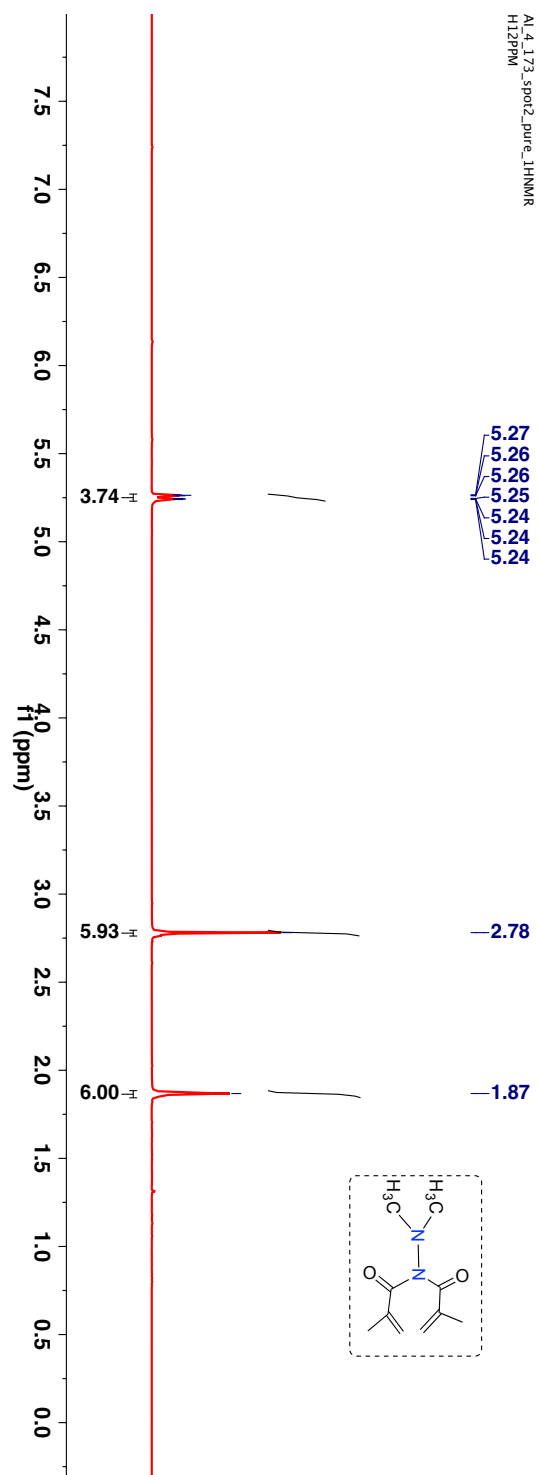
Figure 2.45: ^{1}H-NMR (400 MHz, CDCl$_3$, δ ppm) spectrum of **113i**.

¹³C-NMR (100 MHz, CDCl₃, δ ppm): 18.8, 44.1, 120.2 143.4 and 174.4.
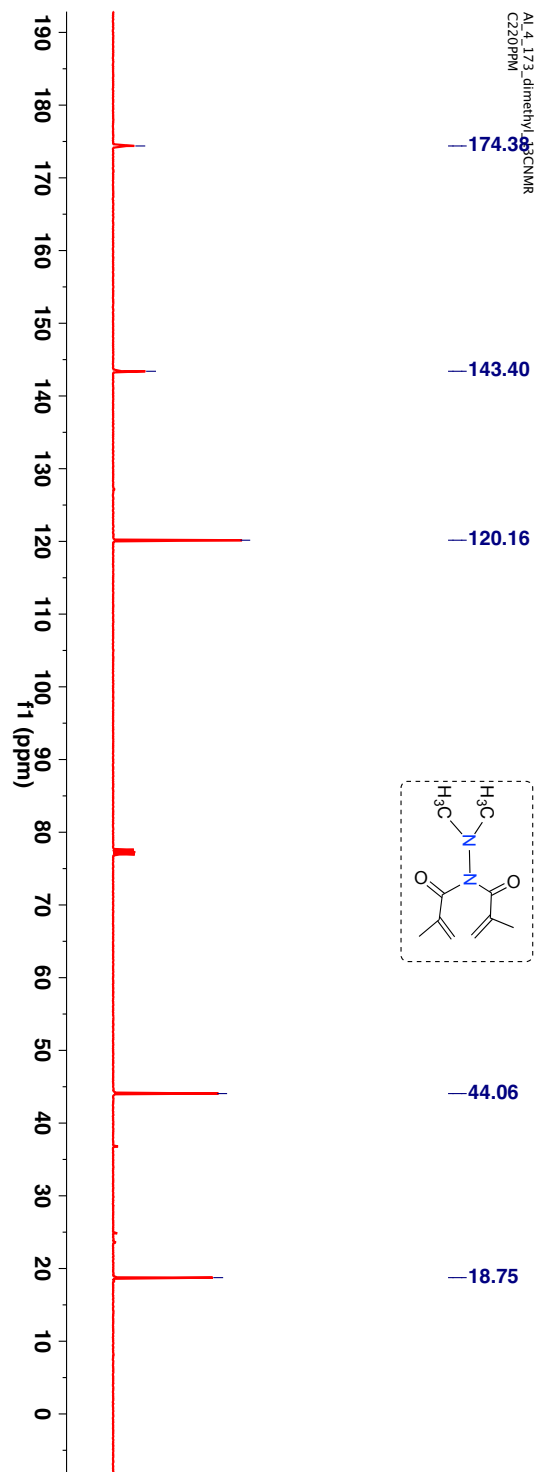
Figure 2.46: ¹³C-NMR (100 MHz, CDCl₃, δ ppm) spectrum of **113i**.

HRMS-ESI (m/z) ([M + Na]$^+$):

Chemical Formula   : C$_{10}$H$_{16}$N$_2$O$_2$

Calculated   : 219.1109

Observed   : 219.1118

|Δm| : 4.1 ppm
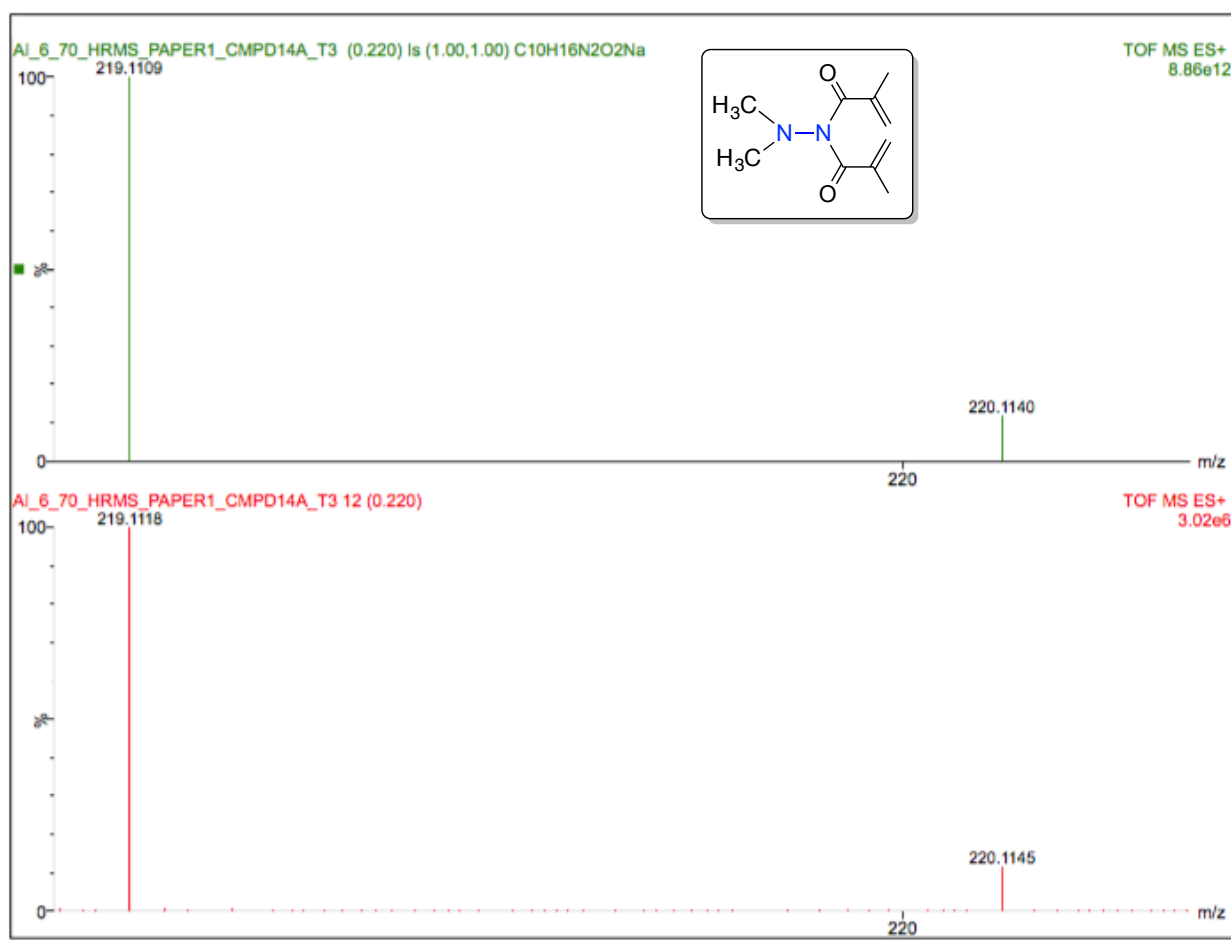
Figure 2.47: HRMS spectra of **113i**.

2.17. Synthesis of primary amine derivative 113k.
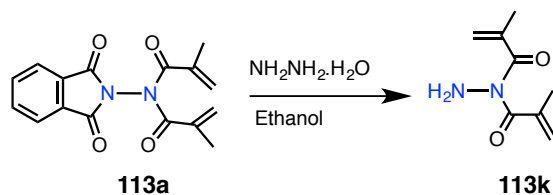
Scheme 2.35: Synthesis of acrylimide derivative **113k**.

Imide derivative **113a** (1 equiv) was dissolved in absolute ethanol. To the reaction mixture hydrazine hydrate (11 equiv) was added and the mixture was refluxed for 45 minutes (monitored by TLC). The solution was filtered through a short celite pad. The crude was diluted with ethyl acetate and was washed with 1M HCl. The aqueous layer was separated and washed with 1N NaOH and the organic layer was washed with brine (2 × 10 mL). The organic layer was dried over anhyd Na_2SO_4, filtered and the solvent was removed under reduced pressure to yield product. The compound was used without further purification. Clear solid (Yield = 16%)

^{1}H-NMR (400 MHz, CDCl$_3$, δ ppm): 1.95 (s, 3H), 3.92 (bs, 2H), 5.34 (s, 1H) and 5.69 (s, 1H).
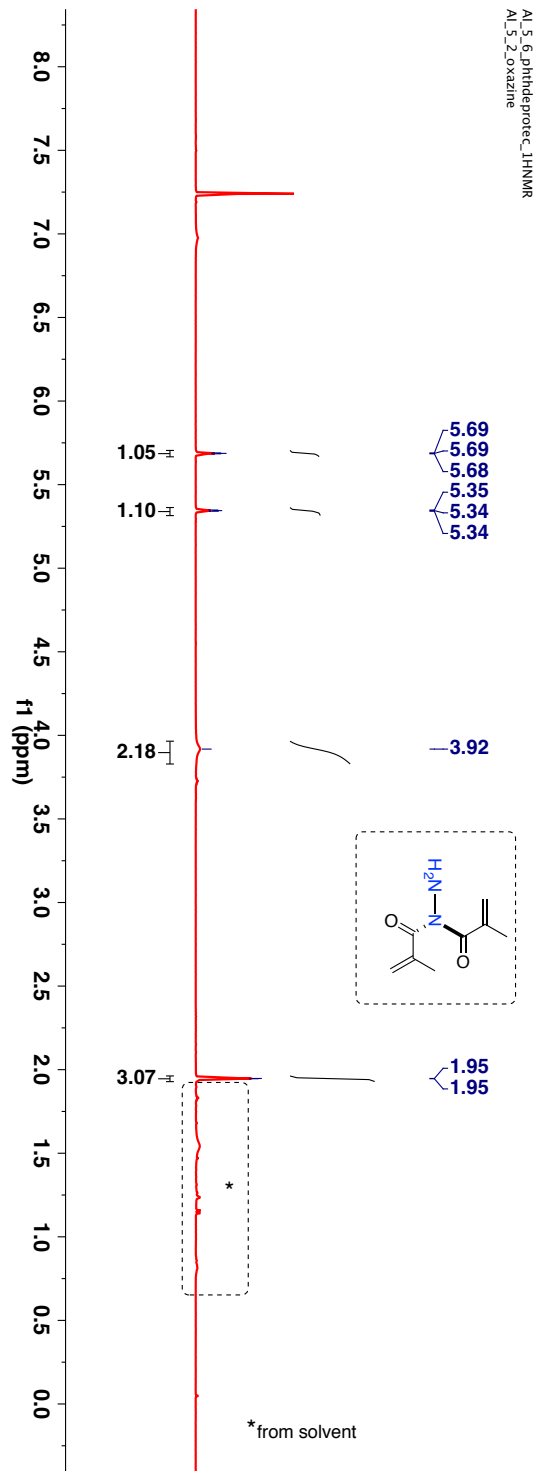
Figure 2.48: ^{1}H-NMR (400 MHz, CDCl$_3$, δ ppm) spectrum of **113k**.

¹³C-NMR (100 MHz, CDCl₃, δ ppm): 18.6, 120.5, 138.3 and 169.6.
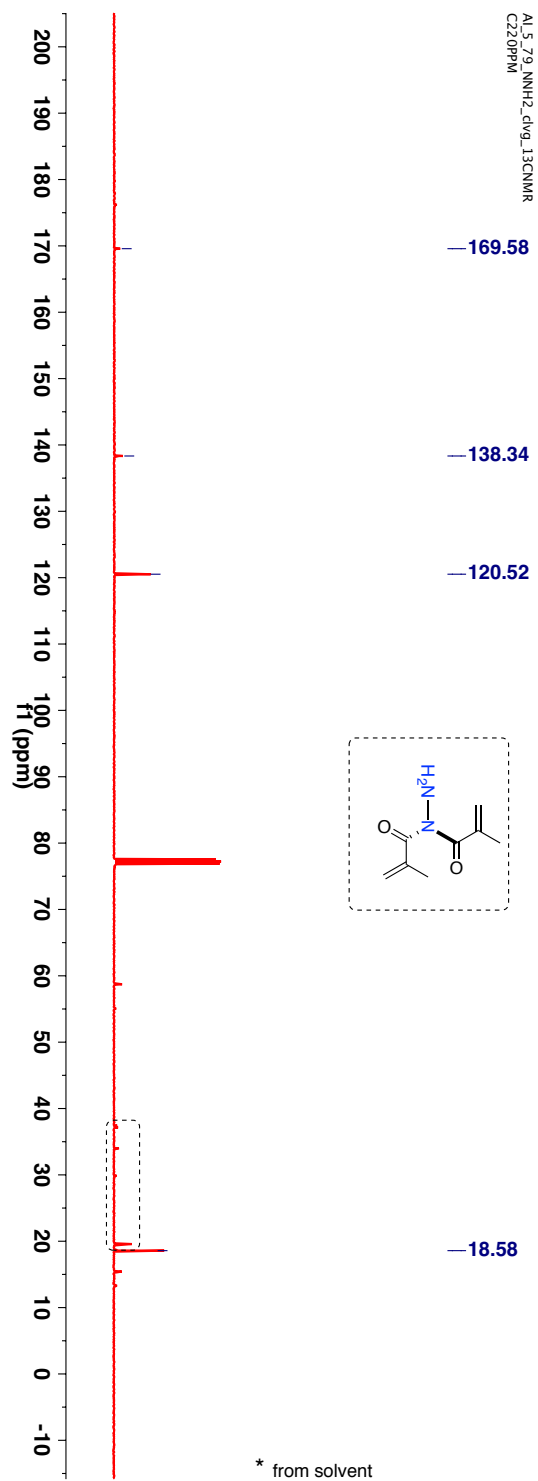
Figure 2.49: ¹³C-NMR (100 MHz, CDCl₃, δ ppm) spectrum of **113k**.

2.18. General procedure followed for irradiation of substrates and characterization of photoproducts

(a)   Procedure for photoreaction:

In a pyrex tube, solution of the desired substrate was dissolved in an appropriate solvent under an inert atmosphere. This was followed by the addition of triplet sensitizer (thioxanthone). The sample was then irradiated at 25 °C in a Rayonet reactor equipped with ~420 nm tubes (16 tubes x 14 Watt). In case of Norrish-Yang cyclization of α-oxoamide derivative the irradiation was performed with Rayonet reactor/CFL lamp (compact fluorescent lamp, 13 W). For the LED photoreaction, a visible light photoreactor was used which was constructed from a commercial purple LED tape (300 LEDs, 4.8 W, 16.4 ft) wound around a beaker.

 (b)   Characterization of photoproduct after photoreaction:

In case of large-scale photoreactions, after irradiation the crude reaction mixture was purified by combiflash using hexanes/ethyl acetate mixtures. The photoproducts were then characterized by NMR spectroscopy and/or single crystal XRD. In certain cases the crude mixture was purified by preparative thin layer chromatography. These substrates showed very weak/negligible fluorescence under UV-light illumination, so by utilizing preparative thin layer chromatography the sensitizer band was removed and remaining band was taken for analyzing with NMR spectroscopy. In some of the cases, the R_f of substrate and the photoproduct did not show appreciable difference during the course of photoreaction. So in order to avoid ambiguity the photoreactions were monitored by ^{1}H-NMR spectroscopy.

2.19. Reaction optimization for [2+2] photoreaction of acrylimide derivative 113a.

113a   **114a**   **117a**
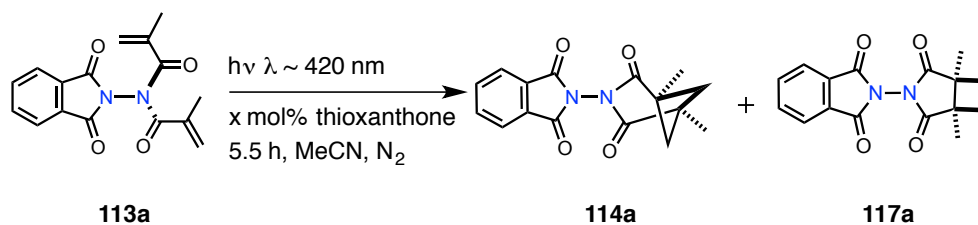
Scheme 2.36: Photoreaction of acrylimide derivative **113a**.

Table 2.10: Sensitizer loading studies for intramolecular [2+2] photoreaction of *N-N* bond based acrylimide derivative **113a**.[a]

Entry	TX (x mol%)	Conversion/%
1	0	0
2	1	8
3	5	39
4	10	100

[a] [**113a**] = 3.35 mM, TX: Thioxanthone

Table 2.11: Solvent screening studies for intramolecular [2+2] photoreaction of *N-N* bond based acrylimide derivative **113a**.[a]

Entry	Solvent	Conversion/%
1	Methanol	100
2	Acetonitrile	100
3	Ethyl acetate	<7
4	Benzene	63
6	Methylcyclohexane	0

[a] [**113a**] = 3.35 mM. The photoreactions were performed with 10 mol% thioxanthone loading.

2.19.1. Effect of sensitizer on [2+2] photoreaction of acrylimide derivative 113a
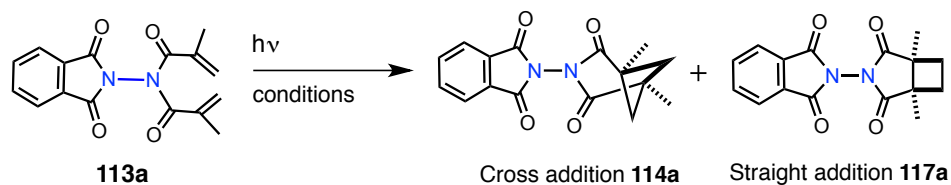
Scheme 2.37: Photoreaction of acrylimide derivative **113a** under different reaction conditions.

Table 2.12: Intramolecular [2+2] photoreaction of *N-N* bond based acrylimide derivative **113a** under different conditions.[a]

Entry	Conditions	Conversion/%[d]	**114a:117a**[d]
1	$\lambda > 290$ nm, Acetone, 3h	100	>99:1
2	$\lambda > 290$ nm, MeCN, 3h	100	95:5
3	$\lambda \sim 350$ nm, 10 mol% benzophenone, MeCN, 5.5h	100	96:4
4	$\lambda \sim 350$ nm, 10 mol% xanthone, MeCN, 8h	100	96:4
5	$\lambda \sim 420$ nm, 10 mol% thioxanthone, MeCN, 8h	100	91:9

[a] Irradiations were performed at room temperature unless otherwise noted. The solvents utilized for irradiation were of HPLC grade with no optical density at irradiation wavelength. [b] [**113a**] = 3.35 mM, [c] Rayonet reactor equipped ~420 nm (16 tubes × 14 W each). [d] % conversion/NMR yield (±5% error) calculated by ^{1}H-NMR spectroscopy using triphenylmethane as internal standard.

TLC condition - R$_f$ = 0.4 (20% ethyl acetate:hexanes), Crystalline solid (Yield = 71%).

^{1}H-NMR (400 MHz, CDCl$_3$, δ ppm): 1.40 (s, 6H), 2.22-2.41 (m, 2H), 2.79-2.81 (m, 2H), 7.77-7.79 (dd, 2H, J_1 5.6Hz, J_2 3.2Hz) and 7.90-7.92 (dd, 2H, J_1 5.6Hz, J_2 3.2Hz).
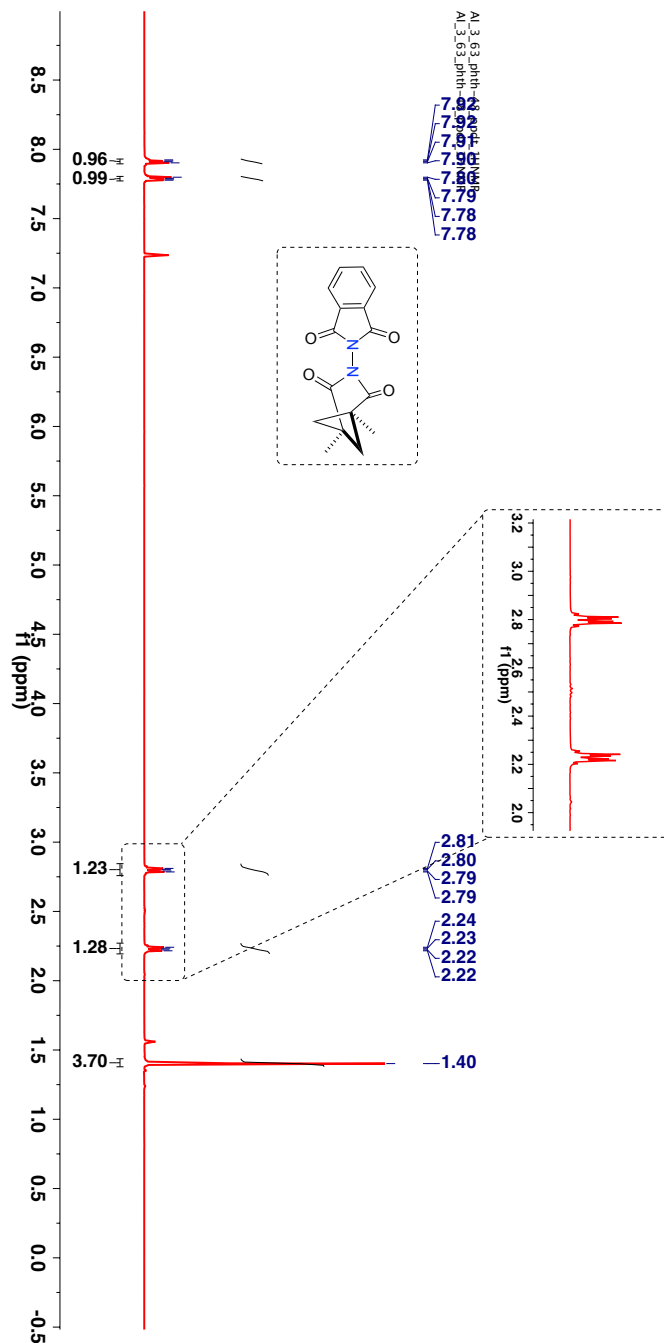
Figure 2.50: ^{1}H-NMR (400 MHz, CDCl$_3$, δ ppm) spectrum of **114a**.

^{13}C-NMR (100 MHz, CDCl$_3$, δ ppm): 19.5, 43.6, 46.0, 124.4, 130.4, 134.9, 163.9 and 174.7.
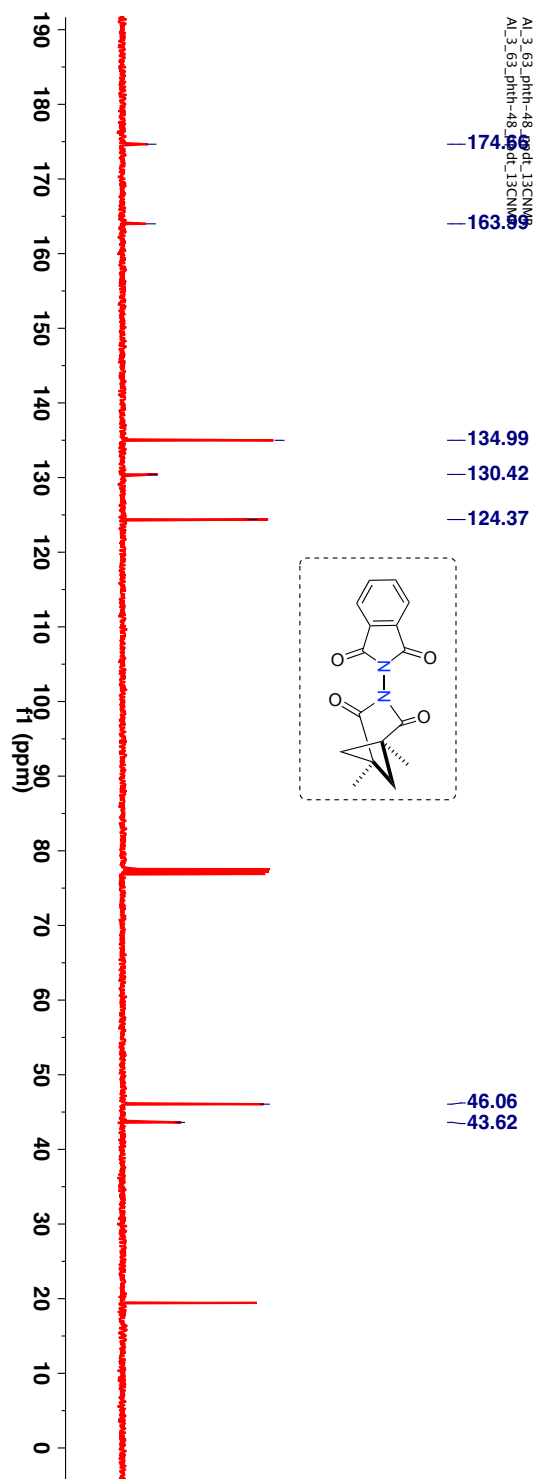
Figure 2.51: ^{13}C-NMR (100 MHz, CDCl$_3$, δ ppm) spectrum of **114a**.

2.19.2. UV-VIS spectra of acrylimide derivative 113a and photoproduct 114a
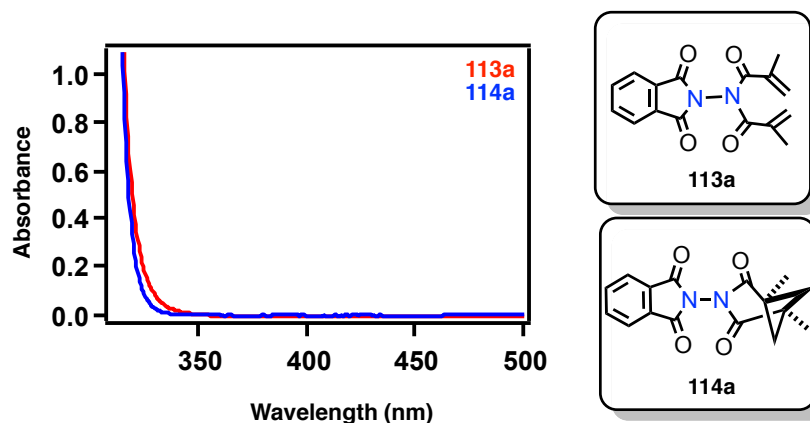
Figure 2.52: UV-Vis spectra of *N-N* bond based acrylimide derivative **113a** (concn = 3.34 mM) and photoproduct **114a** (concn = 3.34 mM) recorded at the reaction concentration in acetonitrile.

HRMS-ESI (m/z) ([M + Na]$^+$):

Chemical Formula   : $C_{16}H_{14}N_2O_4$

Calculated   : 321.0851

Observed   : 321.0869

|Δm| : 5.6 ppm
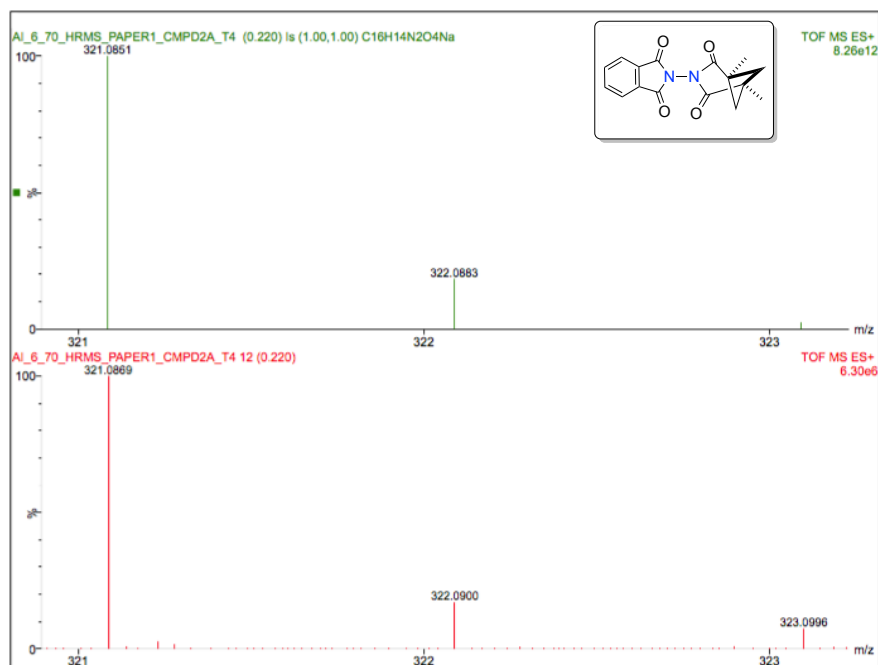
Figure 2.53: HRMS spectra of **113a**.

2.20. Removal of phthalimide ring of acrylimide based photoproduct 114a
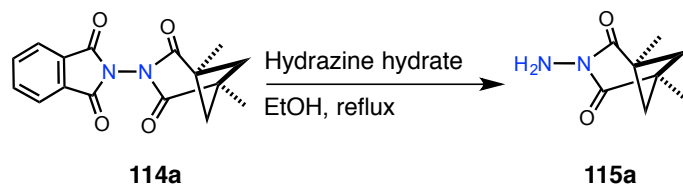
Scheme 2.38: Removal of phthalimide ring in acrylimide based photoproduct **114a**.

Following the modified procedure reported by Michael et al. the photoproduct **114a** (1 equiv) was charged in a vial equipped with a teflon cap.[42] The compound was dissolved in absolute ethanol (5 mL per 100 mg of photoproduct) and hydrazine monohydrate (11.9 equiv) was added. The solution was stirred for 5 min and refluxed for 30 min (until TLC showed complete consumption of starting material). The solution was brought to room temperature and diluted with ethyl acetate. The solution was sonicated for 15 min and then filtered through a short celite plug. The filtrate was concentrated under reduced pressure to obtain the crude product. The crude product was purified using a prep TLC with hexanes and ethyl acetate mixture as eluting solvents to obtain *N*-Amino photoproduct. Crystalline solid, Yield = 81%.

^{1}H-NMR (400 MHz, CDCl$_3$, δ ppm): 1.33 (s, 6H), 2.06-2.09 (m, 2H), 2.42-2.44 (m, 2H) and 4.40 (bs).
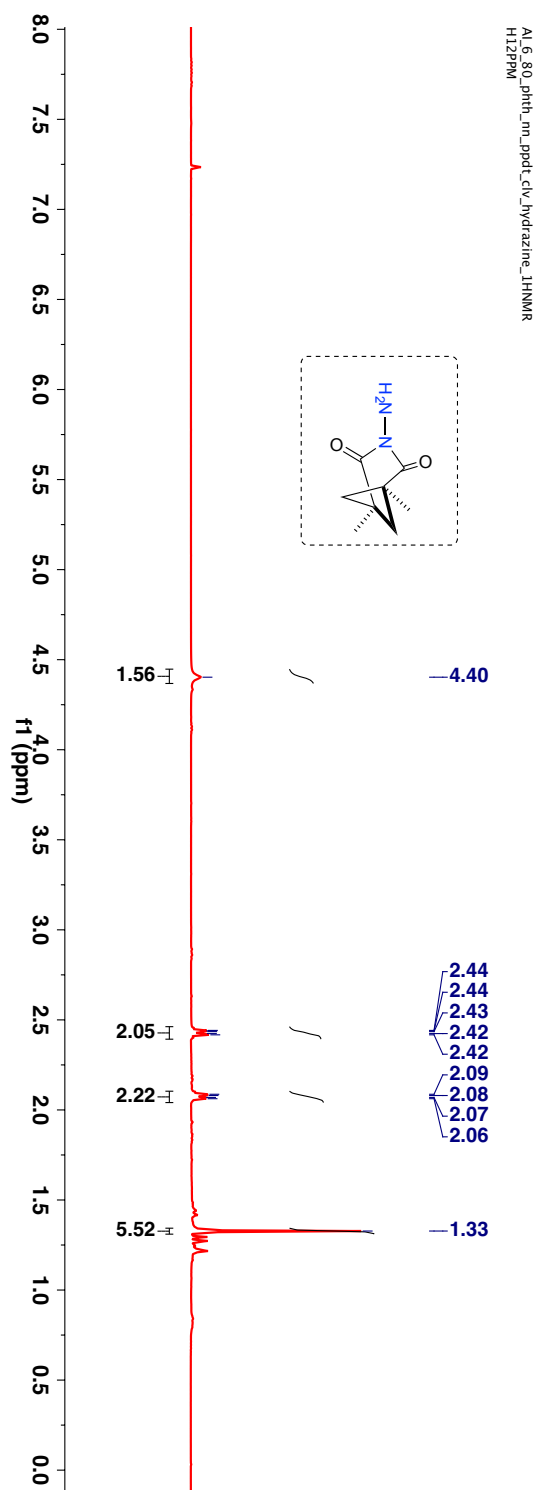
Figure 2.54: ^{1}H-NMR (400 MHz, CDCl$_3$, δ ppm) spectrum of **115a**.

¹³C-NMR (100 MHz, CDCl₃, δ ppm): 19.6, 43.2, 47.2 and 176.4.
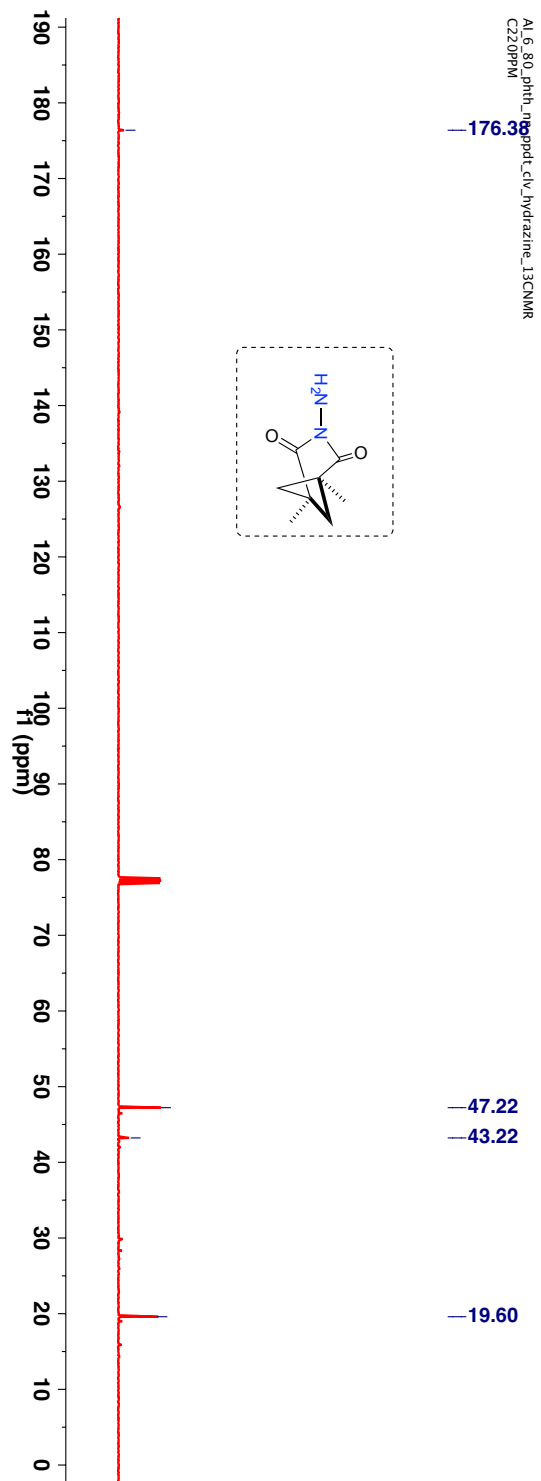
Figure 2.55: ¹³C-NMR (100 MHz, CDCl₃, δ ppm) spectrum of **115a**.

HRMS-ESI (m/z) ([M + H]$^+$):

Chemical Formula   : C$_8$H$_{12}$N$_2$O$_2$

Calculated   : 169.0977

Observed   : 169.0963

|Δm| : 2.0 ppm
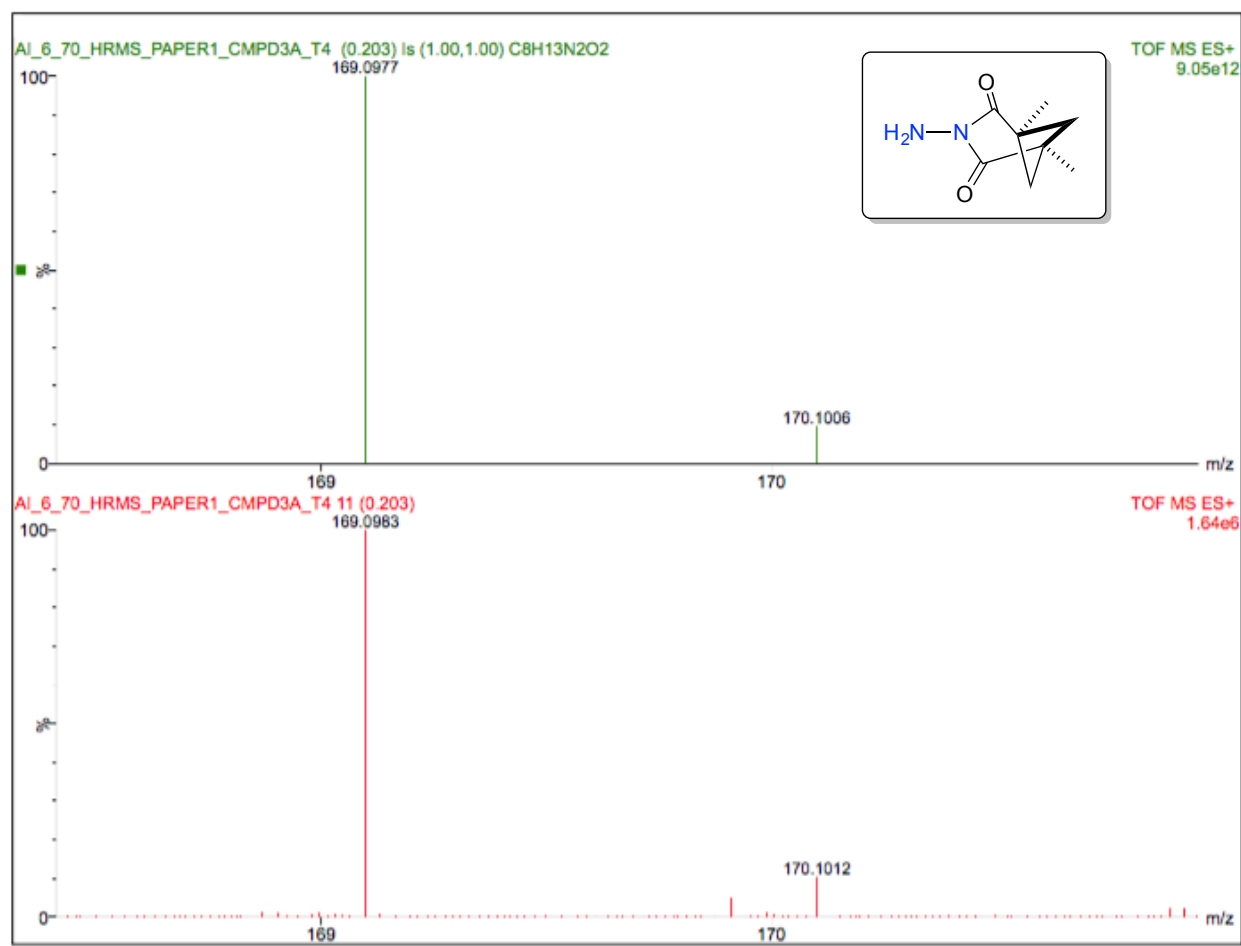
Figure 2.56: HRMS spectra of **115a**.

2.21. Reaction optimization for Paternò-Büchi reaction of α-oxoamide derivative 113b

113b   **114b**
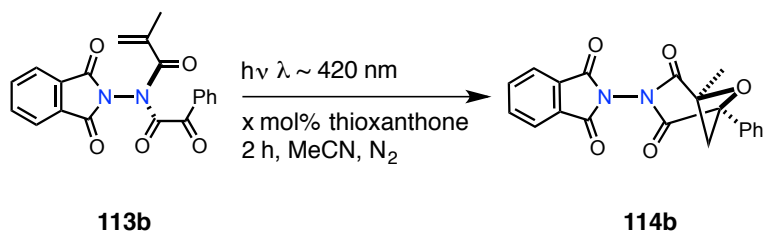
Scheme 2.39: Photoreaction of α-oxoamide derivative **113b**.

Table 2.13: Sensitizer loading studies for Paternò-Büchi reaction of *N-N* bond based α-oxoamide derivative **113b**.[a]

Entry	TX (x mol%)	Conversion/%
1	0	19
2	1	26
3	5	100
4	10	100

[a] [**113b**] = 3.33 mM, TX : Thioxanthone

Table 2.14: Solvent screening studies for Paternò-Büchi reaction of *N-N* bond based α-oxoamide derivative **113b**.[a]

Entry	Solvent	Conversion/%
1	Methanol	Decomposition
2	Acetonitrile	100
3	Ethyl acetate	78
4	Benzene	100
6	Methylcyclohexane	71

[a] [**113b**] = 3.33 mM. The photoreactions were performed with 10 mol% thioxanthone loading.

Table 2.15: Effect of reaction atmosphere for Paternò-Büchi reaction of *N-N* bond based α-oxoamide derivative **113b**.[a]

Entry	Conditions	Conversion/% [d]
1	λ ~ 420 nm, MeCN, N$_2$, 2h	19
2	λ ~ 420 nm, MeCN, O$_2$, 2h	23

[a] [**113b**] = 3.33 mM.

TLC condition - R$_f$ = 0.5 (50% ethyl acetate:hexanes), Pale yellow solid (Yield = 88%).

^{1}H-NMR (400 MHz, CDCl$_3$, δ ppm): 1.74 (s, 3H), 3.43-3.52 (ABq, 2H), 7.36-7.44 (m, 5H), 7.78-7.80 (m, 2H), and 7.90-7.94 (m, 2H).
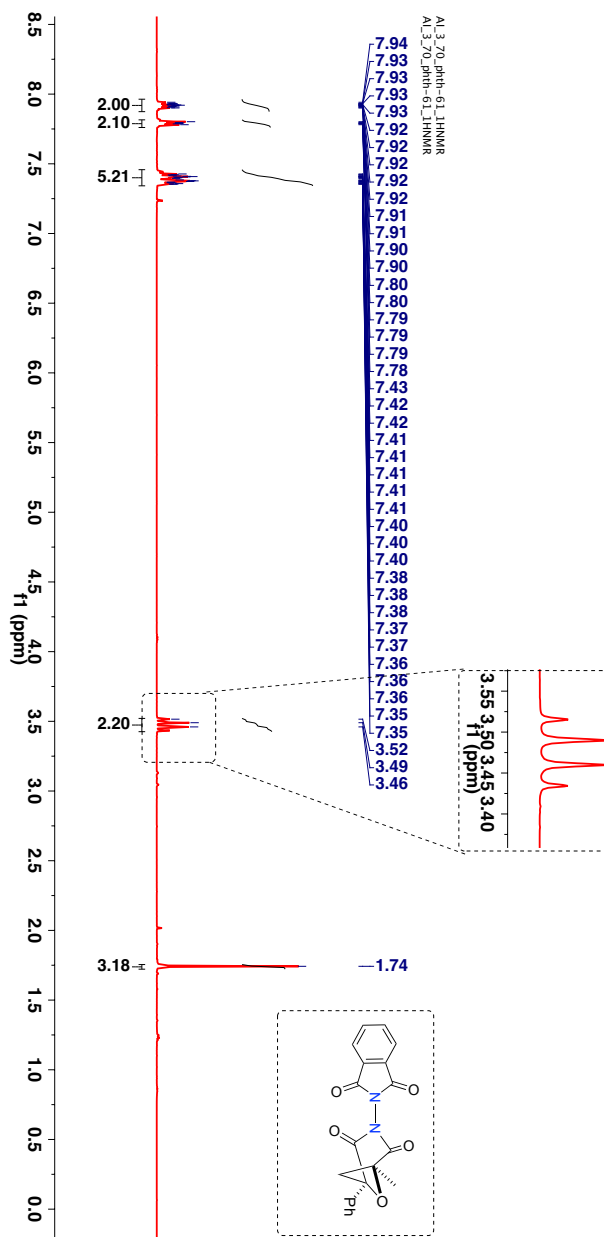
Figure 2.57: ^{1}H-NMR (400 MHz, CDCl$_3$, δ ppm) spectrum of **114b**.

^{13}C-NMR (100 MHz, CDCl$_3$, δ ppm): 19.9, 48.7, 83.0, 84.8, 124.5, 124.7, 125.5, 129.5, 130.1, 135.2, 135.3, 163.3, 163.9, 169.3 and 170.3.
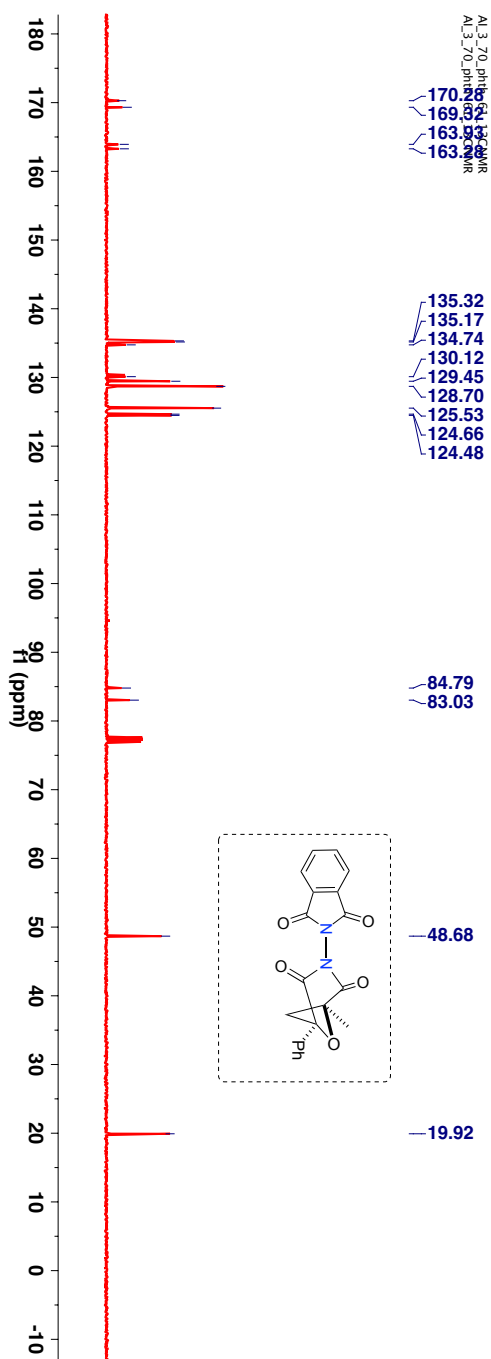
Figure 2.58: ^{13}C-NMR (100 MHz, CDCl$_3$, δ ppm) spectrum of **114b**.

2.21.1. UV-VIS spectra of α−oxoamide derivative 113b and photoproduct 114b
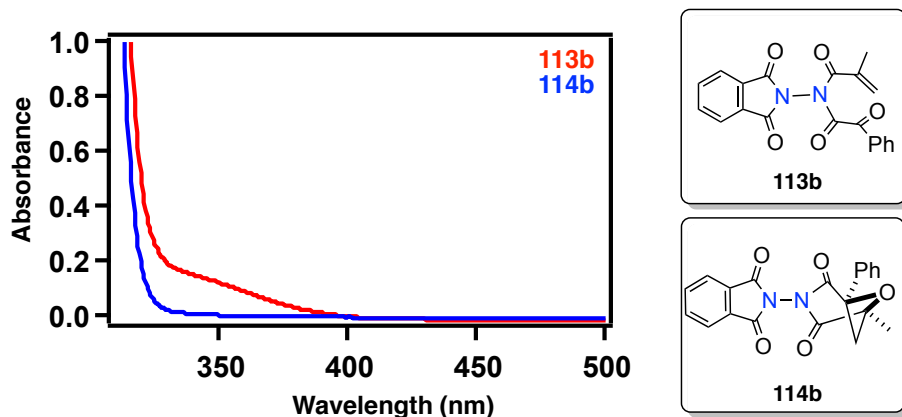
Figure 2.59: UV-Vis spectra of *N-N* bond based α−oxoamide derivative **113b** (concn = 1.32 mM) and photoproduct **114b** (concn = 1.32 mM) recorded in acetonitrile.

HRMS-ESI (m/z) ([M + Na]$^+$):

Chemical Formula	: C$_{20}$H$_{14}$N$_2$O$_5$
Calculated	: 385.0800
Observed	: 385.0820
|Δm|	: 5.2 ppm
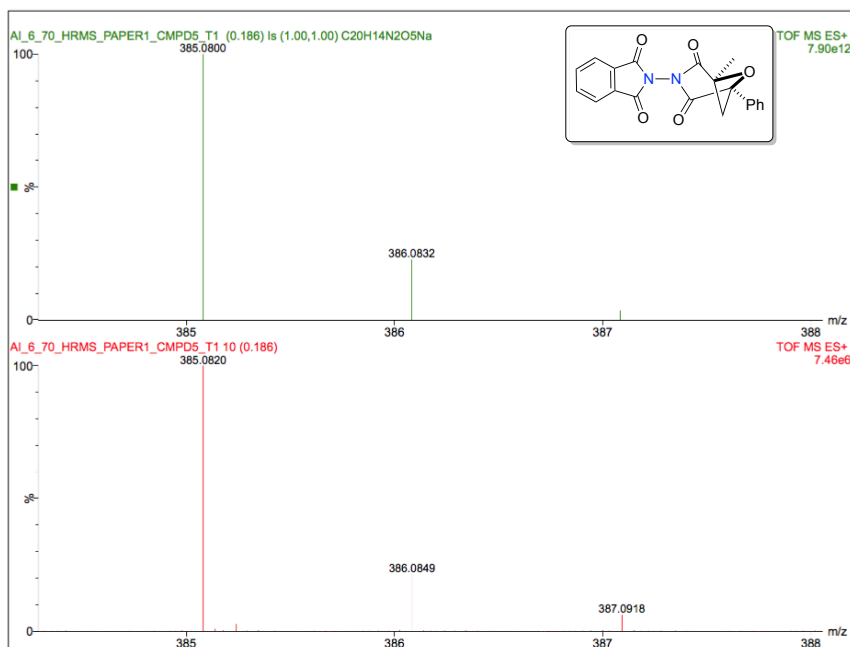
Figure 2.60: HRMS spectra of **114b**.

2.22. Reaction optimization for 6π photocyclization of acrylanilide derivative 113d
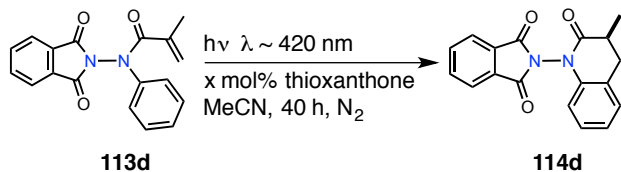
Scheme 2.40: 6π Photocyclization of acrylanilide derivative **113d**.

Table 2.16: Sensitizer loading studies for 6π photocyclization of acrylanilide derivative of *N-N* bond based acrylanilide derivative **113d**.[a]

Entry	TX (x mol%)	Conversion/%
1	0	7
2	1	88
3	5	46
4	10	90

[a] [**113d**] = 3.26 mM, TX: thioxanthone

Table 2.17: Solvent screening studies for 6π photocyclization of acrylanilide derivative of *N-N* bond based acrylanilide derivative **113d**.[a]

Entry	Solvent	Conversion/%
1	Methanol	91
2	Acetonitrile	90
3	Ethyl acetate	100
4	Benzene	60
6	Methylcyclohexane	71

[a] [**113d**] = 3.26 mM.

TLC condition - R$_f$ = 0.4 (50% ethyl acetate:hexanes), Crystalline solid (Yield = 62%).

^{1}H-NMR (400 MHz, CDCl$_3$, δ ppm): 1.34 (d, 3H), 2.94-3.12 (m, 3H), 6.67 (d, 1H, J 8Hz), 7.02-7.06 (m, 1H), 7.13-7.17 (m, 1H), 7.21 (d, 1H, J 8Hz), 7.79-7.82 (m, 2H) and 7.91-7.96 (m, 2H).
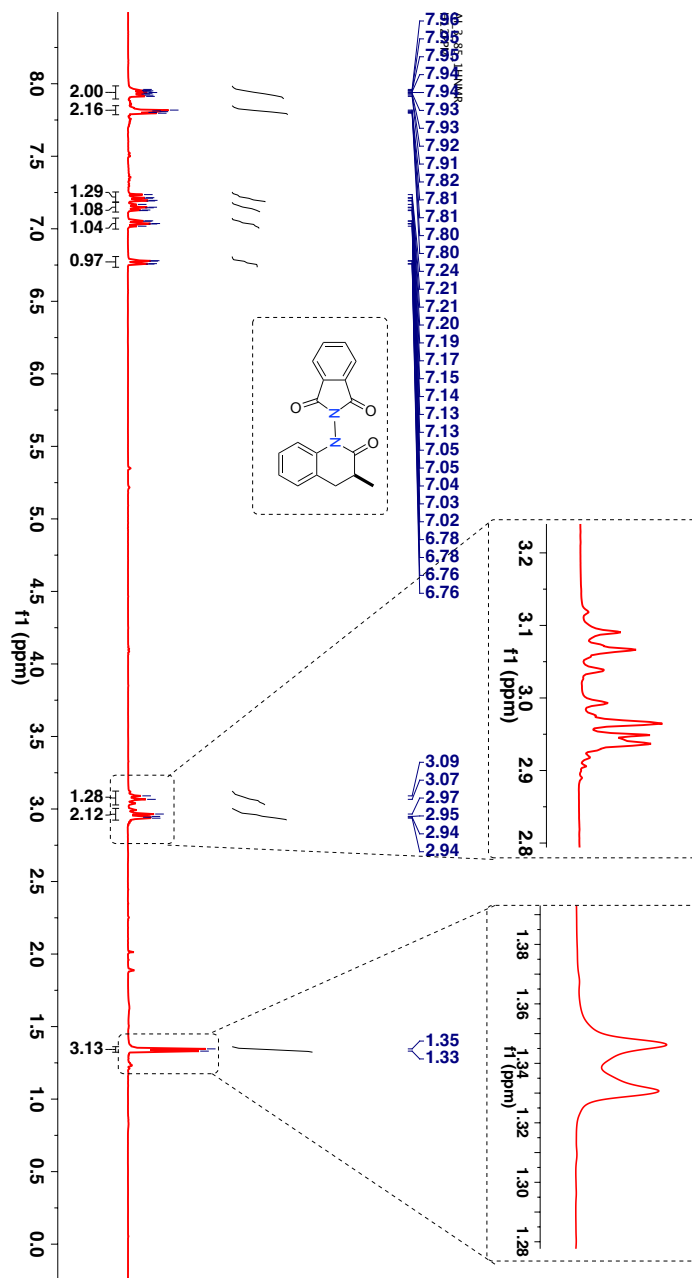
Figure 2.61: ^{1}H-NMR (400 MHz, CDCl$_3$, δ ppm) spectrum of **114d**.

^{13}C-NMR (100 MHz, CDCl$_3$, δ ppm): 15.5, 33.2, 35.8, 113.3, 124.4, 124.4, 124.4, 124.6, 127.9, 128.4, 130.3, 130.4, 135.1, 135.1, 139.0, 164.7, 165.2 and 170.4.
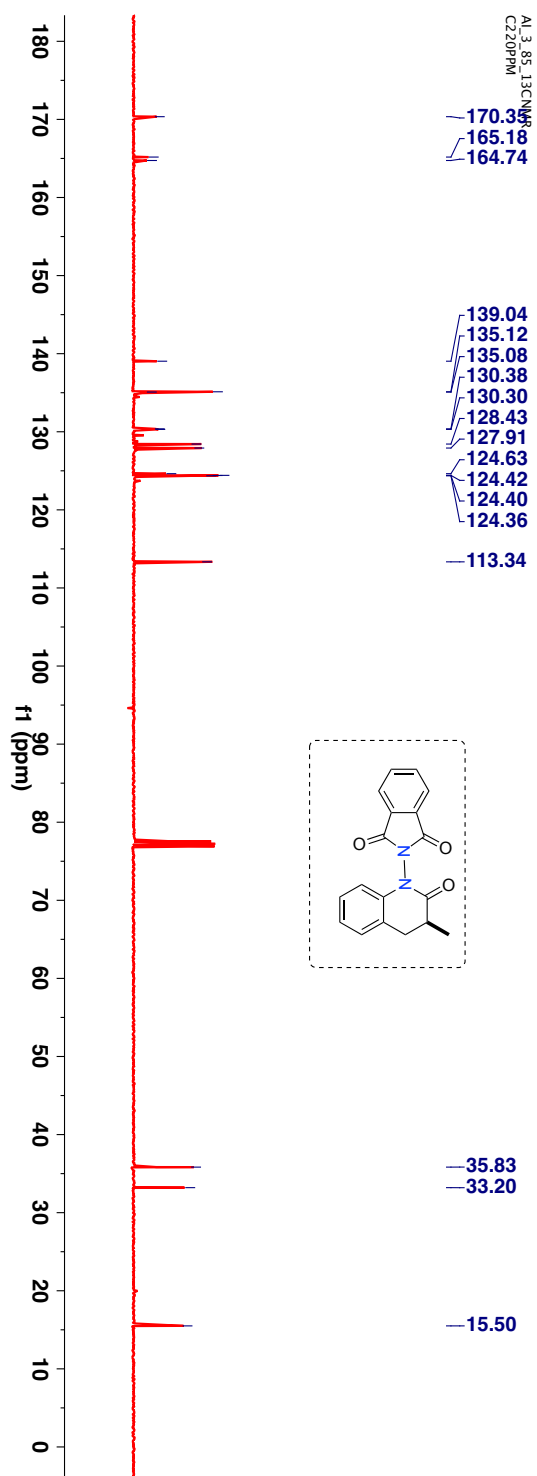
Figure 2.62: ^{13}C-NMR (100 MHz, CDCl$_3$, δ ppm) spectrum of **114d**.

2.22.1. UV-VIS spectra of acrylanilide derivative 113d and photoproduct 114d
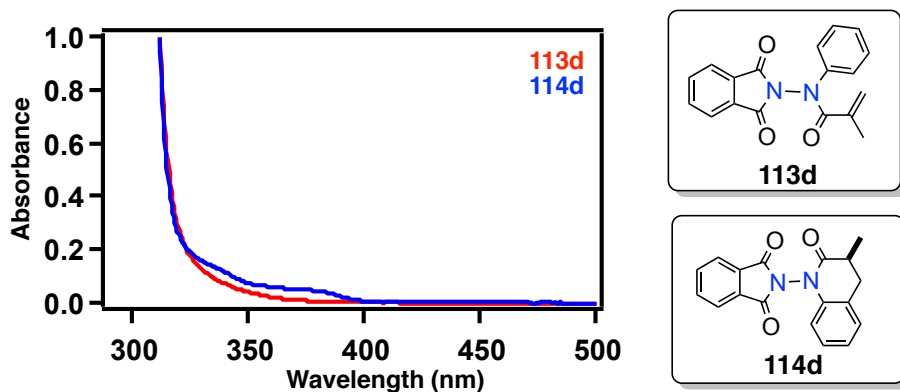
Figure 2.63: UV-Vis spectra of *N-N* bond based acrylanilide derivative **113d** (concn = 1.24 mM) and photoproduct **114d** (concn = 1.24 mM) recorded in acetonitrile.

HRMS-ESI (m/z) ([M + Na]$^+$):

Chemical Formula	: C$_{18}$H$_{14}$N$_2$O$_3$
Calculated	: 329.0902
Observed	: 329.0911
|Δm|	: 2.7 ppm
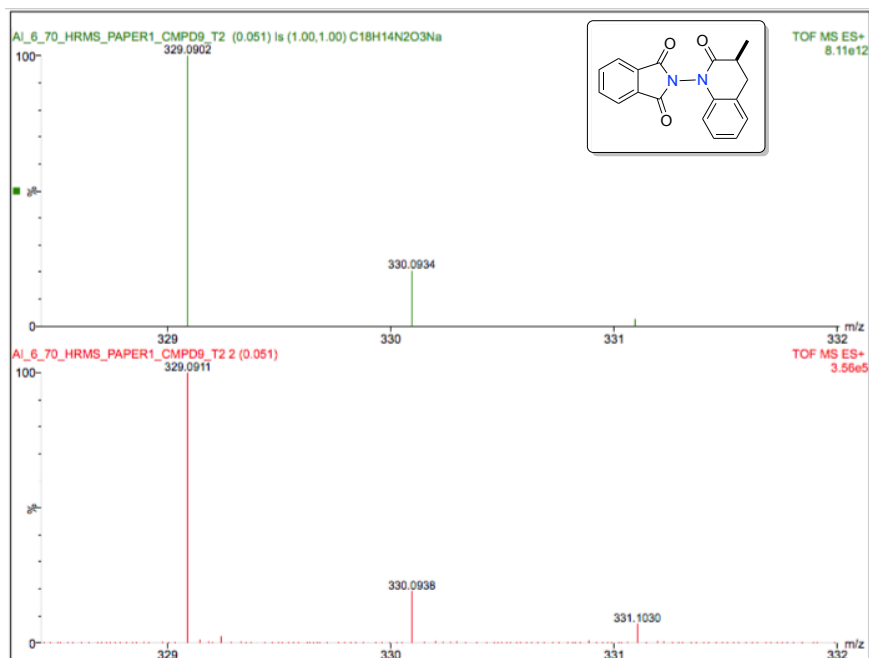
Figure 2.64: HRMS spectra of **113d**.

2.23. Removal of phthalimide ring in acrylanilide based photoproduct 114d
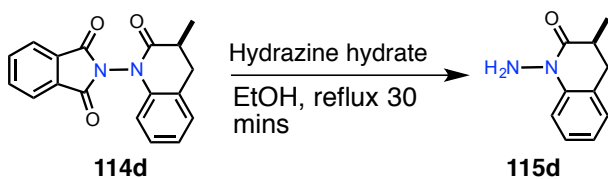
Scheme 2.41: Removal of phthalimide ring in acrylanilide based photoproduct **114d**.

Following the modified procedure reported by Michael et al. the photoproduct **114d** (1 equiv) was charged in a vial equipped with a teflon cap.[42] The compound was dissolved in absolute ethanol (5 mL per 100mg of photoproduct) and hydrazine monohydrate (11.9 equiv) was added. The solution was stirred for 5 min and refluxed for 30 min (until TLC showed complete consumption of starting material). The solution was brought to room temperature and diluted with ethyl acetate. The solution was sonicated for 15 min and then filtered through a short celite plug. The filtrate was concentrated under reduced pressure to obtain the crude product. The crude product was purified using a prep TLC with hexanes and ethyl acetate mixture as eluting solvent to obtain i.e. *N*-Amino dihydroquinolinone derivative **115d**.

Crystalline solid (Yield = 74%).

^{1}H-NMR (400 MHz, CDCl$_3$, δ ppm): 1.25 (d, 3H, *J* 6.4Hz), 2.62-2.72 (m, 2H), 2.87-2.95 (m, 1H), 4.48 (bs, 2H), 6.95-6.97 (m, 1H), 7.06-7.10 (m, 1H), 7.21-7.25 (m, 1H) and 7.49-7.52 (m, 1H).
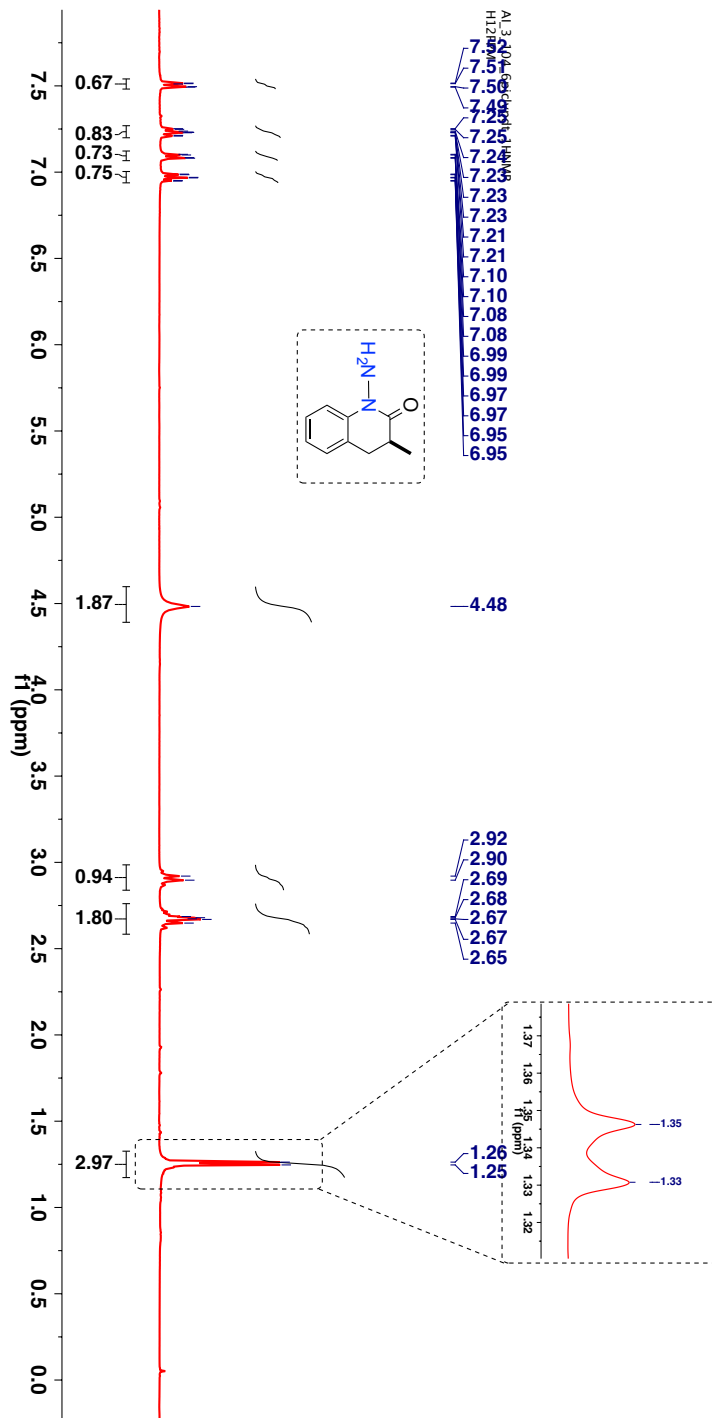
Figure 2.65: ^{1}H-NMR (400 MHz, CDCl$_3$, δ ppm) spectrum of **115d**.

^{13}C-NMR (100 MHz, CDCl$_3$, δ ppm): 15.9, 33.2, 35.8, 114.9, 123.1, 124.2, 127.6, 127.8, 140.1 and 172.1.
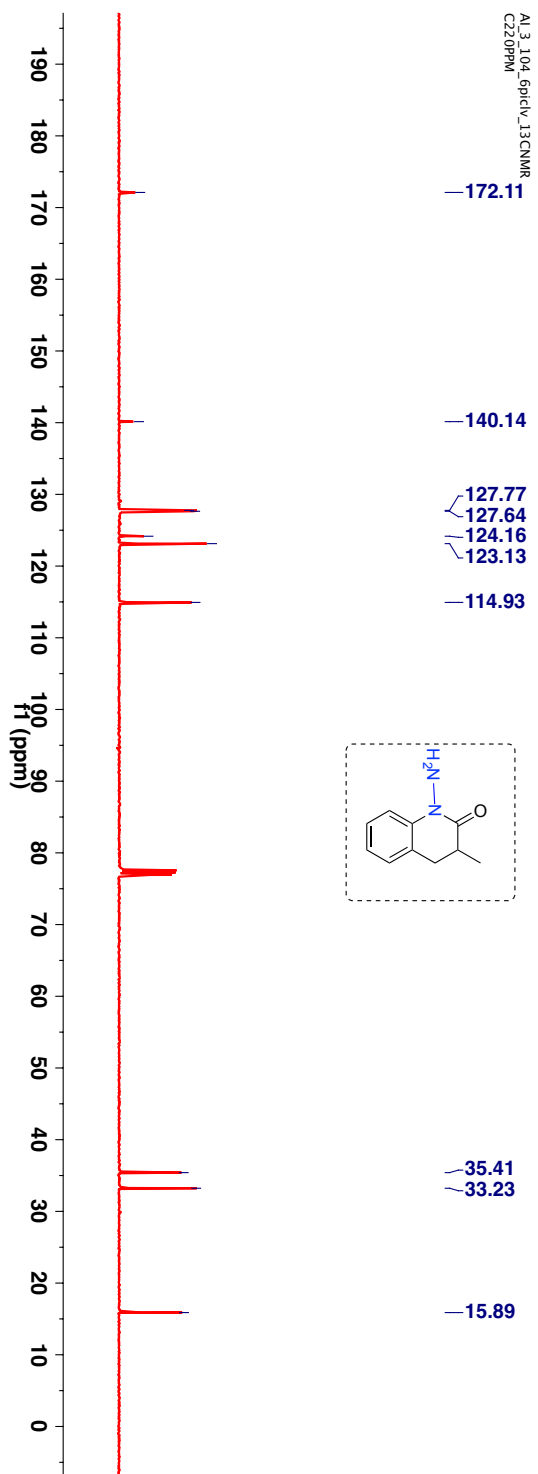
Figure 2.66: ^{13}C-NMR (100 MHz, CDCl$_3$, δ ppm) spectrum of **115d**.

HRMS-ESI (m/z) ([M + Na]$^+$):

Chemical Formula	: $C_{10}H_{12}N_2O$
Calculated	: 199.0847
Observed	: 199.0857
$|\Delta m|$	: 5.0 ppm
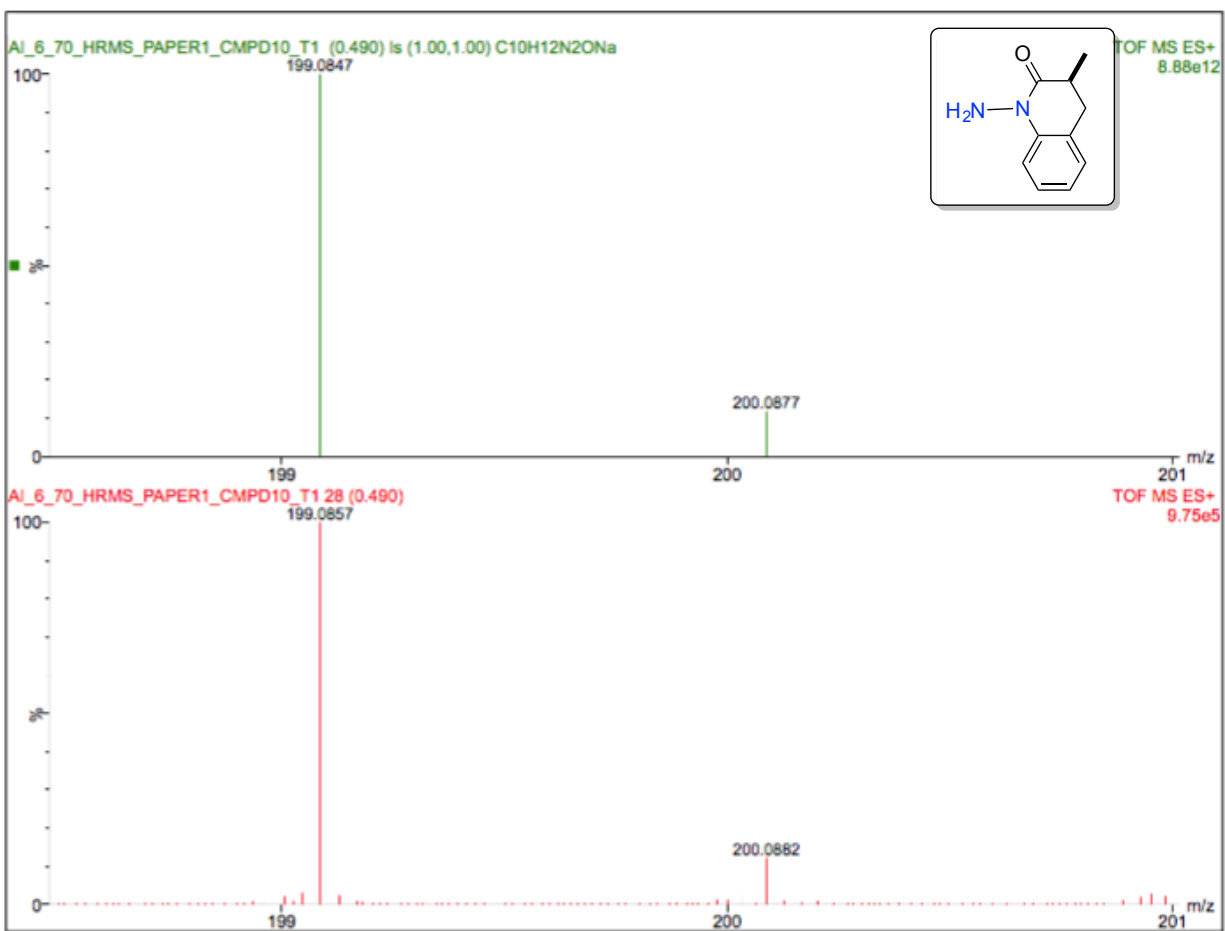
Figure 2.67: HRMS spectra of **115d**.

2.24. Reaction optimization for Norrish-Yang cyclization of α-oxoamide derivative 113c
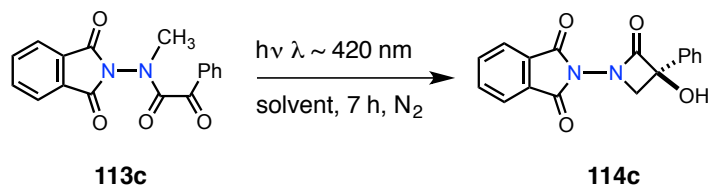
Scheme 2.42: Photoreaction of α-oxoamide derivative **113c**.

Table 2.18: Solvent screening studies for Norrish-Yang cyclization of α-oxoamide derivative **113c**.[a]

Entry	Solvent	Conversion/%
1	Methanol	decomposition
2	Acetonitrile	16
3	Ethyl acetate	55
4	Benzene	63
6	Methylcyclohexane	No reaction

[a] [**113c**] = 3.24 mM.

Crude NMR Photoreaction performed with purple LED as the light source. ^{1}H-NMR (400 MHz, CDCl$_3$, δ ppm): 4.04-4.20 (ABq, 2H), 7.37-7.47 (m, 3H), 7.69-7.72 (m, 2Hz), 7.80-7.82 (m, 2H) and 7.91-7.93 (m, 2H).
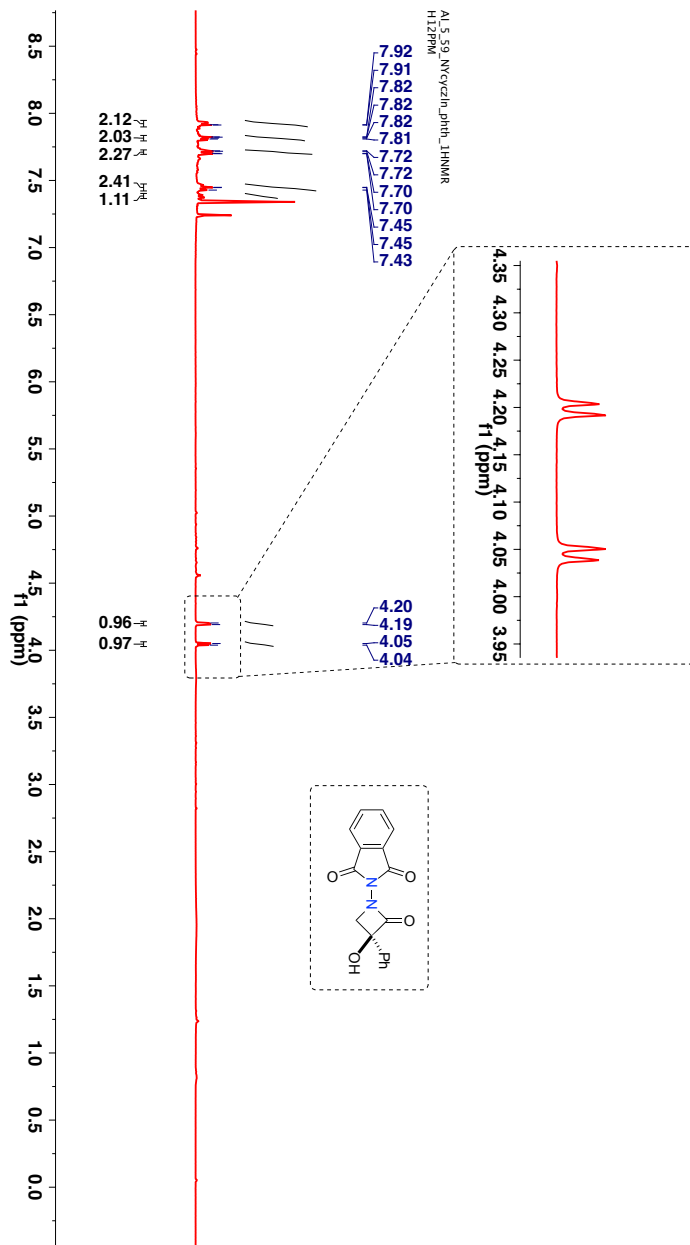
Figure 2.68: ^{1}H-NMR (400 MHz, CDCl$_3$, δ ppm) spectrum of **114c**.

CRUDE NMR aromatic region has thioxanthone peaks (sensitizer)

^{13}C-NMR (100 MHz, CDCl$_3$, δ ppm): 63.3, 85.2, 123.5, 123.9, 124.4, 125.3, 127.8, 128.3, 128.5, 128.9, 128.9, 129.8, 130.2, 134.4, 134.9, 135.2, 136.8, 163.9 and 169.5.
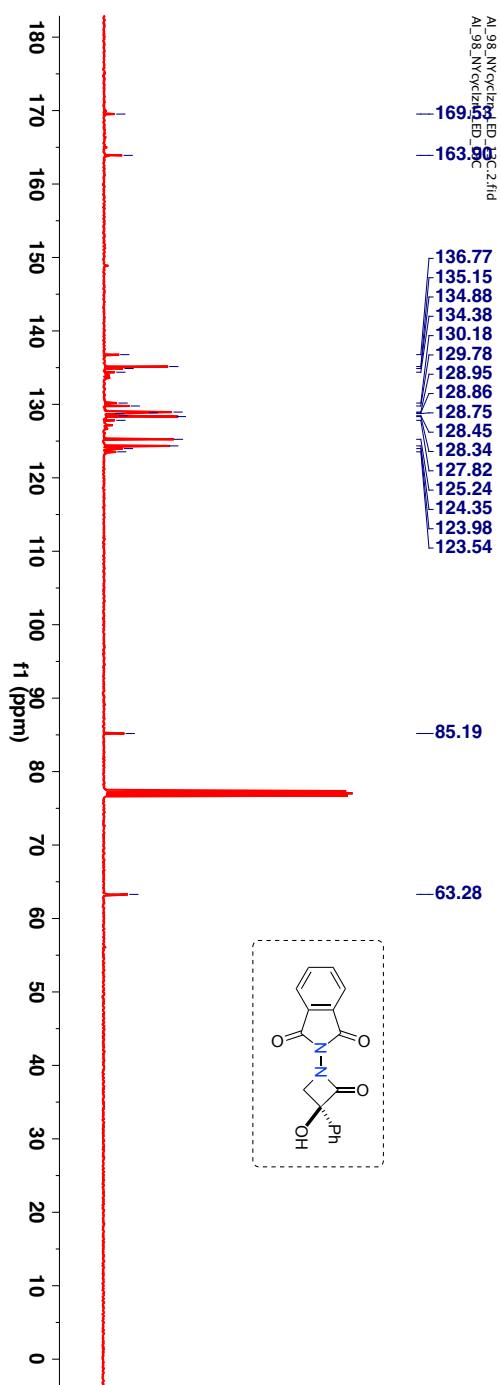
Figure 2.69: ^{13}C-NMR (100 MHz, CDCl$_3$, δ ppm) spectrum of **114c**.

2.24.1. UV-VIS spectra of α–oxoamide derivative 113c
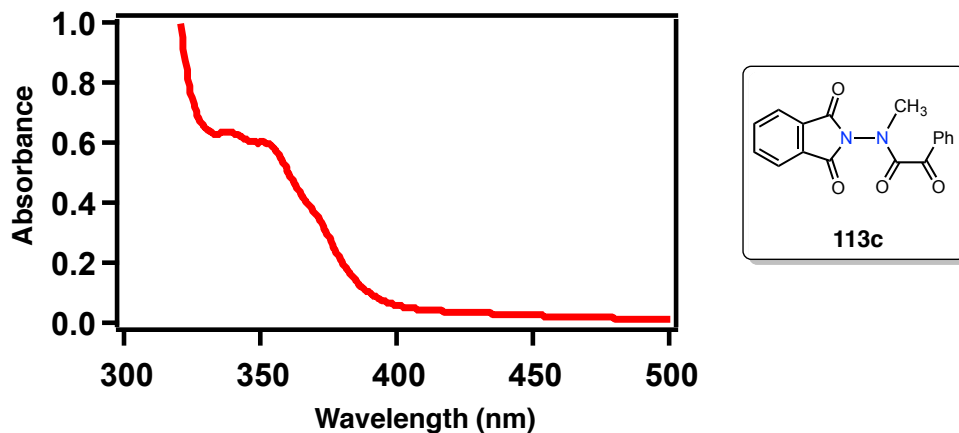
Figure 2.70: UV-Vis spectra of *N-N* bond based α–oxoamide derivative **113c** (concn = 3.2 mM) recorded at the reaction concentration in benzene.
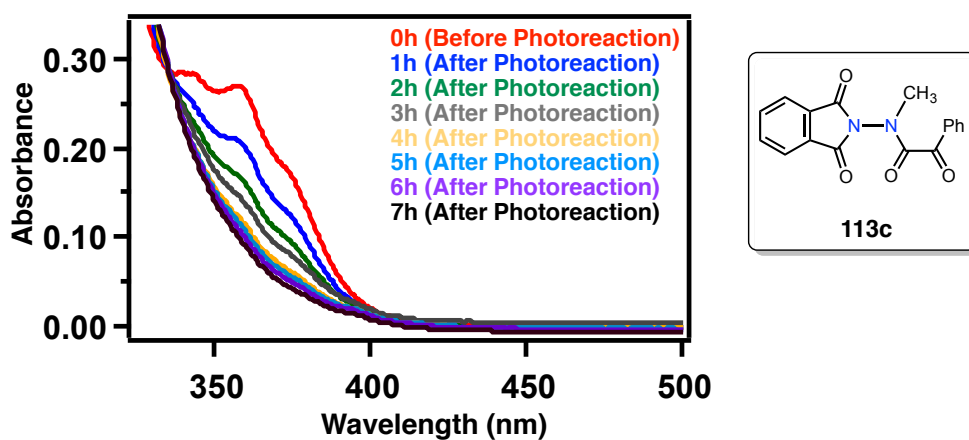
Figure 2.71: UV-Vis spectra of *N-N* bond based α–oxoamide derivative **113c** recorded in benzene during the course of photoreaction under CFL lamp illumination; [**113c**] = 3.2 mM (before photoreaction).

HRMS-ESI (m/z) ([M + Na]$^+$):

Chemical Formula	: C$_{17}$H$_{12}$N$_2$O$_4$
Calculated	: 331.0695
Observed	: 331.0705
|Δm|	: 3.0 ppm
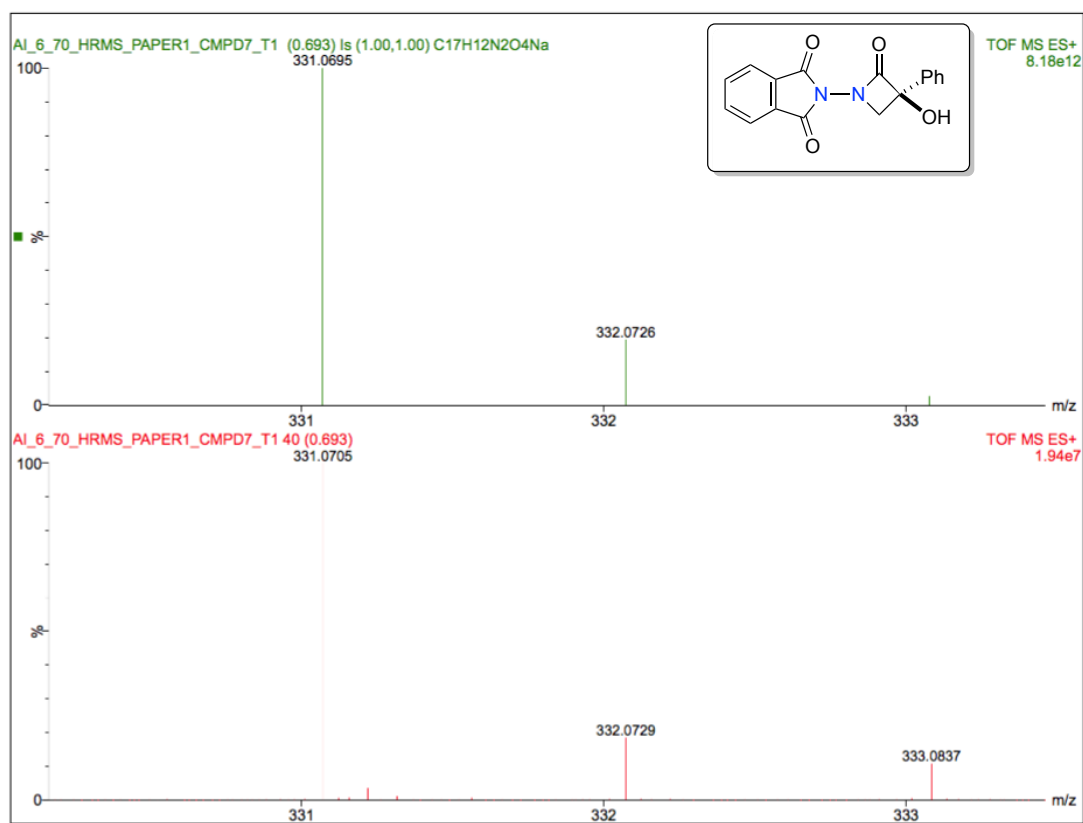
Figure 2.72: HRMS spectra of **114c**.

2.25. Reaction optimization for [2+2] photoreaction of tertiary amine derivative 113i
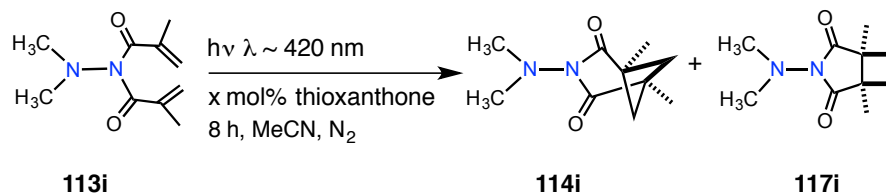
Scheme 2.43: [2+2] Photoreaction of tertiary amine (acrylimide) derivative **113i**.

Table 2.19: Sensitizer loading studies for [2+2] photoreaction of tertiary amine derivative **113i**.[a]

Entry	TX (x mol%)	Conversion/%
1	0	0
2	1	74
3	5	93
4	10	95

[a] [**113i**] = 5.1 mM, TX: Thioxanthone

Table 2.20: Solvent screening studies for [2+2] photoreaction of tertiary amine derivative **113i**.[a]

Entry	Solvent	Conversion/%	NMR yield/%	**114i:117i**
1	Methanol	-[b]	-[b]	-[b]
2	Acetonitrile	95	40	70:30
3	Ethyl acetate	55	27	75:25
4	Benzene	52	28	75:25
6	Methylcyclohexane	Decomposition	-	-

[a] [**113i**] = 5.1 mM. [b] Difficult to interpret because of overlapping peaks.

TLC condition - R$_f$ = 0.2 (20% ethyl acetate:hexanes), Solid (Yield = 24%).

^{1}H-NMR (400 MHz, CDCl$_3$, δ ppm, mixture of regioisomers): 1.26 (s), 1.31 (s, 6H), 2.00-2.02 (m, 2H), 2.03-2.20 (m), 2.31-2.34 (m, 2H), 2.89 (s, 6H) and 2.92 (s).
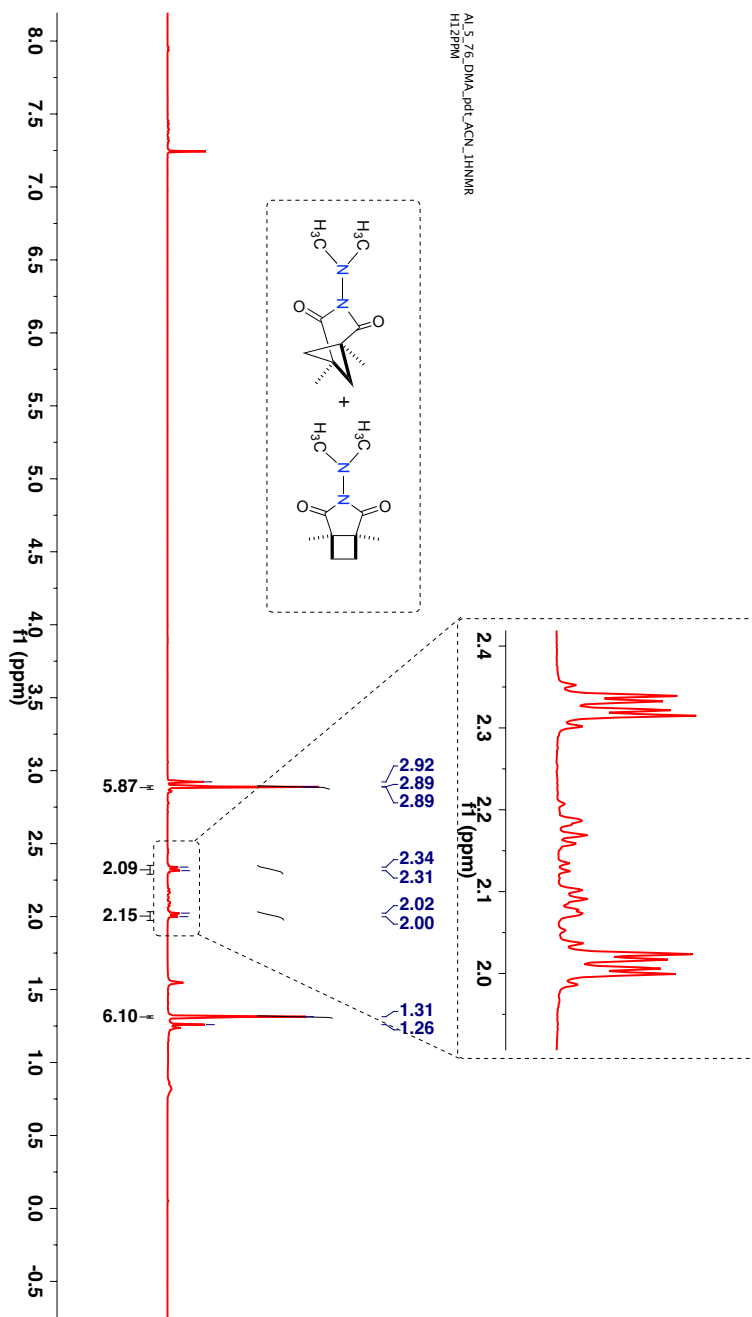
Figure 2.73: ^{1}H-NMR (400 MHz, CDCl$_3$, δ ppm) spectrum of **114i** and **117i**.

^{13}C-NMR (100 MHz, CDCl$_3$, δ ppm, mixture of regioisomers): 15.8, 19.8, 28.6, 43.3, 43.9, 44.0 and 177.6.
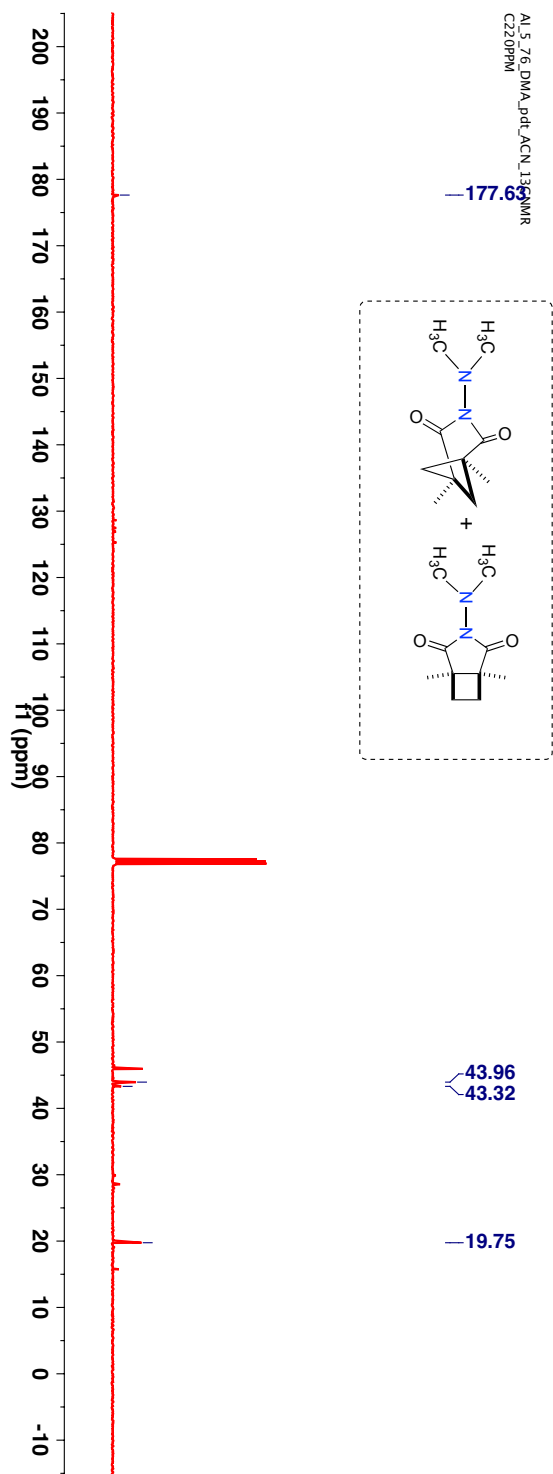
Figure 2.74: ^{13}C-NMR (100 MHz, CDCl$_3$, δ ppm) spectrum of **114i** and **117i**.

2.25.1. UV-VIS spectra of tertiary amine derivative 113i
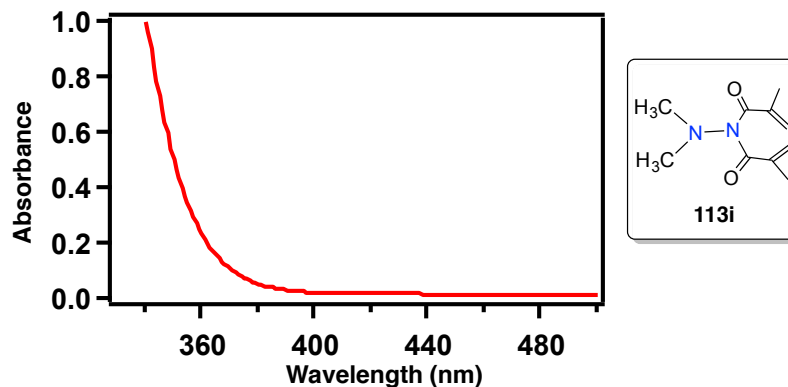
Figure 2.75: UV-Vis spectra of tertiary amine derivative **113i** (concn = 5.1 mM) recorded at the reaction concentration in acetonitrile.

HRMS-ESI (m/z) ([M + Na]$^+$):

Chemical Formula   : $C_{10}H_{16}N_2O_2$

Calculated   : 219.1109

Observed   : 219.1118

|Δm| : 4.1 ppm
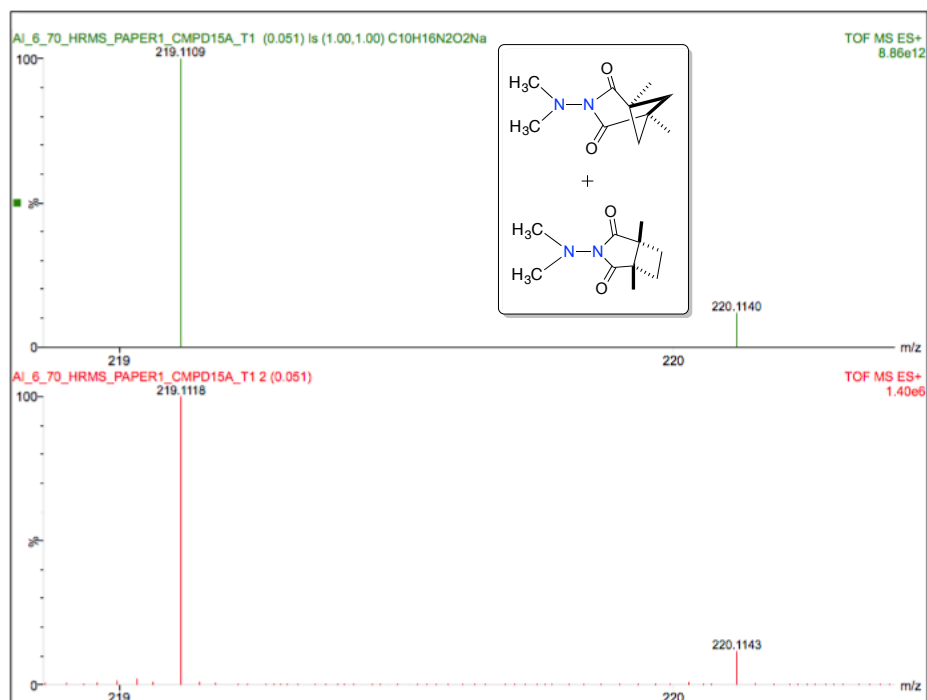
Figure 2.76: HRMS spectra of **114i** and **117i**.

2.26. Reaction optimization for [2+2] photoreaction of secondary amine derivative 113j

113j   **114j**   **117j**
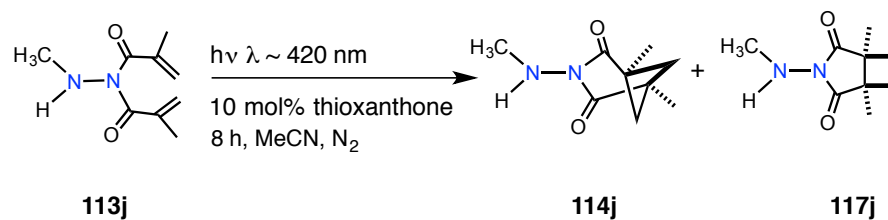
Scheme 2.44: [2+2] Photoreaction of secondary amine derivative **113j**.

Table 2.21: [2+2] Photoreaction of secondary amine derivative **113j**.[a]

Entry	Solvent	Conversion/%	NMR yield/%	**113j:117j**
1	Acetonitrile	>99	40	80:20

[a] [**113j**] = 5.49 mM.

Thick oil (Yield = 35%).

^{1}H-NMR (400 MHz, CDCl$_3$, δ ppm, mixture of regioisomers): 1.29 (s), 1.34 (s, 6H), 2.07-2.09 (m, 2H), 2.10-2.20 (m), 2.39-2.42 (m, 2H), 2.65 (s, 3H) and 2.72 (s).
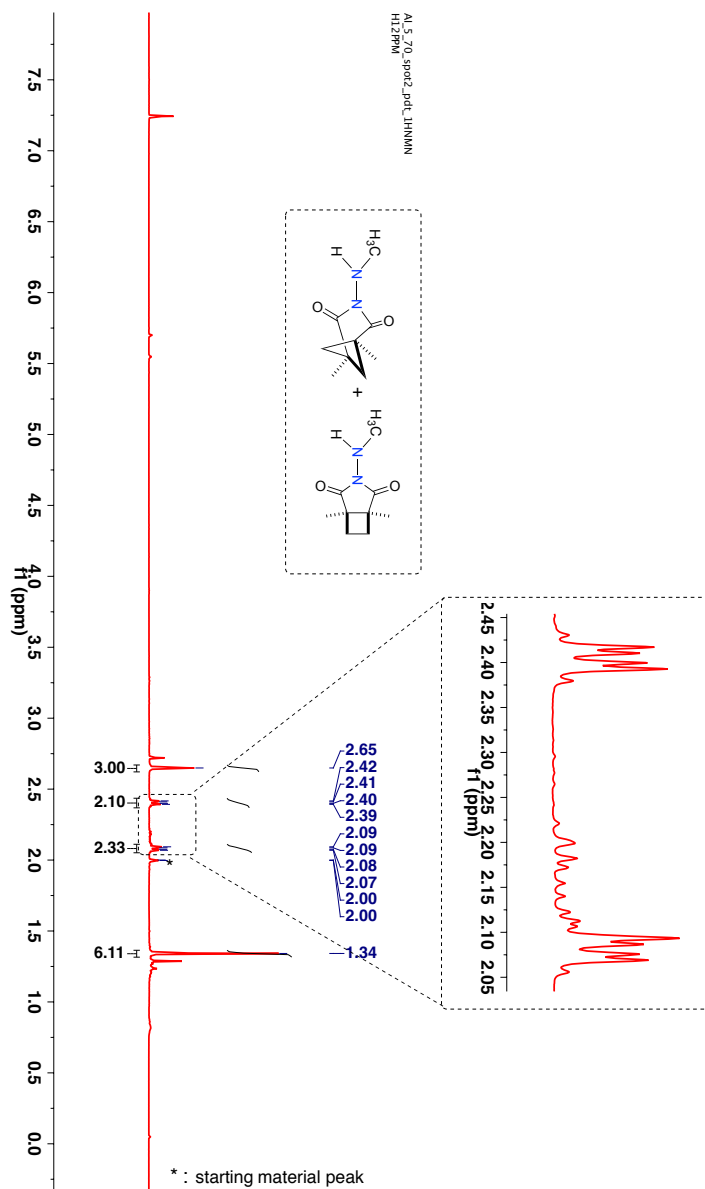
Figure 2.77: ^{1}H-NMR (400 MHz, CDCl$_3$, δ ppm) spectrum of **114j** and **117j**.

¹³C-NMR (100 MHz, CDCl₃, δ ppm, mixture of regioisomers): 19.6, 37.9, 43.1, 46.8 and 176.6.
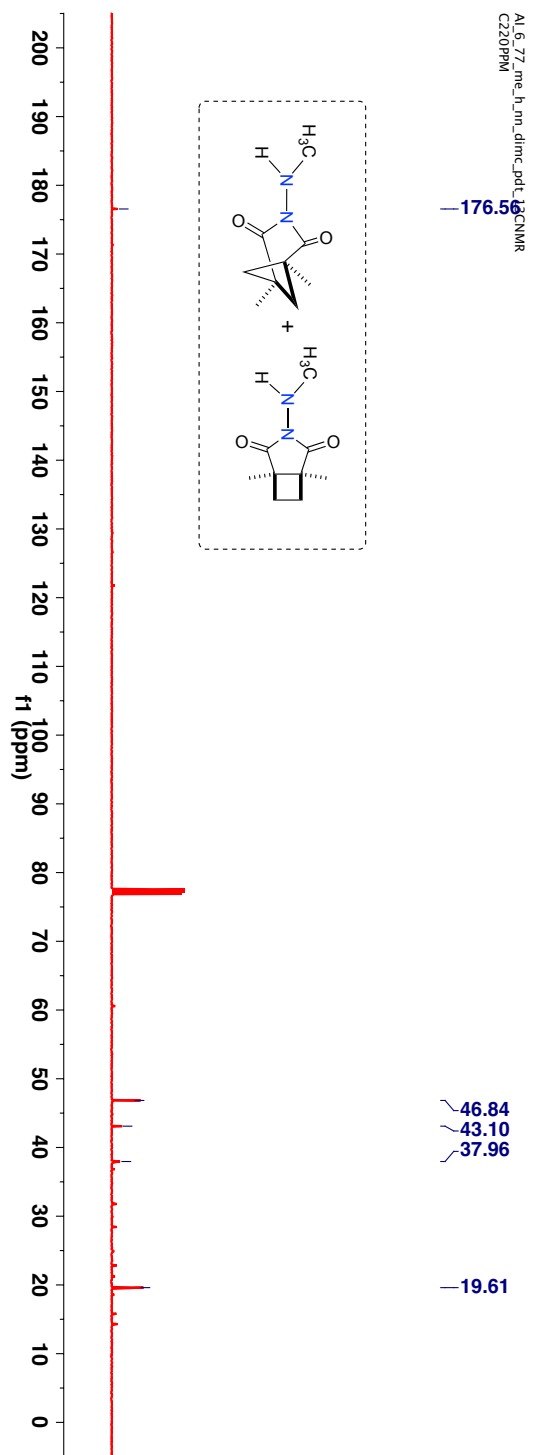
Figure 2.78: ¹³C-NMR (100 MHz, CDCl₃, δ ppm) spectrum of **114j** and **117j**.

2.26.1. UV-VIS spectra of secondary amine derivative 113j
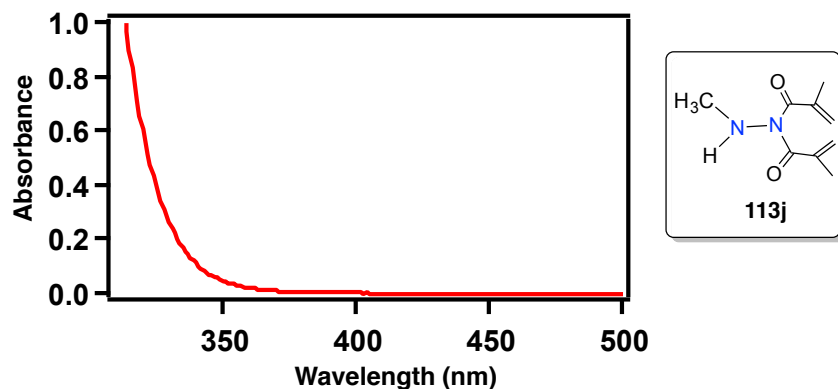
Figure 2.79: UV-Vis spectra of secondary amine derivative **113j** (concn = 5.49 mM) recorded at the reaction concentration in acetonitrile.

HRMS-ESI (m/z) ([M + Na]$^+$):

Chemical Formula	: $C_9H_{14}N_2O_2$
Calculated	: 205.0963
Observed	: 205.0960
$|\Delta m|$	: 1.5 ppm
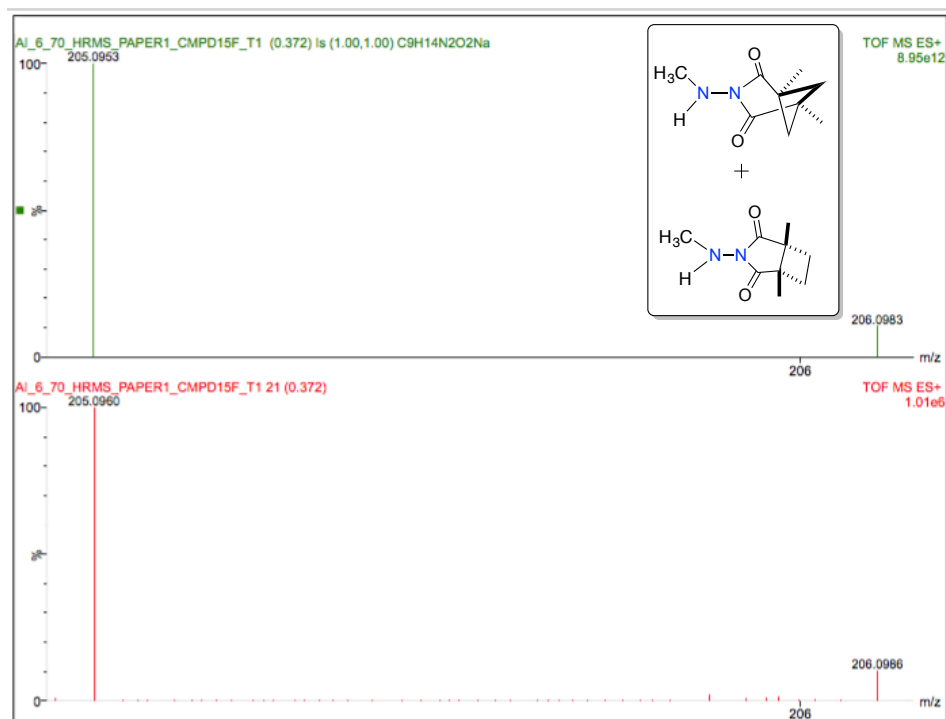
Figure 2.80: HRMS spectra of **114j** and **117j**.

2.27. Reaction optimization for [2+2] photoreaction of imide based derivative 113e
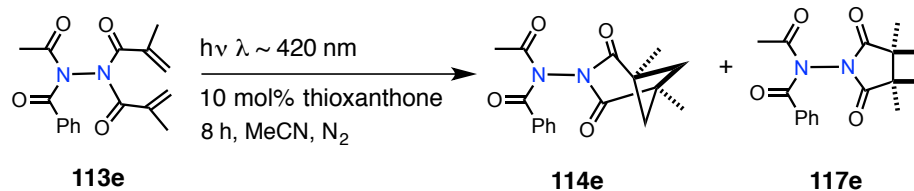
Scheme 2.45: [2+2] Photoreaction of imide based derivative **113e**.

Table 2.22: [2+2] Photoreaction of imide based derivative **113e**.[a]

Entry	Solvent	Conversion/%	NMR yield/%	114e:117e
1	Acetonitrile	56	52	-[b]

[a] [**113e**] =3.18 mM. [b] Ratios not reported due to overlapping peaks in ^{1}H NMR spectroscopy

TLC condition - R$_f$ = 0.2 (10% ethyl acetate:hexanes), Thick oil (Yield = 45%).

^{1}H-NMR (400 MHz, CDCl$_3$, δ ppm, mixture of rotamers): 0.99 (s), 1.29 (s), 1.30 (s), 1.39-1.45 (m), 1.51-1.55 (m), 1.85-1.88 (m), 2.08-2.11 (m), 2.42-2.46 (m), 2.67 (s), 2.72-2.79 (m) and 7.39-7.56 (m).
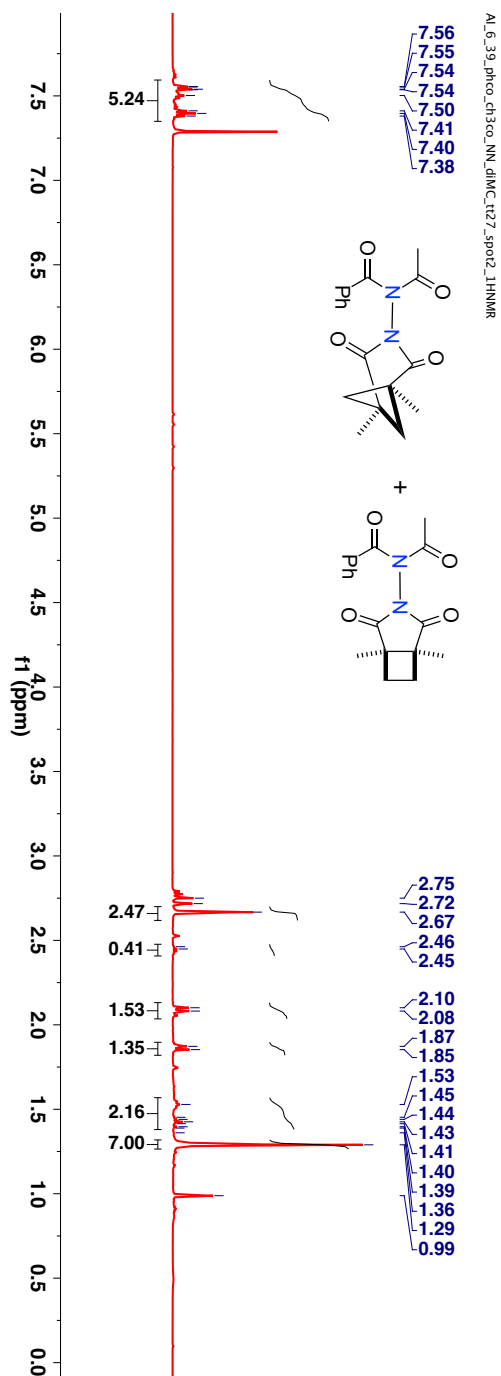
Figure 2.81: ^{1}H-NMR (400 MHz, CDCl$_3$, δ ppm) spectrum of **114e** and **117e**.

^{13}C-NMR (100 MHz, CDCl$_3$, δ ppm, all peaks are reported together): 15.3, 15.7, 19.3, 25.3, 25.5, 27.8, 28.3, 43.3, 44.2, 45.5, 126.8, 126.8, 127.0, 128.4, 128.4, 128.4, 128.7, 129.0, 129.2, 131.9, 132.1, 132.2, 132.9, 134.2, 169.7, 171.2 and 174.8.
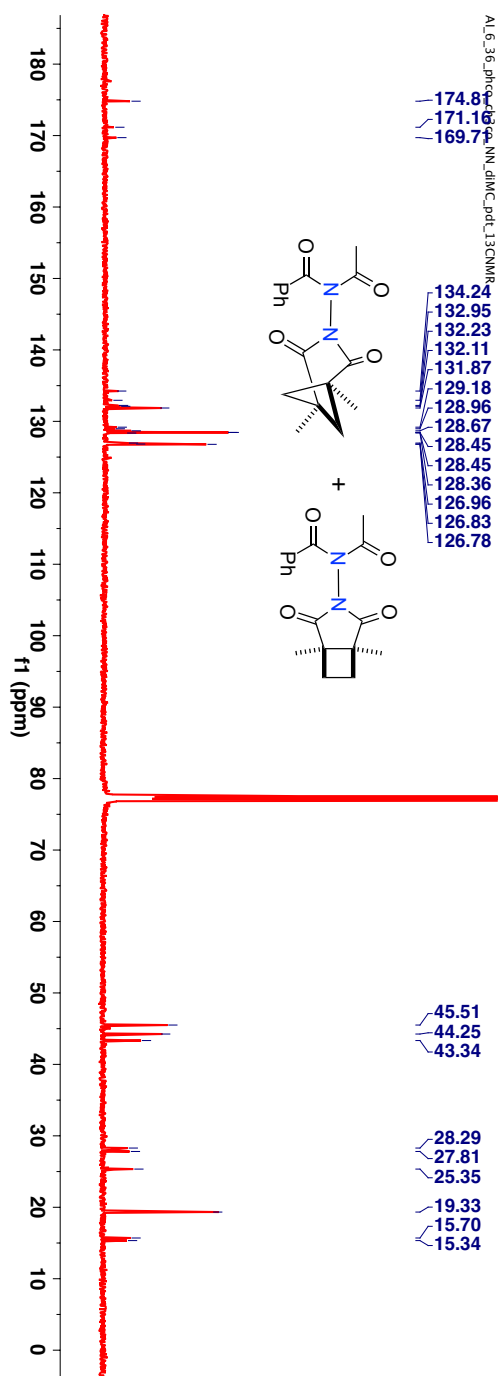
Figure 2.82: ^{13}C-NMR (100 MHz, CDCl$_3$, δ ppm) spectrum of **114e** and **117e**.

2.27.1. UV-VIS spectra of imide based derivative 113e
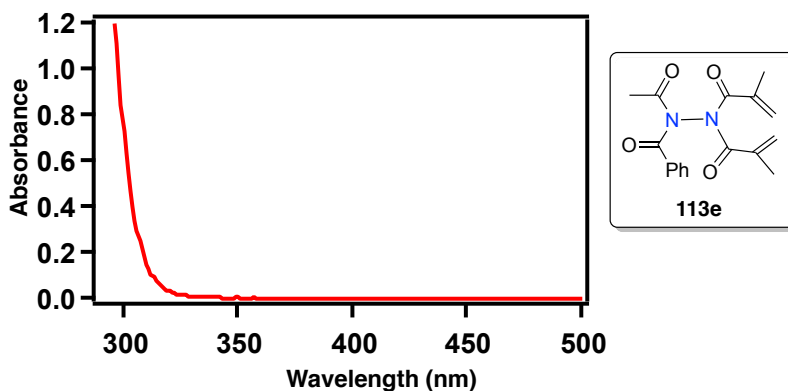
Figure 2.83: UV-Vis spectra of imide based derivative **113e** (concn = 3.18 mM) recorded at the reaction concentration in acetonitrile.

HRMS-ESI (m/z) ([M + Na]$^+$):

Chemical Formula : $C_{17}H_{18}N_2O_4$

Calculated : 337.1177

Observed : 337.1164

$|\Delta m|$: 3.8 ppm
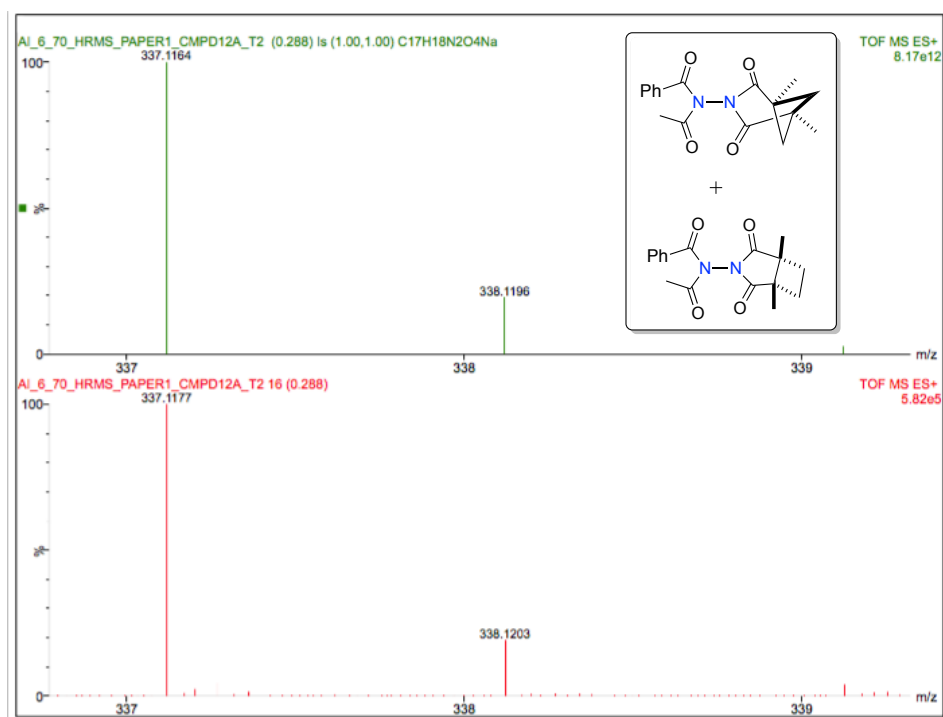
Figure 2.84: HRMS spectra of **114e** and **117e**.

2.28. Reaction optimization for [2+2] photoreaction of carbamate derivative 113h
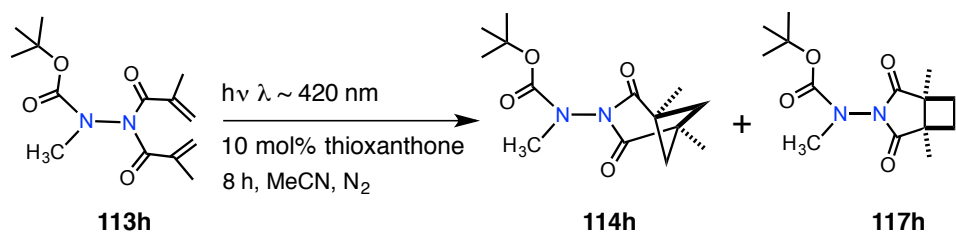
Scheme 2.46: [2+2] Photoreaction of carbamate derivative **113h**.

Table 2.23: [2+2] Photoreaction of carbamate derivative **113h**.[a]

Entry	Solvent	Conversion/%	**114h:117h**
1	Acetonitrile	82	– [b]

[a] [**113h**] = 3.54 mM. [b] Difficult to determine due to overlapping peaks

TLC condition - R_f = 0.3 (20% ethyl acetate:hexanes), Thick oil (Yield = 73%).

^{1}H-NMR (400 MHz, CDCl$_3$, δ ppm, mixture of regioisomers): 1.25 (s), 1.28 (s), 1.32 (s), 1.34 (s), 1.36 (s), 1.45 (s), 2.02-2.10 (m), 2.36-2.46 (m), 2.66-2.71 (m), 3.10 (s), 3.11 (s), 3.14 (s) and 3.15 (s).
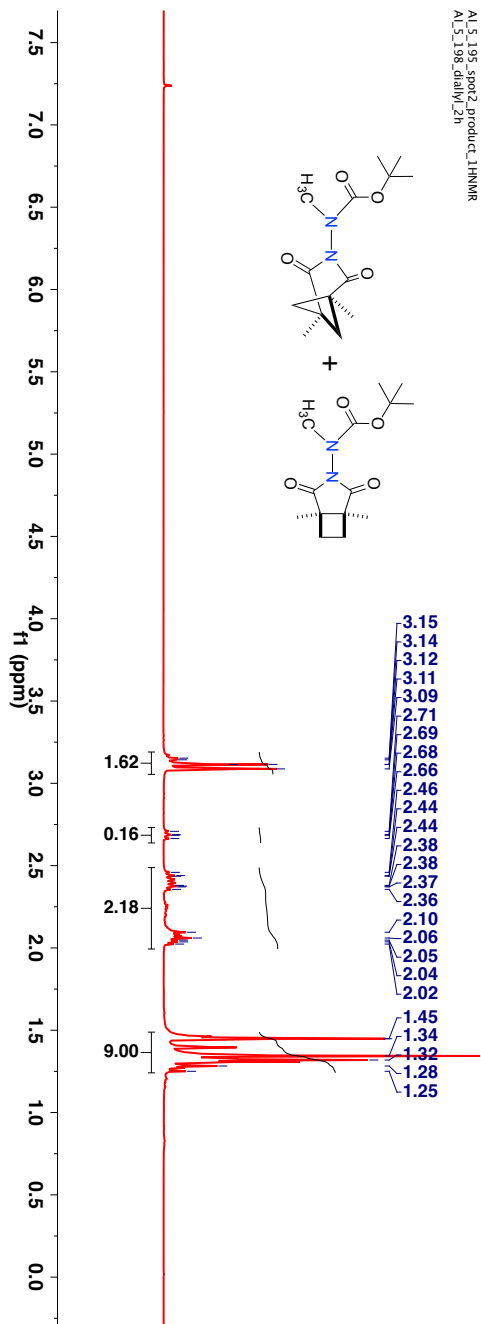
Figure 2.85: ^{1}H-NMR (400 MHz, CDCl$_3$, δ ppm) spectrum of **114h** and **117h**.

^{13}C-NMR (100 MHz, CDCl$_3$, δ ppm, mixture of regioisomers): 15.6, 15.7, 15.8, 19.5, 28.2, 28.4, 35.9, 37.4, 43.0, 43.1, 44.7, 45.2, 45.6, 45.7, 45.7, 81.7, 82.2, 82.6, 153.4, 154.1, 154.2, 175.1, 175.7 and 178.1.
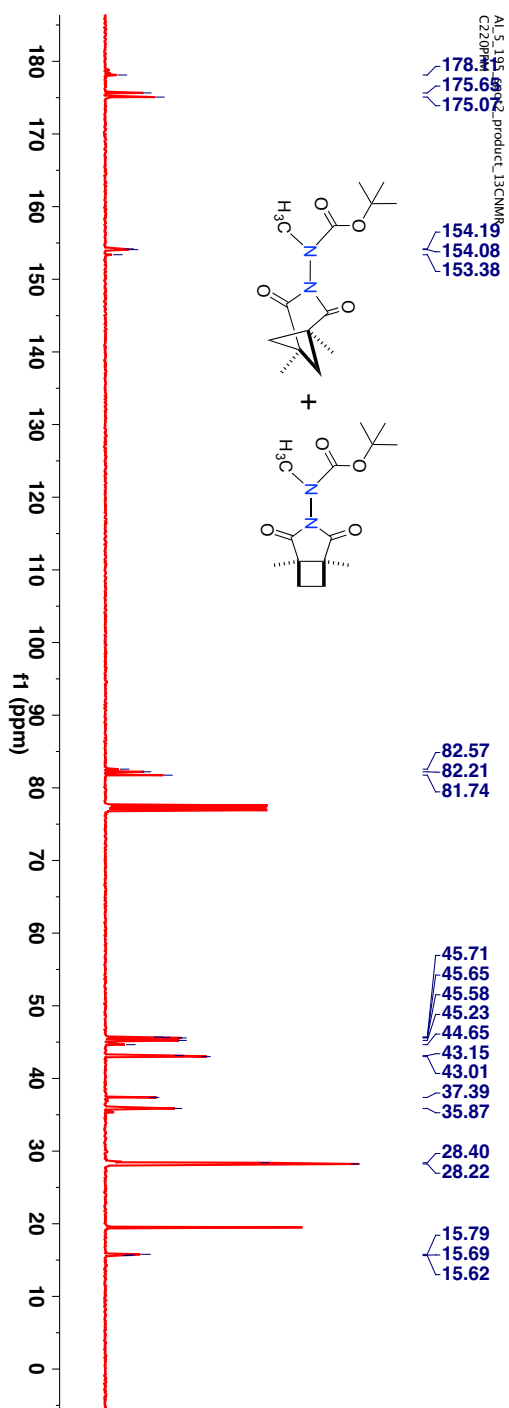
Figure 2.86: ^{13}C-NMR (100 MHz, CDCl$_3$, δ ppm) spectrum of **114h** and **117h**.

2.28.1. UV-VIS spectra of carbamate derivative 113h
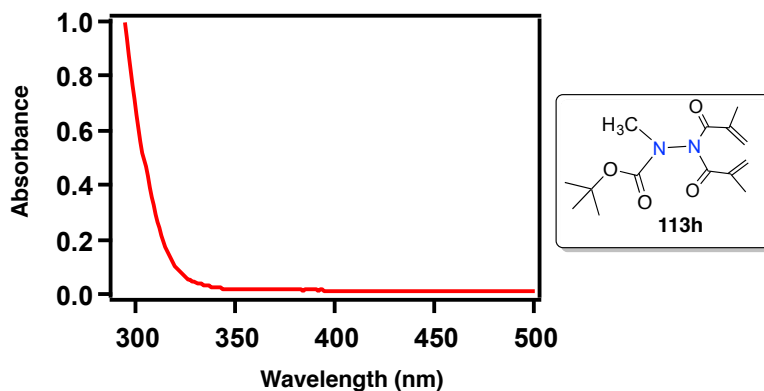
Figure 2.87: UV-Vis spectra of carbamate derivative **113h** recorded at the reaction concentration in acetonitrile (concn= 3.5 mM).

HRMS-ESI (m/z) ([M + Na]$^+$):

Chemical Formula	: $C_{14}H_{22}N_2O_4$
Calculated	: 305.1477
Observed	: 305.1493
|Δm|	: 5.6 ppm
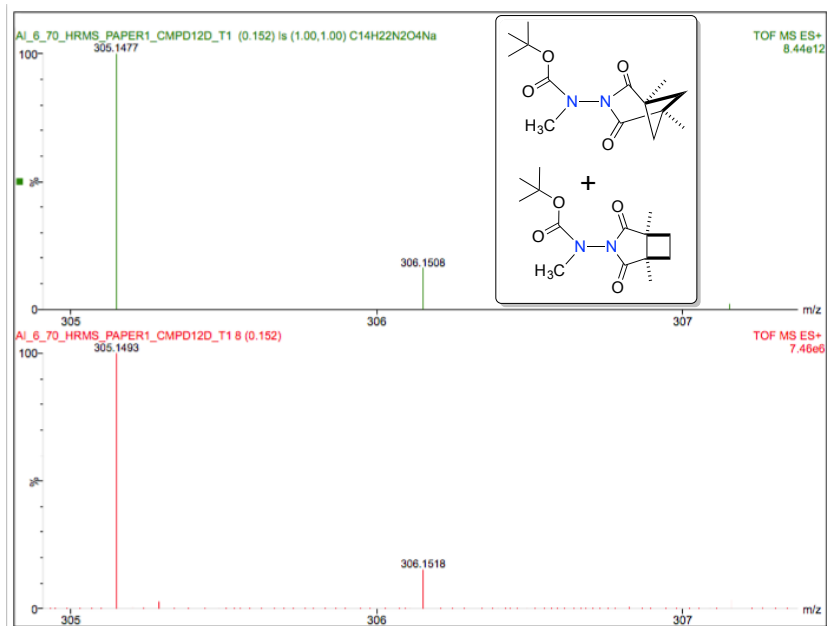
Figure 2.88: HRMS spectra of **114h** and **117h**

2.29. Phosphorescence spectra of hydrazides
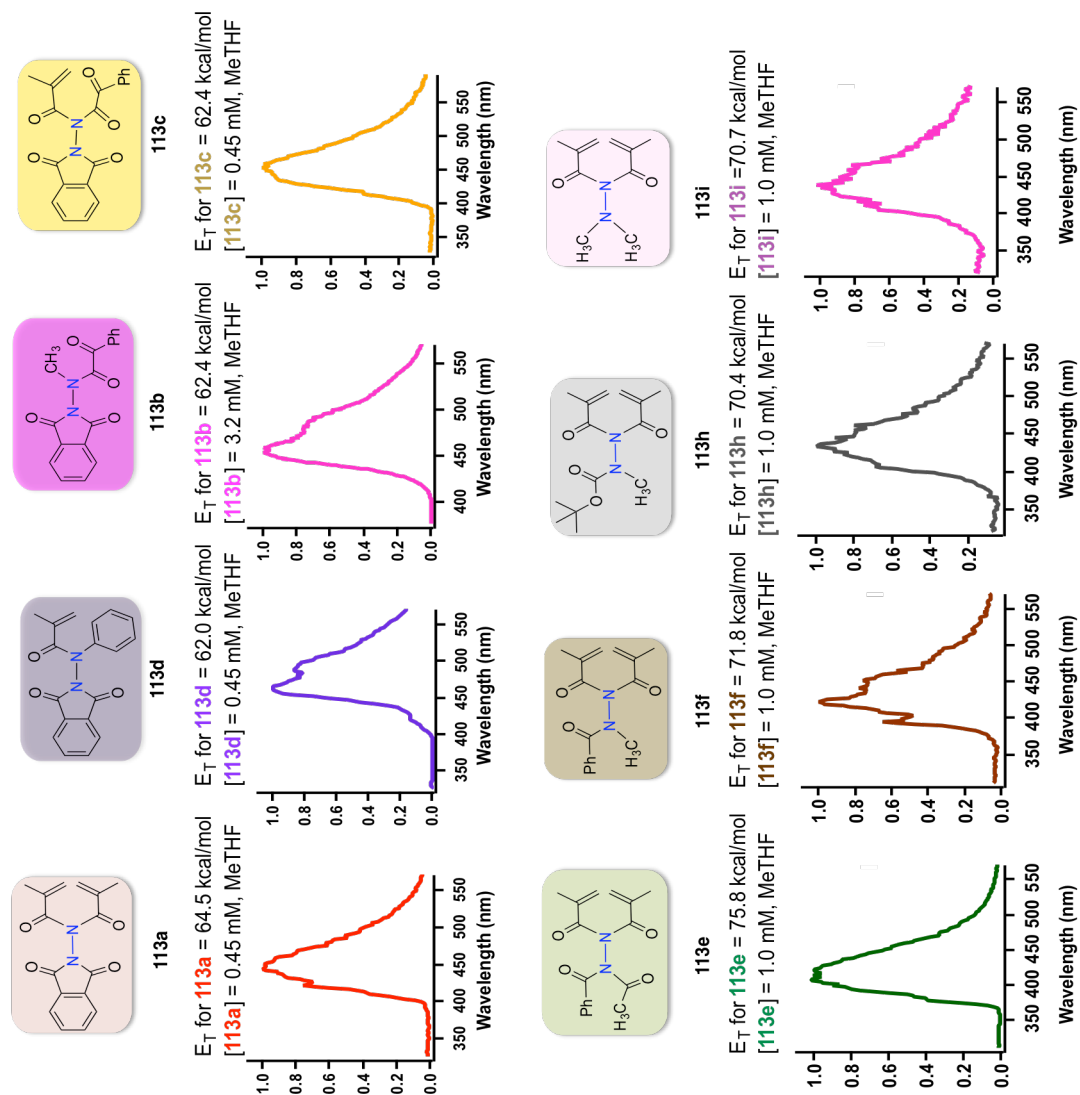
Figure 2.89: Phosphorescence spectra of hydrazides **113a-k** recorded in glass matrix of 2-MeTHF.

2.30. References

(1)   Forbes, M. D. E. *ACS Central Science* **2015**, *1*, 354-63.

(2)   Kärkäs, M. D.; Porco, J. A.; Stephenson, C. R. J. *Chem. Rev.* **2016**

10.1021/acs.chemrev.5b00760

(3)   Schultz, D. M.; Yoon, T. P. *Science* **2014**, *343*.

(4)   Du, J.; Skubi, K. L.; Schultz, D. M.; Yoon, T. P. *Science* **2014**, *344*, 392-96.

(5)   Bock, C. R.; Connor, J. A.; Gutierrez, A. R.; Meyer, T. J.; Whitten, D. G.; Sullivan, B. P.; Nagle, J. K. *J. Am. Chem. Soc.* **1979**, *101*, 4815-24.

(6)   Brimioulle, R.; Lenhart, D.; Maturi, M. M.; Bach, T. *Angew. Chem. Int. Ed.* **2015**, *54*, 3872-90.

(7)   Fagnoni, M.; Dondi, D.; Ravelli, D.; Albini, A. *Chem. Rev.* **2007**, *107*, 2725-56.

(8)   Dauben, W. G.; Salem, L.; Turro, N. J. *Acc. Chem. Res.* **1975**, *8*, 41-54.

(9)   Bach, T. *Synthesis* **1998**, *1998*, 683-703.

(10)   Turro, N. J.; Ramamurthy, V.; Scaiano, J. C. *Modern Molecular Photochemistry of Organic Molecules*; University Science Books: Sausalito, CA, 2010.

(11)   Cuthbertson, J. D.; MacMillan, D. W. C. *Nature* **2015**, *519*, 74-77.

(12)   Blair, L. M.; Sperry, J. *J. Nat. Prod.* **2013**, *76*, 794-812.

(13)   Majumdar, P.; Pati, A.; Patra, M.; Behera, R. K.; Behera, A. K. *Chem. Rev.* **2014**, *114*, 2942-77.

(14)   Vincent-Rocan, J.-F.; Ivanovich, R. A.; Clavette, C.; Leckett, K.; Bejjani, J.; Beauchemin, A. M. *Chem. Sci.* **2016**, *7*, 315-28.

(15)   Rosen, B. R.; Werner, E. W.; O'Brien, A. G.; Baran, P. S. *J. Am. Chem. Soc.* **2014**, *136*, 5571-74.

(16)   Zheng, Z.; Ma, S.; Tang, L.; Zhang-Negrerie, D.; Du, Y.; Zhao, K. *J. Org. Chem.* **2014**, *79*, 4687-93.

(17)   Chen, J.-R.; Hu, X.-Q.; Lu, L.-Q.; Xiao, W.-J. *Chem. Soc. Rev.* **2016**, *45*, 2044-56.

(18)   Rees, C. W.; Gilchrist, T. L.; Stanton, E. *J. Chem. Soc. C* **1971**, 988-93.

(19)   Nelson, S. F.; Pladziewicz, J. R. Intermolecular Electron Transfer Reactivity Determined from Cross Rate Studies. http://www.chem.uwec.edu/pladzijr/Pages/Accts(revised).pdf (accessed 17 August 2016).

(20)   Ferroud, C.; Cocquet, G.; Guy, A. *Tetrahedron Lett.* **1999**, *40*, 5005-08.

(21)   Cocquet, G.; Ferroud, C.; Guy, A. *Tetrahedron* **2000**, *56*, 2975-84.

(22)   Ferroud, C.; Rool, P.; Santamaria, J. *Tetrahedron Lett.* **1998**, *39*, 9423-26.

(23)   Cocquet, G.; Ferroud, C.; Simon, P.; Taberna, P.-L. *Journal of the Chemical Society, Perkin Transactions 2* **2000**, 1147-53.

(24)   Lebrun, S.; Couture, A.; Deniau, E.; Grandclaudon, P. *Synlett* **2009**, *2009*, 2621-24.

(25)   Watterson, A. C.; Shama, S. A. *J. Org. Chem.* **1975**, *40*, 19-24.

(26)   Greulich, T. W.; Daniliuc, C. G.; Studer, A. *Org. Lett.* **2015**, *17*, 254-57.

(27)   Miyazawa, K.; Koike, T.; Akita, M. *Chem. Eur. J.* **2015**, *21*, 11677-80.

(28)   Chen, Y.; Kamlet, A. S.; Steinman, J. B.; Liu, D. R. *Nat Chem* **2011**, *3*, 146-53.

(29)   Hu, X.-Q.; Chen, J.-R.; Wei, Q.; Liu, F.-L.; Deng, Q.-H.; Beauchemin, A. M.; Xiao, W.-J. *Angew. Chem. Int. Ed.* **2014**, *53*, 12163-67.

(30)   Zhu, M.; Zheng, N. *Synthesis* **2011**, *2011*, 2223-36.

(31)   Ghosh, K.; Karmakar, R.; Mal, D. *Eur. J. Org. Chem.* **2013**, *2013*, 4037-46.

(32)   Mahmoud, E.; Watson, D. A.; Lobo, R. F. *Green Chemistry* **2014**, *16*, 167-75.

(33)   Iyer, A.; Jockusch, S.; Sivaguru, J. *J. Phys. Chem. A* **2014**, *118*, 10596-602.

(34)   Aoyama, H.; Sakamoto, M.; Kuwabara, K.; Yoshida, K.; Omote, Y. *J. Am. Chem. Soc.* **1983**, *105*, 1958-64

(35)   Rehm, D.; Weller, A. *Isr. J. Chem.* **1970**, *8*, 259-71.

(36)   Chesta, C. A.; Whitten, D. G. *J. Am. Chem. Soc.* **1992**, *114*, 2188–97.

(37)   Deng, W.; Wang, Y.-F.; Zou, Y.; Liu, L.; Guo, Q.-X. *Tetrahedron Lett.* **2004**, *45*, 2311-15.

(38)   Natarajan, A.; Mague, J. T.; Ramamurthy, V. *J. Am. Chem. Soc.* **2005**, *127*, 3568-76.

(39)   Yagci, Y.; Jockusch, S.; Turro, N. J. *Macromolecules* **2007**, *40*, 4481-85.

(40)   Abbas, C.; Pickaert, G.; Didierjean, C.; Grégoire, B. J.; Vanderesse, R. *Tetrahedron Lett.* **2009**, *50*, 4158-60.

(41)   Aoki, Y.; Saito, Y.; Sakamoto, T.; Kikugawa, Y. *Synth. Commun.* **2000**, *30*, 131-40.

(42)   Hoover, J. M.; DiPasquale, A.; Mayer, J. M.; Michael, F. E. *J. Am. Chem. Soc.* **2010**, *132*, 5043-53.

CHAPTER 3. DEVELOPING ATROPISOMERIC HYDRAZIDES FOR VISIBLE LIGHT MEDIATED PHOTOCATALYSIS

3.1. Introduction

Hydrazides are a class of organic compounds that comprise of functional group characterized by a covalent *N-N* bond and having four substituents, wherein at least one of the substituents is an acyl group.[1] The hydrazides are also commonly termed as *N*-acyl hydrazides. Hydrazides are the derivatives of hydrazines and their history dates back to 1850 in the literature.[2] Since then there have been numerous reports on synthesis of hydrazides and analogs, as these constitute versatile reagents in chemical synthesis.[3] The hydrazide possess general structure classified as $(Y=X)(R^1)N-N(R^2)(R^3)$ **124a-d**, where the $R^1/R^2/R^3$ groups are frequently hydrogen(s) (Scheme 3.1). Changing substitution on X from carbon to sulfur or phosphorus results in useful hydrazide analogs viz sulfonyl hydrazides **124b** and phosphohydrazide **124c** respectively.[1] In addition on changing the heteroatom from oxygen to sulfur affords thiohydrazides **124d**. Depending on the R^1/R^2 groups/substitution on the *N* atom, the hydrazides exhibit varied thermal stability.[4]
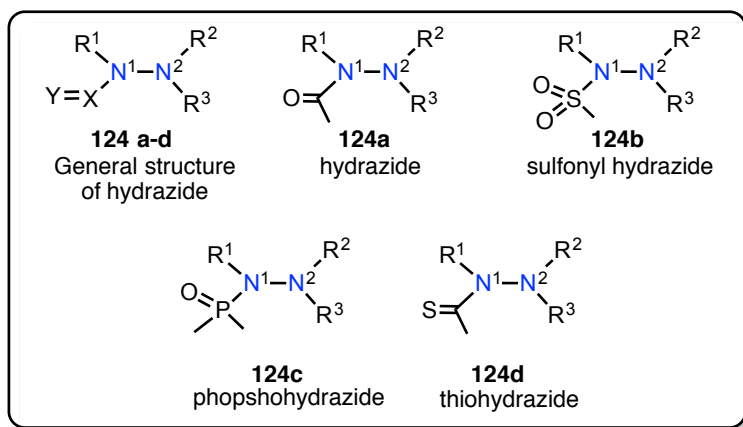
Scheme 3.1: General structure of hydrazides **124a-d** and analogs.

It is important to note that hydrazides are important class of compounds as they are useful precursors for various heterocycles. [3,5-7] In the field of biochemical sciences, hydrazides have extensive application in protein chemical synthesis to overcome the limitations of protein expression and for accessing proteins with predesigned changes.[8-9] In addition this functionality is commonly found in synthetically useful compounds/macromolecules like polymers, drugs **125-130** (Scheme 3.2) and agrochemicals [6,10-11] Chiral hydrazides find extensive application as organocatalysts for asymmetric reactions.[12]

125

NIALAMDE
Antidepressant

126

GLICLAZIDE
Hypoglycemic drug

127

ATAZANAVIR
HIV

128

LINATINE
Cytotoxic towards
CaCo-2 colon cancer
cells.

129

MARPLAN
Monoamine oxidase
inhibitor (MAO)

130

DYNOHYDRAZIDE B
Inhibition of
mammalian cancer
cells
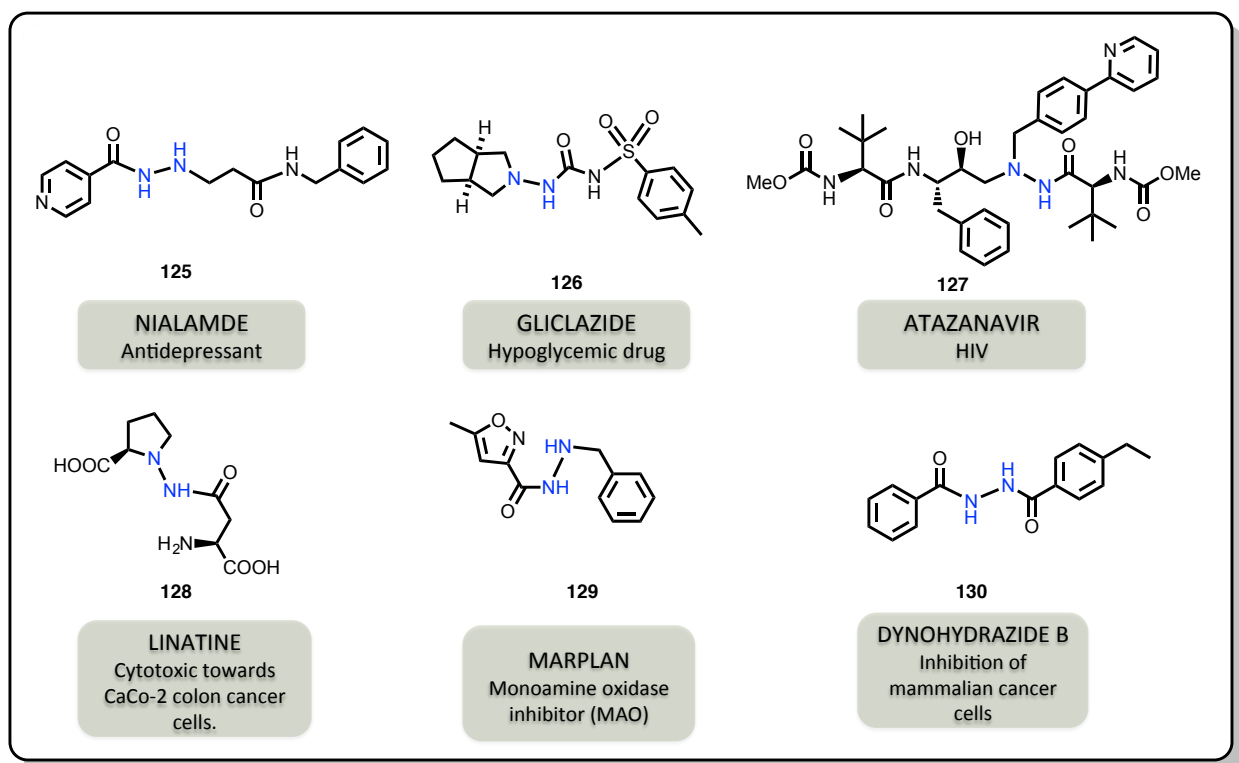
Scheme 3.2: Few important hydrazide derivatives that have potential biological activity.

3.2. Synthesis of hydrazides

The structural feature that imparts unique reactivity and challenging synthetic protocol predominantly includes *N-N* bond and *N*-acyl substitution. A look at the retrosynthetic analysis (Scheme 3.3) suggests hydrazide synthesis can be broadly classified into two categories viz (1) One *N* synthon approach and (2) Two *N* synthon approach. Each of the approaches is discussed in detail in the following section.
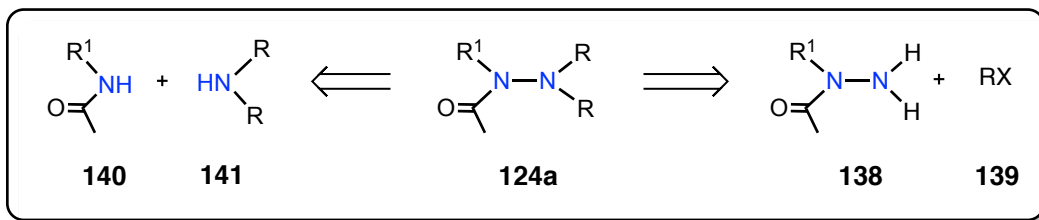
Scheme 3.3: Retrosynthetic analysis for hydrazide.
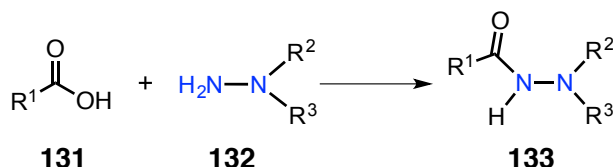
Scheme 3.4: Direct condensation of hydrazines to yield hydrazides.

The easiest way to synthesize hydrazides is the acylation/alkylation of corresponding hydrazine. Direct condensation of hydrazines **132** with carboxylic acids **131** (Scheme 3.4) or acylation under low temperature results in hydrazides **133** [13] The reaction of hydrazines with alkyl halides is a difficult process to control and often results in mixture of products. Măeorg et al. have reported an elegant strategy of converting substituted hydrazines **134** into corresponding hydrazides **136/137** through sequential lithiation reaction (Scheme 3.5).[14] This method affords a convenient access to substituted hydrazides with control over regioselectivity.
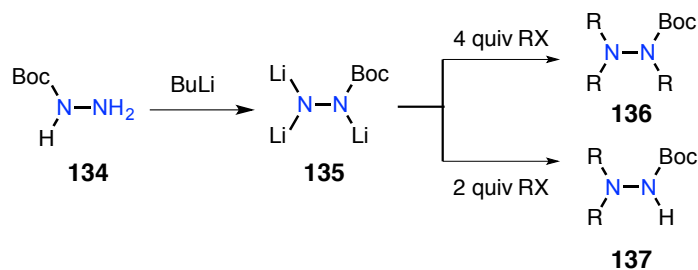
Scheme 3.5: Lithiation of hydrazines for selective alkylation.

3.2.1. One *N* synthon approach
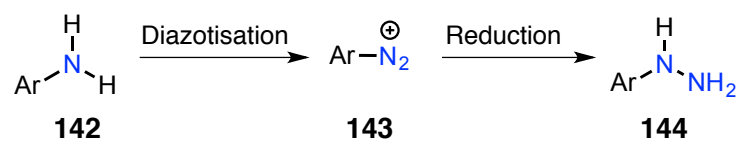
Scheme 3.6: Diazotisation of anilines for accessing hydrazines.

Diazotisation followed by reduction: The simplest and oldest way to access aryl hydrazines **144** that can easily be converted to hydrazides involves the process of diazotization (Scheme 3.6).[15-16] Diazotization of aryl amine **142** is a convenient chemical reaction that often proceeds in quantitative yields to yield desired product. The diazonium salt **143** formed during diazotization can be easily reduced to the corresponding hydrazines by mild reducing agents such as sodium bisulfite, stannous chloride or zinc dust.
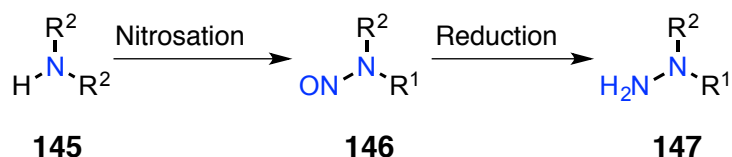
Scheme 3.7: Nitrosation of anilines for accessing hydrazines.

Nitrosation followed by reduction: Another synthetic methodology to access hydrazines **147** starting from secondary amines **145** involves nitrosation (Scheme 3.7). The main drawback with the synthesis of nitrosamines **146** is the associated with its toxicity. After nitrosation of the amine the reaction is followed by reduction with zinc/acetic acid or mild reducing agents like hydrogen in the presence of a catalyst, $LiAlH_4$, $NaHSO_3$ etc. that makes this method to have wide scope.[16-17] The amines **145** utilized can be aliphatic, mixed aliphatic/aromatic and aromatic 1,1-disubstituted hydrazines to afford the corresponding hydrazine **147** in moderate to high yield.[18]
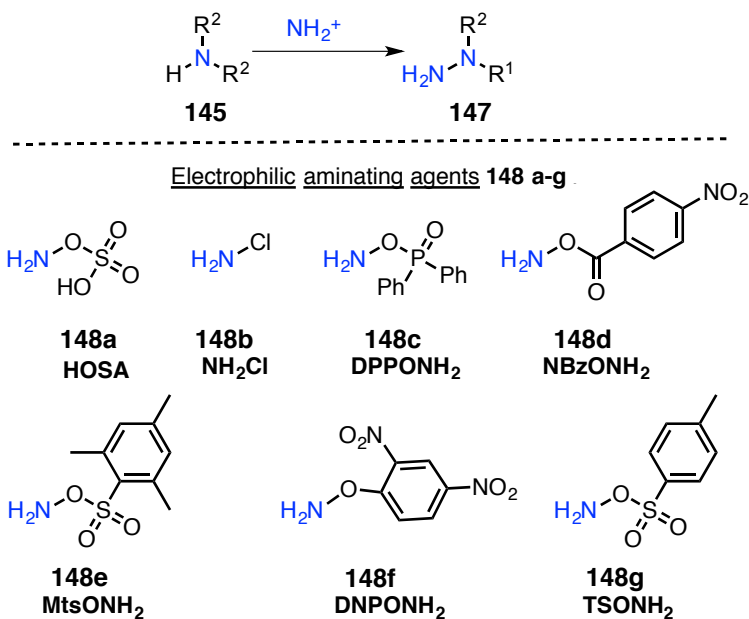
Scheme 3.8: *N*-Amination of amines for synthesis of hydrazines.

N-Amination: Electrophilic *N*-amination is a useful strategy to for accessing for hydrazines. There are a number of aminating reagents **148a-g** (Scheme 3.8) investigated in literature that vary in their relative amination strength.[19-22] Hydroxylamine derivatives are efficient electrophilic NH_2^+ donors of amino group. Among the various aminating reagents hydroxylamine-*O*-sulfonic acid (**148a**, HOSA) is most often employed for *N*-amination. The other reagents evaluated for direct amination of amines include monochloramine (**148b**, NH_2Cl), *O*-(diphenylphosphinyl)hydroxylamine (**148c**, DPPONH_2), *O*-(*p*-nitrobenzoyl)hydroxylamine (**148d**, NbzONH_2), *O*-(mesitylenesulfonyl)hydroxylamine (**148e**, MtsONH_2), *O*-dinitrophenylhydroxylamine (**148f**, DNPONH_2) and *O*-*p*-tolylsulfonylhydroxylamine (**148g**, TSONH_2).[21,23-24]
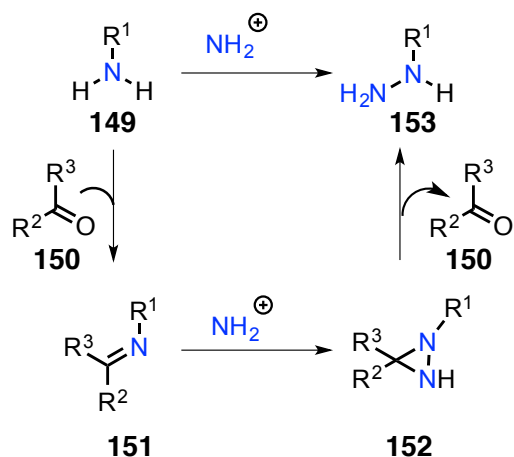
Scheme 3.9: Hydrazine synthesis via diaziridine.

Amination via diaziridines: Carbonyl compounds either aldehydes or ketones **150** (Scheme 3.9) in presence of primary amines **149** and an aminating reagent **148a-g** give rise to alkyldiaziridines. Aminating reagent frequently employed for the synthesis of diaziridine is chloramine **148b** (Scheme 3.8) or hydroxylamine-*O*-sulfonic acid **148a** (Scheme 3.8).[25-26] The diaziridines **152** (Scheme 3.9) are insensitive to the aminating agent. After the cleavage of the diaziridine, the carbonyl compound **150** gets regenerated. Diaziridines provide a generally applicable method for the synthesis of alkylhydrazines **153**.[26]
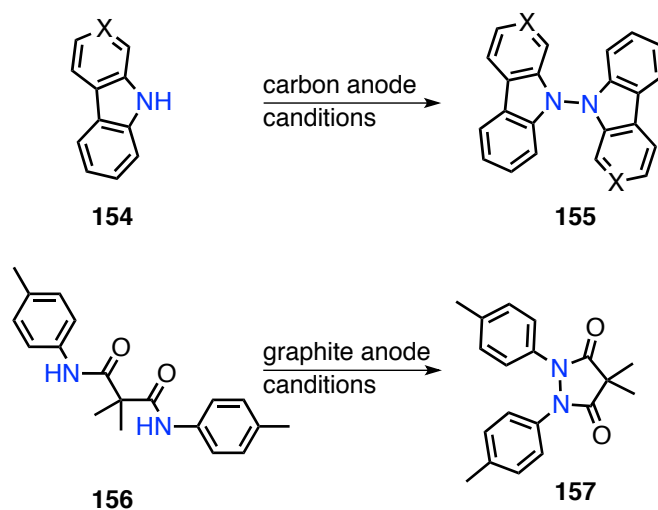
Scheme 3.10: Anodic *N-N* bond formation.

    Electrochemical methods: Stitching the two nitrogens by electrochemical means, has been useful to target the synthesis of many heterocycles. Efforts by Baran and coworkers in developing electrochemical techniques for constructing *N-N* bond has received lot of attention in the recent years (Scheme 3.10).[27-28] One of the possible limitation of this methodology stems from the requirement of dimeric/symmetrical systems to be the final product.

3.2.2. Two *N* synthon approach
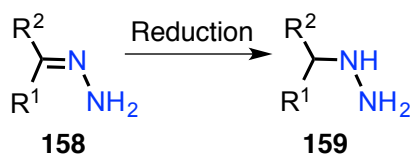
Scheme 3.11: Reduction of hydrazones for synthesis of hydrazines.

    Reduction of hydrazones: Hydrazones **158** can be reduced to give hydrazines **159** that can then be utilized to access hydrazides (Scheme 3.11). A major challenge in this strategy relates to *N–N* bond cleavage during the process of reduction.[16] So in order to avoid further reduction, the distal nitrogen is generally protected. Alternatives to catalytic hydrogenation for mild reduction of hydrazones include $NaBH_4$ and $NaBH_3CN$.

3.3.   Atropisomeric hydrazides

The hindered rotation in certain molecules about single bond results in molecularly chiral isomers/atropisomers.[29] The restricted rotation about a single bond results from sterics and as a result the molecules adopts a non-planar conformation to minimize the repulsive interactions. The most extensively studied atropisomers displaying hindered single bond rotation are the compounds with hindered C–C bond rotation while there are few other atropisomeric systems with hindered rotation about C–*N* and *N*–*N* bond.[30]

The atropisomers are separable on a chiral column when the barrier to single bond rotation is sufficiently high.[29] Stereochemical aspects presented by *N*–*N* bond are unique for hydrazides.[31] The maximum barrier to rotation around *N-N* bond is observed when both the nitrogen is acylated.[32-33] The increased barrier to rotation around *N-N* single bond (Figure 3.1) can be rationalized in terms of a destabilizing interaction arising from eclipsing of the filled orbitals on each nitrogen (sp^2). To sum up, any steric barriers that arise from bulky substitution is outweighed by an electronic barrier and with rigidity enforced by incorporation of the acyl carbonyl groups. [30]

The electronic preference forces the molecule to adopt a torsion angle ~ 90° provided each nitrogen bears different substituents that leads to chirality in the molecule. In addition to experimental evidences, high level *AB* initio calculations have bolstered the role of electronic preferences.[34] The very first report by Riggs and Korsch discussing the plausible reasons for this restricted rotation dates back to 1966. [35]
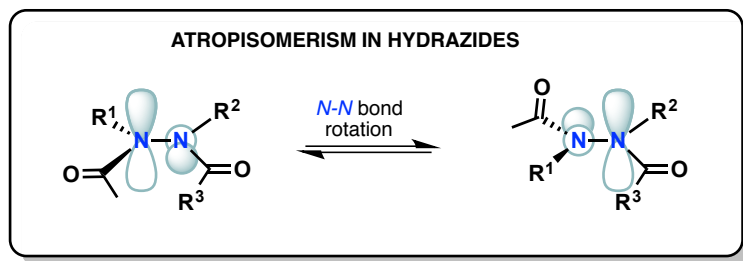
Figure 3.1: Eclipsing of the filled orbitals on nitrogen atoms in hydrazides.

The first report on the restricted bond rotation in acyclic hydrazides **160 a-b** (Chart 3.1) has been documented in the literature by Sutherland and coworkers.[33] Cyclic tetracylhydrazide derivative **160e** studied by the same group reported a barrier to N–N bond rotation of 20 kcalmol^{-1}.[33,36] In case of benzoxazolinone **160f** and quinolinone **160g-h** based hydrazides a low rotational barrier of 18.4 kcalmol^{-1} and 26.2 kcalmol^{-1} was observed.[37]

160a, 23.4 kcal/mol
T_c = 188 °C

160b, 23.5 kcal/mol
T_c = 192 °C

160c, 28 kcal/mol

160d, 23.2 kcal/mol
T_c = 170 °C

160e, 20 kcal/mol
T_c = 120 °C

160f, 18.4 kcal/mol
T_c = 95 °C

160g, 25.3 kcal/mol

160h, 26.1 kcal/mol

160i, 29 kcal/mol
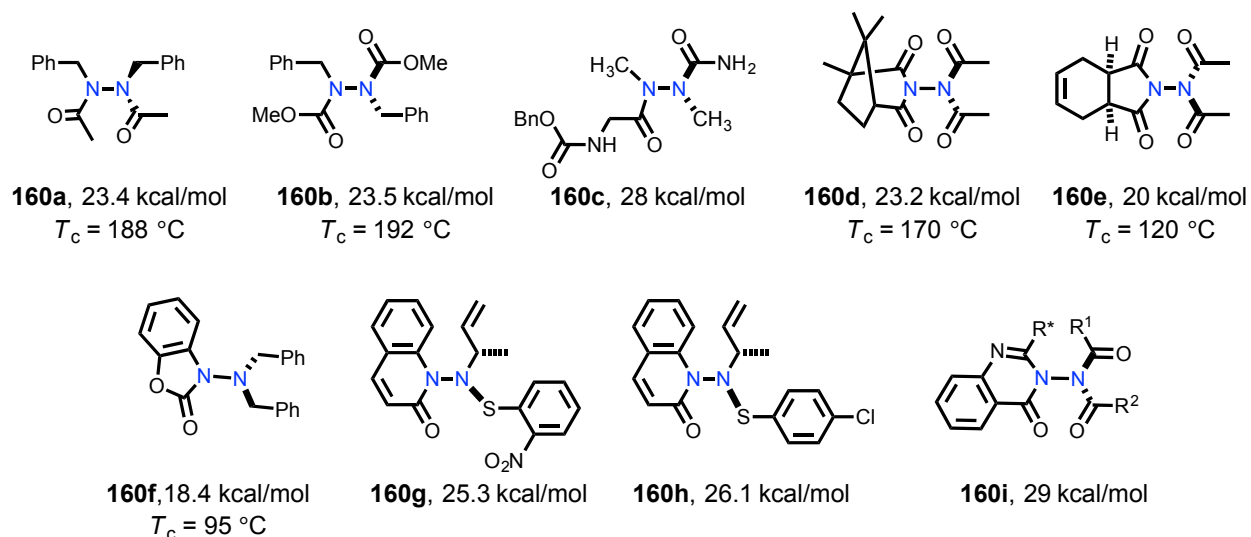
Chart 3.1: Atropisomeric hydrazides **160a-i** and their corresponding rotational barriers reported in the literature.

Verma and Prasad have studied N–N bond rotation in N,N-diacetylcamphorimide **160d** and have reported a barrier to rotation in excess of 18-20 kcalmol^{-1} from variable temperature NMR spectral measurements.[38] Atkinson et al. have reported high barrier (~29 kcalmol^{-1}) to rotation in 3-(Diacylamino)quinazolinones (**160i**, DAQs).[32,37,39-50] The group utilized DAQs as an effective enantioselective acylating agent. On differentially substituting the acyl groups in DAQ, **160i** the N–N bond acted as a chiral axis wherein the planes containing the quinazolinone ring and imide moieties were orthogonal to one another. The barrier to N–N bond rotation was sufficiently high to allow separation of diastereoisomers when a chiral center was incorporated in DAQ. In a recent communication, Gütschow and coworkers reported their study on chiral azapeptides **160c** resulting from chiral N–N bond (Chart 3.1).[51] The group synthesized and analyzed structurally reduced model azapeptides. They observed that the size of the aza-amino acid residue was related to stereochemical stability of atropisomers.

161   **162**
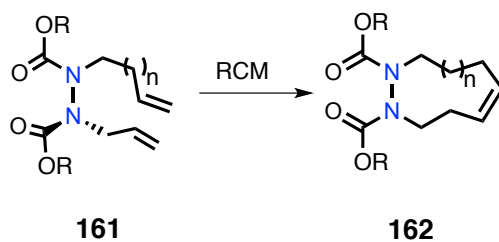
Scheme 3.12: Utilizing *N–N* bond stereodynamics for the synthesis of lactam.

Another interesting report on atropisomeric hydrazides (Scheme 3.12) came from Lee and Kim.[52] The group exploited *N–N* bond stereodynamics to facilitate ring closing metathesis (RCM). CO-*N-N*-CO Dihedral angles of 90° in hydrazide results in *N,N''*-vicinal substituents **161** to be close proximity that sets the geometry in a *gauche*-like arrangement to the desired RCM reaction. Based on these reports we became interested to evaluate atropisomeric hydrazides for classical photoreactions.

3.4. 6π-Photocyclization based on employing photochiral auxiliaries constituting restricted *N-N* bond rotations.

3.4.1. Background on 6π-photocyclization

Intramolecular light induced electrocyclization in a π-conjugated organic molecule that results in a ring system is referred to as 6π-photocyclization.[53-54] The process of electrocyclization occurs via a concerted mechanism. This class of photochemical reactions fall under category of unimolecular pericyclic reactions where in a terminal conjugated π-system is replaced with a new σ-bond. In case of 6π-photocyclization the conrotatory ring closure of π-orbitals (Figure 3.2) on the terminal alkene atoms proceeds in same direction (either clockwise or anti-clockwise).
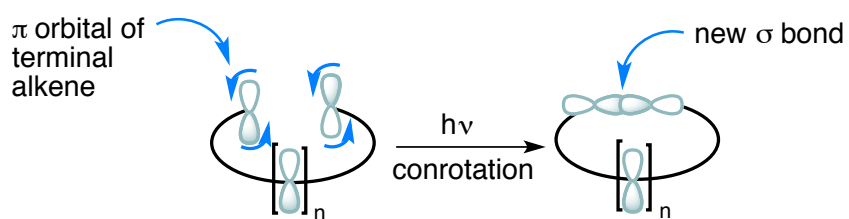
Figure 3.2: Conrotatory ring closure of π-orbitals in photoinduced cyclization.

3.4.2. 6π-Photocyclization of acrylanilides

Studies on photoinduced conrotatory 6π ring closure of acrylanilides has been well documented in the literature as they provide an easy route to access dihydroquinolinone derivatives.[55-58] Dihydroquinolinones belong to class of privileged heterocycles as they are found in many biologically active compounds.[59] The skeleton of dihydroquinolinone is embedded within a large number of pharmaceutical targets, and hence its synthesis has attracted the attention of scientists for a long time. The first report on 6π photocyclization of acrylanilide was reported by Chapman and coworkers.[4] Their work focused on non-oxidative photocyclization of alkyl-substituted acrylic acid anilide **163** (Scheme 3.13).
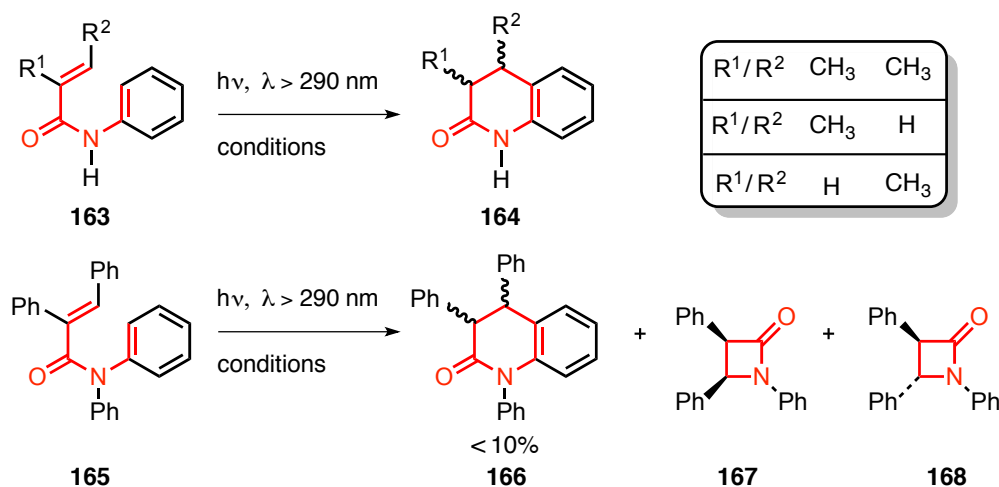
Scheme 3.13: 6π-Photocyclization in acrylanilides reported by Chapman and coworkers.

For irradiation purposes they utilized a 550 W mercury arc lamp equipped with pyrex cut off. They observed that the 6π photocyclization of alkyl-substituted acrylanilides **163** resulted in diastereomeric photoproducts viz *cis* and *trans* 3,4-dihydroquinoline derivatives **164**. However the irradiation of aryl-substituted acrylanilide **165** gave the dihydroquinolinone-based photoproduct **166** as only a minor side product.
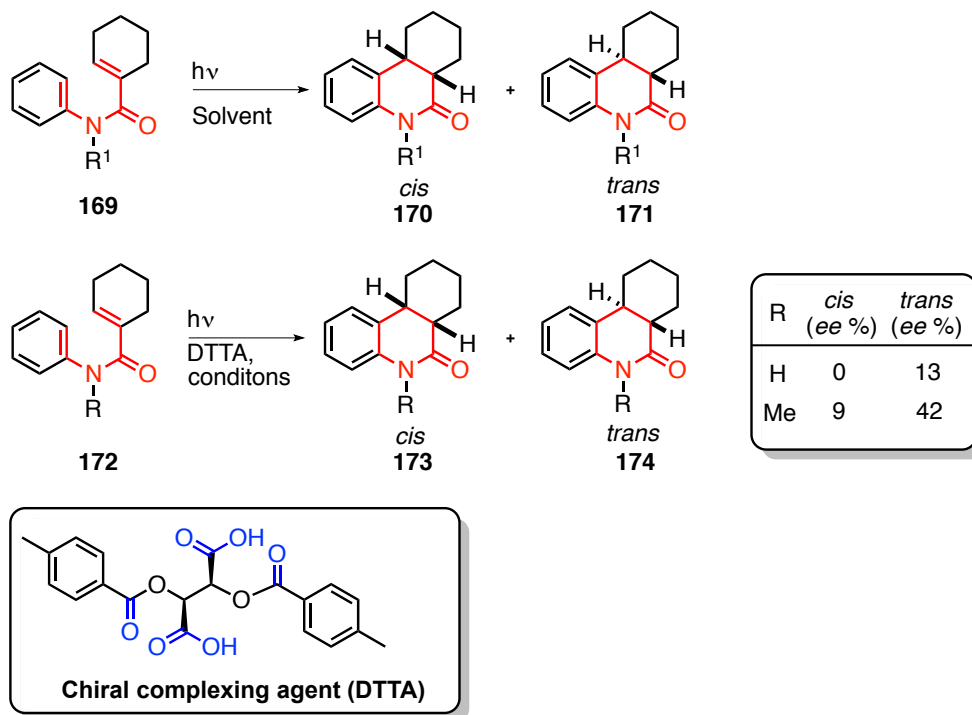
Scheme 3.14: Enantioselective 6π-photocyclization of acrylanilides reported by Ninomiya and coworkers.

In a later report Ninomiya et al. performed an in depth study on 6π-photocyclization of acrylanilides **169** (Scheme 3.14).[58,60-69]They evaluated the influence of the substituents and the role of solvents in affecting the ratio of *cis/trans* photoproducts (**170/171** Scheme 3.14). Their study revealed that employing aprotic solvent afforded the *trans* product **171** and the use of protic solvent yielded the *cis* photoproduct **170**. The initial efforts to evaluate enantioselective 6π-photocyclization of acrylanilides came from Toda and coworkers.[70-71] They studied asymmetric solid-state 6π-photocyclization using inclusion crystal of acrylanilides with tartaric acid-derived 1,4-dioxaspiro-[4.4]-nonanes and 1,4-dioxaspiro-[4.5]-decanes. The photocyclization in the crystalline environment afforded *trans* photoproduct with 98 % enantioselectivity.[70-71] Naito and Ninomiya reported the first enantioselective 6π-photocyclization of acrylanilides in solution.[72] The photocyclization was performed in the presence of a chiral dibasic acid (DTTA) to afford optically active dihydroquinolone **173/174** in low to moderate optical yields (13 - 42%, Scheme 3.14).

Based on chiral supramolecular approach adopted by Toda and coworkers and asymmetric photoreaction performed by Ninomiya and coworkers in solution, Bach and coworkers developed chiral H-bonding catalyst for enantioselective 6π-photocyclization of acrylanilides in solution.[73] The group developed novel chiral Kemp triacid host system (KT) that gave a 57 % *ee* for the *trans* photoproduct **176** and 45% *ee* for *cis* photoproduct **175** (Scheme 3.15).

X	*cis* (% *ee*)	*trans* (% *ee*)
C	30	57
N	10	25

R^1	% *ee*
H	13
CH_3	0

Chiral complexing agent (KT)

Chiral complexing agent (TU)
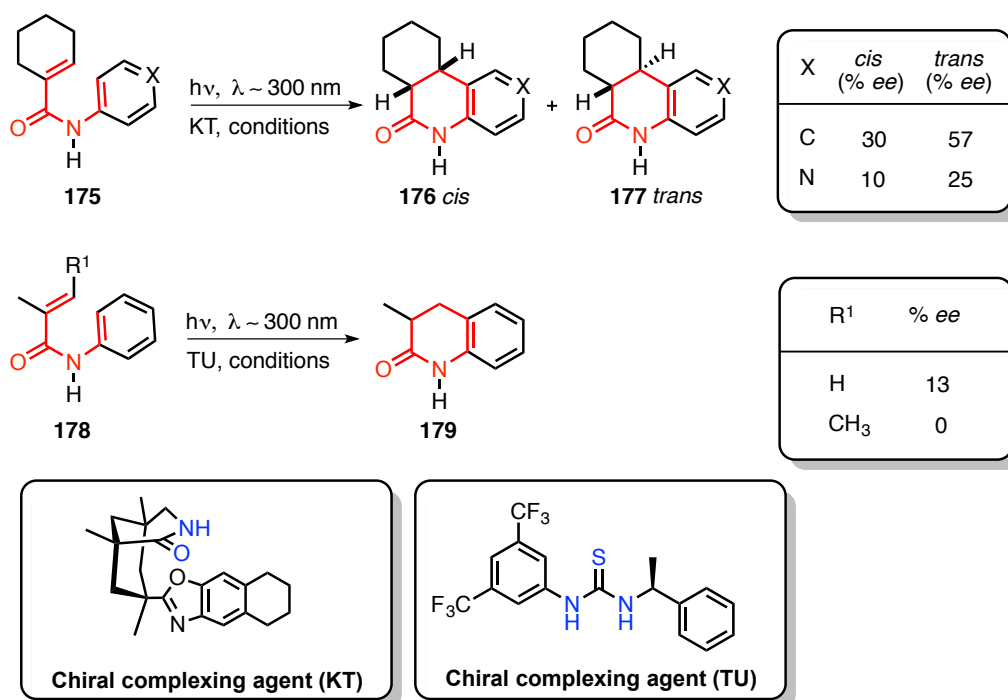
Scheme 3.15: Templated enantioselective 6π-photocyclization of acrylanilides in solution.

Using a similar approach, Sivaguru and coworkers utilized chiral H-bonding thiourea (TU) derived catalyst for 6π-photocyclization of achiral acrylanilides **178** in solution (Scheme 3.15).[74] The photochemical reaction afforded the 3,4-dihydroquinolin-2-one photoproduct **179** with low enantioselectivity (~13% ee). Detailed photophysical studies were performed that explained reasons for low chiral induction during photocyclization. The group reasoned the formation of an enol intermediate that eroded the chirality during the photocyclization and the reactivity of the zwitterionic intermediate that could possibly compete with enol formation and direct hydrogen atom migration for the low enantioselectivity.
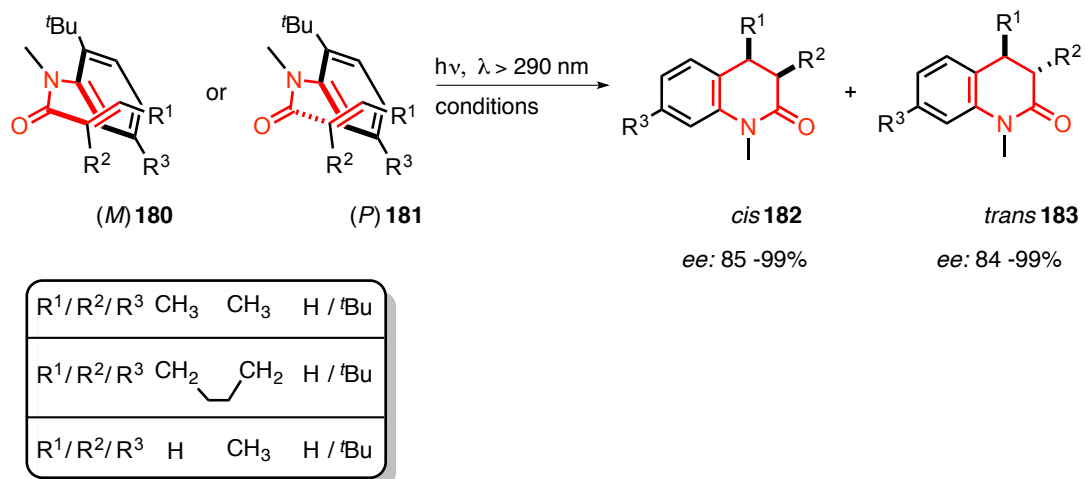
Scheme 3.16: Atropselective 6π-photocyclization of acrylanilides reported by Sivaguru and coworkers.

Sivaguru and coworkers has also evaluated axially chiral chromophores that afforded the highest enantioselectivity so far reported in the literature for 6π-photocyclization in solution.[75-77] They utilized atropisomeric acrylanilides **180**-**181** to achieve conformational restriction during photocyclization (84-99 % ee, Scheme 3.16). In addition they have elaborated the role of confinement (solid-state photoreaction), effect of heavy atom and reactive spin states on 6π-photocyclization of axially chiral acrylanilides.[78]
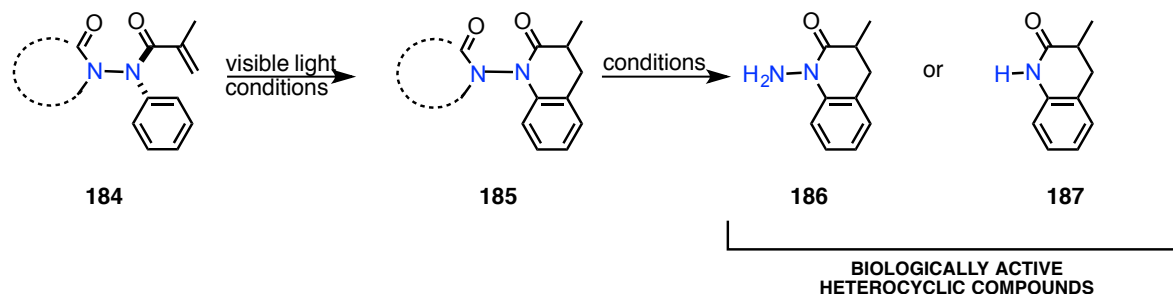
Scheme 3.17: Working paradigm for 6π-photocyclization of *N-N* bond based acrylanilides.

Based on our detailed photochemical investigation on hydrazides (documented in chapter-2) we evaluated novel atropisomeric *N-N* bond based acrylanilides towards sensitized visible light irradiation. In addition the incorporation of chiral *N-N* axis in the acrylanilides could be utilized to understand the role of axial chirality in stereoselective 6π-photocyclization (Scheme 3.17).

After the photocyclization, the dihydroquinolinone-based photoproduct **185** could be subjected to chemical/photochemical modification to afford the *N*-amino **186** or *N*-H derivative **187** (Scheme 3.17). Both the products are useful heterocycles and exhibit biological activity.[59,79-80] Ucar and co-worker have reported the *N*-amino dihydroquinolinones (**186a-b**, AQ) to have potential inhibitory activity against mono-amine oxidase (MAO inhibitor).[81] The diazoheterocyclic **186b**, (R^1 = H) possessing a free amine group, inhibited rat liver MAO-B competitively and reversibly indicating that the small molecule was able to effectively interact with the active site channel of the enzyme. They suggested that the chemical structure of **186b** was similar to that of MAO substrates, which results in strong interaction with the active site channel of MAO-B. The other model compounds evaluated in their study, that lacked the free amine group inhibited the rat liver MAO-B non-competitively and non-reversibly.

3.4.3. Evaluating *N-N* stereodynamics in acrylanilides

The literature precedents on chiral *N-N* axis set the path for us to investigate atropisomeric acrylanilides (Chart 3.2). We started out our initial attempts by first exploring the stereochemistry in acyclic hydrazide **184a**.

184a R^1 = Ph
184g R^1 = Me

184b R^2 = R^3 = Me
(*R*)-**184f** R^2 = Me; R^3 = H
(*R* isomer)

184e R^4 = H
184c R^4 = Me

184d

185a R^1 = Ph
185g R^1 = Me

185b R^2 = R^3 = Me
185f R^2 = Me; R^3 = H
(*R* isomer)

185e R^4 = H
185c R^4 = Me

185d

184h

184i

184j

186

188a R^5=H
188b R^5=Me

189a X = CH$_2$
189b X = CH$_3$

190

191

192

193a

193b

194

195a X = CH$_2$
195b X = CH$_3$

196

197

198a X = CH$_2$
198b X = CH$_3$

199

200
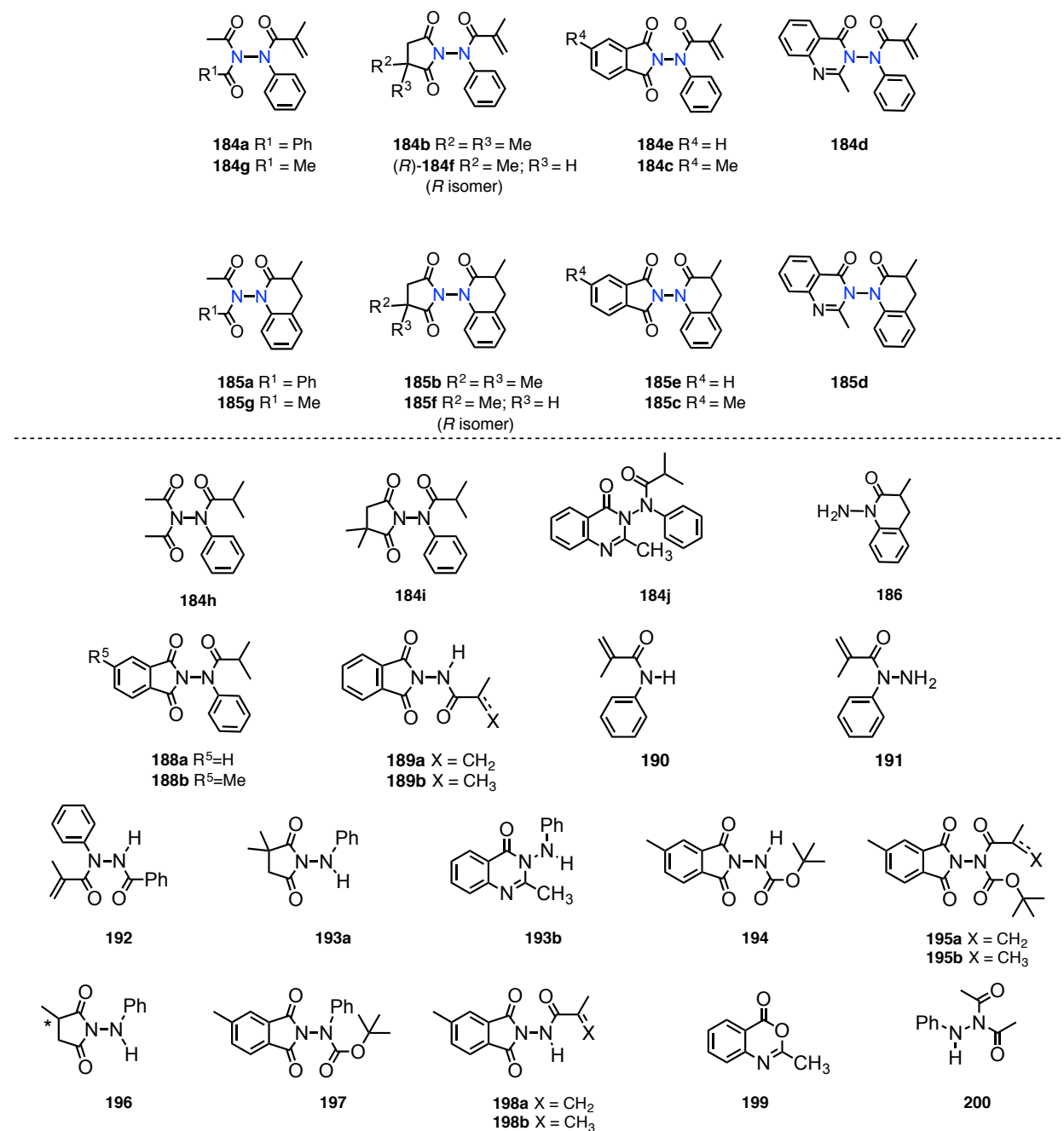
Chart 3.2: *N-N* bond based acrylanilides **184a-g** synthesized for the study, their corresponding photoproducts and other intermediates/reactants utilized in the synthesis of atropisomeric acrylanilides.

It has been reported that if both the nitrogen atoms are monoacylated the *N-N* bond becomes axially chiral in acyclic hydrazides ($\Delta G^{\ddagger}_{rac} \sim$ 23 kcal/mol, T_c = 188 $^{\circ}$C).[33,82] Keeping that in mind we were hoping for an appreciable rotational barrier of asymmetrically substituted acrylanilide which is a triacylated hydrazide. However, to our disappointment we could not observe separation of the atropisomers by HPLC analysis on a chiral stationary phase (Scheme 3.18). We then shifted our focus to develop cyclic hydrazides in order to evaluate the effect of tethering one of the nitrogen atoms. Verma and coworkers have extensively documented studied on restricted *N-N* bond rotation in camphorimide/other dimidyl based hydrazides and have mentioned moderate to high rotational barrier by NMR spectral analysis.[83-88] In case of succinimide **184b** tethered acrylanilide we observed a fast rotation around the *N-N* bond on a separation time scales.[89] The peak shape characteristics reflected two resolved peaks that do not reach the baseline (plateau).[90] This gave us some lead in developing our chiral acrylanilides. We then resorted to design and develop model hydrazides where the plane containing tethered nitrogen atom becomes completely rigid and planar.
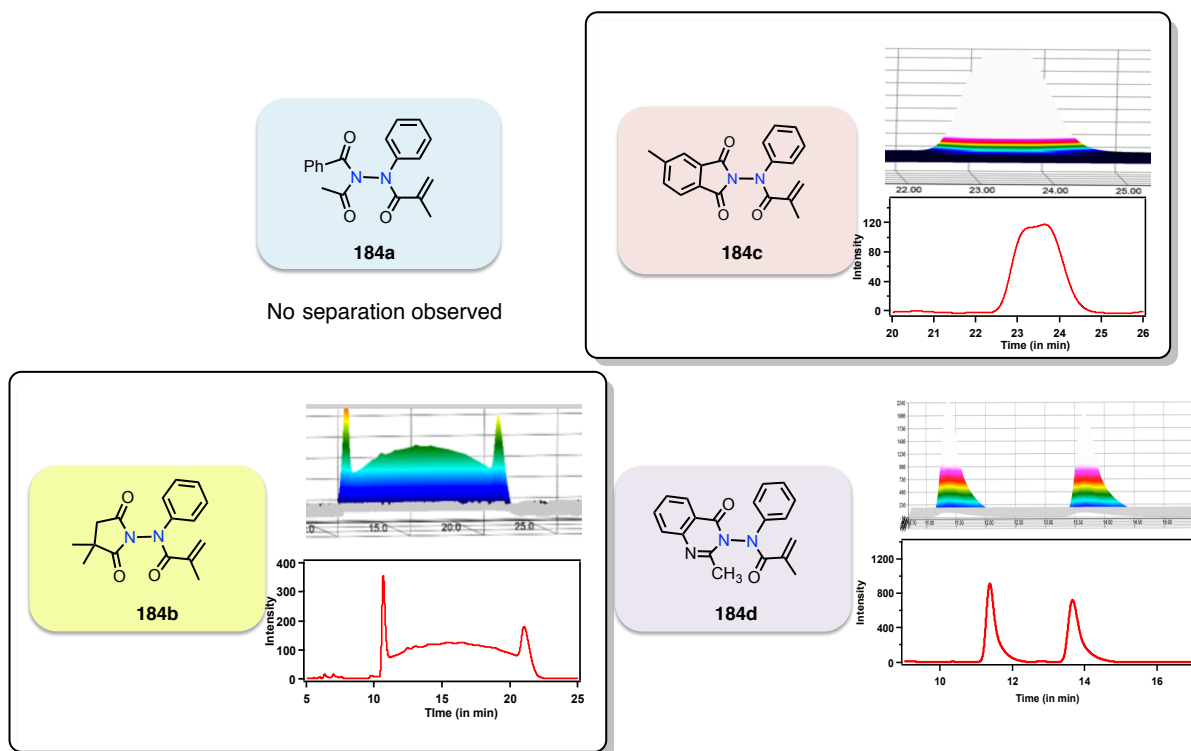
Scheme 3.18: HPLC analysis of chiral *N-N* bond based acrylanilides.

We synthesized chiral phthalimide-derived hydrazide **184c** and the HPLC analysis was again futile for this system. The HPLC trace showed a shallow valley, which alas did not show any base-to-base separation at room temperature (Scheme 3.18). The 5,6-fused aromatic ring system in phthalimide **184c** was then altered to a 6,6-fused aromatic ring system of quinazolinone-based acrylanilide **184d**. In the past, quinazolinone based diacylated hydrazides have been shown to yield stable atropisomers. [37,39,42] [31,46-50] Based on chiral stationary phase based HPLC analysis, the quinazolinone derived hydrazide **184d** showed well-resolved peaks for the individual *P* and *M* atropisomers (Scheme 3.18). It then became critical to ascertain the barrier for racemization, kinetic studies (Table 3.1) revealed a moderate single bond rotation at 45 ^{o}C indicating an appreciable barrier for *N-N* bond rotation at room temperature. The barrier for racemization ($\Delta G^{\ddagger}_{rac}$) in ethyl acetate (polar solvent) was found to be ~24.2 kcal/mol at 45 ^{o}C with a racemization rate constant (k_{rac}) of 16.4×10^{-5} s^{-1} that corresponded to a half-life of racemization ($\tau_{1/2}$) of 1.2 days. Changing the solvent from ethyl acetate to benzene (non-polar solvent), the kinetic data was not effected much. The activation barrier for racemization ($\Delta G^{\ddagger}_{rac}$) at 45 ^{o}C was found to be ~23.9 kcal/mol with a racemization rate constant (k_{rac}) of 2.15×10^{-5} s^{-1} that corresponded to a half-life of racemization ($\tau_{1/2}$) of 0.89 day. This suggests that the *N-N* bond based optically pure atropisomers behave like an inert model system where the molecular movements/interaction from the solvent is negligible.

Table 3.1: Kinetic parameters of racemization barrier for atropisomeric acrylanilide **184d**.[a]

Entry	Hydrazide	Solvent	Kinetic parameters		
			$\tau_{1/2}$ (days)	k_{rac} (s^{-1})	$\Delta G^{\ddagger}_{rac}$ (kcal·mol^{-1})
1	**184d**	Benzene	0.89	2.15×10^{-5}	23.9
2		Ethyl acetate	1.20	16.4×10^{-5}	24.2

[a] Values carry an error of ±5%. The racemization kinetics was followed at 45 ^{o}C by HPLC analysis on a chiral stationary phase.

3.4.4. Synthesis of *N-N* bond based acrylanilides

For the synthesis of acyclic hydrazides **184a** and **184g**, the approach was straightforward. We began our synthesis from *N,N* amino acrylanilide and then constructed the full skeleton (Scheme 3.19). *N*-amination was useful for the synthesis of target hydrazides.[21]
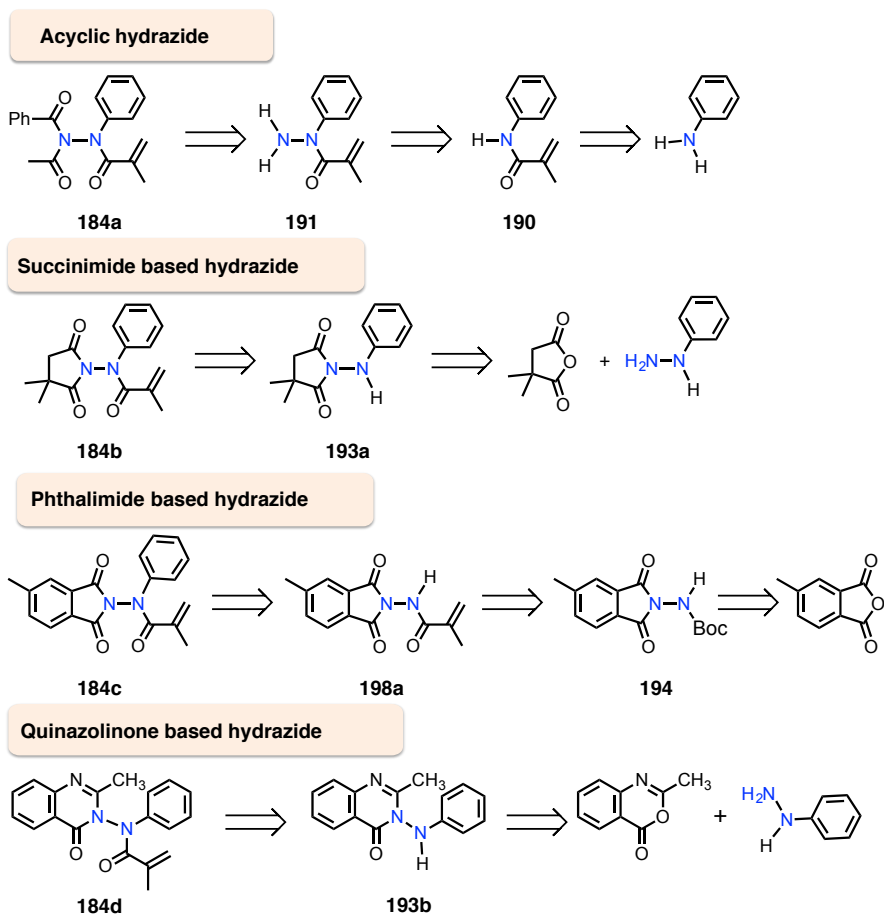
Scheme 3.19: Retrosynthetic analysis for synthesis of atropisomeric *N-N* bond based acrylanilides.

We resorted to monochloramine as the source for NH_2^+ owing to the ease in reagent preparation. In addition, we wanted to circumvent the stability issues related to the synthesis of traditional electrophilic aminating agents.[19-20] The *N*-aminated acrylanilides were found to be unstable for storage and was taken to the next step. The acylated hydrazides showed to be highly stable at room temperature. In case of succinimide based hydrazide **184b** we turned our attention to phenyl hydrazine as the two-nitrogen synthon. Despite of existing literature precedence for the synthesis of *N*-Phenylaminopyrrolidine-2,5-dione derivative[91], we wanted to ascertain that the other likely product of reaction i.e. tetrahydrophenylpyridazinedione[92] derivative was not formed while heating a cyclic imide with phenyl hydrazine under dehydrating conditions. In addition, Conley and coworkers have reported several single crystal XRD structures showcasing ambiguity in literature in regards to the existing synthetic routes for *N*-*N* bond based imides.[93] The synthesis of desired imide based anilide **193a** was confirmed by single crystal XRD analysis. The next step in synthesis was acylation with methacryloyl chloride.

The acylation was not straightforward and required the deprotonation of the *N*-H̲ hydrogen by a strong base. The desired acrylanilide **184b** was successfully synthesized from sequential two steps in high yields. In comparison to succinimide-based hydrazide **184b** the synthesis of phthalimide-based hydrazide **184c** was easier and straightforward. We utilized 2-*tert*-butyl carbazate as the source of two-*N* synthon. The reaction gave us quantitative yields of desired *N*-(tert-Butoxycarbonylamino)phthalimide derivative. The extensive work related to *tert*-Butyl (1,3-dioxoisoindolin-2-yl)carbamate derivatives by groups of Abbas[94] and Brosse[95] were helpful in the synthesis. For phthalimide-based hydrazide the construction of *N*-C(Aryl) bond to synthesize the desired acrylanilide was challenging. Our only concern in regards to synthesis was the radical reactions that could possibly be initiated by double bond in methacryloyl functionality. Our initial trials focused on *N*-arylation with Pd(OAc)$_2$/P(^{t}Bu)$_3$ system was not successful.[96] The seminal work of Barton[97-99] and other groups[96,100-103] directed our attention towards the use of copper/triarylbismuth in the combination with tertiary amine as an effective system for *N*-arylation of hydrazides.

For quinazolinone based hydrazide **184d** the synthetic route adopted was similar to the synthesis of succinimide-based hydrazide **184b**. We started with anthranilic acid, which on ring cyclization afforded us the benzoxazine derivative. Again phenyl hydrazine was utilized as the two-*N* synthon for hydrazide synthesis, starting from the appropriate benzoxazine derivative. It was required to heat phenyl hydrazine with benzoxazine derivative in a pressure tube to obtain the hydrazide **193b** in good yields. The acylation of the hydrazide with traditional acylating reagents was ineffective. Lithiation with *n*-BuLi followed by quenching with acyl chloride was easy and clean. The synthesis of target acrylanilide **184d** was accomplished in three simple and high yielding steps.

3.4.5. 6π-Photocyclization of *N-N* bond based acrylanilides in solution
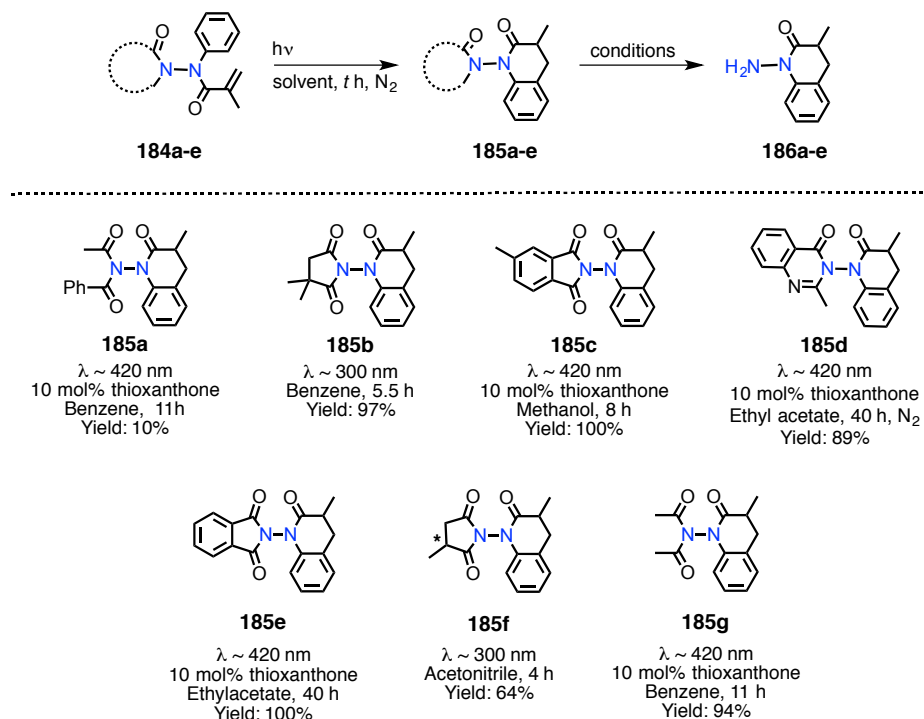
Scheme 3.20: 6π-Photocyclization of *N-N* bond based acrylanilides **185a-g** in solution.

The 6π-photocyclization of *N-N* bond based acrylanilides **184a-g** by UV/Visible light irradiation was facile at room temperature (Scheme 3.20). Except for the succinimide based hydrazide **185b**/**185f** all the other substrates underwent a facile visible light mediated photocyclization. The sensitizer employed for the visible light irradiation was thioxanthen-9-one. The photochemical reactions were clean which was reflected in excellent yields in dihydroquinolinone-based photoproducts **185b-185e**.

For each hydrazide a systematic solvent screening was performed to arrive at the optimized reaction conditions that was suitable for achieving high yields of the photoproducts (Table 3.2). The photocyclization of *N-N* bond based acrylanilides **184a-g** was facile at room temperature by visible light irradiation with thioxanthone (TX) acting as a sensitizer (Scheme 3.20; Table 3.2). Inspection of Table 3.3 and Scheme 3.20 shows that for the acylic hydrazide (**184g**, Table 3.3), phthalimide based hydrazide (**184c**, Table 3.3) and quinazolinone based hydrazide (**184d**, Table 3.3) underwent visible light initiated photocyclization with 1-10 mol% of TX as the photocatalyst/sensitizer to the corresponding dihydroquinolinone photoproduct **185** (Scheme 3.20).

For example, in the case of **184c**, the conversion was 88% and 90% (with 62% isolated yield) for visible light initiated photocyclization with 1-mol% and 10-mol% thioxanthone, respectively (Table 3.3). Succinimide based hydrazide **184b** and **184f** underwent cyclization under direct irradiation (~ 300 nm) as TX sensitization was ineffective. A systematic solvent screening (Table 3.2) was performed to arrive at the conditions that were suitable for achieving high yields of dihydroquinolinone based photoproduct **185**. In the case of acylic hydrazide, benzene was employed as the solvent for large-scale photoreactions. For example in **184a**, 93% conversion was observed under visible light initiated photocyclization with 10-mol% of TX. For cyclic hydrazides, both polar and non-polar solvents were suitable for photocyclization (under direct irradiation). For phthalimide based hydrazides **184e-c** both polar and non-polar solvents were effective with near quantitative conversions (Table 3.2). In case of the quinazolinone based acrylanilide **184d** the EtOAc and MeCN were an optimal solvents with 90% and 76% conversions (Table 3.2), respectively solvent for sensitized 6π photocyclization for all the substrates under study. Large-scale visible light initiated photocyclization of acrylanilide **184e** was performed under optimized conditions (EtOAc as solvent) in Rayonet Reactor equipped with ~420 nm tube lights with 10-mol% TX that gave product photoproduct **186** in 40% yield.

The large-scale sensitized photocyclization of acrylanilide **184c** (Scheme 3.21) was performed under optimized conditions in Rayonet Reactor equipped with ~420 nm tube lights. The photoproduct **185c** was then subjected to hydrazine hydrate to remove the phthalimide ring and the reaction proceeded in quantitative yields. This provided us a convenient access to *N*-amino-3,4-dihydroquinoline-(1H)-2-one) **186** which happens to have inhibitory activity (Scheme 3.21).[81]
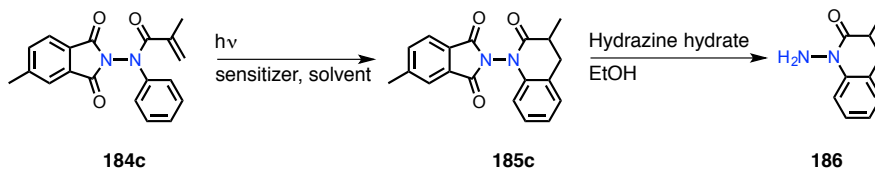
Scheme 3.21: Synthesis of *N*-amino-dihydroquinolinone **186** derivative by removal of photo-auxiliary.

Table 3.2: Solvent screening studies for 6π-photocyclization of *N-N* bond based acrylanilides.[a]

Entry	Solvent	% Conversion				
		184a	**184b**[b]	**184c**	**184d**	**184g**
1	Methanol	35	72	100	0	18
2	Acetonitrile	-[c]	93	94	76	0
3	Ethyl acetate	8	80	69	90	18
4	Benzene	93	96	93	<10	12
5	Methylcyclohexane	-[c]	51	-[c]	0	-[c]

[a] Irradiations at ~420 nm in a Rayonet reactor (16 tubes × 14 W each) with HPLC grade solvents with 10 mol% thioxanthone. [**184a**] = 3.84 mM, hν time = 11 h; [**184b**] = 3.84 mM, hν time = 5.5 h; [**184c**] = 3.12 mM, hν time = 8 h, [**184d**] = 3.84 mM, hν time = 30 h and [**184g**] = 3.1 mM, hν time = 11 h. Reported values are an average of a minimum of 3 trials (±5% error). % Conversions were calculated by ^{1}H-NMR spectroscopy using triphenylmethane as an internal standard. [b] Irradiations at ~300 nm in a Rayonet reactor (16 tubes × 12 W each). [c] Decomposition was observed.

Table 3.3: Visible-light mediated photocyclization of *N-N* bond based acrylanilides with different loading levels of the thioxanthone (TX). [a]

Entry	TX(mol%)	% Conversion[b]			
		184c	**184d**	**184e**	**184g**
1	0	7	0	0	0
2	1	88	0	32	13
3	5	-	80	69	63
4	10	90(62)	90(40)	94(76)	88(49)

[a] Irradiations at ~420 nm in a Rayonet reactor (16 tubes × 14 W each) with HPLC grade solvents with 10 mol% thioxanthone. [**184e**] = 3.26 mM, hν time = 40 h; [**184g**] = 3.84 mM, hν time = 11 h; [**184c**] = 3.12 mM, hν time = 8 h and [**184d**] = 3.84 mM, hν time = 30 h. Reported values are an average of a minimum of 3 trials (±5% error). % Conversions were calculated by ^{1}H-NMR spectroscopy using triphenylmethane as an internal standard. [b] Isolated yields reported in parenthesis.

3.4.6. Atropselective photoreaction of *N-N* bond based acrylanilides in solution

The phthalimide-derived hydrazide **184c** was evaluated towards enantioselective 6π-photocyclization. Since the HPLC separation of the hydrazide showed a peak with a shallow valley, the tail ends of the broad peaks were separated using HPLC on a chiral stationary phase.

stereoisomer **184c**   racemic photoproduct **185c**
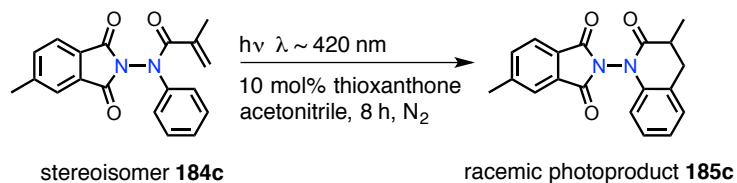
Scheme 3.22: 6π-Photocyclization of chiral phthalimide based *N-N* bond derivative.

The sensitized photoreaction of the separated hydrazide resulted in racemic product (Scheme 3.22). There were two possible explanations for that to happen: (a) the separated hydrazide could have undergone racemization during irradiation (as we did not have racemization barrier for this hydrazide) or (b) the photocyclization step could have ended by an enol-tautomerization (Scheme 3.23) step that could have eroded the optical purity during phototransformation.

racemic mixture of photoproducts
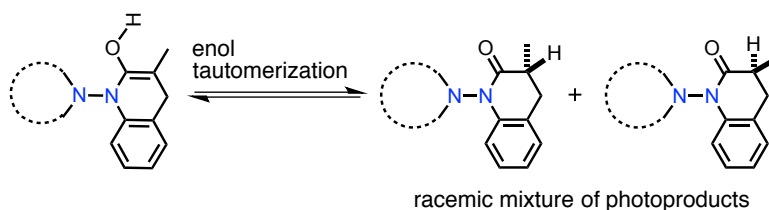
Scheme 3.23: Plausible enol-tautomerization during 6π-photocyclization of acrylanilides.

In order to have an idea of the racemization barrier in phthalimide derived acrylanilide **184c** a corresponding anilide derivative was synthesized **197** (Figure 3.3). However the novel *N-N* bond based anilide did not show any base-to-base separation on any of the available chiral columns (Figure 3.3).
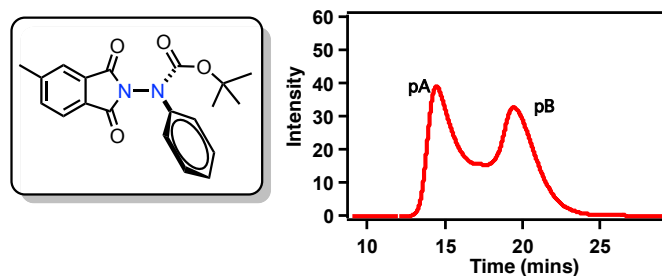
Figure 3.3: Investigating chirality in atropisomeric anilide **197**.

We also evaluated the optically pure quinazolinone-based acrylanilide **184d** towards atropselective 6π-photocyclization. We knew the photocyclization took 40 h to undergo a conversion of ~89% and the racemization barrier was ~24.2 kcal/mol at 45 $^{\circ}$C ($\Delta G^{\ddagger}_{rac}$) in ethyl acetate. We irradiated the optically pure *P* and *M* atropisomers in solution of ethyl acetate at -10 $^{\circ}$C for 6 h with ~15 mol% of thioxanthone loading. The HPLC traces and NMR spectral analysis confirmed the unconsumed starting material (Scheme 3.24).
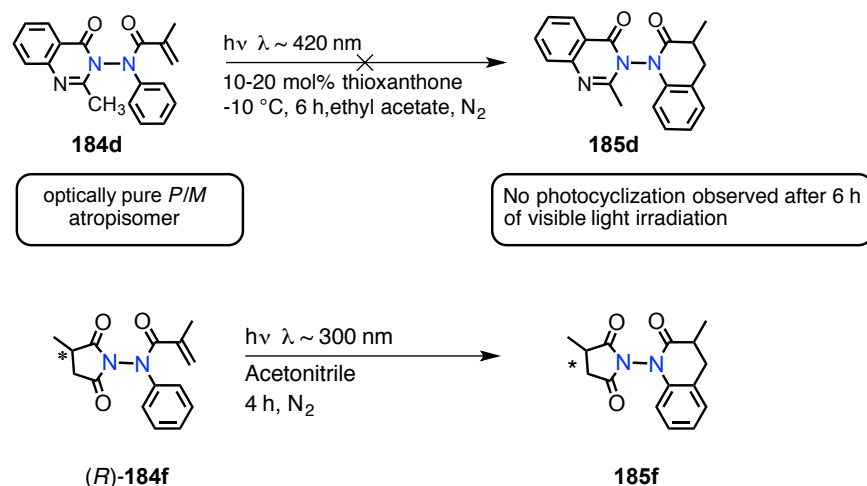
Scheme 3.24: Evaluating chiral acrylanilides for 6π-photocyclization.

In case of succinimide based acrylanilide the direct irradiation of (*R*)-**184f** in acetonitrile afforded the crude reaction mixture. However due to overlapping peaks of the NMR signals, it was difficult to ascertain the role of point chirality and/or axial chirality on the selectivity in the photoproduct.

3.4.7. 6π-Photocyclization of *N-N* bond based acrylanilides in solid state

Since we were successful in obtaining good quality crystals for single crystal XRD analysis for **185b**, **185c** and **185d** we became interested to evaluate hydrazide based acrylanilides towards solid-state phototransformation. DFT calculations were performed at B3LYP/6-31G* level of theory using the cartesian obtained from single crystal XRD structures. The LUMO+1 states for succinimide based acrylanilide showed negligible orbital localization on the C_2 carbon ($C_1=C_2$) of methacryloyl functionality when compared to that observed for phthalimide and quinazolinone derived acrylanilide (Figure 3.4). In the latter two cases an appreciable orbital density was observed on the terminal alkenyl carbon. A closer look at the conformation suggests that only in the case of succinimide based hydrazide, the terminal alkene carbon points away from the phenyl group. Further the measured bond distances from the single crystal XRD structures for the distances between C1/C6 carbon atom(s) of the phenyl ring to the terminal alkenyl carbon for **184c** and **184d** were both within the Schmidt distance (r1 = 3.635 Å and r2 = 3.746 Å; 7, r1 = 3.670 Å and r2 = 3.388 Å). But in case of acrylanilide **184c** the measured bond distance was slightly larger the optimal distance for C6 (phenyl) - C2 (C1=C2) bond (r1 = 3.685 Å and r2 = 4.974 Å).

The photocyclization were conducted under the conditions of direct irradiation. The solid state photocyclization for acrylanilide 5 was performed at two different wavelengths viz. λ~300 nm and λ~245 nm. In both the cases we were unable to observe product formation by ^{1}H NMR analysis. The crystal was stable towards decomposition/change during the irradiation. The stability of the crystal was monitored until 72 h from single crystal XRD analysis. However in case of hydrazides **184c** and **184d**, the solid state photocyclization underwent smoothly and the products were characterized by ^{1}H NMR analysis. The bond distances for photocyclization and/or the conformation of the acrylanilides in the crystalline lattice could be the plausible reason that explains the inability of the substrate to undergo solid-state photocyclization.

Another important feature shown by these hydrazides is the pyramidalization of the nitrogen atom that constitutes the part of ring system. There are a couple of reports in the literature on the single XRD analysis for *N-N* bond based compounds that confirms our observation. Those studies describe such hydrazides to fall under the category of what are called as class of atypical compounds.[104]
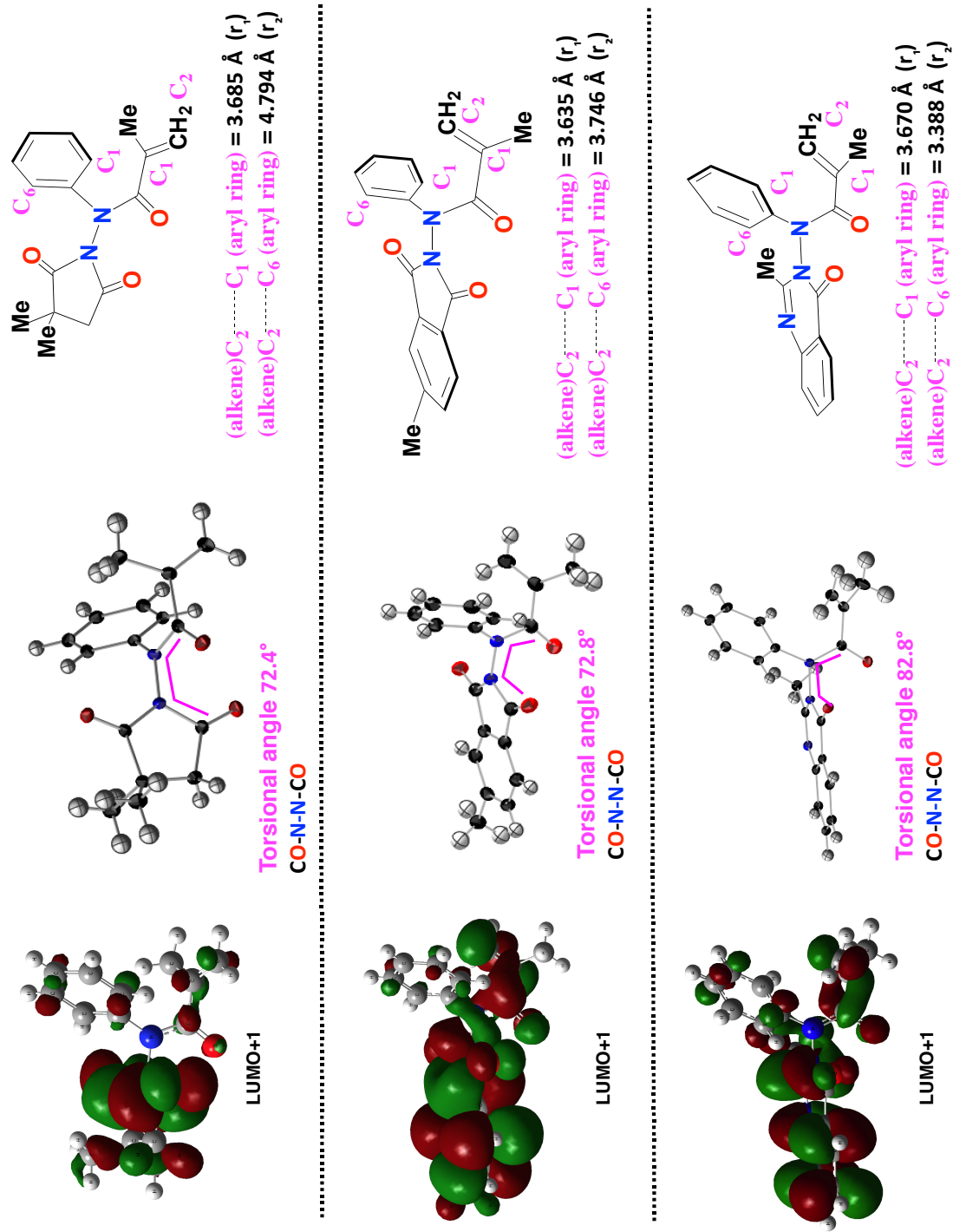
Figure 3.4: Understanding the solid state photochemical reactivity based on orbital density computed with Gaussian 09 at B3LYP/6-31G* and single crystal X-ray structure of **184b**, **184c** and **184d**.

Aitken and coworkers attribute the *N-N* bond twist in *N*-(Acetylamino)phthalimide to intermolecular H-bonding interactions.[104] They observe an unusually large torsional angle θ (CO-*N*-*N*-CO) of ~86º that explains the orthogonality between the two planes containing each nitrogen atom. The torsional angles θ (CO-*N*-*N*-CO) for **185b** was ~72.4º and for **185c** was ~72.8º (Table 3.4). For quinazolinone based hydrazide **185d** the measured torsional angles θ (CO-*N*-*N*-CO) was ~82.8º. In all the cases the planes of the groups on the two nitrogen atoms were almost perpendicular. This is expected from the repulsive interactions between the lone pair of on the two heteroatoms.

Table 3.4: Torsional angle (θ) in atypical crystals of acrylanilides.

Entry	*N-N* bond based acrylanilide	Torsional angle (θ)
1	**185b**	72.4°
2	**185c**	72.8°
3	**185d**	82.8°

To bias the restricted bond rotation towards one atropisomer, (*R*)-**184f** with a point chiral center was evaluated both in solution and in the solid state. To our surprise, the presence of the chiral center, forced crystallization (Figure 3.5, top) of the (*R,M*)-isomer of **184f** leading to optical resolution of the diastereomers. Inspection of the crystal structures showed four molecules per unit cell (Figure 3.5, top), with both *s-cis* (Figure 3.5A and 3.5D) and *s-trans* (Figure 3.5B and 3.5C) OC-C rotamer in the same unit cell. The structural over lay (Figure 3.5-right) indicates that the *N*-phenyl ring exhibits different orientation within the individual rotamers.

As the cyclization distance was optimal in the crystalline state, irradiation of the crystals of (*R*, *M*)-(*R*)-**184f** resulted in the photocyclized product with good diastereomeric ratio ((*R*)-**185f**, based on the HPLC analysis). Slow rotation of *N-N* bond leading to diasteromerization was observed during analysis of the photoproduct (*R*)-**185f** that eroded the diastereoselectivity. Nevertheless, the results clearly showed that combination of restricted bond rotation around *N-N* bond and crystalline confinement can lead to good stereoenrichment in the photoproduct.
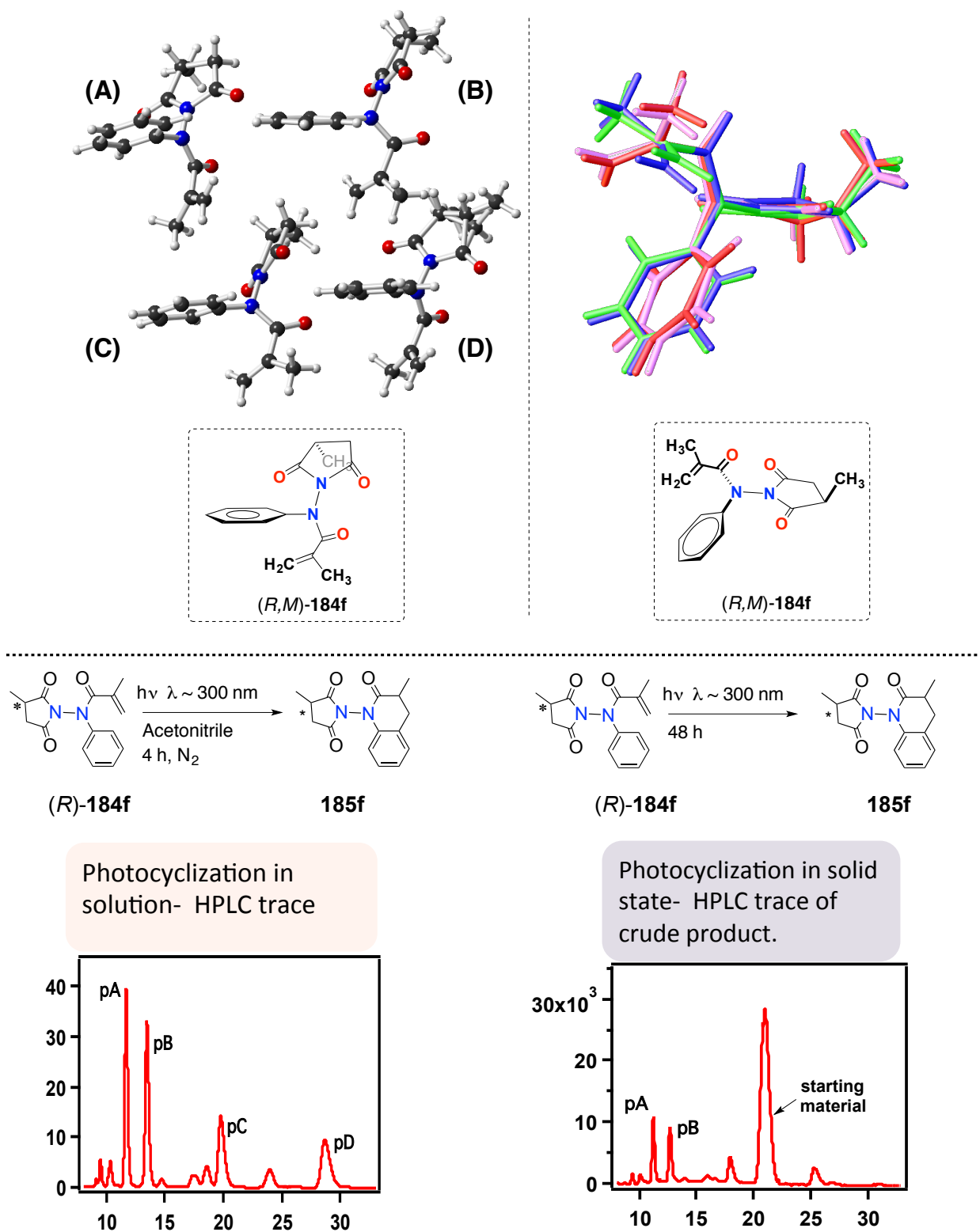
Figure 3.5: (top) Single crystal XRD of (*R*)-**184f** showing the OC-C in the rotamers in the same unit cell. The presence a chiral handle enabled crystallization of optically pure *M*-isomer. (bottom) HPLC traces of the reaction mixture from the photoreaction of chiral acrylanilide derivative in solution and in crystalline environement.

3.4.8. Photophysical investigation on *N-N* bond based acrylanilides

In order to understand the role of *N-N* bond in visible light mediated we performed photophysical studies on all the hydrazides. The triplet energies were calculated from the phosphorescence spectra, the luminescence lifetime confirmed the observed steady-state luminescence was from phosphorescence. Photophysical substrates **184h-j**, and **188a** were synthesized to their influence on the luminescence studies. Based on phosphorescence experiments (Figure 3.6) it was evident that absence/presence of C=C bond in methacryloyl unit in acrylanilides had little to no effect on the triplet energies.
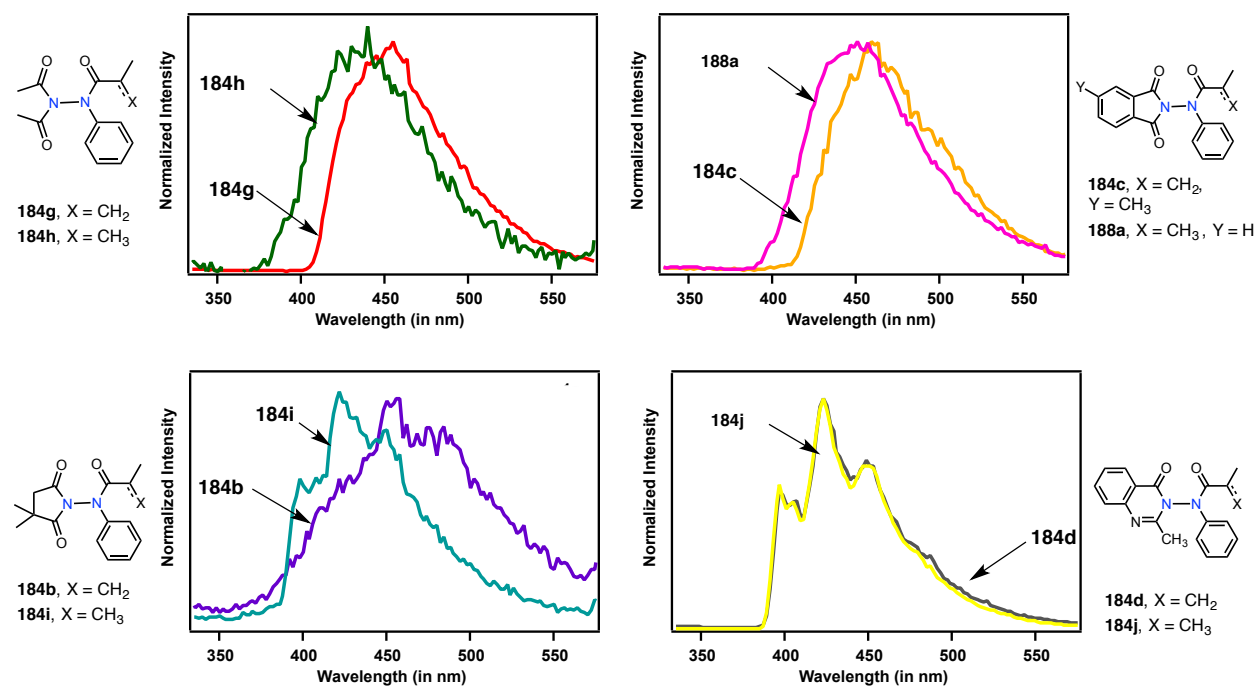
Figure 3.6: Phosphorescence spectra of *N-N* bond based acrylanilides.

3.5. Mechanistic rationale for visible light mediated 6π-photocyclization of *N-N* bond based acrylanilides

The sensitized photocyclization could occur via an energy transfer or electron transfer or a combination of both from photoexcited sensitizer. To understand/study the possibility of electron transfer we carried out electrochemical studies (Table 3.5). The free energy ΔG_{eT} for electron transfer calculated using the Rehm-Weller equation was either close to zero or negative, indicating a possibility of electron transfer mechanism.

Table 3.5: Triplet energy (E_T) and free energy for electron transfer from thioxanthone for various *N-N* bond based acrylanilides.[a]

Entry	Compd	E_{red} (eV)[a]	E_{ox} (eV)[a]	ΔG_{eT} (kcal/mol)[b]	E_T (kcal/mol)[c]	k_q (M^{-1}s^{-1})[d]
1	**184a**	-1.07	1.2	-3.0	-[d]	-
2	**184b**	-1.26	-	1.4	62.7	$(2.2\pm0.1) \times 10^7$
3	**184c**	-1.30	-	2.3	62.3	$(9.7\pm0.2) \times 10^8$
4	**184d**	-1.28	2.05	1.8	72.0	$(1.5\pm0.1) \times 10^7$
5	**184g**	-1.14	2.17	-1.4	62.8	$(2.1\pm0.1) \times 10^7$
6	**184f**	-1.19	-	-0.2	-[d]	-
7	**184e**	-1.26	-	1.4	62.4	$(3.1\pm0.1) \times 10^8$

[a] vs. SEC, working electrode glassy carbon; solvent used was MeCN; [**184a**] = 0.93 mM; [**184b**] = 1.0 mM; [**184c**] = 0.89 mM; [**184d**] = 0.47 mM; [**184g**] = 0.58 mM; [**184f**] = 1.10 mM; and [**184e**] = 0.49 mM. [b] ΔG_{eT} calculated from E_{ox} of thioxanthone of 1.7 V using Rehm-Weller equation. [c] Based on phosphorescence spectra recorded in 2-Methyl THF glass at 77 K. [d] Phosphorescence spectra recorded was not recorded for these entries. [d] TX triplet quenching rate constants determined by laser flash photolysis in acetonitrile.

To ascertain the reaction pathway we carried detailed photophysical studies as well as ascertained the oxidation and reduction potential for examining the feasibility of electron transfer in our system (Table 3.5). The oxidation and reduction potentials of TX and hydrazides **184a-g** were established by cyclic voltammetry measurements (Table 3.5).[105] The free energy for electron transfer from excited TX to **184a-g** was calculated using the Rehm-Weller equation.[105-106] For hydrazides **184a**, **184g** and **184f** the free energy for electron transfer (ΔG_{eT}) was negative (Table 3.5; entries 1, 5 and 6), indicating that an electron transfer mechanism was indeed feasible.[105] For other hydrazides, the free energy for electron transfer (ΔG_{eT}) was positive (Table 3.5; entries 2, 3, 4 and 7), indicating that endergonic electron transfer.[105]

Phosphorescence measurements were performed at 77 K in Me-THF glass to ascertain the triplet energy of acyclic hydrazide **184b**, cyclic hydrazide **184c**, phthalimide based hydrazide **184e-c** and quinazolinone hydrazide **184d**. The Triplet energies (E_T) were calculated from the phosphorescence spectra (Table 3.5).[105] Based on the triplet energy of TX ($E_T \approx 63$ kcal/mol),[107] triplet energy transfer from TX to hydrazide **184a-g** is feasible as their E_T was found be between 62-63 kcal/mol (except of **184d**). The E_T for **184d** was found to be ~72 kcal/mol indicating a triplet energy transfer from excited TX is unlikely.
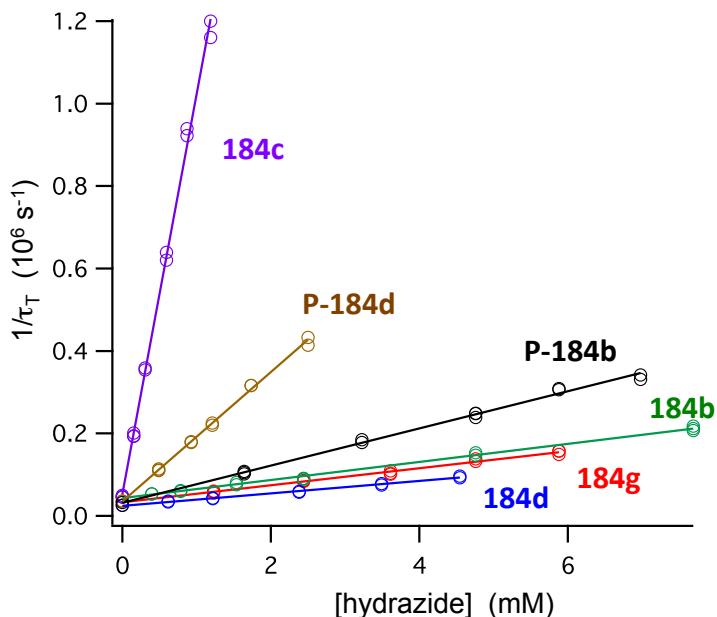
Figure 3.7: Determination of the bimolecular quenching rate constants k_q of quenching of thioxanthone triplet states by hydrazide derivatives using laser flash photolysis (λ_{ex} = 355 nm, 7 ns pulse width). Inverse thioxanthone triplet lifetime determined from triplet absorption decay traces monitored at 620 nm vs. varying hydrazide concentrations in argon saturated acetonitrile solutions.

As photocyclization of **184a-g** was efficient with TX, we investigated its role in promoting the reaction using transient absorption spectroscopy. Laser excitation (λ_{ex} = 355 nm; 7 ns pulse width) of TX in the presence of varying concentrations of **184a-g** in argon saturated acetonitrile solution was investigated to ascertain the bimolecular quenching rate constant (k_q; Figure 3.7). In the case of phthalimide-based system **184e-c** the bimolecular quenching rate constant (k_q) was an order higher in magnitude than the quinazolinone derivative **184d** (Table 3.5; Compare k_q for entries 3 and 7 with 4). As the triplet energy of **184d** is higher than TX the lower k_q is expected. The k_q for acyclic and cyclic substrates **184g** and **184b** were an order lower than the corresponding phthalimide derivative, even though their triplet energies are optimal for energy transfer from TX. In spite of quenching the TX triplet as well as possessing a favorable E_T photocyclization of **184b** failed to occur under visible light irradiation (Table 3.5) but occurred effectively under direct irradiation. We believe that the molecular geometry and/or the non-radiative pathway to be responsible for the diminished reactivity in solution for **184b**.
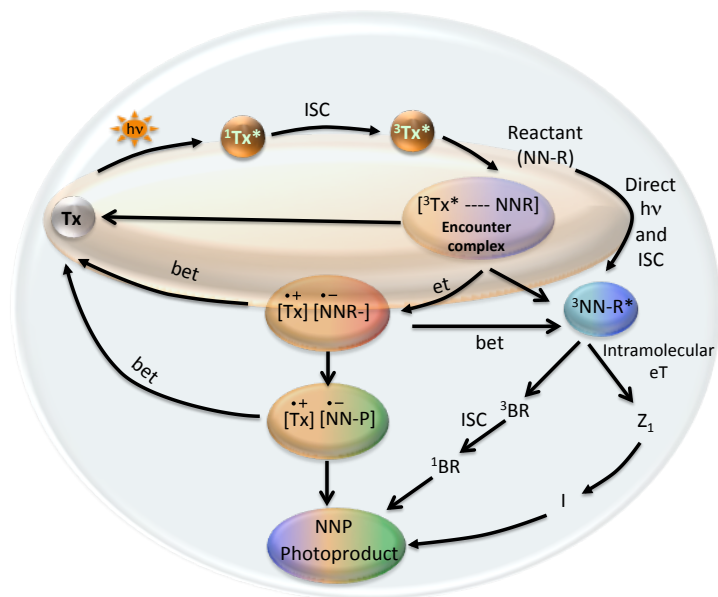
Figure 3.8: Mechanistic model for visible light mediated photocyclization of hydrazide-based acrylanilides.

Based on our reactivity model (Figure 3.8) proposed for hydrazides we can hypothesize the mechanistic details of 6π-photocyclization of hydrazide-acrylanilides. The acrylanilides **184** can either adopt an electron or energy transfer (eT or ET) pathway depending on the electrochemical potential and triplet energy of the hydrazides. If the hydrazide adopts the eT pathway (Figure 3.10) the photoexcited thioxanthone (^{3}TX*) can get reduced to the corresponding TX$^{+\bullet}$ and subsequently afford the hydrazide based radical anion species (**184**$^{-\bullet}$). This hydrazide radical can undergo cyclization followed by re-aromatization by another eT to TX$^{+\bullet}$ to regenerate TX thus making it act as photocatalyst/photosensitizer. This sequential eT results in the formation of photocyclized product **185**. Another possibility that explains the formation of the observed dihydroquinolinone based products **185** by ET mechanism (Figure 3.10).

In ET pathway the photoexcited TX can populate the triplet of hydrazides ^{3}[**184**]* which yields the corresponding 1,2 triplet biradical (1,2-TBR-**184**). This 1,2 biradical species undergoes ring cyclization to afford the 1,4 triplet biradical (1,4-TBR-**184**). The latter undergoes an intersystem crossing to afford the singlet biradical (SBR-**184**). This singlet biradical intermediate undergoes isomerization to give zwitterionic intermediate (ZW-**184**), which can lead to the photoproducts **185** either by a process of re-aromatization followed by tautomerization or by proton transfer.

For direct irradiation, reaction likely proceeds *via* a singlet excited state via ZW-**184** leading to product **185** (Figure 3.10). For direct irradiation, reaction likely proceeds via a triplet excited state through diradical pathway as we observed 77% and 0% conversions for hydrazide **184b** when irradiated for 2 h under nitrogen and oxygen atmosphere, respectively (Figure 3.9). The singlet excited state can also intersystem cross to the triplet albeit with low efficiency and take a pathway as detailed for triplet sensitization with thioxanthone. In the solid state, direct irradiation likely proceeds *via* a singlet-excited state leading to high diastereomeric ratio in product.
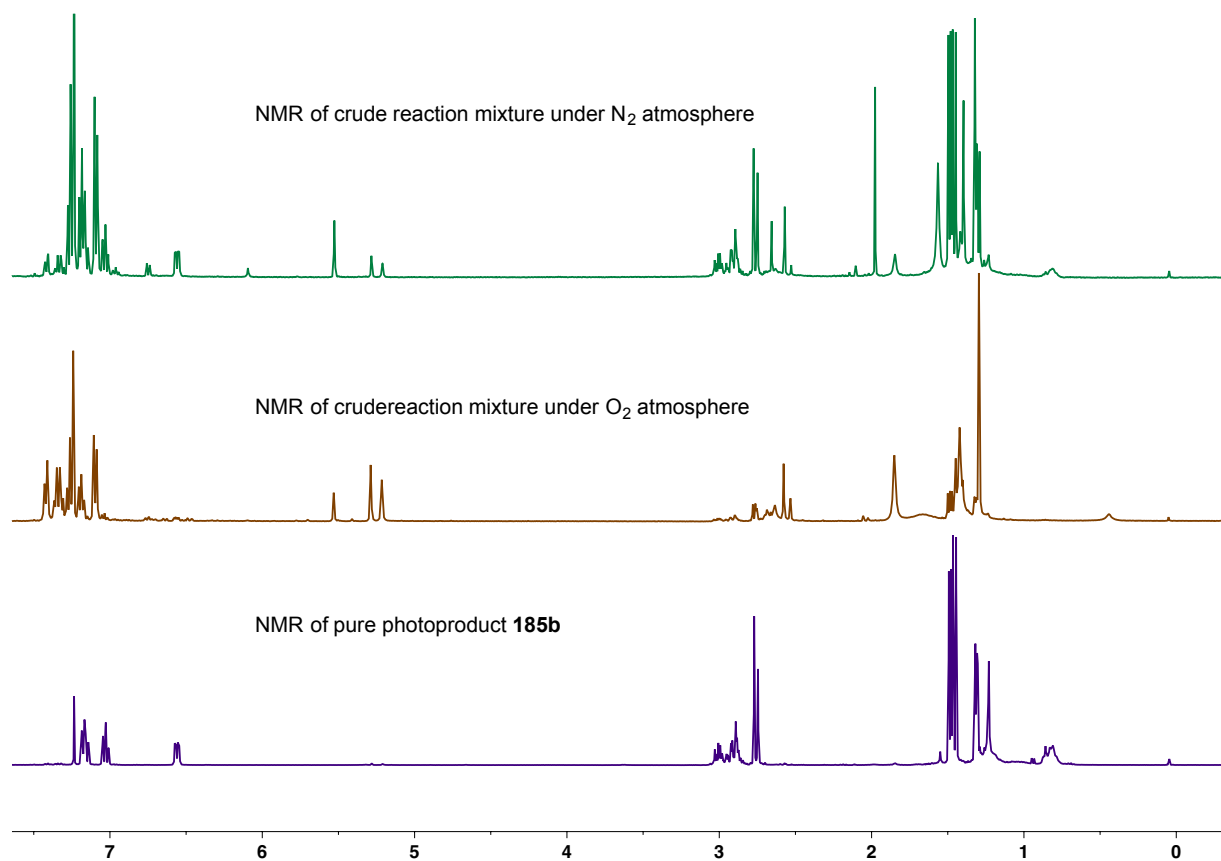
Figure 3.9: NMR traces of reaction mixture for direct photoreaction of **184b** under various reaction atmospheres.
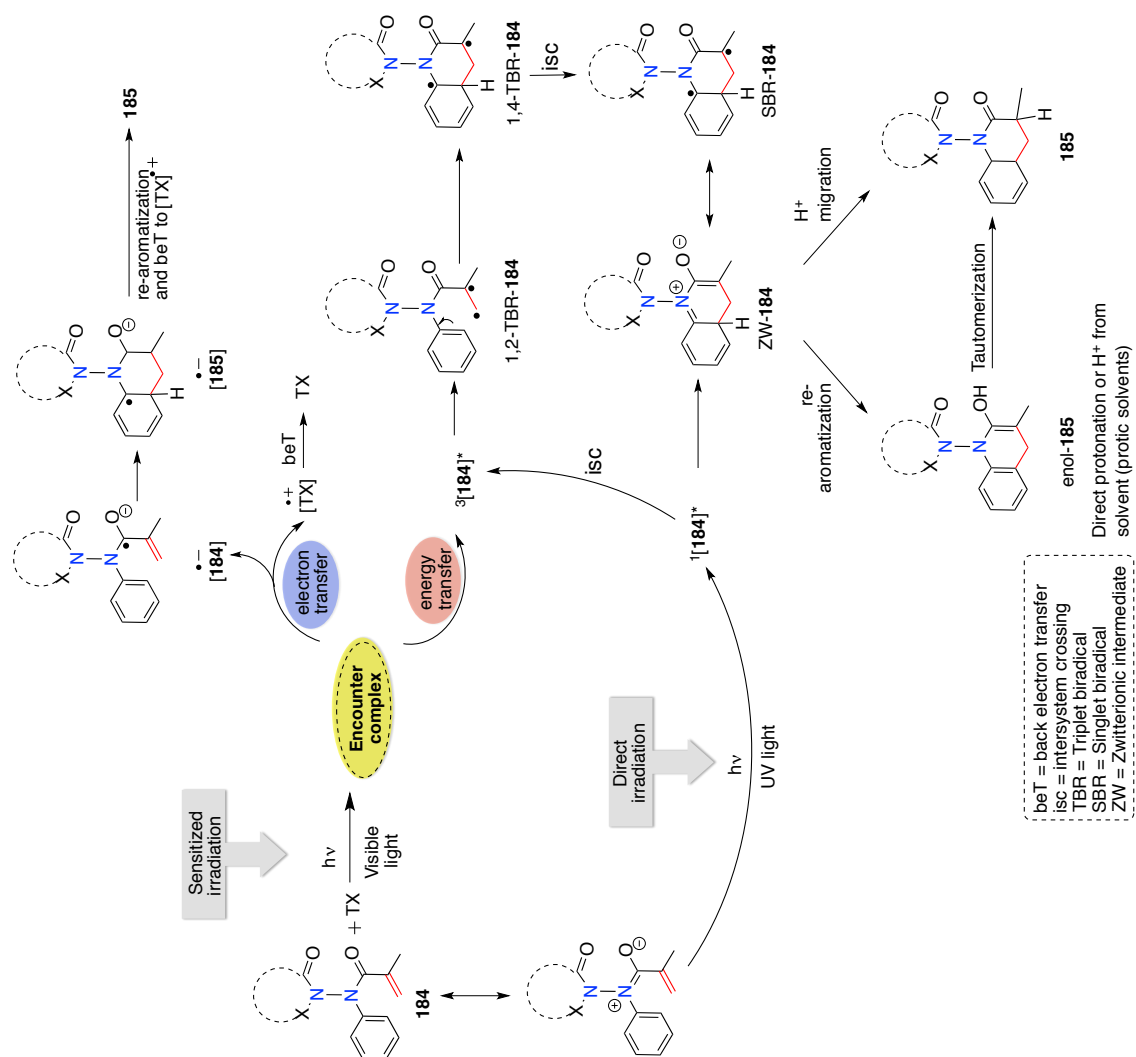
Figure 3.10: Plausible mechanism for visible light mediated photocyclization of hydrazide-based acrylanilides.

224

3.6. X-Ray crystal structure data of hydrazide

Structure determination: Single crystal X-ray diffraction data of the compounds **15, 1** and **2** were collected on a Bruker Apex Duo diffractometer equipped with a Apex 2 CCD area detector at T = 100K. Cu radiation was used in all the cases. All structures were processed using Apex 2 v2010.9-1 software package. Direct method was used to solve the structures after multi-scan absorption corrections.
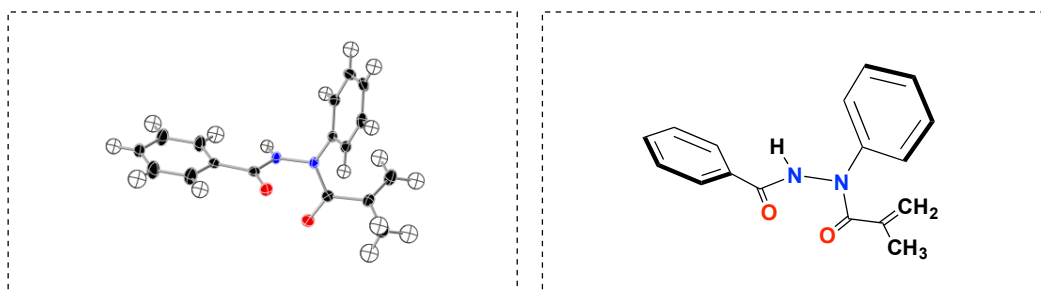
Figure 3.11: Crystal structure of **192** (Crystallized from: hexanes/ethylacetate).
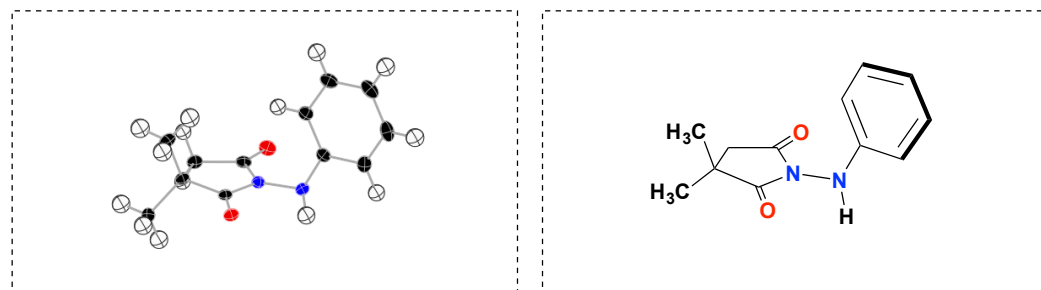
Figure 3.12: Crystal structure of **193a** (Crystallized from: hexanes/dichloromethane).
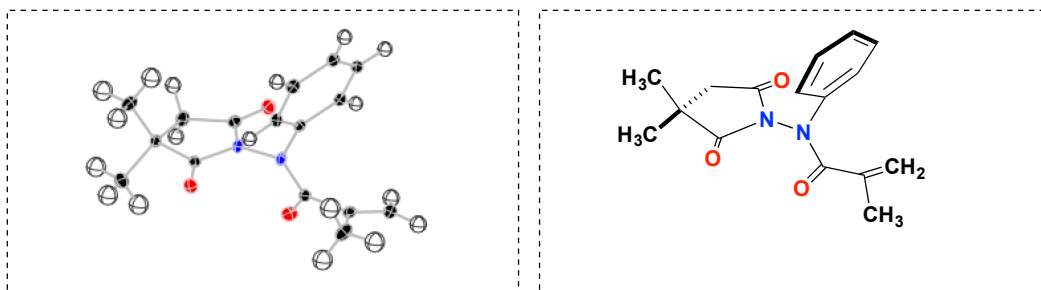
Figure 3.13: Crystal structure of **184b** (Crystallized from: hexanes/ethylacetate).

225
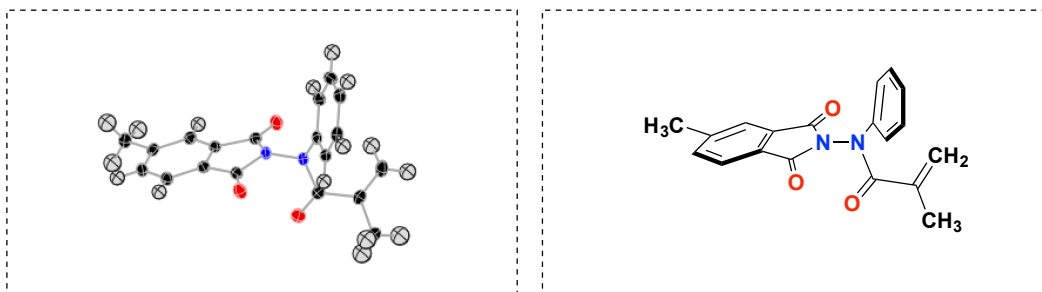
Figure 3.14: Crystal structure of **184c** (Crystallized from: hexanes/ethylacetate).
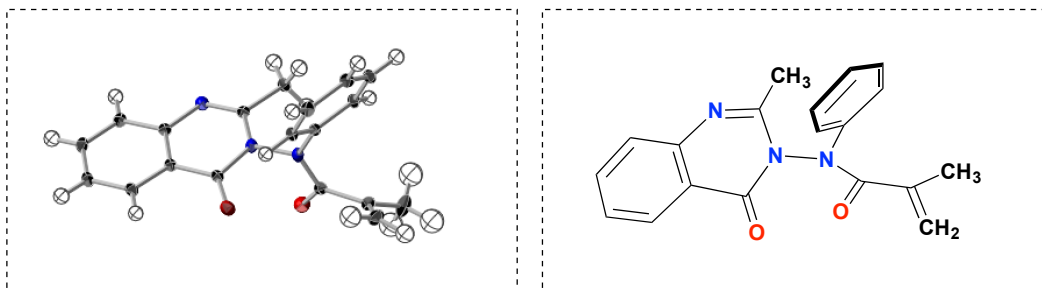
Figure 3.15: Crystal structure of **184d** (Crystallized from: hexanes/ethylacetate).

Table 3.6: Structural parameter table for hydrazides **192**, **193** and **184b**.

Crystals	192	193a	184b
Formula	$C_{16}H_{17}N_2O_2$	$C_{12}H_{14}N_2O_4$	$C_{16}H_{18}N_2O_3$
Formula Weight	280.32	219.26	286.32
Space Group, Z	P 1 21/n 1	P 1 21/c 1	P 1 21/n 1
a/Å	11.0260(4)	9.4560(4)	9.4606(3)
b/Å	7.7415(2)	10.7425(5)	12.6354(4)
c/Å	16.8380(6)	11.1944(5)	12.7086(4)
α /°	90	90	90
β/°	96.290(2)	99.483(2)	105.269
γ /°	90	90	90
V (Å^3)	1428.60(8)	1121.60(9)	1465.54(8)
h, k , l$_{max}$	13, 9,19	11,12,13	11,15,15
ρ$_{calc}$ [mg/mm^3]	1.303	1.298	1.298
μ [mm^{-1}]	0.698	0.728	0.739
Radiation type	CuKα (λ = 1.54178)	CuKα (λ = 1.54178)	CuKα (λ = 1.54178)
F(000)	592.0	468.0	608.0
No. of measured reflections	2489	1980	2582
No. of independent reflections	2172	1793	2429
Final R indexes (I ≥ 2 σ)	R$_1$ = 0.0406, wR$_2$ = 0.1088	R$_1$ = 0.0398, wR$_2$ = 0.1192	R$_1$ = 0.0875, wR$_2$ = 0.0340
R1/wR2 (I ≥ 2 σ) [%]	0.0406/0.1088	0. 0398/0.1192	0.0875/0.0340

Table 3.7: Structural parameter table for hydrazides **184c** and **184d**.

Crystals	184c	184d
Formula	$C_{19}H_{16}N_2O_3$	$C_{19}H_{17}N_3O_2$
Formula Weight	320.34	320.36
Space Group, Z	P -1	P 1 21/c 1
a/Å	8.2022(6)	14.7749(5)
b/Å	8.6904(6)	12.4865(4)
c/Å	12.6628(10)	8.8566(3)
α /°	87.880(3)	90
β/°	75.115(4)	93.211(1)
γ /°	64.0641(3)	90
V (Å^3)	781.49(10)	1631.36(9)
h, k , l$_{max}$	9,10,15	17,14,10
ρ$_{calc}$ [mg/mm^3]	1.361	1.304
μ [mm^{-1}]	0.762	0.698
Radiation type	CuKα (λ = 1.54178)	CuKα (λ = 1.54178)
F(000)	336.0	676.0
No. of measured reflections	2666	2867
No. of independent reflections	2400	2597
Final R indexes (I ≥ 2 σ)	R_1 = 0.0407, wR_2 = 0.1079	R_1 = 0.0368, wR_2 = 0.0990
R1/wR2 (I ≥ 2 σ) [%]	0.0407/0.1079	0. 0368/0. 0990

228

3.7.   Summary and outlook

We have performed a systematic study on novel acrylanilides and what it takes to make stable *N-N* bond based chiral hydrazides. Our work suggested the presence of 6,6 fused ring system results in separable atropisomers. The visible light mediated sensitized photocyclization afforded the dihydroquinolinone derivative in high yields. 6π-photocyclization of novel acrylanilides were also evaluated in solid state to understand the role of conformational preferences in effecting the reactivity in crystalline media. The detailed photochemical, photophysical studies and electrochemical studies confirm our mechanistic model for hydrazides.

Our study has uncovered the unique feature of *N-N* in which restricted bond rotation not only leads to atropisomerism but also the distinctive photochemical features leads to visible light reactivity from the excited state. This combination lends itself to a new approach in which *N-N* bond based substrates can be utilized as a "photochiral auxiliary" as the *N-N* bond can be easily modified after phototransformation. The presence of the point chiral unit enables for resolution of the atropisomers circumventing the use of chiral stationary phase to separate the atropisomers and employ them for photoreactions. The future efforts required are to evaluate other 6,6 fused ring systems for enantioselective 6π-photocyclization.

3.8.   General methods and materials

All commercially obtained reagents/solvents were used as received; chemicals that were purchased from Alfa Aesar®, Sigma – Aldrich®, Acros®, TCI® America, Mallinckrodt®, and Oakwood Products® were used as received without further purification. Spectroscopic grade acetonitrile purchased from EMD® were used for photoreactions and for recording absorbance spectra of various substrates. Unless otherwise stated dichloromethane and acetone were freshly distilled from CaH_2 and potassium carbonate before employing in a reaction. Unless stated otherwise, reactions were conducted in oven-dried glassware under an atmosphere of nitrogen using anhydrous solvents; Photoreactions were performed under N_2 or O_2 atmosphere.

^1H NMR and ^{13}C NMR spectra were recorded on Varian 400 MHz (100 MHz) and on 500 MHz (125 MHz) spectrometers. The residual solvent signal was used as reference. ($CDCl_3$: δ_H = 7.26 ppm, δ_C = 77.2 ppm). Data for ^1H NMR spectra are reported as follows: chemical shift (δ ppm), multiplicity, coupling constant (Hz) and integration. The following abbreviations were used to explain the multiplicities: s = singlet, d = doublet, t = triplet, q = quartet, m = multiplet, quin = quintuplet, sext = sextet, sep = septet, b = broad. In many instances, it was not possible to obtain a signal for the carbonyl carbon, despite long relaxation times and concentrated samples. However these signals are reported wherever possible.

HPLC analyses were performed on Waters® HPLC equipped with 2525 pump or on Dionex® Ultimate 3000 HPLC. Waters® 2767 sample manager was used for automated sample injection. All HPLC injections were monitored using a Waters® 2487 dual wavelength absorbance detector at 254 nm and 270 nm. Analytical and semi-preparative injections were performed on chiral stationary phase using various columns indicated below:

i. Regis® PIRKLE COVALENT (R,R) WHELK–01

     a) 25 cm x 4.6 mm column for analytical injections

     b) 25 cm x 10 mm column for semi-preparative injections.

ii. CHIRACEL® OD-H

     a) 0.46 cm x 25 cm column for analytical injections

     b) 25 cm x 10 mm column for semi-preparative injections.

iii. CHIRALPAK® IC

     a) 0.46 cm x 25 cm column for analytical injections

     b) 10 mm x 25 cm column for semi-preparative injections

iv. CHIRALPAK® AD-H

     a) 0.46 cm x 25 cm column for analytical injections

     b) 25 cm x 10 mm column for semi-preparative injections

Masslynx software version 4.1 was used to analyze/process the HPLC injections. Masslynx software version 4.1 was used for analyzing HPLC injections on Waters®. Chromeleon 7.0 software was used for analyzing HPLC injections on Dionex ® HPLC. Igor Pro® Software version 3.0 was used for processing HPLC chromatograms. The reactants and photoproducts were purified by flash chromatography using silica gel (by standard technique with solvents as indicated. RediSep®, silica gel standard grade: Porosity 60 Å, Particle size: 230 x 400 mesh, Average particle size: 60 to 70 micron). The Retardation Factor (R_f) values were recorded using various combination of solvent systems as mobile phase (as mentioned in the text) and on SORBENT TECHNOLOGIES® Silica Gel TLC plates (200 µm thickness w/UV_{254}).

3.8.1. Photophysical methods

Spectrophotometric solvents were used wherever necessary unless otherwise mentioned. UV-Vis spectra were recorded using Shimadzu 2501PC UV-Vis spectrometer equipped with UV quality fluorimeter cells (with range until 190 nm) were purchased from Luzchem. Absorbance measurements were performed using a Shimadzu UV-2501PC UV-Vis spectrophotometer. Laser flash photolysis experiments employed the pulses from a Spectra Physics GCR-150-30 Nd:YAG laser (355 nm, *ca.* 5 mJ/pulse, 7 ns pulse length or 266 nm, ca 5 mJ/pulse, 5 ns pulse length) and a computer controlled system that has been described elsewhere.

3.8.2 Electrochemistry

Cyclic voltammograms was using HPLC grade acetonitrile as the solvent on a CH instrument. Working electrode employed was glassy carbon, reference electrode was silver chloride and counter electrode was platinum electrode. A solution of tetrabutylammonium hexafluorophosphate (TBAP) was used as the supporting electrolyte. The experiments were performed under constant flow of nitrogen.

3.9. Synthesis of phthalimide based achiral acrylanilide derivative 184e
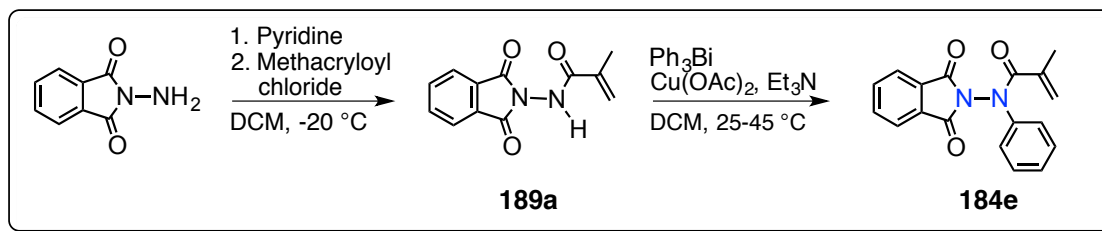
Scheme 3.25: Synthesis of phthalimide based achiral acrylanilide derivative **184e**.

STEP 1
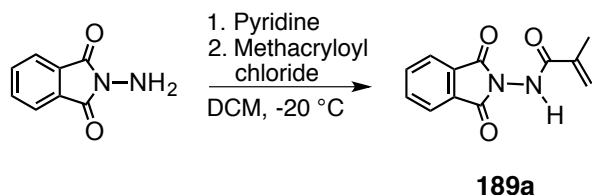
Scheme 3.26: Synthesis of amide derivative **189a**.

N-Aminophthalimide (1 equiv) was dissolved in freshly distilled dichloromethane (DCM) under N_2 atmosphere. To this solution, 1.5 equiv of pyridine was added and the reaction mixture was then cooled to -20 °C, followed by the dropwise addition of methacryloyl chloride (1.2 equiv). After stirring for 15 min, the mixture was brought to room temperature and stirred for 1 h (reaction was monitored by TLC). The reaction was quenched with 5 mL of H_2O, stirred and the organic layer was separated. The organic layer was sequentially washed with DI water (2 × 10 mL), saturated $NaHCO_3$ (2 × 10 mL) and finally with brine. The organic layer was dried over anhyd Na_2SO_4, filtered and the solvent was removed under reduced pressure to yield crude product. The crude product was purified by combiflash using hexanes and ethyl acetate mixture to get the desired amide. The product was characterized by NMR spectroscopy.

TLC condition - R_f = 0.7 (50% ethyl acetate:hexanes). Crystalline solid (Yield = 65%).

^{1}H-NMR (400 MHz, CDCl$_3$, δ ppm): 2.04 (s, 3H), 5.57 (bs, 1H), 5.97 (bs, 1H), 7.74 (bs, 1H), 7.76-7.78 (dd, *J* = 5.6 Hz, 3.2 Hz, 2H) and 7.88-7.90 (dd, *J* = 5.6 Hz, 3.2 Hz, 2H).

Figure 3.16: ^{1}H-NMR (400 MHz, CDCl$_3$, δ ppm) spectrum of **189a**.

<u>STEP 2</u>
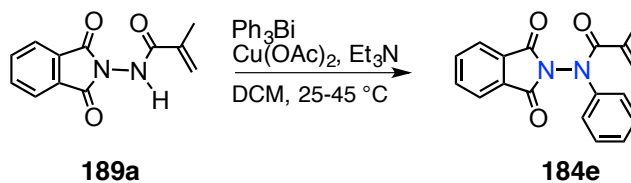
Scheme 3.27: Synthesis of acrylanilide derivative **184e**.

Following the modified procedure reported by Kikugawa et al., a mixture of amide **189a** (1 equiv), triphenylbismuth (2 equiv), cupric acetate (1.5 equiv), and triethylamine (1.5 equiv) was stirred in freshly distilled dichloromethane (DCM) for 1.5 h at room temperature under N_2 protection and then refluxed for 20 h.[103] After completion of the reaction, the solution was diluted with ethyl acetate (20 mL) and filtered through a short celite pad. The filtrate was evaporated under reduced pressure. The crude product was chromatographed on a flash column using ethyl acetate and hexane as eluting solvents.

TLC condition - R_f = 0.7 (50% ethyl acetate:hexanes). Crystalline solid (Yield = 33%).

^{1}H-NMR (400 MHz, CDCl$_3$, δ ppm): 1.89 (s, 9H), 5.22 (s, 1H), 5.35 (s, 1H), 7.28-7.37 (m, 3H), 7.50-7.52 (m, 2H), 7.74-7.76 (m, 1H), and 7.86-7.88 (m, 1H).
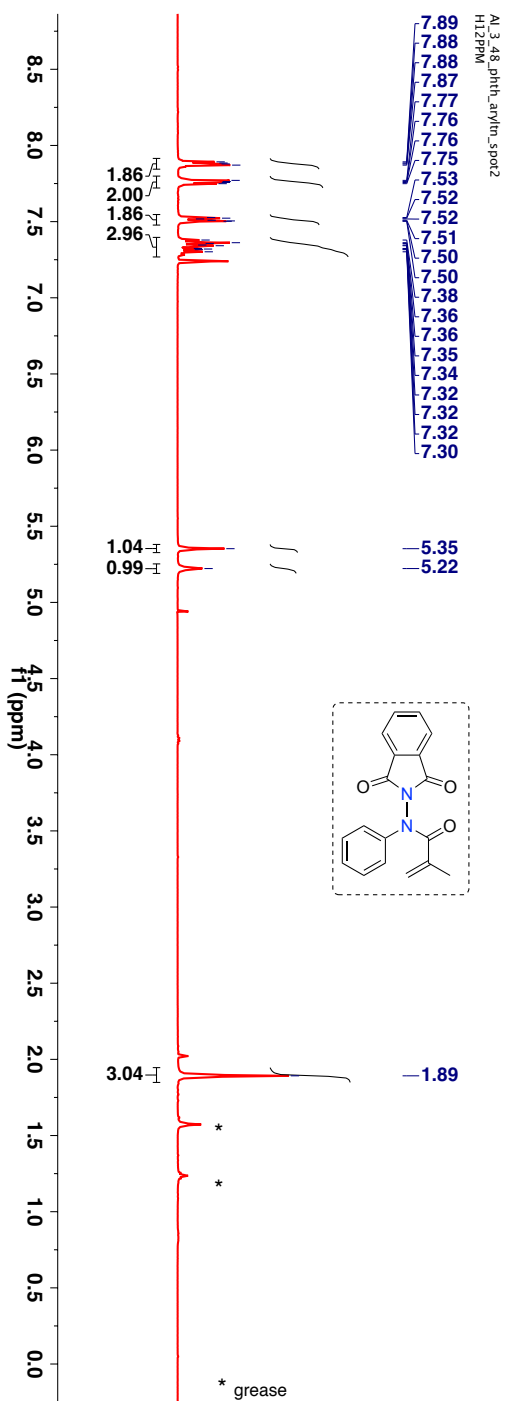
Figure 3.17: ^{1}H-NMR (400 MHz, CDCl$_3$, δ ppm) spectrum of **184e**.

3.10. Synthesis of photophysical acrylanilide derivative 188a
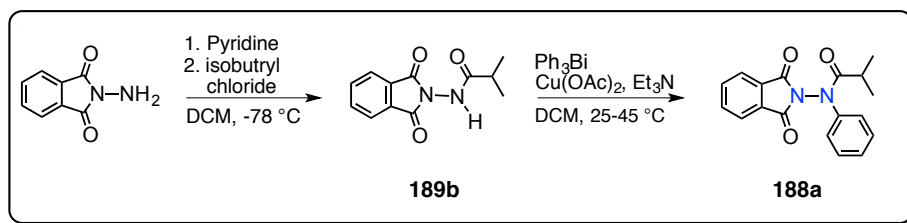
Scheme 3.28: Synthesis of phthalimide based achiral acrylanilide derivative **188a**.

STEP 1
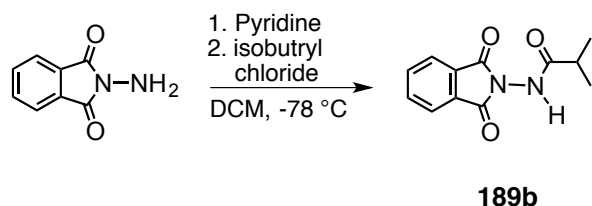
Scheme 3.29: Synthesis of amide derivative **189b**.

N-Aminophthalimide (1 equiv) was dissolved in freshly distilled dichloromethane (DCM) under N_2 atmosphere. To this solution, 1.5 equiv of pyridine was added and the reaction mixture was then cooled to -78 °C, followed by the dropwise addition of isobutryl chloride (1.2 equiv). After stirring for 25 min, the mixture was slowly brought to room temperature. The reaction was quenched with 5 mL of H_2O, stirred and the organic layer was separated. The organic layer was sequentially washed with DI water (2 × 10 mL), saturated $NaHCO_3$ (2 × 10 mL) and finally with brine. The organic layer was dried over anhyd Na_2SO_4, filtered and the solvent was removed under reduced pressure to yield crude product. The crude product was purified by combiflash using hexanes and ethyl acetate mixture to get the desired amide. The product was characterized by NMR spectroscopy.

TLC condition - R_f = 0.3 (50% ethyl acetate:hexanes). Crystalline solid (Yield = 72%).

^{1}H-NMR (400 MHz, CDCl$_3$, δ ppm): 1.19 (d, *J* 6.8 Hz, 6H), 2.56 – 2.63 (sep, *J* 6.8 Hz, 1H), 7.70-7.71 (m, 2H), 7.79-7.82 (m, 2H) and 8.19 (bs, 1H).
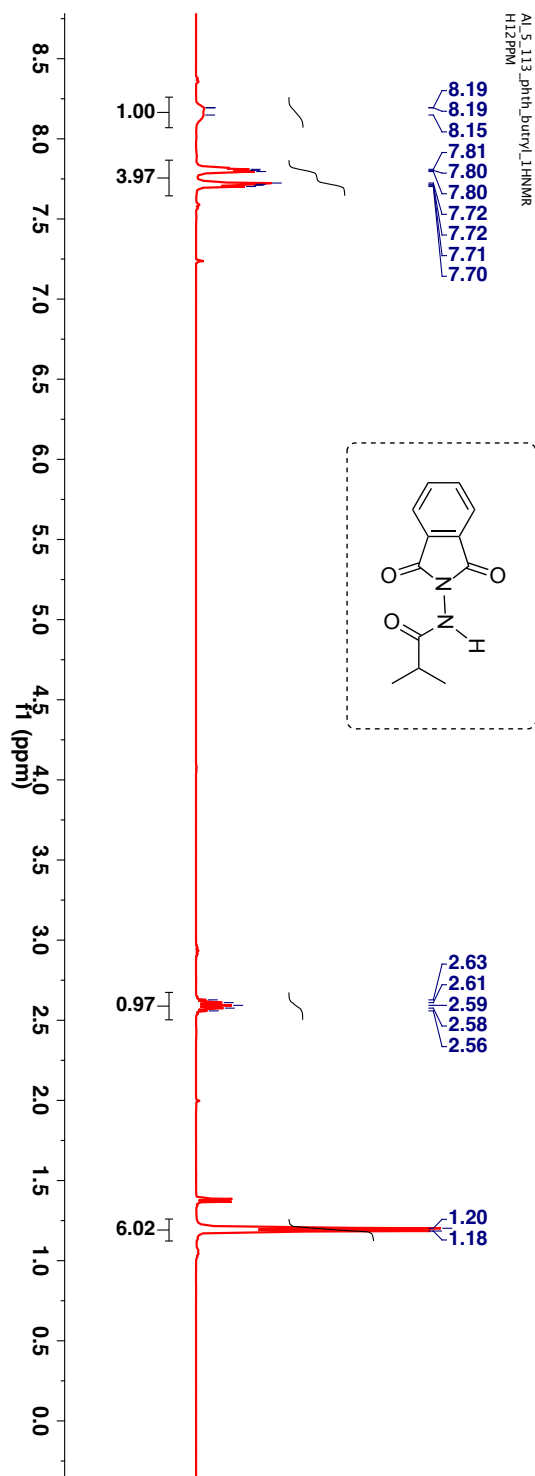
Figure 3.18: ^{1}H-NMR (400 MHz, CDCl$_3$, δ ppm) spectrum of **189b**.

^{13}C-NMR (100 MHz, CDCl$_3$, δ ppm): 19.4, 33.5, 124.1, 130.2, 134.8, 165.5 and 176.4.
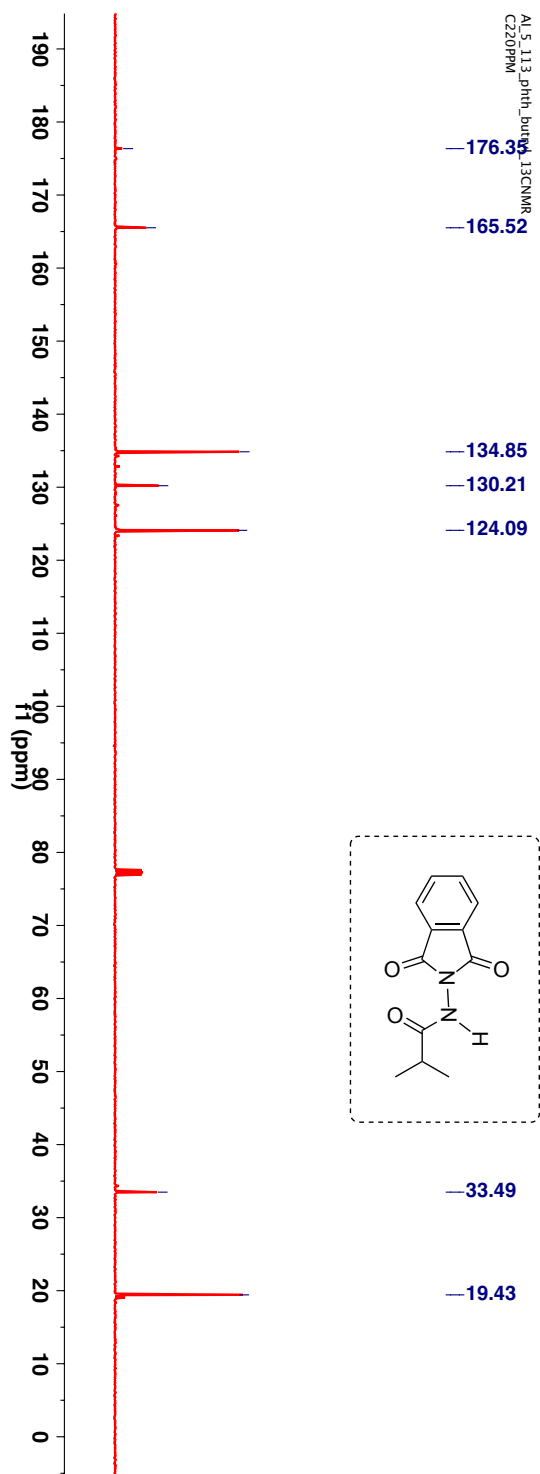
Figure 3.19: ^{13}C-NMR (100 MHz, CDCl$_3$, δ ppm) spectrum of **189b**.

<u>Step 2</u>
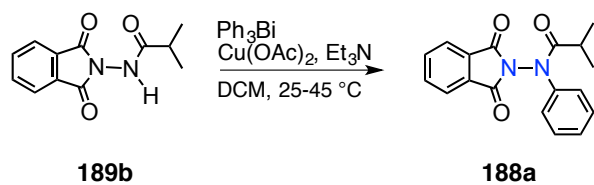
Scheme 3.30: Synthesis of acrylanilide derivative **188a**.

Following the modified procedure reported by Kikugawa et al., a mixture of amide **189b** (1 equiv), triphenylbismuth (2 equiv), cupric acetate (1.5 equiv), and triethylamine (1.5 equiv) was stirred in freshly distilled dichloromethane (DCM) for 1.5 h at room temperature under N_2 protection and then refluxed for 20 h.[103] After completion of the reaction, the solution was diluted with ethyl acetate (20 mL) and filtered through a short celite pad. The filtrate was evaporated under reduced pressure. The crude product was chromatographed on a flash column using ethyl acetate and hexane as eluting solvents.

TLC condition - R_f = 0.5 (20% ethyl acetate:hexanes). Crystalline solid (Yield = 58%).

^{1}H-NMR (400 MHz, CDCl$_3$, δ ppm): 1.09 (d, *J* 7.6 Hz, 6H), 2.64 – 2.71 (sep, *J* 6.8 Hz, 1H), 7.39-7.44 (m, 3H), 7.66 - 7.71 (m, 4H) and 7.81 – 7.84 (m, 2H).
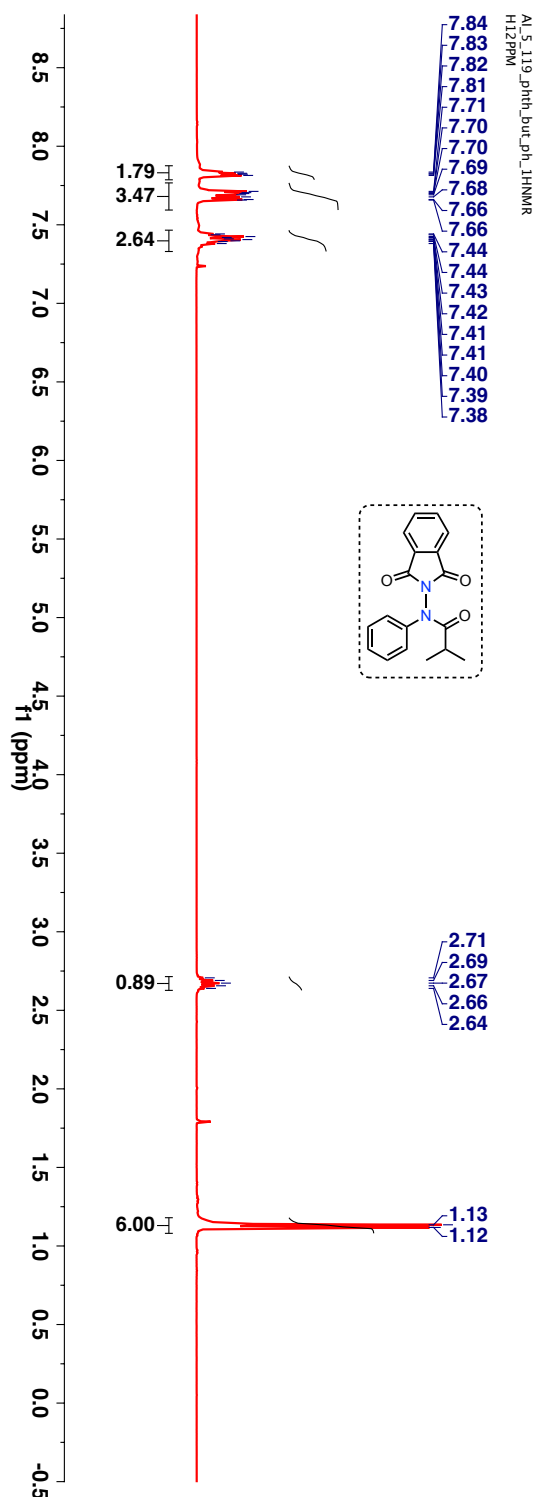
Figure 3.20: ^{1}H-NMR (400 MHz, CDCl$_3$, δ ppm) spectrum of **188a**.

¹³C-NMR (100 MHz, CDCl₃, δ ppm): 19.5, 31.1, 124.1, 129.1, 129.7, 130.0, 130.3, 134.8 and 140.5.
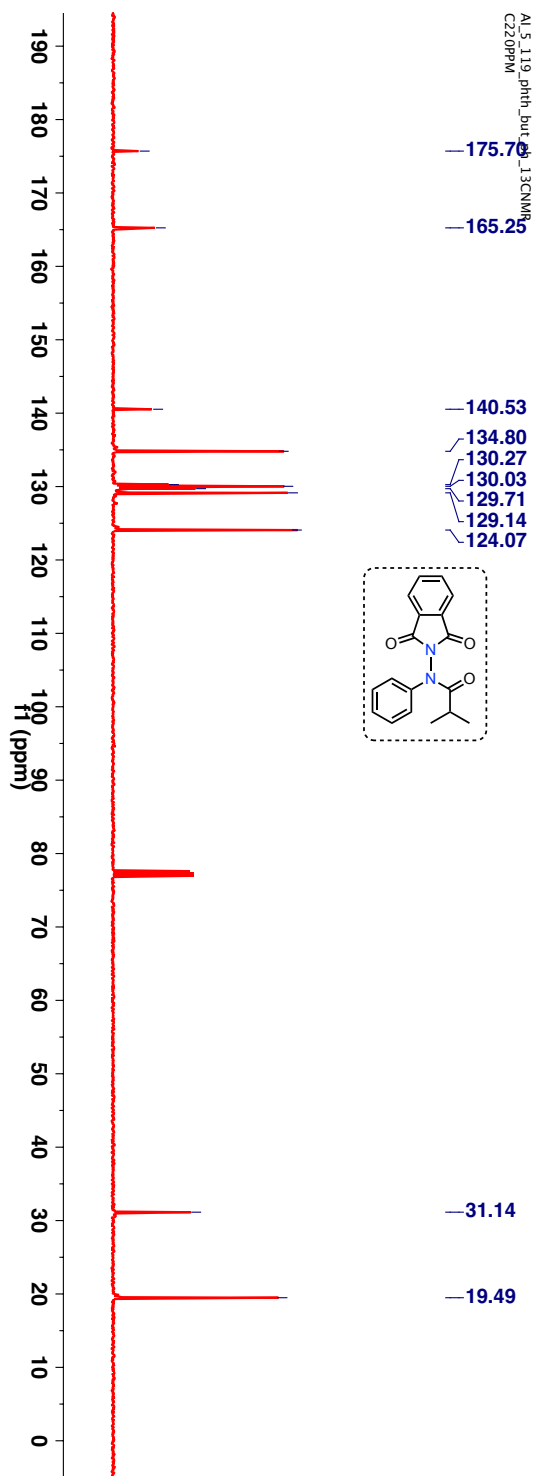
Figure 3.21: ¹³C-NMR (100 MHz, CDCl₃, δ ppm) spectrum of **188a**.

3.11. Synthesis of imide based achiral acrylanilide derivative 184g
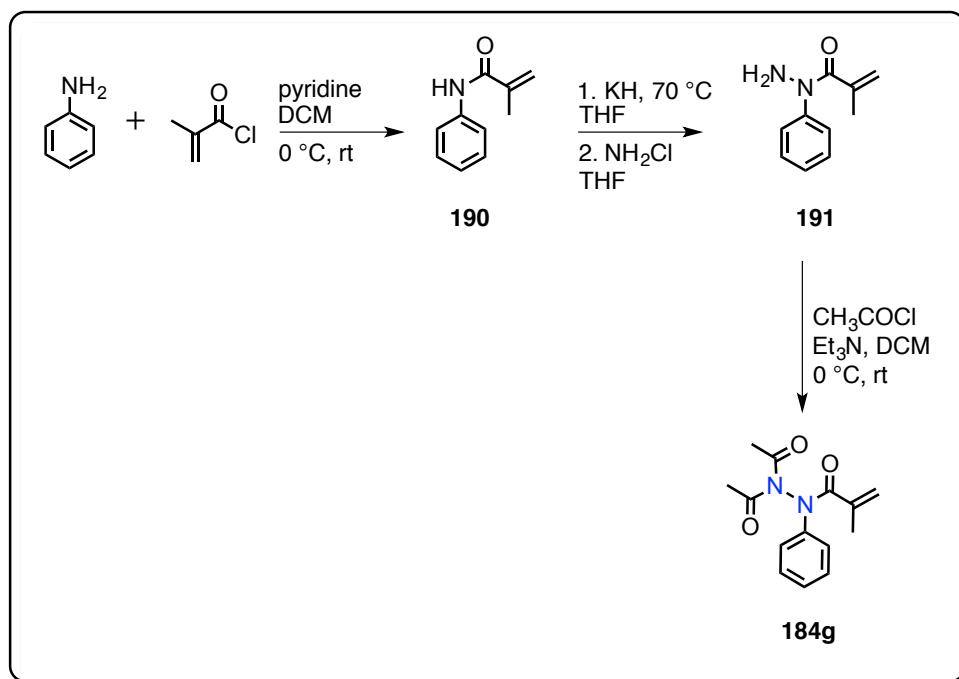
Scheme 3.31: Synthesis of phthalimide based achiral acrylanilide derivative **184g**.
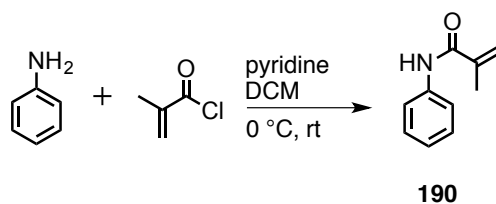
Scheme 3.32: Synthesis of acrylanilide derivative **190**.

Following the modified procedure reported by Iyer et al.*,* aniline (1 equiv) was dissolved in freshly distilled dichloromethane (DCM) under N_2 atmosphere.[108] To this solution, 1.5 equiv of pyridine was added and the reaction mixture was then cooled to 0 °C, followed by the dropwise addition of methacryloyl chloride (1.2 equiv). After stirring for 15 min, the mixture was brought to room temperature and stirred for 16 h. The reaction was quenched with 10 mL of DI water, stirred and the layers were separated. The organic layer was sequentially washed with DI water (2 × 10 mL**)**, saturated $NaHCO_3$ (2 × 10 mL**)** and finally with brine. The organic layer was dried over anhyd Na_2SO_4, filtered and the solvent was removed under reduced pressure to yield crude product. The crude product was purified by column chromatography using hexanes and ethyl acetate mixture to get the desired amide. The product was characterized by NMR spectroscopy and mass spectrometry.

TLC condition - R_f = 0.3 (20% ethyl acetate: hexanes). White solid (Yield = 71%).

^{1}H-NMR (400 MHz, CDCl$_3$, δ ppm): 2.05 (s, 3H), 5.44 (s, 1H) 5.78 (s, 1H), 7.09-7.13 (m, 1H), 7.30-7.34 (m, 1H), 7.55-7.57 (m, 1H) and 7.67 (bs, 1H).
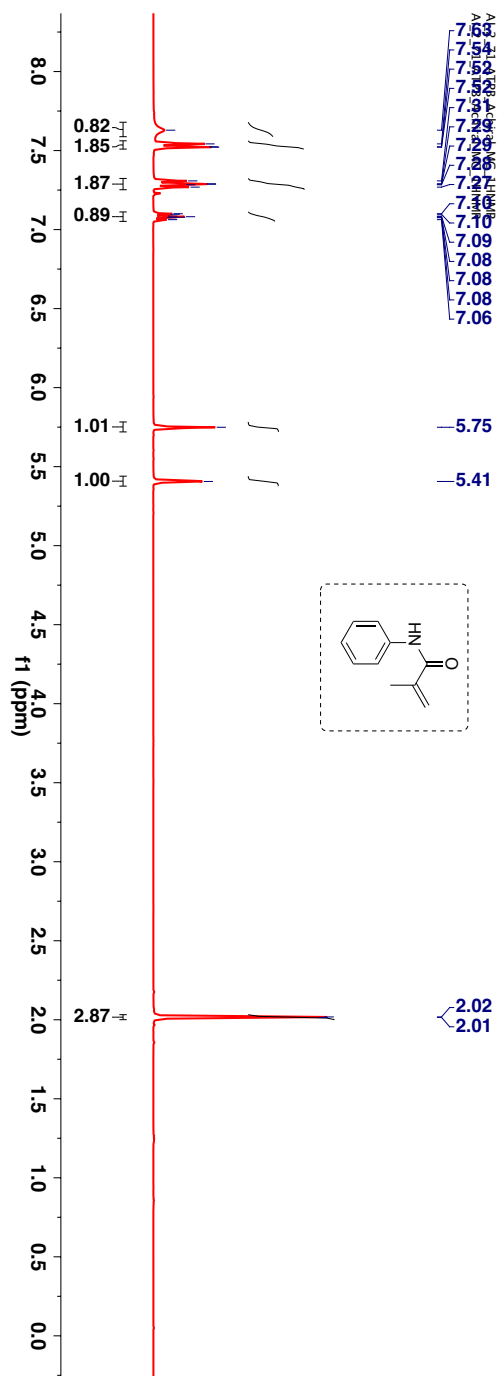
Figure 3.22: ^{1}H-NMR (400 MHz, CDCl$_3$, δ ppm) spectrum of **190**.

¹³C-NMR (100 MHz, CDCl₃, δ ppm): 18.9, 119.9 120.2, 124.6, 129.1, 138.0, 141.1 and 166.9.
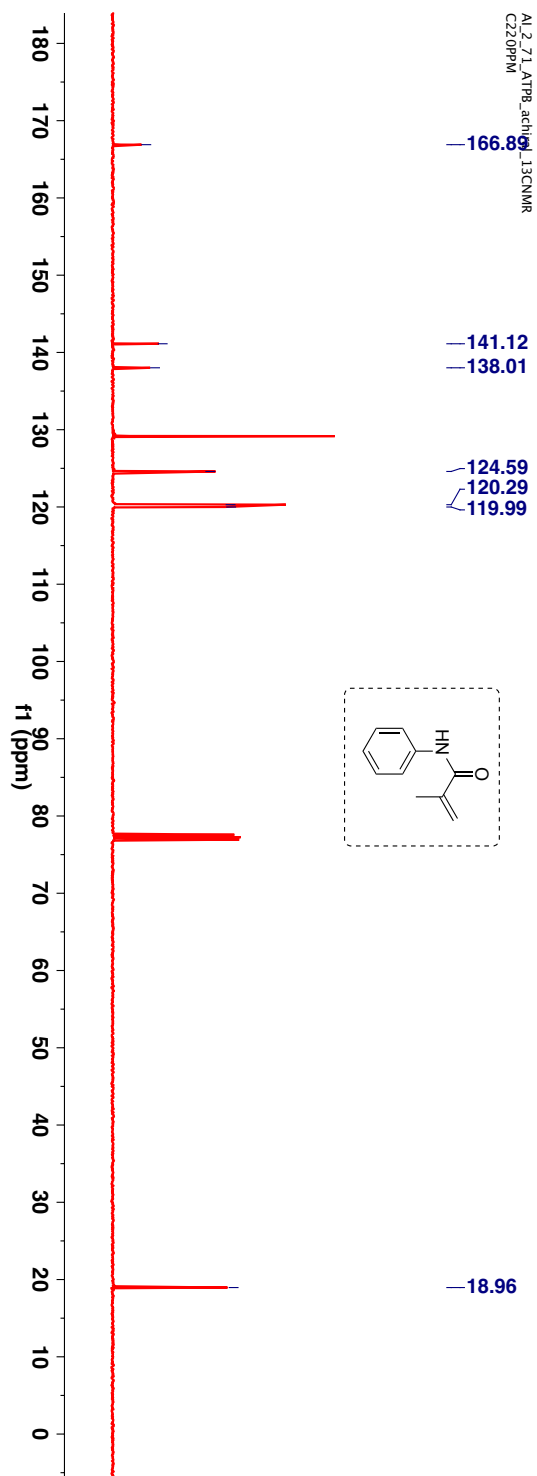
Figure 3.23: ¹³C-NMR (100 MHz, CDCl₃, δ ppm) spectrum of **190**.

<u>STEP 2</u>
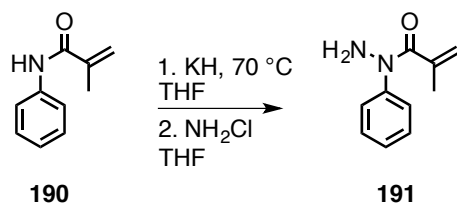
Scheme 3.33: Synthesis of *N*-amino acrylanilide derivative **191**.

N-amination was performed using a modified procedure stated by Hynes et al.[20]

Preparation of Anhydrous Ethereal Monochloramine: NH_4Cl (3 g, 56 mmol) in diethyl ether (110 mL) was cooled to -5 °C, and to this slurry, concentrated NH_4OH (4.7 mL) was added via pipette. Commercial bleach (72 mL) was then added slowly. The mixture was stirred for 15-20 min, the layers were separated, and the organic layer was washed with brine (1 × 35 mL). The organic layer was dried over powdered $CaCl_2$ in a freezer for 1 h and stored at -80 °C until consumed.

To a solution of amide in freshly distilled THF, 1.1 equiv of KH was added. The mixture was stirred at 70 °C for 1 h and then cooled to room temperature. To this freshly prepared ethereal monochloramine (1.1 equiv) was added. The mixture was stirred at room temperature for 20 h followed by column chromatography using hexanes and ethyl acetate mixture to get the desired *N*-amino derivative.

TLC condition - R_f = 0.3 (50% hexanes: ethyl acetate). Viscous pale yellow liquid. Product yield varied from 65-85% depending on the concentration of ethereal chloramine.

Note: The *N*-amino derivative **191** was unstable and was used immediately after purification the same day without leaving it in refrigerator for perusal. In some cases the crude was filtered through a short celite pad, which was then subjected to column chromatography.

¹H-NMR (400 MHz, CDCl₃, δ ppm): 1.77 (s, 3H), 4.65 (bs, 2H), 5.05 (s, 1H), 5.09 (s, 1H), 7.18-7.23 (m, 3H) and 7.28-7.32 (m, 2H).
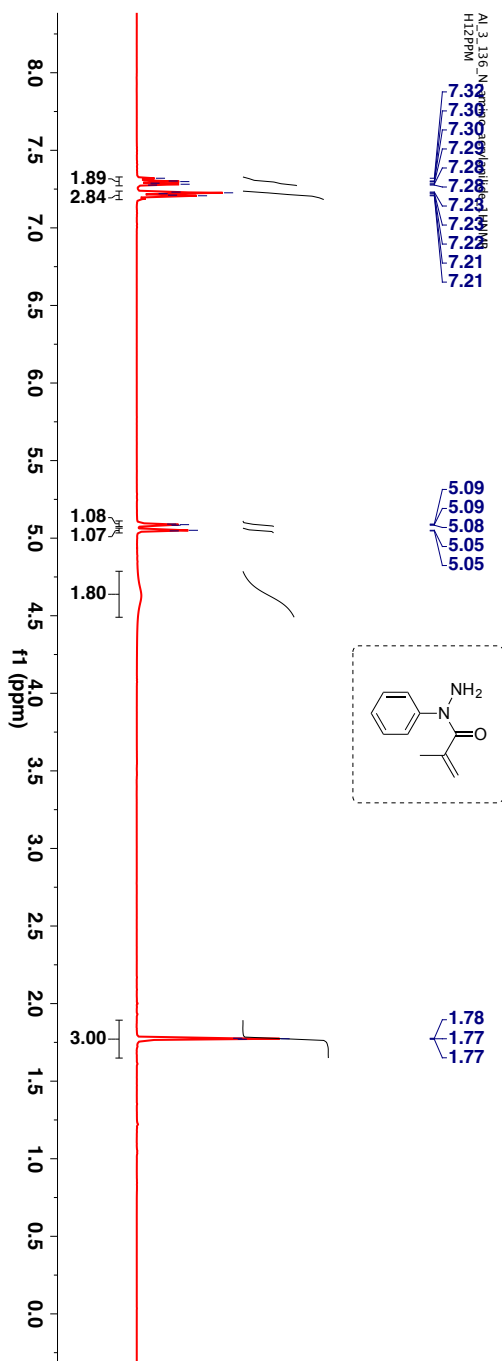
Figure 3.24: ¹H-NMR (400 MHz, CDCl₃, δ ppm) spectrum of **191**.

^{13}C-NMR (100 MHz, CDCl$_3$, δ ppm): 20.1, 120.7 125.9, 127.2, 129.1, 139.9, 143.4 and 170.9.
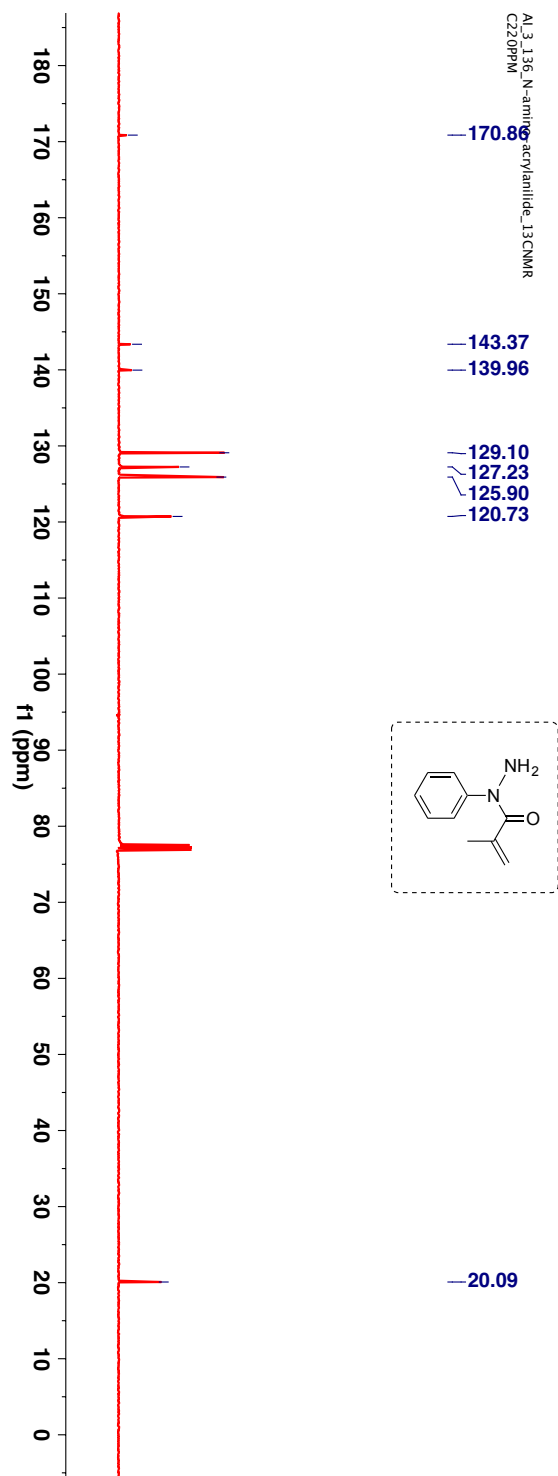
Figure 3.25: ^{13}C-NMR (100 MHz, CDCl$_3$, δ ppm) spectrum of **191**.
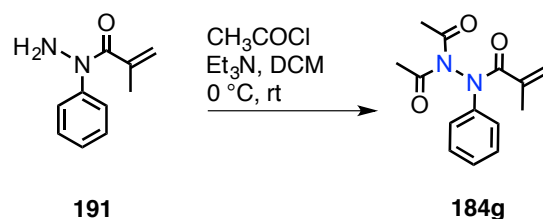
Scheme 3.34: Synthesis of *N,N* diacylated hydrazide derivative **184g**.

N-amino derivative **191** (1 equiv) was dissolved in freshly distilled dichloromethane (DCM) and to this mixture anhydrous Et$_3$N (4 equiv) was added. The solution was cooled to 0 °C. Freshly distilled acetyl chloride (2.2 equiv) was added dropwise and the solution was stirred at to 0 °C for additional one hour after which the reaction mixture was brought to room temperature. The mixture was stirred at room temperature for 20 h. The reaction was quenched with 10 mL of DI water, stirred and the layers were separated. The organic layer was sequentially washed with DI water (2 × 10 mL), saturated NaHCO$_3$ (2 × 10 mL) and finally with brine. The organic layer was dried over anhyd Na$_2$SO$_4$, filtered and the solvent was removed under reduced pressure to yield the crude product. The crude product was purified by column chromatography using hexanes and ethyl acetate mixture to get the desired *N–N* acrylanilide derivative.

TLC condition - R$_f$ = 0.6 (50% hexanes:ethyl acetate). Viscous clear liquid (Yield = 34%).

^{1}H-NMR (400 MHz, CDCl$_3$, δ ppm): 1.83 (s, 3H), 2.41 (s, 6H), 5.25 (s, 1H), 5.33 (s, 1H), 7.13-7.16 (m, 2H), 7.20-7.23-7.25 (m, 1H) and 7.30-7.34 (m, 2H).
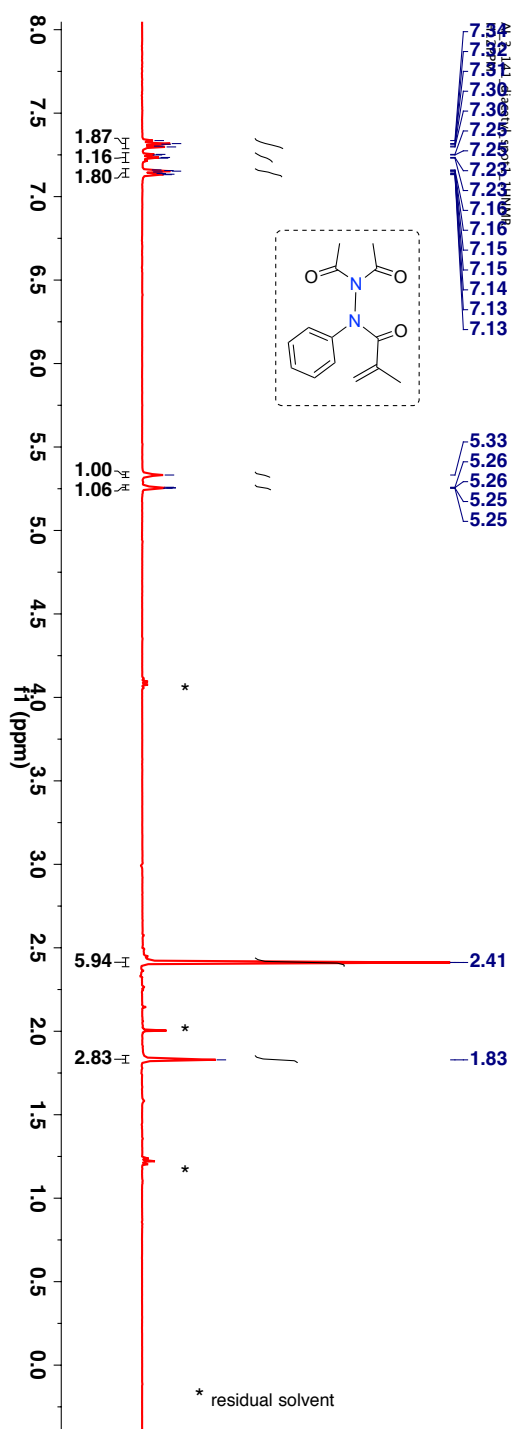
Figure 3.26: ^{1}H-NMR (400 MHz, CDCl$_3$, δ ppm) spectrum of **184g**.

^{13}C-NMR (100 MHz, CDCl$_3$, δ ppm): 19.5, 23.3, 124.6, 127.4, 138.9 and 171.7.
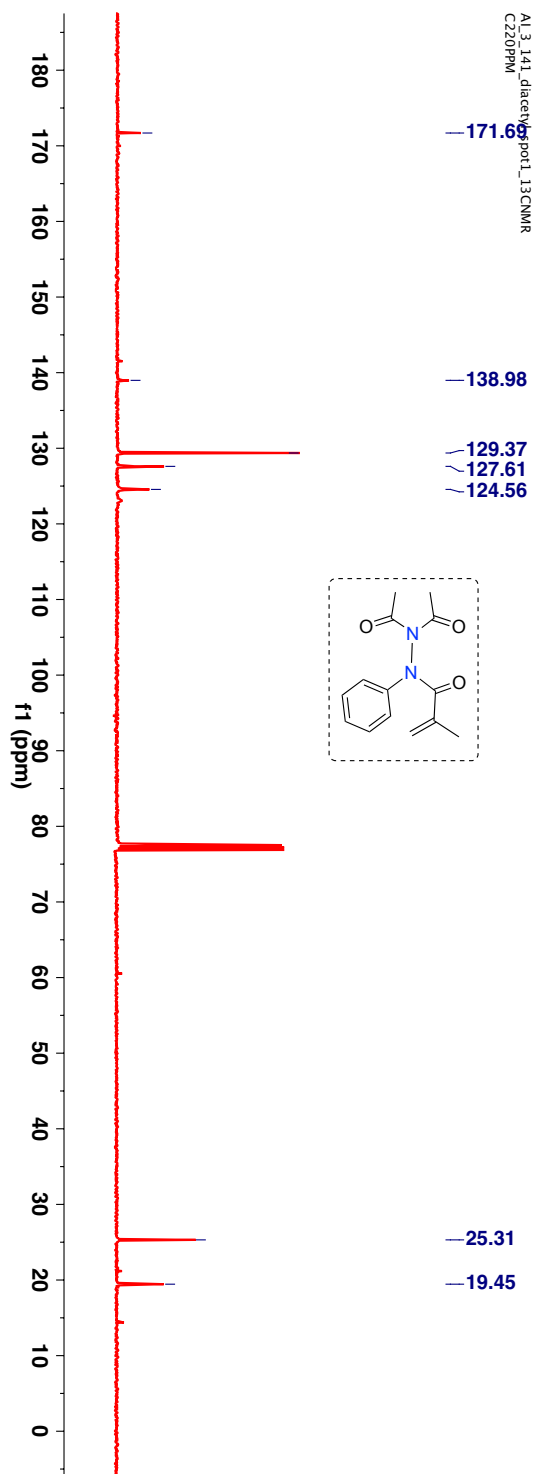
Figure 3.27: ^{13}C-NMR (100 MHz, CDCl$_3$, δ ppm) spectrum of **184g**.

HRMS-ESI (m/z) ([M + Na]):

Chemical Formula: $C_{14}H_{16}N_2O_3$

Calculated   : 283.1059

Observed   : 283.1071

|Δm| : 4.2 ppm
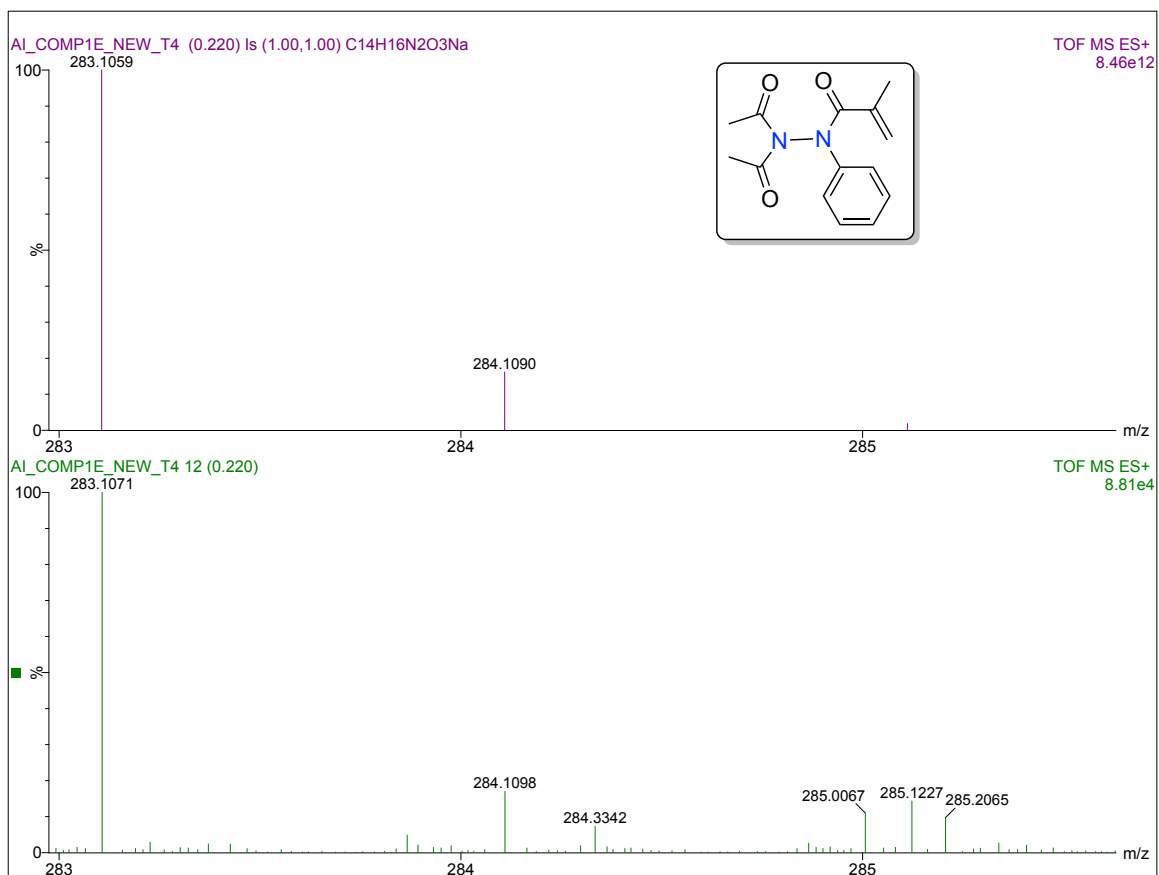
Figure 3.28: HRMS spectra of **184g**.

3.12. Synthesis of photophysical substrate 184h
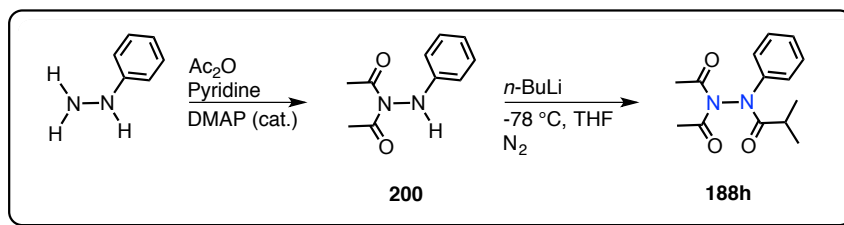
Scheme 3.35: Synthesis of anilide derivative **188h**.

STEP-1
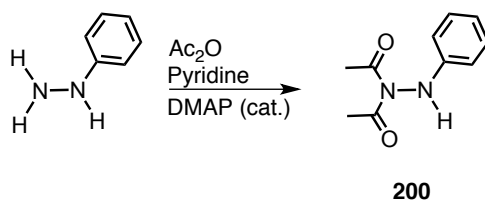
Scheme 3.36: Synthesis of hydrazide derivative **200**.

Phenylhydrazine (1 equiv) was dissolved in acetic anhydride (2.2 equiv). To this mixture 20 mol% of DMAP was added slowly at 0 °C. The solution was stirred at this temperature for an hour after which the solution was slowly brought to room temperature. The solution was quenched with ~10 mL of water and given a 2N HCl wash. The solution was diluted with ethyl acetate and the organic layer was neutralized with 2N HCl solution and then sequentially washed with DI water (2 × 10 mL), saturated NaHCO$_3$ (2 × 10 mL) and finally with brine. The organic layer was dried over anhyd Na$_2$SO$_4$, filtered and the solvent was removed under reduced pressure to yield crude product. After concentrating the organic layer, the crude product was purified by combiflash using hexanes and ethyl acetate mixture to get the desired compound.

TLC condition - R$_f$ = 0.4 (50% ethyl acetate:hexanes). Solid (Yield = 12%).

^{1}H-NMR (400 MHz, CDCl$_3$, δ ppm): 2.5 (s, 6H), 6.68 (bs, 1H), 6.77 (d, *J* 6Hz, 2H), 6.98–7.0 (m, 1H) and 7.28–7.31 (m, 2H).
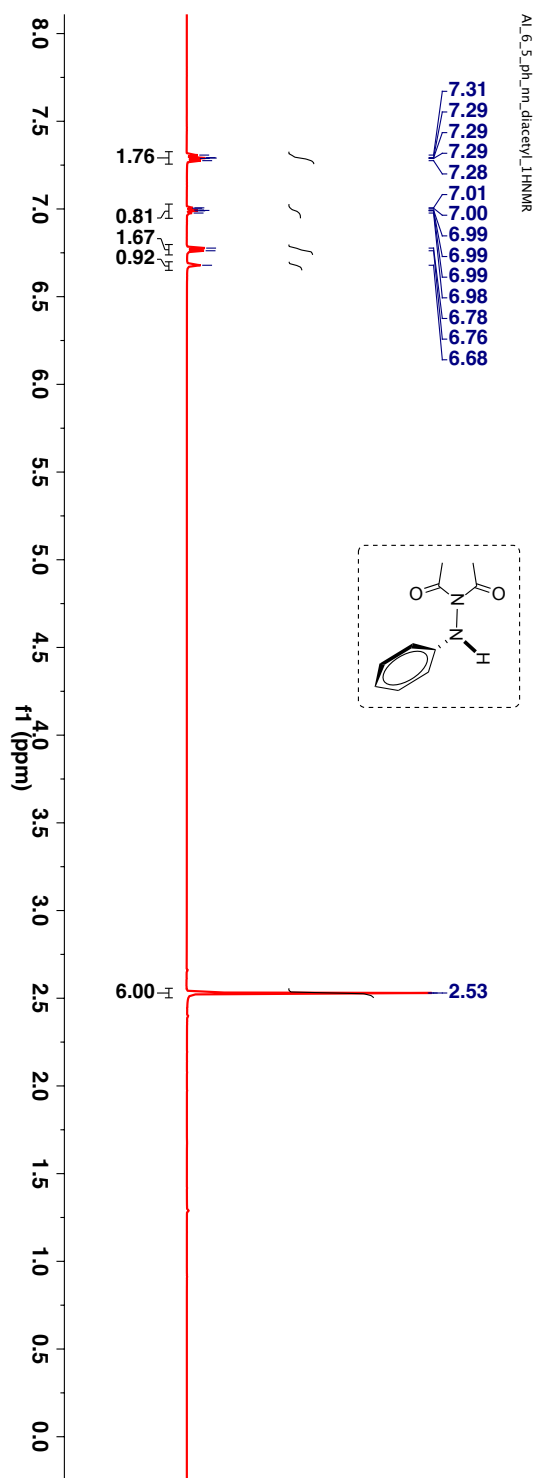
Figure 3.29: ^{1}H-NMR (400 MHz, CDCl$_3$, δ ppm) spectrum of **200**.

^{13}C-NMR (100 MHz, CDCl$_3$, δ ppm): 25.7, 113.5, 122.4, 129.7, 146.9 and 173.7.
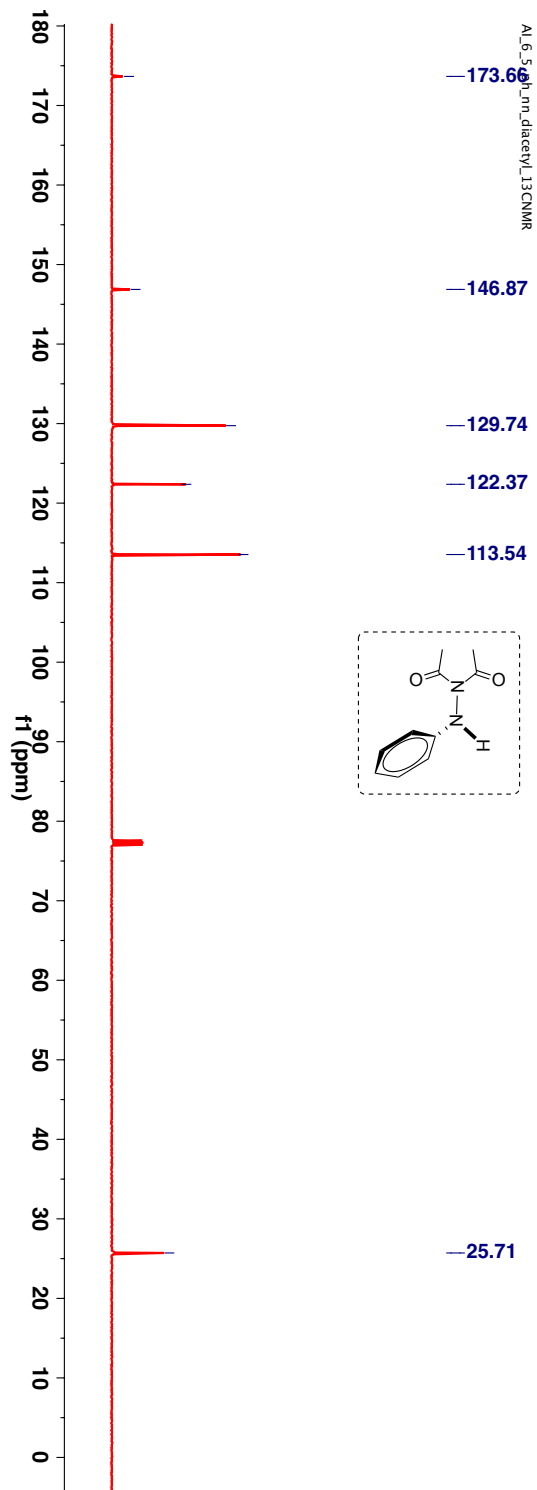
Figure 3.30: ^{13}C-NMR (100 MHz, CDCl$_3$, δ ppm) spectrum of **200**.

<u>STEP-2</u>
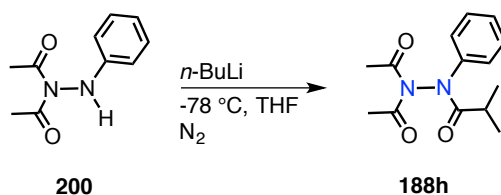
Scheme 3.37: Synthesis of imide based acrylanilide derivative **188h**.

Hydrazide derivative **200** (1 equiv) was dissolved in anhydrous THF under an inert atmosphere. The solution was then cooled to -78 °C. To this cold solution *n*-BuLi (2.5 M, 1.1 equiv) was added slowly. The mixture was stirred at this temperature for 20 min. The reaction was quenched with anhydrous freshly distilled acetyl chloride (1.1 equiv). The stirring was continued for another 2 h after which the reaction was slowly brought to room temperature. The solution was then quenched with slow addition of ~10 mL of saturated NH$_4$Cl. The solution was diluted with diethyl ether and the organic layer was sequentially washed with DI water (2 × 10 mL), saturated NaHCO$_3$ (2 × 10 mL) and finally with brine. The organic layer was dried over anhyd Na$_2$SO$_4$, filtered and the solvent was removed under reduced pressure to yield crude product. After concentrating the organic layer, the crude product was purified by combiflash using hexanes and ethyl acetate mixture to get the desired compound.

TLC condition - R$_f$ = 0.5 (50% ethyl acetate:hexanes). Solid (Yield = 71%).

^{1}H-NMR (400 MHz, CDCl$_3$, δ ppm): 1.09 (d, J 5.2 Hz, 6H), 2.78–2.84 (sep, J 5.2 Hz, 1H) and 7.34–7.42 (m, 5H).

Figure 3.31: ^{1}H-NMR (400 MHz, CDCl$_3$, δ ppm) spectrum of **188h**.

^{13}C-NMR (100 MHz, CDCl$_3$, δ ppm): 19.3, 25.4, 31.3, 126.7, 128.9, 129.9, 141.1, 171.8 and 176.4.
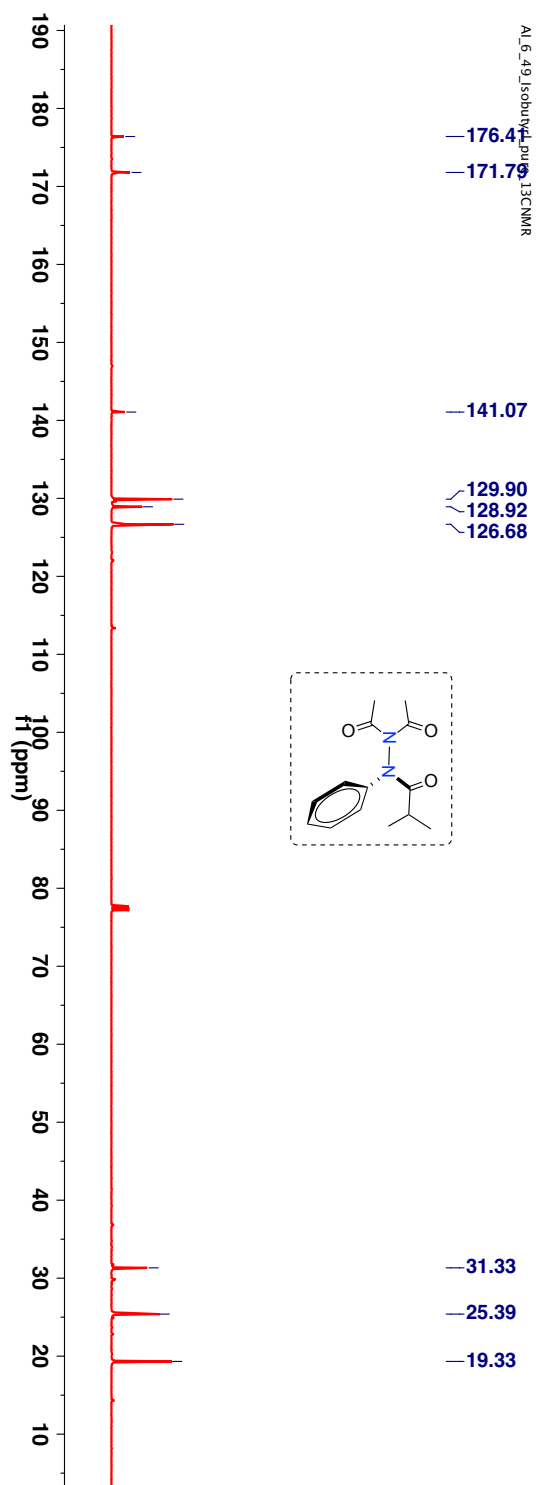
Figure 3.32: ^{13}C-NMR (100 MHz, CDCl$_3$, δ ppm) spectrum of **188h**.

3.13. Synthesis of chiral *N-N* bond based acrylanilide derivatives
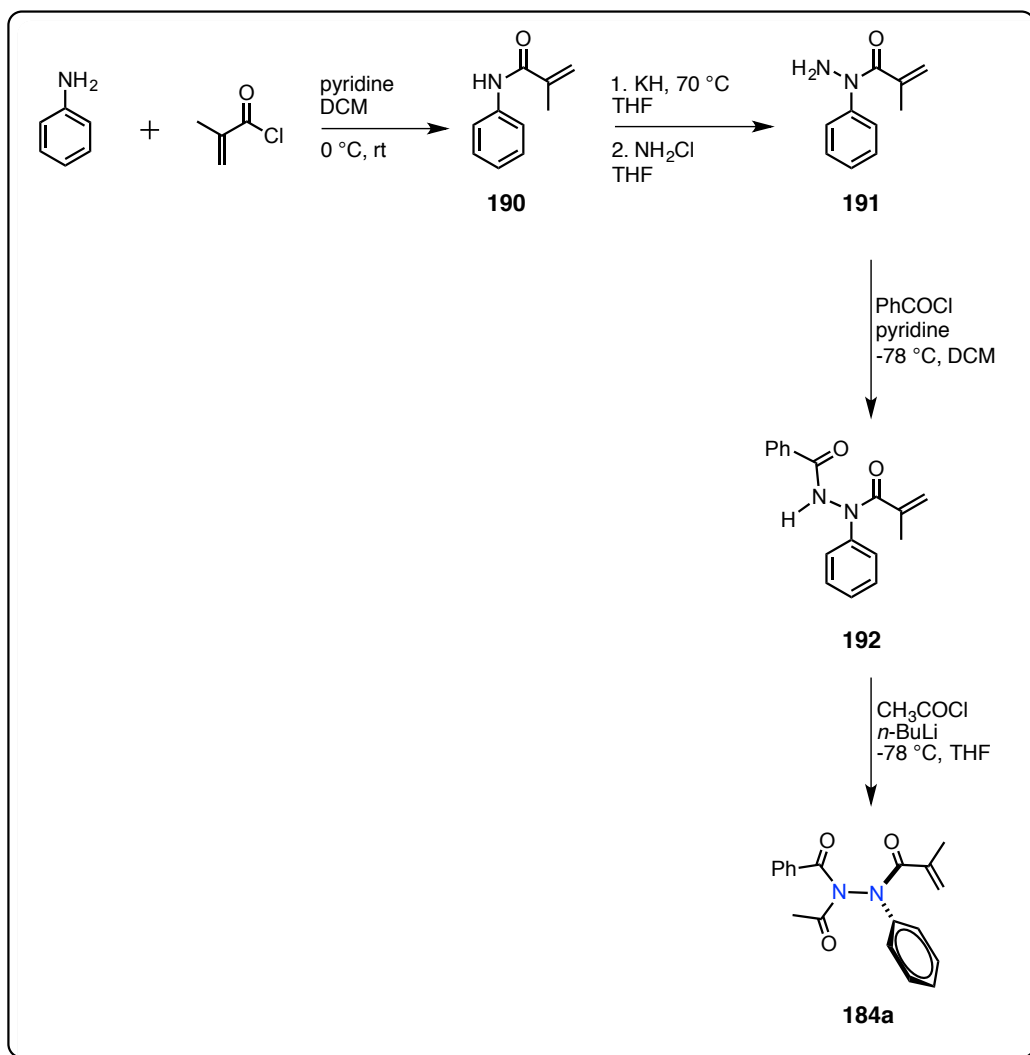
Scheme 3.38: Synthesis of imide based acrylanilide derivative **184a**.
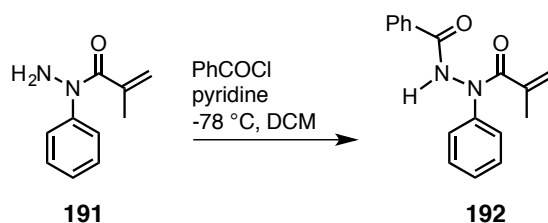
Scheme 3.39: Synthesis of acrylanilide **192**.

N-amino anilide derivative **191** (1 equiv) was dissolved in freshly distilled dichloromethane (DCM) and to this mixture anhydrous pyridine (4 equiv) was added. The solution was cooled to -78 °C and benzoyl chloride (1.2 equiv) was added dropwise and the solution was stirred at this temperature for additional two hours after which the reaction mixture was quenched with 10 mL of DI water (at -78 °C), stirred and the layers were separated. The organic layer was sequentially washed with DI water (2 × 10 mL), saturated $NaHCO_3$ (2 × 10 mL) and finally with brine. The organic layer was dried over anhyd Na_2SO_4, filtered and the solvent was removed under reduced pressure to yield crude product. The crude product was purified by column chromatography using hexanes and ethyl acetate mixture to get the desired acrylanilide derivative.

TLC condition - R_f = 0.5 (20% ethyl acetate:hexanes). Crystalline solid (Yield = 89%).

^{1}H-NMR (400 MHz, CDCl$_3$, δ ppm): 1.86 (s, 3H), 5.21 (s, 1H), 5.32 (s, 1H), 7.23-7.47 (m, 8H), 7.79 (d, 2H,

J 9.6Hz), 8.06 (d, 1H, *J* 8.4Hz) and 8.99 (bs, 1H).
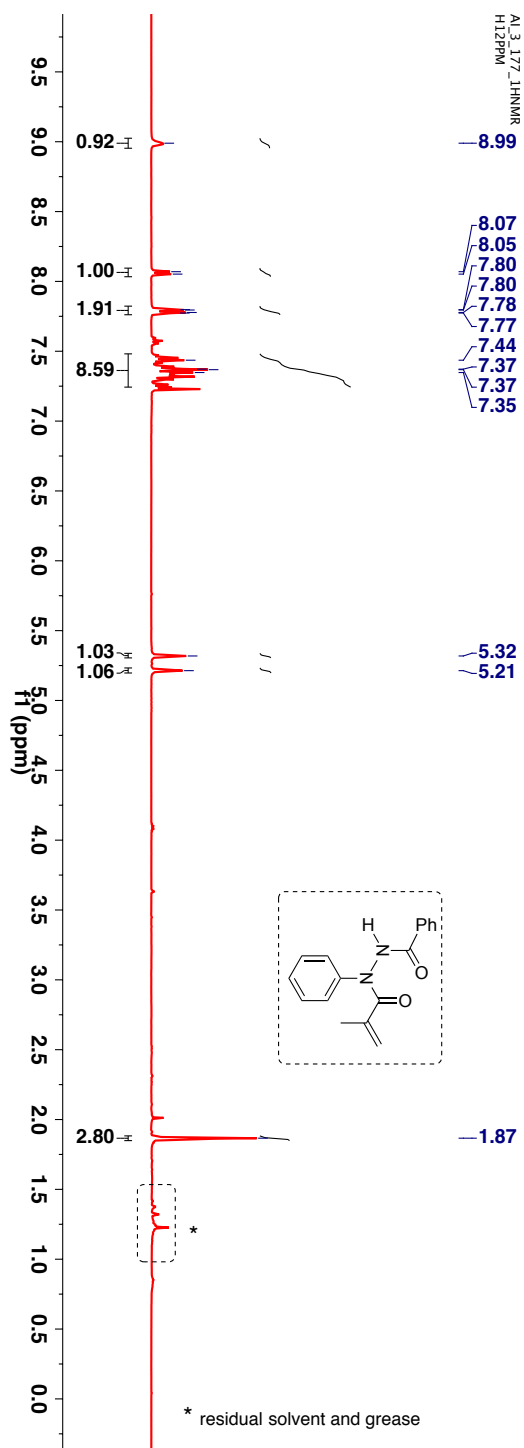
Figure 3.33: ^{1}H-NMR (400 MHz, CDCl$_3$, δ ppm) spectrum of **192**.

^{13}C-NMR (100 MHz, CDCl$_3$, δ ppm): 19.9, 121.6, 126.2, 127.6, 127.8, 128.7, 128.8, 129.2, 130.3, 131.3, 1331.9, 132.5, 133.8, 139.4, 142.7, 167.1 and 171.7.
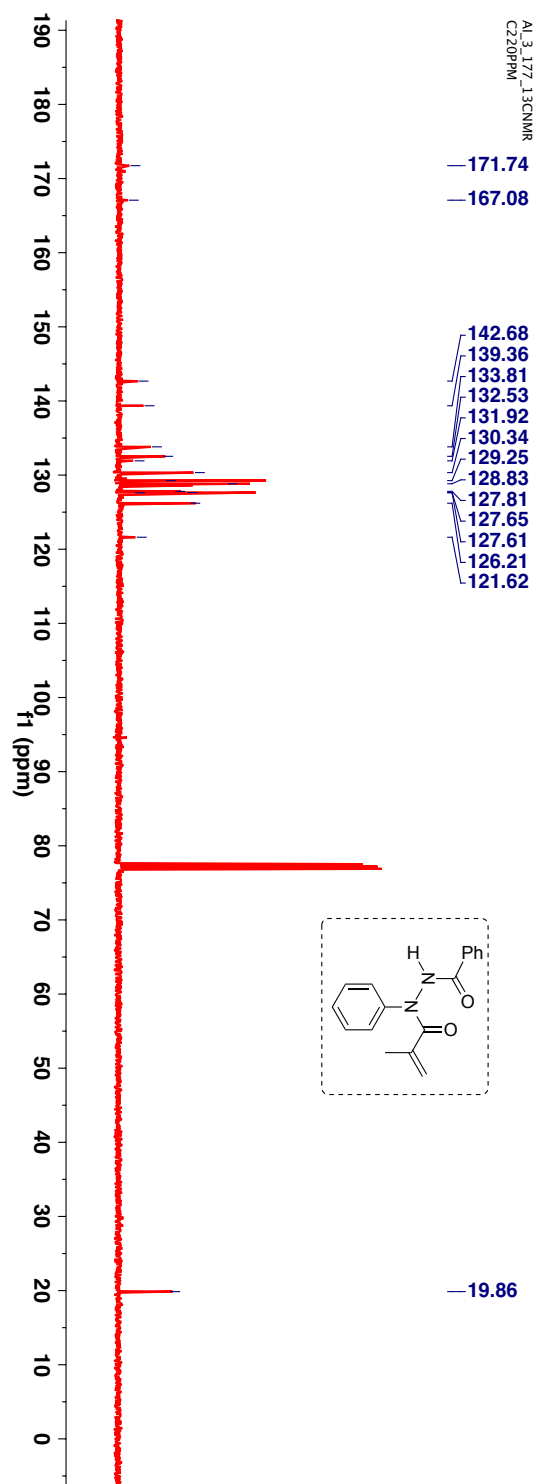
Figure 3.34: ^{13}C-NMR (100 MHz, CDCl$_3$, δ ppm) spectrum of **192**.
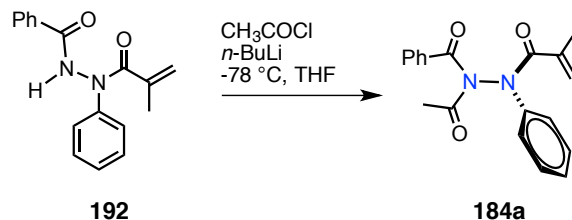
Scheme 3.40: Synthesis of imide based acrylanilide derivative **184a**.

Hydrazide derivative **192** (1 equiv) was dissolved in anhydrous THF under an inert atmosphere. The solution was then cooled to -78 °C. To this cold solution *n*-BuLi (2.5 M, 1.1 equiv) was added slowly. The mixture was stirred at this temperature for 45 min. The reaction was quenched with anhydrous freshly distilled acetyl chloride (1.3 equiv). The stirring was continued for another 3 h after which the solution was quenched with slow addition of ~10 mL of saturated NH$_4$Cl. (Note: the solution was quenched at -78 °C). The solution was further stirred for 35 min and then diluted with diethyl ether and the organic layer was sequentially washed with DI water (2 × 10 mL), saturated NaHCO$_3$ (2 × 10 mL) and finally with brine. The organic layer was dried over anhyd Na$_2$SO$_4$, filtered and the solvent was removed under reduced pressure to yield crude product. After concentrating the organic layer, the crude product was purified by combiflash using hexanes and ethyl acetate mixture to get the desired compound.

TLC condition - R$_f$ = 0.5 (50% ethyl acetate:hexanes). Viscous clear liquid, which on cooling turns into a crystalline solid (Yield = 77%).

^{1}H-NMR (400 MHz, CDCl$_3$, δ ppm): 1.73 (s, 3H), 2.45 (s, 3H), 5.10-5.13 (m, 2H), 6.88-6.89 (m, 2H), 7.16-7.18 (m, 3H), 7.33-7.37 (m, 2H), 7.47-7.49 (m, 1H) and 7.55-7.57 (m, 2H).
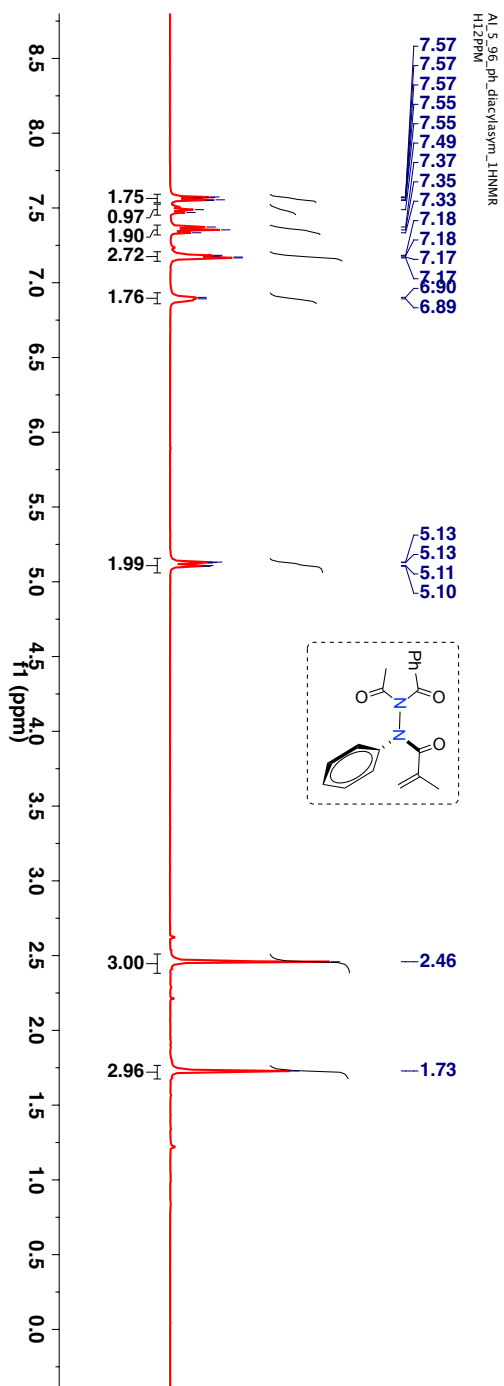
Figure 3.35: ^{1}H-NMR (400 MHz, CDCl$_3$, δ ppm) spectrum of **184a**.

^{13}C-NMR (100 MHz, CDCl$_3$, δ ppm): 19.5, 25.2, 122.1, 125.8, 127.8, 128.0, 128.5, 128.5, 129.2, 132.4, 143.7, 138.9, 141.7, 169.9, 171.0 and 171.8.
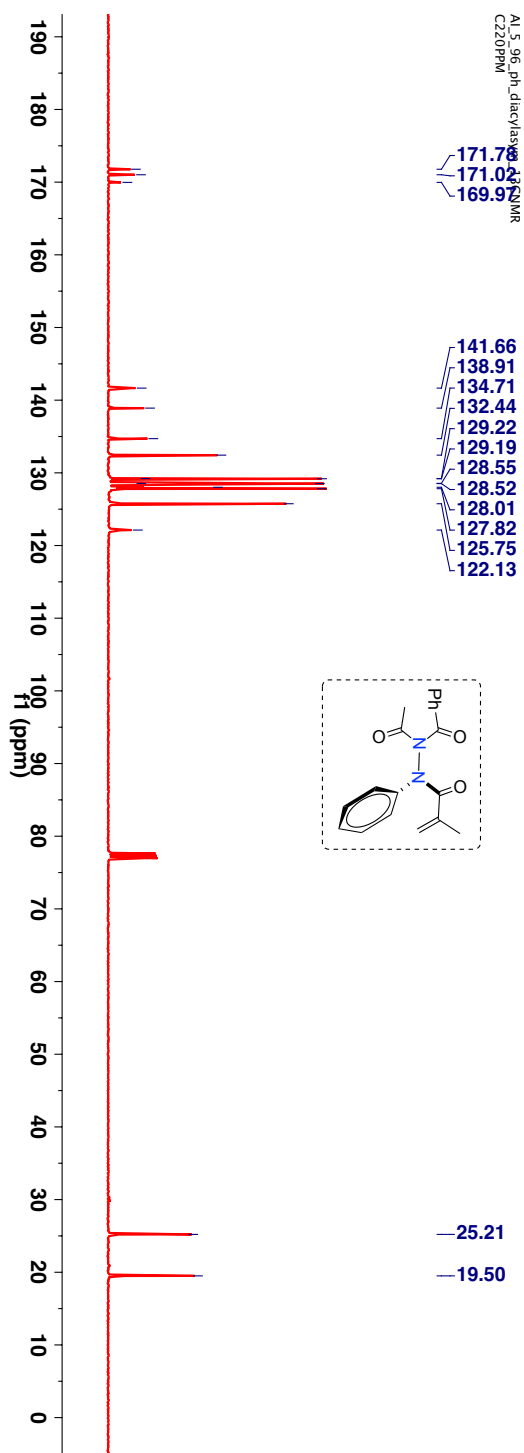
Figure 3.36: ^{13}C-NMR (100 MHz, CDCl$_3$, δ ppm) spectrum of **184a**.

HRMS-ESI (m/z) ([M + Na]):

Chemical Formula: $C_{19}H_{18}N_2O_3$

Calculated   : 345.1215

Observed   : 345.1230

|Δm| : 4.3 ppm
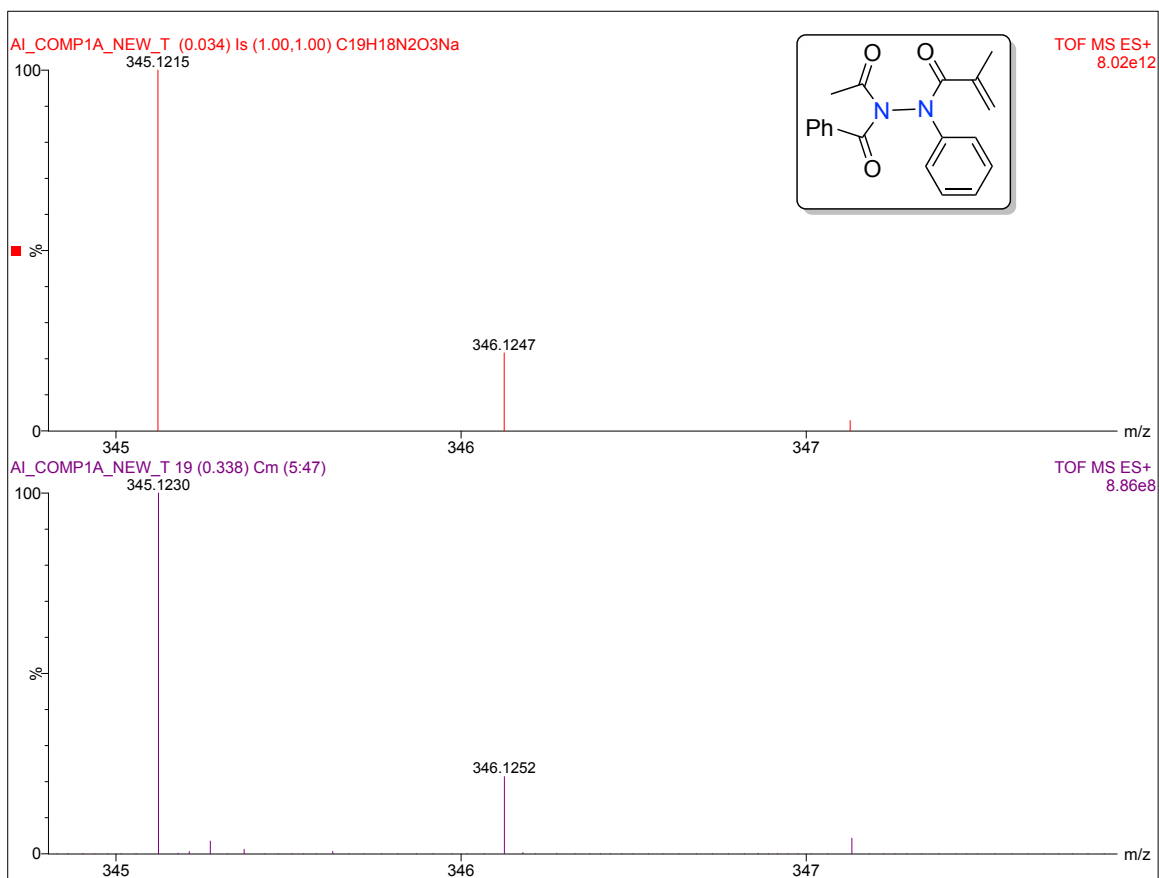
Figure 3.37: HRMS spectra of **184a**.

3.14. Synthesis of phthalimide based acrylanilide derivative 184c/188b
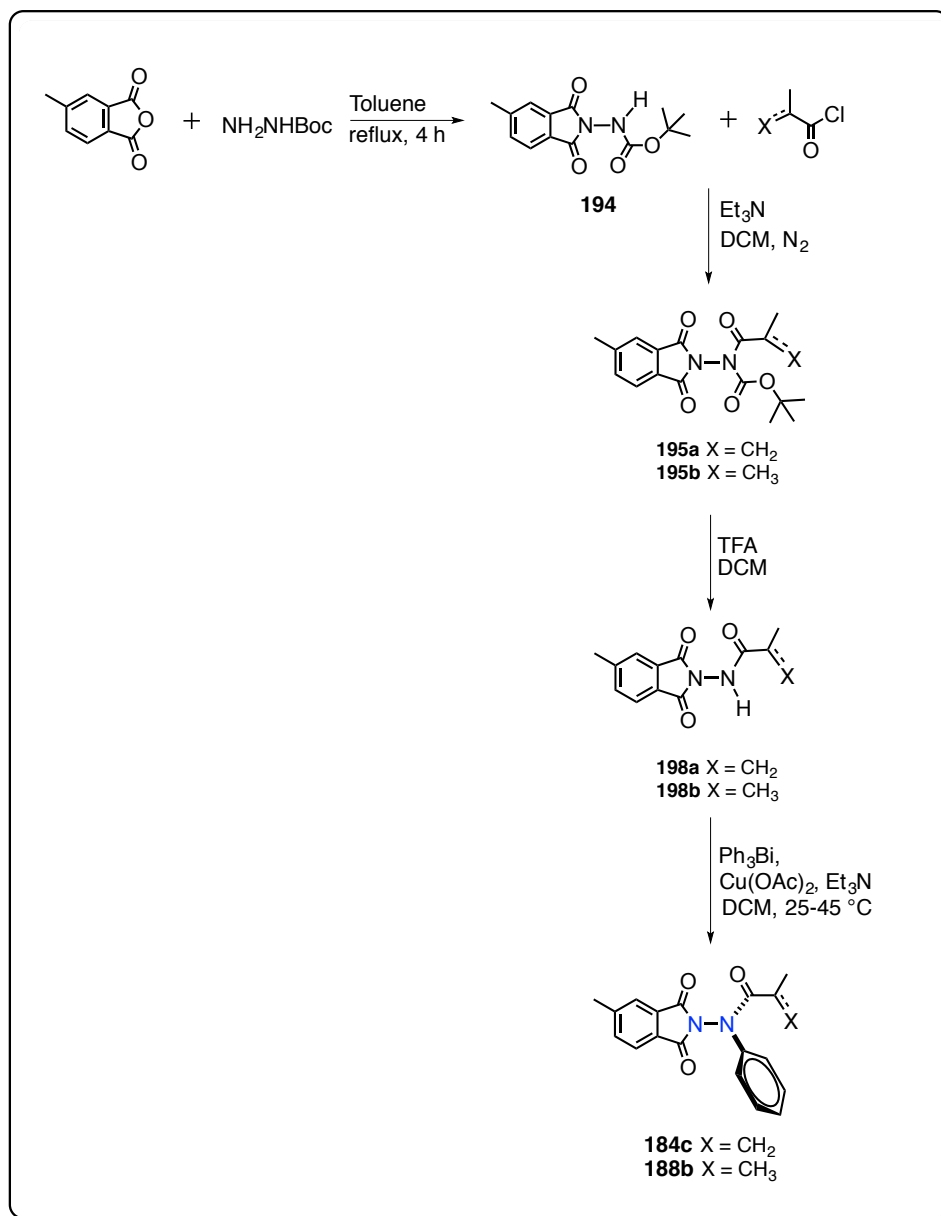
Scheme 3.41: Synthesis of phthalimide based acrylanilide derivative **184c/188b**.

194
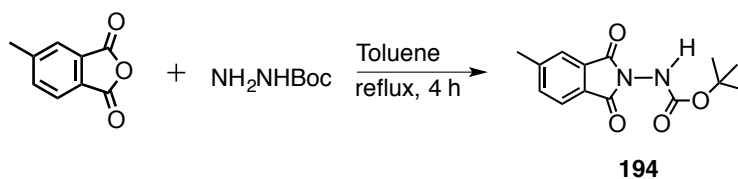
Scheme 3.42: Synthesis of amide derivative **194**.

Modifying a procedure reported by Cécile et al., to a suspension of 4-methyl phthalic anhydride (1 equiv) and *tert*-butylcarbazate (1 equiv) in toluene, equipped in a two-necked flask was heated under reflux in a Dean-Stark trap.[94] The reflux was continued for 4h. The mixture was cooled and concentrated. The crude product was purified by column chromatography using hexanes and ethyl acetate mixture to get the desired amide **194**.

TLC condition - R_f = 0.3 (20% ethyl acetate:hexanes). Crystalline clear solid (Yield = 96%).

^{1}H-NMR (400 MHz, CDCl$_3$, δ ppm): 1.46 (bs, 9H), 2.49 (s, 3H), 6.64 (s, 1H), 7.53 (d, 1H, *J* 7.6Hz), 7.66 (s, 1H) and 7.74 (d, 1H, *J* 7.6Hz).
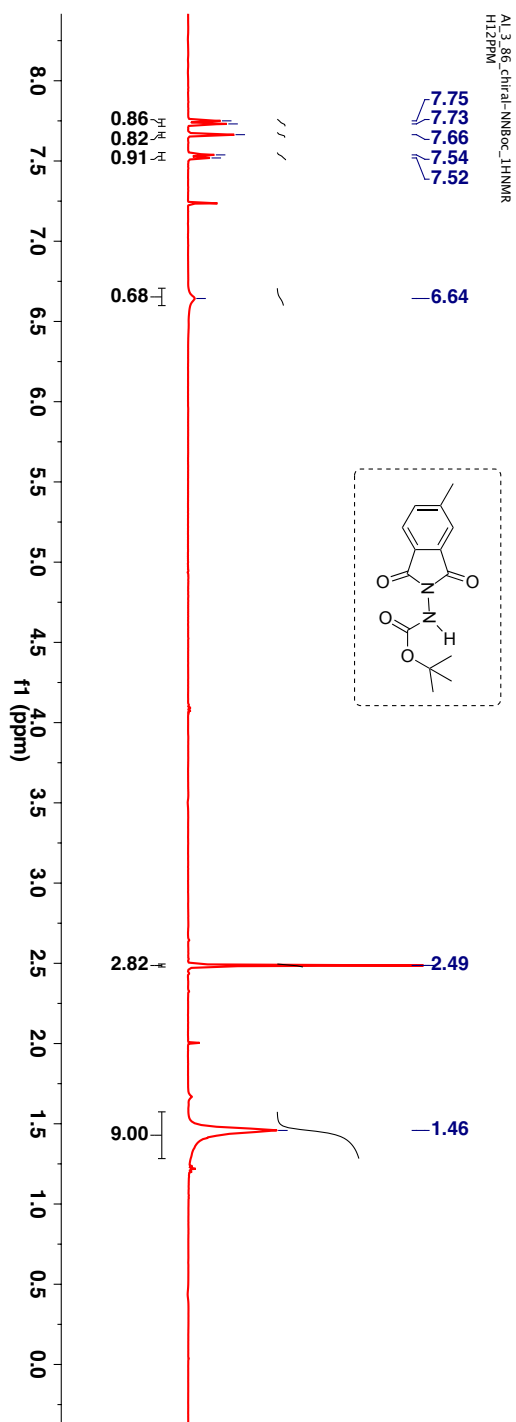
Figure 3.38: ^{1}H-NMR (400 MHz, CDCl$_3$, δ ppm) spectrum of **194**.

^{13}C-NMR (100 MHz, CDCl$_3$, δ ppm): 22.3, 28.2, 83.1, 124.1, 124.6, 1247.5, 130.5, 135.4, 146.3, 153.6 and 165.7.
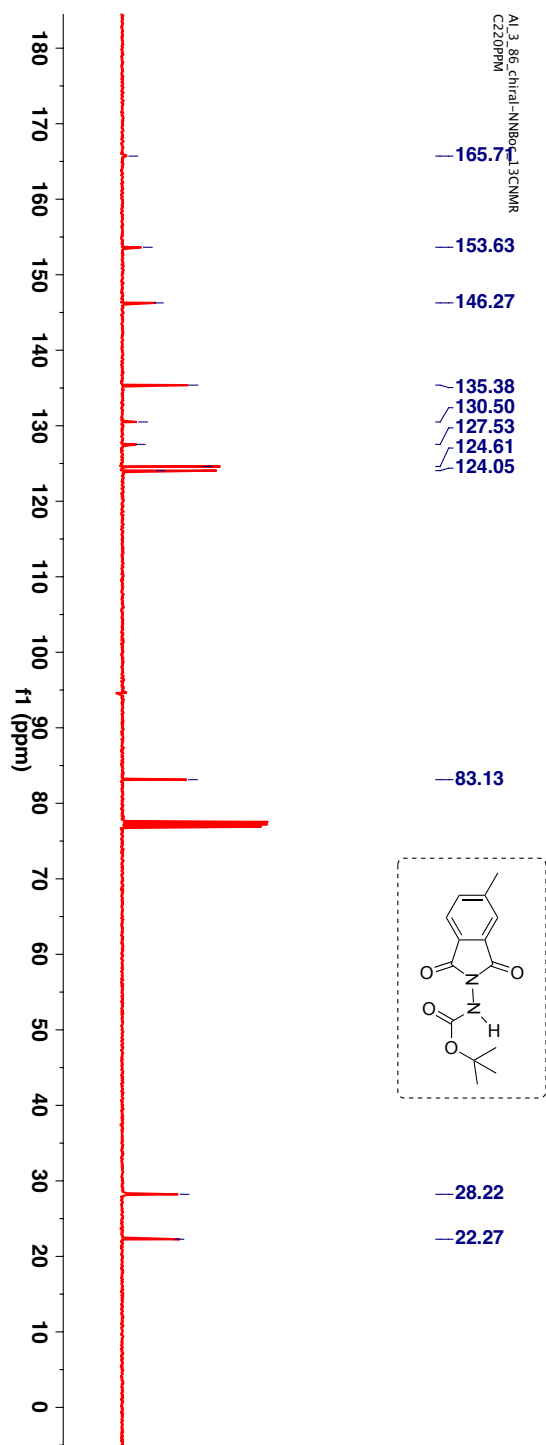
Figure 3.39: ^{13}C-NMR (100 MHz, CDCl$_3$, δ ppm) spectrum of **194**.

STEP 2
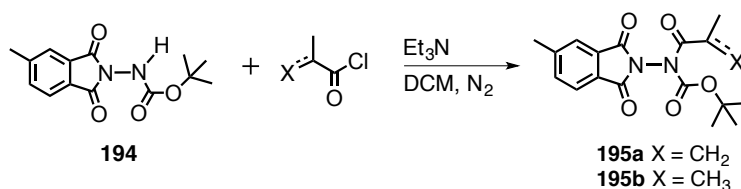
Scheme 3.43: Synthesis of imide derivative **195a/195b**.

Amide derivative **194 (**1 equiv) was dissolved in freshly distilled dichloromethane (DCM) and to this mixture Et$_3$N **(**2 equiv) was added. The solution was cooled to -50 °C. Acid chloride (1.2 equiv) was added dropwise and the solution was stirred at this temperature for additional one hour after which the reaction mixture was brought to room temperature and stirred for 20 h. The reaction was quenched with 5 mL of H$_2$O, stirred and the organic layer was separated. The organic layer was sequentially washed with DI water (2 × 10 mL), saturated NaHCO$_3$ (2 × 10 mL) and finally with brine. The organic layer was dried over anhyd Na$_2$SO$_4$, filtered and the solvent was removed under reduced pressure to yield crude product. The crude product was purified by combiflash using hexanes and ethyl acetate as the eluting solvents.

195a, TLC condition - R$_f$ = 0.4 (20% hexanes:ethyl acetate). Crystalline clear solid (Yield = 83%).

195b, TLC condition - R$_f$ = 0.4 (20% hexanes:ethyl acetate). Crystalline clear solid (Yield = 81%).

^{1}H-NMR (400 MHz, CDCl$_3$, δ ppm): 1.44 (s, 9H), 2.06 (s, 3H), 2.50 (s, 3H), 5.46 (s, 1H), 5.68 (s, 1H), 7.55 (d, J 7.6Hz, 1H), 7.69 (s, 1H) and 7.76 (d, J 7.6Hz, 1H).
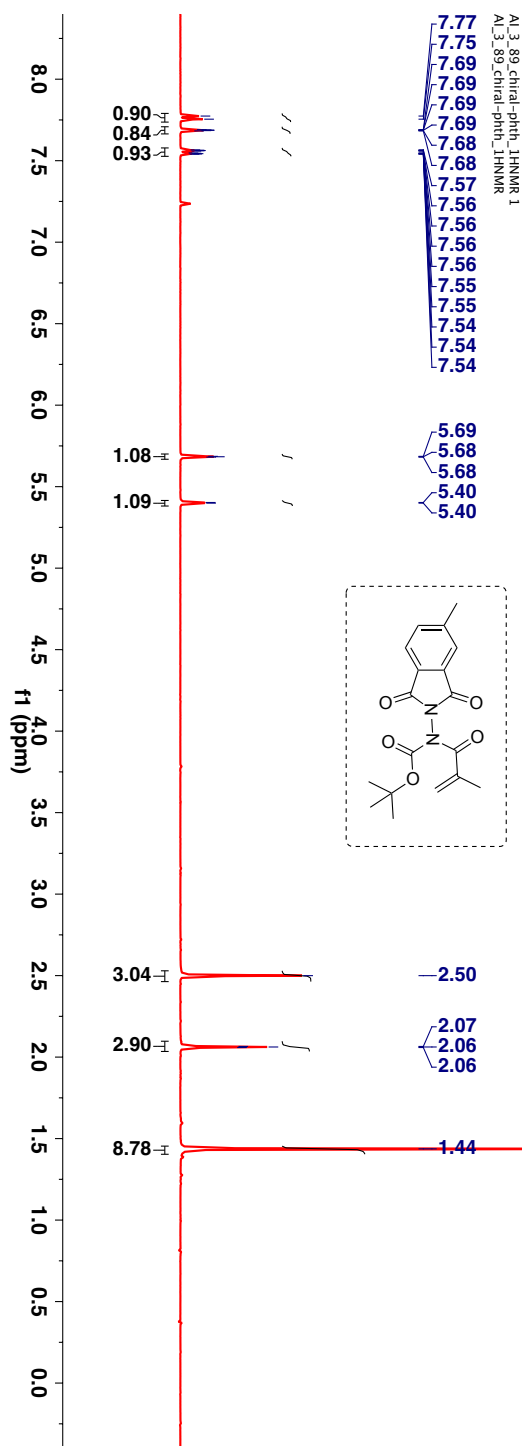
Figure 3.40: ^{1}H-NMR (400 MHz, CDCl$_3$, δ ppm) spectrum of **195a**.

^{13}C-NMR (100 MHz, CDCl$_3$, δ ppm): 22.3, 28.2, 83.1, 124.1, 124.6, 127.5, 130.5, 135.4, 146.3, 153.6 and 165.7.
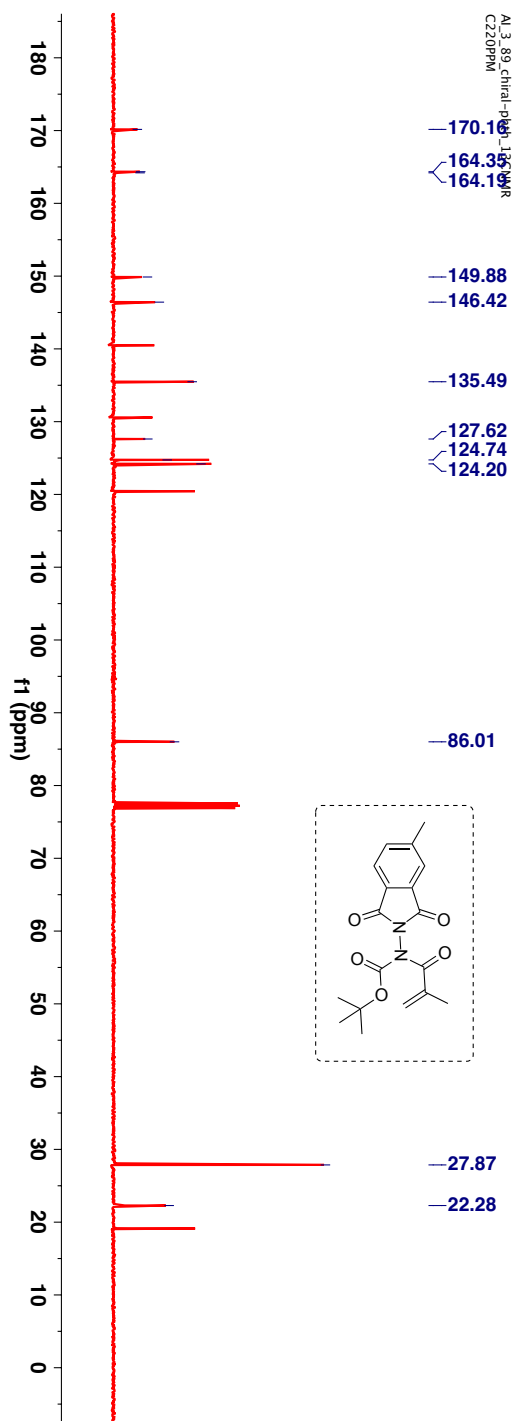
Figure 3.41: ^{13}C-NMR (100 MHz, CDCl$_3$, δ ppm) spectrum of **195a**.

^{1}H-NMR (400 MHz, CDCl$_3$, δ ppm): 1.75 (d, *J* 6.8Hz, 6H), 1.36 (s, 9H), 2.42 (s, 3H), 3.65–3.74 (sep, *J* 6.8Hz, 1H), 7.48 (d, *J* 7.6Hz, 1H), 7.60 (s, 1H) and 7.67 (d, *J* 7.6Hz, 1H).
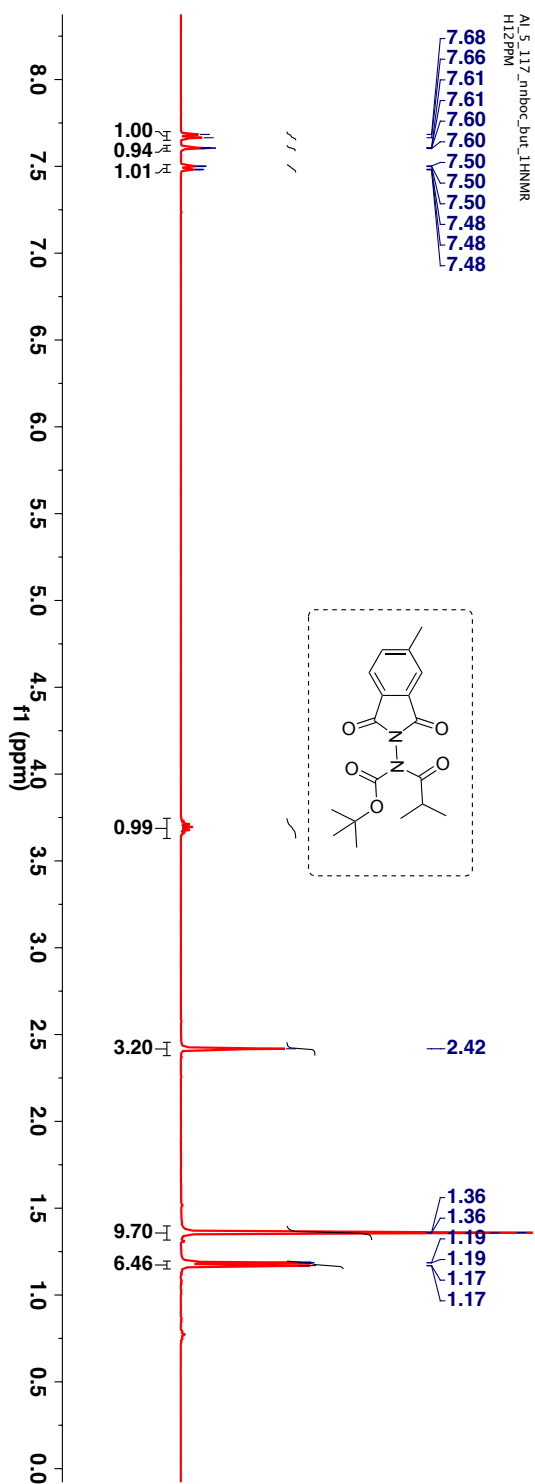
Figure 3.42: ^{1}H-NMR (400 MHz, CDCl$_3$, δ ppm) spectrum of **195b**.

^{13}C-NMR (100 MHz, CDCl$_3$, δ ppm): 19.5, 22.2, 22.8, 34.6, 85.1, 124.0, 124.6, 127.5, 130.5, 146.4, 149.9, 164.1, 164.3 and 176.3.
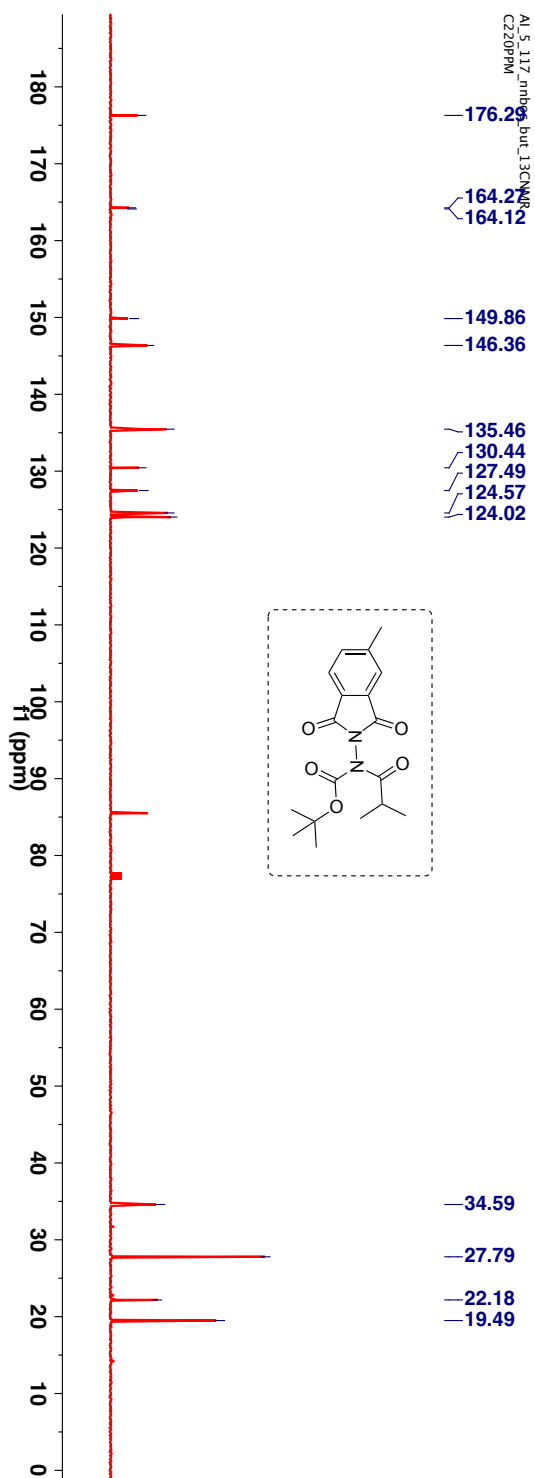
Figure 3.43: ^{13}C-NMR (400 MHz, CDCl$_3$, δ ppm) spectrum of **195b**.

STEP 3

195a X = CH$_2$
195b X = CH$_3$

198a X = CH$_2$
198b X = CH$_3$
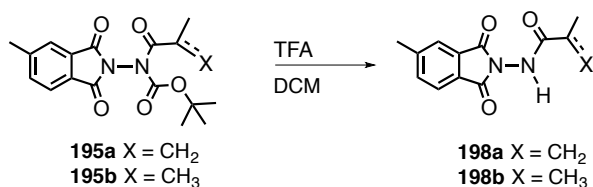
Scheme 3.44: Synthesis of amide derivative **198a/198b**.

Modifying a procedure reported by Cécile et al., to a solution of imide derivative **195a/195b** (1 equiv) in freshly distilled dichloromethane (DCM) was added small volumes of trifluoroacetic acid (8% in DCM) (25 equiv) at 0°C.[94] The mixture was stirred overnight and if necessary more TFA was added until complete consumption of starting material was observed. The solution was concentrated under vacuum. The crude reaction mixture was dissolved in ethyl acetate and the organic layer was sequentially washed with DI water (2 × 10 mL), saturated NaHCO$_3$ (2 × 10 mL) and finally with brine. The organic layer was dried over anhyd Na$_2$SO$_4$, filtered and the solvent was removed under reduced pressure to yield crude product. After concentrating the organic layer, the crude product was purified by combiflash using hexanes and ethyl acetate as the eluting solvents.

198a, TLC condition - R$_f$ = 0.2 (20% ethyl acetate:hexanes). Crystalline clear solid (Yield = 86%).

198b, TLC condition - R$_f$ = 0.2 (20% ethyl acetate:hexanes). Clear solid (Yield = 92%).

^{1}H-NMR (400 MHz, CDCl$_3$, δ ppm): 2.02 (s, 3H), 2.49 (s, 3H), 5.54 (s, 1H), 5.96 (s, 1H), 7.54 (d, 1H, J 7.6Hz), 7.67 (s, 1H), 7.75 (d, 1H, J 7.6Hz) and 7.96 (bs, 1H).
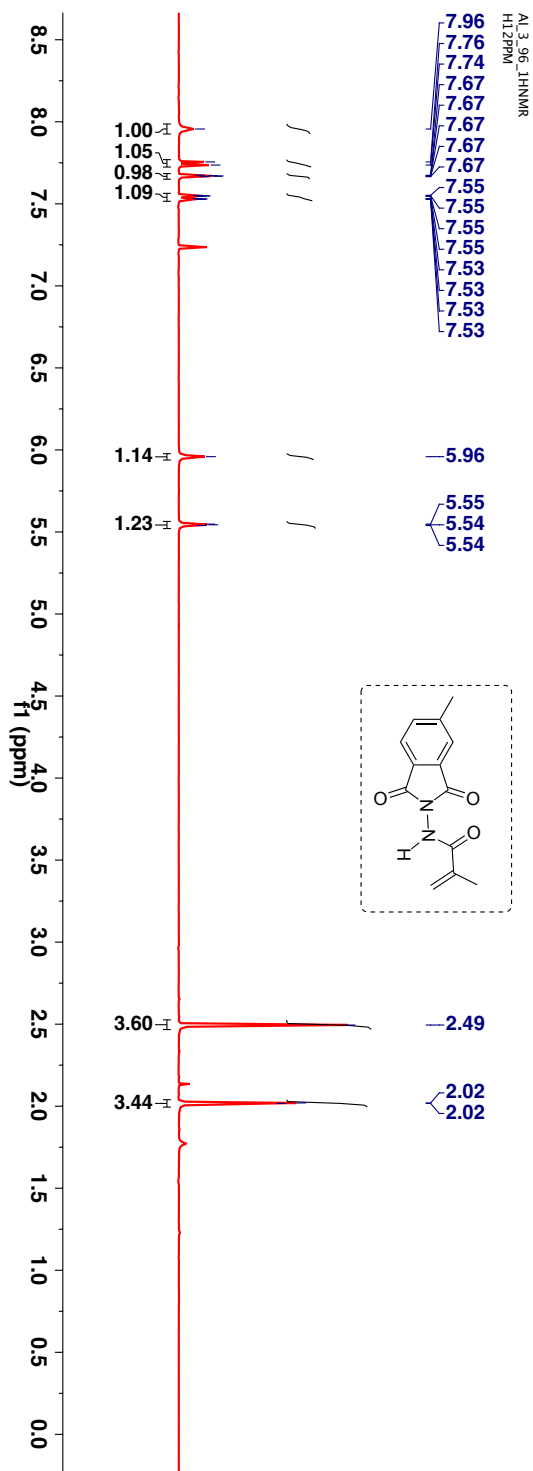
Figure 3.44: ^{1}H-NMR (400 MHz, CDCl$_3$, δ ppm) spectrum of **198a**.

^{13}C-NMR (100 MHz, CDCl$_3$, δ ppm): 18.6, 22.3, 94.6, 122.9, 124.1, 124.7, 124.7, 127.6, 130.6, 135.4, 137.2 and 146.4.
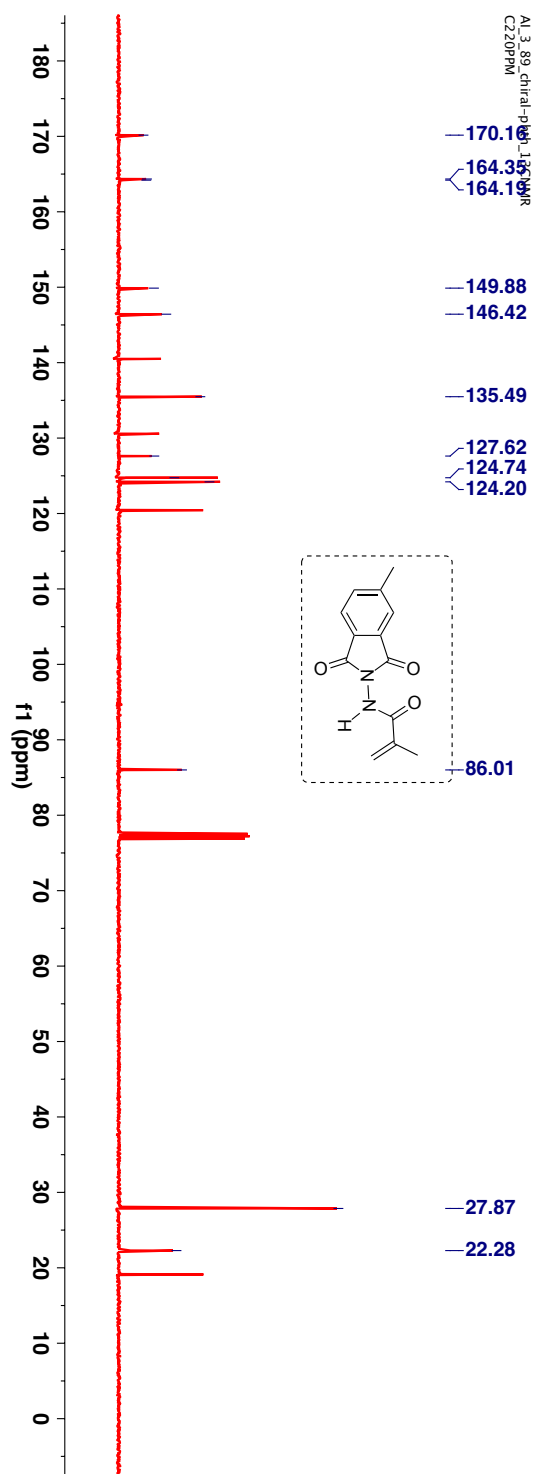
Figure 3.45: ^{13}C-NMR (100 MHz, CDCl$_3$, δ ppm) spectrum of **198a**.

^{1}H-NMR (400 MHz, CDCl$_3$, δ ppm): 1.29 (d, *J* 6.8Hz, 6H), 2.54 (s, 3H), 2.61–2.72 (sep, *J* 6.8Hz, 1H), 7.57 (d, *J* 8Hz, 1H), 7.69–7.7 (m, 2H) and 7.77 (d, *J* 7.6Hz, 1H).
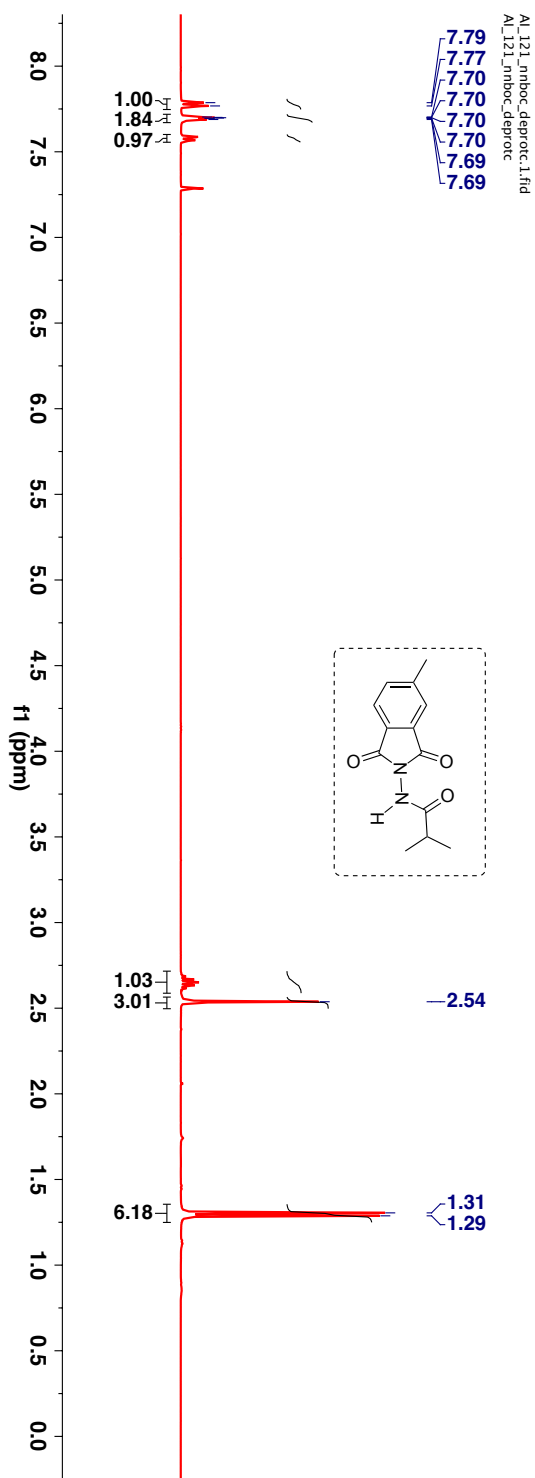
Figure 3.46: ^{1}H-NMR (400 MHz, CDCl$_3$, δ ppm) spectrum of **198b**.

¹³C-NMR (100 MHz, CDCl₃, δ ppm): 19.3, 22.1, 33.4, 123.9, 124.5, 135.2, 146.2, 165.4, 165.5 and 175.8.
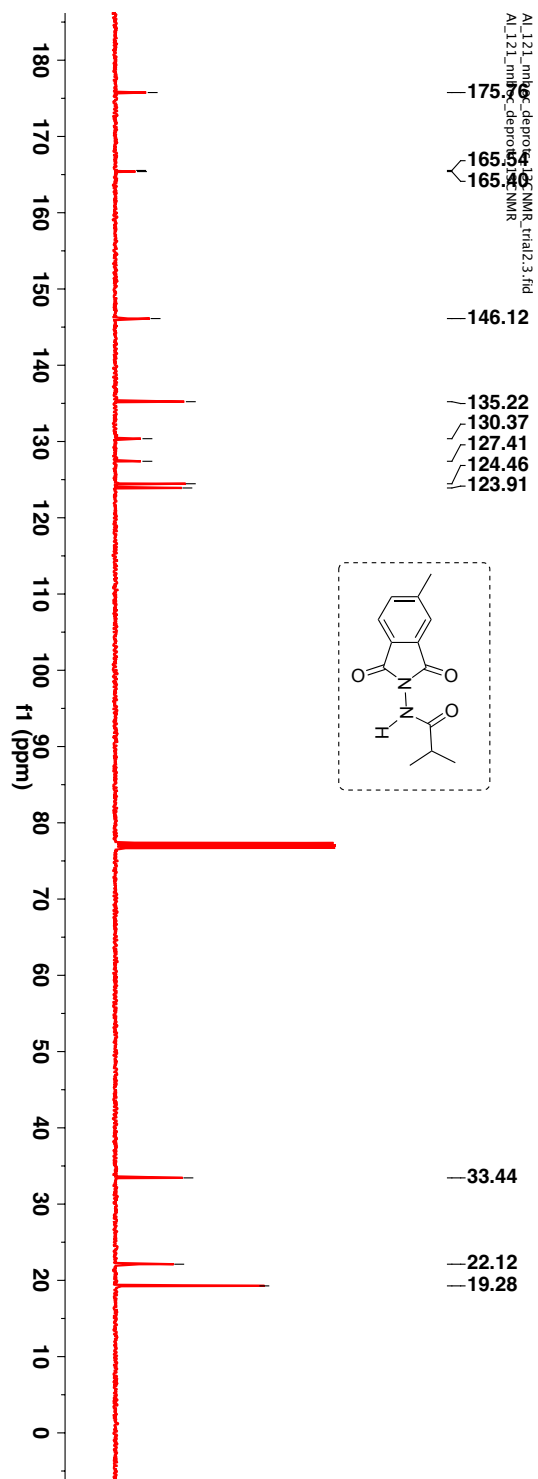
Figure 3.47: ¹³C-NMR (100 MHz, CDCl₃, δ ppm) spectrum of **198b**.

198a X = CH$_2$
198b X = CH$_3$

184c X = CH$_2$
188b X = CH$_3$
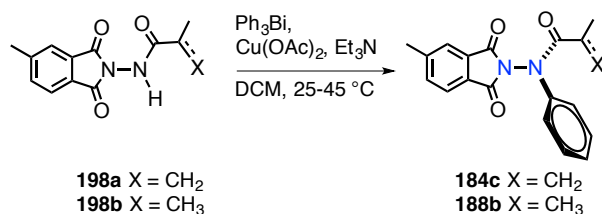
Scheme 3.45: Synthesis of phthalimide based acrylanilide derivative **184c/188b**.

Following the modified procedure reported by Kikugawa et al. A mixture of amide derivative **198**(1 equiv), triphenylbismuth (2 equiv), cupric acetate (1.5 equiv), and triethylamine (1.5 equiv) was stirred in freshly distilled dichloromethane (DCM) for 1.5 h at room temperature under N$_2$ protection and then refluxed for 15 h.[103] After completion of the reaction, the solution was diluted with ethyl acetate (20 mL) and filtered through a short celite pad. The filtrate was evaporated under reduced pressure. The crude product was chromatographed with a flash column using ethyl acetate and hexane as the eluting solvents.

184c, TLC condition - R$_f$ = 0.5 (20% ethyl acetate:hexanes). Crystalline clear solid (Yield = 63%).

188b, TLC condition - R$_f$ = 0.5 (20% ethyl acetate:hexanes). Crystalline solid (Yield = 86%).

^{1}H-NMR (400 MHz, CDCl$_3$, δ ppm): 1.88 (s, 3H), 2.48 (s, 3H), 5.19 (s, 1H), 5.33 (s, 1H), 7.28-7.35 (m, 3H), 7.49-7.54 (m, 3H), 7.66 (s, 1H) and 7.74 (d, 1H, *J* 7.6Hz).
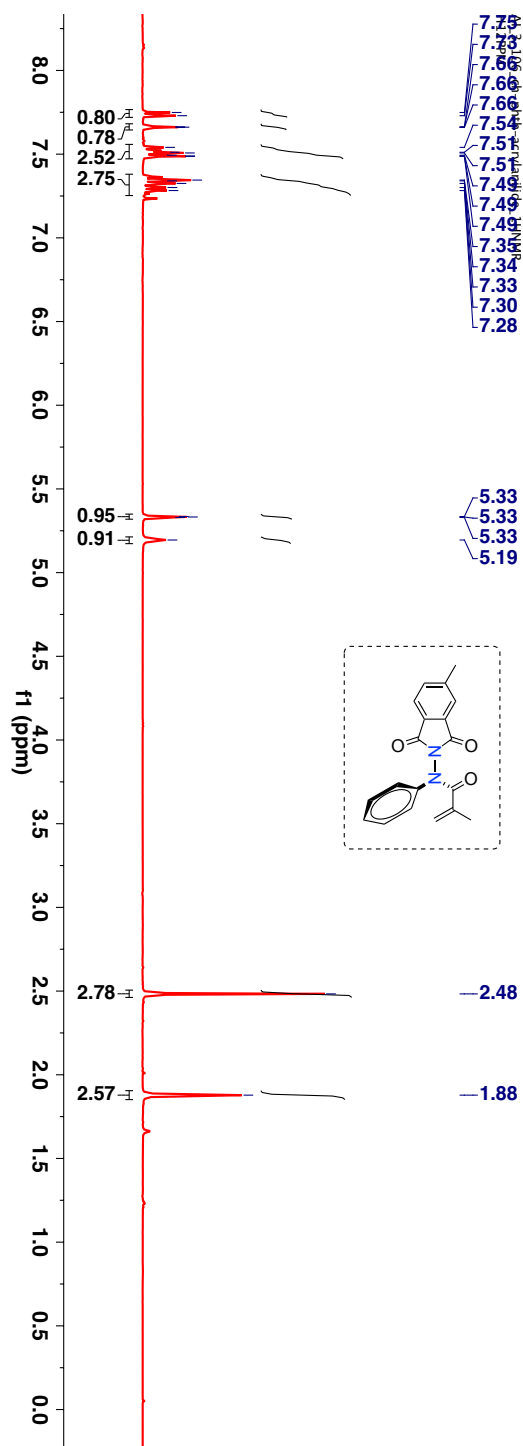
Figure 3.48: ^{1}H-NMR (400 MHz, CDCl$_3$, δ ppm) spectrum of **184c**.

^{13}C-NMR (100 MHz, CDCl$_3$, δ ppm): 19.9, 22.3, 124.2, 124.2, 124.7, 127.6, 126.7, 129.5, 130.5, 132.1, 135.5, 136.9, 138.5, 146.4, 165.2 and 165.3.

Figure 3.49: ^{13}C-NMR (100 MHz, CDCl$_3$, δ ppm) spectrum of **184c**.

HRMS-ESI (m/z) ([M + Na]):

Chemical Formula: $C_{19}H_{16}N_2O_3$

Calculated : 343.1059

Observed : 343.1070

|Δm| : 3.2 ppm
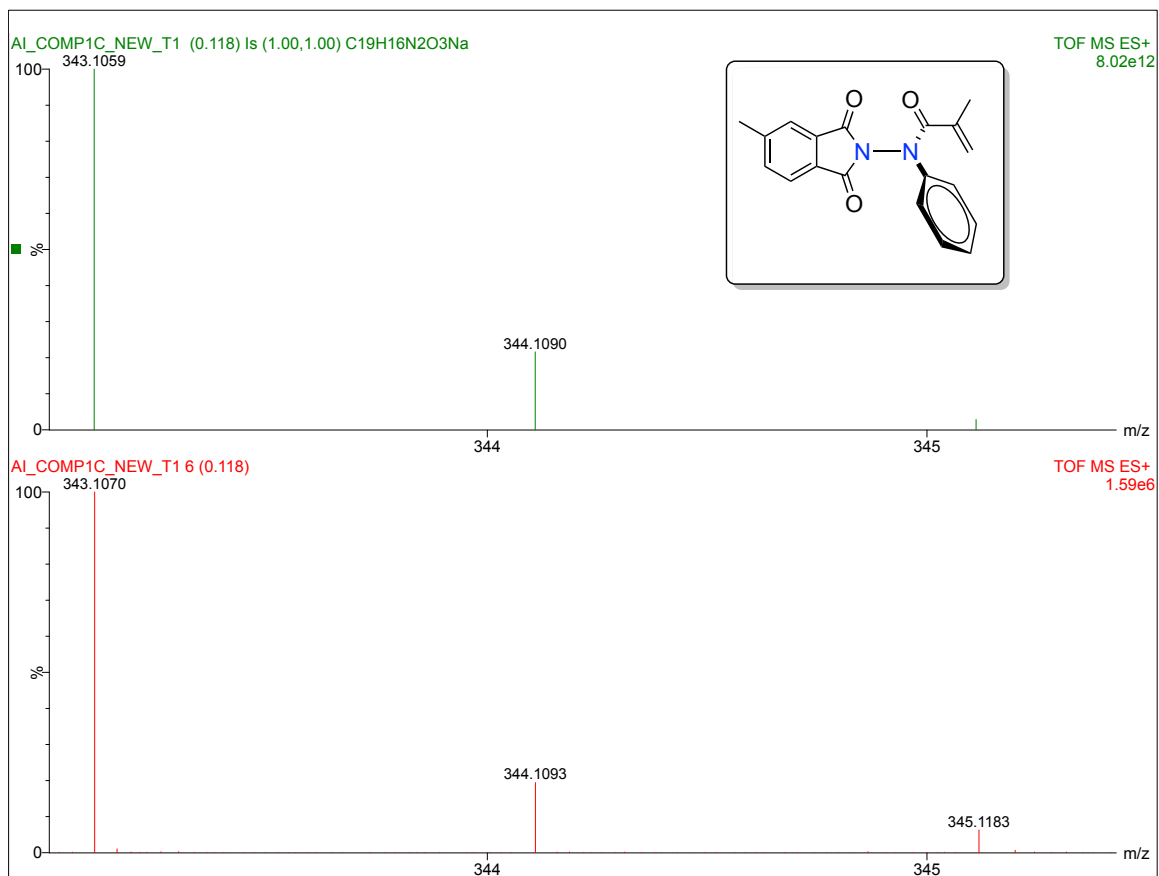
Figure 3.50: HRMS spectra of **184c**.

¹H-NMR (400 MHz, CDCl₃, δ ppm): 1.11 (d, *J* 6.8Hz, 6H), 2.39 (s, 3H), 2.59–2.68 (sep, *J* 6.8Hz, 1H), 7.32–7.45 (m, 4H), 7.56 (m, 1H) and 7.63–7.65 (m, 3H).
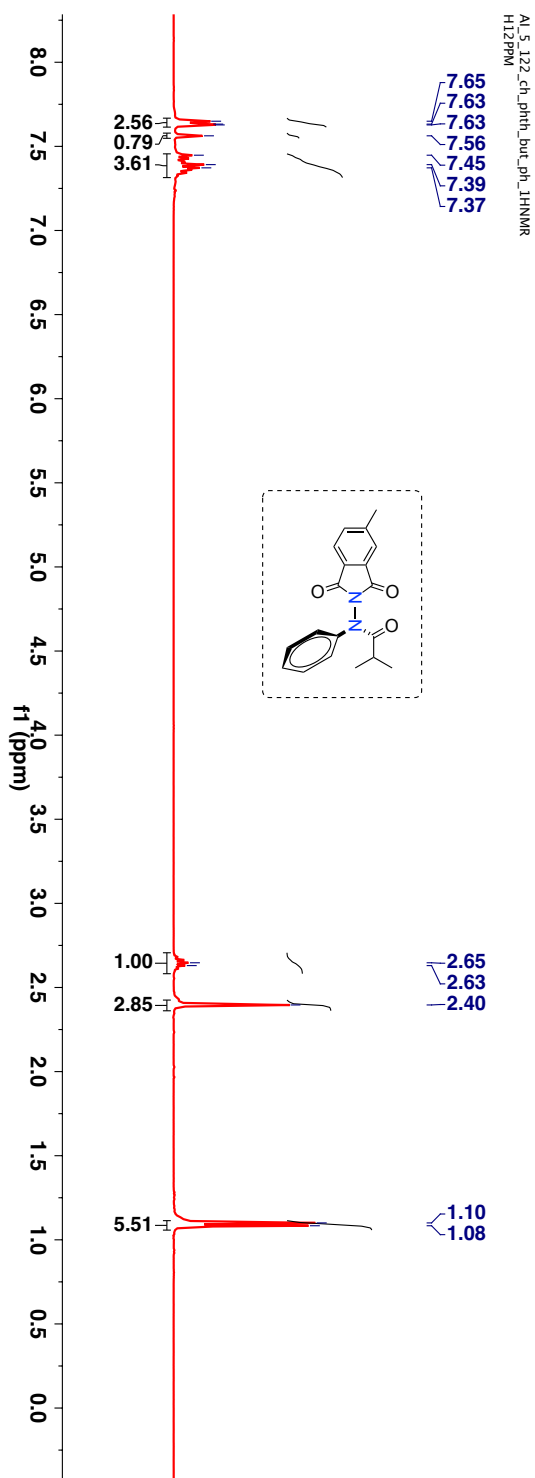
Figure 3.51: ¹H-NMR (400 MHz, CDCl₃, δ ppm) spectrum of **188b**.

^{13}C-NMR (100 MHz, CDCl$_3$, δ ppm): 19.5, 22.2, 31.1, 123.9, 124.5, 127.6, 129.1, 129.7, 130, 130.5, 135.4, 140.6, 146.2, 165.3, 164.4 and 175.6.
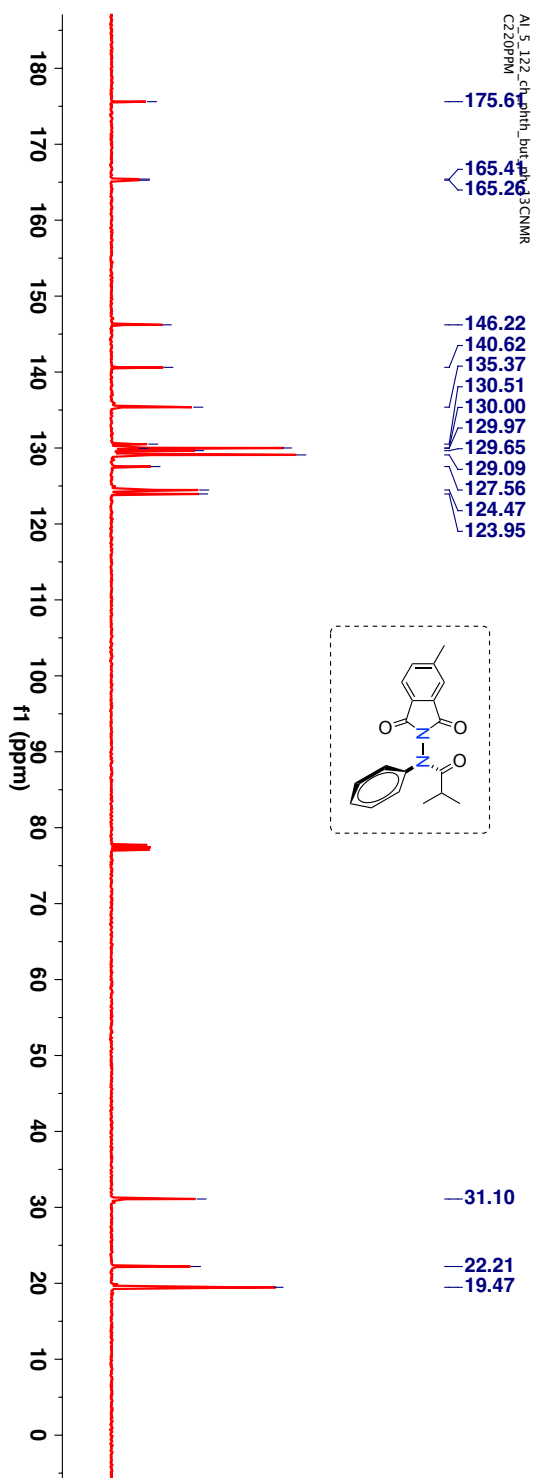
Figure 3.52: ^{13}C-NMR (100 MHz, CDCl$_3$, δ ppm) spectrum of **188b**.

3.15. Synthesis of phthalimide based anilide derivative 197
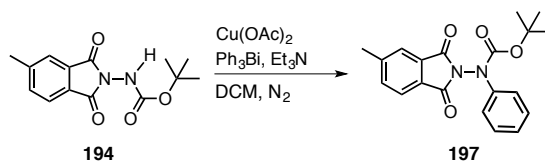
Scheme 3.46: Synthesis of anilide derivative **197**.

Following the modified procedure reported by Kikugawa et al. A mixture of amide derivative **194** (1 equiv), triphenylbismuth (2 equiv), cupric acetate (1.5 equiv), and triethylamine (1.5 equiv) was stirred in freshly distilled dichloromethane (DCM) for 1.5 h at room temperature under N_2 protection and then refluxed for 20 h.[103] After completion of the reaction, the solution was diluted with ethyl acetate (20 mL) and filtered through a short celite pad. The filtrate was evaporated under reduced pressure. The crude product was chromatographed with a flash column using ethyl acetate and hexane as the eluting solvents.

TLC condition - R_f = 0.5 (20% ethyl acetate:hexanes). Crystalline clear solid (Yield = 74%).

¹H-NMR (400 MHz, CDCl₃, δ ppm): 1.40 (s, 9H), 2.50 (s, 3H), 7.21-7.24 (m, 1H), 5.33 (s, 1H), 7.33 (t, 2H, *J* 7.6Hz), 7.52-7.56 (m, 3H), 7.69 (s, 1H) and 7.77 (d, 1H, *J* 7.6Hz).
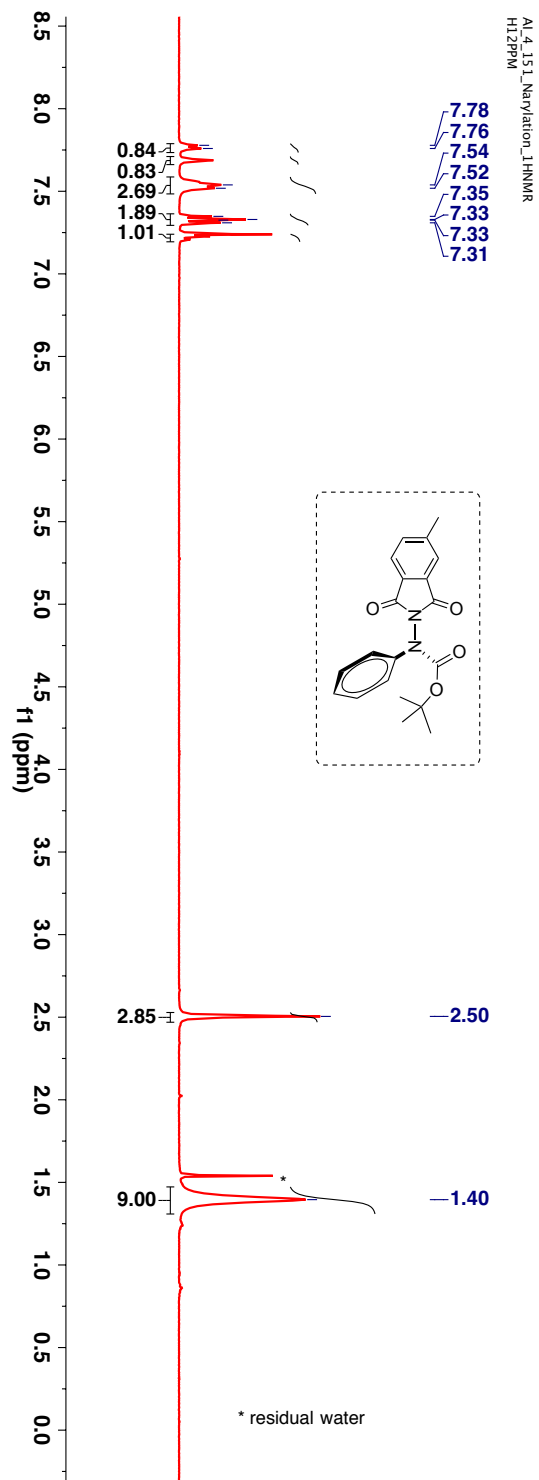
Figure 3.53: ¹H-NMR (400 MHz, CDCl₃, δ ppm) spectrum of **197**.

^{13}C-NMR (100 MHz, CDCl$_3$, δ ppm): 22.3, 28.17, 124.1, 124.6, 129.1, 130.5, 135.5 and 146.4.
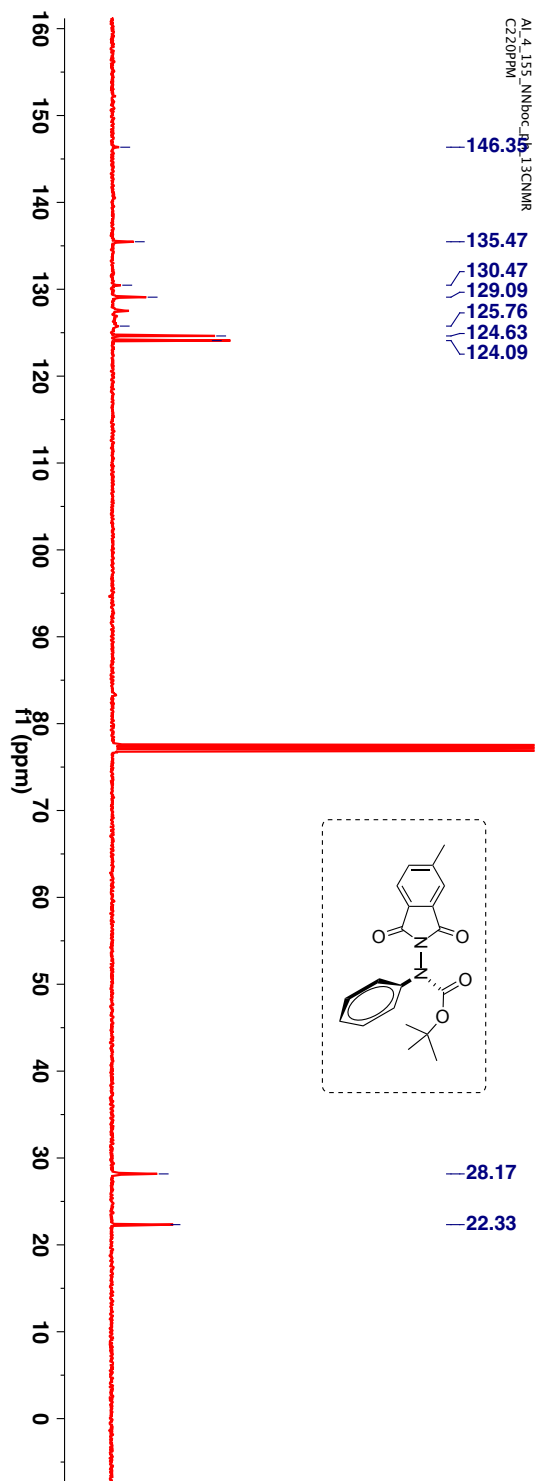
Figure 3.54: ^{13}C-NMR (100 MHz, CDCl$_3$, δ ppm) spectrum of **197**.

3.16. Synthesis of succinimide based acrylanilide derivative 184b/184i
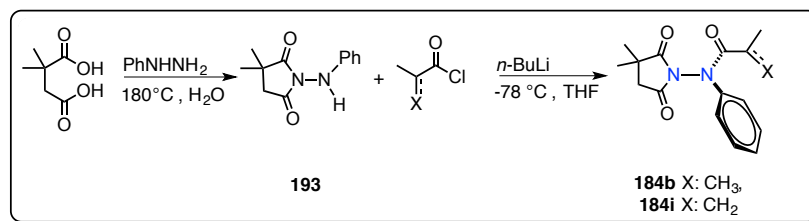
Scheme 3.47: Synthesis of acrylanilide derivative **184b/184i**.

STEP 1
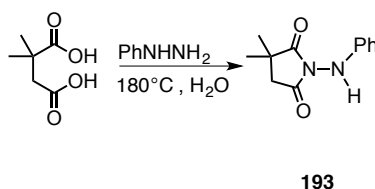
Scheme 3.48: Synthesis of anilide derivative **193**.

Following the modified procedure reported by Kamiński et al., a suspension of 2,2-dimethyl-succinic acid (1 equiv) in water (10 mL per gram of acid derivative), phenylhydrazine (1 equiv) was added.[91] The mixture was heated in an oil bath at 180 °C with simultaneous removal of water. After 1 h, the mixture was brought to room temperature and the crude was diluted with ethyl acetate and the organic layer was sequentially washed with 10% HCl, (2 × 10 mL), DI water (2 × 10 mL), saturated NaHCO$_3$ (2 × 10 mL) and finally with brine. The organic layer was dried over anhyd Na$_2$SO$_4$, filtered and the solvent was removed under reduced pressure to yield crude product. After concentrating the organic layer, the crude product was purified by combiflash using hexanes and ethyl acetate mixture to get the desired compound.

TLC condition - R$_f$ = 0.3 (30% ethyl acetate:hexanes). Crystalline solid (Yield = 33%).

^{1}H-NMR (400 MHz, CDCl$_3$, δ ppm): 1.48 (s, 6H), 2.62 (s, 2H), 6.21 (bs, 1H), 6.70-6.73 (m, 2H), 6.93 (m, 2H) and 7.19 (m, 1H).
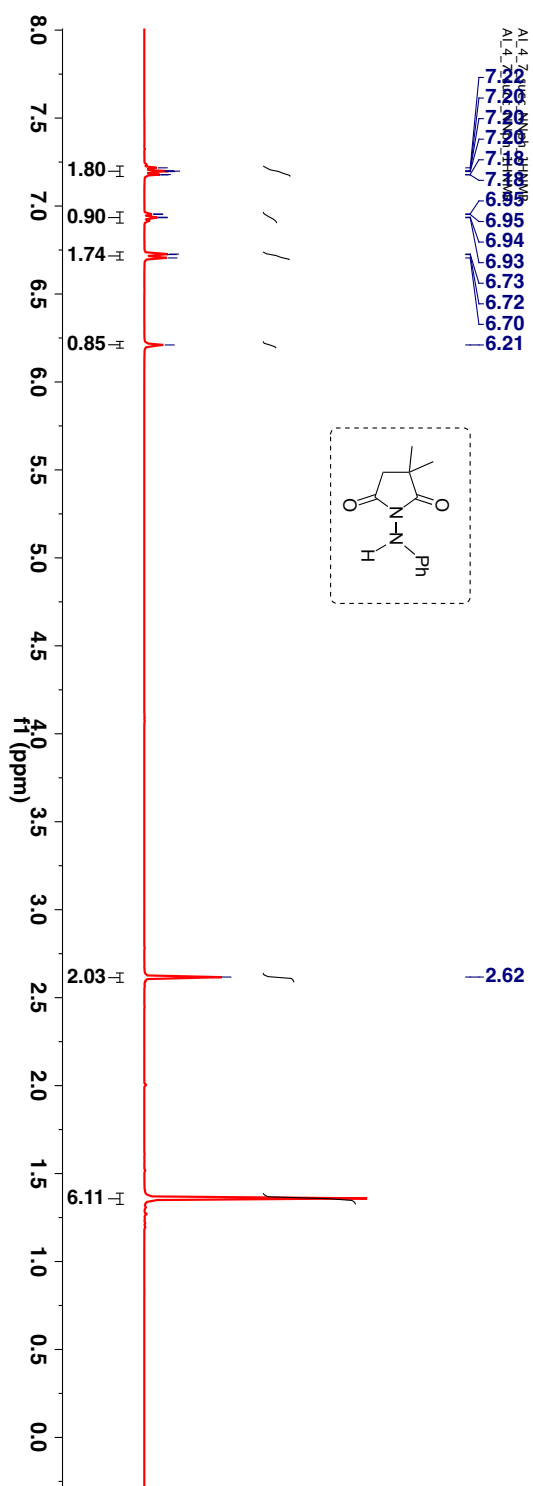
Figure 3.55: ^{1}H-NMR (400 MHz, CDCl$_3$, δ ppm) spectrum of **193**.

STEP 2
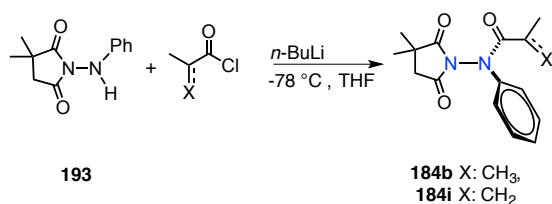
Scheme 3.49: Synthesis of acrylanilide derivative **184b/184i**.

Hydrazide derivative **193** (1 equiv) was dissolved in anhydrous THF under an inert atmosphere. The solution was then cooled to -78 °C. To this cold solution *n*-BuLi (2.5 M, 1.1 equiv) was added slowly. The mixture was stirred at this temperature for 1 h. The reaction was quenched with anhydrous appropriate acid chloride (1 equiv). The stirring was continued for another 2 h after which the solution was quenched with slow addition of ~10 mL of saturated NH_4Cl. (Note: the solution was quenched at -78 °C). The solution was further stirred for 35 min and then diluted with diethyl ether and the organic layer was sequentially washed with DI water (2 × 10 mL), saturated $NaHCO_3$ (2 × 10 mL) and finally with brine. The organic layer was dried over anhyd Na_2SO_4, filtered and the solvent was removed under reduced pressure to yield crude product. After concentrating the organic layer, the crude product was purified by combiflash using hexanes and ethyl acetate mixture to get the desired compound.

184b, TLC condition - R_f = 0.3 (50% ethyl acetate:hexanes). Crystalline solid (Yield = 88%).

184i, TLC condition - R_f = 0.5 (50% ethyl acetate:hexanes). Solid (Yield = 61%).

¹H-NMR (400 MHz, CDCl₃, δ ppm): 1.27 (s, 3H), 1.40 (bs, 3H), 1.83 (bs, 3H), 2.51-2.61 (m, 2H), 5.19 (s, 1H), 5.26 (s, 1H), 7.30-7.33 (m, 3H) and 7.39-7.41 (m, 2H).
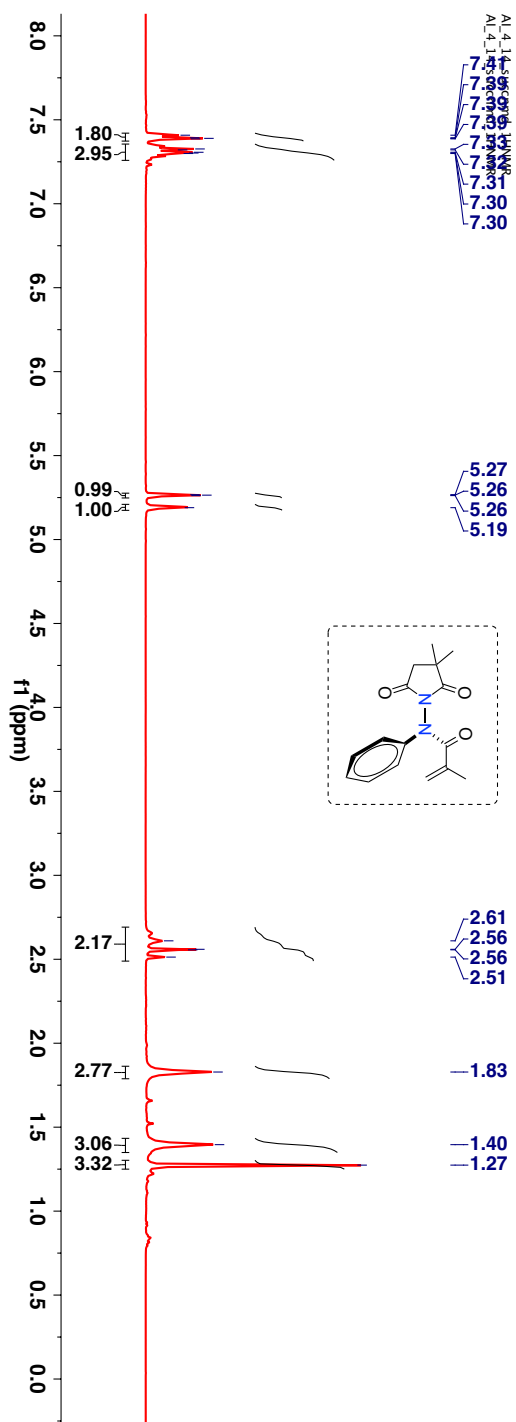
Figure 3.56: ¹H-NMR (400 MHz, CDCl₃, δ ppm) spectrum of **184b**.

^{13}C-NMR (100 MHz, CDCl$_3$, δ ppm): 19.9, 25.3, 42.2, 127.5, 128.8, 129.6, 173.5 and 179.5.
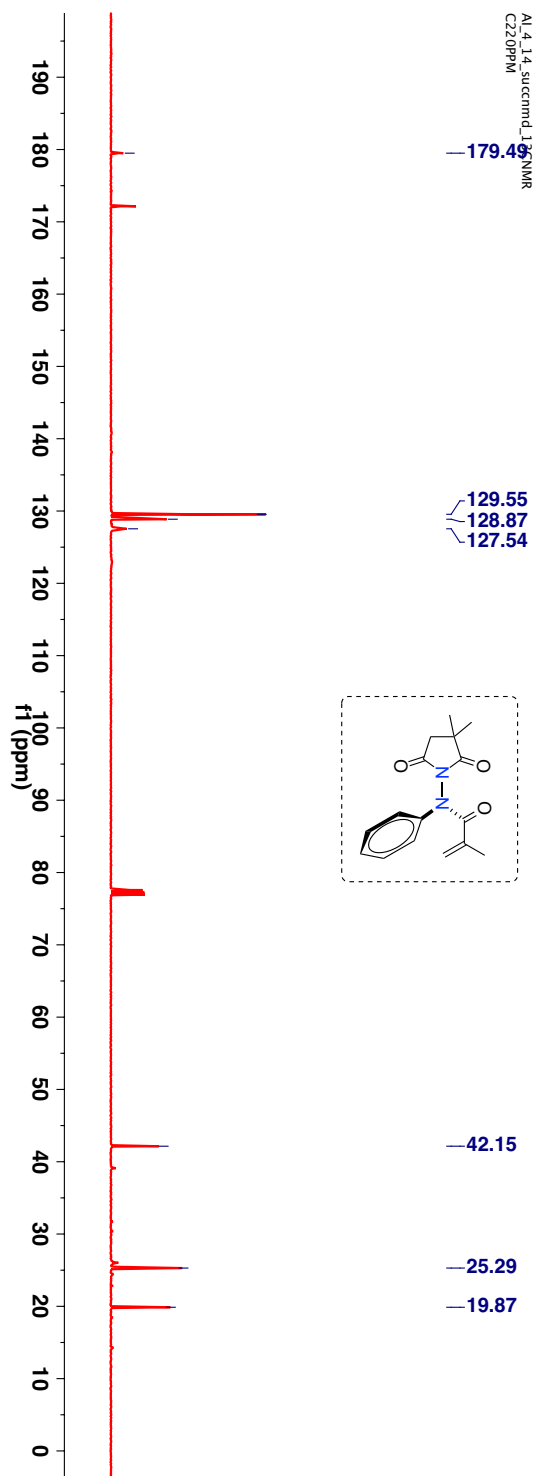
Figure 3.57: ^{13}C-NMR (100 MHz, CDCl$_3$, δ ppm) spectrum of **184b**.

HRMS-ESI (m/z) ([M + Na]):

Chemical Formula: $C_{16}H_{18}N_2O_3$

Calculated   : 343.1059

Observed   : 343.1070

|Δm| : 3.2 ppm
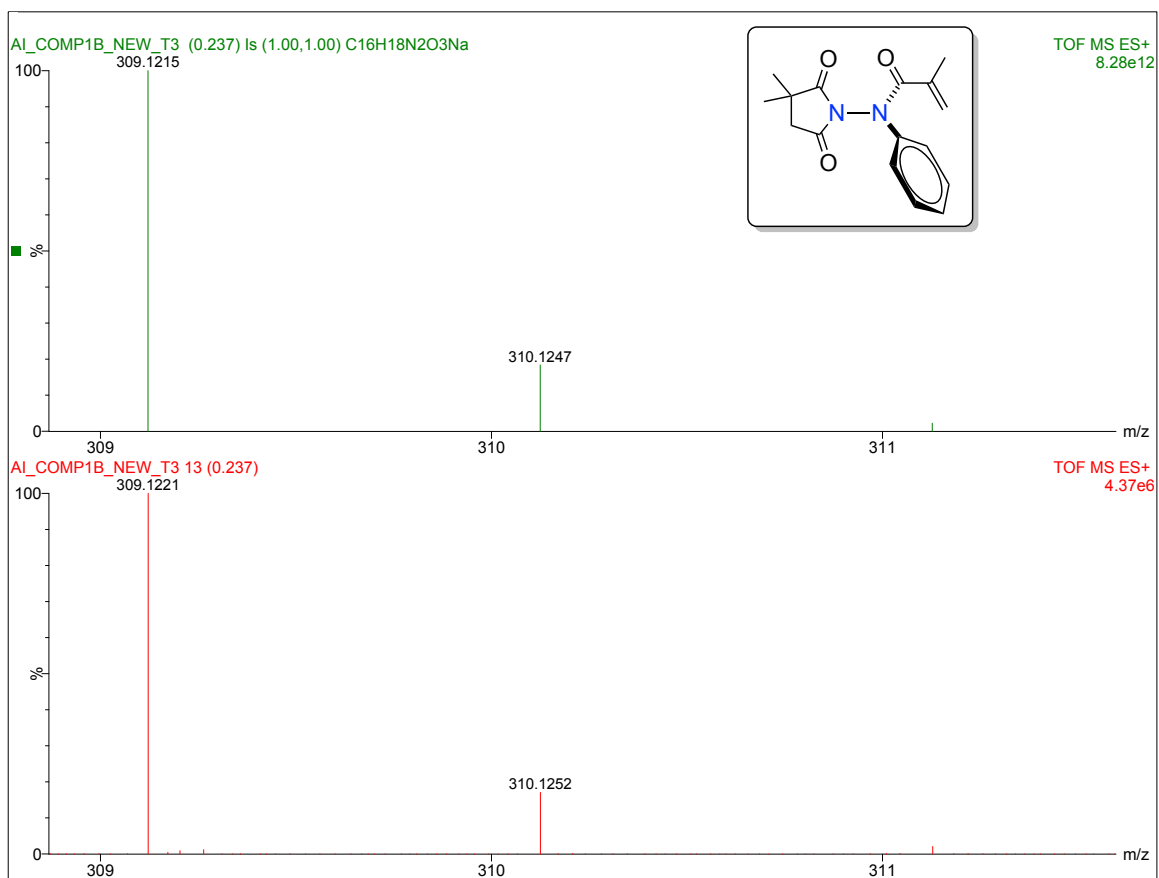
Figure 3.58: HRMS spectra of **184b**.

^{1}H-NMR (400 MHz, CDCl$_3$, δ ppm): 1.29 (dd, J_1 3.2 Hz, J_2 2.4 Hz, 6H), 1.30 (s, 3H), 1.47 (s, 3H), 2.53-2.69 (m, 3H), 7.44-7.48 (m, 3H) and 7.62-7.64 (m, 2H).
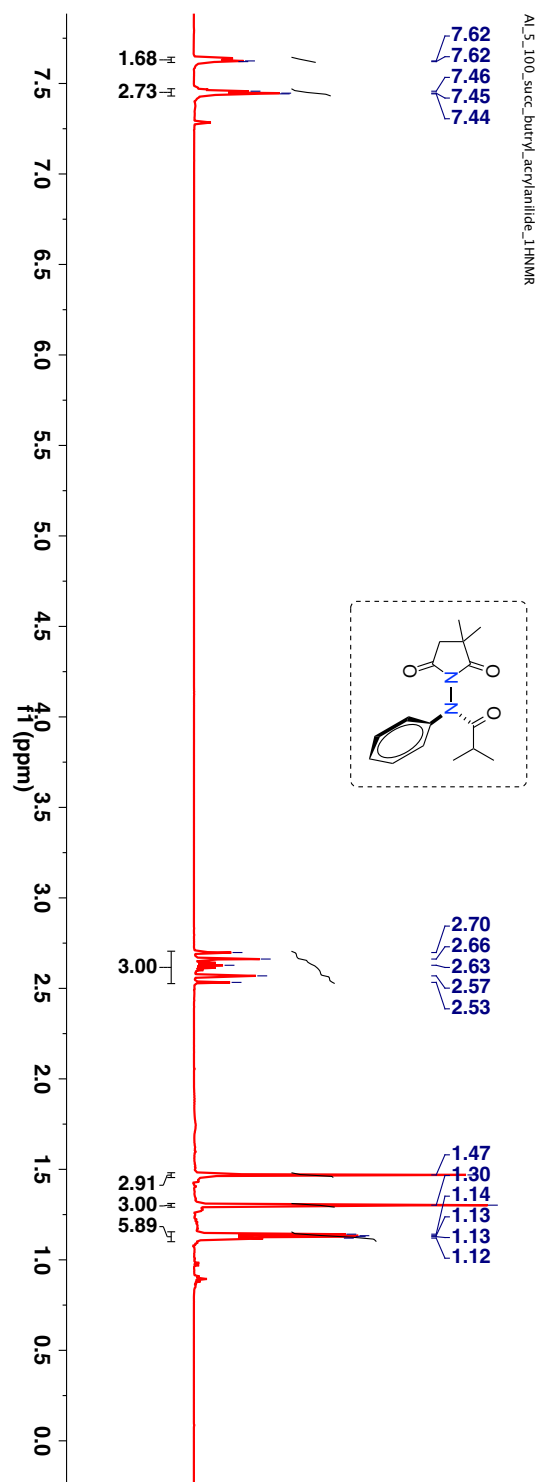
Figure 3.59: ^{1}H-NMR (400 MHz, CDCl$_3$, δ ppm) spectrum of **184i**.

^{13}C-NMR (100 MHz, CDCl$_3$, δ ppm): 19.4, 25.2, 26.4, 30.9, 39.1, 42.2, 129.1, 129.8, 129.9, 139.8, 172.3, 175.1 and 179.8.
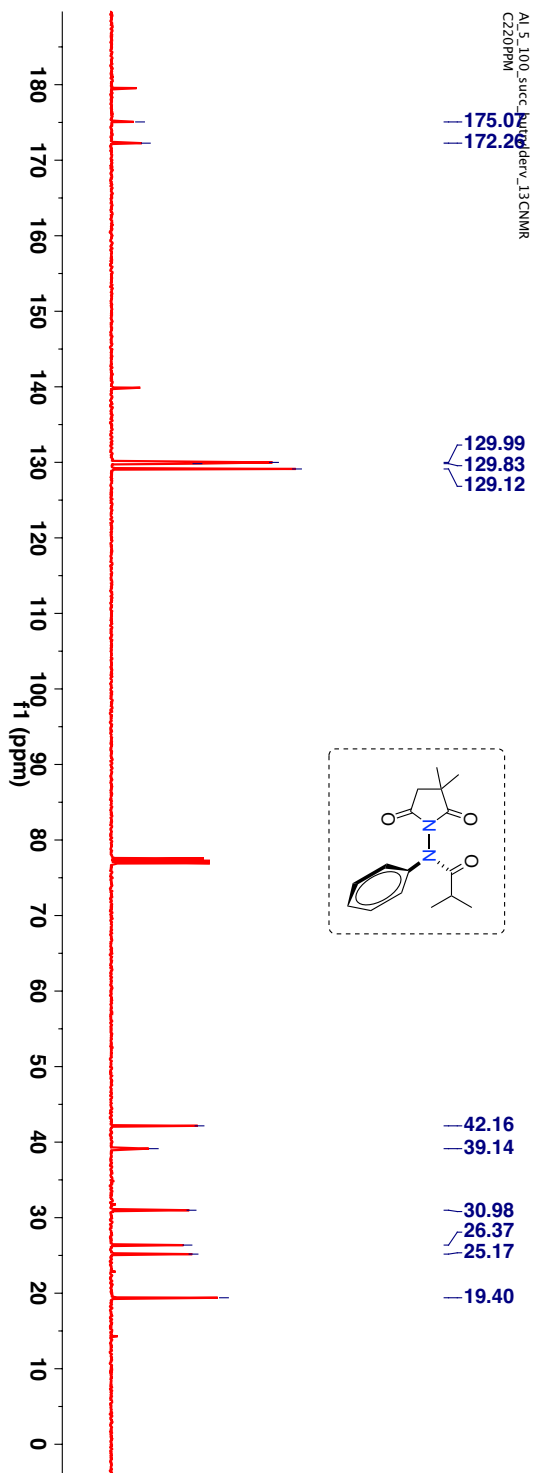
Figure 3.60: ^{13}C-NMR (100 MHz, CDCl$_3$, δ ppm) spectrum of **184i**.

3.17. Synthesis of point chiral succinimide based acrylanilide derivative 184f.
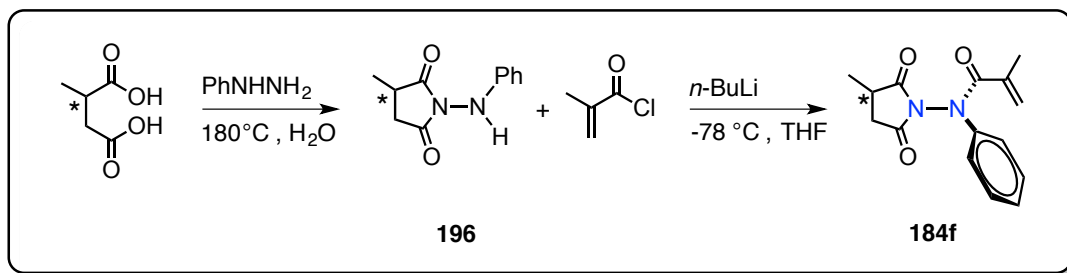
Scheme 3.50: Synthesis of acrylanilide derivative (R)-**184f**.

<u>STEP 1</u>
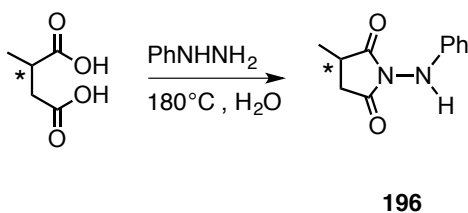
Scheme 3.51: Synthesis of anilide derivative **196**.

Following the modified procedure reported by Kamiński et al., a suspension of (R)-(+)-methyl-succinic acid (1 equiv) in water (10 mL per gram of acid), phenyl hydrazine (1 equiv) was added.[91] The mixture was heated in an oil bath at 180 °C with simultaneous removal of water. After 1 h, the mixture was brought to room temperature and the crude was diluted with ethyl acetate and the organic layer was sequentially washed with 10% HCl, (2 × 10 mL), DI water (2 × 10 mL), saturated $NaHCO_3$ (2 × 10 mL) and finally with brine. The organic layer was dried over anhyd Na_2SO_4, filtered and the solvent was removed under reduced pressure to yield crude product. After concentrating the organic layer, the crude product was purified by combiflash using hexanes and ethyl acetate mixture to get the desired compound.

TLC condition - R_f = 0.3 (50% ethyl acetate:hexanes). Crystalline solid (Yield = 40%)

^{1}H-NMR (400 MHz, CDCl$_3$, δ ppm): 1.41 (d, 3H, *J* 7.2Hz), 2.44 (dd, 1H, *J$_1$* 17.6Hz, *J$_2$* 3.6Hz), 2.95-3.07 (m, 2H), 6.09 (bs, 1H), 6.76 (d, 2H, *J* 8Hz), 6.97 (t, 1H, *J* 7.6Hz) and 7.21-7.25 (m, 2H).
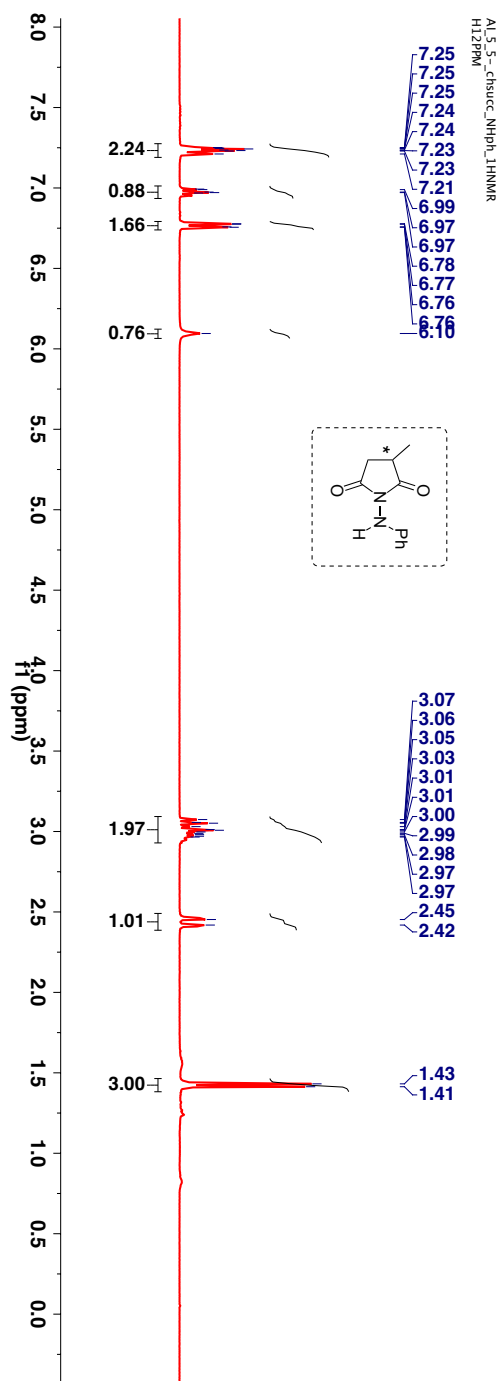
Figure 3.61: ^{1}H-NMR (400 MHz, CDCl$_3$, δ ppm) spectrum of **196**.

^{13}C-NMR (100 MHz, CDCl$_3$, δ ppm): 17.2, 34.3, 34.9, 114.9, 123.0, 129.6, 145.3, 174.1 and 179.4.

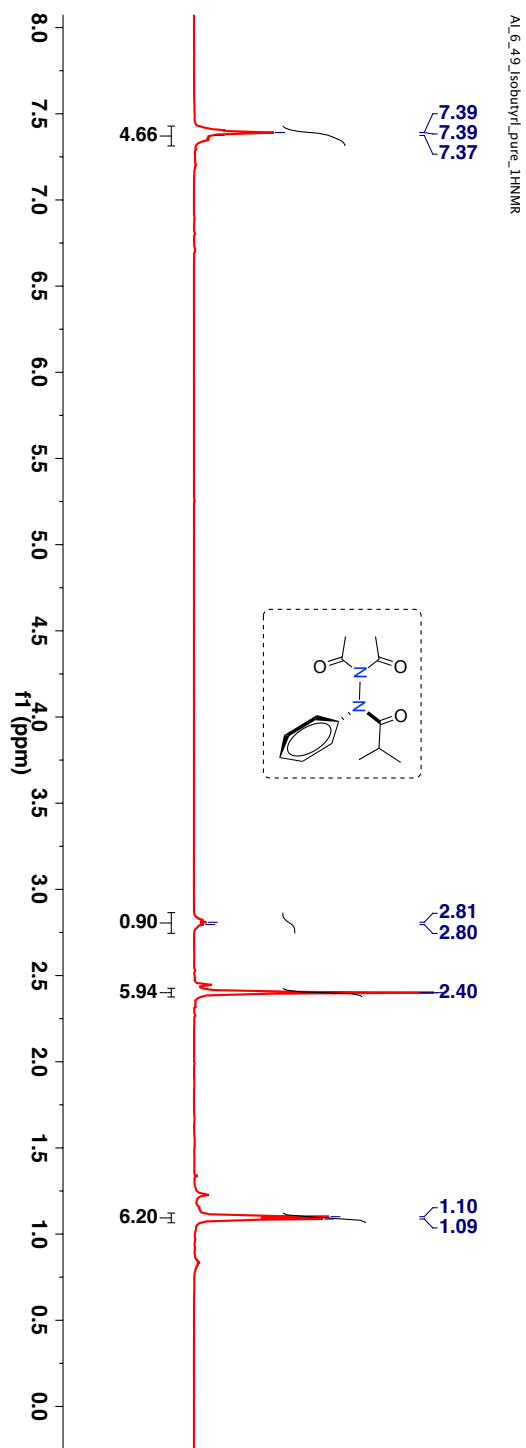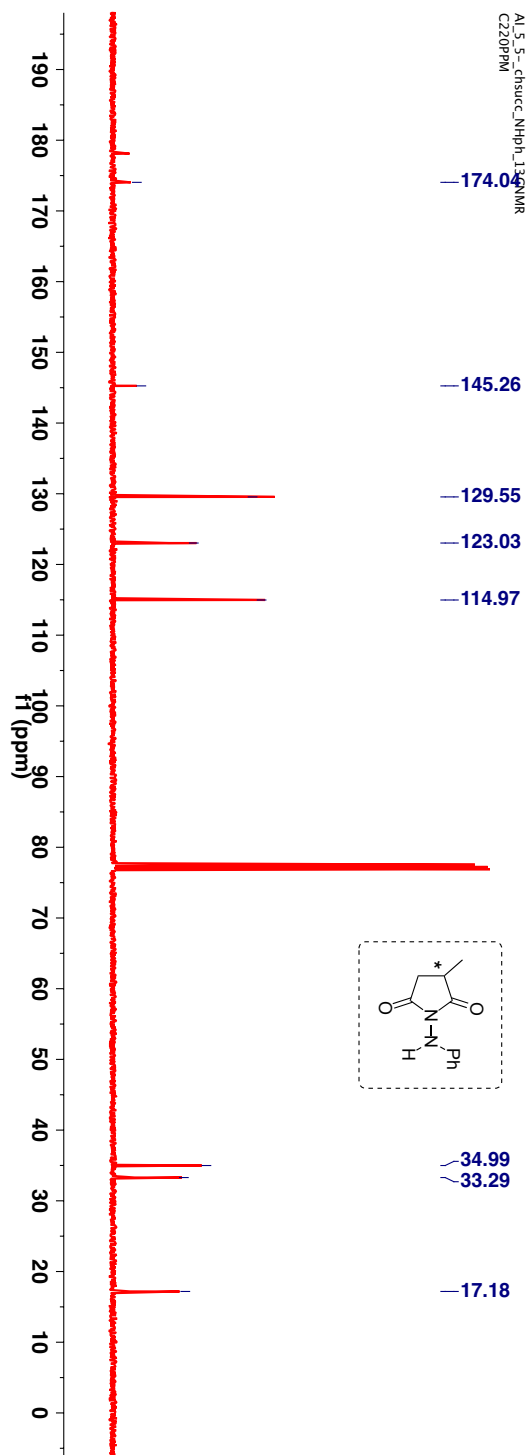**Figure 3.62:** ^{13}C-NMR (100 MHz, CDCl$_3$, δ ppm) spectrum of **196**.

STEP 2
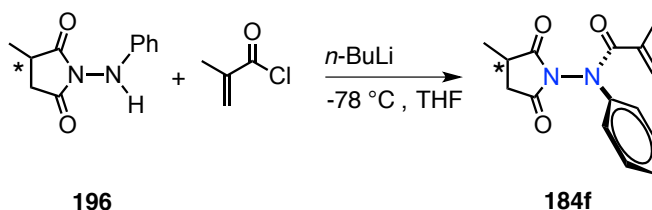
Scheme 3.52: Synthesis of acrylanilide derivative (*R*)-**184f**.

Hydrazide derivative **196** (1 equiv) was dissolved in anhydrous THF under an inert atmosphere. The solution was then cooled to -78 °C. To this cold solution *n*-BuLi (2.5 M, 1.1 equiv) was added slowly. The mixture was stirred at this temperature for 1 h. The reaction was quenched with anhydrous methacryloyl chloride (1.3 equiv). The stirring was continued for another 2 h after which the solution was quenched with slow addition of ~10 mL of saturated NH$_4$Cl. (Note: the solution was quenched at -78 °C). The solution was further stirred for 35 min and then diluted with diethyl ether and the organic layer was sequentially washed with DI water (2 × 10 mL), saturated NaHCO$_3$ (2 × 10 mL) and finally with brine. The organic layer was dried over anhyd Na$_2$SO$_4$, filtered and the solvent was removed under reduced pressure to yield crude product. After concentrating the organic layer, the crude product was purified by combiflash using hexanes and ethyl acetate mixture to get the desired compound.

TLC condition - R$_f$ = 0.6 (50% ethyl acetate:hexanes). Crystalline clear solid (Yield = 75%).

Figure 3.63: Crude ^{1}H-NMR (400 MHz, CDCl$_3$, δ ppm) spectrum of (*R*)-**184f**.

^{1}H-NMR (400 MHz, CDCl$_3$, δ ppm, rotamer peaks are reported together): 1.29 (d, *J* 6.8 Hz), 1.39-1.43 (m), 1.83 (bs), 2.28-2.45 (m), 2.84-3.05 (m), 5.19 (s), 5.27 (m), 7.29-7.35 (m) and 7.40-7.43 (m).
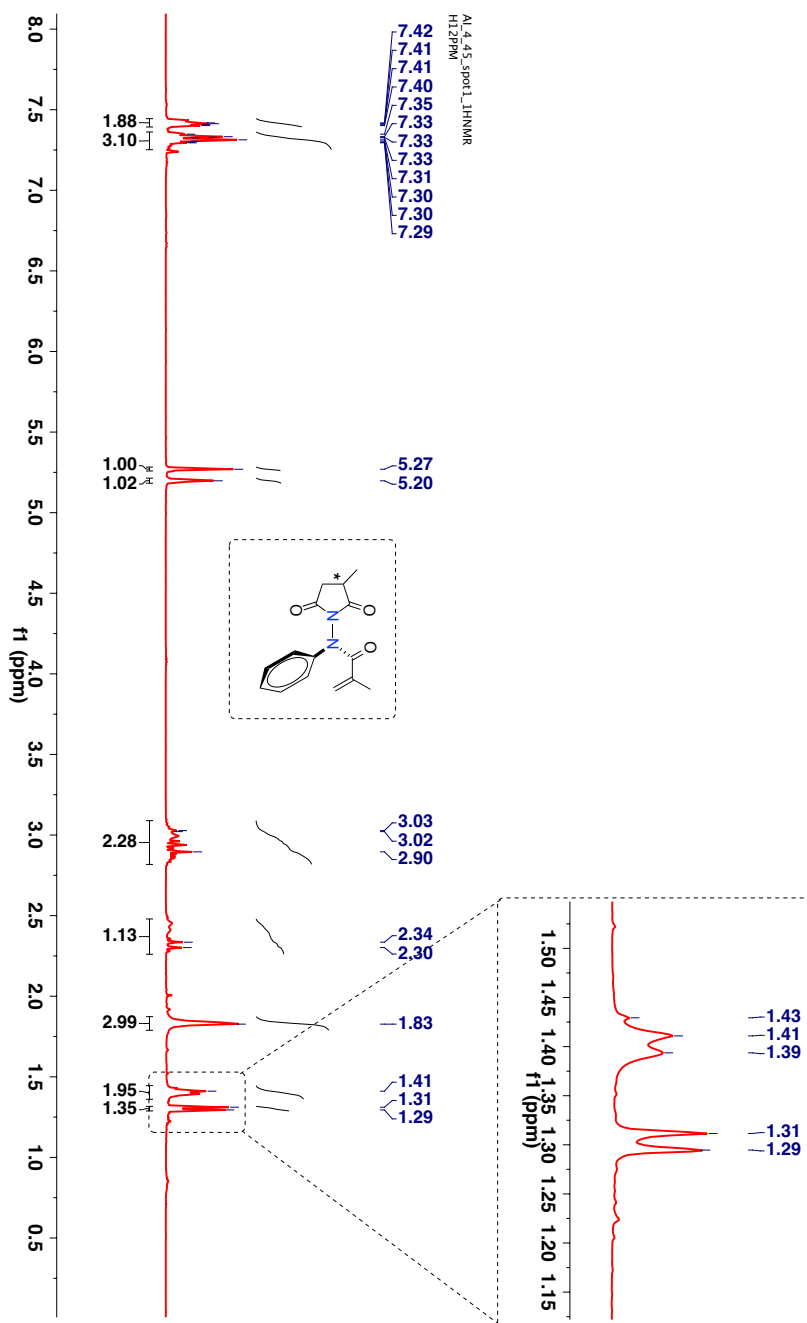
Figure 3.64: ^{1}H-NMR (400 MHz, CDCl$_3$, δ ppm) spectrum of (*R*)-**184f**.

Parameters

	Parameter	Value (f2, f1)
1	Origin	Bruker BioSpin GmbH
2	Solvent	CDCl3
3	Temperature	298.2
4	Experiment	COSY
5	Probe	5 mm PABBO BB/ 19F–1H/ D Z–GRD Z108618/ 0645
6	Number of Scans	4
7	Receiver Gain	197
8	Relaxation Delay	2.0000
9	Pulse Width	14.7000
10	Acquisition Date	2015–07–29T12:52:02
11	Spectrometer Frequency	(400.13, 400.13)
12	Spectral Width	(5341.9, 5341.9)
13	Lowest Frequency	(–265.3, –265.3)
14	Nucleus	(1H, 1H)
15	Acquired Size	(1024, 128)
16	Spectral Size	(1024, 1024)

Parameters

	Parameter	Value (f2, f1)
1	Origin	Bruker BioSpin GmbH
2	Solvent	CDCl3
3	Temperature	298.2
4	Experiment	COSY
5	Probe	5 mm PABBO BB/ 19F–1H/ D Z–GRD Z108618/ 0645
6	Number of Scans	4
7	Receiver Gain	197
8	Relaxation Delay	2.0000
9	Pulse Width	14.7000
10	Acquisition Date	2015–07–29T12:52:02
11	Spectrometer Frequency	(400.13, 400.13)
12	Spectral Width	(5341.9, 5341.9)
13	Lowest Frequency	(–265.3, –265.3)
14	Nucleus	(1H, 1H)
15	Acquired Size	(1024, 128)
16	Spectral Size	(1024, 1024)

Figure 3.65: COSY (400 MHz, CDCl$_3$, δ ppm) spectrum of (*R*)-**184f**.

Figure 3.66: NOESY (400 MHz, CDCl₃, δ ppm) spectrum of (*R*)-**184f**.

^{13}C-NMR (100 MHz, CDCl$_3$, δ ppm, rotamer peaks are reported together): 21.7, 22.0, 22.1, 38.4, 38.5, 39.9, 40.0, 41.9, 131.6, 132.7, 132.9, 133.8, 133.9, 133.9, 134.3, 134.5, 134.6, 177.5, 177.7, 181.6 and 181.7.
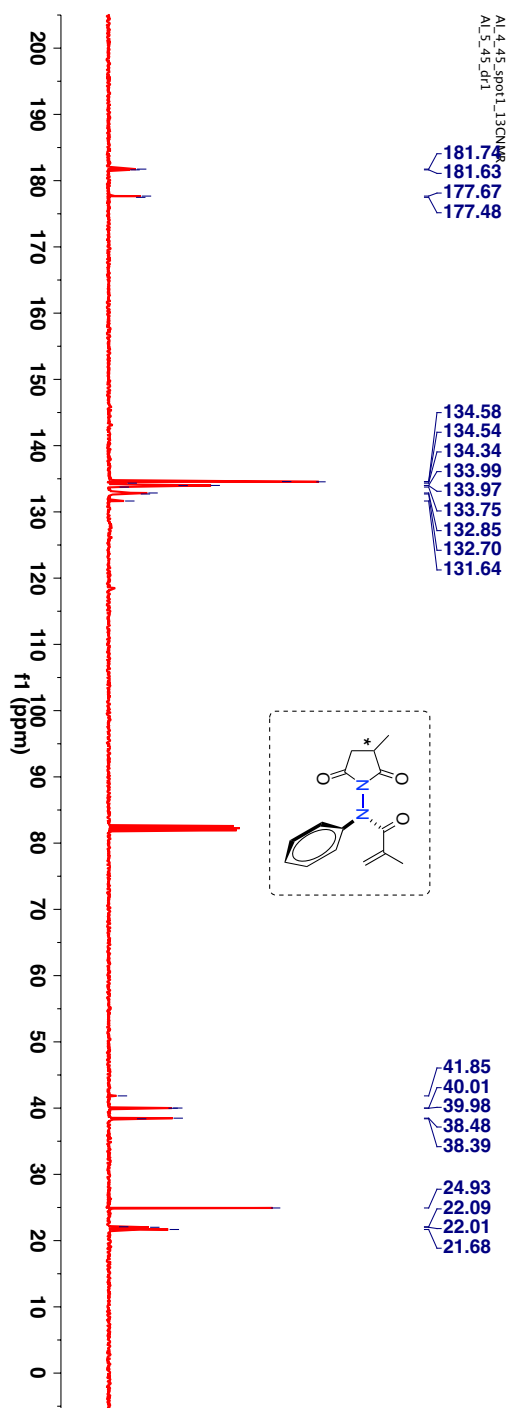
Figure 3.67: ^{13}C-NMR (100 MHz, CDCl$_3$, δ ppm) spectrum of (*R*)-**184f**.

HRMS-ESI (m/z) ([M + Na]):

Chemical Formula: $C_{16}H_{20}N_2O_3$

Calculated : 295.1059

Observed : 295.1073

|Δm| : 4.7 ppm
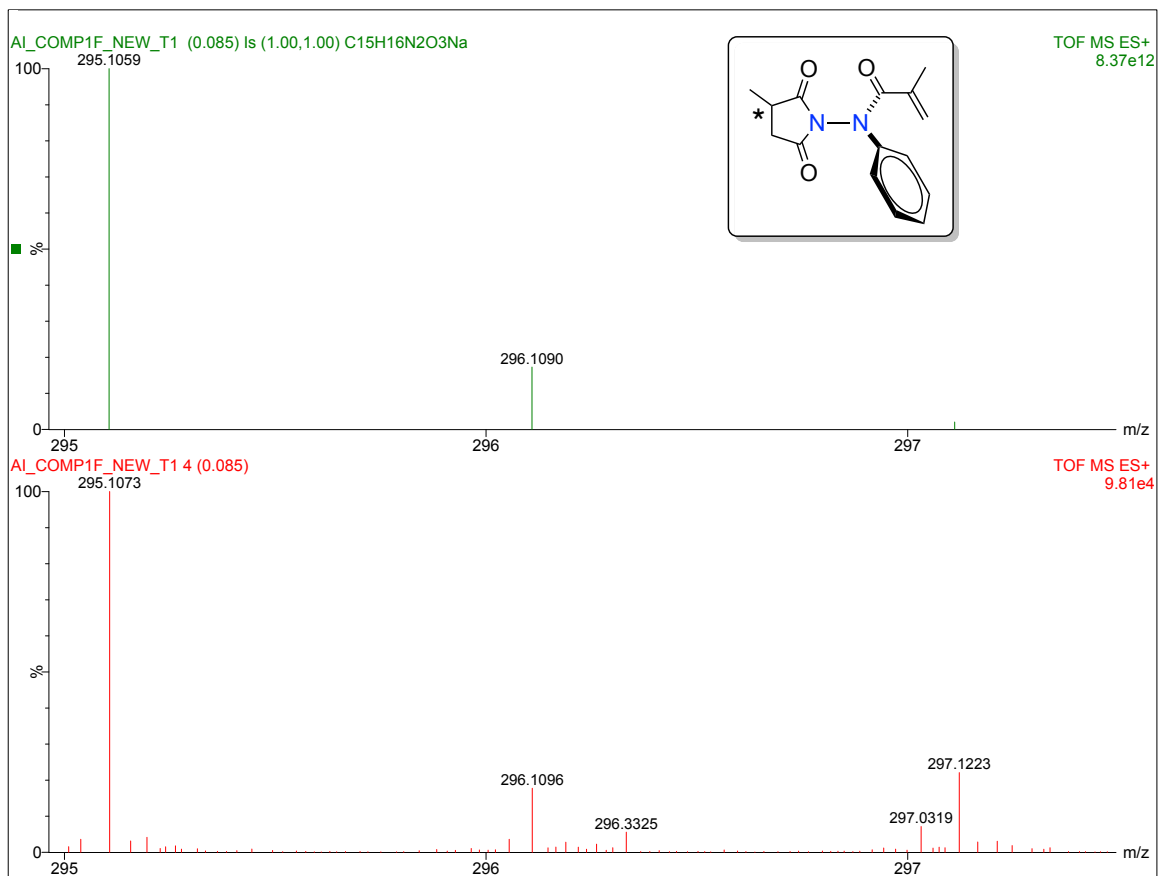
Figure 3.68: HRMS spectra of (*R*)-**184f**.

3.18. Synthesis of quinazolinone based acrylanilide derivative
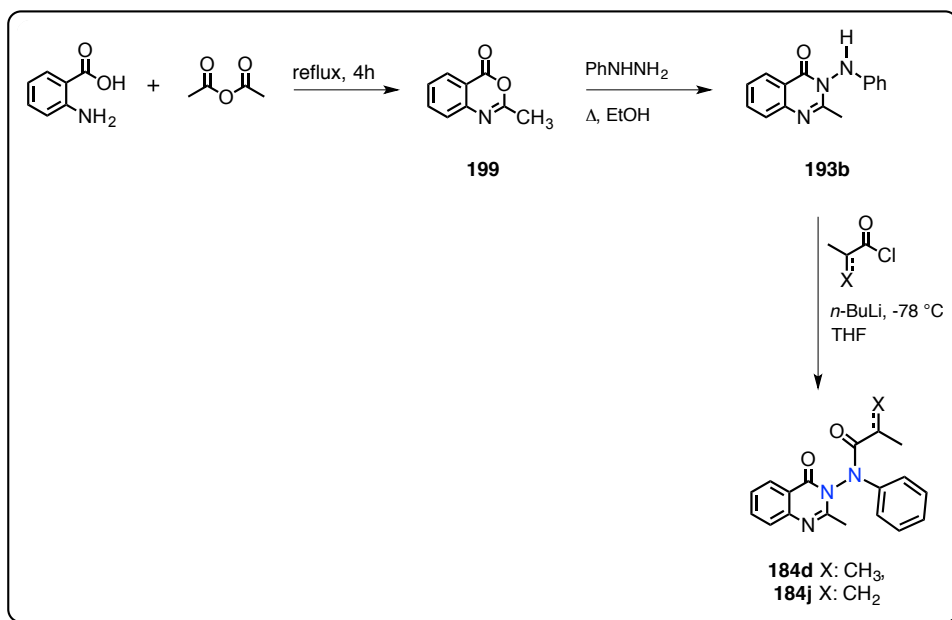
Scheme 3.53: Synthesis of quinazolinone based acrylanilide **184d/184j**.

199
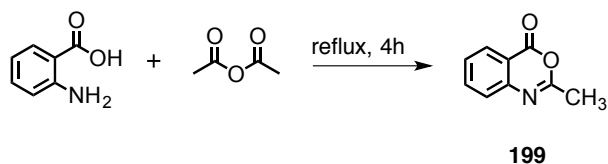
Scheme 3.54: Synthesis of 2-methyl-3,1-benzoxazin-4-one **199**.

Following the modified procedure reported by Jain et al. a mixture of anthranilic acid (1 equiv) and acetic anhydride (2 equiv) was stirred for 15 minutes.[109] The mixture was then refluxed for 4 hours under anhydrous conditions. The solution was then brought to room temperature and the excess of acetic anhydride was removed under reduced pressure. The crude was diluted with ethyl acetate and then the solution was washed with excess of saturated $NaHCO_3$ (4 × 10 mL) and finally with brine. The organic layer was dried over anhyd Na_2SO_4, filtered and the solvent was removed under reduced pressure to yield product. The product was used without further purification.

Solid (Yield = 98%).

^{1}H-NMR (400 MHz, CDCl$_3$, δ ppm): 2.45 (s, 3H), 7.47 (m, 1H), 7.52 (d, 1H, J 8Hz), 7.45-7.79 (m, 1H) and 8.16-8.18 (m, 1H).
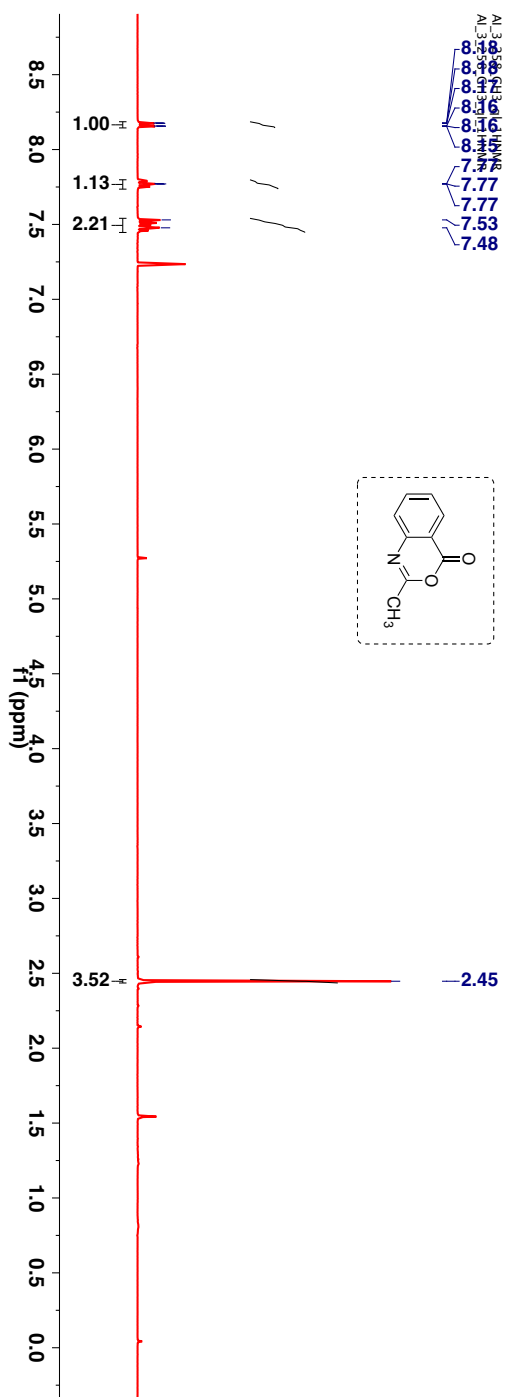
Figure 3.69: ^{1}H-NMR (400 MHz, CDCl$_3$, δ ppm) spectrum of **199**.
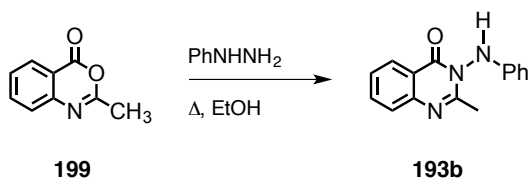
Scheme 3.55: Synthesis of anilide derivative **193b**.

Benzoxazine derivative **199** (1 equiv) was dissolved in absolute ethanol (20 ml per gram of **199**). The solution was heated at 135 °C in a pressure tube for 18 h. After 18 h, the mixture was brought to room temperature and ethanol was removed under reduced pressure. The crude was diluted with ethyl acetate and the organic layer was sequentially washed with 10% HCl, (3 × 10 mL), DI water (2 × 10 mL), saturated NaHCO$_3$ (2 × 10 mL) and finally with brine. The organic layer was dried over anhyd Na$_2$SO$_4$, filtered and the solvent was removed under reduced pressure to yield crude product. After concentrating the organic layer, the crude product was purified by combiflash using hexanes and ethyl acetate mixture to get the desired compound.

TLC condition - R$_f$ = 0.6 (50% ethyl acetate:hexanes). Yellow solid (Yield = 22%).

^{1}H-NMR (400 MHz, CDCl$_3$, δ ppm): 2.64 (s, 3H), 6.71 (d, 2H, J 8.8Hz), 6.97 (t, 1H, J 7.6Hz), 7.15 (s, 1H), 7.22-7.24 (m, 3H), 7.41-7.46 (t, 1H), 7.69-7.70 (m, 1H), 7.74-7.78 (m, 1H) and 8.18-8.21 (m, 1H).
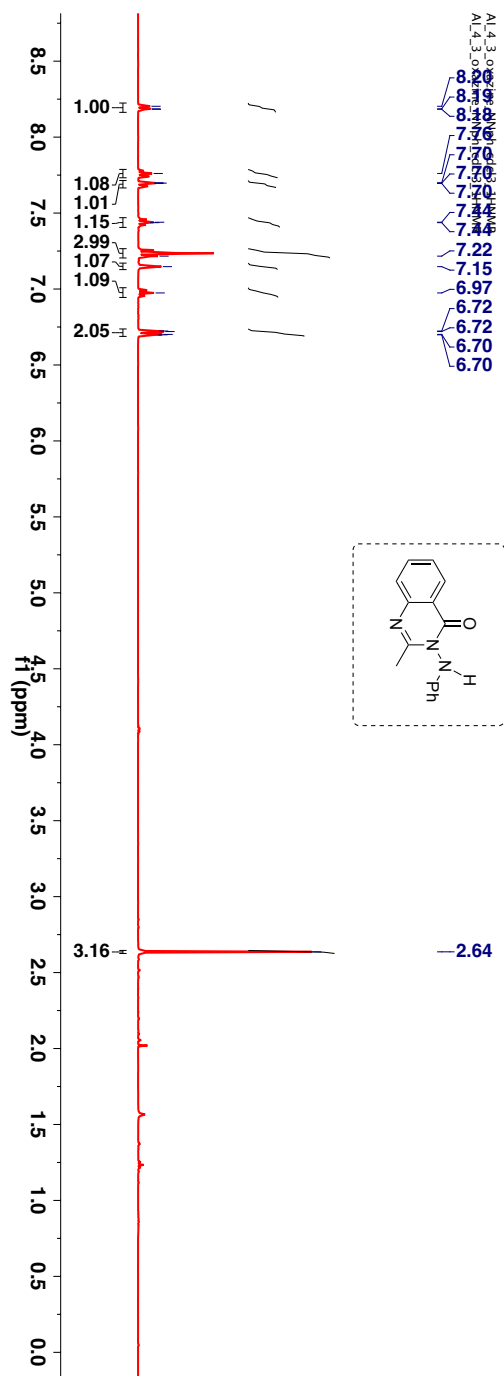
Figure 3.70: ^{1}H-NMR (400 MHz, CDCl$_3$, δ ppm) spectrum of **193b**.
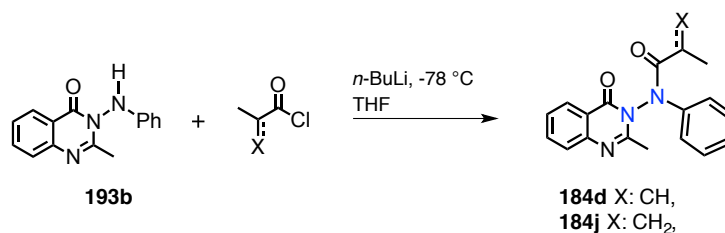
Scheme 3.56: Synthesis of acrylanilide derivative **184d/184j**.

Hydrazide derivative **193b** (1 equiv) was dissolved in anhydrous THF under an inert atmosphere. The solution was then cooled to -78 °C. To this cold solution *n*-BuLi (2.5 M, 1.1 equiv) was added slowly. The mixture was stirred at this temperature for 30 min. The reaction was quenched with anhydrous methacryloyl chloride (1.1 equiv). The stirring was continued for another 1.5 h after which the solution was slowly brought to room temperature and stirred for 12 h. The solution was quenched with saturated NH$_4$Cl (~5 mL) and then diluted with diethyl ether and the organic layer was sequentially washed with DI water (2 × 10 mL), saturated NaHCO$_3$ (2 × 10 mL) and finally with brine. The organic layer was dried over anhyd Na$_2$SO$_4$, filtered and the solvent was removed under reduced pressure to yield crude product. After concentrating the organic layer, the crude product was purified by combiflash using hexanes and ethyl acetate mixture to get the desired compound.

184d, TLC condition - R$_f$ = 0.5 (50% ethyl acetate:hexanes). Crystalline solid (Yield = 76%).

184j, TLC condition - R$_f$ = 0.4(50% ethyl acetate:hexanes). Crystalline solid (Yield = 94%).

^{1}H-NMR (400 MHz, CDCl$_3$, δ ppm): 1.96 (s, 3H), 2.58 (s, 3H), 5.37 (bs, 1H), 5.53 (bs, 1H), 7.29-7.30 (m, 1H), 7.36-7.37 (m, 4H), 7.48-7.51 (m, 1H), 7.67-7.69 (m, 1H), 7.77-7.80 (m, 1H) and 8.28-8.30 (m, 1H).
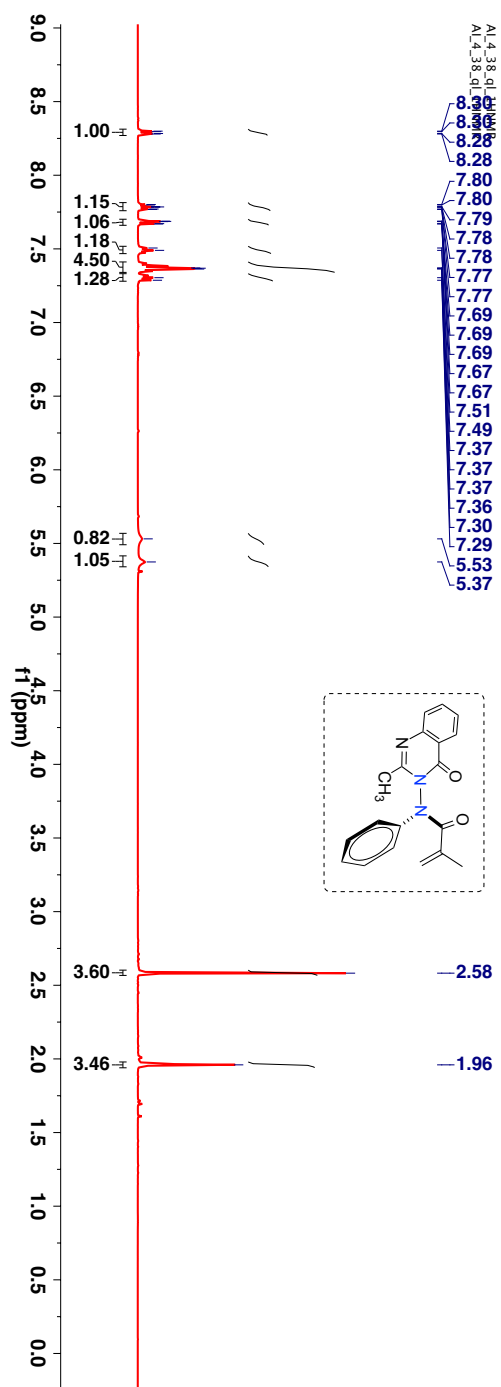
Figure 3.71: ^{1}H-NMR (400 MHz, CDCl$_3$, δ ppm) spectrum of **184d**.

^{13}C-NMR (100 MHz, CDCl$_3$, δ ppm): 19.6, 21.9, 113.0, 121.7, 123.7, 125.1, 127.0, 127.4, 127.5, 127.9, 129.5, 135.2, 138.8, 147.1, 155.5 and 160.2.
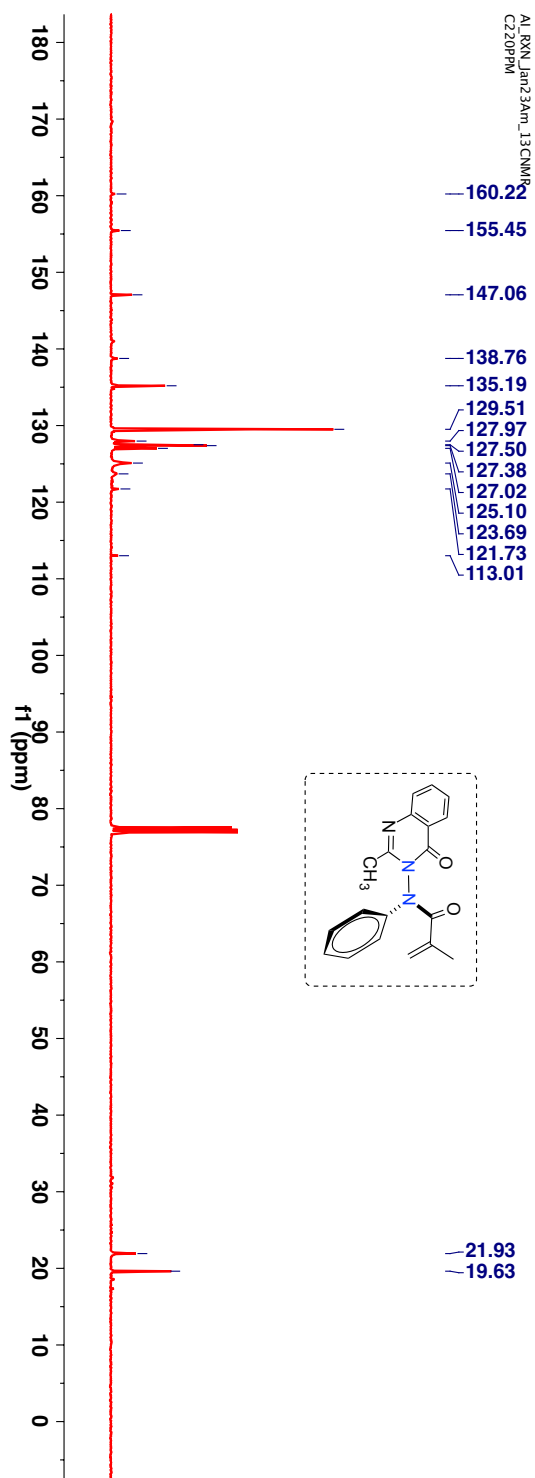
Figure 3.72: ^{13}C-NMR (100 MHz, CDCl$_3$, δ ppm) spectrum of **184d**.

HRMS-ESI (m/z) ([M + Na]):

Chemical Formula	: $C_{19}H_{17}N_3O_2$
Calculated	: 342.1219
Observed	: 342.1233
|Δm|	: 4.1 ppm
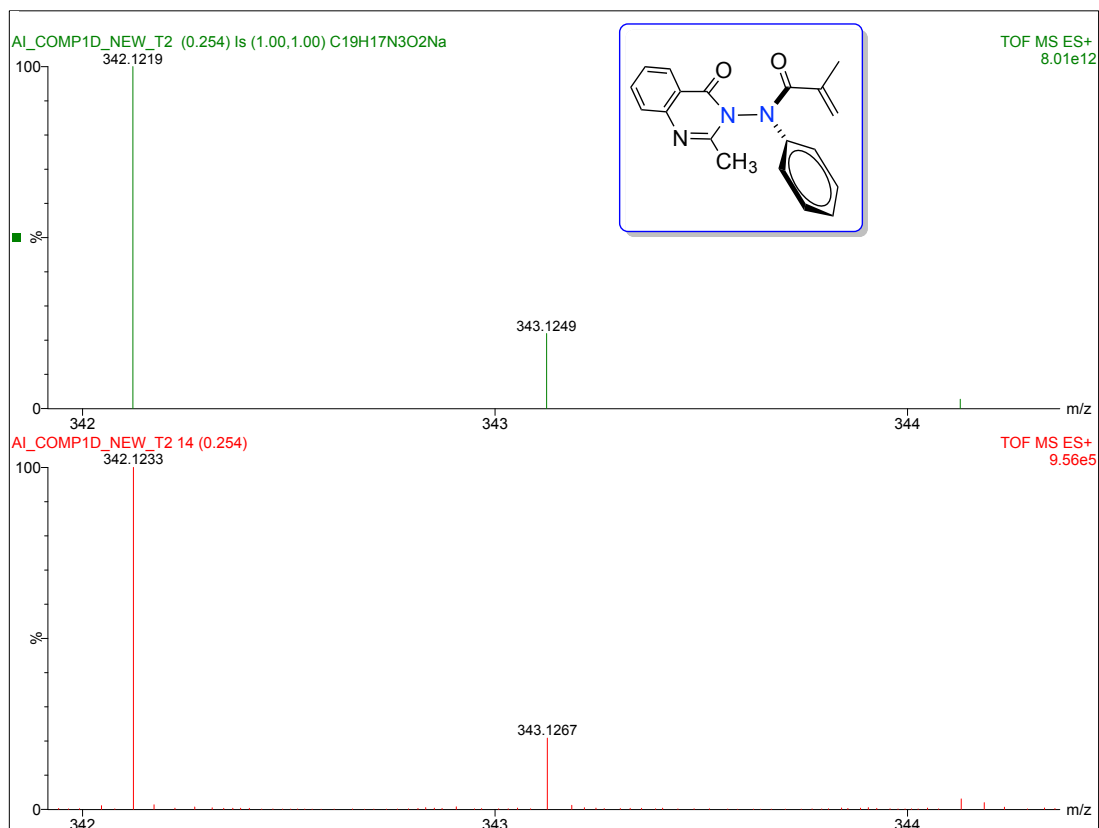
Figure 3.73: HRMS spectra of **184d**.

¹H-NMR (400 MHz, CDCl₃, δ ppm): 1.17 – 1.21 (m, 6H), 2.56 (s, 3H), 2.85–2.95 (sep, *J* 6.8Hz 1H), 7.31-7.43 (m, 4H), 7.56-7.61 (m, 3H), 7.66-7.72 (m, 1H) and 8.23-8.25 (m, 1H).
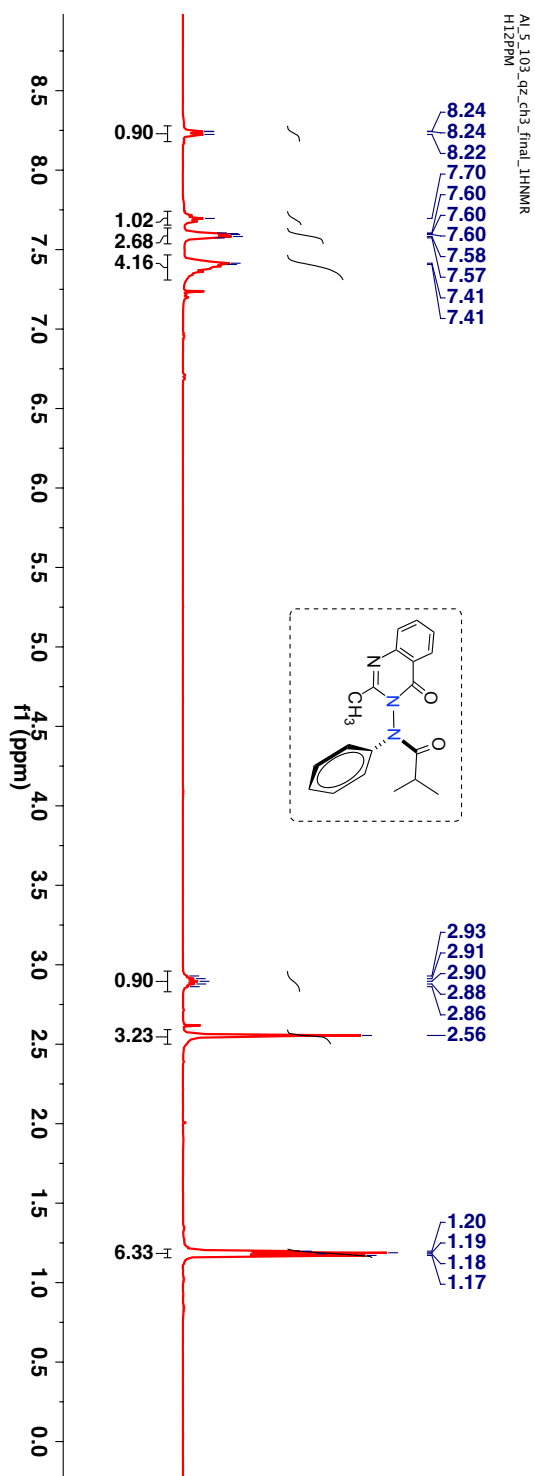
Figure 3.74: ¹H-NMR (400 MHz, CDCl₃, δ ppm) spectrum of **184j**.

^{13}C-NMR (100 MHz, CDCl$_3$, δ ppm): 19.4, 19.5, 31.5, 114.1, 121.9, 126.8, 127.0, 127.2, 127.3, 127.5, 129.3, 129.7, 129.9, 135.0, 140.6, 146.9, 155.6, 160.2 and 176.1.
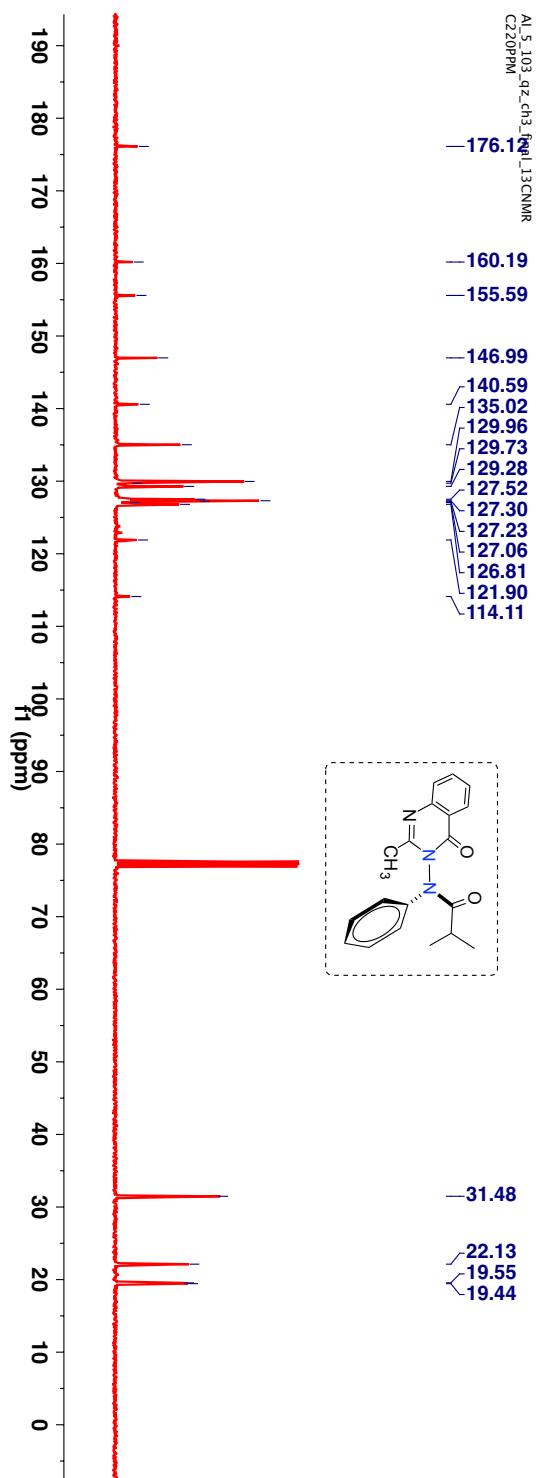
Figure 3.75: ^{13}C-NMR (100 MHz, CDCl$_3$, δ ppm) spectrum of **184j**.

3.19. General procedure followed for irradiation of substrates and characterization of photoproducts

3.19.1. Procedure for photoreactions in solution

(a) Sensitized irradiation: In a pyrex tube, solution of the desired substrate was dissolved in an appropriate solvent under an inert atmosphere. This was followed by the addition of triplet sensitizer (thioxanthone). The sample was then irradiated at ambient conditions in a Rayonet reactor equipped with ~420 nm tubes (16 tubes x 14 Watt).

(b) Direct irradiation: In a pyrex tube, solution of the desired substrate was dissolved in an appropriate solvent under an inert atmosphere. The sample was then irradiated at ambient conditions in a Rayonet reactor equipped with ~300 nm/ ~350 nm tubes (16 tubes x 12 Watt). After irradiation, triphenylmethane was added as internal standard and the solvent was evaporated under reduced pressure. Conversion and mass balance was determined using the following equation by NMR spectroscopy:

$$mol_a = mol_i \times \left(\frac{Integral\ of\ analyte}{Integral\ of\ internal\ standard} \right) \times \frac{N_a}{N_i}$$

Where, N_a and N_i are the number of nuclei giving rise to the relevant analyte and internal standard peaks respectively. Similarly, mol_a and mol_i are the number of moles of analyte and the internal standard respectively.

3.19.2. Characterization of photoproduct(s) after photoreaction

In case of large-scale photoreactions, after irradiation the mixture was purified by combiflash using hexanes/ethyl acetate mixtures. The photoproducts were then characterized by NMR spectroscopy and/or single crystal XRD. In case of photoreactions done on small scale (<60 mg) the mixture was purified by preparative thin layer chromatography. The course of photoreaction was monitored by ^{1}H-NMR spectroscopy.

3.20. Photoreaction of achiral phthalimide derivative 184e
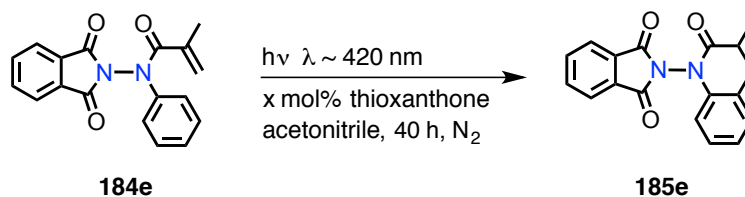
Scheme 3.57: 6π Photocyclization of acrylanilide derivative **184e**.

Table 3.8: Sensitizer loading studies for 6π photocyclization of acrylanilide derivative in acetonitrile **184e**.[a]

Entry	TX (x mol%)	Conversion/%
1	0	7
2	1	88
3	5	46
4	10	90

[a] [**184e**] = 3.26 mM. Values based on ^{1}H-NMR spectroscopy (±5% error), each experiment was performed for three trials, % conversion and mass balance calculated using triphenylmethane as internal standard. TX: thioxanthone

Table 3.9: Solvent screening studies for 6π photocyclization of *N-N* bond based acrylanilide derivative **184e**.[a]

Entry	Solvent	Conversion/%
1	Methanol	91
2	Acetonitrile	90
3	Ethyl acetate	100
4	Benzene	60
6	Methylcyclohexane	71

[a] [**184e**] = 3.26 mM. Values based on ^{1}H-NMR spectroscopy (±5% error), each experiment was performed for three trials, % conversion and mass balance calculated using triphenylmethane as internal standard. TX: thioxanthone

TLC condition - R$_f$ = 0.4 (50% ethyl acetate:hexanes). Crystalline solid (Yield = 62%).

^{1}H-NMR (400 MHz, CDCl$_3$, δ ppm): 1.34 (s, 3H), 2.94-3.12 (m, 3H), 6.67 (d, 1H, *J* 8Hz), 7.02-7.06 (m, 1H), 7.13-7.17 (m, 1H), 7.21 (d, 1H, *J* 8Hz), 7.79-7.82 (m, 2H) and 7.91-7.96 (m, 2H).
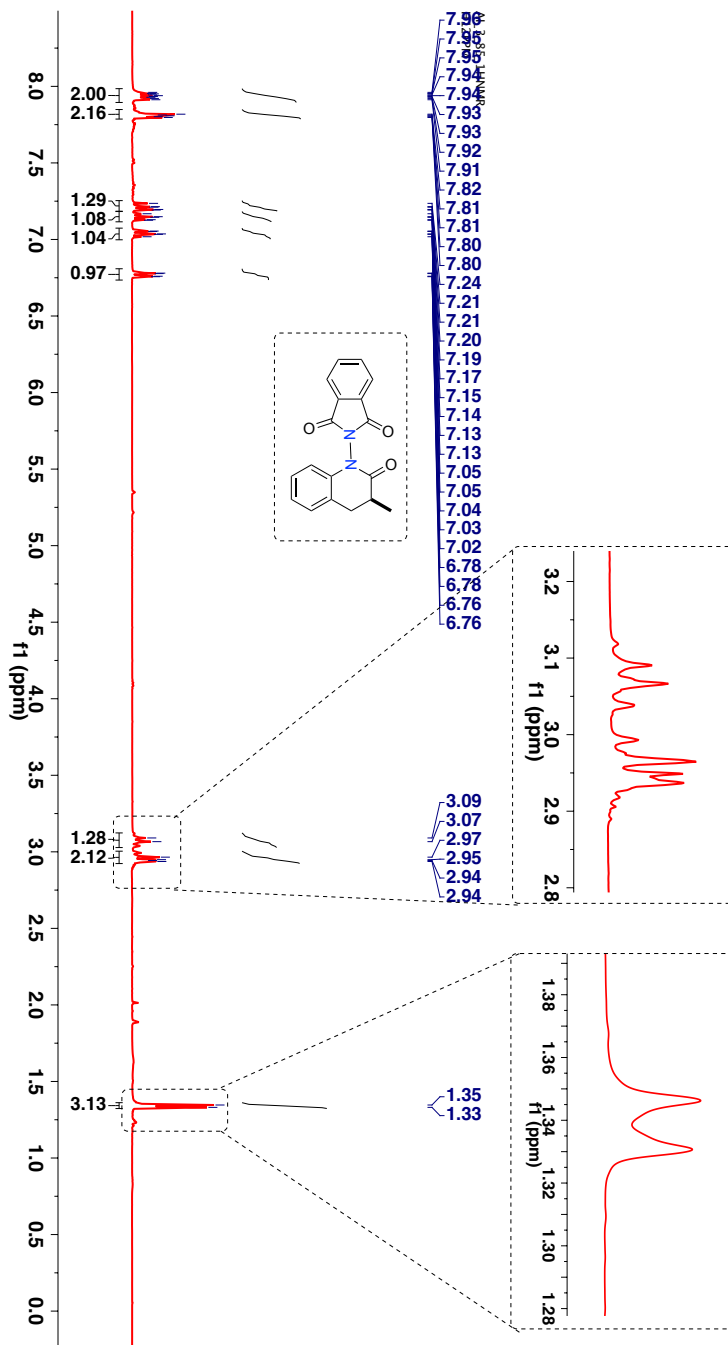
Figure 3.76: ^{1}H-NMR (400 MHz, CDCl$_3$, δ ppm) spectrum of **185e**.

3.20.1. UV-Vis spectra of acrylanilide derivative 184e
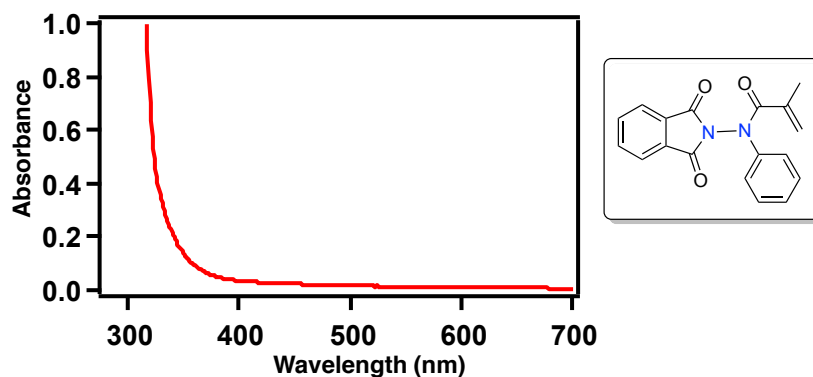
Figure 3.77: UV-Vis spectra of *N-N* bond based acrylanilide derivative **184e** recorded at the reaction concentration (concn = 3.26 mM) in acetonitrile.

HRMS-ESI (m/z) ([M + Na]$^+$):

Chemical Formula	: $C_{18}H_{14}N_2O_3$
Calculated	: 329.0902
Observed	: 329.0911
|Δm|	: 2.7 ppm
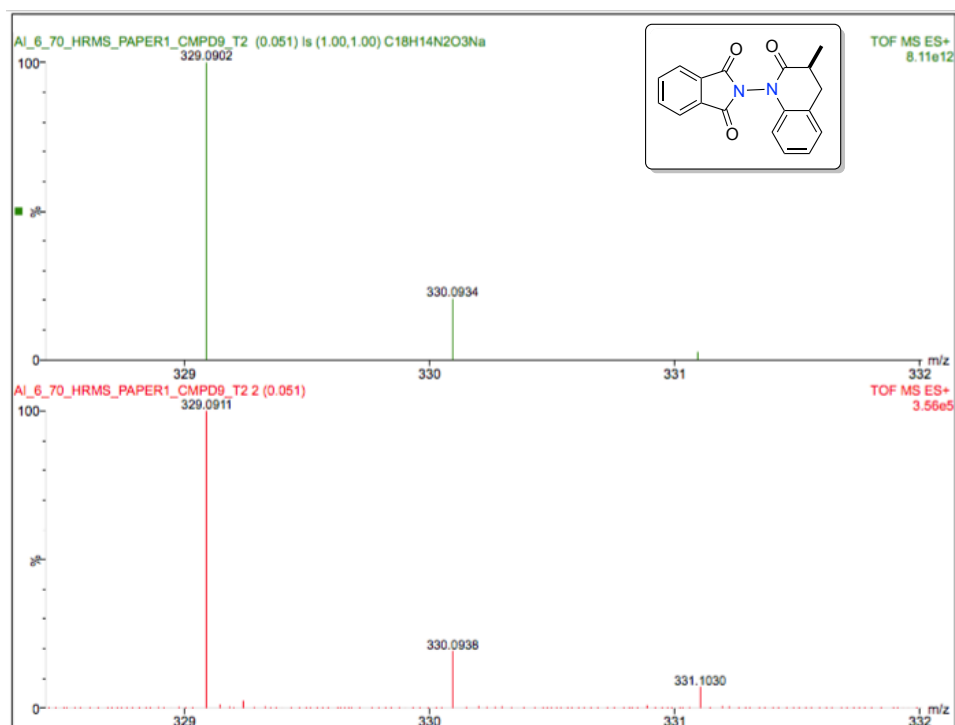
Figure 3.78: HRMS spectra of **185e**.

3.21. Phthalimide deprotection in the photoproduct 185e
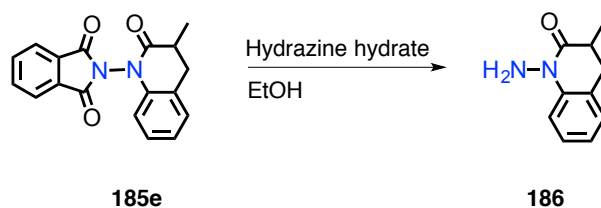
185e   **186**

Scheme 3.58: Synthesis of *N*-amino-3,4-dihydroquinoline-(1H)-2-one **186**.

Following the modified procedure reported by Kikugawa et al. the photoproduct **185e** (1 equiv) was charged in a vial equipped with a teflon cap.[103] The compound **185e** was dissolved in absolute ethanol (5 mL per 100 mg of **185e**) and hydrazine monohydrate (11.9 equiv) was added. The solution was stirred for 5 min and refluxed for 30 min (until TLC showed complete consumption of starting material). The solution was brought to room temperature and diluted with ethyl acetate. The solution was sonicated for 15 min and then filtered through a short celite plug. The filtrate was concentrated under reduced pressure to obtain the desired product, i.e. *N*-amino dihydroquinolinone derivative.

Crystalline solid (Yield = 74%).

^{1}H-NMR (400 MHz, CDCl$_3$, δ ppm): 1.25 (d, 3H, *J* 6.4Hz), 2.62-2.72 (m, 2H), 2.87-2.95 (m, 1H), 4.85 (bs, 2H), 6.95-6.97 (m, 1H), 7.06-7.10 (m, 1H), 7.21-7.25 (m, 1H) and 7.49-7.52 (m, 1H).
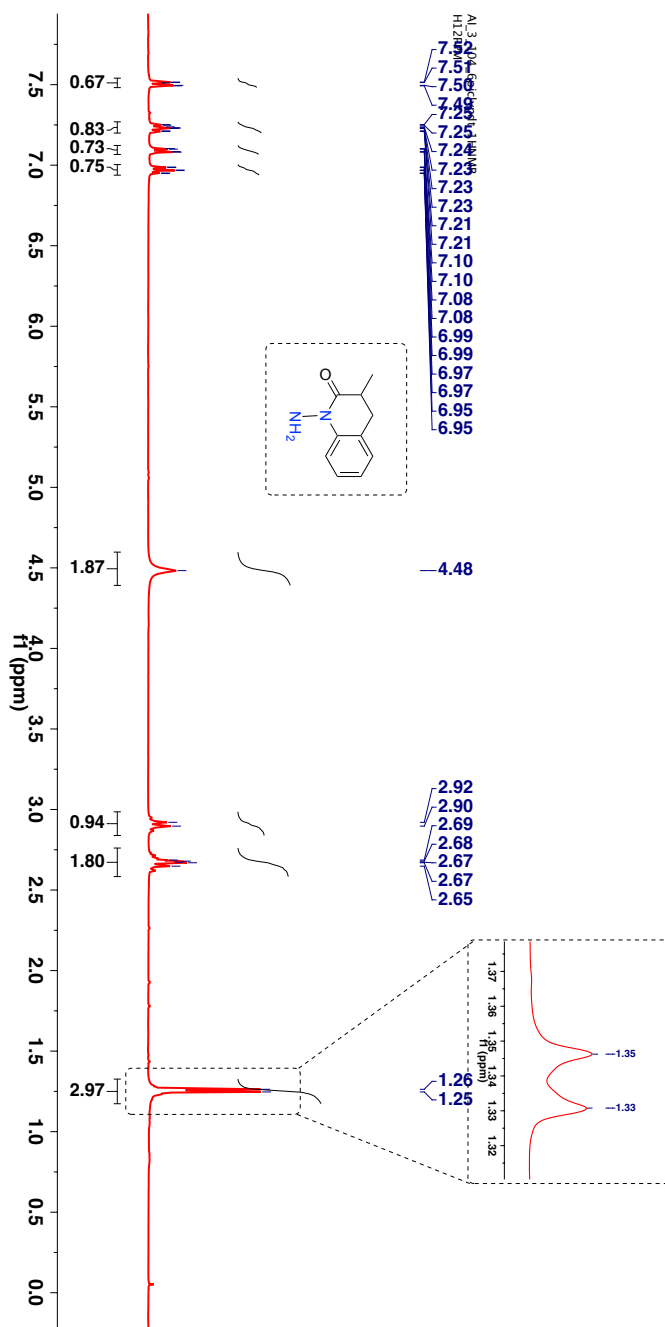
Figure 3.79: ^{1}H-NMR (400 MHz, CDCl$_3$, δ ppm) spectrum of **186**.

¹³C-NMR (100 MHz, CDCl₃, δ ppm): 15.9, 33.2, 35.8, 114.9, 123.1, 124.2, 127.6, 127.8, 140.1, and 172.1.
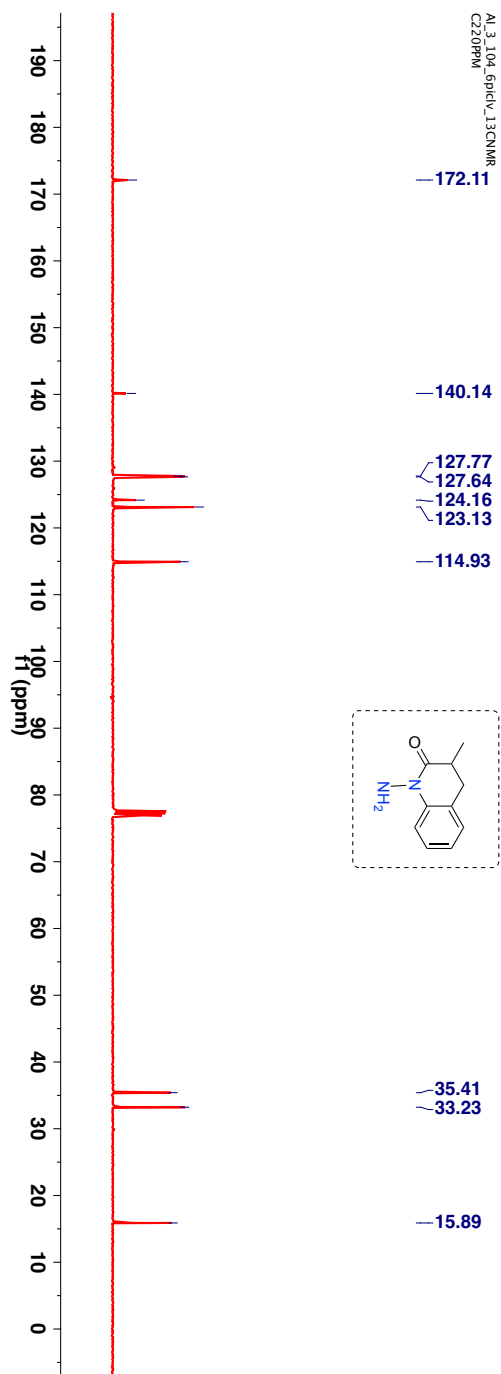
Figure 3.80: ¹³C-NMR (100 MHz, CDCl₃, δ ppm) spectrum of **186**.

HRMS-ESI (m/z) ([M + Na]$^+$):

Chemical Formula   : $C_{10}H_{12}N_2O$

Calculated   : 199.0847

Observed   : 199.0857

|Δm| : 5.0 ppm
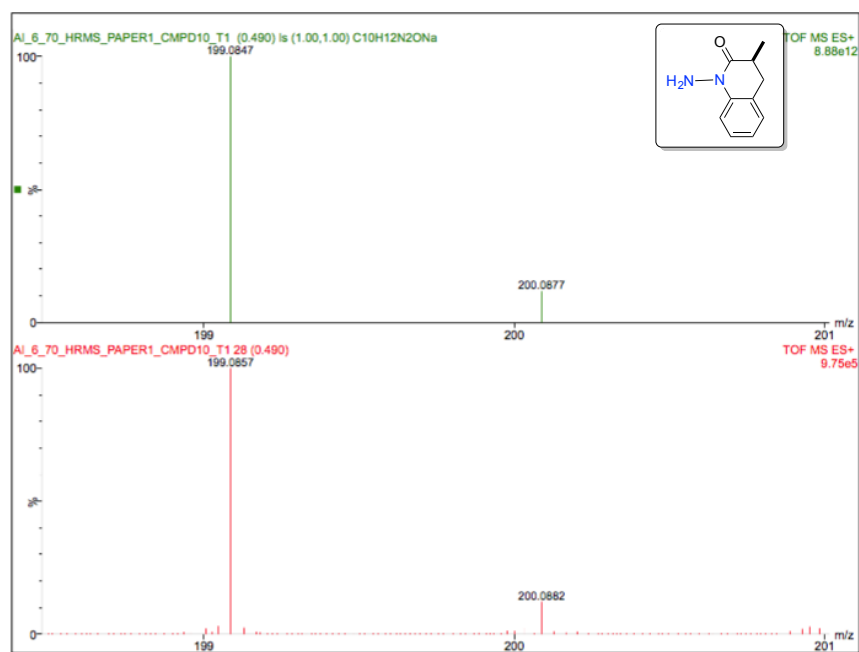
Figure 3.81: HRMS spectra of **186**.

3.21.1. HPLC analysis conditions for 186
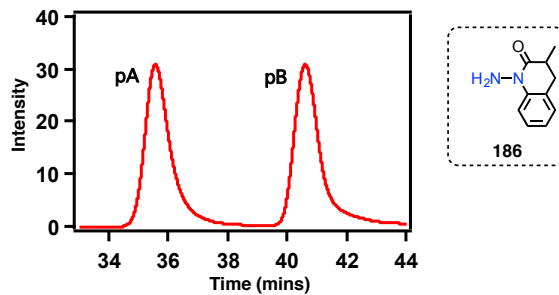
For analytical conditions,

Column   : CHIRACEL® ASH

Abs. detector wavelength   : 254 nm and 313 nm

Mobile phase   : Hexanes:2-propanol = 97:03

Flow rate   : 1.0 mL/min

Retention times (min)   : pA 35.5 and pB 40.5

Relative area   : pA = 50% and pB = 50%

3.22. Photoreaction of achiral diacetyl hydrazide derivative 184g

184g **185g**
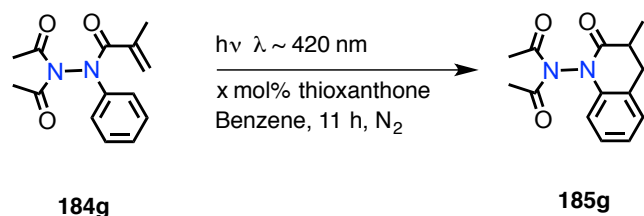
Scheme 3.59: 6π Photocyclization of acrylanilide derivative **184g**.

Table 3.10: Sensitizer loading studies for 6π photocyclization diacetyl hydrazide derivative **184g** in benzene.[a]

Entry	TX (x mol%)	Conversion/%
1	0	0
2	1	13
3	5	63
4	10	88

[a] [**184g**] = 3.84 mM. Values based on ^{1}H-NMR spectroscopy (±5% error), each experiment was performed for three trials, % conversion and mass balance calculated using triphenylmethane as internal standard, TX: thioxanthone.

Table 3.11: Solvent screening studies for 6π photocyclization of diacetyl hydrazide derivative **184g**.[a]

Entry	Solvent	Conversion/%
1	Methanol	35
2	Acetonitrile	decomposition
3	Ethyl acetate	8
4	Benzene	93
6	Methylcyclohexane	decomposition

[a] [**184g**] = 3.84 mM. Values based on ^{1}H-NMR spectroscopy (±5% error), each experiment was performed for three trials, % conversion and mass balance calculated using triphenylmethane as internal standard, TX: thioxanthone.

3.22.1. UV-Vis spectra of diacetyl hydrazide derivative 184g
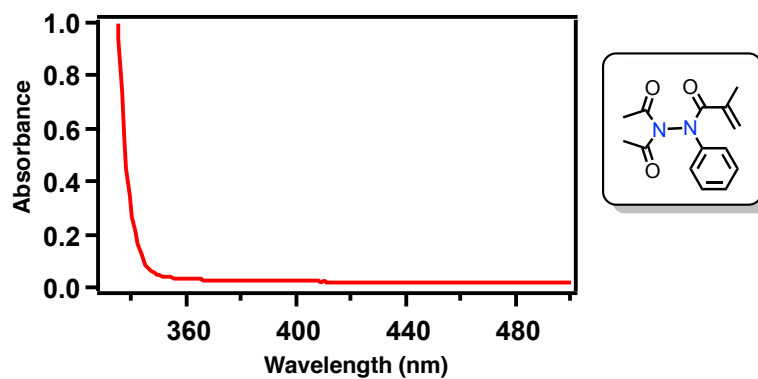
Figure 3.82: UV-Vis spectra of *N-N* bond based diacetyl hydrazide derivative **184g** recorded at the reaction concentration (concn = 3.84 mM) in acetonitrile.

TLC condition - R$_f$ = 0.3 (20% ethyl acetate:hexanes). Thick oil (Yield = 49%).

^{1}H-NMR (400 MHz, CDCl$_3$, δ ppm): 1.36 (d, 3H, *J* 8Hz), 2.37 (s, 3H), 2.48 (s, 3H), 2.88-2.91 (m, 2H), 3.10-3.12 (m, 1H), 6.69-6.72 (m, 1H), 7.09-7.12 (m, 1H) and 7.24-7.28 (m, 2H).
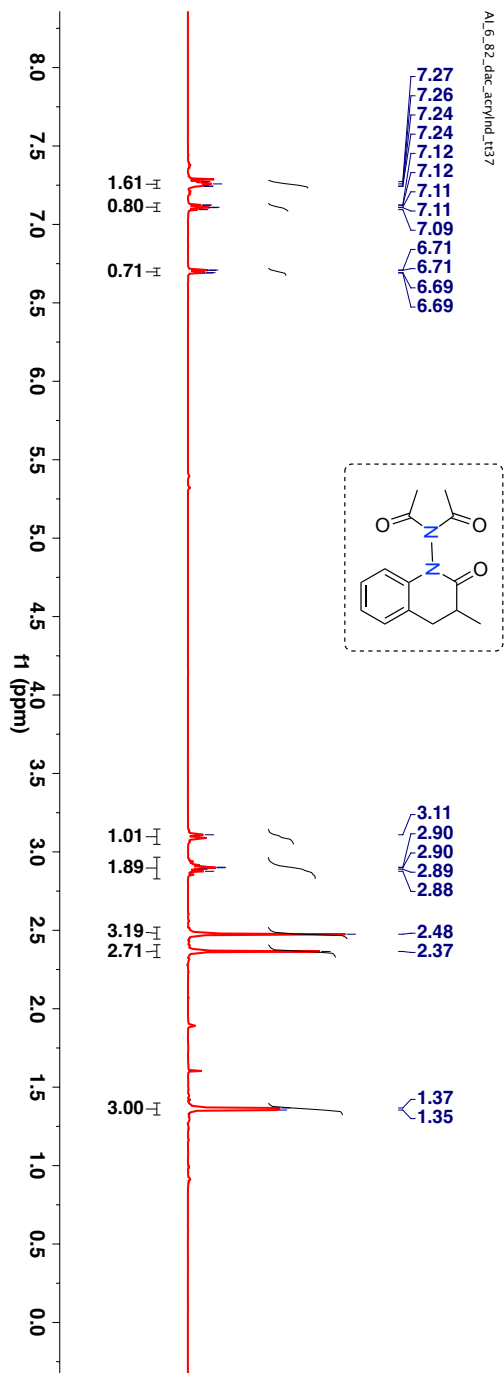
Figure 3.83: ^{1}H-NMR (400 MHz, CDCl$_3$, δ ppm) spectrum of **185g**.

^{13}C-NMR (100 MHz, CDCl$_3$, δ ppm): 15.4, 24.6, 24.9, 32.9, 35.9, 112.7, 124.5, 124.7, 128.2, 128.7, 138.8, 170.7, 170.9 and 171.0.
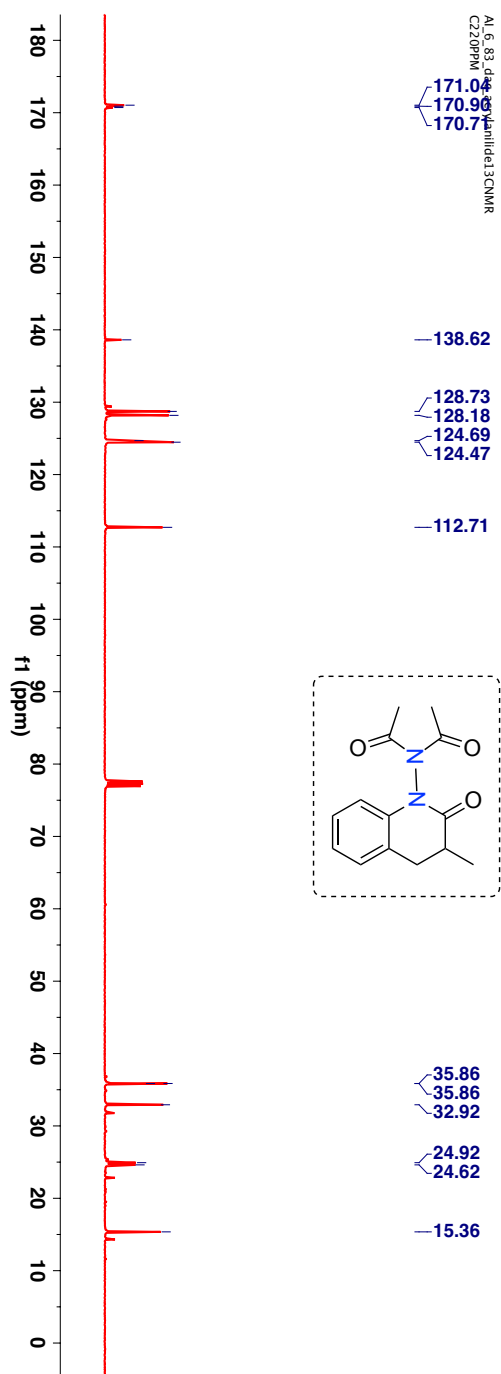
Figure 3.84: ^{13}C-NMR (100 MHz, CDCl$_3$, δ ppm) spectrum of **185g**.

HRMS-ESI (m/z) ([M + Na]$^+$):

Chemical Formula: $C_{14}H_{16}N_2O_3$

Calculated   : 283.1059

Observed   : 283.1075

|Δm| : 5.7 ppm
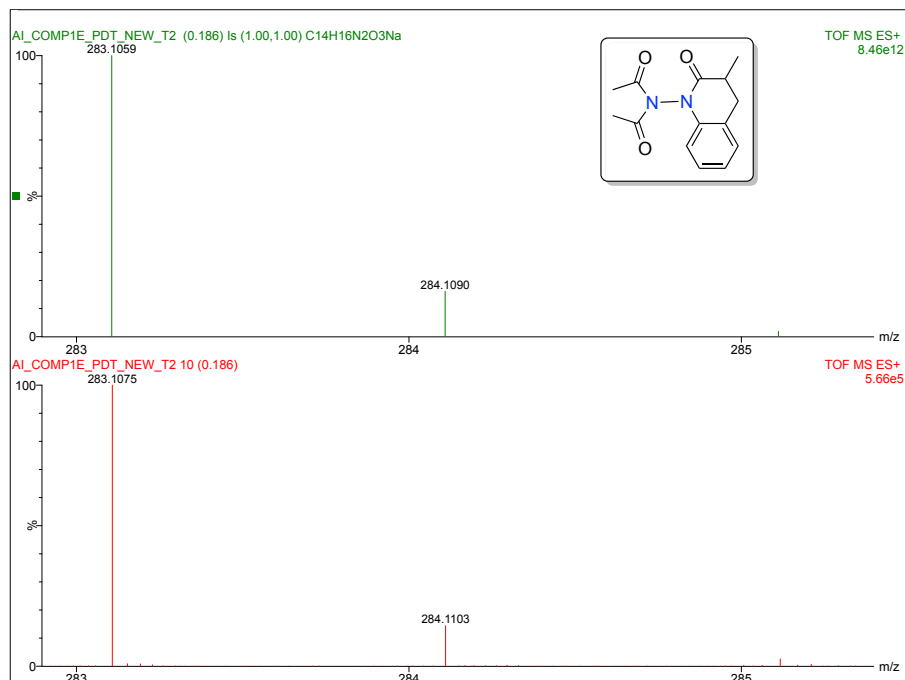
Figure 3.85: HRMS spectra of **185g**.

3.22.2. HPLC analysis conditions for 185g
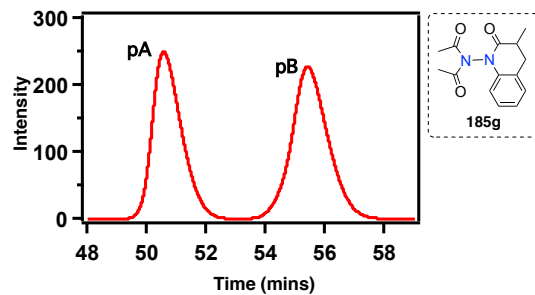
For analytical conditions,

Column	: CHIRALPAK$^{\circledR}$ IC
Abs. detector wavelength	: 254 nm and 313 nm
Mobile phase	: Hexanes:2-propanol = 95:05
Flow rate	: 0.8 mL/min
Retention time (min)	: pA = 47% and pB = 52%

3.23. Photoreaction of asymmetrically substituted hydrazide derivative 184a

184a → **185a**

hν λ ~ 420nm
10 mol% Thioxanthone
11 h, solvent, N₂
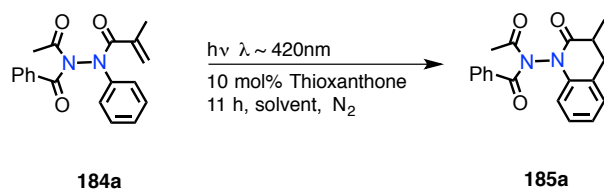
Scheme 3.60: 6π Photocyclization of acrylanilide derivative **184a**.

Table 3.12: Solvent screening studies for 6π photocyclization of asymmetrically substituted hydrazide derivative **184a**. [a]

Entry	Solvent	Conversion/%
1	Methanol	18
2	Acetonitrile	0
3	Ethyl acetate	18
4	Benzene	10
6	Methylcyclohexane	decomposition

[a]**[184a]** = 3.1 mM. Values based on ¹H-NMR spectroscopy (±5% error), each experiment was performed for three trials; %Conversion and mass balance calculated using triphenylmethane as internal standard.

3.23.1. UV-Vis spectra of asymmetrically substituted hydrazide derivative 184a
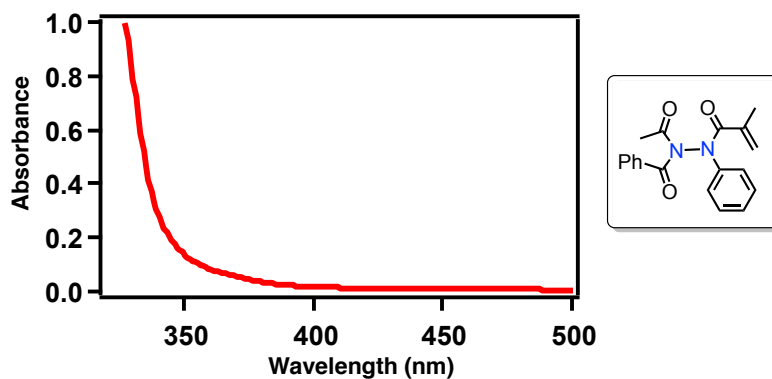
Figure 3.86: UV-Vis spectra of *N-N* bond based diacetyl hydrazide derivative **184a** recorded at the reaction concentration (concn = 3.1 mM) in acetonitrile.

3.24. Photoreaction of chiral phthalimide derivative 184c

184c   **185c**
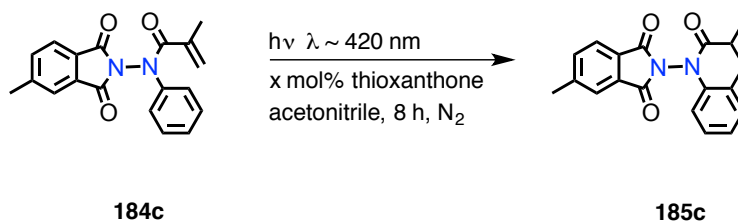
Scheme 3.61: 6π Photocyclization of acrylanilide derivative **184c**.

Table 3.13: Sensitizer loading studies for 6π photocyclization of acrylanilide derivative **184c** in acetonitrile. [a]

Entry	TX (x mol%)	Conversion/%
1	0	0
2	1	32
3	5	69
4	10	94

[a] [**184c**] = 3.12 mM. Values based on ^{1}H-NMR spectroscopy (±5% error), each experiment was performed for three trials, % conversion and mass balance calculated using triphenylmethane as internal standard, TX: thioxanthone.

Table 3.14: Solvent screening studies for 6π photocyclization of *N-N* bond based acrylanilide derivative **184c**. [a]

Entry	Solvent	Conversion/%
1	Methanol	100
2	Acetonitrile	94
3	Ethyl acetate	69
4	Benzene	93
6	Methylcyclohexane	decomposition

[a] [**184c**] = 3.12 mM. Values based on ^{1}H-NMR spectroscopy (±5% error), each experiment was performed for three trials, % conversion and mass balance calculated using triphenylmethane as internal standard, TX: thioxanthone.

TLC condition - R$_f$ = 0.2 (50% ethyl acetate:hexanes). Clear solid (Yield = 48%).

^{1}H-NMR (400 MHz, CDCl$_3$, δ ppm): 1.35 (d, 1H, J 6 Hz), 2.94-2.97 (m, 2H), 3.07-3.09 (m, 1H), 6.76 (d, 1H, J 8Hz), 7.03 (t, 1H J 6 Hz), 7.13 (t, 1H J 8 Hz), 7.19-7.2 (m, 1H), 7.79-7.82 (m, 2H) and 7.91-7.96 (m, 2H).
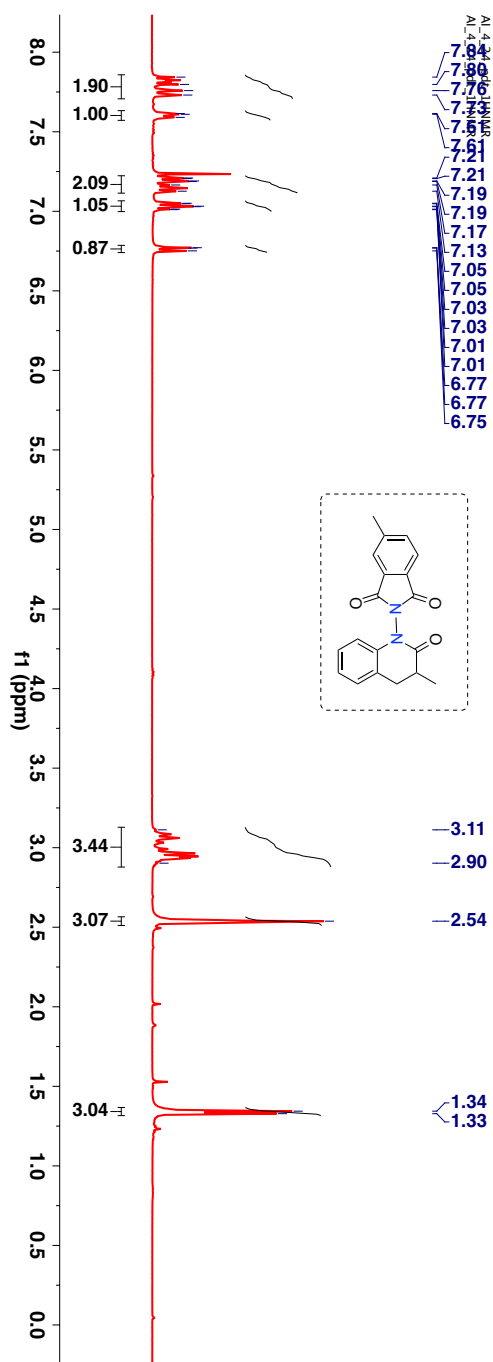
Figure 3.87: ^{1}H-NMR (400 MHz, CDCl$_3$, δ ppm) spectrum of **185c**.

^{13}C-NMR (100 MHz, CDCl$_3$, δ ppm): 15.5, 33.2, 35.8, 113.3, 124.3, 124.4, 124.4, 124.6, 127.9, 128.4, 130.3, 130.4, 135.1, 139.0, 165.7, 165.2 and 170.4.
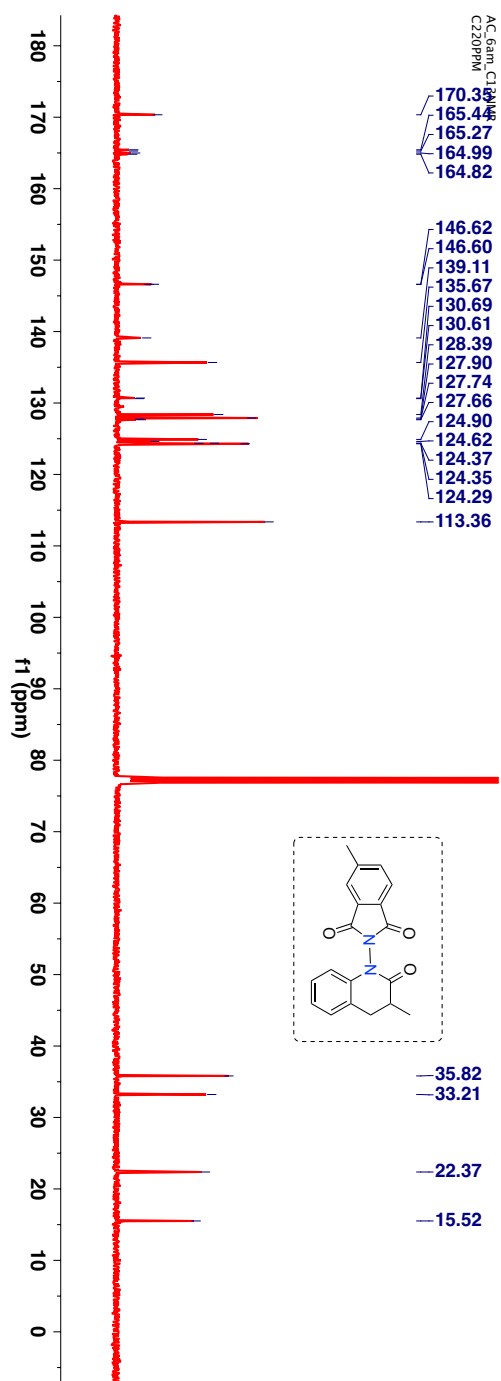
Figure 3.88: ^{13}C-NMR (100 MHz, CDCl$_3$, δ ppm) spectrum of **185c**.

HRMS-ESI (m/z) ([M + Na]$^+$):

Chemical Formula:	$C_{19}H_{16}N_2O_3$
Calculated	: 343.1059
Observed	: 343.1072
$|\Delta m|$	: 3.8 ppm
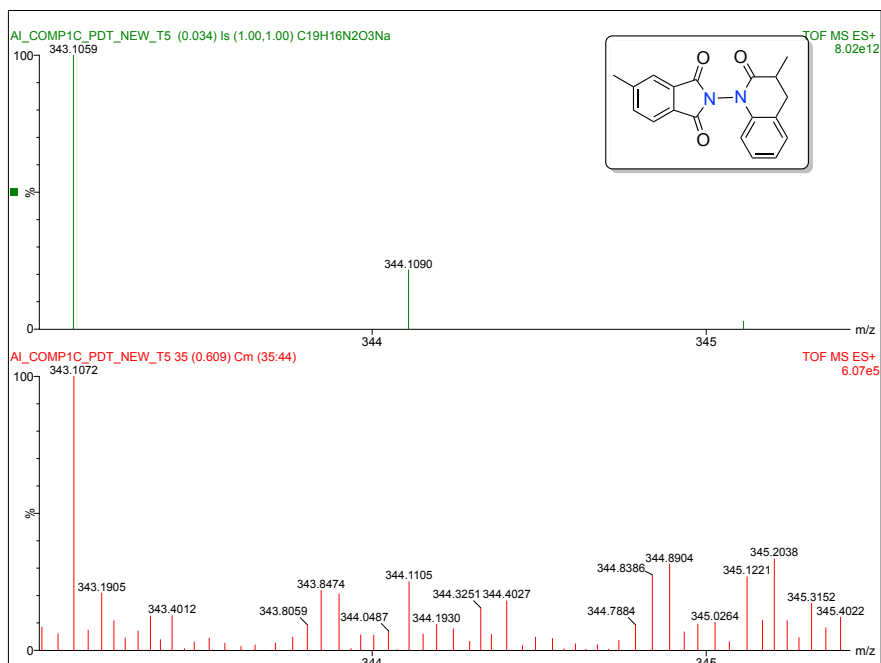
Figure 3.89: HRMS spectra of **185c**.

3.24.1. UV-Vis spectra of acrylanilide derivative 184c.
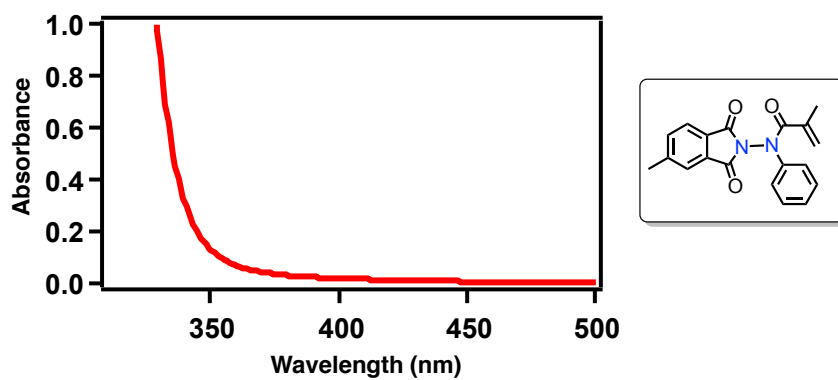
Figure 3.90: UV-Vis spectra of *N-N* bond based acrylanilide derivative **184c** recorded at the reaction concentration (concn = 3.12 mM) in acetonitrile.

3.25. Phthalimide deprotection in photoproduct 185c
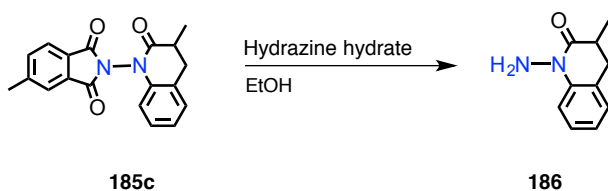
Scheme 3.62: Synthesis of *N*-amino-3,4-dihydroquinoline-(1H)-2-one **185c**.

Following the modified procedure reported by Kikugawa et al. the photoproduct **185c** (1 equiv) was charged in a vial equipped with a teflon cap.[103] The compound **185c** was dissolved in absolute ethanol (5 mL per 100mg **185c**) and hydrazine monohydrate (11.9 equiv) was added. The solution was stirred for 5 min and refluxed for 30 min (until TLC showed complete consumption of starting material). The solution was brought to room temperature and diluted with ethyl acetate. The solution was sonicated for 15 min and then filtered through a short celite pad. The filtrate was concentrated under reduced pressure to obtain the crude product. The crude product was purified using a prep TLC with hexanes and ethyl acetate mixture as eluting solvent to obtain i.e. *N*-amino dihydroquinolinone derivative.

Crystalline solid (Yield = 76%).

^{1}H-NMR (400 MHz, CDCl$_3$, δ ppm): 1.27 (d, 3H, J 6.4Hz), 2.62-2.72 (m, 2H), 2.87-2.95 (m, 1H), 4.48 (bs, 2H), 6.96-6.97 (m, 1H), 7.06-7.10 (m, 1H), 7.21-7.25 (m, 1H) and 7.49-7.52 (m, 1H).
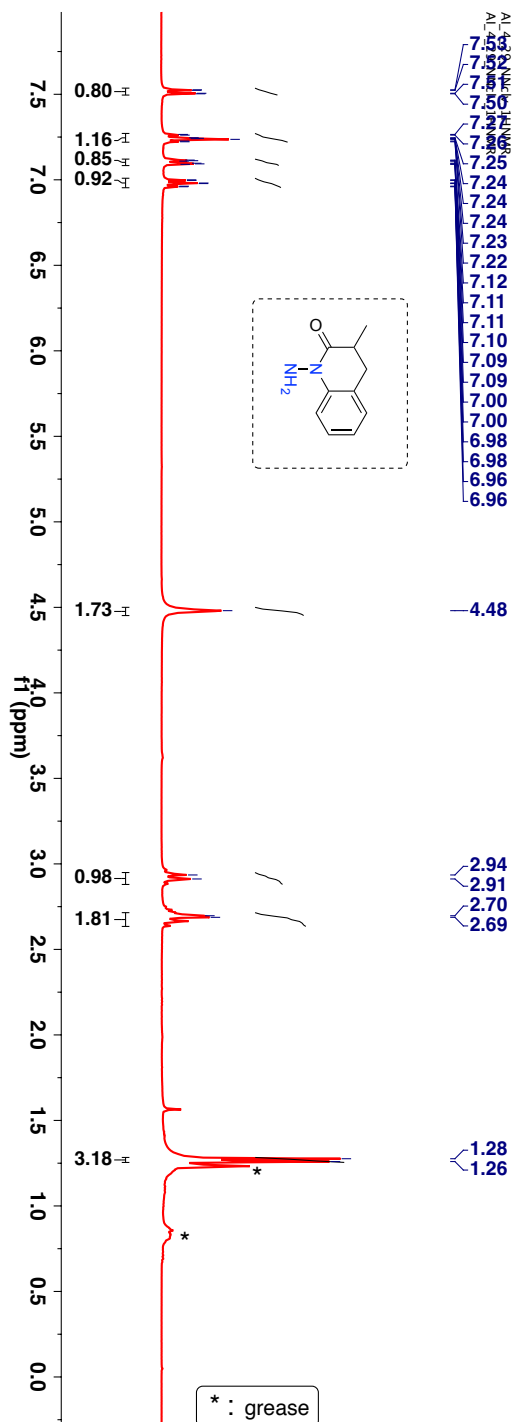
Figure 3.91: ^{1}H-NMR (400 MHz, CDCl$_3$, δ ppm) spectrum of **186**.

3.25.1. HPLC analysis conditions for 184c
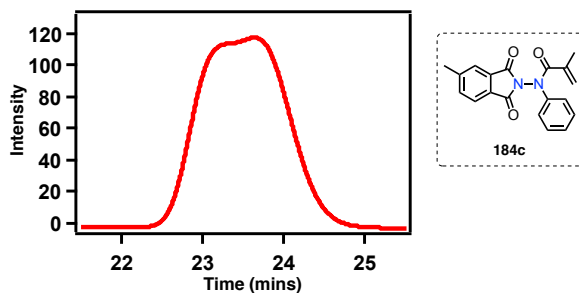
For analytical conditions,

Column	: CHIRALPAK® IC
Abs. detector wavelength	: 254 nm and 313 nm
Mobile phase	: Hexanes:2-propanol = 70:30
Flow rate	: 0.8 mL/min
Retention time (min)	: broad peak from 22.4 – 25.0

3.25.2. HPLC analysis conditions for 185c
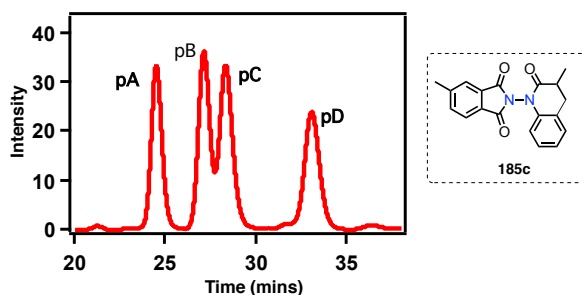
For analytical conditions,

Column	: CHIRALPAK® IC
Abs. detector wavelength	: 254 nm and 270 nm
Mobile phase	: Hexanes:2-propanol = 70:30
Flow rate	: 0.8 mL/min
Retention times (min)	: pA 24.5, pB 27.1, pC 26.7 and pD 22.4
Relative area	: pA ~ 23%, pB ~ 27%, pC ~ 27, pD ~ 23%

3.25.3. HPLC analysis conditions for 186
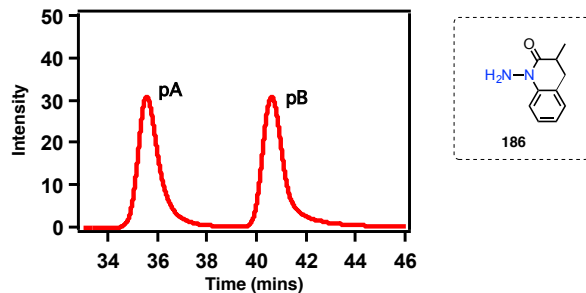
For analytical conditions,

Column	: CHIRACEL® ASH
Abs. detector wavelength	: 254 nm and 270 nm
Mobile phase	: Hexanes:2-propanol = 97:03
Flow rate	: 1.0 mL/min
Retention times (min)	: pA 34.2 and pB 39.4
Relative area	: pA ~ 50% and pB ~ 50%

3.25.4. HPLC analysis conditions for 197
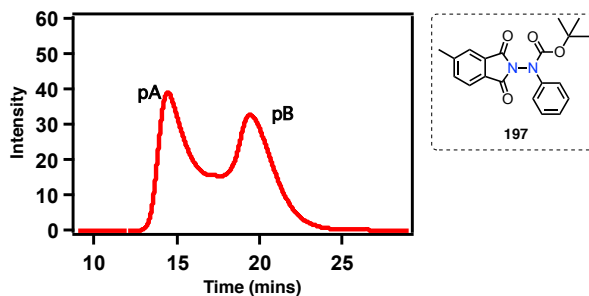
For analytical conditions,

Column	: CHIRALPAK® IC
Abs. detector wavelength	: 254 nm and 270 nm
Mobile phase	: Hexanes:2-propanol = 98:02
Flow rate	: 0.8 mL/min
Retention times (min)	: pA 14.3 and pB 19.4
Relative area	: pA ~ 50% and pB ~ 50%

3.26. Photoreaction of chiral succinimide derivative 184b

184b → **185b**

hν λ ~ 300 nm

5.5 h, solvent, N_2
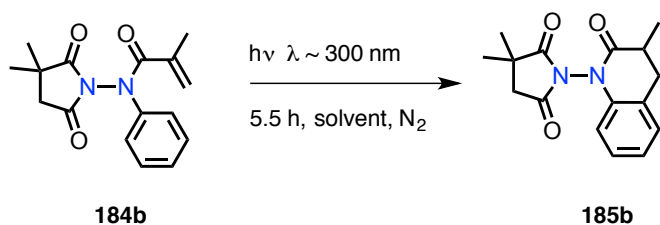
Scheme 3.63: 6π Photocyclization of acrylanilide derivative **184b**.

Table 3.15: Solvent screening studies for 6π photocyclization of *N-N* bond based acrylanilide derivative **184b**.[a]

Entry	Solvent	Conversion/%
1	Methanol	72
2	Acetonitrile	93
3	Ethyl acetate	80
4	Benzene	96
6	Methylcyclohexane	51

[a] [**184b**] = 3.84 mM. Values based on ^{1}H-NMR spectroscopy (±5% error), each experiment was performed for three trials, %conversion and mass balance calculated using triphenylmethane as internal standard.

Table 3.16: 6π Photocyclization of *N-N* bond based acrylanilide derivative **184b** in different reaction atmospheres.[a]

Entry	Reaction conditions	Conversion/%
1	hν~ 300 nm, MeCN, 2 h, O_2	0
2	hν~ 300 nm, MeCN, 2 h, N_2	77

[a] [**184b**] = 3.84 mM. Values based on ^{1}H-NMR spectroscopy (±5% error), each experiment was performed for two trials, %conversion and mass balance calculated using triphenylmethane as internal standard.

TLC condition - R$_f$ = 0.5 (50% ethyl acetate:hexanes). Clear solid (Yield = 89%).

^{1}H-NMR (400 MHz, CDCl$_3$, δ ppm, peaks of diastereomers are reported together): 1.30-1.32 (m, 3H), 1.45-1.49 (m, 6H), 2.74-2.77 (m, 2H), 2.84-3.03 (m, 3H), 6.54-6.58 (m, 1H), 7.01-7.05 (m, 1H) and 7.14-7.19 (m, 1H).
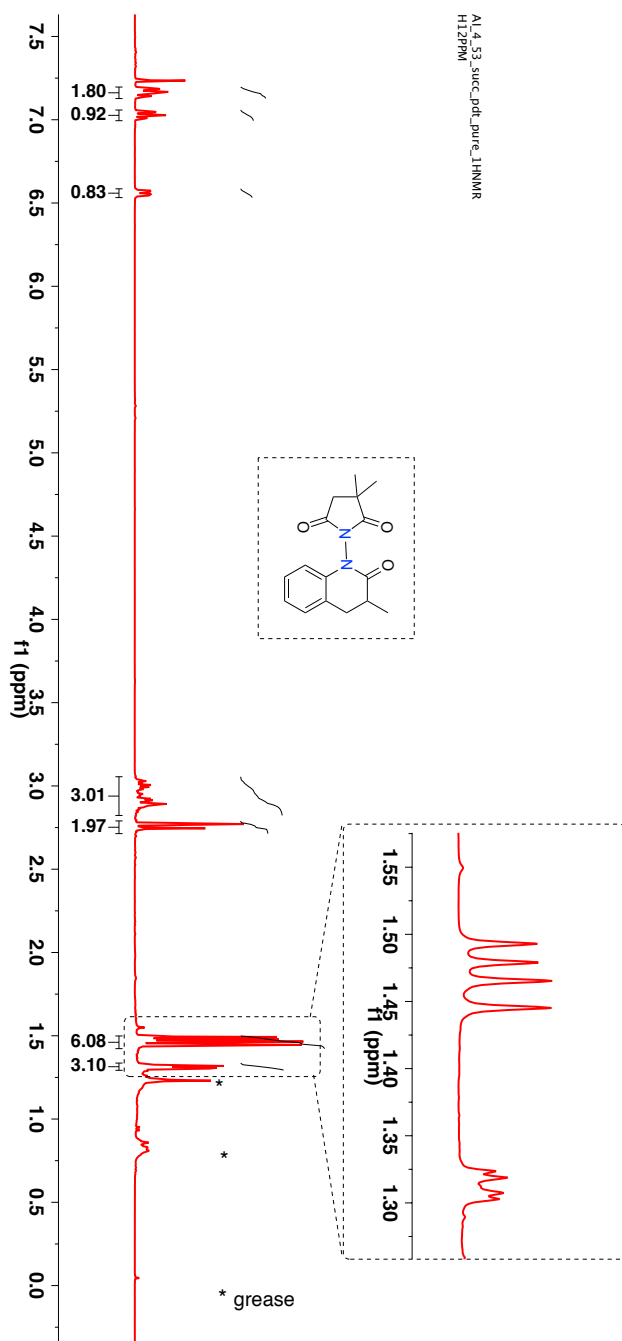
Figure 3.92: ^{1}H-NMR (400 MHz, CDCl$_3$, δ ppm) spectrum of **185b**.

^{13}C-NMR (100 MHz, CDCl$_3$, δ ppm, peaks of diastereomers are reported together): 14.5, 15.4, 25.9, 26.0, 26.2, 29.9, 33.2, 33.2, 35.7, 35.7, 39.5, 39.5, 42.4, 42.3, 112.7, 112.7, 124.4, 124.7, 124.7, 127.9, 128.5, 128.5, 138.1, 138.2, 169.7, 169.7, 171.6, 172.1, 178.9 and 179.5.
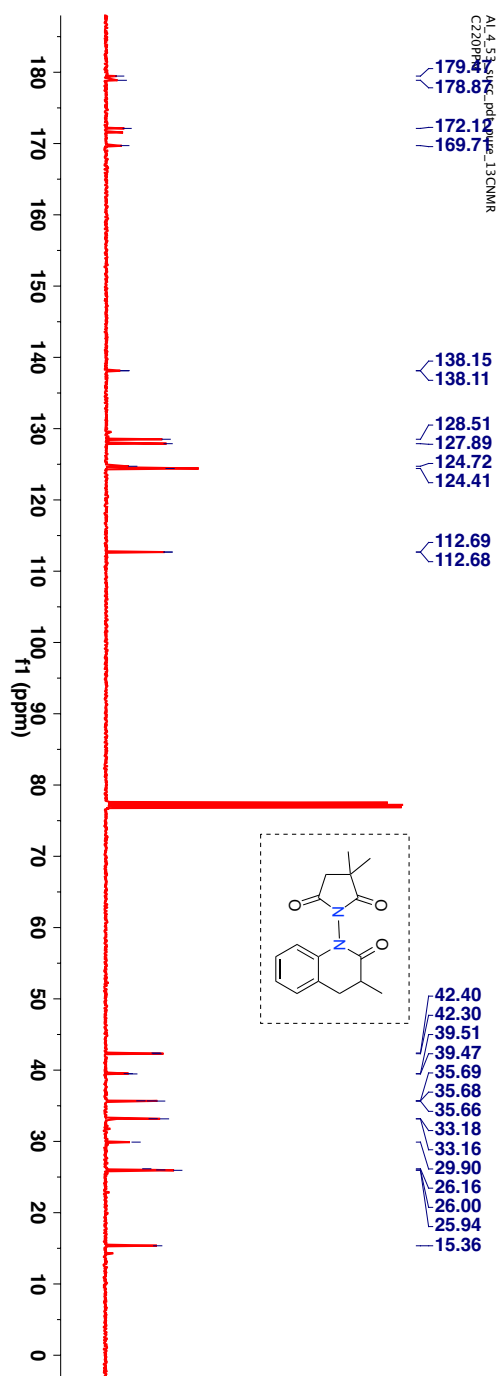
Figure 3.93: ^{13}C-NMR (100 MHz, CDCl$_3$, δ ppm) spectrum of **185b**.

HRMS-ESI (m/z) ([M + Na]$^+$):

Chemical Formula	: $C_{16}H_{18}N_2O_3$
Calculated	: 309.1215
Observed	: 309.1233
$|\Delta m|$	: 5.8 ppm
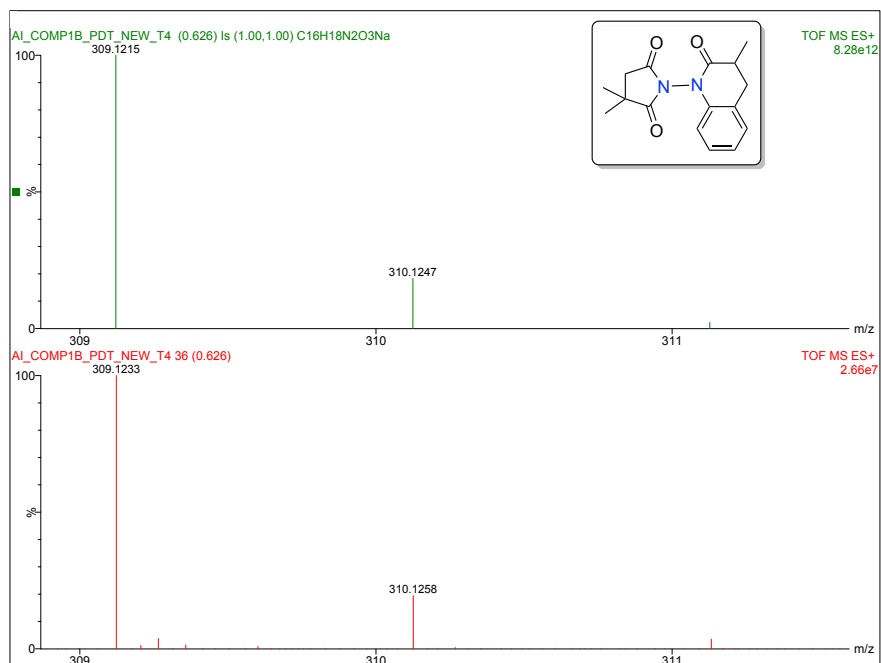
Figure 3.94: HRMS spectra of **185b**.

3.26.1. UV-Vis spectra of acrylanilide derivative 184b
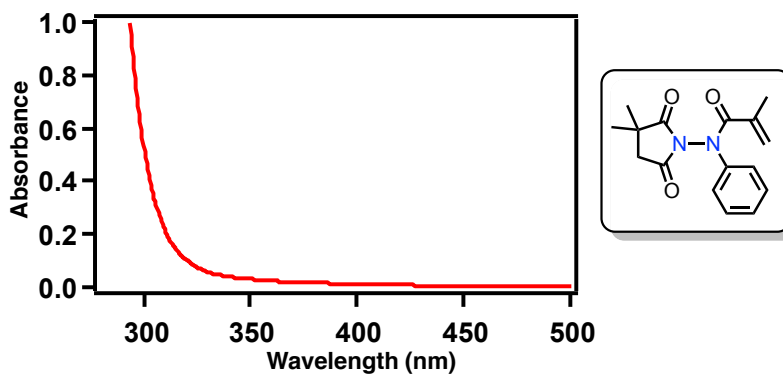
Figure 3.95: UV-Vis spectra of *N-N* bond based acrylanilide derivative **184b** recorded at the reaction concentration (concn = 3.49 mM) in acetonitrile.

3.26.2. HPLC analysis conditions for 184b
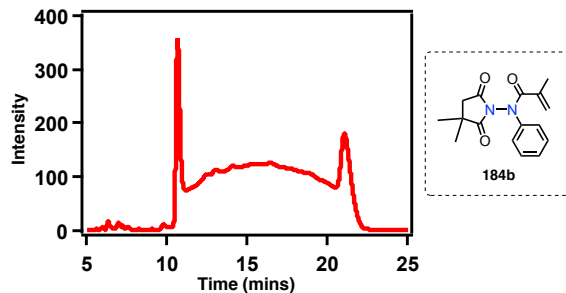
For analytical conditions,

Column	: CHIRALPAK ® IC
Abs. detector wavelength	: 254 nm and 313 nm
Mobile phase	: Hexanes:2-propanol = 70:30
Flow rate	: 1.0 mL/min
Retention times (min)	: pA 10.6 and pB 20.9

3.26.3. HPLC analysis conditions for 185b
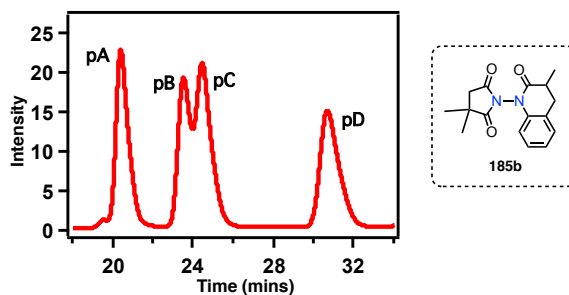
For analytical conditions,

Column	: CHIRALPAK ® AD3
Abs. detector wavelength	: 254 nm and 313 nm
Mobile phase	: Hexanes:2-propanol = 90:10
Flow rate	: 0.8 mL/min
Retention times (min)	: pA 20.3, pB 23.4, pC 24.4 and pD 30.7
Relative area	: pA ~ 25%, pB ~ 22%, pC ~ 28.0 and pD ~ 25%

3.27. Photoreaction of point chiral succinimide derivative (*R*)-184f

(*R*)-**184f**   **185f**
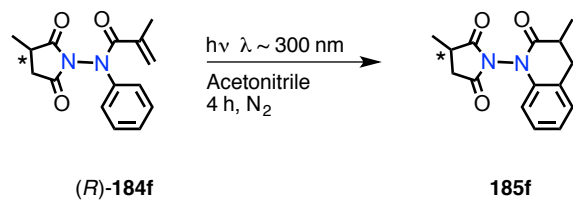
Scheme 3.64: 6π Photocyclization of acrylanilide derivative (*R*)-**184f** by direct irradiation.

(*R*)-**184f**   **185f**
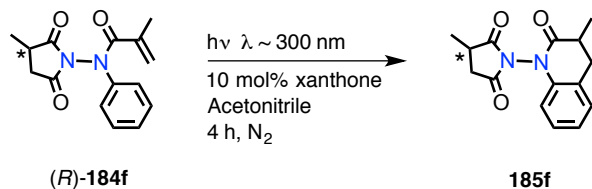
Scheme 3.65: 6π Photocyclization of acrylanilide derivative (*R*)-**184f** by sensitized irradiation with xanthone as the triplet sensitizer.
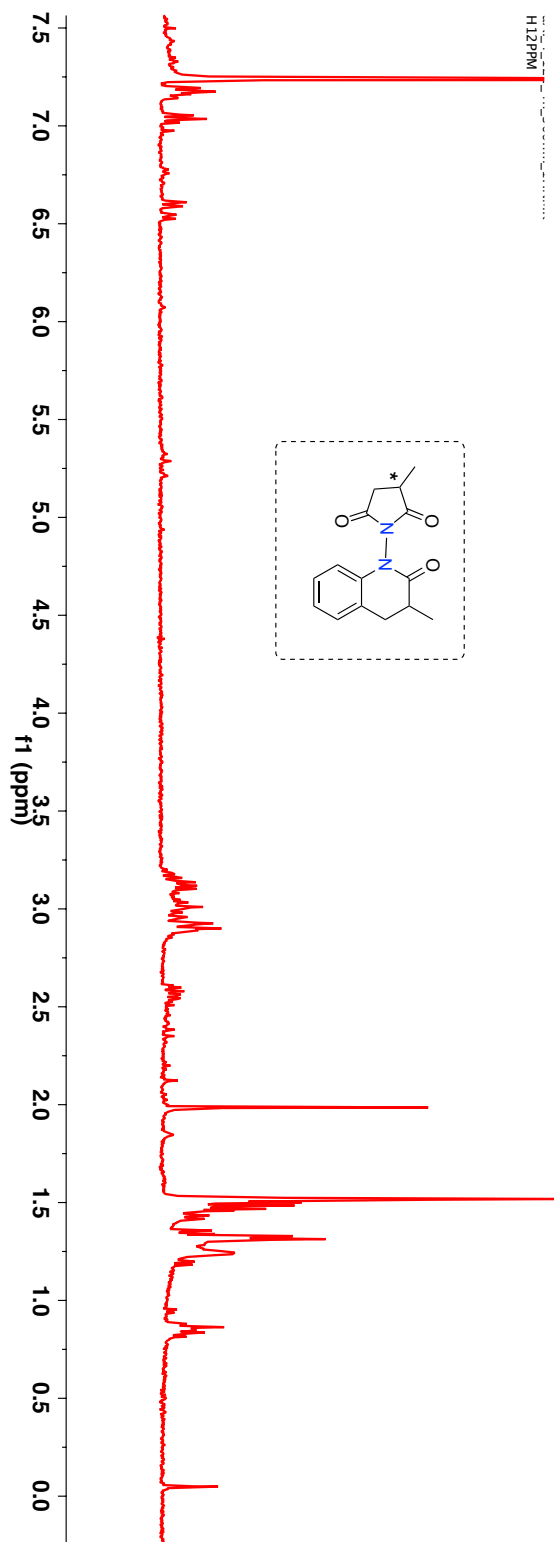
Figure 3.96: ^{1}H-NMR (400 MHz, CDCl$_3$, δ ppm) spectrum of (*R*)-**185f** (of crude reaction mixture).

TLC condition - R$_f$ = 0.4 (50% hexanes:ethyl acetate). Clear solid (Yield = 75%).

^{1}H-NMR (400 MHz, CDCl$_3$, δ ppm): 1.31-1.33 (m), 1.46-1.52 (m), 2.52-2.61(m), 2.90-3.18 (m), 6.53-6.61 (m), 7.01-7.05 (m) and 7.14-7.20 (m).
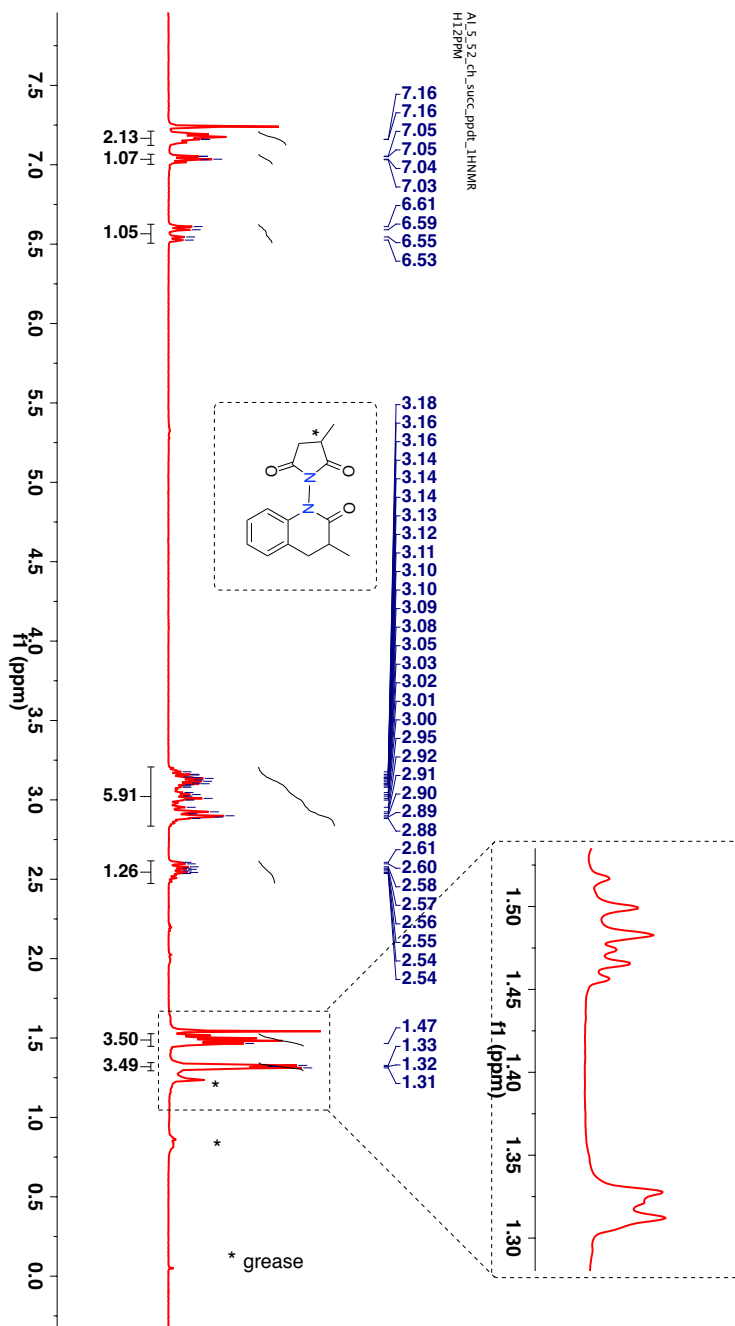
Figure 3.97: ^{1}H-NMR (400 MHz, CDCl$_3$, δ ppm) spectrum of (*R*)-**185f**.

^{13}C-NMR (100 MHz, CDCl$_3$, δ ppm): 15.4, 15.4, 17.1, 17.3, 17.4, 17.4, 33.1, 33.2, 33.6, 33.7, 33.8, 35.1, 35.2, 35.2, 35.3, 35.7, 35.7, 112.6, 112.7, 112.9, 112.9, 124.4, 124.7, 124.7, 127.9, 127.9, 127.9, 128.5, 128.5, 128.6, 138.1, 169.6, 169.6, 172.1, 172.7, 175.9, 176.2 and 176.8.
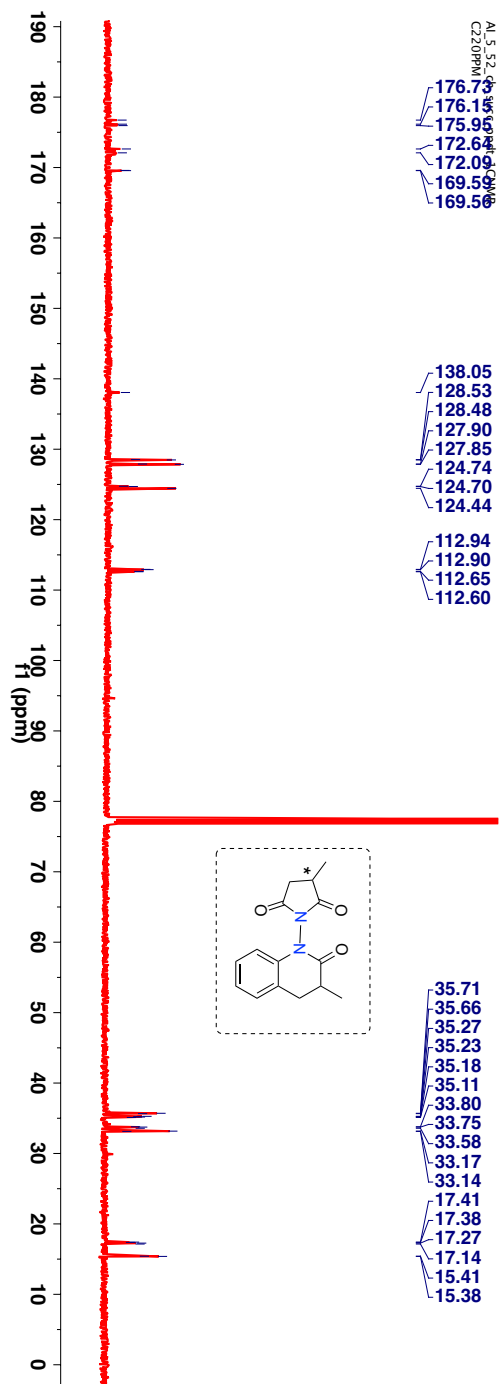
Figure 3.98: ^{13}C-NMR (100 MHz, CDCl$_3$, δ ppm) spectrum of (*R*)-**185f**.

3.27.1. UV-Vis spectra of acrylanilide derivative 184f
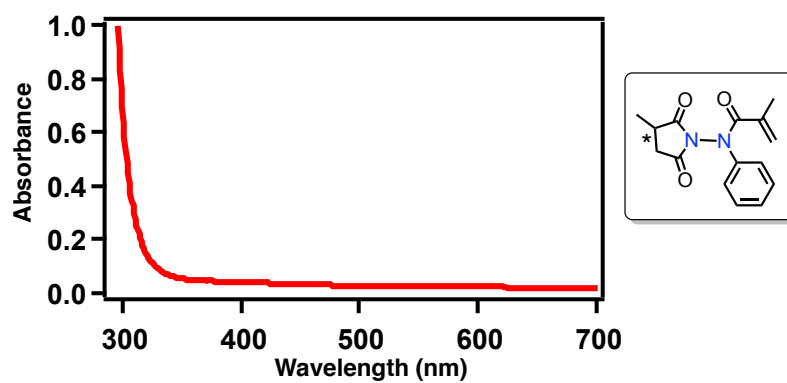
Figure 3.99: UV-Vis spectra of *N-N* bond based acrylanilide derivative (*R*)-**184f** recorded at the reaction concentration (concn = 4.9 mM) in acetonitrile.

3.27.2. HPLC analysis conditions for 196
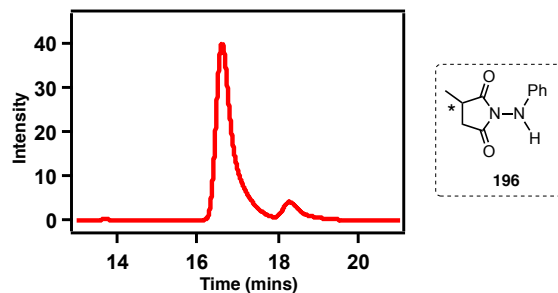
For analytical conditions,

Column	: CHIRALPAK® AD-H
Abs. detector wavelength	: 254 nm and 270 nm
Mobile phase	: Hexanes:2-propanol = 80:20
Flow rate	: 0.8 mL/min
Retention times (min)	: pA 16.6 and pB 18.3
Relative area	: pA ~ 94% and pB ~ 6%

3.27.3 HPLC analysis conditions for 184f
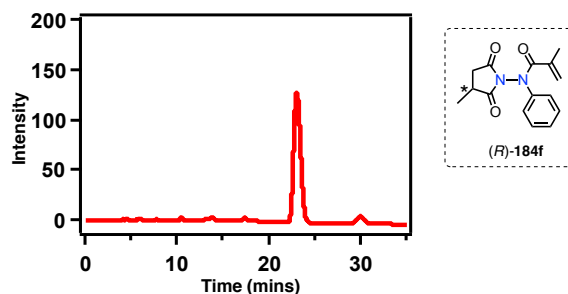
Column	: CHIRALPAK® IC
Abs. detector wavelength	: 254 nm and 270 nm
Mobile phase	: Hexanes:2-propanol = 70:30
Flow rate	: 0.8 mL/min
Retention times (min)	: pA ~23.0

3.27.4 HPLC analysis conditions for 185f by direct irradiation (crude sample was injected)
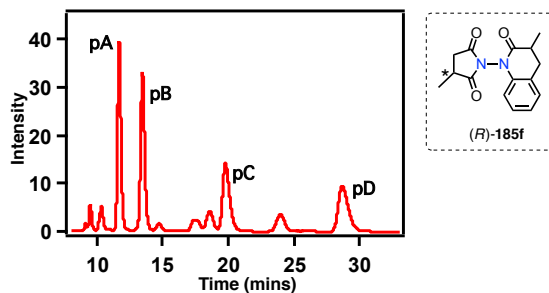
For analytical conditions,

Column	: CHIRALPAK® IC
Abs. detector wavelength	: 254 nm and 270 nm
Mobile phase	: Hexanes:2-propanol = 70:30
Flow rate	: 0.8 mL/min
Retention times (min)	: pA 11.6, pB 13.4, pC 19.7 and 28.6
Relative area	: pA ~ 29%, pB ~ 29%, pC = 21%, pD ~ 21%

3.27.5 HPLC analysis conditions for 185f by sensitized irradiation (crude sample was injected)
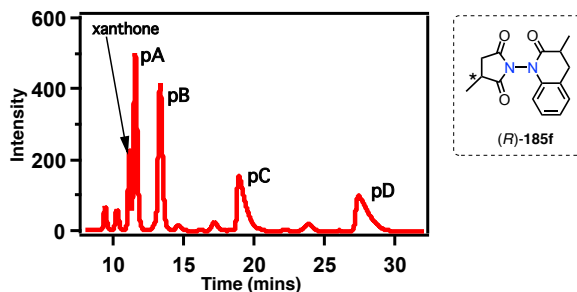
Column	: CHIRALPAK® IC
Abs. detector wavelength	: 254 nm and 270 nm
Mobile phase	: Hexanes:2-propanol = 70:30
Flow rate	: 0.8 mL/min
Retention times (min)	: pA 11.6, pB 13.4, pC 19.7 and 28.6
Relative area	: pA ~ 29%, pB ~ 29%, pC ~ 21%, pD ~ 21%

3.28. Photoreaction of quinazolinone derivative 184d

184d   **185d**
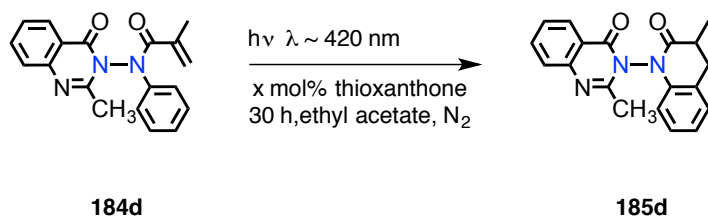
Scheme 3.66: 6π Photocyclization of acrylanilide derivative **184d** by sensitized irradiation.

Table 3.17: Sensitizer loading studies for 6π photocyclization of quinazolinone derivative **184d** in ethyl acetate.[a]

Entry	TX (x mol%)	Conversion/%
1	0	0
2	1	0
3	5	80
4	10	90

[a] [**184d**] = 3.84 mM. Values based on ^{1}H-NMR spectroscopy (±5% error), each experiment was performed for three trials, %conversion and mass balance calculated using triphenylmethane as internal standard. TX: thioxanthone.

Table 3.18: Solvent screening studies for 6π photocyclization of quinazolinone derivative **184d**.[a]

Entry	Solvent	Conversion/%
1	Methanol	0
2	Acetonitrile	76
3	Ethyl acetate	90
4	Benzene	<10
6	Methylcyclohexane	0

[a] [**184d**] = 3.84 mM. Values based on ^{1}H-NMR spectroscopy (±5% error), each experiment was performed for three trials, %conversion and mass balance calculated using triphenylmethane as internal standard. TX: thioxanthone.

TLC condition - R$_f$ = 0.6 (50% hexanes:ethyl acetate). Solid (Yield = 40%).

^{1}H-NMR (400 MHz, CDCl$_3$, δ ppm): 1.37-1.39 (m), 2.35 (s), 2.42 (s), 2.54 (s), 2.85-3.17 (m), 6.54-6.51(m), 7.05-7.17 (m), 7.25-7.27 (m), 7.32-7.33 (m), 7.43-7.49 (m) 7.68-7.69 (m), 7.76-7.81 (m) and 8.19-8.26 (m).
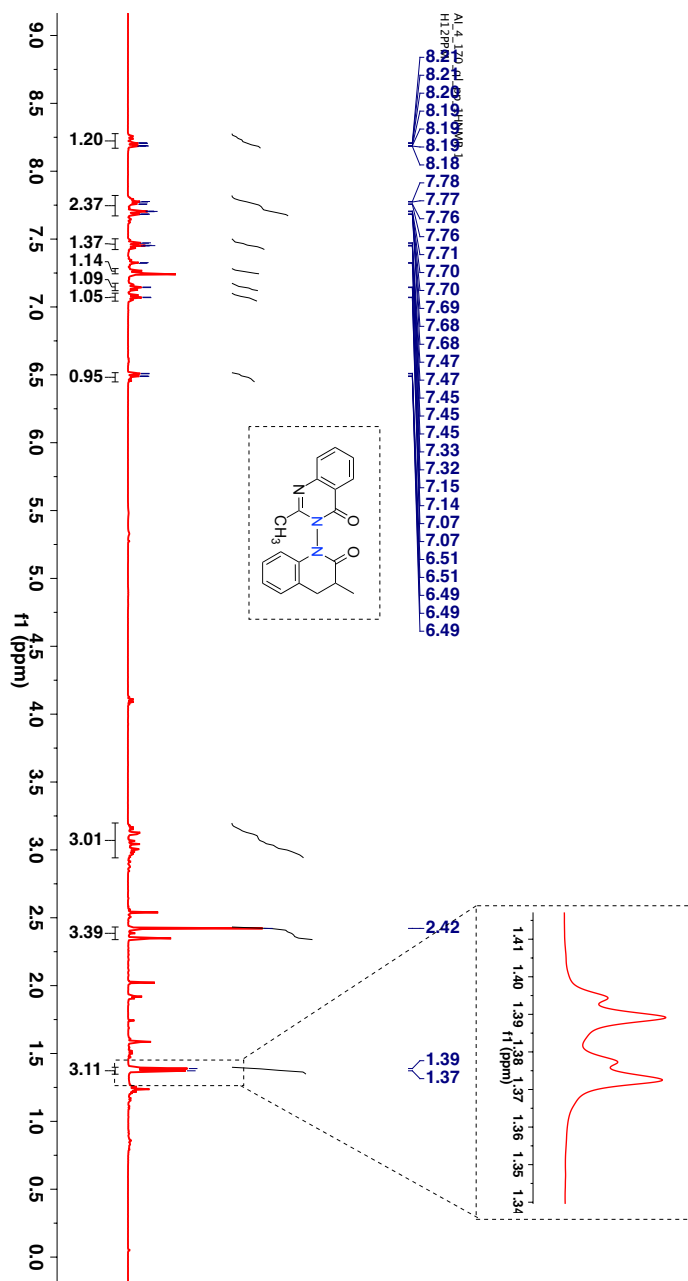
Figure 3.100: ^{1}H-NMR (400 MHz, CDCl$_3$, δ ppm) spectrum of **185d**.

^{13}C-NMR (100 MHz, CDCl$_3$, δ ppm): 15.4, 15.5, 20.9, 20.0, 33.1, 33.2, 33.8, 36.3, 112.6, 112.8, 121.6, 124.6, 124.7, 124.8, 127.1, 127.5, 127.6, 128.2, 128.3, 128.7, 128.9, 128.5, 135.3, 135.3, 137.9, 138.3, 147.2, 147.3, 155.2, 155.4, 158.7, 158.9, 170.5 and 170.8.
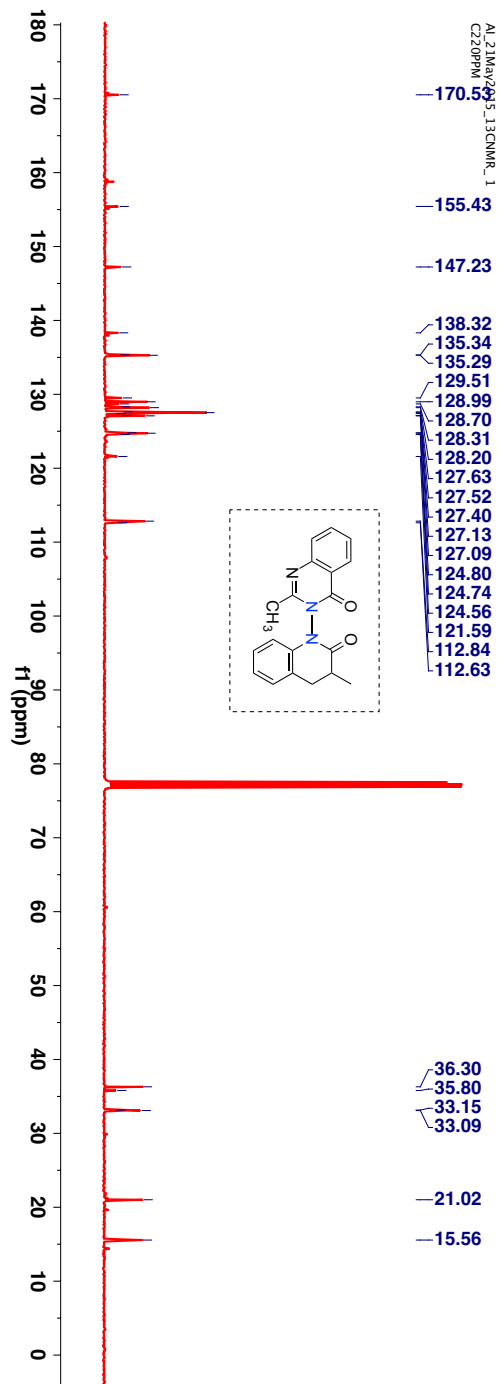
Figure 3.101: ^{13}C-NMR (100 MHz, CDCl$_3$, δ ppm) spectrum of **185d**.

HRMS-ESI (m/z) ([M + Na]$^+$):

Chemical Formula	: C$_{19}$H$_{17}$N$_3$O$_2$
Calculated	: 342.1219
Observed	: 342.1236
|Δm|	: 4.9 ppm
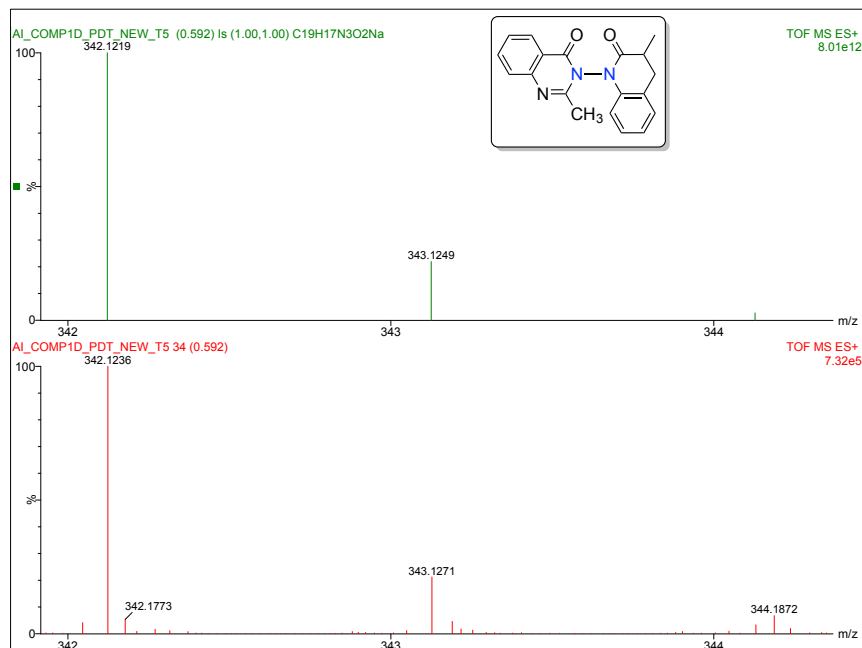
Figure 3.102: HRMS spectra of **185d**.

3.28.1 UV-Vis spectra of acrylanilide derivative 184d
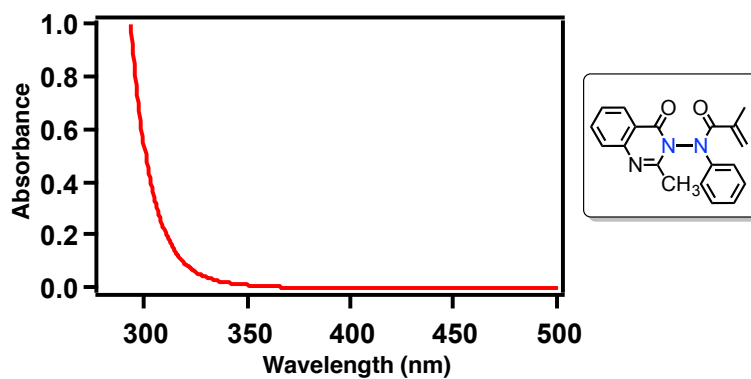
Figure 3.103: UV-Vis spectra of *N-N* bond based acrylanilide derivative **184d** recorded at the reaction concentration (concn = 3.13 mM) in acetonitrile.

3.28.2 HPLC analysis condition for 184d
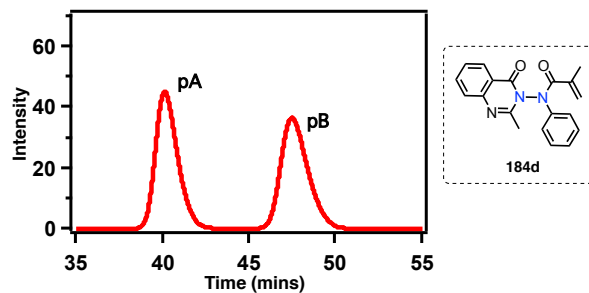
For analytical conditions,

Column	: CHIRALPAK® AD-H
Abs. detector wavelength	: 254 nm and 313 nm
Mobile phase	: Hexanes:2-propanol = 70:30
Flow rate	: 0.8 mL/min
Retention times (min)	: pA 11.4 and pB 13.7

For preparative conditions,

Column	: CHIRACEL® OD-H
Abs. detector wavelength	: 254 nm and 313 nm
Mobile phase	: Hexanes:2-propanol = 80:20
Flow rate	: 2.0 mL/min
Retention times (min)	: pA 19.9 and pB 24.3

3.28.3   HPLC analysis condition for 185d
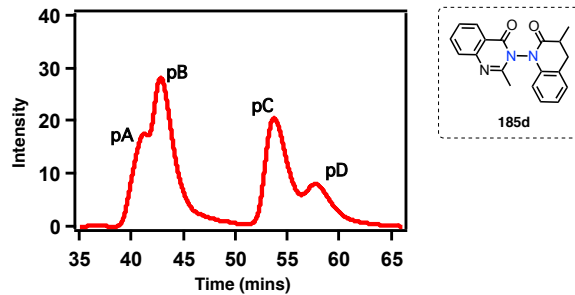
For analytical conditions,

Column	: Regis® PIRKLE COVALENT (R,R) WHELK–01
Abs. detector wavelength	: 254 nm and 270 nm
Mobile phase	: Hexanes:2-propanol = 80:20
Flow rate	: 0.8 mL/min

3.29. Racemization kinetics of acrylanilide 184d
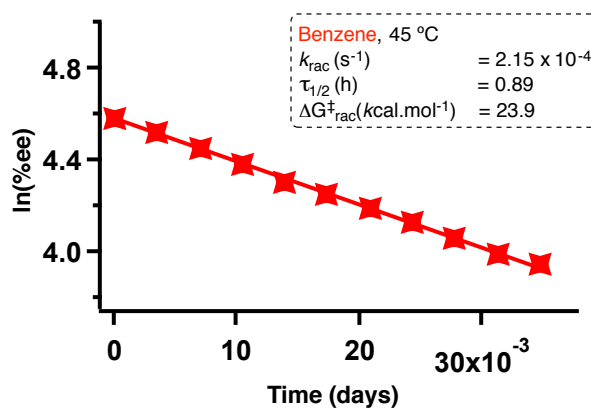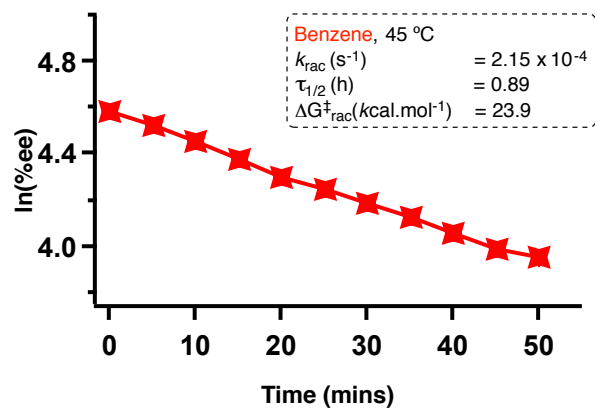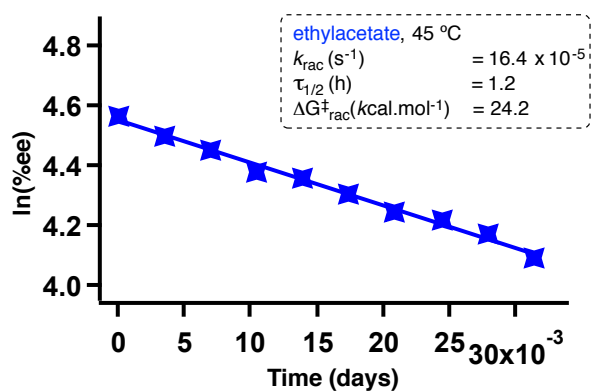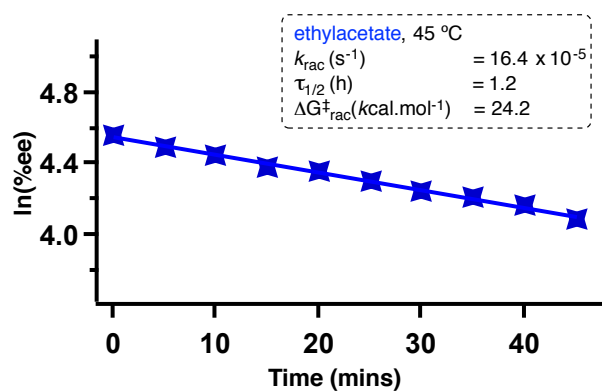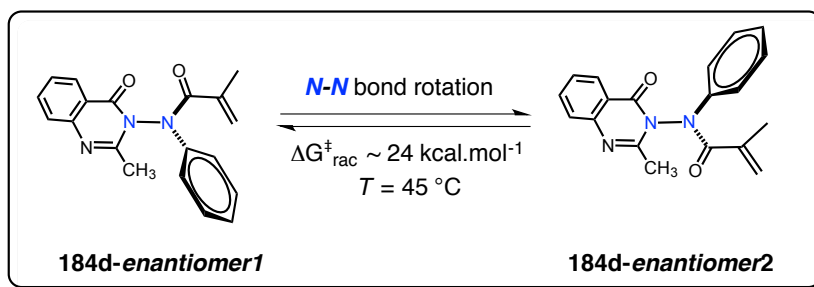
Figure 3.104: Racemization kinetics for optically pure quinazolinone based *N-N* atropisomer **184d** in benzene and ethyl acetate.

3.30. Phosphorescence spectra of *N-N* bond based acrylanilides recorded at 77 K

E$_T$ for **184g** = 62.8 kcal/mol
[**184g**] = 0.45 mM, MetTHF

E$_T$ for **184c** = 62.3 kcal/mol
[**184c**] = 0.45 mM, MetTHF

E$_T$ for **184b** = 62.7 kcal/mol
[**184b**] = 0.45 mM, MetTHF

E$_T$ for **184d** = 72.0 kcal/mol
[**184d**] = 0.45 mM, MetTHF
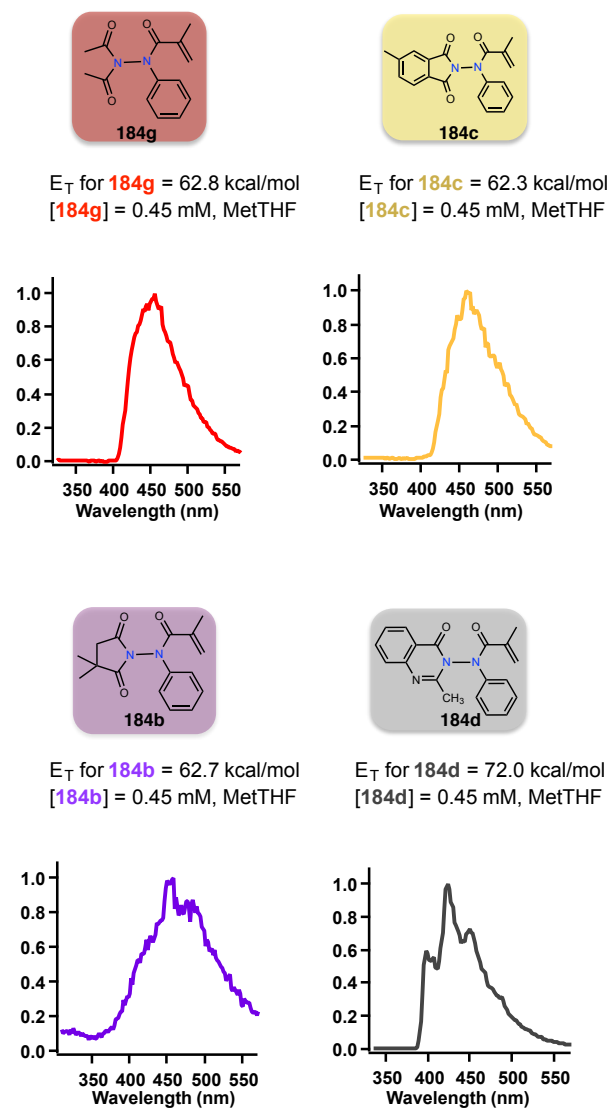
Figure 3.105: Phosphorescence spectra of *N-N* bond based acrylanilides recorded at 77 K in 2-Met THF glass matrix.

3.31.   References

(1)   McNaught, A. D.; Wilkinson, A.; Blackwell Scientific Publications, Oxford 1997, 10.1351/goldbook.

(2)   Schöfer, K.; Schwan, S. *J. Prak. Chem.* **1850**, *51*, 185.

(3)   Saha, A.; Kumar, R.; Kumar, R.; Devakumar, C. *Indian J. Chem., Sect B* **2010**, *49*, 526-31.

(4)   Loiseau, F., University of Ottawa, 2013.

(5)   Majumdar, P.; Pati, A.; Patra, M.; Behera, R. K.; Behera, A. K. *Chem. Rev.* **2014**, *114*, 2942-77.

(6)   Vincent-Rocan, J.-F.; Ivanovich, R. A.; Clavette, C.; Leckett, K.; Bejjani, J.; Beauchemin, A. M. *Chem. Sci.* **2016**, *7*, 315-28.

(7)   Roveda, J.-G.; Clavette, C.; Hunt, A. D.; Gorelsky, S. I.; Whipp, C. J.; Beauchemin, A. M. *J. Am. Chem. Soc.* 2009, *131*, 8740-41.

(8)   Fang, G.-M.; Li, Y.-M.; Shen, F.; Huang, Y.-C.; Li, J.-B.; Lin, Y.; Cui, H.-K.; Liu, L. *Angew. Chem. Int. Ed.* 2011, *50*, 7645-49.

(9)   Zheng, J.-S.; Tang, S.; Qi, Y.-K.; Wang, Z.-P.; Liu, L. *Nat. Protocols* 2013, *8*, 2483-95.

(10)   Yale, H. L.; Losee, K.; Martins, J.; Holsing, M.; Perry, F. M.; Bernstein, J. *J. Am. Chem. Soc.* 1953, *75*, 1933-42.

(11)   Blair, L. M.; Sperry, J. *J. Nat. Prod.* 2013, *76*, 794-812.

(12)   Gould, E.; Lebl, T.; Slawin, A. M. Z.; Reid, M.; Davies, T.; Smith, A. D. *Organic & Biomolecular Chemistry* 2013, *11*, 7877-92.

(13)   Hoover, J. M.; DiPasquale, A.; Mayer, J. M.; Michael, F. E. *J. Am. Chem. Soc.* 2010, *132*, 5043-53.

(14)   Bredihhin, A.; Groth, U. M.; Mäeorg, U. *Org. Lett.* 2007, *9*, 1097-99.

(15)   Fischer, E. *Berichte der deutschen chemischen Gesellschaft* 1875, *8*, 589-94.

(16)   Ragnarsson, U. *Chem. Soc. Rev.* 2001, *30*, 205-13.

(17)   Lunn, G.; Sansone, E. B.; Keefer, L. K. *J. Org. Chem.* 1984, *49*, 3470-73.

(18)   Hayes, B. T.; Stevens, T. S. *J. Chem. Soc. C: Org.* 1970, 10.1039/J39700001088, 1088-89.

(19)   Draghici, C., The University of Vermont, 2009.

(20)   Hynes, J.; Doubleday, W. W.; Dyckman, A. J.; Godfrey, J. D.; Grosso, J. A.; Kiau, S.; Leftheris, K. *J. Org. Chem.* 2004, *69*, 1368-71.

(21)   Shen, Y.; Friestad, G. K. *J. Org. Chem.* 2002, *67*, 6236-39.

(22)   Rozgowska, E. J., The University of Edingburgh, 2011.

(23)   Tamura, Y.; Minamikawa, J.; Sumoto, K.; Fujii, S.; Ikeda, M. *J. Org. Chem.* 1973, *38*, 1239-41.

(24)   Glover, E. E.; Rowbottom, K. T. *J. Chem. Soc., Perkin Trans. 1* 1976, 10.1039/P19760000367, 367-71.

(25)   Schmitz, E. *Angew. Chem. Intd. Ed.* 1964, *3*, 333-41.

(26)   Strong, B., Western Michigan University, 2012.

(27)   Rosen, B. R.; Werner, E. W.; O'Brien, A. G.; Baran, P. S. *J. Am. Chem. Soc.* 2014, *136*, 5571-74.

(28)   Gieshoff, T.; Schollmeyer, D.; Waldvogel, S. R. *Angew. Chem. Int. Ed.* 2016, 10.1002/anie.201603899, n/a-n/a.

(29)   Wolf, C. *Dynamic Stereochemistry of Chiral Compounds. Principles and Applications*; RSC publishing: Cambridge, UK, 2008.

(30)   Coogan, M. P.; Passey, S. C. *J. Chem. Soc., Perkin Trans.* 2000, 10.1039/b004457l, 2060-66.

(31)   Arthur, R. J.; Coogan, M. P.; Casadesus, M.; Haigh, R.; Headspith, D. A.; Francesconi, M. G.; Laye, R. H. *CrystEngComm* 2009, *11*, 610-19.

(32)   Atkinson, R. S.; Barker, E.; Edwards, P. J.; Thomson, G. A. *J. Chem. Soc., Perkin Trans. 1* 1996, 10.1039/P19960001047, 1047-55.

(33)   Bishop, G. J.; Price, B. J.; Sutherland, I. O. *Chem. Commun.* 1967, 10.1039/C19670000672, 672-74.

(34)   Reynolds, C. H.; Hormann, R. E. *J. Am. Chem. Soc.* 1996, *118*, 9395-401.

(35)   Korsch, B. H.; Riggs, N. V. *Tetrahedron Lett.* 1966, *7*, 5897-903.

(36)   Price, B.; Sutherland, I. O.; Williamson, F. G. *Tetrahedron* 1966, *22*, 3477-90.

(37)   Atkinson, R. S.; Judkins, B. D. *Tetrahedron Lett.* 1979, *20*, 4001-02.

(38)   Verma, S. M.; Prasad, R. *J. Org. Chem.* 1973, *38*, 1004-10.

(39)   Atkinson, R. S.; Judkins, B. D.; Patwardhan, B. *J. Chem. Soc., Perkin Trans.* 1979, 10.1039/P29790001490, 1490-95.

(40)   Atkinson, R. S.; Edwards, P. J.; Thomson, G. A. *J. Chem. Soc., Chem. Commun.* 1992, 10.1039/C39920001256, 1256-57.

(41)   Atkinson, R. S.; Kelly, B. J.; Williams, J. *Tetrahedron* 1992, *48*, 7713-30.

(42)   Atkinson, R. S.; Barker, E.; Price, C. J.; Russell, D. R. *J. Chem. Soc., Chem. Commun.* 1994, 10.1039/C39940001159, 1159-60.

(43)   Atkinson, R. S.; Barker, E.; Sutcliffe, M. J. *Chem. Commun.* 1996, 10.1039/CC9960001051, 1051-52.

(44)   Atkinson, R. S.; Ayscough, A. P.; Gattrell, W. T.; Raynham, T. M. *Tetrahedron Lett.* 1998, *39*, 4377-80.

(45)   S. Atkinson, R.; Barker, E.; K. Meades, C.; S. Atkinson, R.; K. Meades, C.; A. Albar, H. *Chem. Commun.* 1998, 10.1039/A706283D, 29-30.

(46)   Al-Sehemi, A. G.; Atkinson, R. S.; Fawcett, J.; Russell, D. R. *J. Chem. Soc., Perkin Trans. 1* 2000, 10.1039/b005814i, 4413-21.

(47)   Al-Sehemi, A. G.; Atkinson, R. S.; Fawcett, J.; Russell, D. R. *Tetrahedron Lett.* 2000, *41*, 2243-46.

(48)   Al-Sehemi, A. G.; Atkinson, R. S.; Fawcett, J.; Russell, D. R. *Tetrahedron Lett.* 2000, *41*, 2239-42.

(49)   Al-Sehemi, A. G.; Atkinson, R. S.; Fawcett, J.; Russell, D. R. *Chem. Commun.* 2000, 10.1039/A907970J, 43-44.

(50)   Atkinson, R. S.; Draycott, R. D.; Hirst, D. J.; Parratt, M. J.; Raynham, T. M. *Tetrahedron Lett.* 2002, *43*, 2083-85.

(51)   Ottersbach, P. A.; Schnakenburg, G.; Gutschow, M. *Chem. Commun.* 2012, *48*, 5772-4.

(52)   Kim, Y. J.; Lee, D. *Org. Lett.* 2004, *6*, 4351-53.

(53)   Braslavsky, S. E. In *Pure Appl. Chem.* 2007; Vol. 79, p 293.

(54)   Turro, N. J.; Ramamurthy, V.; Scaiano, J. C. *Modern Molecular Photochemistry of Organic Molecules*; University Science Books: Sausalito, CA, 2010.

(55)   Baumgarten, H. E.; Creger, P. L.; Zey, R. L. *J. Am. Chem. Soc.* 1960, *82*, 3977-82.

(56)   Cleveland, P. G.; Chapman, O. L. *Chemical Communications (London)* 1967, 10.1039/C19670001064, 1064-65.

(57)   Chapman, O. L.; Adams, W. R. *J. Am. Chem. Soc.* 1968, *90*, 2333-42.

(58)   Naito, T.; Tada, Y.; Nishiguchi, Y.; Ninomiya, I. *J. Chem. Soc., Perkin Trans. 1* 1985, 10.1039/P19850000487, 487-91.

(59)   Zhang, L.; Sonaglia, L.; Stacey, J.; Lautens, M. *Org. Lett.* 2013, *15*, 2128-31.

(60)   Ninomiya, I.; Kiguchi, T.; Yamauchi, S.; Naito, T. *J. Chem. Soc., Perkin Trans.* 1976, 10.1039/P19760001861, 1861-65.

(61)   Ninomiya, I.; Yamauchi, S.; Kiguchi, T.; Shinohara, A.; Naito, T. *J. Chem. Soc., Perkin Trans. 1* 1974, 10.1039/P19740001747, 1747-51.

(62)   Ninomiya, I.; Naito, T.; Mori, T. *J. Chem. Soc., Perkin Trans. 1* 1973, 10.1039/P19730000505, 505-09.

(63)   Ninomiya, I.; Yamauchi, S.; Kiguchi, T.; Shinohara, A.; Naito, T. *Journal of the Chemical Society, Perkin Transactions 1* 1974, 10.1039/P19740001747, 1747-51.

(64)   Ninomiya, I.; Kiguchi, T.; Naito, T. *Heterocycles* 1978, *8*.

(65)   Ninomiya, I.; Kiguchi, T.; Yamauchi, S.; Naito, T. *J. Chem. Soc., Perkin Trans. 1* 1980, 10.1039/P19800000197, 197-202.

(66)   Ninomiya, I.; Yamamoto, O.; Naito, T. *J. Chem. Soc., Perkin Trans. 1* 1983, 10.1039/P19830002165, 2165-70.

(67)   Fodor, L.; Szabó, J.; Bernáth, G.; Sohár, P.; Maclean, D. B.; Smith, R. W.; Ninomiya, I.; Naito, T. *J. Heterocycl. Chem.* 1989, *26*, 333-37.

(68)   Naito, T.; Kojima, N.; Miyata, O.; Ninomiya, I.; Inoue, M.; Doi, M. *J. Chem. Soc., Perkin Trans. 1* 1990, 10.1039/P19900001271, 1271-80.

(69)   Naito, T.; Yuumoto, Y.; Kiguchi, T.; Ninomiya, I. *J. Chem. Soc., Perkin Trans. 1* 1996, 10.1039/P19960000281, 281-88.

(70)   Tanaka, K.; Toda, F. *Chem. Rev.* 2000, *100*, 1025-74.

(71)   Tanaka, K.; Kakinoki, O.; Toda, F. *J. Chem. Soc., Chem. Commun.* 1992, 10.1039/C39920001053, 1053-54.

(72)   Naito, T. T., Y.; Ninomiya, I. *Heterocycles* 1984, *22*, 237-40.

(73)   Bach, T.; Grosch, B.; Strassner, T.; Herdtweck, E. *J. Org. Chem.* 2003, *68*, 1107-16.

(74)   Raghunathan, R.; Jockusch, S.; Sibi, M. P.; Sivaguru, J. *J. Photochem. Photobio. A*, http://dx.doi.org/10.1016/j.jphotochem.2015.12.023.

(75)   Ayitou, A. J.-L.; Sivaguru, J. *J. Am. Chem. Soc.* 2009, *131*, 5036-37.

(76) Ayitou, A. J.-L.; Sivaguru, J.; Ugrinov, A. *Photochem. Photobiol. Sci.* 2009, *8*, 751-54.

(77) Ayitou, A. J.-L.; Sivaguru, J. *Chem. Commun.* 2011, *47*, 2568-70.

(78) Ayitou, A. J.-L.; Clay, A.; Kumarasamy, E.; Jockusch, S.; Sivaguru, J. *Photochem. Photobiol. Sci.* 2014, *13*, 141-44.

(79) Hayashi, H.; Miwa, Y.; Miki, I.; Ichikawa, S.; Yoda, N.; Ishii, A.; Kono, M.; Suzuki, F. *J. Med. Chem.* 1992, *35*, 4893-902.

(80) Carling, R. W.; Leeson, P. D.; Moore, K. W.; Smith, J. D.; Moyes, C. R.; Mawer, I. M.; Thomas, S.; Chan, T.; Baker, R. *J. Med. Chem.* 1993, *36*, 3397-408.

(81) Sunal, S. G.; Yabanoglu, S.; Yesilada, A.; Ucar, G. *J Neural Transm* 2007, *114*, 717-19.

(82) Moriarty Sr, R. M.; Murphy, M. R.; Druck, S. J.; May, L. *Tetrahedron Lett.* 1967, *8*, 1603-09.

(83) Verma, S. M.; Rao, S. O.; K.O.P., S. *Bull. Chem. Soc. Jap.* 1974, *47*.

(84) Verma, S. M.; Sinha, K. O. P.; Rao, C. K. *Can. J. Chem.* 1974, *52*, 2399-402.

(85) Verma, S. M.; Singh, R. M. *Aust. J. Chem.* 1976, *29*.

(86) Verma, S. M.; Singh, M. D. *J. Org. Chem.* 1977, *42*, 3736-40.

(87) Verma, S. M.; Singh, R. M. *Bull. Chem. Soc. Jap.* 1978, *51*.

(88) Srivastava, A.; Samtani, S.; Verma, S. M. *Proc. Indian. Natn. Sci. Acad.* 1994, *60*.

(89) Trapp, O. *Top. Curr. Chem.* 2013, *341*, 231-69.

(90) D'Acquarica, I.; Gasparrini, F.; Pierini, M.; Villani, C.; Zappia, G. *J. Sep. Sci.* 2006, *29*, 1508-16.

(91) Kamiński, K.; Obniska, J. *Biorg. Med. Chem.* 2008, *16*, 4921-31.

(92) Bourel, L.; Tartar, A.; Melnyk, P. *Tetrahedron Lett.* 1996, *37*, 4145-48.

(93) Conley, N. R.; Hung, R. J.; Willson, C. G. *J. Org. Chem.* 2005, *70*, 4553-55.

(94) Abbas, C.; Pickaert, G.; Didierjean, C.; Grégoire, B. J.; Vanderesse, R. *Tetrahedron Lett.* 2009, *50*, 4158-60.

(95) Brosse, N.; Pinto, M.-F.; Bodiguel, J.; Jamart-Grégoire, B. *J. Org. Chem.* 2001, *66*, 2869-73.

(96) Lim, Y.-K.; Lee, K.-S.; Cho, C.-G. *Org. Lett.* 2003, *5*, 979-82.

(97) Barton, D. H. R.; Finet, J.-P.; Khamsi, J. *Tetrahedron Lett.* 1986, *27*, 3615-18.

(98) Barton, D. H. R.; Finet, J.-P.; Khamsi, J. *Tetrahedron Lett.* 1988, *29*, 1115-18.

(99) Barton, D. H. R.; Ozbalik, N.; Ramesh, M. *Tetrahedron Lett.* 1988, *29*, 857-60.

(100)   Chan, D. M. T. *Tetrahedron Lett.* 1996, *37*, 9013-16.

(101)   Anderson, J. C.; Cubbon, R.; Harding, M.; James, D. S. *Tetrahedron: Asymmetry* 1998, *9*, 3461-90.

(102)   Táubrik, O.; Máeorg, U.; Sillard, R.; Ragnarsson, U. *Tetrahedron* 2004, *60*, 8363-73.

(103)   Aoki, Y.; Saito, Y.; Sakamoto, T.; Kikugawa, Y. *Synth. Commun.* 2000, *30*, 131-40.

(104)   Aitken, K. M.; Aitken, R. A.; Slawin, A. M. Z. *J. Chem. Crystallogr.* 2013, *44*, 25-29.

(105)   *Chemical photocatalysis*; Berlin: Walter de Gruyter GmbH & Co. KG., 2013.

(106)   Rehm, D.; Weller, A. *Isr. J. Chem.* 1970, *8*, 259-71.

(107)   Dadashi-Silab, S.; Aydogan, C.; Yagci, Y. *Polymer Chemistry* 2015, *6*, 6595-615.

(108)   Iyer, A.; Jockusch, S.; Sivaguru, J. *J. Phys. Chem. A* 2014, *118*, 10596-602.

(109)   Palak Jain, V. G., Arun Parikh and Hansa Parikh *Pharma Science Monitor: Int. J. Pharm. Sci.* 2012, *3*.

CHAPTER 4. METAL-FREE VISIBLE LIGHT MEDIATED CHLOROMETHYLATION OF ATROPISOMERIC HYDRAZIDES

4.1. Introduction

Discovery of natural products has revolutionized the field of medicinal chemistry. Among the most noted drugs that has been extensively studied and utilized by humans include: penicillin from mold, aspirin derived from willow, steroids extracted from Mexican yam, morphine from opium and taxol from yew tree.[1] The importance of natural products has led the path for many chemists over the years to investigate and develop methodologies for accessing them. Many natural products possessing trihalomethyl or dichloromethyl groups exhibit wide range of biologically activity (Chart 4.1). [2-7] There are more than 2100 natural products extracted from marine organisms that are known to have organochlorine skeleton.[1]

201 dysithiazolamide	**202** sinkotamide A	**203** dysamide A
204 barbamide	**205** muironolide A	**206** neodysidenin
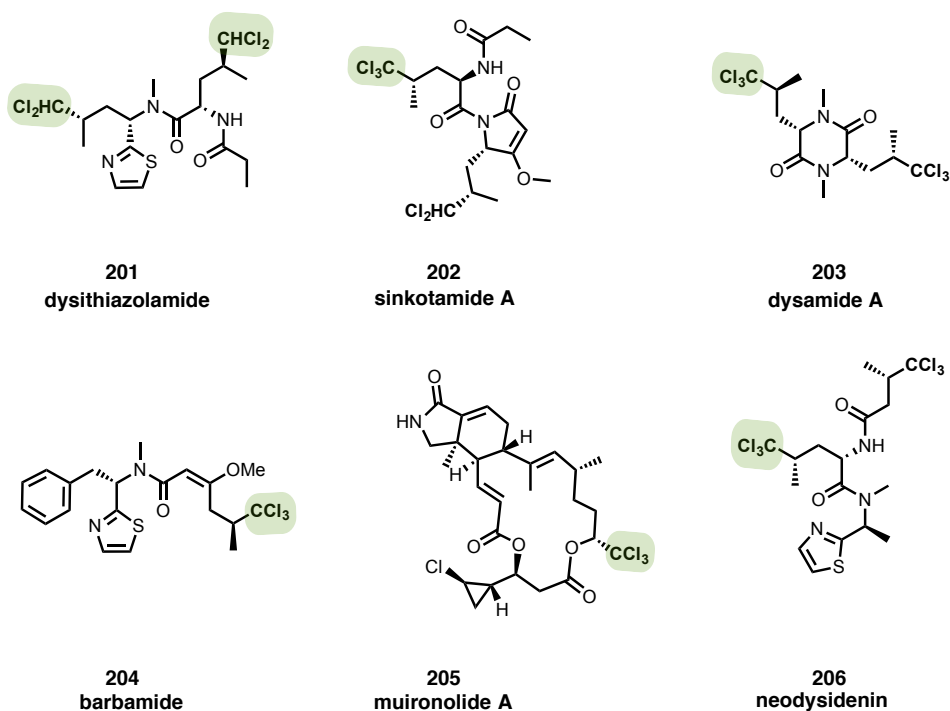
Chart 4.1: Some of the natural products possessing di and tri-chloromethyl groups.

Attention towards strategies for chloromethylation did not garner attention of chemists until the seminal work performed by Zakarian and coworkers.[8-12] The group has developed an efficient methodology that requires the use of titanium enolates (Scheme 4.1) for radical addition of trichloromethyl radical. The reaction proceeds in high yields with complete control over diastereoselectivity. The chloromethylation required the use of $[Ph_3P]_3RuCl_2$ as the redox catalyst for electron transfer. Trichlorobromomethane proved to the most efficient haloalkylating agent while titanium tetrachloride was utilized for accessing the enolate.
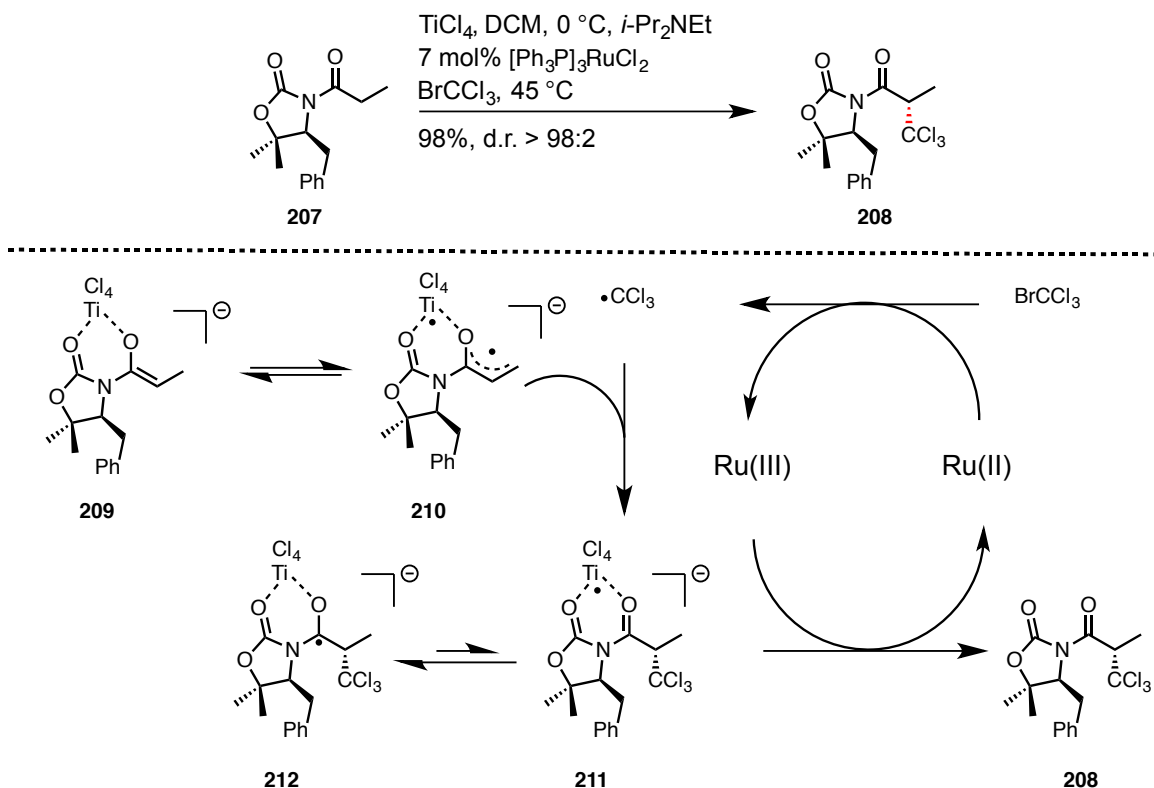
Scheme 4.1: Catalytic radical haloalkylation of titanium enolates illustrated by Zakarian and coworkers.

The reaction mechanism (Scheme 4.1) involves a Ru-catalyzed reductive generation of haloalkyl radical, which then adds to biradical valence tautomeric pair **210/209**. This leads to the formation of tautomeric ketyl pair **211/212** which initiates a SET to regenerate the Ru(II) catalyst and thus forming the desired product **208**. The work describes a practical and an efficient way for stereoselective chloroalkylation of titanium enolates. In order to showcase the applicability of their methodology the group demonstrated the total synthesis of neodysidenin and sintokamides A, B and E.

Following the work of Zakarian et al., the Meggers group utilized photoredox chemistry to afford trichloromethyl radical (Scheme 4.2).[13] They demonstrated visible light mediated catalytic trichloromethylation of 2-acyl imidazoles and 2-acyl pyridines with high enantiomeric excess. The chiral induction originated from the chiral iridium complex and trichlorobromomethane was utilized as the chloromethylating agent.
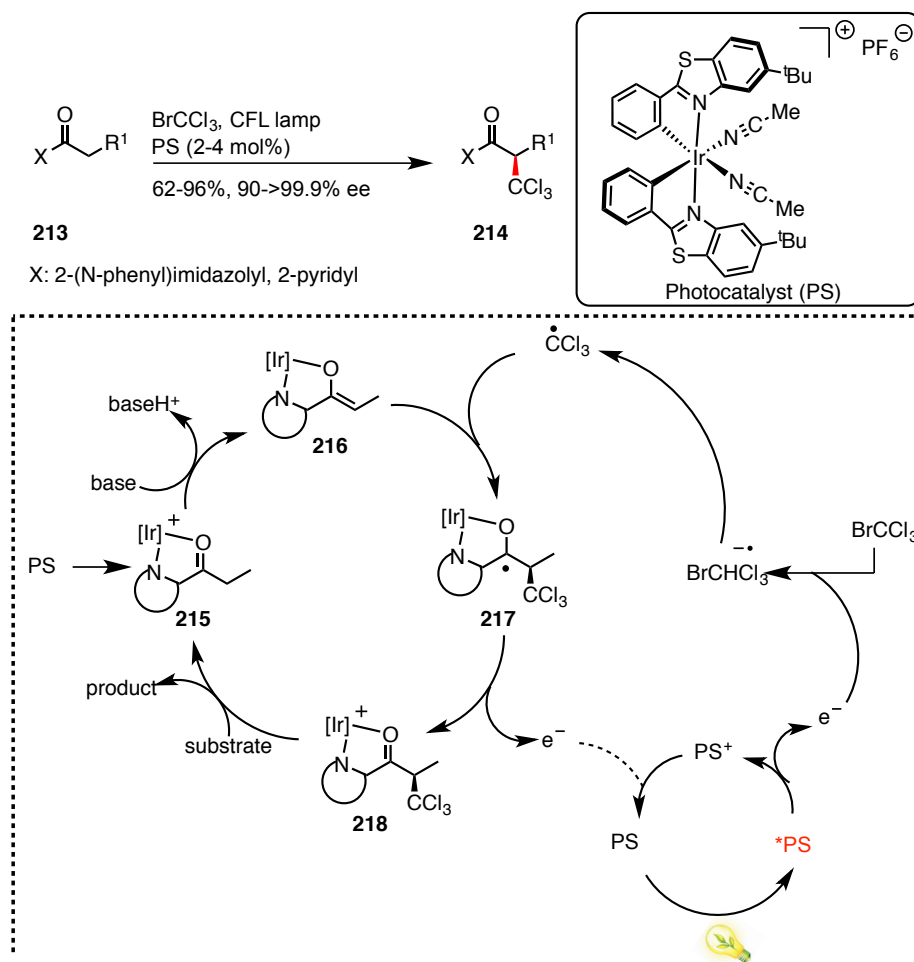
Scheme 4.2: Photoredox catalysis for performing chloromethylation showcased by Meggers group.

In the view of expanding the library of chemical methods and in order to understand the role of *N-N* bond in mediating chloromethylation, we began our initial studies with atropisomeric acrylanilides. There are two reports in the literature that have employed acrylanilides for visible light mediated chloromethylation.[14-15] Li and co-workers utilized photoredox chemistry to generate haloalkane radical species (Scheme 4.3) for 1,2-alkylarylation of activated alkenes. The reaction proceeds *via* a scission of $(sp^3)C$ –H bond adjacent to halide atom which leads to the formation of halo-substituted alkyl radical. This radical leads to the formation of polyhalo-substituted oxindoles in good to excellent yields.
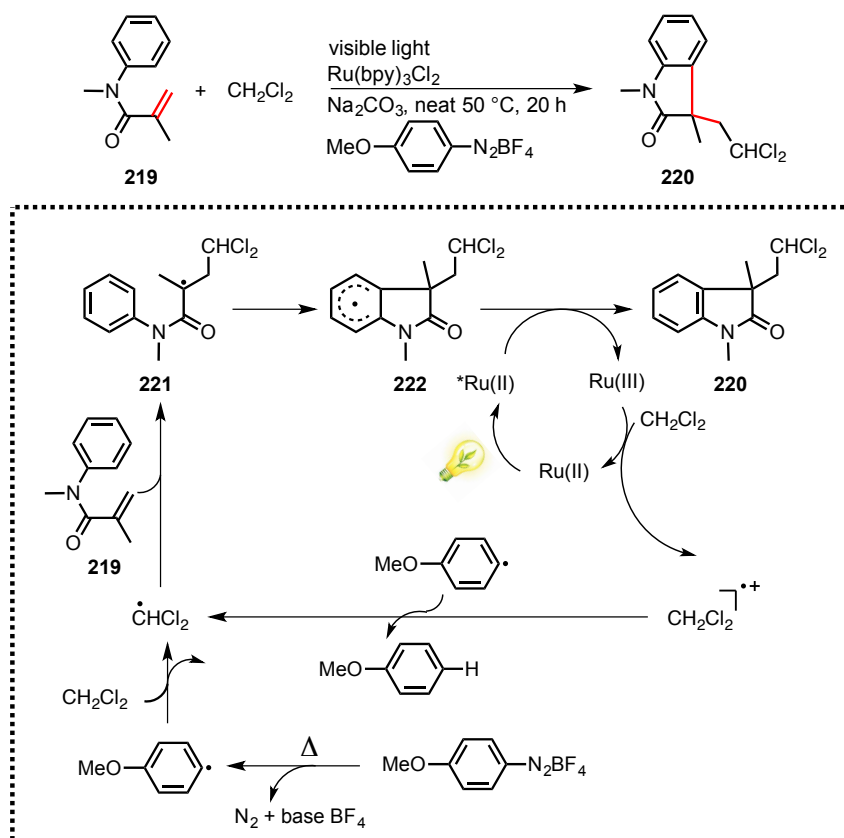
Scheme 4.3: Visible light mediated chloromethylation of acrylanilide showcased by Li and coworkers.

The group evaluated a variety of alkyl halides for chloromethylation (Scheme 4.4) and found the reaction was effected by the choice of chloromethylating agent to afford the substituted oxindole product. For example, the monochloro-substituted 1-chlorobutane yielded only trace amount of corresponding oxindole product.
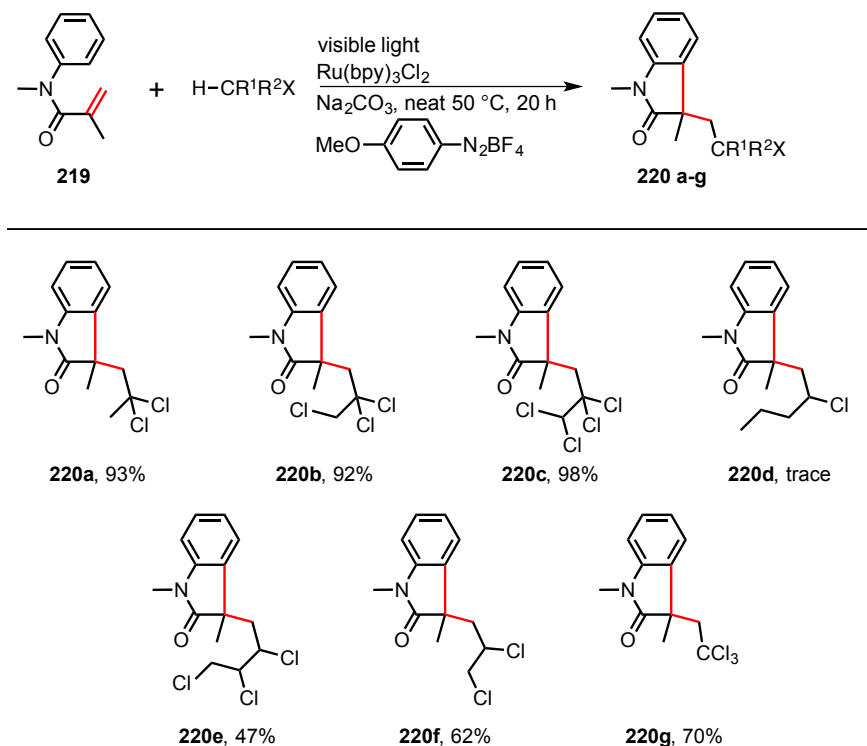
Scheme 4.4: Scope of chloroalkylating agent for chloromethylation of acrylanilide by photoredox chemistry.

The work performed by Fu and Zhu highlights the addition of tetrachloromethane (Scheme 4.5) to acrylanilides by photoredox chemistry. The reaction showed compatibility to both electron donating and withdrawing groups. Unlike the report of Li and coworkers, this strategy of chloromethylation required mild operating conditions and worked efficiently room temperature.
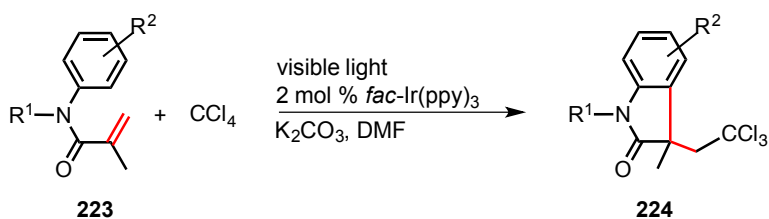
Scheme 4.5: Trichloromethylation of acrylanilides under visible light irradiation by Fu and Zhu.

It is noteworthy to point that the chloromethylation of acrylanilides by visible light reported by the two groups yielded the oxindole-based product exclusively. Many research groups, utilizing electron transfer reagents and heat to initiate chloromethylation also observed the oxindole product.[16-18] None of the reports suggests an atom transfer radical addition (ATRA) of the chloromethylating agent (Scheme 4.6) on the double bond. In other words, none of the research groups observed the ring opened anilide product in their reaction.
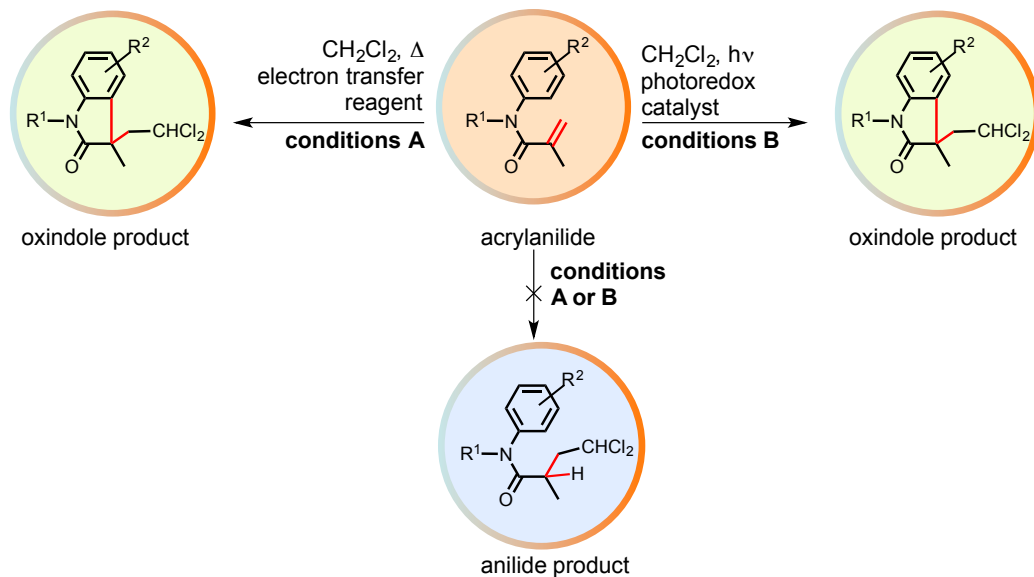
Scheme 4.6: Schematic representation of attempted chloromethylation of acrylanilides in literature.

4.2. Evaluating *N-N* bond based acrylanilides for visible light mediated chloromethylation

The acrylanilides that were studied for chloromethylation have been listed in chart 4.2.

| **184a** | **184b** | **184c** |

| **184d** | **184g** | **184e** |
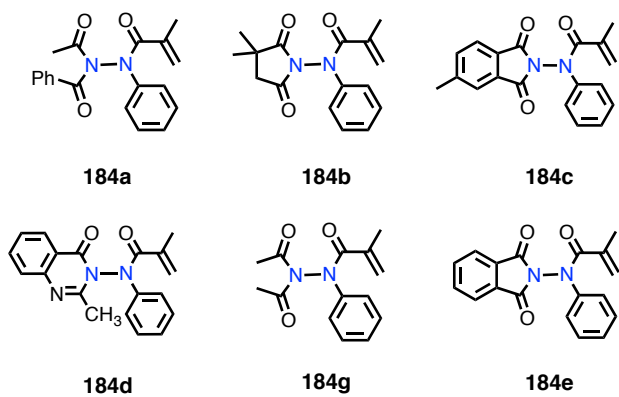
Chart 4.2: *N-N* bond based acrylanilides **184a-e** investigated for chloromethylation.

4.3. Reaction optimization studies for chloromethylation of *N-N* bond based acrylanilides

The trichloromethylation of *N-N* bond based acrylanilides proceeded smoothly with moderate to excellent yields under visible light irradiation (Scheme 4.7). The light induced addition of haloalkane was facilitated in the presence of thioxanthone as the sensitizer/catalyst. Chloroform was employed both as a chloromethylating reagent and as a solvent. It was surprising to note that the chloromethylation of atropisomeric acrylanilides yielded the anilide product **226a-g**. The isolated yields of the chloromethylated photoproducts ranged from 34-93%

184 a-g

hν, λ ~ 420 nm
10 mol% TX, CHCl$_3$, N$_2$

226 a-g

226e

226e
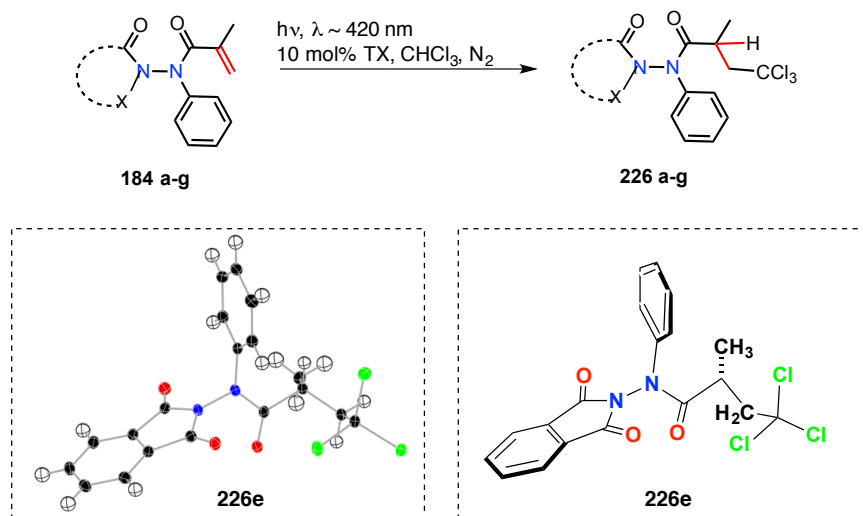
Scheme 4.7: Trichloromethylation of *N-N* bond based acrylanilides.

The course of reaction was monitored by thin layer chromatography and all the products were characterized by ^{1}H and ^{13}C NMR spectroscopy and HRMS. The single crystal XRD analysis for **226e** (Scheme 4.7) was performed to overcome any ambiguity in structural elucidation of the chloromethylated product. A closer inspection of the photoproduct reveals that the chloromethylation had occurred at the β-carbon. To understand the features necessary for chloromethylation reaction, we systematically varied the functionality around the hydrazide chromophore.

As we had established restricted bond rotations around of *N-N* bond (refer to Chapter-2 for details), we synthesized **184c** by introducing a methyl group on the phthalimide ring to evaluate influence of atropisomerism during chloromethylation. Chloromethylation of **184c** resulted in 75% isolated yield with a diastereomeric ratio of 2:1 (in **226c** from crude ^{1}H NMR spectroscopy analysis after the photoreaction, Table 4.1). We then synthesized acyclic imides **184g** and **184a** that underwent chloromethylation to yield **226g** and **226b** respectively with 36% and 50% isolated yields (Table 4.1). Due to restricted *N-N* bond rotations, the diastereomeric ratio in **184d** was found to 1.5:1. Cyclic imides **184b** underwent chloromethylation efficiently leading to 93% isolated yield. The aromatic quinozilinone derivate **184d** gave the corresponding chloromethylated product **226d** in 80% isolated yield

Table 4.1: Reaction optimization studies for chloromethylation of atropisomeric acrylanilides.[a]

Entry	Substrate	Yield/%[b]	*dr*[c]	t(h)
1	**184a**	50	1.5:1	11
2	**184b**	93	-[d]	9
3	**184c**	75	~2:1	8
4	**184d**	80	1.5:1	30
5	**184e**	34	-	40
6	**184g**	36	-	11

[a] Photoreactions were performed with 10 mol% of thioxanthone loading, [**184a**] = 3.10 mM. [**184b**] = 3.49 mM, [**184c**] = 3.12 mM, [**184d**] = 3.13 mM, [**184e**] =3.49 mM, [**184g**] = 3.84 mM. [b] Values based on ^{1}H-NMR spectroscopy (±5% error), each experiment was performed for three trials; isolated yields reported in the paranthesis % conversion and mass balance calculated using triphenylmethane as internal standard. [c] *dr* values are reported based on crude ^{1}H-NMR results. [d] Difficult to determine because of overlapping peaks.

4.4. Role of other haloalkanes in chloromethylation of *N-N* bond based acrylanilides

Having ascertained that the visible light mediated, sensitized addition of chloroform to atropisomeric acrylanilides was working; next we evaluated different chloroalkanes for the reaction (Scheme 4.8). The investigated chloroalkanes were employed as solvent. Achiral phthalimide based acrylanilide **184e** was utilized for the studies as the NMR spectra for crude photoreaction mixture was simpler to interpret.
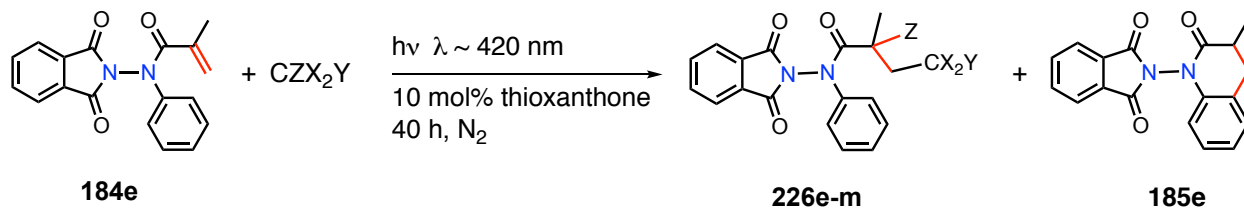
Scheme 4.8: Light induced addition of chloroalkanes to *N-N* bond based acrylanilides.

Table 4.2: Summarized results for intermolecular addition of chloroalkanes to acrylanilide derivative **184e**.[a]

Entry	Chloroalkane	% Conversion[b]	226e : 185e[c]
1	CCl_4	100	1:>99
2	$CHCl_3$	100	>99:1
3	$CDCl_3$	100	1:>99
4	CH_2Cl_2	100	1:2.7
5	CD_2Cl_2	100	1:>99

[a] Photoreactions were performed with 10 mol% of thioxanthone loading, [**184e**] = 3.26 mM. [b] Values based on ¹H-NMR spectroscopy (±5% error), each experiment was performed for three trials, % conversion and mass balance calculated using triphenylmethane as internal standard. [c] Values are reported based on crude ¹H-NMR results.

Use of tetrachloromethane as the solvent for the optimized photoreaction (10 mol% Thioxanthone under N_2 atmosphere) afforded the dihydroquinolinone based photoproduct **185e** exclusively (100% conversion, Table 4.2, entry 1) On the other hand, chloromethylated product **226e** was observed exclusively in $CHCl_3$ (Table 4.2; entry 2). Changing the solvent to CH_2Cl_2 resulted in both **185e** and **226e** in the ratio 1:2.7 (Table 4.2; entry 4). This indicated that the CH hydrogen played a curial role in the chloromethylation reaction. To understand the system we then evaluated the chloromethylation reaction in deuterated solvents viz., $CDCl_3$ and CD_2Cl_2.

Complete reversal of product selectivity was observed in chloroform (**226e** exclusively observed; Table 4.2; entry 2) when compared to chloroform-*d* (**185e** exclusively observed; Table 4.2; entry 3). Similarly changing the solvent from CH_2Cl_2 to CD_2Cl_2 resulted in **185e** exclusively (Table 4.2; compare entries 4 and 5). Our observation with the solvent study indicated that the chloromethylation leading to **226e** and 6π-photocyclization leading to **185e** are competing processes and is dictated by the type of solvent employed. In particular the chemoselectivity was dependent on the acidity of the hydrogen.

4.5. Effect of different reaction atmospheres on the chloromethylation of *N-N* bond based acrylanilides

184e   **226e**   **185e**
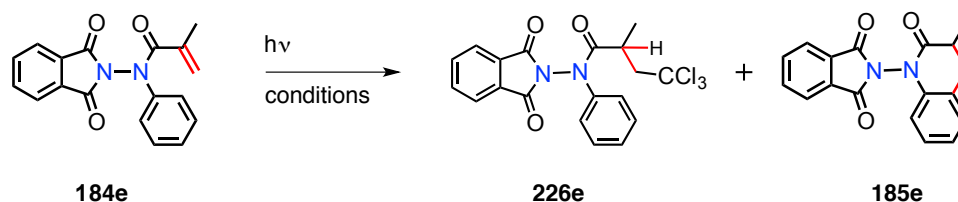
Scheme 4.9: Chloroform addition to *N-N* bond based acrylanilides under different conditions.

The acrylanilide **184e** was subjected to conditions of direct irradiation (Scheme 4.9) in the presence of chloroform as the solvent. The photoreaction when performed under nitrogen atmosphere (Table 4.3) afforded the chloro-substituted anilide based derivative as the major photoproduct **226e**. However, the direct irradiation of oxygen saturated solution of acrylanilide **184e** resulted in the exclusive formation of dihydroquinolinone product **185e**. These results confirmed that the triplet excited states of **184e** was getting generated during photoexcitation under the initial reaction conditions. The triplet excited acrylanilide yielded a mixture of intramolecular addition product **226e** and intermolecular cyclization product **184e**. For the photoreaction performed in oxygen saturated sample the reaction occurred from singlet excited states.

Table 4.3: Summarized results for photoreaction of acrylanilide **184e** under different reaction atmospheres.[a]

Entry	Conditions	Conversion/%[b]	**226e : 185e**[c]
1	λ ~ 300 nm, CHCl₃, 15 h, N₂	89	–[d]
2	λ ~ 300 nm, CHCl₃, 2 h, O₂	17	>99:1

[a] [**184e**] = 3.26 mM. [b] Values based on ¹H-NMR spectroscopy (±5% error), each experiment was performed for three trials, % conversion and mass balance calculated using triphenylmethane as internal standard. [c] Values are reported based on crude ¹H-NMR results. [d] Difficult to determine the photoproduct ratio due to overlapping peaks; **226e** was the major photoproduct.

4.6. Evaluating other hydrazides for chloromethylation under metal free conditions
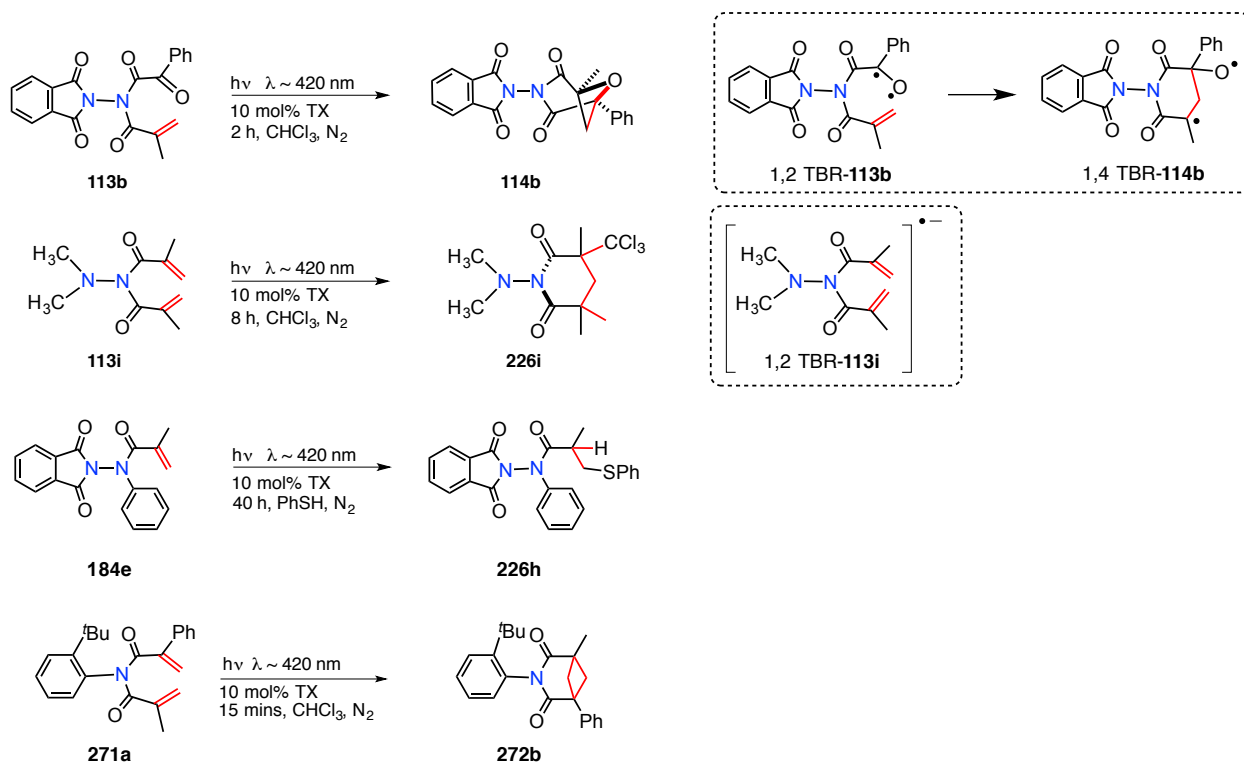
Scheme 4.10: Attempted hydrazides and imide derivatives for chloromethylation under metal free conditions.

The hydrazides **113b** and **113i** were evaluated for visible light mediated chloromethylation (Scheme 4.10). The α-ketoamide based hydrazide **113b** yielded the oxetane based photoproduct **114b** exclusively (>99% conversion). While hydrazide **113i** that features dimethacrylolyl functionality resulted in a cyclized chloromethylated product **226i** (>99% conversion). To comprehend the reactivity of **113b** and **113i** towards chloromethylation, we ascertained a) the triplet energy (ET) to evaluate the feasibility of energy transfer from TX and b) the free energy of electron transfer from excited TX using Rehm-Weller equation. Based on the phosphorescence measurements (at 77 K in Me-THF glass) the triplet energy of **113b** and **113i** was 62.4 kcal/mol and 70.7 kcal/mol. This indicated that exothermic triplet energy transfer from TX triplet to **113b** is feasible.

On the other hand, triplet energy transfer from TX triplet to **113i** is quite unlikely do to energetics. The oxidation and reduction potentials of TX and hydrazides **113b** and **113i** were established by cyclic voltammetry measurements. Based on the Rehm-Weller equation, the free energy for electron transfer from excited TX to **113b** was calculated to be 1.4 kcal/mol indicating an endergonic process. Similarly, electron transfer from excited TX to **113i** was calculated to be -4.8 kcal/mol, revealing an exergonic process.

The formation of substituted hydrazide **226i** confirms the hypothesis that the chloromethylation was not an exclusive observation for *N-N* bond based acrylanilides. The fact that hydrazide **113i** underwent chloromethylation under the optimized conditions, we became certain that the acrylanilide chromophore was not necessary for the photoreaction to occur. While evaluating the scope of solvent addition (Scheme 4.10) to hydrazides we found that thiophenol was able to add to the hydrazide **184e**. The photoreaction was clean and afforded the photoproduct **226h** in good conversions (>99% conversion, 85% isolated yield).

4.7. Evaluating other acrylimides for chloromethylation under metal free conditions

To further understand the reactivity towards chloromethylation we investigated the control substrate **271a** (Scheme 4.10). Irradiation of the imide derivative **271a** that features a restricted bond rotation around *N*-C$_{Aryl}$ bond resulted in the expected cross [2+2]-photocycloadduct **272b** (52% conversion) via diradical mechanism through intermediate int-**271a**.

4.8. Plausible mechanism for sensitized photoreaction of acrylanilides in chloroform
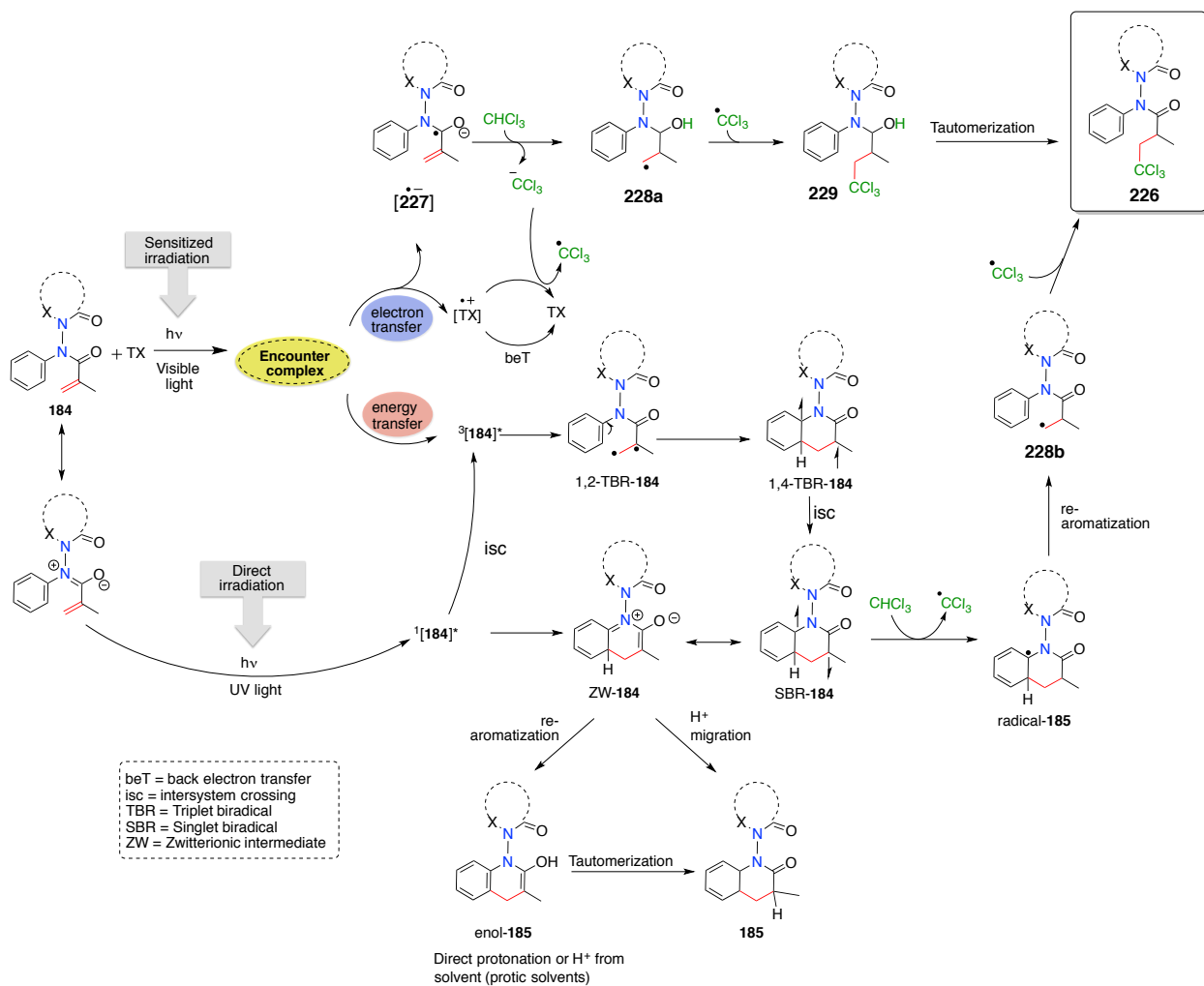
Scheme 4.11: Plausible mechanism for chloromethylation of acrylanilides **184** under the conditions of sensitized irradiation.

The acrylanilides **184** (Scheme 4.11) on visible light irradiation, in the presence of thioxanthone (TX) as the photocatalyst/sensitizer can adopt either an energy transfer pathway or electron transfer pathway depending on the triplet energy/potential of the hydrazide. If the electron transfer pathway is adopted then the photoexcited thioxanthone can do a SET to hydrazide after forming an encounter complex to afford the corresponding radical anion [**227**]$^{\bullet-}$.

The radical intermediate [**227**]$^{\bullet-}$ can abstract a H-radical from chloroform to generate the radical intermediate **228a**. The radical species can add to trichloromethyl radical to yield the trichloromethylated product **229**. The latter can tautomerize to yield the observed chloromethylated anilide based product **226**. If the energy transfer pathway is adopted, the encounter complex can lead to the triplet hydrazide ^{3}[**184**]* which yields the corresponding 1,2 triplet biradical (1,2-TBR-**184**). This 1,2 biradical species can ring cyclize to afford the 1,4 triplet biradical (1,4-TBR-**184**). The latter undergoes an intersystem crossing to afford the singlet biradical (SBR-**184**). This singlet biradical intermediate can isomerize to yield the zwitterionic intermediate (ZW-**184**), which can either lead to the formation of photoproduct **185** or abstract H-radical from chloroform to generate the radical intermediate radical-**185**. The latter can undergo re-aromatization to afford the primary radical **228b**, which finally leads to the formation of trichloromethylated product **226**. This working mechanism explains the observed photoproducts (**226** and/or **185**) during sensitized irradiation of acrylanilides **184** in chloroalkane.

4.9.   X-Ray crystal structure data of hydrazide

Structure determination: Single crystal X-ray diffraction data of the compound **226e** was collected on a Bruker Apex Duo diffractometer with a Apex 2 CCD area detector at T = 100 K. Cu radiation was used in all the cases. All structures were processed using Apex 2 v2010.9-1 software package. Direct method was used to solve the structures after multi-scan absorption corrections.
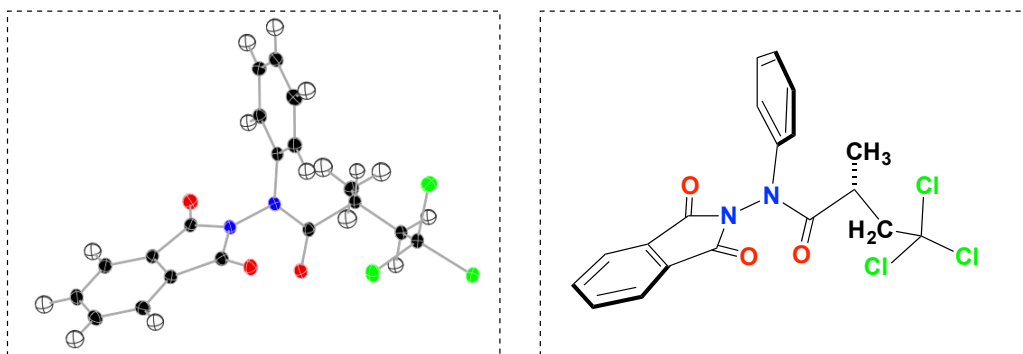
Figure 4.1: Crystal structure of **226e** (Crystallized from: hexanes/dichloromethane).

Table 4.4: Structural parameter table for chloromethylated product **226e**.

Crystal	226e
Formula	$C_{19}H_{15}N_2O_3Cl_3$
Formula Weight	425.68
Space Group, Z	P 1 21/n 1
a/Å	8.0186(3)
b/Å	14.7308(5)
c/Å	16.1335(5)
α /°	90
β/°	91.803(2)
γ /°	90
V (Å^3)	1904.75(11)
h, k , I$_{max}$	9, 17, 19
ρ$_{calc}$ [mg/mm^3]	1.484
μ [mm^{-1}]	4.556
Radiation type	CuKα (λ = 1.54178)
F(000)	872.0
No. of measured reflections	3364
No. of independent reflections	2923
Final R indexes (I ≥ 2 s)	R_1 = 0.0403, wR_2 = 0.1130
R1/wR2 (I ≥ 2 s) [%]	0.0403/0.1130

4.10.   Summary and outlook

We have showcased the facile addition of trichloro/dichloromethyl group to various *N-N* bond based acrylanilides. The optimized photoreactions in chloroform afforded the trichloro-substituted anilide derivative as the major product. Based on the experiments that were carried out in the presence of oxygen, suggested that the acrylanilides that reacted from singlet excited states afforded the dihydroquinolinone product exclusively. The triplet excited acrylanilides gave either the trichloro-substituted anilide derivative or a mixture of substituted anilide and dihydroquinolinone-based photoproduct. Further the fact that acrylimide based hydrazide derivative on irradiating under the optimized conditions for chloromethylation, yielded the trichloro-substituted anilide confirmed hypothesis. We believe that the triplet states of a hydrazide (Scheme 4.12) when populated can afford the intermolecular photoreaction product or the chloromethylated product or a mixture of both. The product yields depend on the rates of intermolecular vs intramolecular addition product.
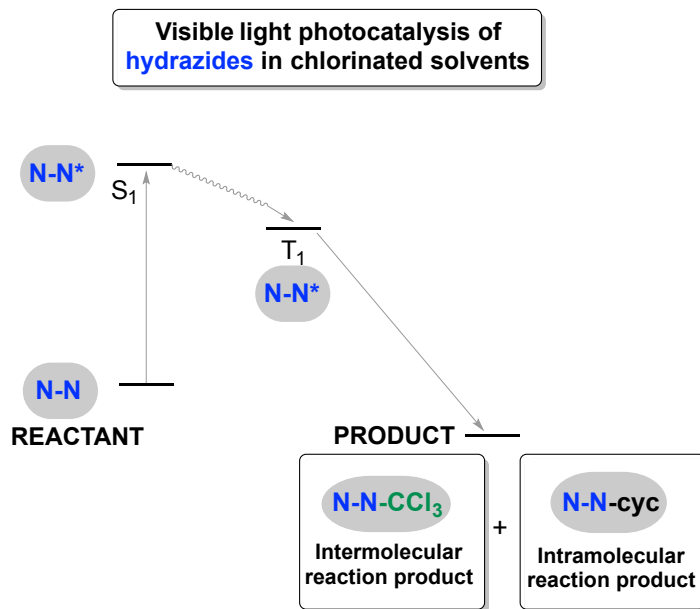
Scheme 4.12: Schematic representation of visible light mediated photochemistry of hydrazides in chlorinated solvent.

This work opens the possibility to add various reagents about the double bond in acrylanilides. In this lieu, we have recently tried and found that a diverse range of organo thio-compounds can be added to acrylanilides under our optimized conditions. Our future efforts are channeled in developing this method to tag biomolecules and showcase a novel application of our methodology.

4.11.   General methods and materials

Unless otherwise stated dichloromethane was freshly distilled from CaH_2 while chloroform and acetone was dried over potassium carbonate before each experiment. Unless stated otherwise, reactions were conducted in oven-dried glassware under an atmosphere of nitrogen using anhydrous solvents; Photoreactions were performed under N_2 or O_2 atmosphere.

^{1}H NMR and ^{13}C NMR spectra were recorded on Varian 400 MHz (100 MHz for ^{13}C NMR) and on 500 MHz (125 MHz for ^{13}C NMR) spectrometers. The residual solvent signal was used as reference. ($CDCl_3$: δ_H = 7.26 ppm, δ_C = 77.2 ppm). Data for ^{1}H NMR spectra are reported as follows: chemical shift (δ ppm), multiplicity, coupling constant (Hz) and integration. In many instances, it was not possible to obtain a signal for the carbonyl carbon, despite long relaxation times and concentrated samples. However these signals are reported wherever possible. High-resolution mass spectrum data was recorded in Electrospray Ionization mode on a Bruker–Daltronics® BioTof mass spectrometer in positive (ESI+) ion mode. The reactants and photoproducts were purified by flash chromatography using silica gel (by standard technique with solvents as indicated. RediSep®, silica gel standard grade: Porosity 60 Å, Particle size: 230 x 400 mesh, Average particle size: 60 to 70 micron). The Retardation Factor (R_f) values were recorded using various combination of solvent systems as mobile phase (as mentioned in the text) and on SORBENT TECHNOLOGIES® Silica Gel TLC plates (200 μm thickness w/UV$_{254}$).

Note: Synthesis of all the acrylanilides and other hydrazides utilized as the starting material for this study have been documented in the Chapter-2 and Chapter-3.

4.11.1. General procedure followed for irradiation of substrates and characterization of photoproducts

(a)   Procedure for photoreaction: In a pyrex tube, solution of appropriate hydrazide was dissolved in the desired solvent (chloroalkane or thiophenol) under an inert atmosphere. This was followed by the addition of appropriate volume of sensitizer (thioxanthone) prepared in the same chlorinated solvent. The sample was then irradiated at ambient conditions in a Rayonet reactor equipped with ~420 nm tubes (16 tubes x 14 Watt).

 (b)   Characterization of photoproduct after photoreaction: In case of large-scale photoreactions, after irradiation the mixture was purified by combiflash using hexanes/ethyl acetate mixtures. In certain cases the crude mixture was purified by preparative thin layer chromatography.

4.12.   Characterization of chloromethylated photoproduct 226e
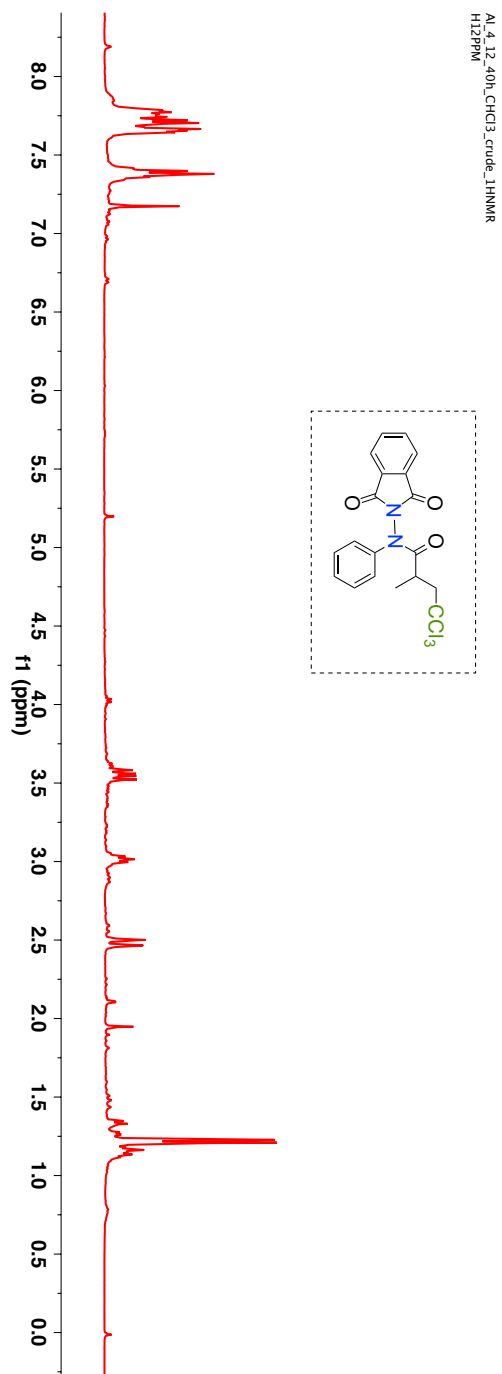
Figure 4.2: Crude ^{1}H-NMR (400 MHz, CDCl$_3$, δ ppm) spectrum of **226e**.

TLC condition - R$_f$ = 0.6 (20% ethyl acetate:hexanes). Crystalline solid (Yield = 34%).

^{1}H-NMR (400 MHz, CDCl$_3$, δ ppm): 1.29 (d, 3H, J = 7.2 Hz), 2.53-2.57 (m, 1H), 3.04-3.12 (m, 1H), 3.59-3.66 (m, 1H), 7.41-7.49 (m, 3H), 7.72 (m, 2H) and 7.72-7.87 (m, 4H).
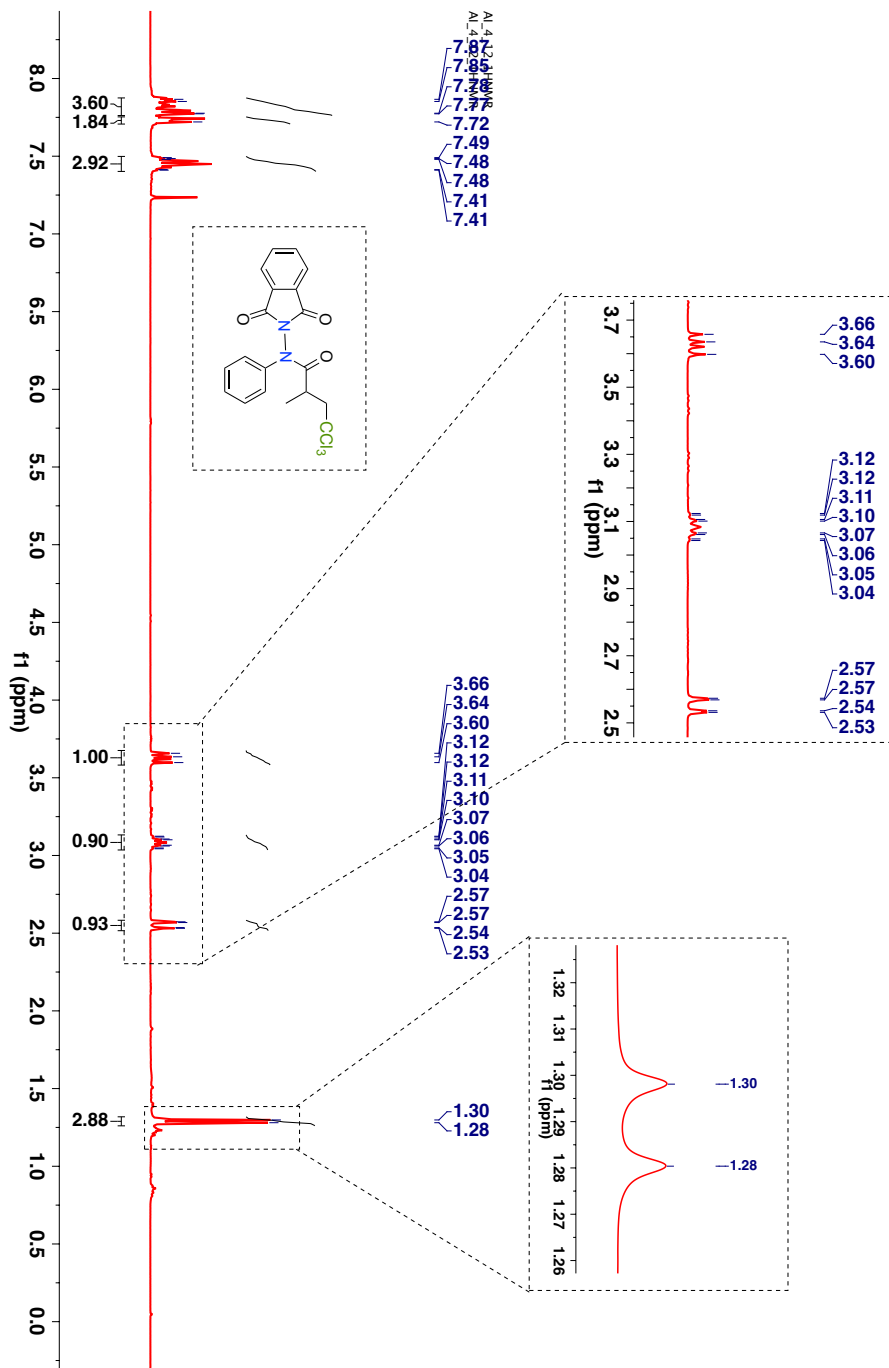
Figure 4.3: ^{1}H-NMR (400 MHz, CDCl$_3$, δ ppm) spectrum of **226e**.

^{13}C-NMR (100 MHz, CDCl$_3$, δ ppm): 19.5, 35.1, 57.9, 98.2, 124.1, 129.5, 130.2, 130.2, 130.2, 134.8, 134.9, 139.9, 164.9, 165.2 and 173.7.
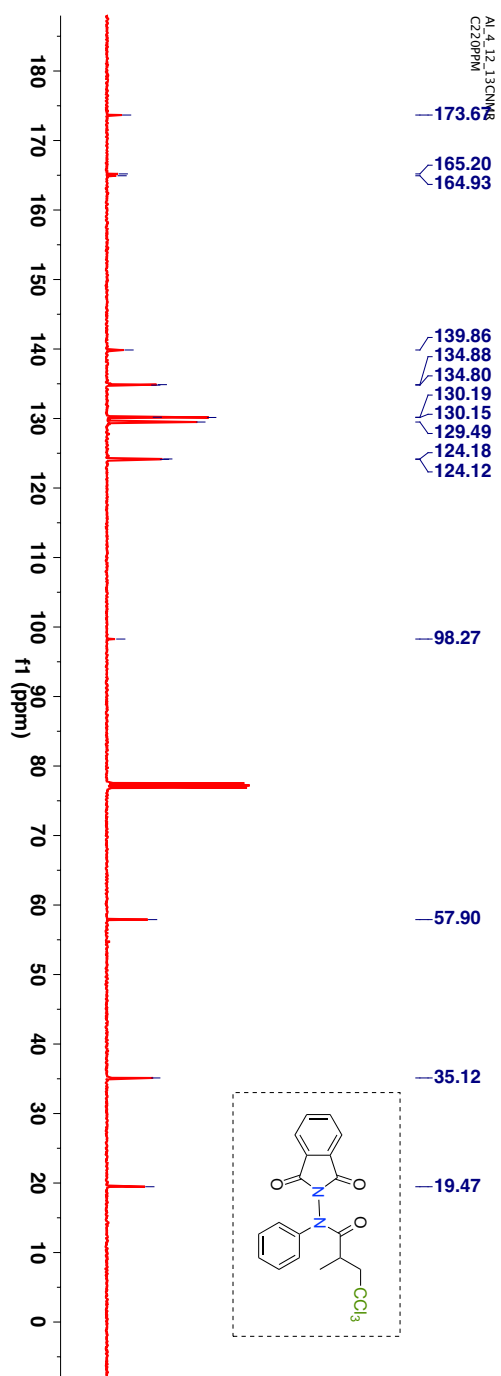
Figure 4.4: ^{13}C-NMR (100 MHz, CDCl$_3$, δ ppm) spectrum of **226e**.

4.12.1. UV-Vis spectra of acrylanilide derivative 184e
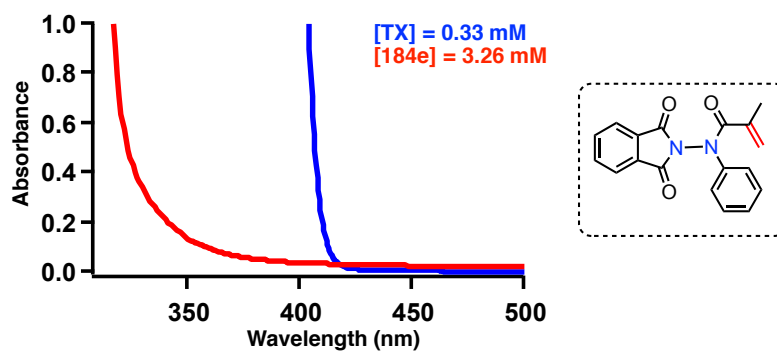
Figure 4.5. UV-Vis spectra of sensitizer/catalyst (TX : thioxanthone) and acrylanilide derivative **184e** (concn = 3.26 mM) recorded at reaction concentration in chloroform as the solvent. (red and blue line represents the absorbance of hydrazide and TX at the reaction concentration)

4.13. Characterization of chloromethylated photoproduct 226g

TLC condition - R$_f$ = 0.3 (20% ethyl acetate:hexanes), Yellow viscous liquid (Yield = 36%).

^{1}H-NMR (400 MHz, CDCl$_3$, δ ppm): 1.24 (d, 3H, J = 5.6 Hz), 2.33 (s, 3H), 2.58–2.61 (m, 4H), 3.30-3.38 (m, 1H), 3.74-3.79 (m, 1H), 7.43-7.51 (m, 3H) and 7.56-7.58 (m, 2H).
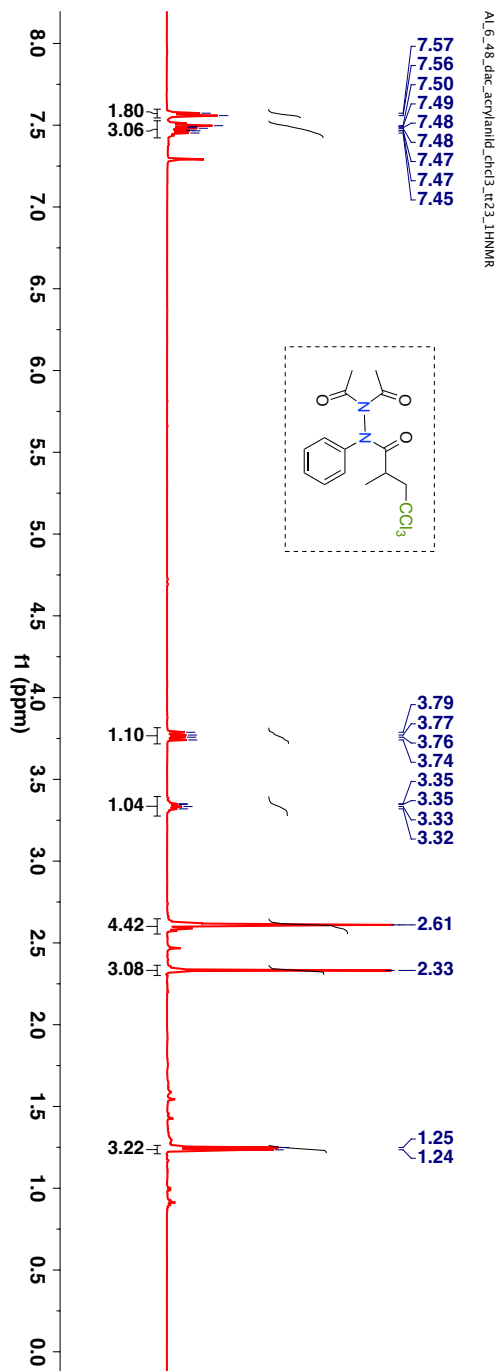
Figure 4.6: ^{1}H-NMR (400 MHz, CDCl$_3$, δ ppm) spectrum of **226g**.

^{13}C-NMR (100 MHz, CDCl$_3$, δ ppm): 19.0, 24.8, 26.3, 35.5, 57.4, 98.8, 127.2, 129.4, 130.1, 140.7, 171.1, 172.9 and 173.7.
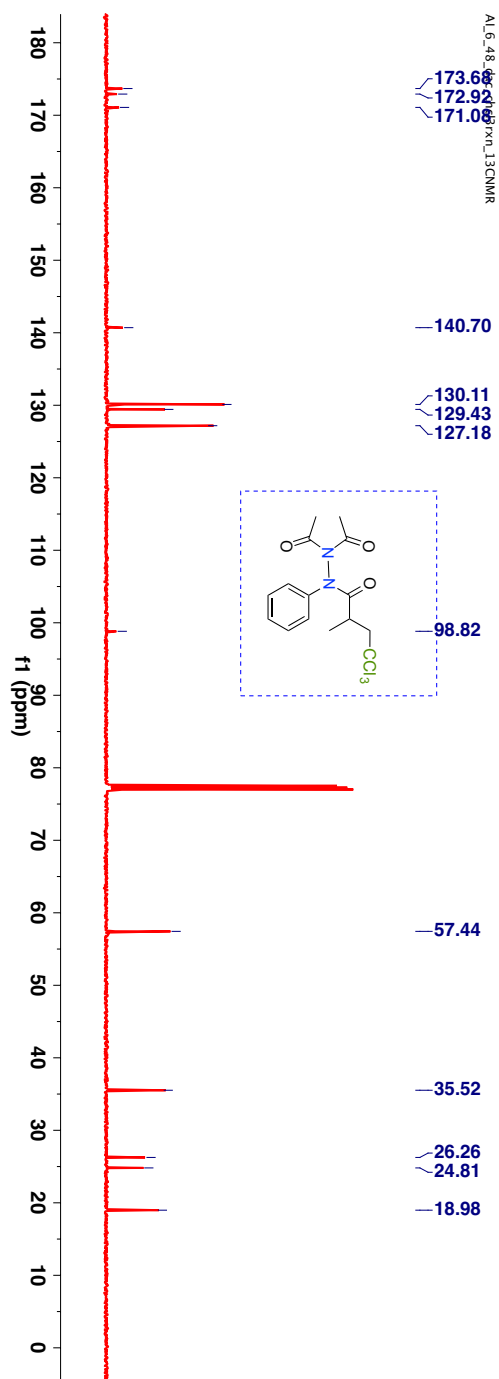
Figure 4.7: ^{13}C-NMR (100 MHz, CDCl$_3$, δ ppm) spectrum of **226g**.

4.13.1. UV-Vis spectra of acrylanilide derivative 184g
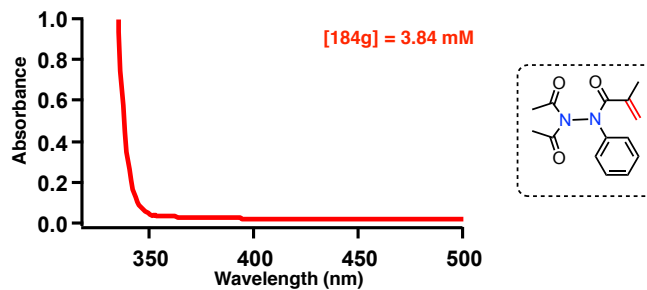
Figure 4.8: UV-Vis spectra of *N-N* bond based acrylanilide derivative **184g** recorded at the reaction concentration (concn = 3.84 mM) in chloroform as the solvent.

HRMS-ESI (m/z) ([M + Na]$^+$):

Chemical Formula	: $C_{15}H_{17}Cl_3N_2O_3$
Calculated	: 401.0194
Observed	: 401.0202
$|\Delta m|$	: 1.9 ppm
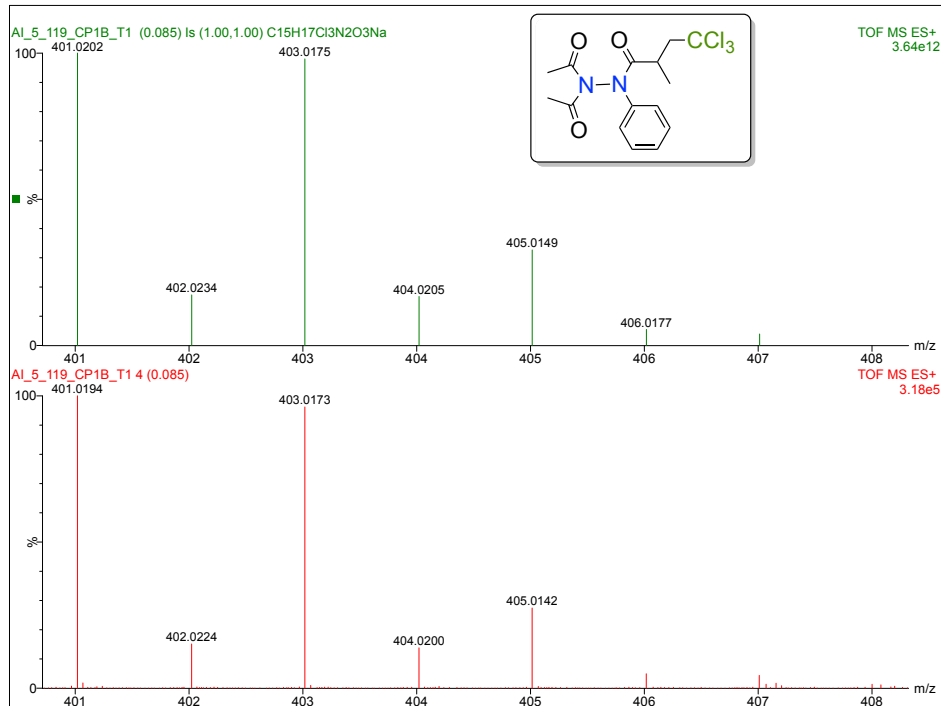
Figure 4.9: HRMS spectra of anilide **226g**.

4.14.   Characterization of chloromethylated photoproduct 226a

TLC condition - R_f = 0.4 (20% ethyl acetate:hexanes) Pale yellow viscous liquid (Yield = 50%).

^{1}H-NMR (400 MHz, CDCl$_3$, δ ppm): 1.19–1.24 (m, 3H), 2.34–2.64 (m, 4H), 2.99–3.11 (m, 1H), 7.09-7.10 (m, 1H), 7.31-7.41 (m, 4H), 7.47–7.50 (m, 1H), 7.55–7.62 (m, 2H) and 7.70-7.72 (m, 1H).
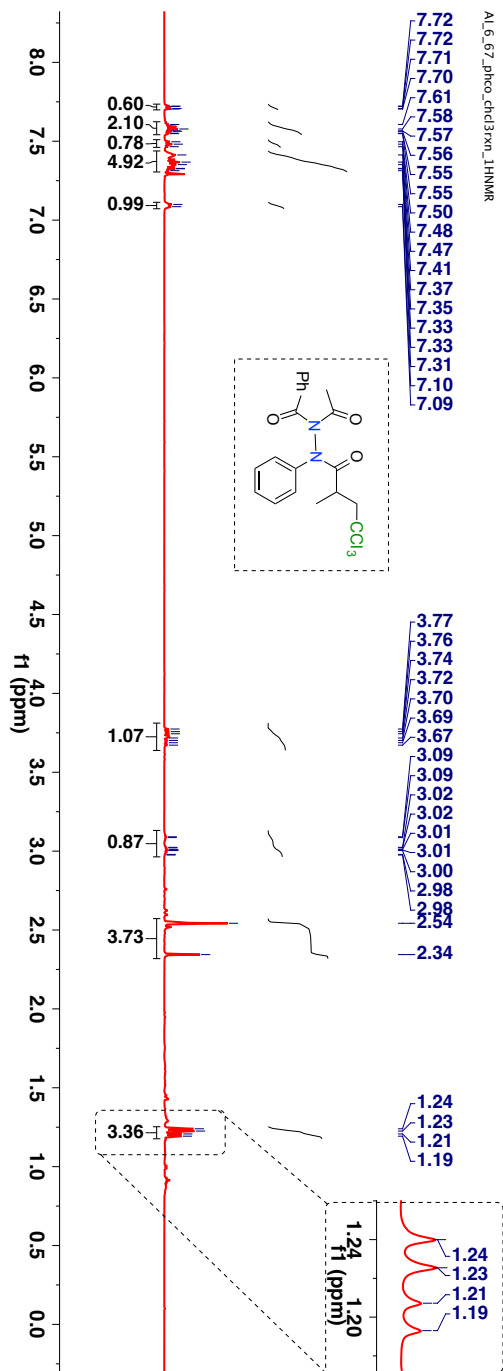
Figure 4.10: ^{1}H-NMR (400 MHz, CDCl$_3$, δ ppm) spectrum of **226a**.

^{13}C-NMR (100 MHz, CDCl$_3$, δ ppm, all peaks are reported together): 19.2, 25.1, 25.5, 35.4, 35.8, 57.5, 57.8 98.5, 127.7, 128.1, 128.3, 128.4, 128.6, 128.8, 129.5, 129.7, 129.8, 130.0, 132.8, 132.8, 134.5, 135.0, 140.6, 171.1, 171.8, 172.2, 173.3 and 173.7.
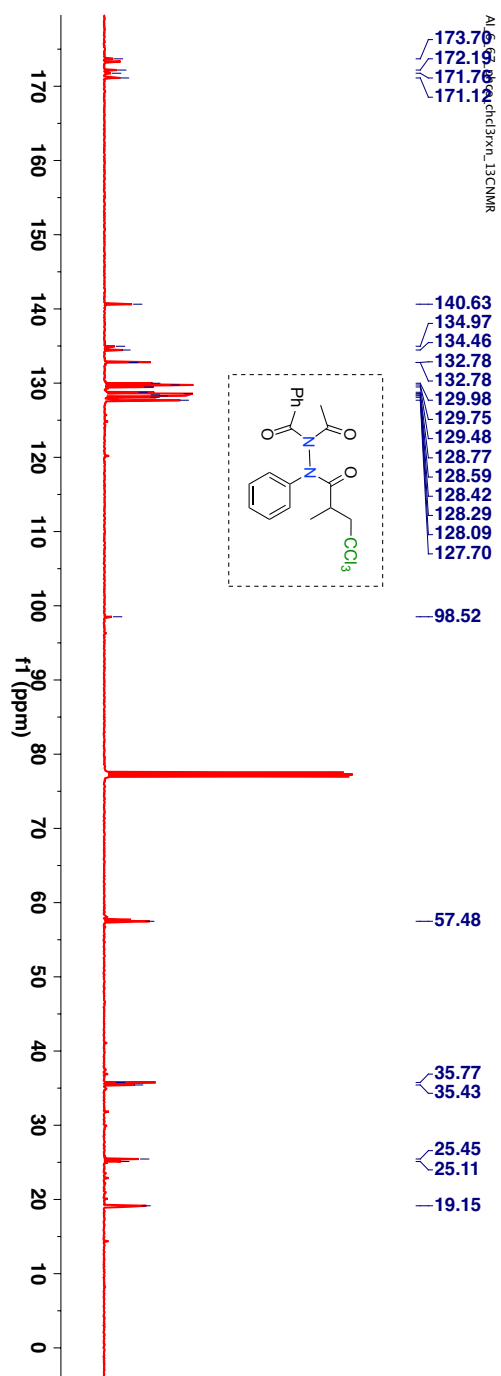
Figure 4.11: ^{13}C-NMR (100 MHz, CDCl$_3$, δ ppm) spectrum of **226a**.

4.15.   UV-Vis spectra of acrylanilide derivative 184a
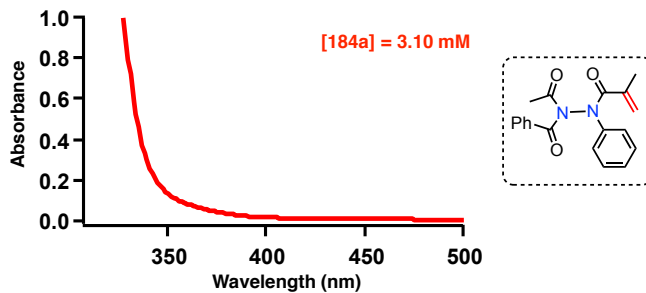
Figure 4.12: UV-Vis spectra of *N-N* bond based acrylanilide derivative **184a** recorded at the reaction concentration (concn = 3.10 mM) in chloroform as the solvent.

HRMS-ESI (m/z) ([M + Na]$^+$):

Chemical Formula   : $C_{20}H_{19}Cl_3N_2O_3$

Calculated   : 463.0354

Observed   : 463.0359

|Δm| : 1.1 ppm
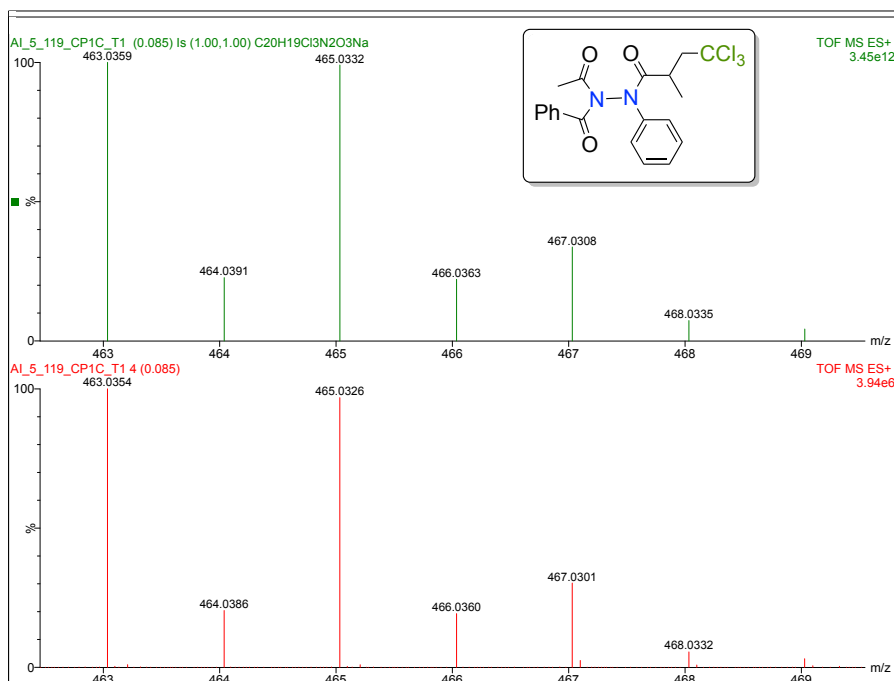
Figure 4.13: HRMS spectra of **226a**.

4.16. Characterization of chloromethylated photoproduct 226c

TLC condition - R$_f$ = 0.3 (20% ethyl acetate:hexanes) Crystalline solid (Yield = 75%).

^{1}H-NMR (400 MHz, CDCl$_3$, δ ppm): 1.34 (d, 3H, *J* = 5.6 Hz), 2.53-2.62 (m, 4H), 3.12-3.15 (m, 1H), 3.67-3.70 (m, 1H), 7.46-7.58 (m, 3H) and 7.67-7.84 (m, 3H).
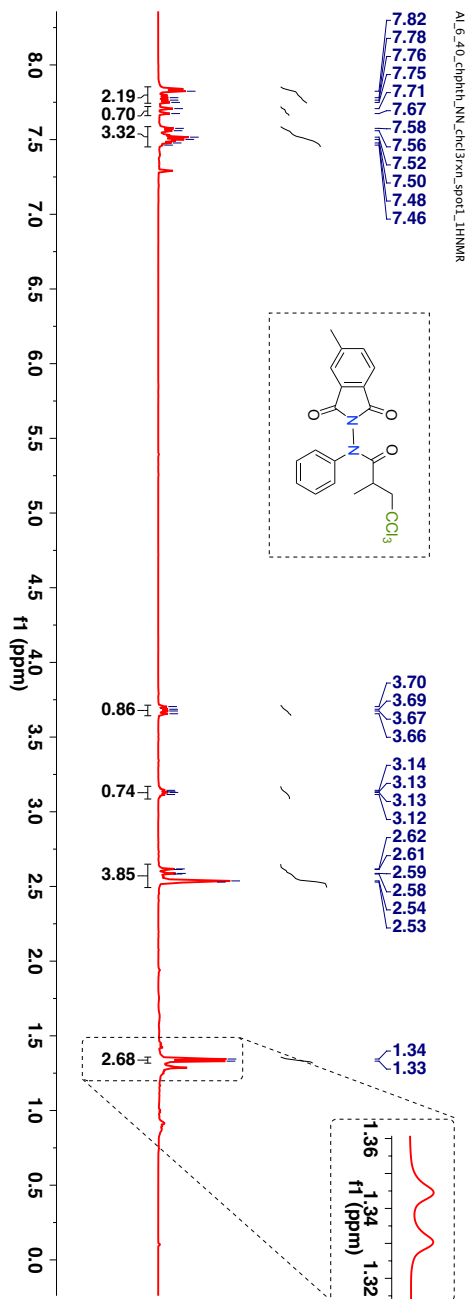
Figure 4.14: ^{1}H-NMR (400 MHz, CDCl$_3$, δ ppm) spectrum of **226c**.

¹³C-NMR (100 MHz, CDCl₃, δ ppm, all peaks are reported together): 19.5, 22.4, 30.0, 35.2, 58.0, 98.3, 124.1, 124.2, 124.6, 124.7, 127.6, 127.7, 129.5, 129.5, 130.1, 130.2, 130.6, 130.6, 135.4, 135.5, 140.0, 146.3, 146.4, 165.1, 165.2, 165.4, 165.5, 173.7.
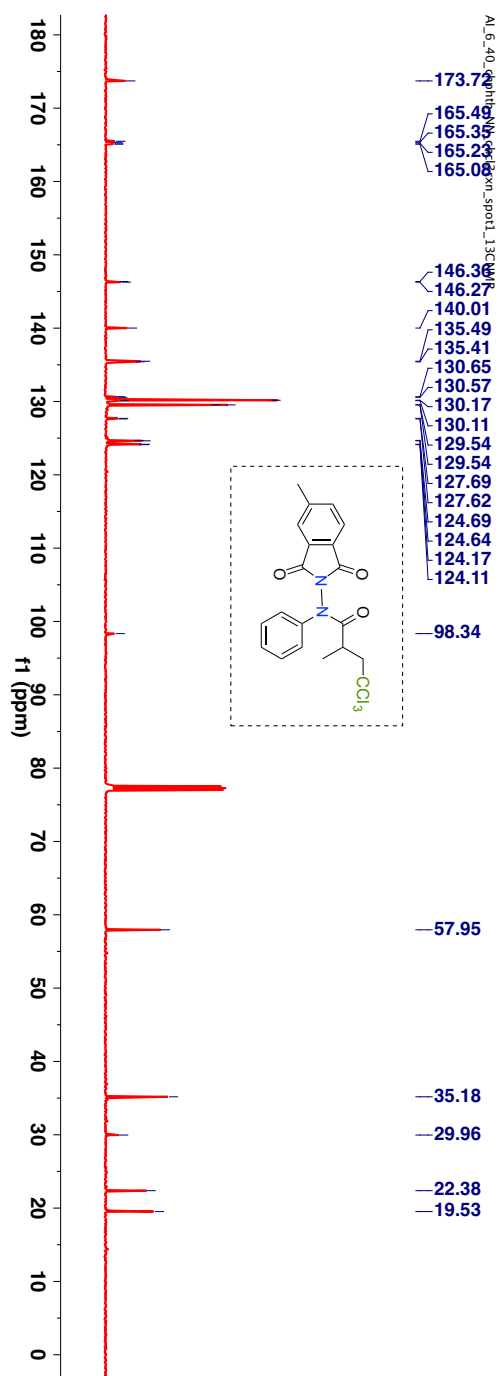
Figure 4.15: ¹³C-NMR (400 MHz, CDCl₃, δ ppm) spectrum of **226c**.

4.16.1. UV-Vis spectra of acrylanilide derivative 184c
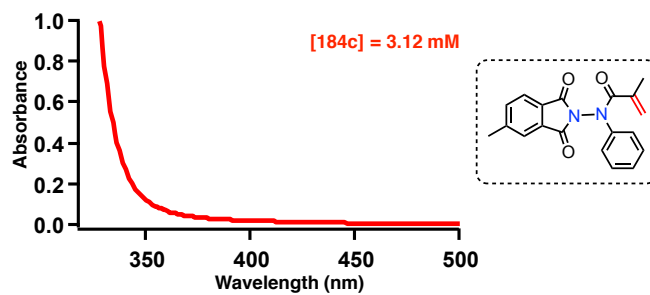
Figure 4.16: UV-Vis spectra of *N-N* bond based acrylanilide derivative **184c** recorded at the reaction concentration in chloroform as the solvent.

HRMS-ESI (m/z) ([M + Na]$^+$):

Chemical Formula	: $C_{20}H_{17}Cl_3N_2O_3$
Calculated	: 463.0175
Observed	: 463. 0176
$|\Delta m|$	: 0.2 ppm
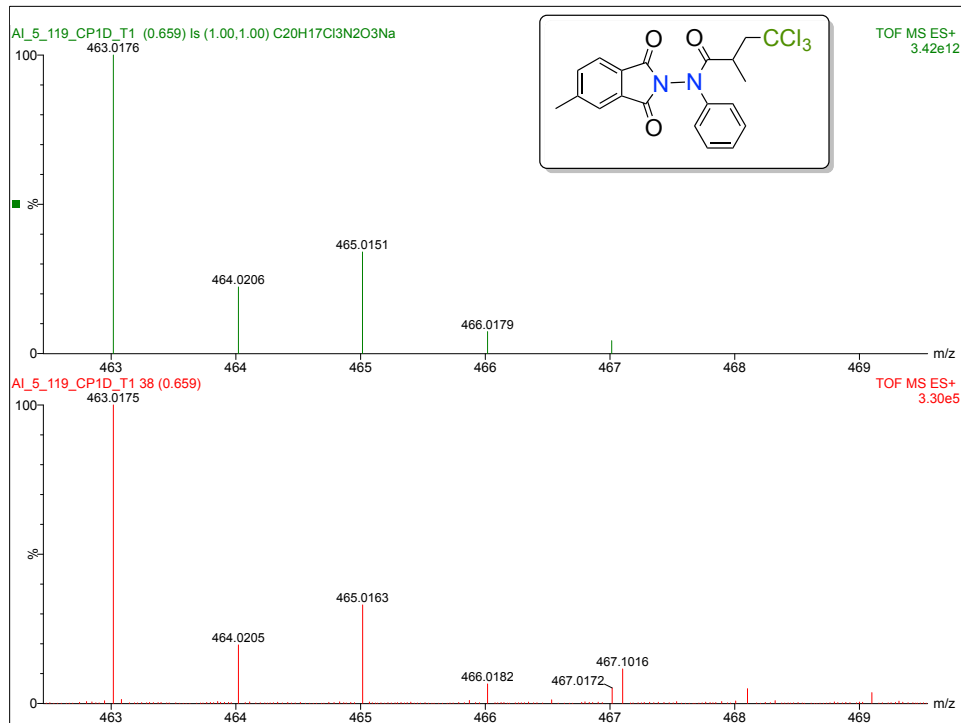
Figure 4.17: HRMS spectra of **226c**.

4.17. Characterization of chloromethylated photoproduct 226b

TLC condition - R_f = 0.3 (20% ethyl acetate:hexanes). Yellow viscous liquid (Yield = 93%).

^{1}H-NMR (400 MHz, CDCl$_3$, δ ppm): 1.24-1.31 (m), 1.46–1.47 (m), 2.52-2.71 (m), 3.02-3.05 (m), 3.61-3.66 (m), 7.47-7.49 (m) and 7.72-7.74 (m).
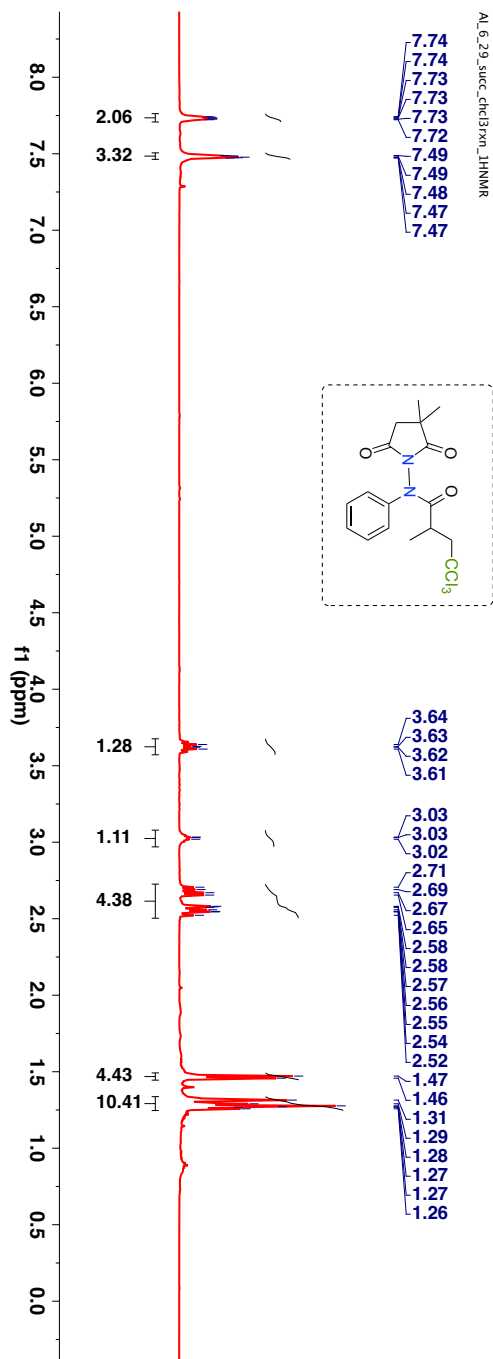
Figure 4.18: ^{1}H-NMR (400 MHz, CDCl$_3$, δ ppm) spectrum of **226b**.

¹³C-NMR (100 MHz, CDCl₃, δ ppm, all peaks are reported together): 19.4, 19.5, 25.2, 26.4, 29.9, 35.0, 35.0, 39.2, 39.2, 42.2, 42.2, 57.8, 57.8, 98.2, 98.3, 129.5, 129.5, 130.2, 130.2, 130.4, 139.3, 171.9, 172.3, 173.0, 173.1, 179.2, 179.6.
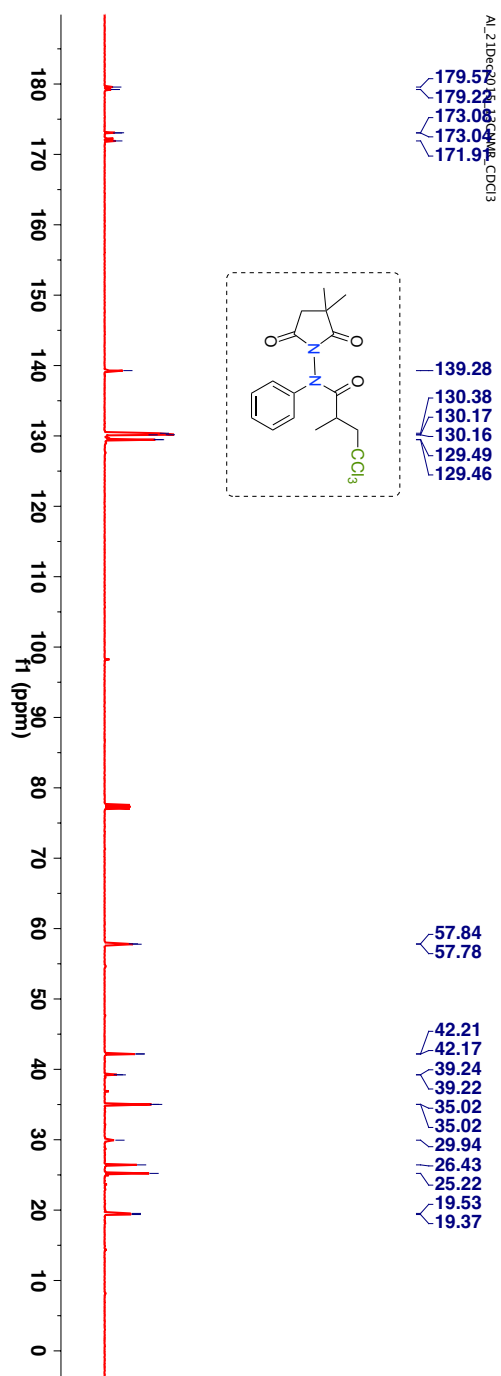
Figure 4.19: ¹³C-NMR (100 MHz, CDCl₃, δ ppm) spectrum of **226b**.

4.17.1. UV-Vis spectra of acrylanilide derivative 184b
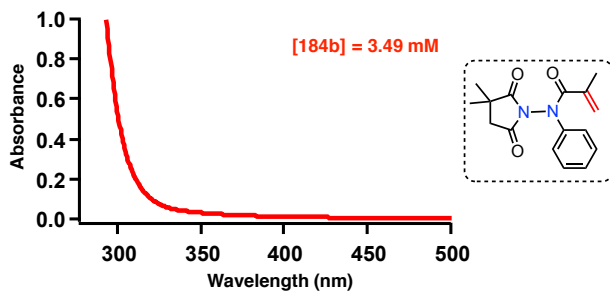
Figure 4.20: UV-Vis spectra of *N-N* bond based acrylanilide derivative **184b** recorded at the reaction concentration (concn = 3.49 mM) in chloroform as the solvent.

HRMS-ESI (m/z) ([M + Na]$^+$):

Chemical Formula	: $C_{17}H_{19}Cl_3N_2O_3$
Calculated	: 427.0383
Observed	: 427.0359
$|\Delta m|$	: 5.6 ppm
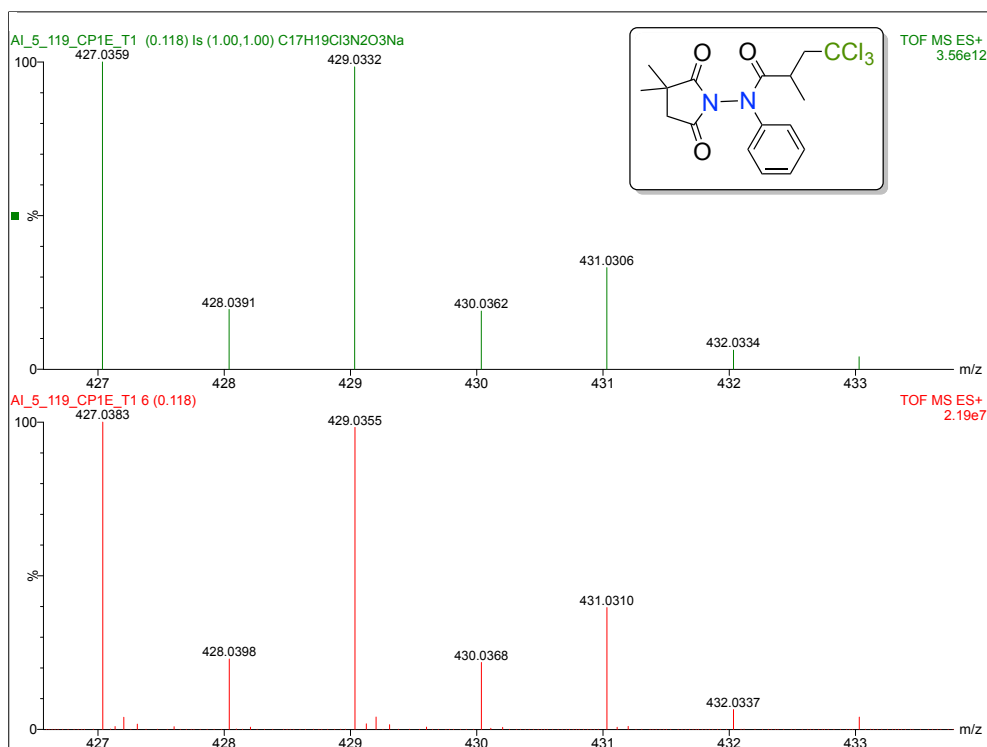
Figure 4.21: HRMS spectra of **226b**.

4.18. Characterization of chloromethylated photoproduct 226d

TLC condition - R$_f$ = 0.5 (50% ethyl acetate:hexanes). Bright yellow solid (Yield = 80%).

^{1}H-NMR (400 MHz, CDCl$_3$, δ ppm): 1.43-1.44 (m, 3H), 2.68 (s, 3H), 3.34-3.38 (m, 1H), 3.68–3.74 (m, 1H), 4.10–4.16 (m, 1H), 7.42-7.52 (m, 4H), 7.62–7.64 (m, 1H), 7.72–7.80 (m, 1H), 7.81–7.82 (m, 2H) and 8.22–8.24 (m, 1H).
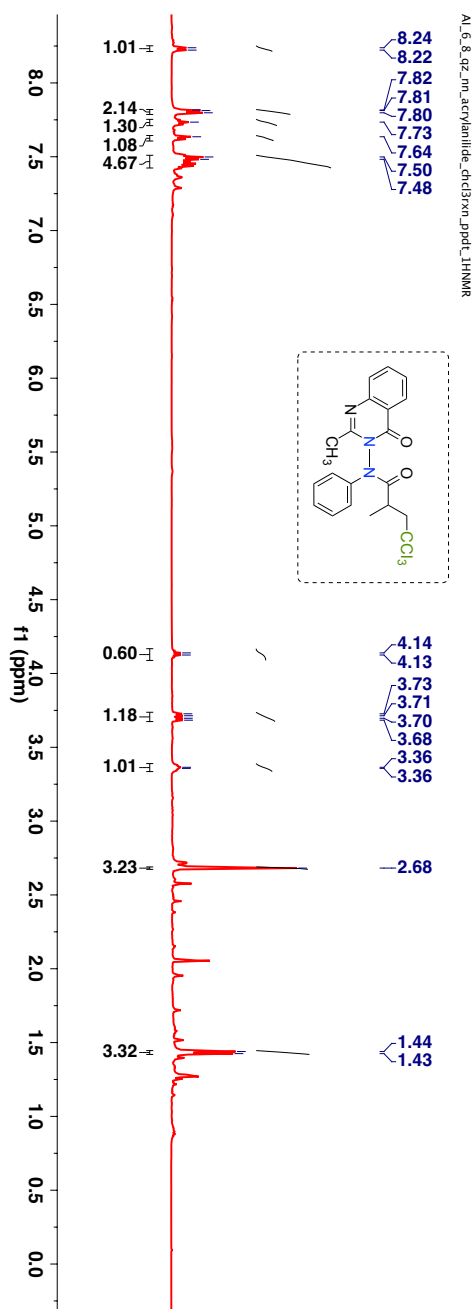
Figure 4.22: ^{1}H-NMR (400 MHz, CDCl$_3$, δ ppm) spectrum of **226d**.

407

^{13}C-NMR (100 MHz, CDCl$_3$, δ ppm, all peaks are reported together): 19.5, 22.2, 35.5, 57.7, 60.6, 98.2, 122.0, 127.0, 127.2, 127.5, 128.3, 129.6, 130.1, 130.1, 135.1, 139.9, 146.8, 155.1, 159.9 and 173.9.
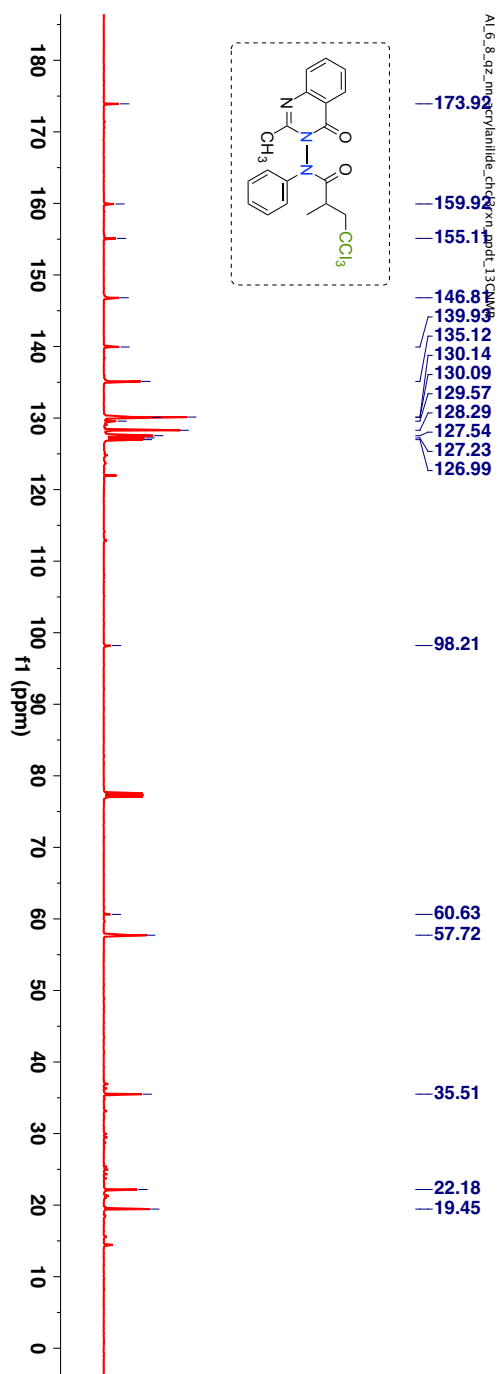
Figure 4.23: ^{13}C-NMR (100 MHz, CDCl$_3$, δ ppm) spectrum of **226d**.

4.18.1. UV-Vis spectra of acrylanilide derivative 184d
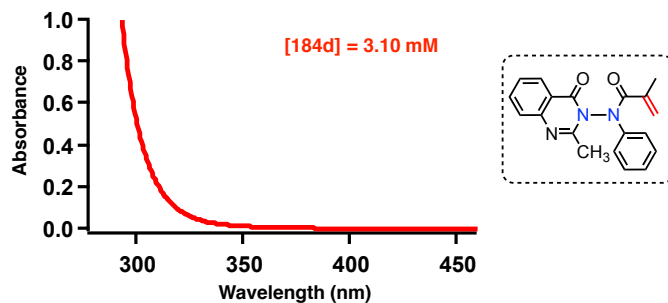
Figure 4.24: UV-Vis spectra of *N-N* bond based acrylanilide derivative **184d** recorded at the reaction concentration (concn = 3.10 mM) in chloroform as the solvent.

HRMS-ESI (m/z) ([M + Na]$^+$):

Chemical Formula	: $C_{20}H_{18}Cl_3N_3O_2$
Calculated	: 460.0360
Observed	: 460.0362
$|\Delta m|$	: 0.4 ppm
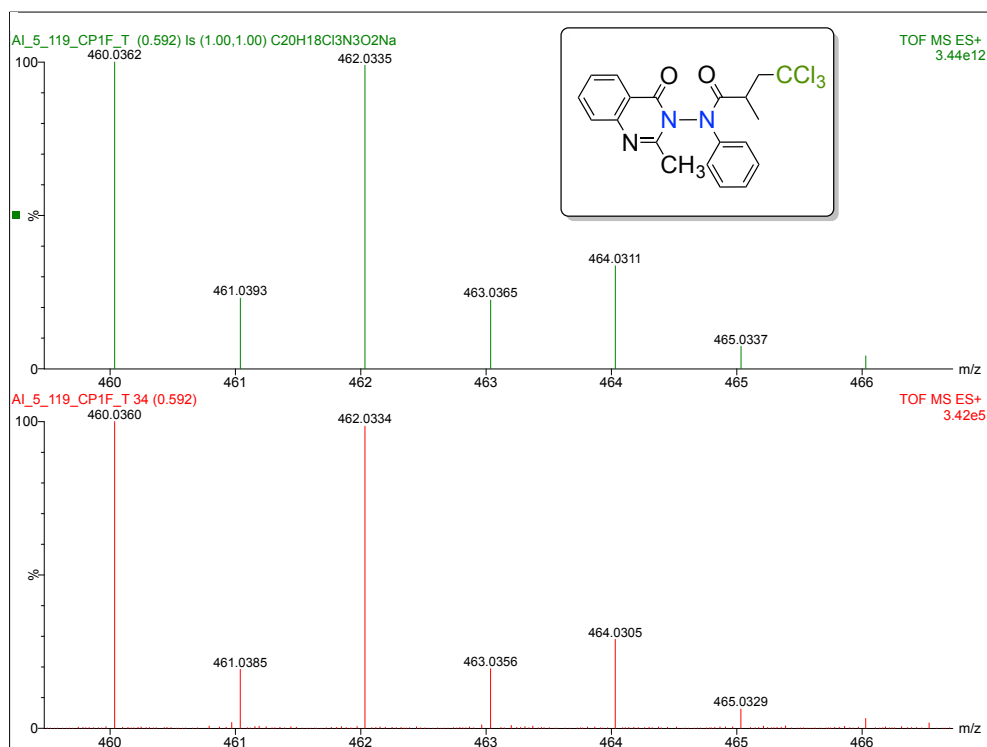
Figure 4.25: HRMS spectra of **226d**.

4.19.   Characterization of chloromethylated photoproduct 226i
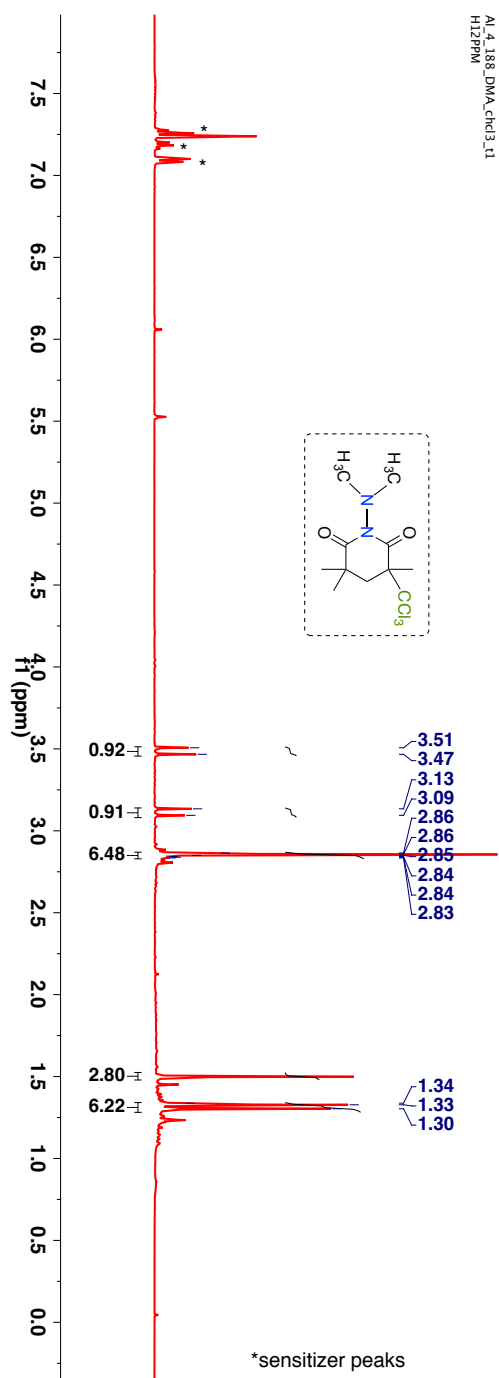
Figure 4.26: Crude ^{1}H-NMR (400 MHz, CDCl$_3$, δ ppm) spectrum of **226i**.

TLC condition R$_f$ = 0.3 (20% hexanes:ethyl acetate). Oil (Yield = 74%).

^{1}H-NMR (400 MHz, CDCl$_3$, δ ppm): 1.30 (s, 3H), 1.33 (s, 3H), 1.50 (s, 3H), 2.85 (s, 6H), 3.09 - 3.50 (ABq, 2H).
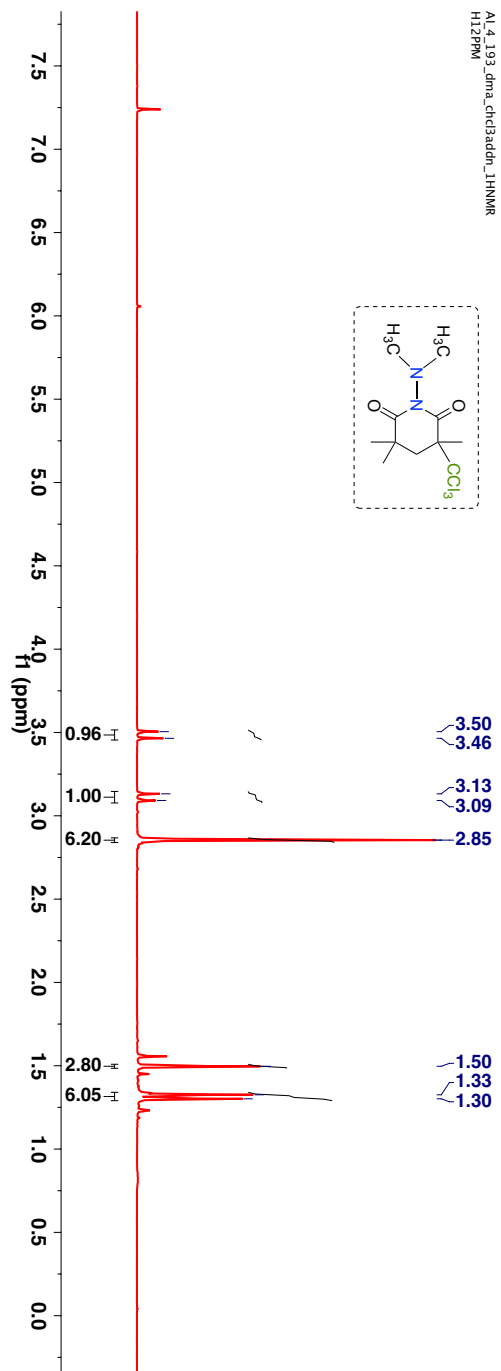
Figure 4.27: ^{1}H-NMR (400 MHz, CDCl$_3$, δ ppm) spectrum of **226i**.

^{13}C-NMR (100 MHz, CDCl$_3$, δ ppm): 19.8, 20.4, 23.1, 43.9, 47.5, 50.8, 56.0, 96.7, 128.1, 178.6 and 180.4.
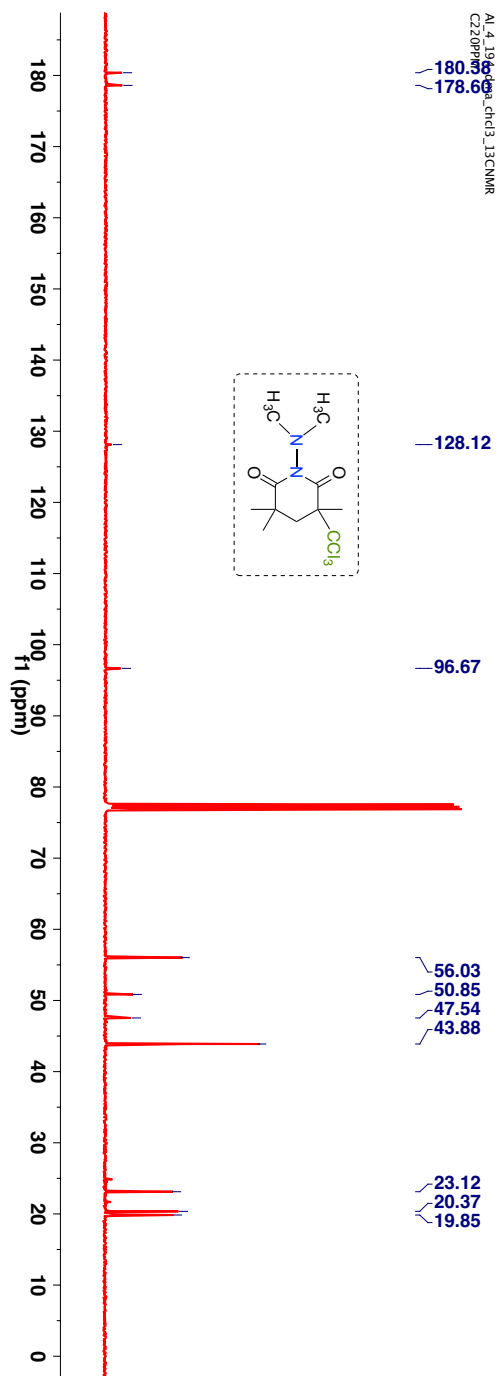
Figure 4.28: ^{13}C-NMR (100 MHz, CDCl$_3$, δ ppm) spectrum of **226i**.

4.19.1. UV-VIS spectra of tertiary amine based hydrazide derivative 113i
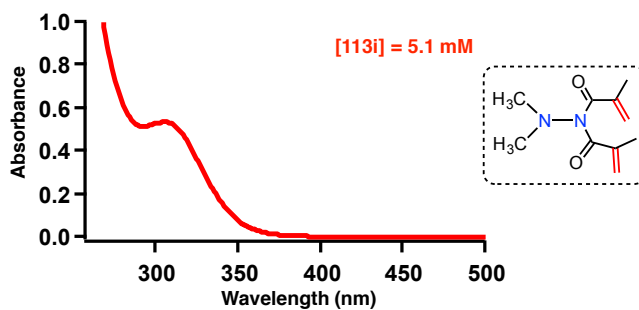
Figure 4.29: UV-Vis spectra of hydrazide based derivative **113i** recorded in chloroform at the reaction concentration (concn = 5.1 mM).

HRMS-ESI (m/z) ([M + Na]$^+$):

Chemical Formula   : $C_{11}H_{17}Cl_3N_2O_2$

Calculated   : 337.0254

Observed   : 337.0253

|Δm| : 0.3 ppm
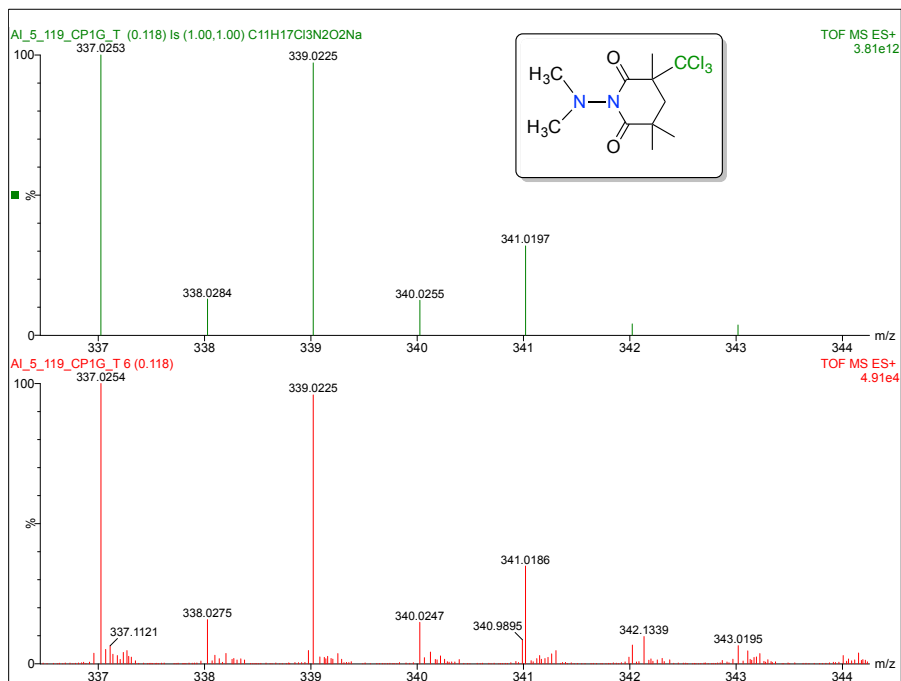
Figure 4.30: HRMS spectra of **226i**.

TLC condition R_f = 0.3 (20% hexanes:ethyl acetate). Oil (Yield = 85%).

^{1}H-NMR (400 MHz, CDCl$_3$, δ ppm): 1.25 (d, J 6.8 Hz, 3H), 2.78 - 2.94 (m, 2H), 3.27 - 3.23 (ABq, 1H), 7.13 - 7.21 (m, 5H), 7.27 – 7.34 (m, 3H), 7.52 – 7.54 (m, 2H), 7.23 – 7.75 (m, 2H) and 7.85 – 7.88 (m, 2H).
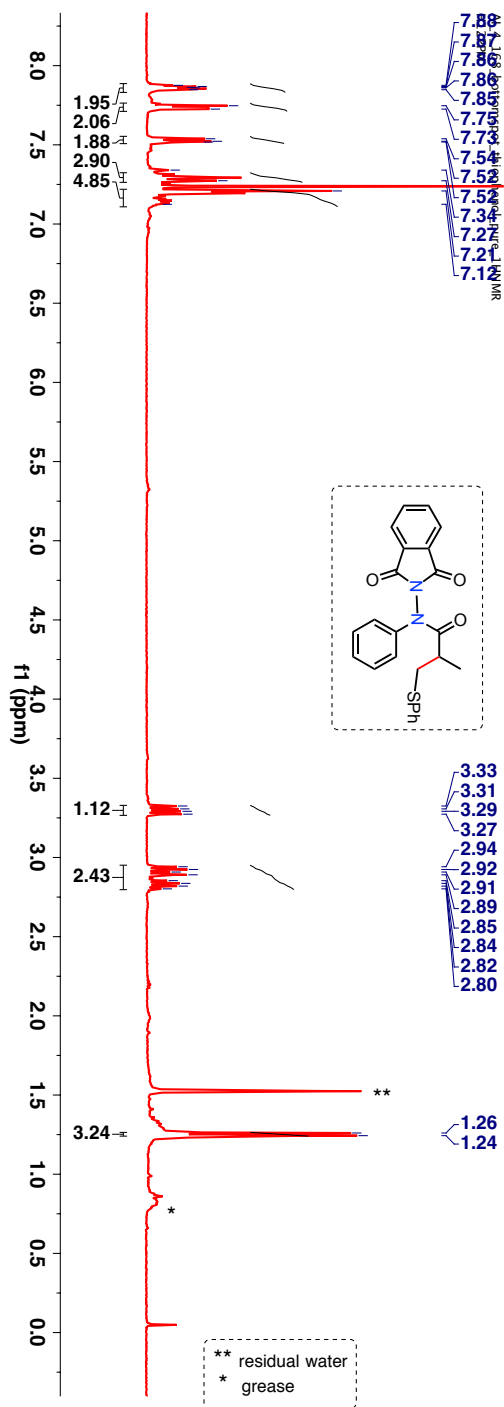
Figure 4.31: ^{1}H-NMR (400 MHz, CDCl$_3$, δ ppm) spectrum of **226h**.

^{13}C-NMR (100 MHz, CDCl$_3$, δ ppm): 17.5, 31.1, 36.6, 37.0, 124.1, 124.1, 126.2, 129.1, 129.4, 129.7, 129.9, 130.3, 130.3, 134.8, 134.8, 136.0, 139.9, 164.9, 165.1 and 173.7.
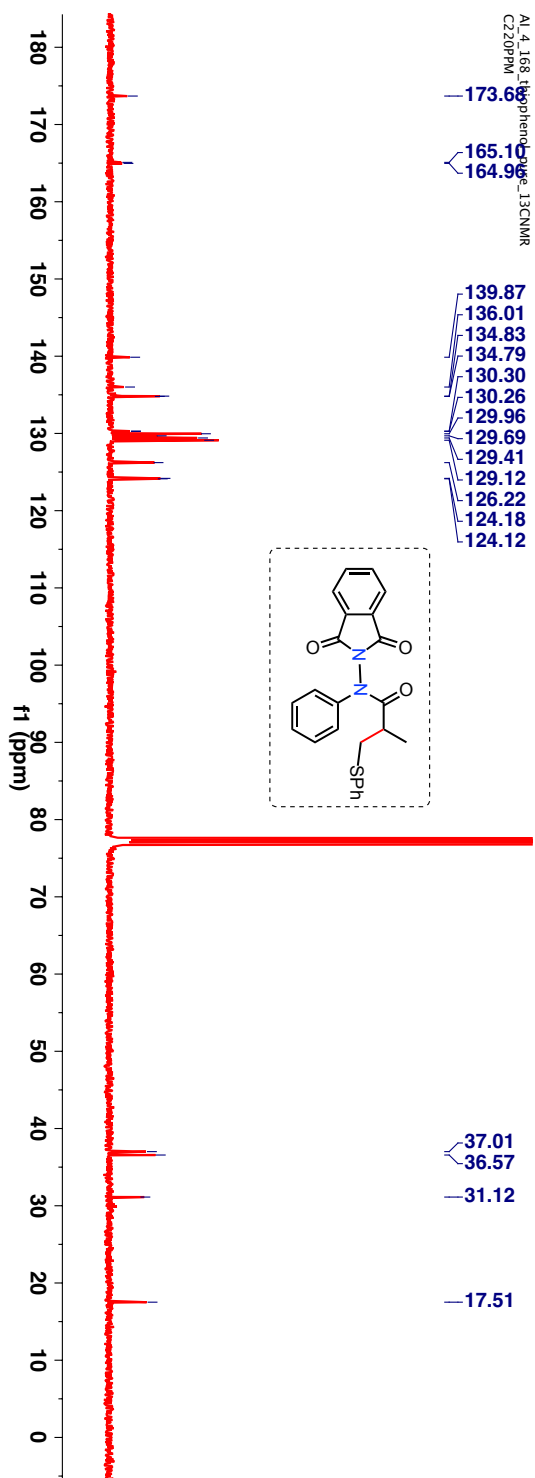
Figure 4.32: ^{13}C-NMR (100 MHz, CDCl$_3$, δ ppm) spectrum of **226h**.

4.19.2. UV-VIS spectra of phthalimide based hydrazide derivative 184e
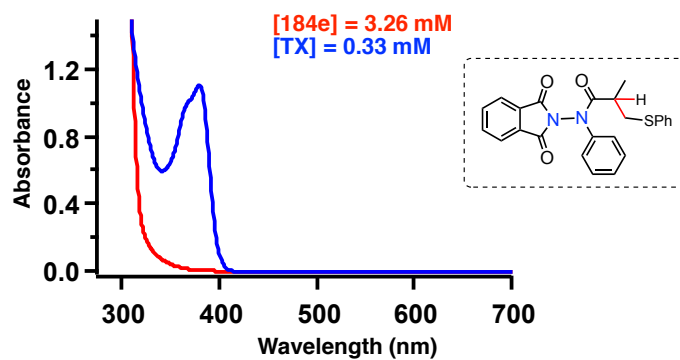
Figure 4.33: UV-Vis spectra of phthalimide based hydrazide **184e** recorded in thiophenol at the reaction concentration (concn = 3.26 mM; red and blue line represents the absorbance trace of hydrazide and TX).

4.20. References

(1)   Gribble, G. W. *J. Chem. Educ.* **2004**, *81*, 1441.

(2)   Su, J.-Y.; Zhong, Y.-L.; Zeng, L.-M.; Wei, S.; Wang, Q.-W.; Mak, T. C. W.; Zhou, Z.-Y. *J. Nat. Prod.* **1993**, *56*, 637-42.

(3)   Orjala, J.; Gerwick, W. H. *J. Nat. Prod.* **1996**, *59*, 427-30.

(4)   Nguyen, V.-A.; Willis, C. L.; Gerwick, W. H. *Chem. Commun.* **2001**, 10.1039/B106087M, 1934-35.

(5)   Arda, A.; Rodra-guez, J.; Nieto, R. M.; Bassarello, C.; Gomez-Paloma, L.; Bifulco, G.; Jimanez, C. *Tetrahedron* **2005**, *61*, 10093-98.

(6)   Durow, A. C.; Long, G. C.; O'Connel, S. J.; Willis, C. L. *Org. Lett.* **2006**, *8*, 5401-04.

(7)   Arda, A.; G. Soengas, R.; Nieto, M. I.; Jimanez, C.; Rodraguez, J. *Org. Lett.* **2008**, *10*, 2175-78.

(8)   Beaumont, S. p.; Ilardi, E. A.; Monroe, L. R.; Zakarian, A. *J. Am. Chem. Soc.* **2010**, *132*, 1482-83.

(9)   Gu, Z.; Zakarian, A. *Angew. Chem. Int. Ed.* **2010**, *49*, 9702-05.

(10)   Gu, Z.; Herrmann, A. T.; Zakarian, A. *Angew. Chem. Int. Ed.* **2011**, *50*, 7136-39.

(11)   Ilardi, E. A.; Zakarian, A. *Chem. Asian J.* **2011**, *6*, 2260-63.

(12)   Herrmann, A. T.; Smith, L. L.; Zakarian, A. *J. Am. Chem. Soc.* **2012**, *134*, 6976-79.

(13)   Huo, H.; Wang, C.; Harms, K.; Meggers, E. *J. Am. Chem. Soc.* **2015**, *137*, 9551-54.

(14)   Liu, Y.; Zhang, J.-L.; Song, R.-J.; Li, J.-H. *Org. Chem. Front.* **2014**, *1*, 1289-94.

(15)   Zhu, M.; Fu, W. *Heterocyc. Comm.* **2015**, *21*, 387-90.

(16)   Lu, M.-Z.; Loh, T.-P. *Org. Lett.* **2014**, *16*, 4698-701.

(17)   Chan, C.-W.; Lee, P.-Y.; Yu, W.-Y. *Tetrahedron Lett.* **2015**, *56*, 2559-63.

(18)   Li, X.; Xu, J.; Gao, Y.; Fang, H.; Tang, G.; Zhao, Y. *J. Org. Chem.* **2015**, *80*, 2621-26.

CHAPTER 5. MISCELLANEOUS WORK

This chapter has been described in three sections that I pursued as side projects involving chemical transformations mediated by visible light irradiations.

5.1.   Visible light mediated metal free polymerization of alkenes mediated by hydrazides

5.1.1.   Introduction for section 5.1

In order to evaluate the scope of *N-N* bond based acrylanilide **184e** towards the addition of various reagents under visible light; we shifted our focus to intermolecular photocycloaddition to alkenes. In the lieu of forming complex cyclobutane based products we attempted photoreactions (Scheme 5.1) of *N-N* bond based acrylanilide with substituted alkenes. To our surprise, we found that the photoreaction was resulting in polymerization of the alkene under study. We were delighted from our preliminary observations as this methodology provides a solvent free, metal free, visible light mediated polymerization of alkenes. The benefits and applications associated with polymers require no introduction.[1-9] There are many groups that have developed synthetic polymers that are as manifold as the natural ones.[2] Man-made polymers can be custom modified for requisite mechanical and physical properties. One of the important features associated with polymers relates to its polydispersity index (PDI).[5]
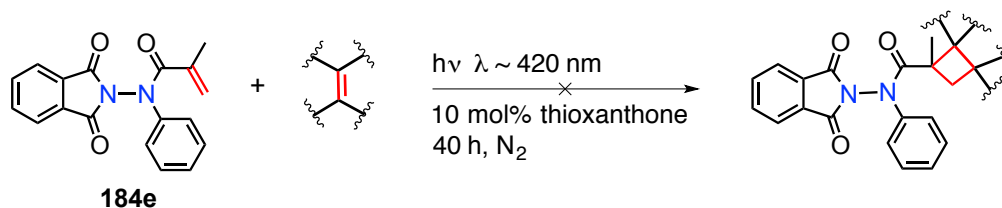
184e

Scheme 5.1: [2+2] Photocycloaddition of alkenes to acrylanilide **184e**.

The material in this section (Section 5.1.1 – 5.1.7) was co-authored by Akila Iyer (AI), Dr. Steffen Jockusch (SJ) and Dr. J. Sivaguru (JS). AI in consultation with JS carried out detailed photochemical and analytical experiments. The future efforts to expand the scope of hydrazides and for elucidating the working mechanism for photopolymerization will be carried out by Sapna Ahuja (SA). SJ and JS have described the conclusions from the preliminary observations described in this chapter.

5.1.2. Concept of average molecular weight[5,10]

Polymers are generally a mixture of molecules of identical or nearly identical make-up, but differing in degree of polymerization (DP) or molecular weight.[10] The polymer chain length is distributed according to a probability function that is governed by the operating mechanism and by the reaction conditions. The concept of average molecular weight, therefore gains importance and is expressed by equation 5.1.

Where, N_i represents the number of polymer chains with a specific molecular weight M_i and $\bar{M}_n$ refers to number average molecular weight.

$$\bar{M}_n = \frac{\sum N_i M_i}{N_i}$$
(Equation 5.1)

Equation 5.1 can be re-written in terms of fractional coefficients that are the mole fractions of the respective polymer chain in the system. The Equation 5.2 provides the weight average molecular weight $\bar{M}_w$.

$$\bar{M}_w = \frac{\sum N_i {M_i}^2}{N_i M_i}$$
(Equation 5.2)

When $\dfrac{\bar{M}_w}{\bar{M}_n}$ = 1;

The conditions suggests a perfectly mono-disperse polymer sample where all the polymer chains are of equal lengths. This ratio is referred to as polydispersity index (PDI). When the PDI is greater than 1, the polymer sample is referred as polydisperse. In addition, deviation from unity is referred to as the distribution ratio and reflects the extent of polydispersity in the sample.
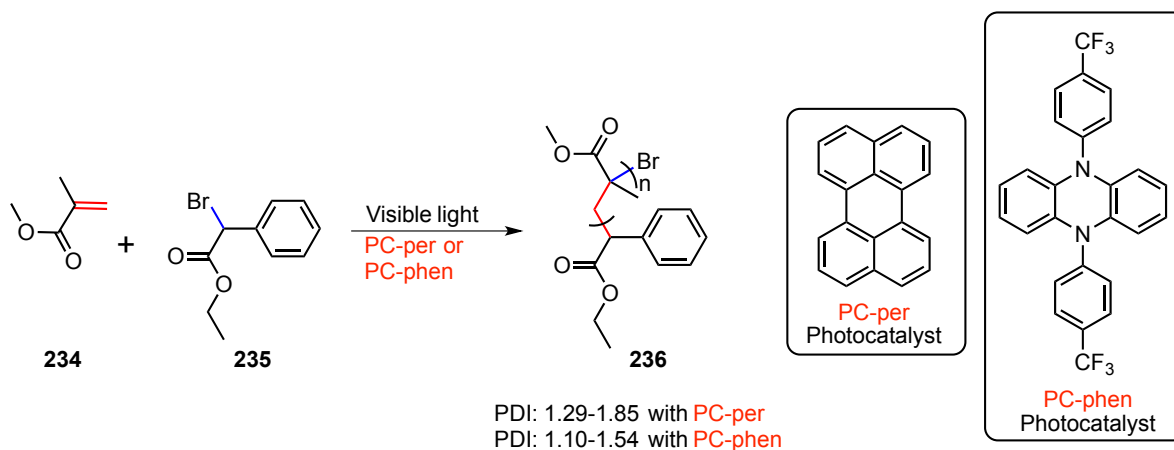
Scheme 5.2: Visible light mediated photopolymerization performed by Miyake and coworkers.

Recently Miyake and co-workers have showcased the use of visible light in the presence of organocatalyst for polymerization of alkenes (Scheme 5.2).[11-12] The first report from the group focused on light driven polymerization of methyl methacrylate **234** in the presence of α-bromophenylacetate **235** and perylene that acted as the photocatalyst/organophotocatalyst/photoorganocatalyst.[12] The photopolymerization resulted in polymer with PDI ranging between 1.29 - 1.85. In the lieu of improvising the reaction conditions to achieve nearly monodisperse polymer samples, the group switched the photocatalyst from perylene to substituted dihydrophenzine.[11] In the presence of a stronger reducing photocatalyst, they observed polymers with low PDI (1.10 - 1.54) that required relatively shorter completion time (6-8 h) under sunlight/white LED illumination. The reports communicated by this group were very similar to our observation on photopolymerization performed with a dual catalyst system composed of *N-N* bond based acrylanilide and thioxanthone (TX).

5.1.3. Visible light mediated photopolymerization of alkenes

The two alkenes that were evaluated for the study were tetramethylethylene and styrene. The photopolymerization were performed in a nitrogen atmosphere with a dual catalyst system (Scheme 5.3). The photoreaction was conducted with alkene acting as both the monomer and as a solvent. The polymerization when performed in any solvent/solvent mixtures yielded the cyclized dihydroquinolinone photoproduct exclusively. The *N-N* bond based acrylanilide was easily accessed from phthalic anhydride, which could be synthesized from biomass-derived furan (Scheme 5.4).[13] For the photopolymerization, ~0.05 equivalents of acrylanilide and TX were added.

233a $R^1 = R^2 = R^3 = R^4 = CH_3$
233b $R^1 = Ph$, $R^2 = R^3 = R^4 = H$
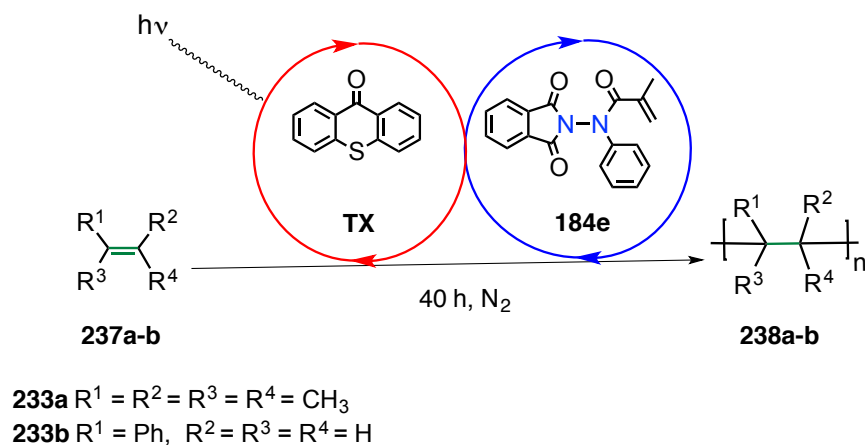
Scheme 5.3: The dual catalyst system for visible light mediated polymerization of alkenes.
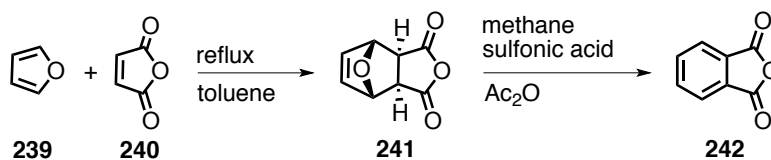
Scheme 5.4: Synthesis of phthalic anhydride starting from furan and maleic anhydride.

5.1.4. General procedure followed for photopolymerization

The polymerization required a simple set-up consisting of CFL lamp as the source of illumination, stirrer and a reaction vessel as illustrated in Figure 5.1. In a sample vial, an appropriate volume of TX (prepared in the alkene under study) was added to 5 mL of alkene. The vials were then sealed and purged with nitrogen and at 25 °C irradiated for 40 h.
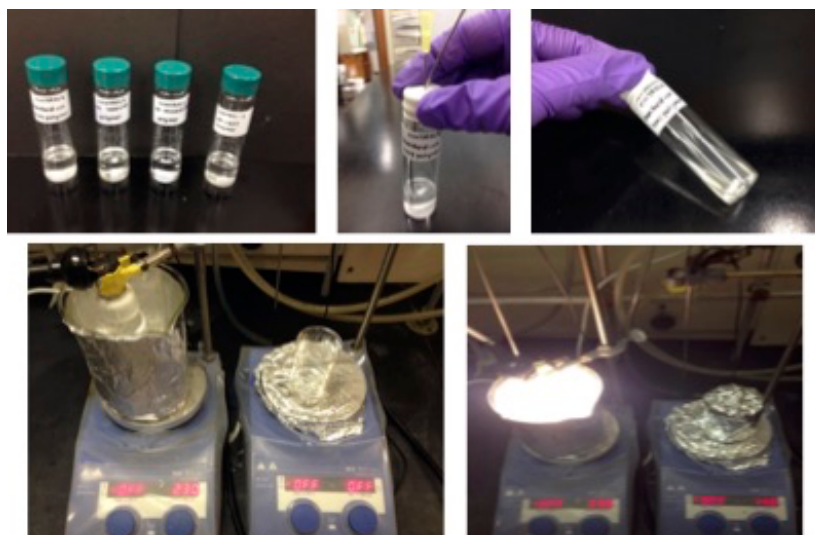
Figure 5.1: The typical experimental set-up for photopolymerization of alkene.
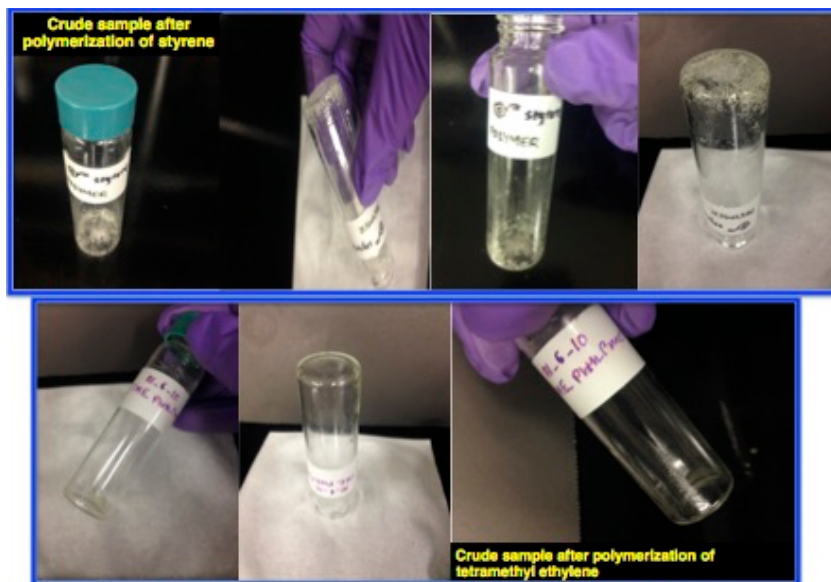
Figure 5.2: The physical appearance of the polymer obtained from the photoreaction.

After the polymerization the excess alkene was removed under reduced pressure. In case of tetramethylethylene as the monomer the corresponding polymer was a thick oily material (Figure 5.2) and for styrene as the monomer the resulting polymer was a sticky solid material. The gel permeation chromatography (GPC) results suggested nearly monodisperse polymers (Table 5.1). The photopolymerization of tetramethylethylene afforded the poly(tetramethylethylene) with a PDI ~1.06. When styrene was used as the monomer the resulting polymer possessed a PDI~1.15.In addition to low PDI values for the monomers under study the $\overline{M}_n$ and $\overline{M}_w$ were appreciably large. The high molecular weight confirmed the observed materials were polymer and not oligomers.

Table 5.1: Molecular weight data for polymers synthesized under visible light irradiation. [a]
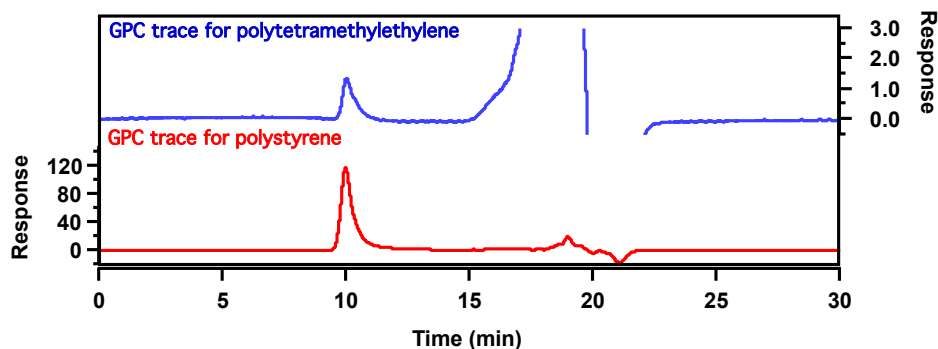
Entry	Polymer	M_n [b]	M_w [b]	M_w /M_n [b]
1	**238a**	41871	44390	1.06
2	**238b**	39736	45570	1.15

[a] The photopolymerization was performed with CFL lamp, hν ~ 400-700 nm, 8W under ambient conditions (TX: thioxanthen-9-one for **237a** and for **237b** was 5×10^{-5} equiv, **184e** for **237a** and for **237b** was 3.8×10^{-4} equiv). [b] The molecular weights were measured using Gel Permeation Chromatography (GPC) with THF as an eluting solvent and at a flow rate of 0.35 mL/min on a Waters Modular system equipped with a refractive Index detector. The system utilized a TSKge; Supermultipore HZ-M*2 column calibrated with polystyrene standards.

5.1.5. Characterization of polymer

The polymers were characterized by thermogravimetric analysis (TGA) and atomic force microscopic (AFM) images. The TGA experiments on poly(tetramethylethylene) suggested the polymer was not stable towards heat. The polymer underwent ~80% weight loss (Figure 5.3) in ~7 minutes with a temperature increase form ~80 °C to 150 °C. Further increase of temperature resulted in complete weight loss at 330 °C in 15 minutes.
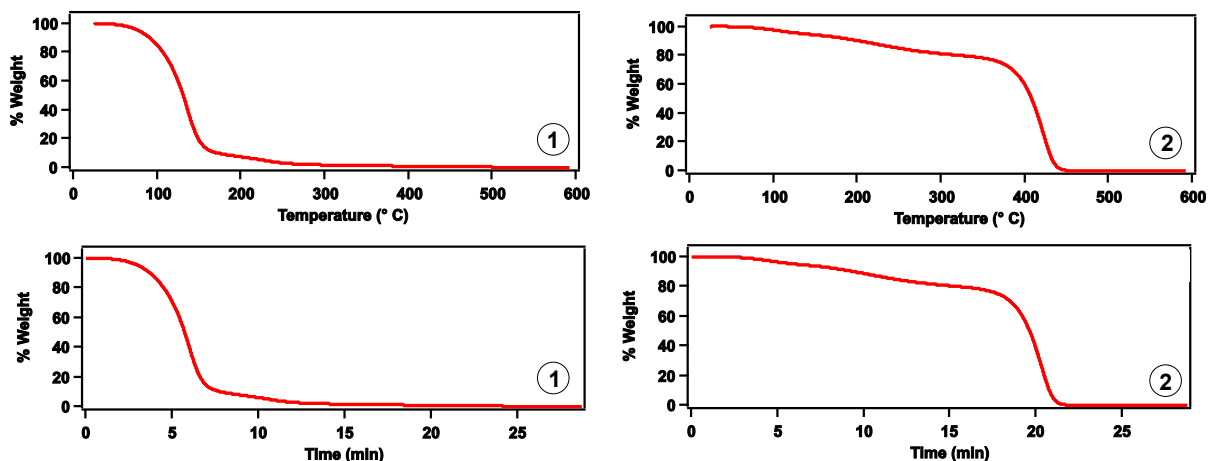
Figure 5.3: TGA results for poly(tetramethylethylene) **238a** and poly(styrene) **238b**.

The poly(styrene) on the other hand was found to be very stable towards heat. The initial weight loss was ~20% over a time period of ~18 minutes with an increase in temperature form ~25 °C to 400 °C (Figure 5.3). A complete weight loss was observed after 22 minutes on increasing the temperature to ~430 °C.

As the poly(styrene) polymer was a solid AFM images were recovered at room temperature. The solid film formed by poly(styrene) suggested that the film possessed cavities with depth of height ranging between ~587 nm-2.1 µm (Figure 5.4).
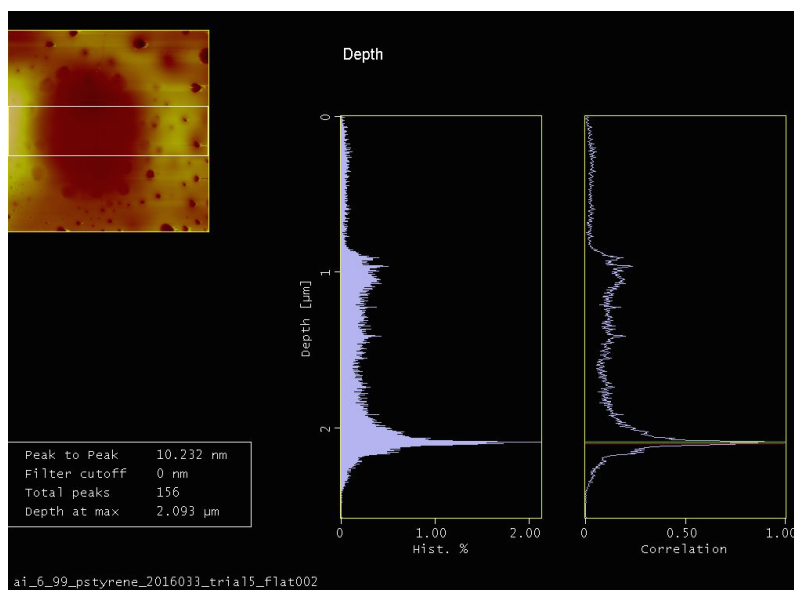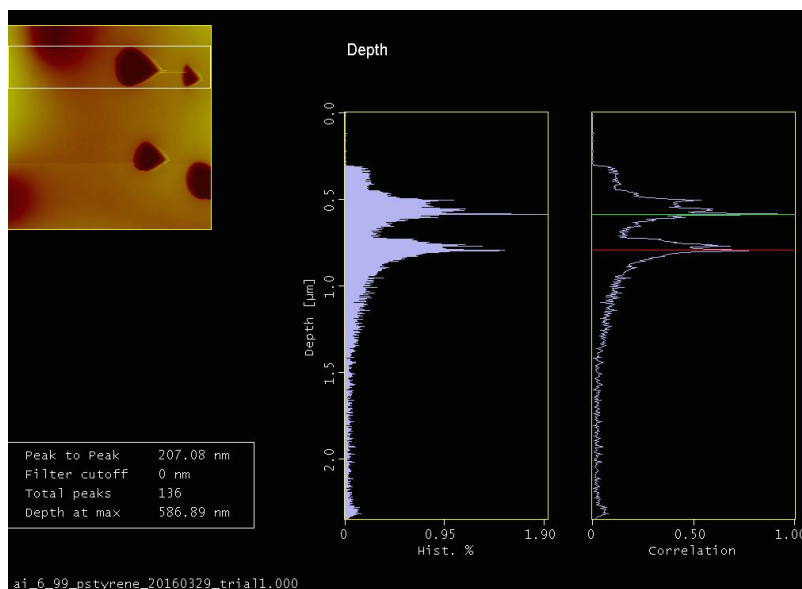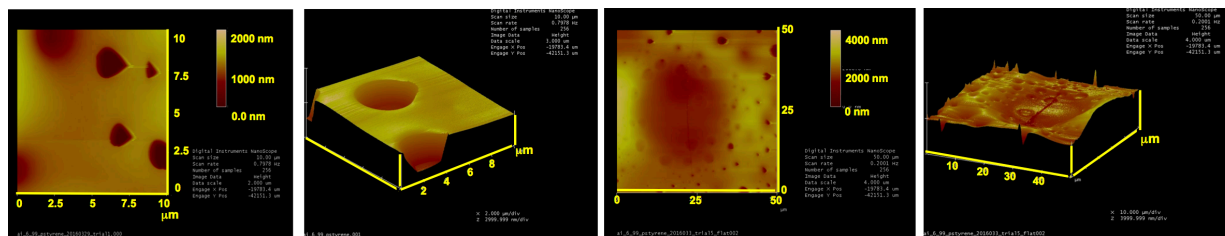
Figure 5.4: AFM images obtained for poly(styrene) films.

5.1.6. Plausible mechanism for photopolymerization under metal free conditions
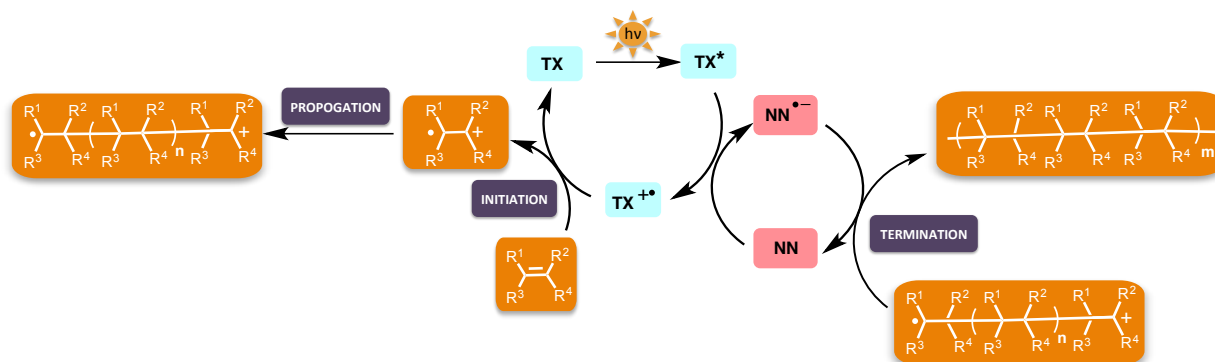
Scheme 5.5: Proposed mechanism for photopolymerization mediated by acrylanilide. (TX: thioxanthone, NN: acrylanilide **184e**).

Based on the electrochemical data and photophysical investigations performed on *N-N* bond based acrylanilide; we believe that both energy and electron transfer from photoexcited TX to acrylanilide catalyst **184e** is possible to generate the hydrazide based radical anion (Scheme 5.5). The TX radical cation that is thus generated can accept an electron from the alkene (e.g. tetramethylethylene) to regenerate TX. This process of electron transfer is accompanied by the subsequent formation of corresponding radical cation of alkene. This radical cation propagates the polymer chain and finally terminates by accepting an electron from the hydrazide. The fact that the polymer samples were nearly monodisperse suggested no side reaction of the propagating polymer chains and is likely a step growth polymerization.

5.1.7. Summary and outlook

Our work highlights the applicability of hydrazides in performing visible light mediated polymerization of alkenes under metal free conditions. The photopolymerization under our optimized conditions afford nearly monodisperse samples. Our future directions are focused on identifying the radical intermediates to bolster the proposed mechanism by electron paramagnetic resonance (EPR) studies. Since the use of solvent was futile for these experiments it was difficult to monitor the course of reaction or the effect of light during polymerization. This suggested us to evaluate other hydrazides for our study and perform in depth investigation to confirm our preliminary studies.

5.2. Developing thioxanthone based sensitizers for visible light mediated metal free photoreactions

5.2.1. Introduction for section 5.2

In our studies we have observed that the presence of *N-N* chromophore in the substrate along with the use of thioxanthone (TX) as the photocatalyst/sensitizer facilitates the visible light mediated photoreaction. Most of the substrates lacking the *N-N* bond do not react under visible light irradiation with TX sensitization. TX is an aromatic ketone based organic compound which is capable of transferring the excited state energy to an acceptor by electron or energy transfer mechanism.[14]

Only the substrates that have matching triplet energies with the triplet energy of TX are capable of getting sensitized by photoexcited triplet TX. In addition TX has a tailing absorption at λ_{on} ~ 420 nm and the absorption maximum is centered at λ_{max} ~ 378 nm, which makes it unpractical for operation under blue/white LED illumination.[15] The optical density (OD) for TX at λ = 420 nm (OD ~ 0.11, for 0.34mM solution in MeCN) is very low. We thought of modifying the thioxanthone skeleton in order to cause a red shift in the absorbance and still maintaining the triplet energy around 60 *k*cal/mol as substituent will lower the triplet energy. One of the important considerations during the design of novel TX based sensitizer, relates to the efficient triplet formation of photoexcitation of TX ($\Phi_{ISC} \approx 1$).[14,16] For this reason we became interested in brominating TX) as it was well known that heavy atom causes an efficient intersystem crossing (ISC).[17-21]

5.2.2. Synthesis of brominated thioxanthone
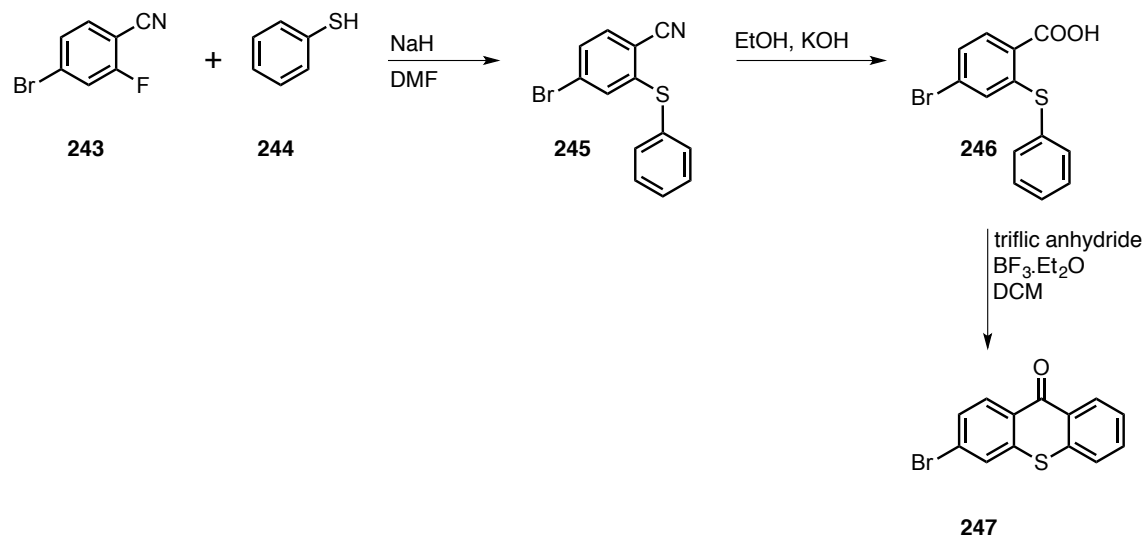
Scheme 5.6: The reported route for synthesis of mono-brominated thioxanthone derivative reported by Gigmes and coworkers.

We initially set out to synthesize (Scheme 5.6) mono brominated TX derivative by following the reported procedure by Gigmes and co-workers.[22-23] To our disappointment the first step of the reported synthesis afforded the thiophenol dimer as the major product, with a ~10% yield of desired 4-bromo-2-(phenylsulfanyl)benzonitrile **245**. Despite of the repeated attempts in optimizing the reaction conditions, we were unable to achieve the desired product in moderate yield.

We then shifted our focus towards the use of traditional electrophilic brominating reagents. The conditions that were best suited involved the use of bromine (Scheme 5.7) with catalytic amounts of Iodine. The reaction resulted in a 55% yield of a mixture of brominated thioxanthone *viz.,* mono and di-brominated TX derivative (**249**/TX-Br1 and **250**/TX-Br2). The brominated product(s) were completely characterized by ^{1}H NMR spectroscopy, HRMS and single crystal XRD analysis.
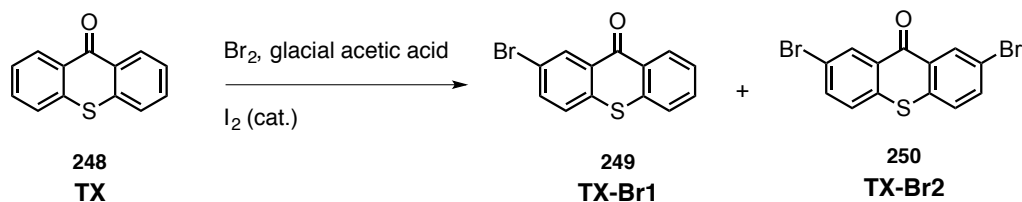
Scheme 5.7: Synthesis of brominated thioxanthone derivatives using electrophilic brominating reagent.

5.2.3. Photophysical aspects of brominated thioxanthones

5.2.3.1. UV-Vis spectra of thioxanthone derivatives

In both polar and non-polar solvents, **250**/TX-Br2 (Figure 5.5) showed a greater red shift in absorbance when compared to TX. In addition, the optical density of **250**/TX-Br2 showed distinct variation depending on the solvent employed.
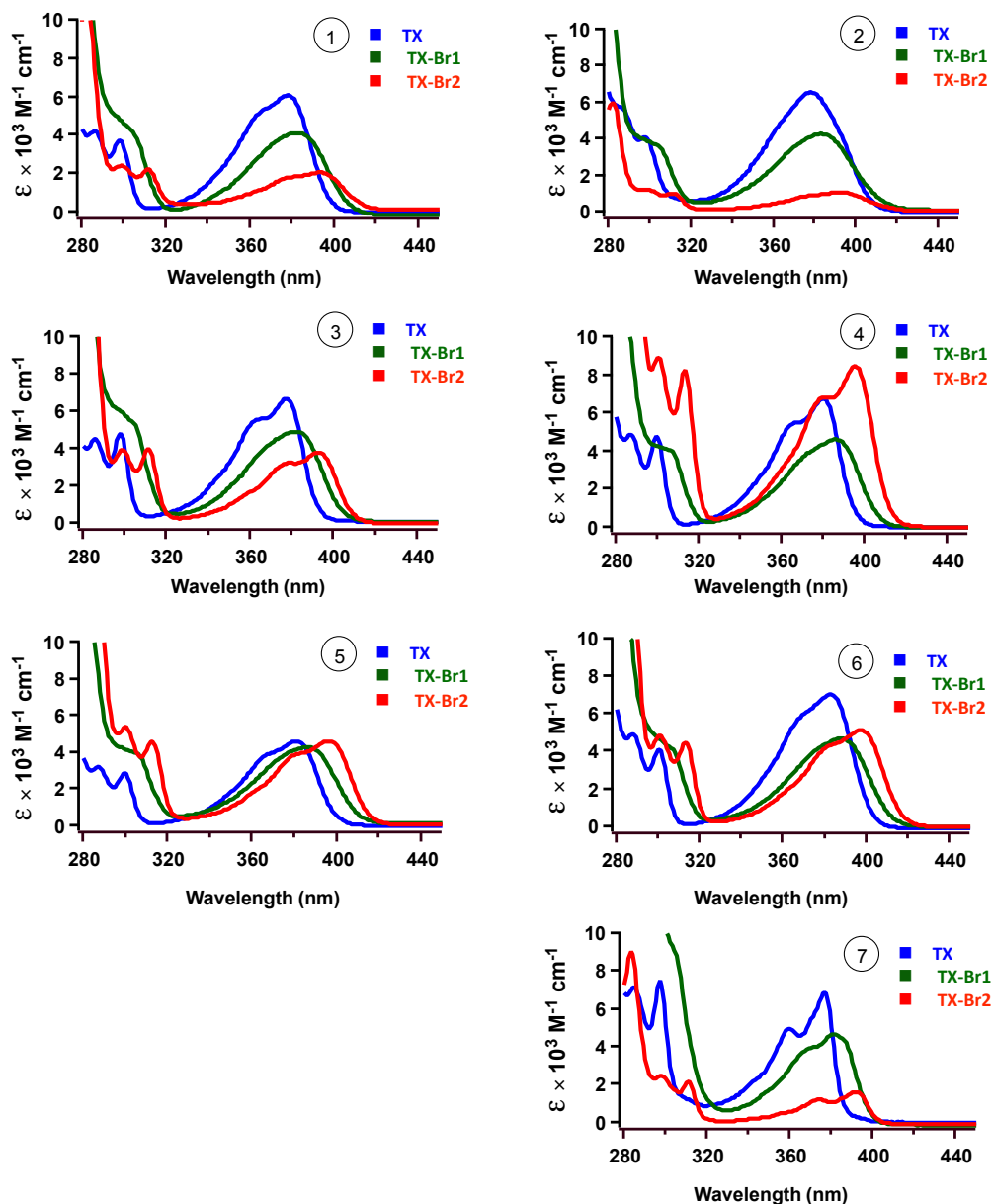
Figure 5.5: UV-Vis spectra of thioxanthone (TX, 0.05 mM) and the corresponding brominated derivatives (**249**/TX-Br1, 0.05 mM; **250**/TX-Br2, 0.05 mM) recorded in (1) acetonitrile, (2) methanol, (3) ethyl acetate, (4) benzene, (5) dichloromethane, (6) chloroform and (7) methylcyclohexane.

5.2.4. Emission spectra of thioxanthone derivatives

Phosphorescence spectra of TX, **249**/TX-Br1 and **250**/TX-Br2 were recorded at 77 K in ethanol (EtOH) and methylcyclohexane (MCH) glass matrix (Figure 5.6). The brominated derivatives (Table 5.2) showed lower triplet energy (E_T) in comparison to TX. Unlike TX that showed a greater effect of solvent on observed E_T the difference was almost negligible in case of **249**/TX-Br1 and **250**/TX-Br2.

Table 5.2: Triplet energy of thioxanthone (TX) and the corresponding brominated derivatives (**249**/TX-Br1 and **250**/TX-Br2) determined from phosphorescence experiments.

Entry	Substrate[a]	Solvent[b]	λ_{max}/(nm)	E_T/(kcal/mol)[c]
1	TX	MCH	441	64.8
		EtOH	464	61.6
2	**249**/TX-Br1	MCH	460	62.2
		EtOH	464	61.6
3	**250**/TX-Br2	MCH	469	61.0
		EtOH	470	60.3

[a] [TX] = 0.05 mM, [**249**/TX-Br1] = 0.05 mM and [**250**/TX-Br2] = 0.05 mM. [b] MCH: methylcyclohexane and EtOH: ethanol. [c] Based on phosphorescence spectra recorded in MCH/EtOH glass at 77 K.
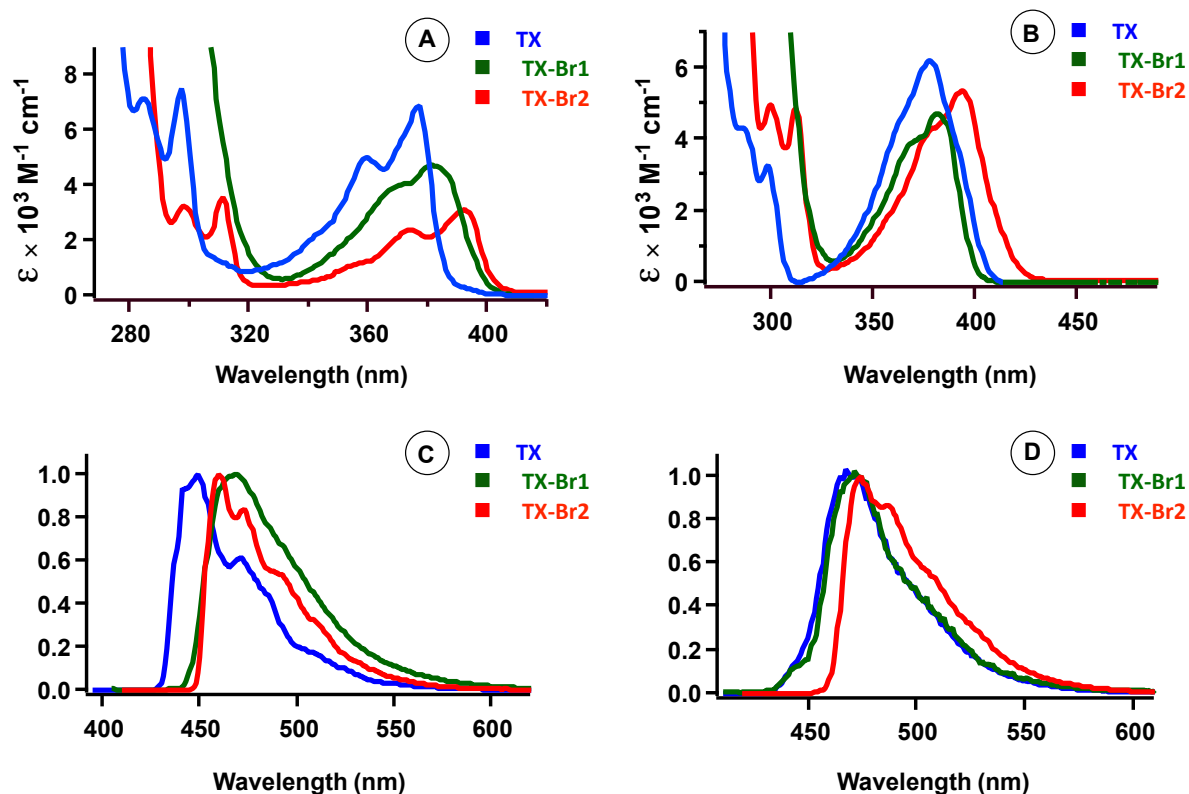
Figure 5.6: A and C refers to UV-Vis and phosphorescence spectra (at 77 K) recorded in MCH (concn = 0.05mM) glass; B and D refers to UV-Vis spectra and phosphorescence spectra (at 77 K) recorded in EtOH glass (concn = 0.05mM).

5.2.5. Electrochemical studies on brominated thioxanthones

The redox potentials obtained for TX matched to the reported values in the literature (Table 5.3).[15] The oxidation potential showed an increasing trend on moving from TX to **249/**TX-Br1 and **250/**TX-Br2. This was indeed expected since the loss of an electron during oxidation process in TX occurs from sulfur atom (Scheme 5.8). However in the presence of halogen the single electron transfer is most likely to occur from the halogen(s) which explains the observed higher oxidation potential. The reduction potential showed a similar trend. The di-brominated thioxanthone TX-Br2 showed the lowest value for reduction potential followed by mono-brominated thioxanthone TX-Br1 as the additional electron dumped into the molecule would be stabilized by halogen atom(s).
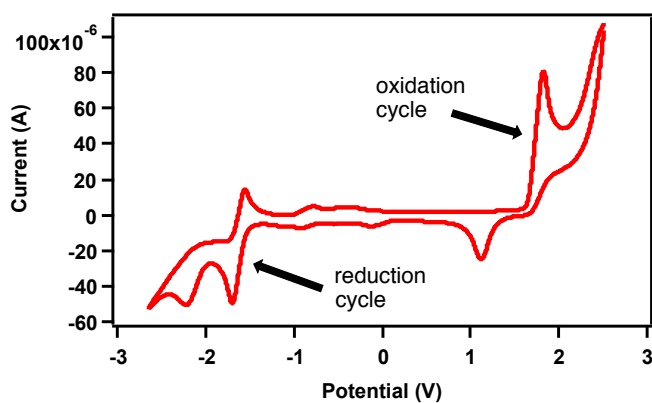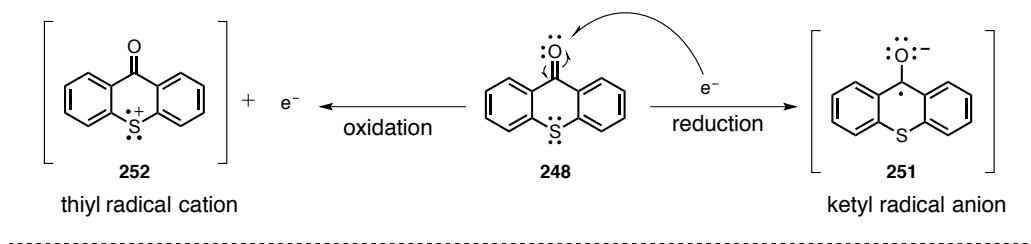
Scheme 5.8: Redox processes involved in electrochemical oxidation/reduction of thioxanthone (TX) **248**; Cyclic voltammogram for TX performed in CH_3CN containing tetrabutylammonium hexafluorophosphate (TBAP) as the supporting electrolyte under constant flow of nitrogen. [TX] = 2.1 mM.

Table 5.3: Redox potentials for thioxanthone (TX) and the corresponding brominated derivatives (**249**/TX-Br1 and **250**/TX-Br2).

ntry	Oxidation cycle [a]	Reduction cycle [a]
1	E(TX/TX$^{\bullet+}$) = 1.70 V	E (TX/TX$^{\bullet-}$) = -1.68 V
2	E(BrTX/BrTX$^{\bullet+}$) =1.88 V	E (BrTX/BrTX$^{\bullet-}$) = -1.09 V
3	E(BrTXBr/BrTXBr$^{\bullet+}$) = 1.90 V	E (BrTXBr/BrTXBr$^{\bullet-}$) = -0.84 V

[a] Determined from cyclic voltammetry performed in CH_3CN containing tetrabutylammonium hexafluorophosphate (TBAP) as the supporting electrolyte. [TX] = 2.1 mM and [TBAP] = 0.025 M; [TX-Br1] = 2.4 mM and [TBAP] = 0.025 M; [TX-Br2] = 1.35 mM and [TBAP] = 0.025 M; The experimental set-up composed of glassy carbon as the working electrode, silver chloride as the reference electrode and the platinum wire as the counter electrode.

5.2.6. Efficiency of di-brominated thioxanthone in photochemical reaction

Based on the substantial red shift observed for TX-Br2 in ethyl acetate (Scheme 5.9), we evaluated the efficiency of the novel sensitizer in facilitating [2+2] photocycloaddition of *N-N* bond based acrylimide (Scheme 5.9). The photoreaction proceeded smoothly with TX-Br2 (20 mol%) to afford the photoproduct in 75% yield under the purple LED illumination. Under the same conditions the TX afforded the photoproduct in ~90% yield. However switching the light source from purple LED to blue LED was futile. No photoreaction was observed and only the starting material was recovered. One of the possible explanations for this could be the low absorptivity of the photocatalyst/sensitizer.
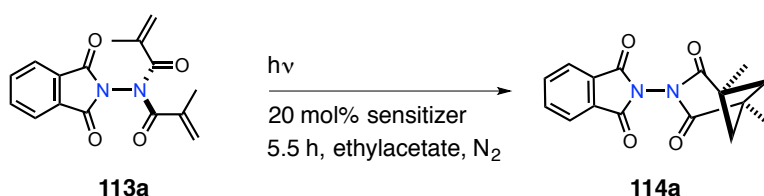
Scheme 5.9: [2+2] Photocycloaddition of phthalimide based acrylimide **113a** performed in the presence of different sensitizers viz. brominated thioxanthone (**250**/TX-Br2) and thioxanthone (TX).

5.2.7. X-Ray crystal structure data of brominated thioxanthone

Structure determination: Single crystal X-ray diffraction data of the compound **250**/TX-Br2 was collected on a Bruker Apex Duo diffractometer with a Apex 2 CCD area detector at T = 100 K. Cu radiation was used in all the cases. All structures were processed using Apex 2 v2010.9-1 software package. Direct method was used to solve the structures after multi-scan absorption corrections.
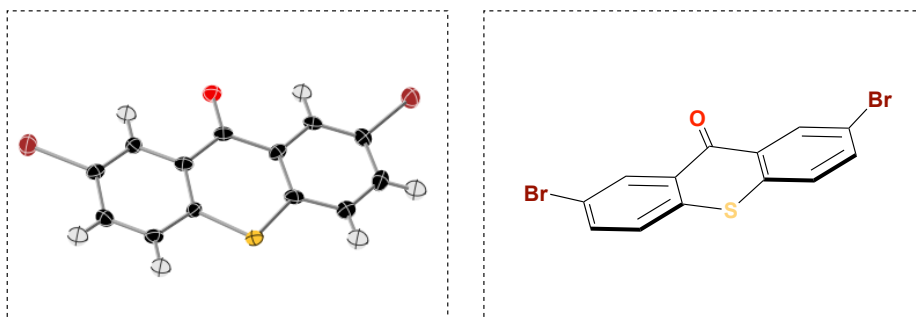
Figure 5.7: Crystal structure of **250**/TX-Br2 (Crystallized from: hexanes/chloroform/ethylacetate).

Table 5.4: Structural parameter table for brominated thioxanthone derivative **250**/TX-Br2.

Crystal	250
Formula	$C_{13}H_6Br_2OS$
Formula Weight	370.06
Space Group, Z	P -1
a/Å	7.4457(4)
b/Å	7.4733(4)
c/Å	12.2345(6)
α /°	87.698(3)
β/°	80.270(3)
γ /°	60.724(2)
V (Å^3)	584.57 (5)
h, k , l$_{max}$	8, 8, 14
ρ_{calc} [mg/mm^3]	2.102
μ [mm^{-1}]	10.280
Radiation type	CuKα (λ = 1.54178)
F(000)	365.0
No. of measured reflections	2019
No. of independent reflections	1746
Final R indexes (I ≥ 2 s)	R_1 = 0.0528, wR_2 = 0.1549
R1/wR2 (I ≥ 2 s) [%]	0.0528/0.1549

5.2.8. Summary and outlook

The brominated thioxanthone derivatives showed phosphorescence proving the effect of heavy atom(s) in facilitating intersystem crossing. The **249/**TX-Br1, **250/**TX-Br2 possessed lower triplet energy and a red shift in absorbance when compared to TX. Despite of the ability for **250/**TX-Br2 to act as a sensitizer or a photocatalyst with similar efficiency as observed for thioxanthone; the novel sensitizer was ineffective in performing under blue LED illumination. The presence of bromo group on the keto-aromatic skeleton provides a handle to build novel sensitizers for various applications (Scheme 5.10). It would be interesting to study thioxanthone-based compounds for visible light mediated reactions and polymerizations.
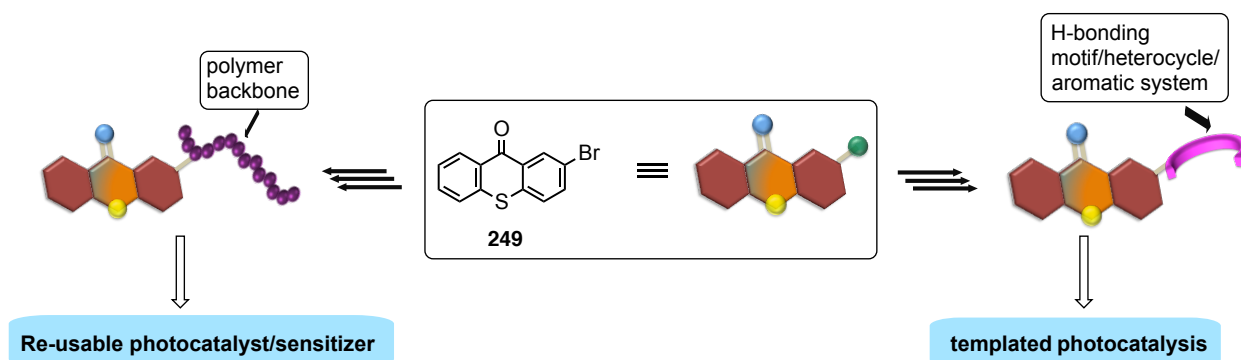
Scheme 5.10: Schematic representation for appending various chromophores to the thioxanthone backbone to access novel photocatalysts/sensitizers.

5.2.9. General methods and materials

Unless stated otherwise, reactions were conducted in oven-dried glassware under an atmosphere of nitrogen using anhydrous solvents; Photoreactions were performed under N_2 or O_2 atmosphere. ^{1}H NMR and ^{13}C NMR spectra were recorded on Varian 400 MHz (100 MHz for ^{13}C NMR) and on 500 MHz (125 MHz for ^{13}C NMR) spectrometers. The residual solvent signal was used as reference. (CDCl$_3$: δ_H = 7.26 ppm, δ_C = 77.2 ppm). Data for ^{1}H NMR spectra are reported as follows: chemical shift (δ ppm), multiplicity, coupling constant (Hz) and integration. High-resolution mass spectrum data was recorded in Electrospray Ionization mode on a Bruker–Daltronics® BioTof mass spectrometer in positive (ESI+) ion mode. The reactants and photoproducts were purified by flash chromatography using silica gel (by standard technique with solvents as indicated. RediSep®, silica gel standard grade: Porosity 60 Å, Particle size: 230 x 400 mesh, Average particle size: 60 to 70 micron). The Retardation Factor (R_f) values were recorded using various combination of solvent systems as mobile phase (as mentioned in the text) on SORBENT TECHNOLOGIES® Silica Gel TLC plates (200 µm thickness w/UV$_{254}$).

5.2.9.1. General procedure followed for irradiation of substrates and characterization of photoproducts

In a pyrex tube, solution of the desired substrate was dissolved in an appropriate solvent under an inert atmosphere. This was followed by the addition of appropriate volume of sensitizer (thioxanthone/brominated thioxanthone) prepared in the same solvent. The sample was then irradiated at 25 °C with an appropriate light source.

5.2.10. Synthesis route to brominated thioxanthone derivatives
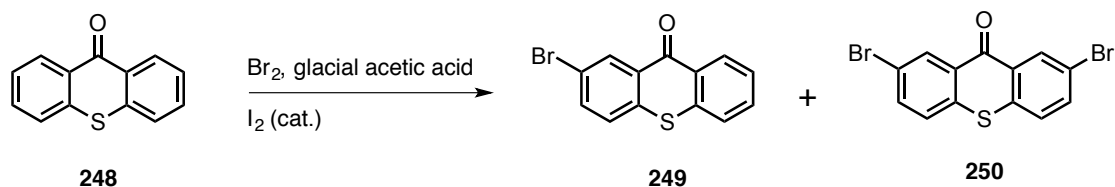
Scheme 5.11: Synthesis of mono/di-brominated thioxanthone derivative.

To the slurry of thioxanthone **250** (1.0 equiv) in glacial acetic acid (7 mL), iodine (1×10^{-3} mol%) was added slowly at 25 $^{\circ}$C under N_2 atmosphere. This was followed by the addition of 2.0 equivalents of bromine. The resulting solution was allowed to reflux 18 hours (until discoloration of bromine color was observed). The reaction was cooled and diluted with chloroform (~20 mL). The organic layer was saturated sodium sulfite solution, stirred for 5 minutes and the layers were separated. The organic layer was washed in sequence with DI water (2 × 10 mL), 1 N NaOH (1 × 15 mL) and finally with brine. The organic layer was dried over anhyd Na_2SO_4, filtered and the solvent was removed under reduced pressure to yield crude product. The crude product was purified by combiflash using hexanes and ethyl acetate mixture to get the desired brominated thioxanthone derivatives as yellow solid.

46% Isolated yield of product mixture.

TLC condition - R$_f$ = 0.3 (50% ethyl acetate:hexanes).

^{1}H-NMR (400 MHz, CDCl$_3$, δ ppm): 7.33 – 7.85 (m, 5H) and 8.54 – 8.68 (m, 2H).
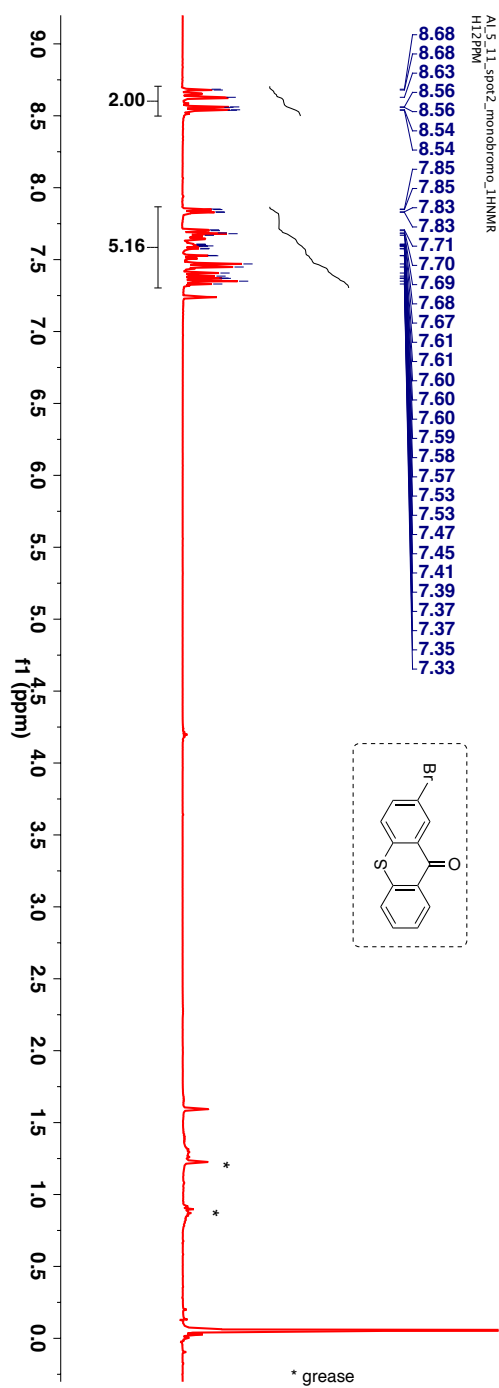
Figure 5.8: ^{1}H-NMR (400 MHz, CDCl$_3$, δ ppm) spectrum of **249**.

¹³C-NMR (100 MHz, CDCl₃, δ ppm): 120.3, 121.0, 126.2, 126.8, 127.1, 127.8, 128.1, 129.4, 130.1, 131.2, 132.6, 132.7 and 178.8.
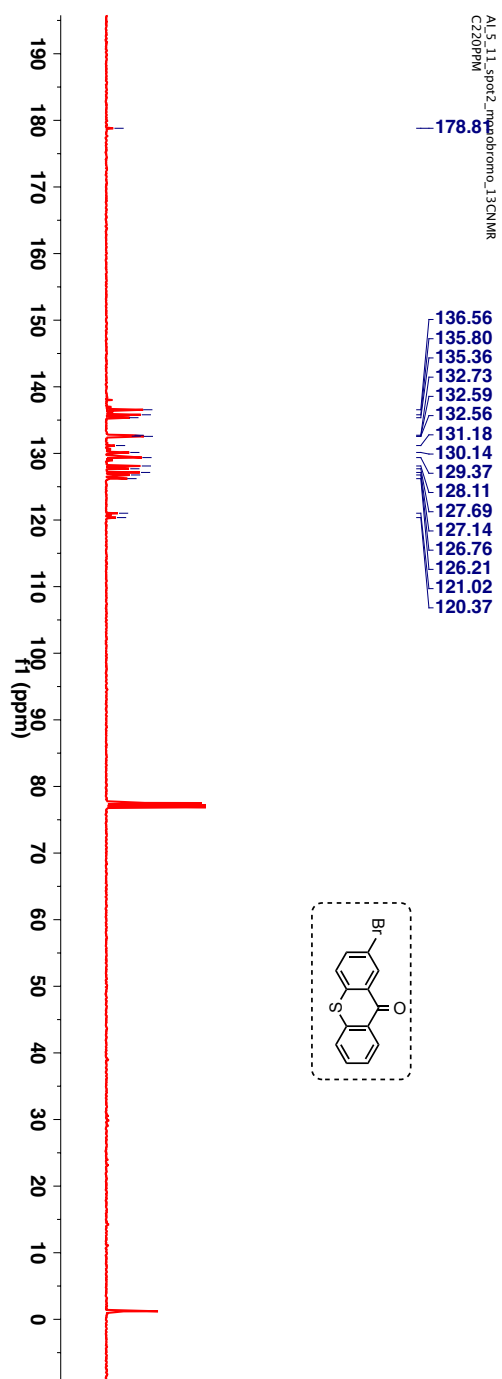
Figure 5.9: ¹³C-NMR (100 MHz, CDCl₃, δ ppm) spectrum of **249**.

HRMS-ESI (m/z) ([M + H]$^+$):

Chemical Formula   : C$_{13}$H$_7$BrOS

Calculated   : 290.9476

Observed   : 290.9479

|Δm| : 1.0 ppm
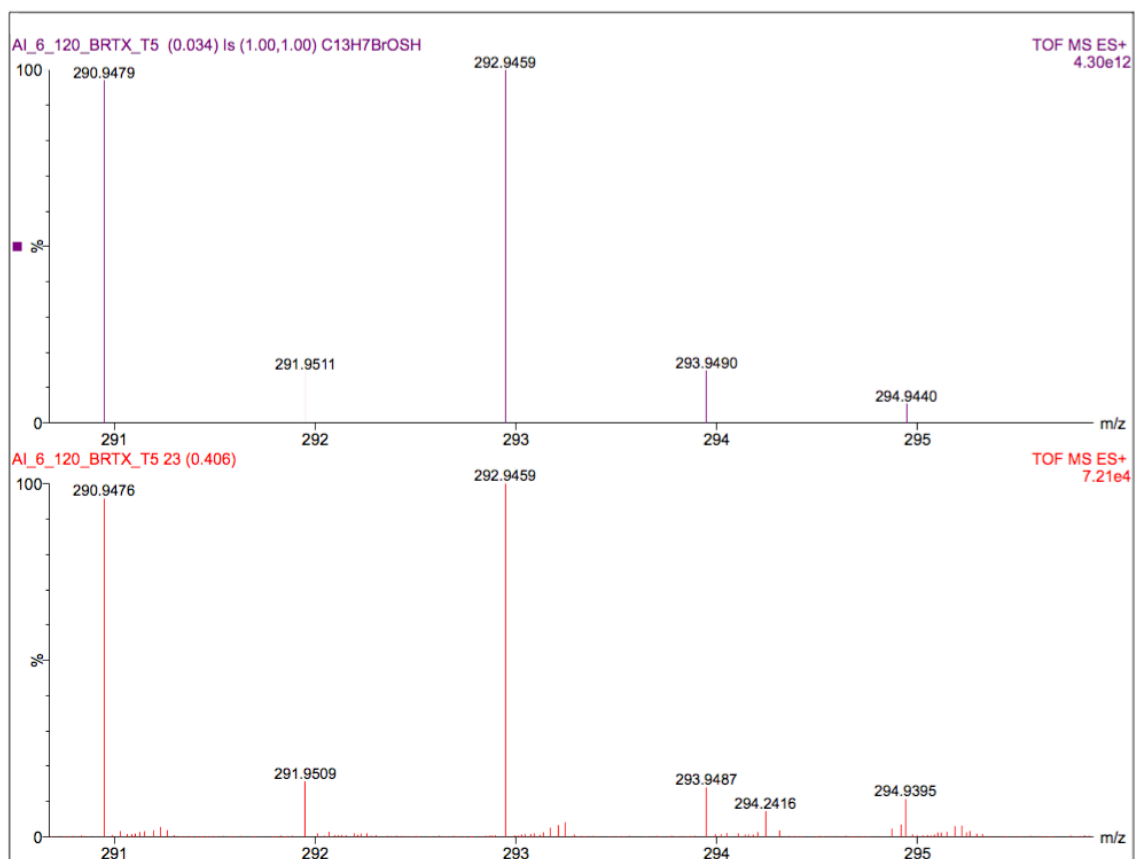
Figure 5.10: HRMS spectra of **249**.

TLC condition - R$_f$ = 0.2 (50% ethyl acetate:hexanes).

^{1}H-NMR (400 MHz, CDCl$_3$, δ ppm): 7.44-7.47 (d, J 8.4 Hz, 1H), 7.71 – 7.74 (dd, J_1 8.8 Hz, J_2 2.4 Hz, 1H) and 7.72-7.87 (d, J 2.4 Hz, 1H).
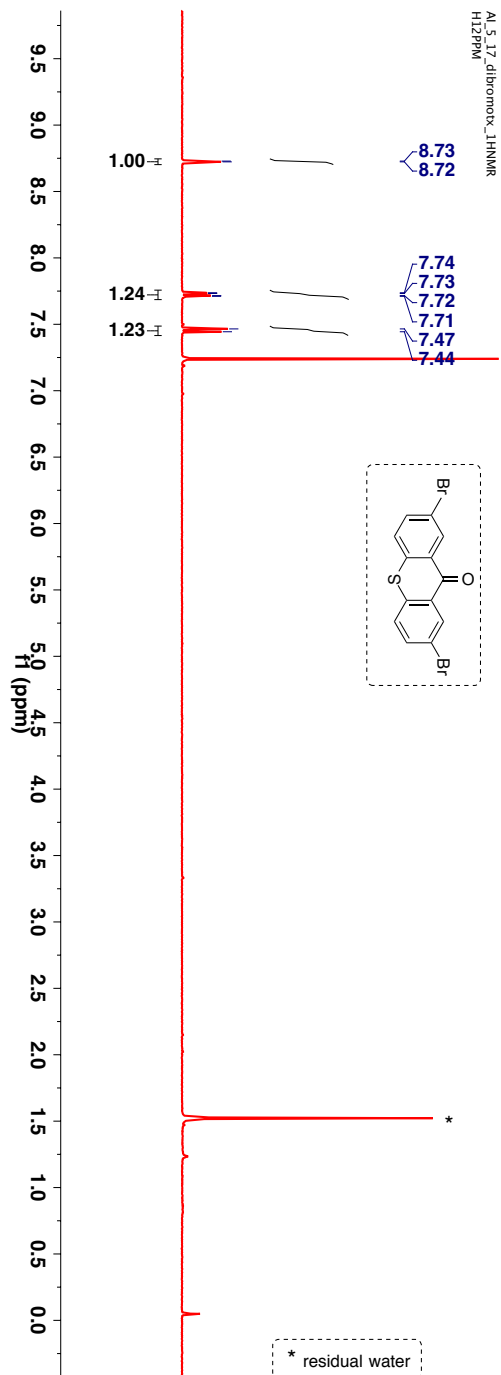
Figure 5.11: ^{1}H-NMR (400 MHz, CDCl$_3$, δ ppm) spectrum of **250**.

^{13}C-NMR (100 MHz, CDCl$_3$, δ ppm): 120.9, 127.9, 130.3, 132.8 and 135.8.
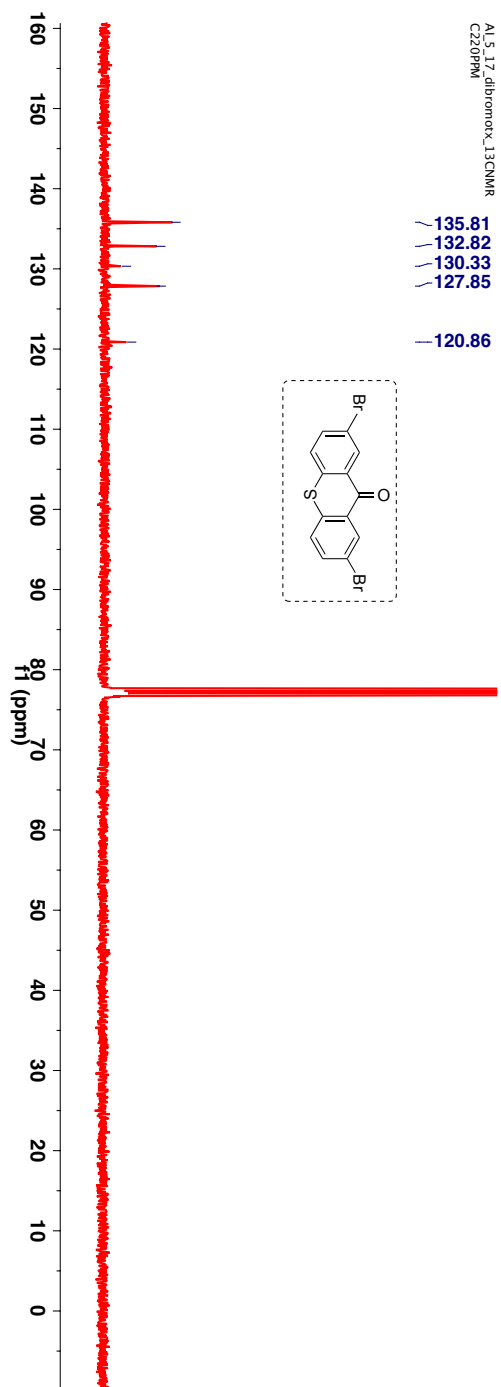
Figure 5.12: ^{13}C-NMR (100 MHz, CDCl$_3$, δ ppm) spectrum of **250**.

HRMS-ESI (m/z) ([M + 3H]$^+$):

Chemical Formula : $C_{13}H_6Br_2OS$

Calculated : 367.8506

Observed : 367.8511

|Δm| : 1.3 ppm
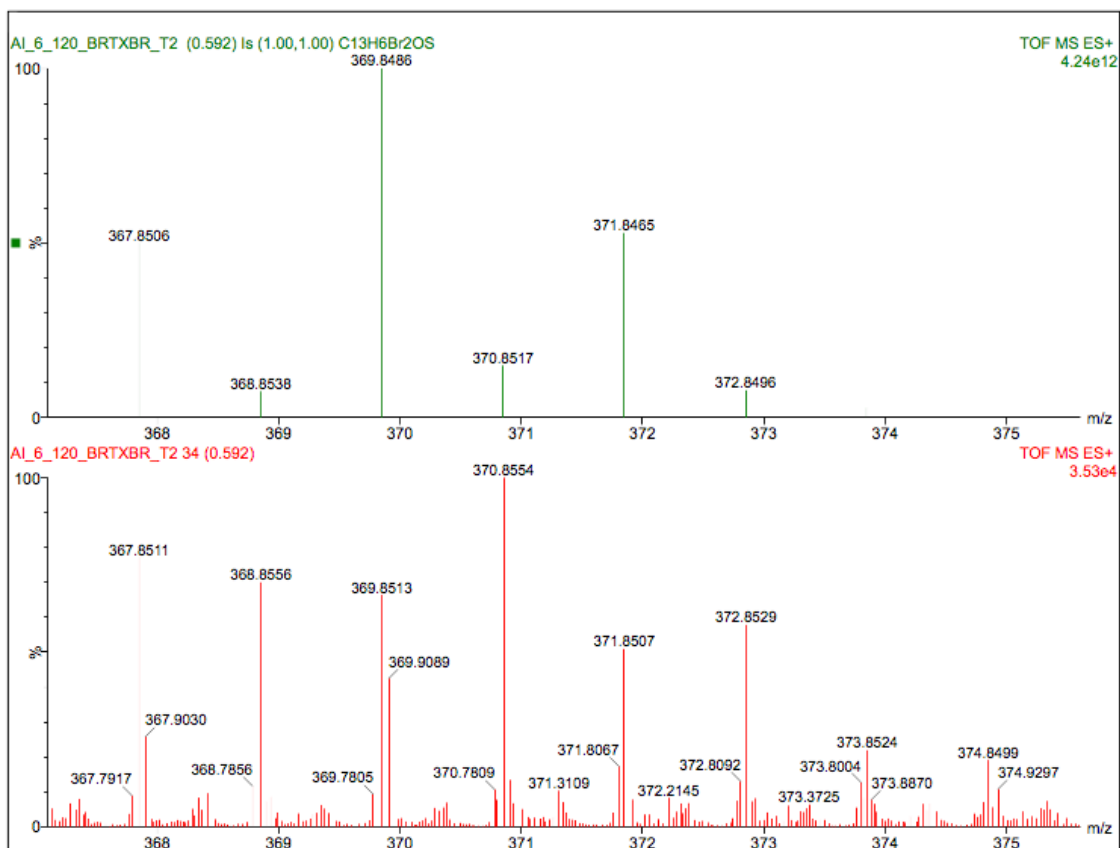
Figure 5.13: HRMS spectra of **250**.

5.3. Visible light mediated enantioselective [2+2] photocycloaddition of atropselective acrylimides

5.3.1. Introduction for section 5.3

Organic photochemistry provides an easy and benign route to access complex scaffolds often in a single step transformation.[24-25] An important class of photochemical reactions that provides an easy access to cyclobutane derivatives is photocycloaddition in particular [2+2] photocycloaddition.[26] Photodimerization of anthracene happens to be the first observation for this class of reaction and dates back to the work from laboratory of Fritzsche in the year 1867.[27-28] His work constituted a simple study utilizing sunlight for organic transformation. His work was later confirmed by single crystal X-ray analysis of the dimer by Linerbarger, Orndorff and Cameron.[29-30] The seminal work from Fritzsche utilizing light to construct conformationally constrained structure led the path for chemists to explore and evaluate olefins towards photocycloaddition. One such example showcased by Liebermann was on the study of [2+2] photocycloaddition of thymoquinone **251** (Scheme 5.12). This work is considered as the milestone in solid state photochemistry.[31]
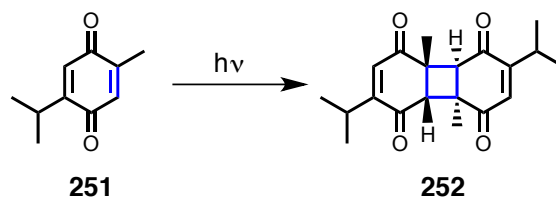
Scheme 5.12: [2+2] Photocycloaddition of thymoquinone.

The material in this section (Section 5.3.3 – 5.3.36) was co-authored by Akila Iyer (AI), Dr. Steffen Jockusch (SJ) and Dr. J. Sivaguru (JS). AI in consultation with JS synthesized all the compounds and carried out photochemical experiments. SJ performed photophysical studies detailed in this chapter. AI and JS came up with the mechanistic rationale and the conclusion described in this chapter.

Photocycloaddition of olefins can be systematically classified in accordance to their mechanistic considerations.[32][33] The first class of photocycloaddition occurs from the direct excitation of an olefin to the first excited singlet state (Scheme 5.13). The excited olefin (**253**, A) either adds to another olefin (**254**, B) molecule (AB heterocycloadduct, **255** or **256**) or adds to another olefin (**253**, A) of the same kind that leads to a heterodimer (AA photoproduct, **257** or **258**. The reaction might occur in a stereospecific manner depending on the nature of the excited state.
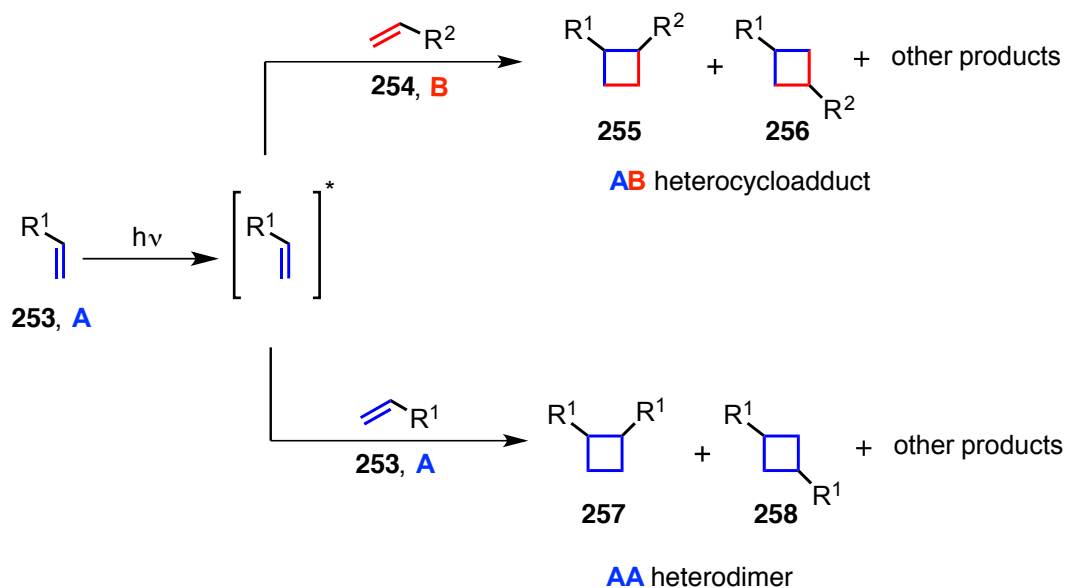
Scheme 5.13: [2+2] Photocycloaddition from direct excitation of an olefin to the first excited singlet state.

In the cases of non-conjugated alkenes the photocycloaddition requires lower wavelength energy for excitation $\lambda \leq 254$ nm. In such cases, the lowest excited state is of $\pi\pi^*$ character and this excited state has various pathways for deactivation thus making the photochemical outcome less efficient. Such a photocycloaddition has been effectively carried out using transition metal complexation (Scheme 5.14).[34] In the presence of metal the [2+2] photocycloaddition is assisted at higher wavelength $\lambda \geq 254$ nm due to metal-to-ligand charge transfer (MLCT) or ligand-to-metal charge transfer (LMCT).
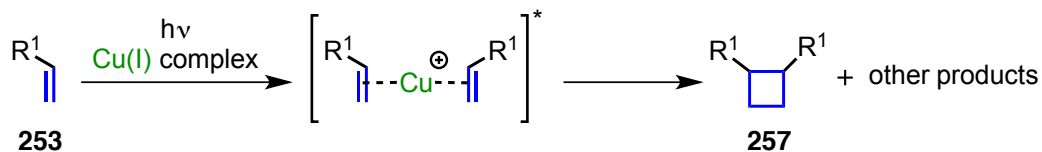
Scheme 5.14: Cu(I) complex mediated [2+2] photocycloaddition of olefins.

Often an intermolecular [2 + 2] photocycloaddition reaction is observed from a triplet excited state, which is relatively long-lived excited state. Such a long-lived excited state is observed for an α,β-unsaturated ketones or an α,β-unsaturated carboxylic acid derivatives.[35] On exciting the enone derivative, the excited S_1 state undergoes an intersystem crossing (ISC) to populate the triplet state and the photocycloaddition reactions then occurs from the lowest-lying triplet state. The triplet state of an alkene can also be accessed by triplet energy transfer (Scheme 5.15). An appropriate organic / inorganic molecule (sensitizer) is employed that can absorb the irradiated energy and populate the triplet state of the alkene from an electron exchange mechanism (Dexter energy transfer mechanism).[36] For the sensitizer, to do triplet energy transfer to an alkene the sensitizer is required to be in a close proximity. In addition, for the triplet sensitization to be in the rate of diffusion-controlled the triplet energy of the sensitizer should be higher than triplet of alkene.[21] Utilizing a triplet energy sensitizer for photocycloaddition reactions provides a handle for employing longer wavelength for irradiation.
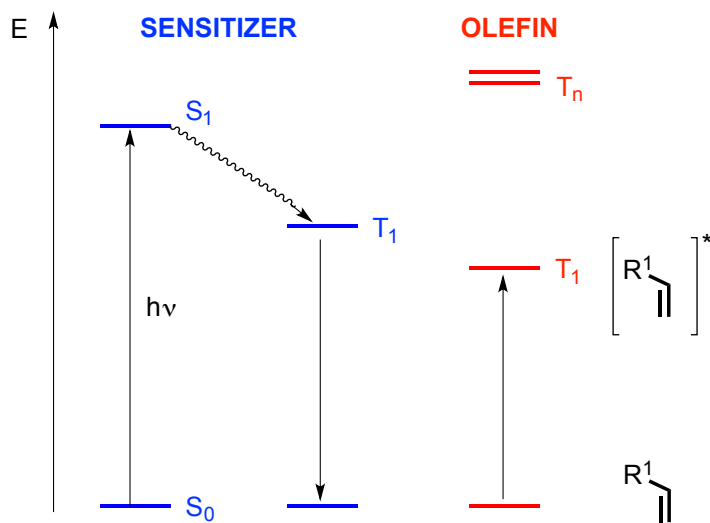
Scheme 5.15: Triplet sensitized [2+2] photocycloaddition of olefins.

Another mechanistic classification in photocycloaddition reactions utilizes a photocatalyst that can initiate single electron transfer (SET). The photocatalyst can be either an organic or inorganic sensitizer and these have been well studied in the literature for photoinduced electron transfer (PET).[37-40] In the past decade there have been numerous reports on chemical transformations catalyzed by single electron transfer from photocatalyst to the substrate undergoing reaction. The process of photoinduced electron transfer is also commonly referred to as photoredox catalysis.[41-47] On absorbing the light, the photocatalyst (P) gets excited and gets reduced/oxidized by SET by a sacrificial electron donor (D)/acceptor (A). The ground state radical cation/anion of photocatalyst is then quenched by the olefin, which is a redox neutral substrate (S) to initiate the desired chemical transformation (Scheme 5.16).
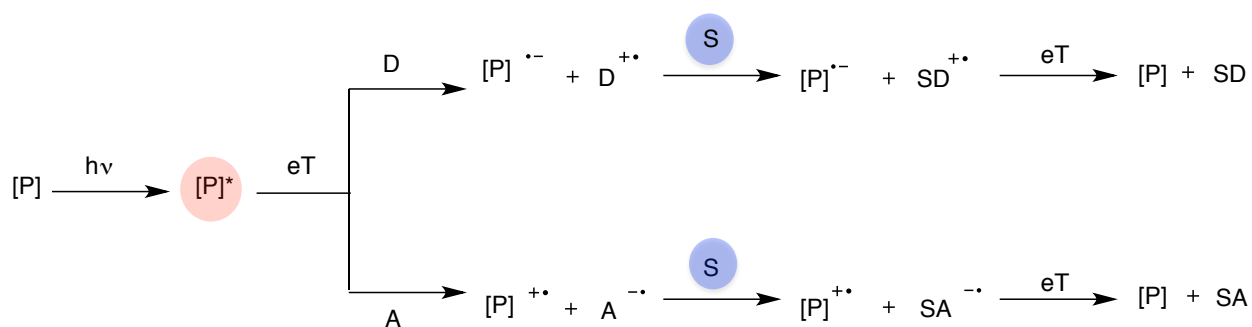
where [P] : photoredox catalyst; D : electron donor; A : electron acceptor; S : olefin (redox neutral substrate), Common donors include (D): amines, alcohols, thiols, ethers, electron rich arenes. Common acceptors (A): carbonyls, halides, electron poor arenes.

Scheme 5.16: [2+2] Photocycloaddition mediated by photocatalyst that can initiate single electron transfer (SET).

Another aspect of [2 + 2] photocycloaddition reaction relates to the asymmetric synthesis. There have been varied approaches adopted by chemists for stereoselective photocycloaddition reactions. These methodologies include supramolecular catalysis, reactions within supramolecular nanocontainers / confinement approach, atropisomeric scaffolds and chiral dual catalysis approach by photoredox chemistry to achieve moderate to very high enantioselectivity in [2 + 2] photocycloaddition reactions.[32-33,46-49] A fine exemplar of supramolecular photocatalysis with atropisomeric H-bonding catalysts, for achieving selectivity in intramolecular [2 + 2] photocycloaddition has been reported by Sivaguru, Sibi and coworkers.[50]

The enantioselective photoreactions occur by an energy sharing mechanism (for low catalyst loading ~1-30 mol%) leading to 69-96% *ee* in the photoproduct **260** at low catalyst (Scheme 5.17).[51-52]
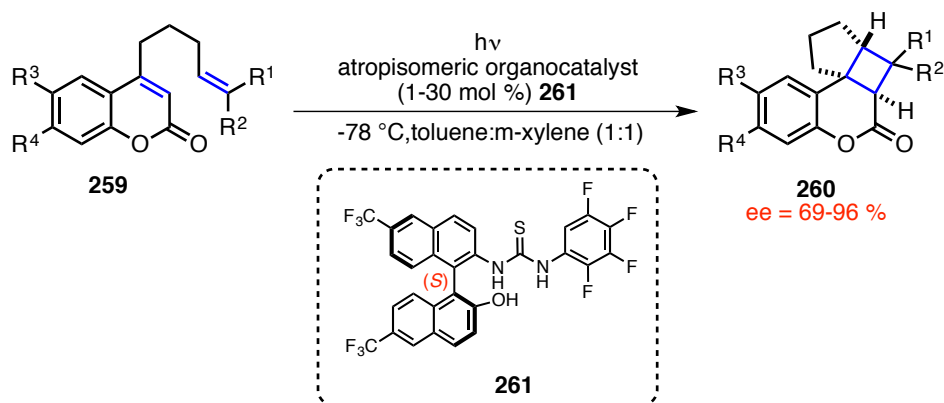
Scheme 5.17: Enantioselective [2+2]-photocycloaddition of coumarin derivatives **259** catalyzed by atropisomeric H-bonding catalyst **261**.

Bach and coworkers have showcased the utility of templated photocatalysis by the use of H-bonding Kemp triacid-based catalyst (KT). They have reported high enantioselectivity (~92% ee) in [2 + 2] photocycloaddition of quinolinone derivative **262** to afford the tetracylic lactam based photoproduct **263** (Scheme 5.18).[33,53-55]
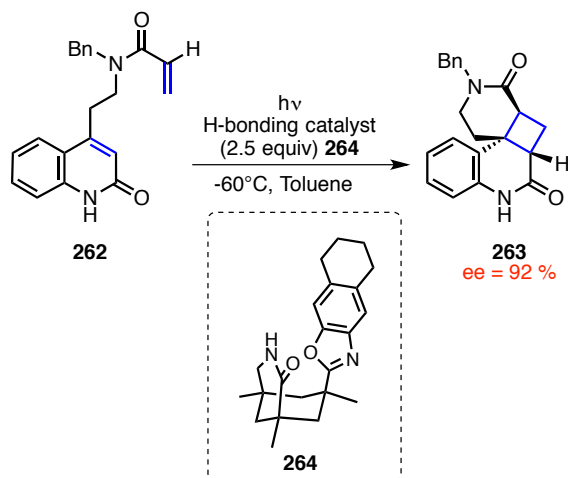
Scheme 5.18: Enantioselective [2+2]-photocycloaddition of quinolinone derivatives **262** catalyzed by H-bonding catalyst **264**.

The present work focuses on exploring optically pure atropisomers and evaluating them towards stereospecific [2 + 2] photocycloaddition. Following those lines, we explored the literature and found that Sivaguru and coworkers have showcased numerous exemplars utilizing atropisomeric scaffolds to achieve very high enantioselectivity in photoproduct. Their first report on intramolecular atropselective [2 + 2] photocycloaddition was on optically pure 3,4-dihydro-2-pyridones **265** (Scheme 5.19). The photocycloaddition proceeded with a very high diastereoselectivity (de > 96%) and high enantioselectivity (ee > 98%) in solution to achieve the cyclobutane-based photoproduct **266**-**267**.[56] A medium pressure Hg lamp fitted with a pyrex cut-off filter was utilized as the light source. The photocycloaddition reactions were carried out in the presence of an appropriate triplet sensitizer to populate the triplet of the enamide photochromophore. In their following communication Sivaguru and coworkers investigated Paternò-Büchi reaction of optically pure α-oxoamides **268** (Scheme 5.20).[57] In their study they employed non-biaryl photochromophore for stereospecific Paternò-Büchi reaction to achieve selectivity both in solution and in the solid-state.
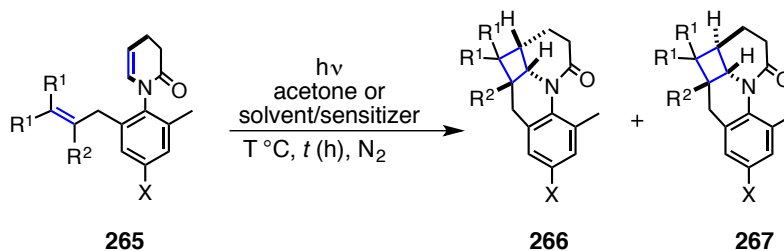
Scheme 5.19: Atropselective [2+2] photocycloaddition of atropisomeric dihydro-2-pyridones **265** in solution.
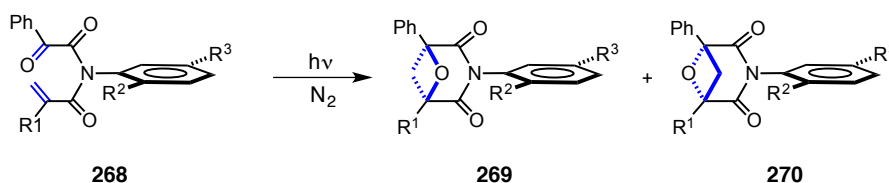
Scheme 5.20: Atropselective [2+2] photocycloaddition of atropisomeric dihydro-2-pyridones **268** in solution and crystalline environment.

The light source employed was either a medium pressure Hg lamp fitted with a pyrex cut-off filter or a Rayonet reactor equipped with ~350 nm tubes. The appropriate source of irradiation excited the keto-amide chromophore of atropisomeric *o-tert*-butyl substituted α-oxoamide. It is the half filled π* orbital of the excited keto-amide photochromophore that triggers the reaction by an intramolecular charge transfer to the π* (LUMO) of the electron deficient alkene leading to oxetane based photoproduct **269** or **270**.[58-59]

The photoreactions proceeded with low to moderate diastereoselectivity and with high enantioselectivity (ee > 97 - 99%) in solution and in solid state. These results prompted us to explore the outcome of [2+2] photocycloaddition in atropisomeric *o-tert*-butyl substituted acrylimides as it will enable us to access cross cyclobutane photoproducts which has are synthetically useful scaffolds.[60] Stanek and coworkers have shown the cross cyclobutane based compounds (Scheme 5.21) to be an effective aromatase inhibitor.[60] Inhibition of aromatase enzyme (a cytochrome P_{-450} dependent enzyme) has been shown to be of practical importance for the treatment of hormone dependent tumors.[60]

aminoglutethimide (AG)
271

3-azabicyclo[3.1.1]heptane-2,4-dione derivative(s)
272
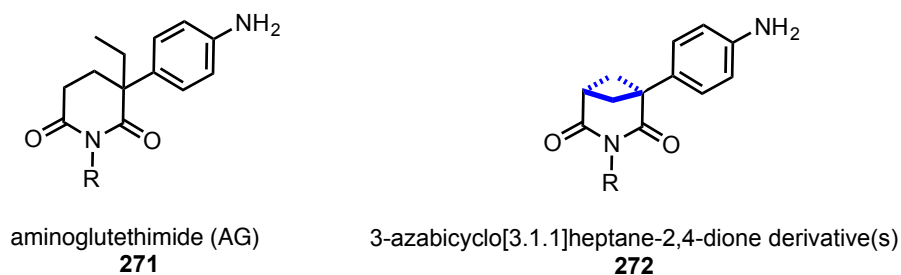
Scheme 5.21: Structure of inhibitors investigated for aromatase inhibition by Stanek et al. (reference 54).

In the study reported by Stanek and coworkers, the activity of cyclobutane-based derivatives were found to be more potent than clinically effective agent aminoglutethimide (AG, Table 5.5).[60]

Table 5.5: Activity of cyclobutane based derivatives towards aromatase enzyme studied in vitro.

Entry	Compound	R	aromatase IC_{50},[a] μmol	Inhibition potency
1	**266a**	H	2.0	0.95
2	**266b**	n-C_3H_7	0.111	17
3	**266c**	$CH_3CH(CH_3)_2$	0.062	30
4	**266d**	n-C_5H_{11}	0.031	61
5	**266e**	n-C_7H_{15}	0.049	39
6	**266f**	n-$C_{10}H_{21}$	0.225	8.5
7	**266g**	n-C_6H_{11}	0.013	140
8	**266h**	$CH_2C_6H_{11}$	0.097	20
9	**265** (AG)	-	1.9	1

[a] Androstenedione as substrate.

In order to broaden the scope of chiral cyclobutane adducts and for developing mechanistic insights highlighting the role of restricted bond rotations in dictating the stereochemical course of the reaction we became interested to study stereospecific cycloaddition of acrylimide photochromophores (Scheme 5.22).
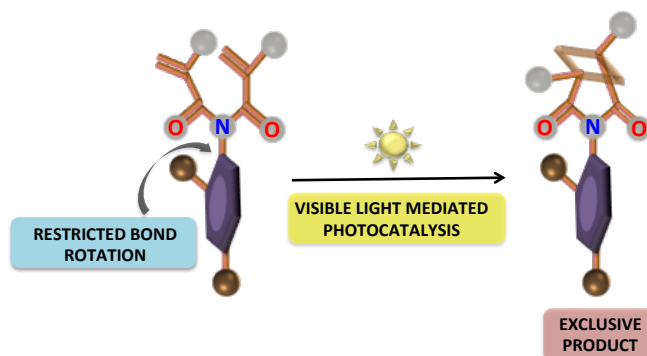
Scheme 5.22: Schematic representation of [2+2] photocycloaddition of atropisomeric acrylimides.

5.3.2. [2+2] Photocycloaddition of acrylimides

The first report on photocycloaddition of acrylimides came in the year 1965 from Lalonde et al.[61] The group studied *N,N*-dimethylacrylylmethacrylamide **273** that underwent [2+2] photocycloaddition to afford cross-addition product in moderate yields (Scheme 5.23). Later Mukuyama and Ishitoku reported a straight addition product for [2+2] photocycloaddition of *N*-methylmethacrylamide.[62] This report was objected from an independent investigation performed by Bellus and coworkers who confirmed the cross-addition product irrespective of the irradiation conditions with aid of various spectroscopic techniques.[63] The controversial reports in the literature on acrylimide photochromophore intrigued us, as it is one of the few systems documented in the literature that leads to cross-addition product. For a typical [2+2] photocycloaddition the straight addition photoproduct is generally preferred in solution and has extensive literature precedence.[64-65]
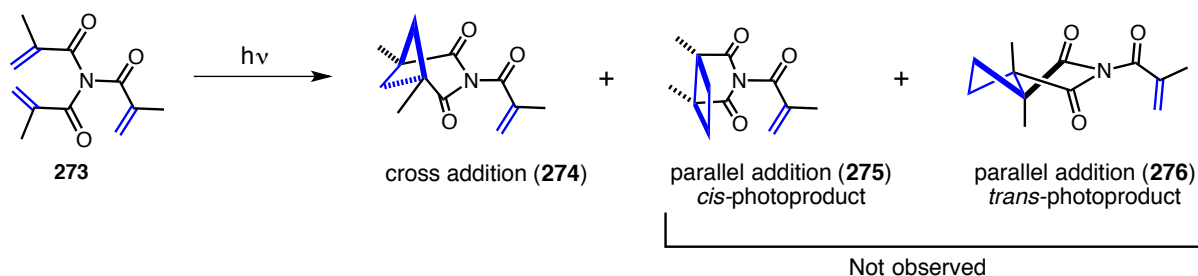
Scheme 5.23: [2+2] Photocycloaddition of *N,N*-dimethylacrylylmethacrylamide **273** reported by Lalonde et al. (reference 55).

The newly synthesized atropisomeric acrylimides and their intermediates are listed in the following Chart 5.1. The atropisomeric acrylimides **279a-b** was synthesized by a two-step sequential acylation from the corresponding aniline derivative and were completely characterized by both NMR spectroscopy, mass spectrometry and single crystal XRD analysis. HPLC analysis confirmed *P* and *M* stereoisomers of **279a-b** originated due to the restricted bond rotation around *N*-C(aryl) axis. *P* and *M* isomers were separated using HPLC on a chiral stationary phase. The optical purity of the isomers was ensured by analysis on a chiral stationary phase.

277   **278**   **279**

a) R^1 = ^{t}Bu; R^2 = H
b) R^1 = ^{t}Bu; R^2 = ^{t}Bu
c) R^1 = R^2 = H

Photoproducts:

280   **281**

a) R^1 = ^{t}Bu; R^2 = H
b) R^1 = ^{t}Bu; R^2 = ^{t}Bu
c) R^1 = R^2 = H

Cleaved photoproducts:

X = H, **282a**
X = ^{t}Bu, **286b**

X = H, **283a**
X = ^{t}Bu, **287b**

284a   **285a**
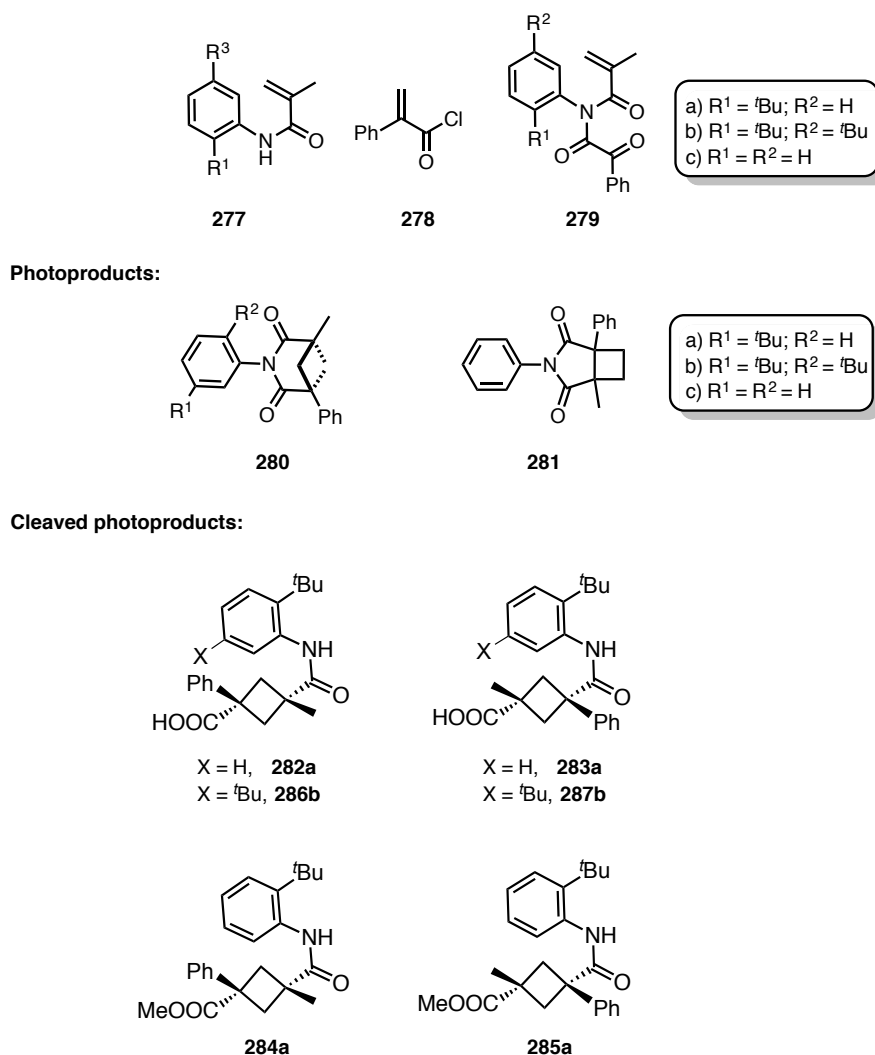
Chart 5.1: Structures of acrylimides **279a-c**, their corresponding photoproducts and the precursors/reactants employed in the study.

5.3.3. Racemization barrier in atropisomeric acrylimides

The temperature at which an optically pure atropisomeric compound undergoes racemization in a given solvent has serious implication on the course of atropselective photoreaction. Racemization can lead to loss of absolute configuration of the atropisomer thus leading to poor selectivity in the desired stereospecific photoreaction. It was therefore important for us to ascertain energy barrier for N-C(aryl) rotation in atropisomeric acrylimides. Due to slow racemization of the optically pure compounds at room temperature, we carried out racemization kinetics of **279a-b** at 45 °C in polar green solvents like acetonitrile (MeCN) and methanol (MeOH). Enantiomeric excess (ee) was monitored using HPLC on a chiral stationary phase over time. The first order kinetic plot of ln(%ee) vs. time (days) gave the rate constant for racemization (k_{rac}). The activation energy barrier, half-life and rate for racemization were calculated from the following equation.[66]

$$k_{rac} = k\left(\frac{k_B T}{h}\right) e^{-\Delta G^{\ddagger}_{rac}/RT}$$

$$\text{and } \Delta G^{\ddagger}_{rac} = -RT \ln\left(\frac{h k_{rac}}{kT k_B}\right)$$

(Equation 5.3)

The half-life of racemization ($\tau_{1/2rac}$), was calculated using the rate constant of racemization k_{rac} (assuming 1-P_0 = 0 at t = 0).

$$\ln\left(\frac{\omega_{eq}}{\omega_{eq} - \omega}\right) = \ln\left(\frac{R_0}{2R - R_0}\right) = \ln\left(\frac{R + S}{R - S}\right) = 2k_{enant} t$$

$$\text{and } \ln\left(\frac{R_0}{R_0 - \omega}\right) = k_{rac} t$$

(Equation 5.4)

Where,

$k_{rac} = 2k_{enant}$; R_0 is the initial concentration of the (R)-enantiomer;

$\omega = R_0 - R$, S (concentration of the racemate at time t); and

k_{rac} is the rate constant for racemization

Note: $R_0 = R + S$

At 50% ee, the equation becomes:

$$\tau_{1/2\,rac} = \frac{\ln 2}{2k_{enant}} \text{ or } \frac{\ln 2}{k_{rac}}$$

(Equation 5.5)

Inspection of Table 5.6 reveals a racemization barrier ($\Delta G^{\ddagger}_{rac}$) of ~26 kcal/mol for the atropisomeric acrylimides **279a-b** with half-life of 1-2 days at 45 $^{\circ}$C in polar solvents. This suggested that atropisomeric acrylimides could be employed for stereospecific photocycloaddition reactions at room temperature without any loss of axial chirality.

Table 5.6: Rate constant, half-life and energy barrier for racemization on atropisomeric acrylimides **279a-b**.[a]

Entry	Compound	Solvent	Kinetic parameters		
			$\tau_{1/2}$ (days)	k_{rac} (s^{-1})	$\Delta G^{\ddagger}_{rac}$ (kcal·mol^{-1})
1	**279a**	MeCN	2.0	4.1×10^{-6}	26.5
2		MeOH	1.9	4.3×10^{-6}	26.5
3	**279b**	MeCN	1.1	7.2×10^{-6}	26.1
4		MeOH	0.9	8.6×10^{-6}	26.0

[a] Values carry an error of ±5%. The racemization kinetics was followed by HPLC analysis on a chiral stationary phase at 45 °C.

5.3.4. Intramolecular [2+2] photocycloaddition of acrylimides 279a-c
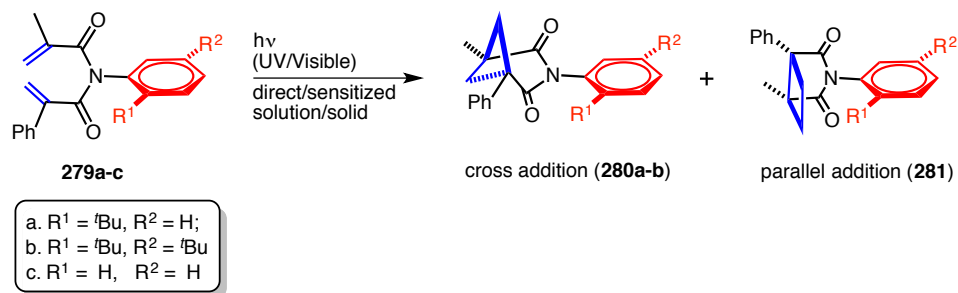
Scheme 5.24: Intramolecular [2+2] photocycloaddition of atropisomeric acrylimides **279a-c**.

In order to evaluate the influence of restricted *N*-C(aryl) bond rotation in solution, we carried out the photoreaction of both atropisomeric **279a-b** and achiral acrylimide **279c** in isotropic media. [2+2]-Photocycloaddition of acrylimides **279a-c** was carried out under different sources of irradiation and was found to proceed smoothly with excellent isolated yields. Three different sets of irradiation conditions were examined *viz.,* a) direct irradiation; b) sensitized irradiation under UV light and c) sensitization under visible light irradiation. After performing the photoreaction, the solvent was removed under reduced pressure and the photoproduct(s) were purified by column or preparative thin layer chromatography. The purified photoproduct(s) were characterized by NMR spectroscopy and HRMS. The enantiomeric excess (ee) in the photoproduct(s) was determined by HPLC analysis on a chiral stationary phase.

Atropisomeric acrylimides **279a** was employed as a model system to optimize the irradiation conditions (Table 5.7). Direct irradiation was carried out using a 450 W medium pressure Hg lamp placed inside a water-cooled jacket with a Pyrex cut off filter or by using a Rayonet reactor equipped with 254 nm tubes (16 tubes × 14 Watts) in acetonitrile under constant flow of nitrogen. In the case of atropisomeric acrylimides **279a-b**, the cross [2+2] photocycloaddition product was formed exclusively as the major product in both MeOH and MeCN with excellent mass balance and conversion. The reaction was found to be very efficient upon changing the irradiations source from a 450 W medium pressure Hg lamp or a Rayonet reactor equipped with 254 nm tubes. The efficiency of the photocycloaddition was unaffected under oxygen (Table 5.7 - entry 3; 68% conversion in 5 min of irradiation) when compared to conversion under nitrogen atmosphere (Table 5.7 - entry 3; 71% conversion in 5 min of irradiation).

Table 5.7: Intramolecular [2+2] photocycloaddition of acrylimides **279a-c**.[a]

Entry	Compd	Irradiation conditions [b]	% Conversion[d]	280:281 [f]
1		Direct irradiation, bb - Pyrex cutoff / 3 h MeCN / N$_2$	97	78
2		Direct irradiation, RR, 254 nm / 5 min / MeCN / N$_2$	71 (70) [e]	
3		Direct irradiation, RR, 254 nm / 5 min / MeCN / O$_2$	68	90
4	**279a**	Direct irradiation, bb - Pyrex cutoff / 3 h / Acetone [c] / N$_2$	100	
5		Benzophenone (10 mol%) / RR ~350 nm / MeCN / 3 h / N$_2$	100	81
6		Xanthone (10 mol%) / RR ~350 nm / 1.5 h / MeCN / N$_2$	100 (71) [e]	
7		Xanthone (10 mol%) / RR ~350 nm / 30 min / MeOH / N$_2$	100	78
8		Thioxanthone (10 mol%) / ~420 nm/ 15 min / MeCN / N$_2$	100	
9		Xanthone (10 mol%) / RR ~350 nm / 1.5 h / MeCN / N$_2$	100 (86) [e]	-
10	**279b**	Xanthone (10 mol%) / RR ~350 nm / MeOH / 30 min / N$_2$	100	-
11		Thioxanthone (10 mol%) / RR ~420 nm / 15 min / MeCN / N$_2$	58	30
12		Xanthone (10 mol%) / RR ~350 nm / 3 h / MeCN / N$_2$	100	
13	**279c** [f]	Xanthone (10 mol%) / RR ~350 nm / 1.5 h / MeCN / N$_2$	100	
14		Xanthone (10 mol%) / RR ~350 nm / 30 min / MeOH / N$_2$	100 (78) [e]	
15		Thioxanthone (10 mol%) / RR ~420 nm / 15 min / MeCN / N$_2$	60	

[a] Irradiation at room temperature unless otherwise noted. Values based on ^{1}H-NMR spectroscopy (±5% error). [**279a**] = 2.88 mM, [**279b**] = 2.48 mM and [**279c**] = 3.43 mM. [b] bb = broadband irradiation performed using 450W mercury lamp with a Pyrex cutoff filter (< 295 nm cutoff); RR = Rayonet reactor equipped with either 254 nm or ~300 nm or ~350 nm or ~420 nm light (16 tubes × 14 Watts). [c] Acetone as solvent and sensitizer. [d] % conversion and mass balance calculated by ^{1}H-NMR spectroscopy using Ph$_3$CH as internal standard. [e] Isolated yield. [f] The values were similar to the one reported in literature for other achiral acrylimides with *N*-aryl substitution. The major and minor photoproducts were assigned based on similarities in ^{1}H and ^{13}C NMR resonances in the reaction mixture. The major photoproduct was characterized by single crystal XRD.

To channel the [2+2] photocycloaddition via triplet excited state, we employed sensitized irradiation using triplet sensitizers of varying triplet energies (E_T) between 78 kcal/mol to 63 kcal/mol.[67] The photocycloaddition was found to be efficient under continuous flow of nitrogen in acetone (E_T between 78 kcal/mol, acting as both solvent and sensitizer) and with benzophenone (10 mol%, E_T between 73 kcal/mol) in MeCN. The photoreaction was equally efficient in MeCN upon changing triplet sensitizer to xanthone (~350 nm irradiation). Visible light irradiation (~420 nm irradiation) with thioxanthone as the photosensitizer afforded the cross photoproduct in ~15 min. Large scale photoreaction of atropisomeric acrylimide **279a** using thioxanthone was performed in gram scale in a round bottom flask with compact fluorescent lamp as the source of illumination (refer to experimental section). The photoreaction of was clean and efficient under triplet sensitization using an artificial visible light source with very high isolated yields in photoproduct (80-90%).

Table 5.8: Enantiospecific intramolecular [2+2] photoreactions of acrylimides **279a-b**. [a]

Entry	Compound	Atropisomer [b]	Solvent	% ee (**280a**)[d]	t (h) [c]
1		*M* - isomer	MeCN	98	1.5
2	**279a**	*P* - isomer	MeCN	98	1.5
3		*M* - isomer	Solid-State	99	11
4		*P* - isomer	Solid-State	99	11
5	**279b**	Pk-A	MeCN	99	1.5
6		Pk-B	MeCN	99	1.5

[a] Irradiation at room temperature using Rayonet reactor equipped with ~350 nm light tubes (16 tubes × 14 Watts) using 10 mol% of xanthone as the triplet sensitizer under constant purging of N_2. [**279a**] = 2.88 mM and [**279b**] = 2.48 mM. [b] Pk-A and Pk-B refers to the elution order of the peaks for a given pair of enantiomers/atropisomers. [c] Photolysis time. [d] ee values (error of ±3%) from HPLC analysis on a chiral stationary phase (Chiralpak IC for **279a** and RR-WHELK-01 for **279b**) with hexanes/2-propanol as mobile phase.

Atropisomeric acrylimides **279a-b** afforded the exclusive formation of cross [2+2]-photocyclized product in excellent isolated yields. The irradiation of achiral imide **279c** on the other hand resulted in both cross and straight [2+2]-photocyclized products. The *N*-C(aryl) restricted bond rotation was responsible for the observed regioselectivity for **279a-b** leading to the exclusive formation of cross [2+2]-photocyclized product. We also evaluated the stereochemical outcome of [2+2] photocycloaddition of optically pure atropisomers of **279a-b** under triplet sensitized conditions with ~350 nm irradiation for xanthone and ~420 nm irradiation for thioxanthone (Table 5.8). HPLC analysis of the reaction mixture revealed a high ee value (>99%) in the photoproduct **280**, highlighting the role of axial chirality in photoreaction. An important point to note is that the cross photoproduct **280** was favored (**280**:**281** = >99:1) with both direct and sensitized irradiations with excellent conversions and high mass balance for axially chiral acrylimides.

As we were able to obtain single crystals of atropisomeric acrylimide **279a**, we investigated the photocycloaddition in the solid state. Single crystal X-ray analysis of the individual atropisomers of the atropisomers of **279a** (4:1 hexanes:chloroform as the crystallizing solvent mixture) provided us with insights into the reactivity in the solid-state. The absolute configuration of individual atropisomers of **279a** (Figure 5.14) was established by Flack parameters.
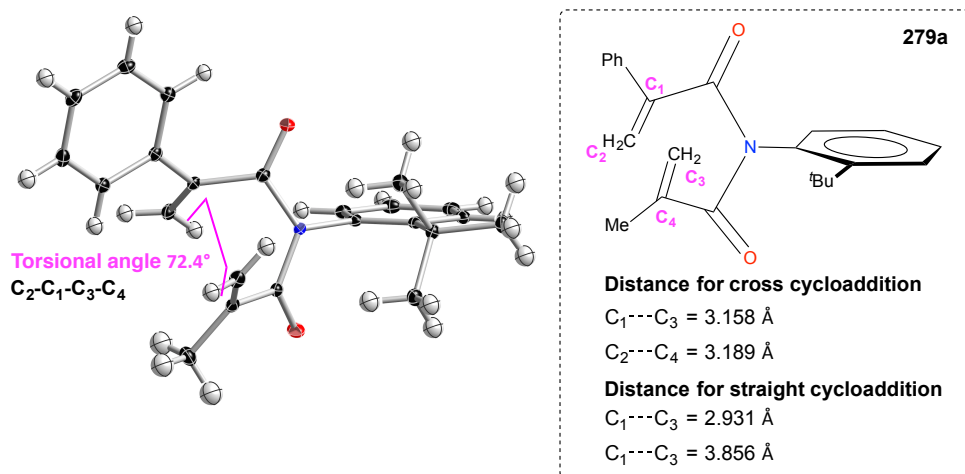
Figure 5.14: Single crystal X-ray structure of **279a**.

Single crystal X-ray structure analysis of the enantiomers of **279a** revealed that the *N*-aryl substituent was perpendicular to the plane of CO-*N*-CO unit. The distance between the alkene carbons is required to be within 4.2 Å (Schmidt distance) for the [2+2]-photoreaction to occur in the solid-state. For acrylimides to afford straight addition product from solid-state photoreaction, the bond formation upon photo-excitation has to occur between the two internal alkene carbon atoms and the two terminal carbon atoms (Figure 5.14-inset. X-ray structure of optically pure **279a** shows that the distance between the two internal alkene carbons i.e., the distance between the C_1 and C_4 carbon is 2.931 Å and the distance between the terminal alkene carbons i.e., the distance between the C_2 and C_3 carbon is 3.856 Å. For cross [2+2]-photocycloaddition of acrylimides, the bond formation upon photo excitation has to occur between the internal alkene carbon and the terminal carbon atom. Examination of the single crystal X-ray structure of **279a** shows that the distance between the internal alkene carbon bearing the phenyl substituent and the terminal alkene carbon bearing the methacryloyl functionality (i.e., the distance between the C_1 and C_3 carbon) is 3.158 Å.

The distance between the internal alkene carbon bearing the methyl substituent and the terminal alkene carbon of the phenylmethacryloyl functionality (i.e., the distance between the C_2 and C_4 carbon) is 3.189 Å. The bond distances for straight addition and cross [2+2]-photocycloaddition are within the Schmidt distance for photoreaction within the solid-state. Additionally, the torsional angle between the double bonds (C_2-C_1-C_3-C_4 torsion angle) was 21.7°. Since the reactive double bonds were within the Schmidt distance, it opened up the possibility to investigate the influence of crystalline environment on the photochemical reactivity of atropisomeric acrylimides.

Optically pure crystals of **279a** were irradiated at room temperature on a Petri dish using a Rayonet reactor equipped with 254 nm tubes (16 tubes × 14 Watts). The reaction was clean with an exclusive formation of the cross photocycloaddition product that was characterized by NMR spectroscopy. The enantiomeric excess of the photoproduct was established by HPLC analysis on a chiral stationary phase that gave enantiomeric excess (ee) of 98% for the photoproduct. To our surprise the cross photoadduct was formed in contrast to straight photoadduct in the solid state as the shortest distance was between C_2 and C_3 (2.931 Å; Figure 5.14). On the other hand, for the formation of the cross photoadduct, the shortest distance was between C_2 and C_3 of 3.158 Å.

The exclusive formation of cross [2+2] photocycloadduct **280a** in the solid state was due to the minimum atomic movements required for the formation of the photoproduct, while the formation of straight [2+2] photoadduct would require drastic atomic movements that would not be preferred within the confined environment of a crystalline matrix. We looked at the excited state of the acrylimide chromophore to develop a quantitative model for understanding the photochemical reactivity of acrylimides leading to cross cyclobutane photoproduct.

5.3.5. Mechanistic rationale for [2+2] photocycloaddition of atropisomeric acrylimides

Based on the single crystal X-ray structure of **279a**, the orbital density in the gas phase was computed using Gaussian 09 at B3LYP/6-31G* level of theory,[68] that showed the excitation was localized at the styrene chromophore (Figure 5.15). One has to be cognizant of the fact that the excited state may have slightly different structure than the ground state in the crystalline environment; one can qualitatively understand the reactivity and/or selectivity.

Torsional angle 72.4°
C₂-C₁-C₃-C₄

279a

Distance for cross cycloaddition
C$_1$---C$_3$ = 3.158 Å
C$_2$---C$_4$ = 3.189 Å
Distance for straight cycloaddition
C$_1$---C$_3$ = 2.931 Å
C$_1$---C$_3$ = 3.856 Å

HOMO   **LUMO**   **LUMO+1**
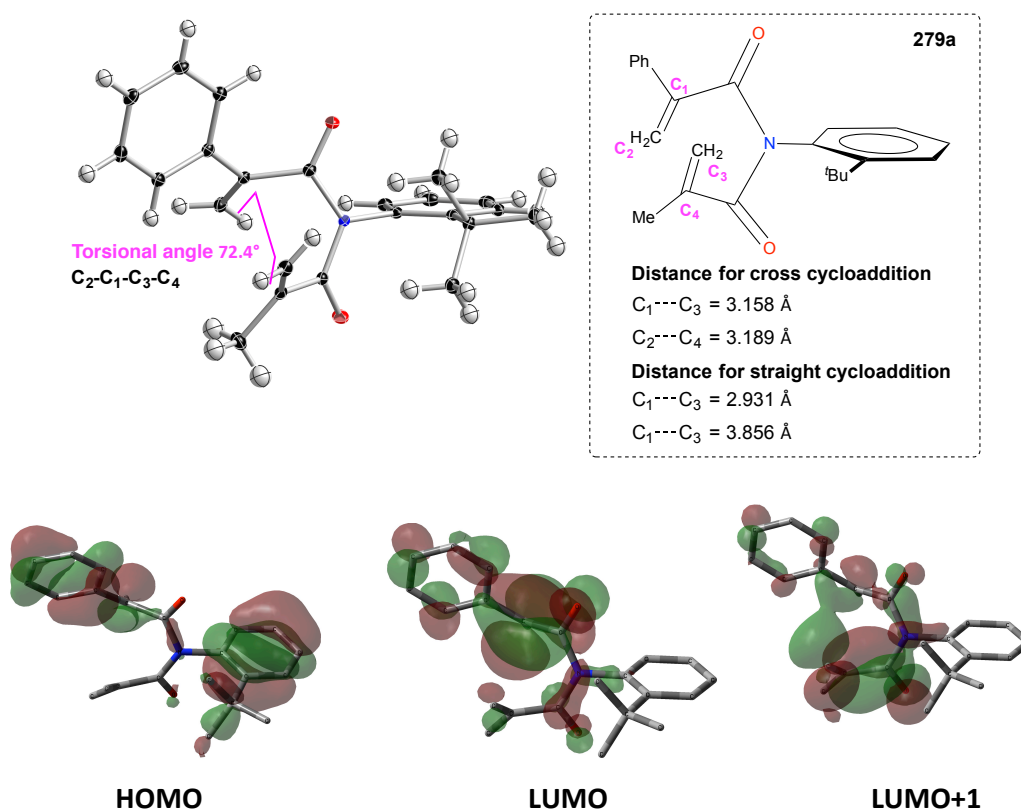
Figure 5.15: Understanding photochemical reactivity based on orbital density computed with Gaussian 09 at B3LYP/6-31G* level.

In accordance to the well established photochemical paradigms[69] for [2+2]-photocycloaddition between electron deficient alkenes, it is likely that the half filled π* orbital of the styrene (conjugated alkene) motif would trigger the photoreaction by interacting with the π* (LUMO) of the electron deficient double bond of methacryloyl unit leading to the photoproduct. In addition, the mixing of the $S_2(\pi\pi^*)$ state will impart a zwitterionic nature.

Due to $\pi\pi^*$ excitation, the electron poor nature of the reactive alkene double bond will interact with the doubly occupied orbital of the zwitterionic species that decays to the photoproduct ($S_1 \rightarrow I(Z)$ or $CI \rightarrow P$). The $\pi^*_{C1=C2} \leftarrow \pi^*_{C3=C4}$ interaction has important consequences on the stereochemical features of the photoproduct as they will be dictated by the orbital overlap (Figure 5.15). A good overlap between the $\pi^*_{C1=C2}$ and $\pi^*_{C3=C4}$ orbitals would initiate the reaction leading to photoproduct formation. Based on the orientation of the double bonds, it is likely that the interactions of the terminal alkene carbon of the methacryloyl unit (C_3 carbon) and the benzylic carbon of the styrene unit (C_1) would initiate the photocycloaddition that locks the conformation leading to cross cyclobutane photoproduct.

5.3.6. Photophysical studies of [2+2] photocycloaddition of atropisomeric acrylimides

Detailed photophysical investigations were carried out to gain more insights into the cross [2+2] photocycloaddition of atropisomeric acrylimides with **279a** as the model system. Steady state luminescence measurements on **279a** were futile as they showed negligible luminescence both at room temperature in solution and at 77 K in solid matrix due to fast decay of excited states. To overcome this limitation, transient absorbance spectra of **279a** was recorded (Figure 5.16) in argon saturated acetonitrile solution using laser flash photolysis (λ_{ex} = 266 nm, 5 ns pulse width).
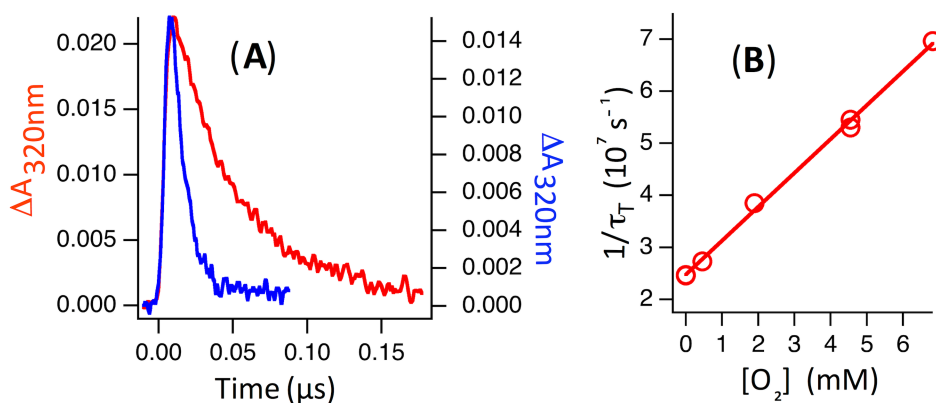
Figure 5.16: (A) Transient absorbance decay traces of **279a** triplet states in argon (red) or oxygen (blue) saturated acetonitrile solutions using laser flash photolysis (λ_{ex} = 266 nm, 5 ns pulse width) monitored at 320 nm. (B) Determination of the bimolecular quenching rate constant k_q of acrylimide **279a** triplet states by molecular oxygen from the slope of the plot of the inverse triplet lifetime vs [O_2].

The concurrent generation of singlet oxygen (Δ^1O_2) was observed by the characteristic phosphorescence at 1270 nm (Figure 5.17). One of the photochromophore in **279a** is styrene skeleton that is known to show triplet-triplet absorption at ~320 nm.[70] Based on oxygen quenching experiment, singlet oxygen generation and similarities with the triplet absorption of styrene, we have assigned the transient absorption shown in Figure 5.17, (C) to the triplet absorption of **279a**. A similar transient absorption was centered at ~320 nm for laser excitation (266 nm) of **279b** and **279c** (refer to experimental section). The atropisomeric acrylimide **279b** having similar structural make-up to that of **279a**, showed a triplet lifetime (τ_T) of 41 ns that was comparable to the τ_T of **279a**, whereas the triplet lifetime of acrylimide **279c** was significantly shorter (~20 ns). The shorter triplet lifetime of **279c** compared to **279a/279b** can be attributed to the free rotation of the N-C(aryl) bond.
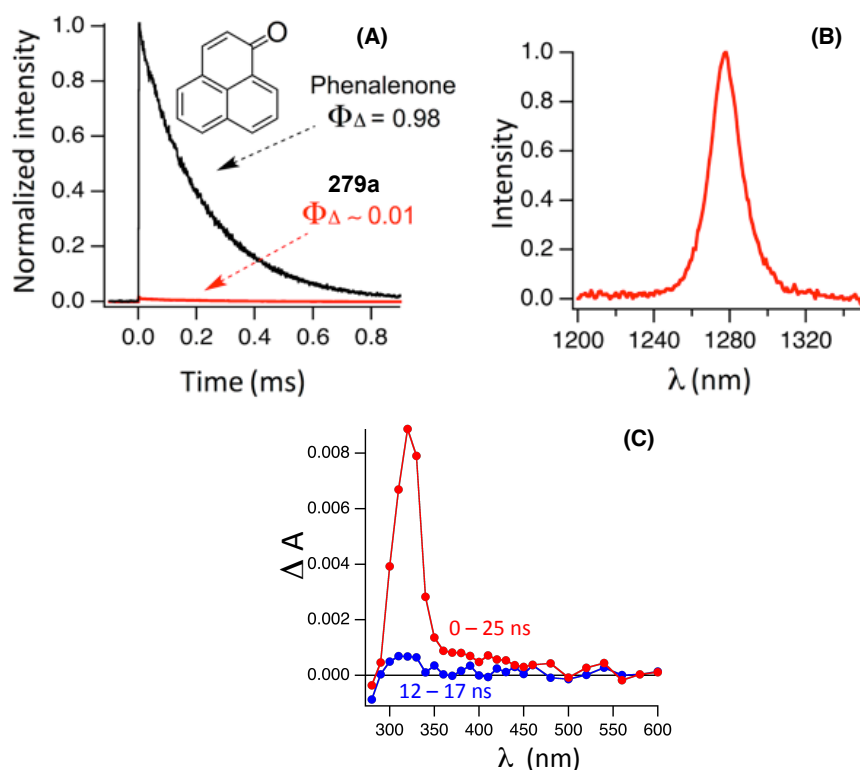
Figure 5.17: (A) Singlet oxygen phosphorescence decay traces monitored at 1270 nm generated by pulsed laser excitation (λ_{ex} = 266 nm, 5 ns pulse length) of O_2 saturated CCl_4 solutions of acrylimide **279a** or phenalenone with matching optical density of 0.3 at 266 nm. (B) Singlet oxygen phosphorescence spectrum generated by steady-state irradiation (355 nm) of acrylimide **279a** in O_2 saturated CCl_4 solution. (C) Transient absorption decay traces of **279a** at 266 nm in argon saturated solution using laser flash photolysis.
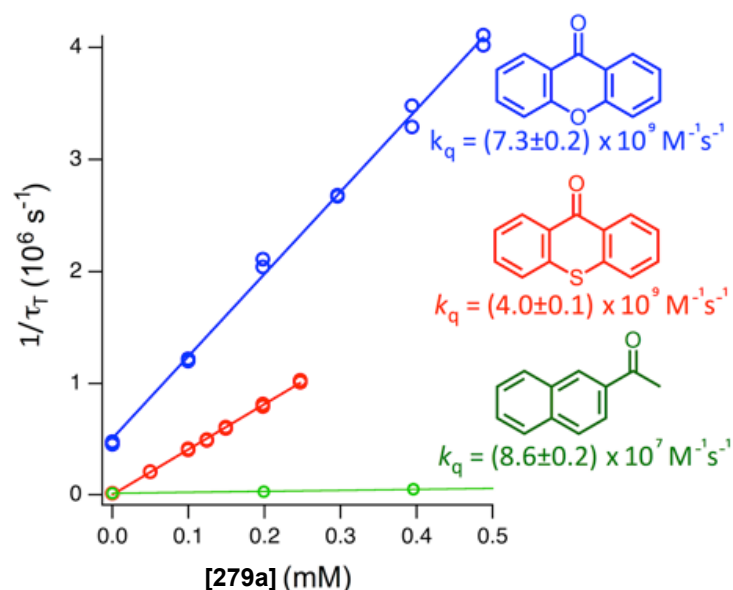
Figure 5.18: Determination of the bimolecular quenching rate constants k_q of sensitizer triplet states by acrylimide **279a** using laser flash photolysis (λ_{ex} = 355 nm, 7 ns pulse width). Plot of inverse triplet lifetime determined from triplet absorption decay traces monitored at 620 nm for xanthone (blue) and thioxanthone (red) and 425 nm for 2-acetonaphthone (green) with varying concentration of **279a** in argon saturated acetonitrile solutions.

Since the photocycloaddition of acrylimides was more efficient in the presence of triplet sensitizers, such as xanthone (~350 nm irradiation) and thioxanthone (~420 nm irradiation) we studied the energy transfer kinetics by laser flash photolysis. The bimolecular rate constants of quenching of sensitizer triplet states by **279a** were determined by monitoring the sensitizer triplet absorption decays after pulsed laser excitation (355 nm) in the presence of varying concentrations of **279a**. The slope obtained from the plot of the inverse sensitizer triplet lifetime ($1/\tau_T$) vs. the quencher concentration [**279a**] gave the bimolecular quenching rate constants (Figure 5.18). For xanthone as the triplet sensitizer, which has a triplet energy of E_T ~73 kcal/mol,[26] a rate constant close to the diffusion limit of k_q = 7.3±0.2 × 10^9 $M^{-1}s^{-1}$ was observed (Figure 5.18, blue). In case of thioxanthone (E_T ~63 kcal/mol),[26] k_q decreased by approximately half to 4.0±0.1 × 10^9 $M^{-1}s^{-1}$ (Figure 5.18, red). On resorting to 2-acetonaphthone as the sensitizer with low triplet energy (E_T ~59.5 kcal/mol),[26] a drop of two-order in magnitude was observed (k_q to 8.6±0.2 × 10^7 $M^{-1}s^{-1}$) (Figure 5.18, green). The dramatic decrease in quenching showed that the triplet energy of **279a** was close to 63 kcal/mol. This triplet energy is in agreement with the triplet energy of styrene (62 kcal/mol),[71] the main chromophore in acrylimides.

Photocycloaddition of acrylimides proceeds efficiently from the triplet state when a triplet sensitizer is used with sufficiently high triplet energy. An important question that remains unanswered is the nature of the reactive spin state (singlet or triplet excited state) that is responsible for reactivity upon direct irradiation of acrylimides to generate cross photocycloaddition products. Laser flash photolysis experiments showed that triplet states of **279a** are generated by direct excitation (Figure 5.18) that was quenched by molecular oxygen to produce singlet oxygen. The quantum yield of singlet oxygen generation (Φ_Δ) upon direct excitation of **279a** was estimated in oxygen saturated Carbon tetrachloride solution using phenalenone as the standard[72] and was found to be as low as ~ 0.01. Considering that not all triplet states of **279a** are quenched in oxygen saturated solutions due to the short triplet lifetime (Figure 5.18), the triplet quantum yield of **279a** is estimated to be in the order of Φ_T ~ 0.02. The low triplet quantum yield under direct irradiation is consistent with photoreaction studies in the absence and presence of molecular oxygen. Upon changing the reaction atmosphere from N_2 to O_2, only a 3% decrease in conversion was observed (which is within our experimental error).

If in case we overlook the experimental error and assume that the intersystem crossing to be compete, a concerted reaction from the singlet manifold to some degree, the 3% decrease could be attributed to the quenching of the triplet excited state upon direct irradiation. Based on low triplet quantum yield and relatively low impact of oxygen quenching on photoproduct yields, we hypothesize that upon direct excitation of **279a**, [2+2] photocycloaddition proceeds mostly from the singlet-excited state in a concerted fashion. The low triplet quantum yield is reasonable due to large singlet-triplet gap in $\pi\pi^*$ excited state of acrylimide that is similar to that of the styrene chromophore.

5.3.7. Synthetic transformation of cyclobutane based photoproduct
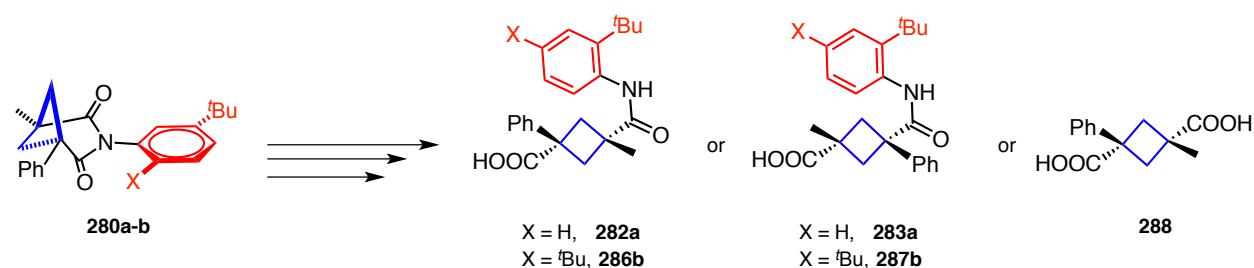
Scheme 5.25: Proposed synthesis of cyclobutane based product.

The [2+2] photocycloaddition of atropisomeric acrylimides provides a convenient access to exclusive formation of cross addition product. Cleavage of C-*N*(aryl) bond in the photoproduct can afford 1,3 disubstituted cyclobutanes. The 1,3 disubstituted cyclobutane derivatives are known to be potential receptors for lipid A.[73] A partial hydrolysis of photoproduct **280a-b** can lead to the formation of 1,3 disubstituted cyclobutanes (**282a/283a**) derivatives with an intact auxiliary (Scheme 5.25). There are numerous natural products possessing cyclobutane skeleton that have been accessed from 1,3 disubstituted cyclobutane derivatives. Baran and co-workers have extensively studied various 1,3 disubstituted cyclobutane derivatives to target several natural products (Scheme 5.26).[74-75] A similar work based on C-H arylation of 1-substituted cyclobutane derivatives for affording cyclobutane based natural products was reported by Babu and coworkers.[76]
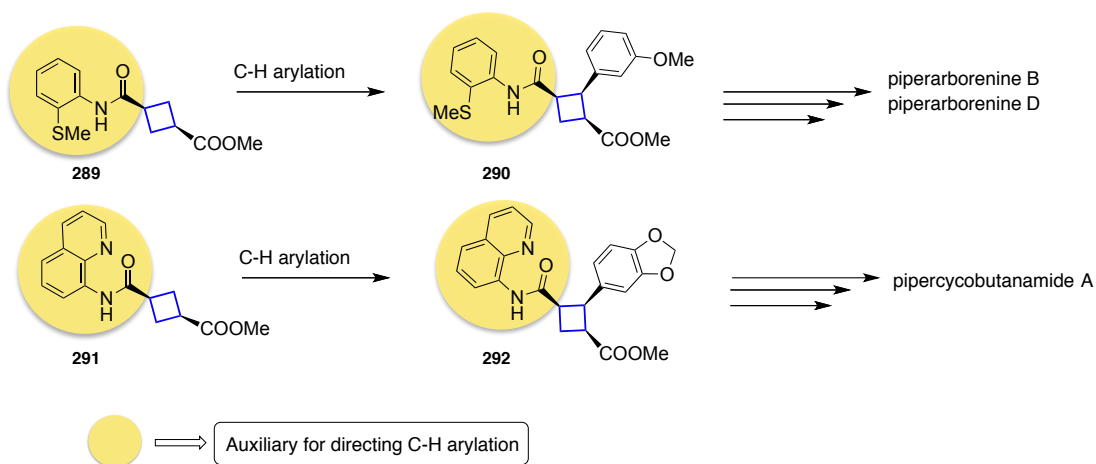
Scheme 5.26: Auxiliary directed approach for affording cyclobutane based natural products.

Knowing the potential utility of 1,3 disubstituted cyclobutanes we became interested to evaluate the outcome from the hydrolysis of photoproduct. Base catalyzed hydrolysis of photoproduct **280a** occurred in good yields and afforded a mixture of 1,3 disubstituted products (**282a/283a**) (Scheme 5.27). In order to further explore the scope of synthetic transformation we converted the acid mixture to the corresponding ester derivative. This work indicates the possibility of synthetic transformation of photoproducts to 1,3 disubstituted cyclobutane derivatives.
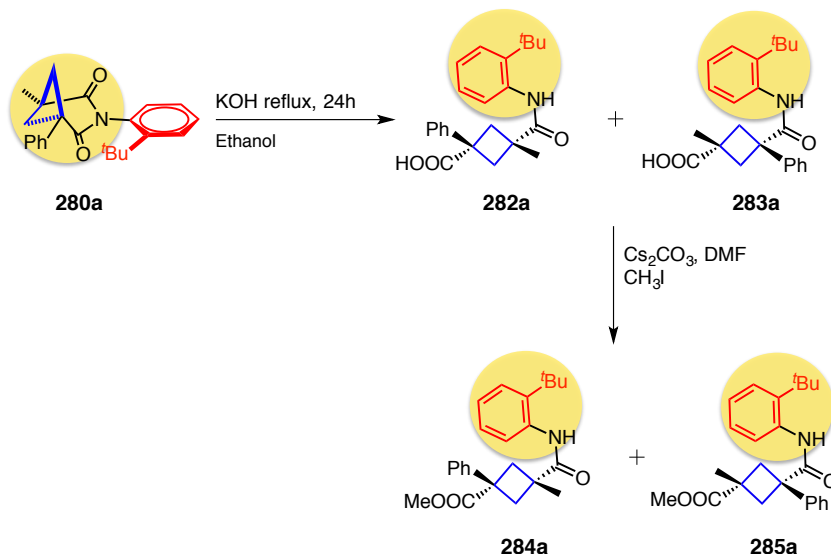
Scheme 5.27: Base hydrolysis of photoproduct to afford 1,3 disubstituted cyclobutane derivatives

We also attempted to remove the auxiliary (atropisomeric unit) to afford the corresponding 1,3 diacid derivative. The only report in literature on mild hydrolysis of aryl amides is reported by Cao and workers.[77] The group showcased a diverse range of aromatic amides underwent facile hydrolysis in the presence of thionyl chloride and pyridine to yield corresponding aniline based products (Scheme 5.28). The authors describe the reaction to involve a two-step protocol. Reaction of aromatic amides with thionyl chloride in the presence of pyridine gave chloro-imine **294** derivatives that hydrolyzed to yield the corresponding aromatic amine **295**.
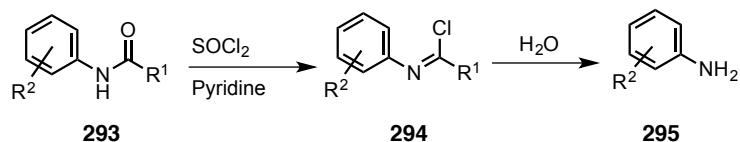
Scheme 5.28: Hydrolysis of aromatic amides using thionyl chloride and pyridine to yield aromatic anilines.

The hydrolysis of 1,3 disubstituted products (**284a/285a**) under the reported conditions by Cao and co-workers afforded a polar fraction that was difficult to interpret with all spectroscopic techniques. The reaction did not afford the desired 1,3 diacid derivative (Scheme 5.29).
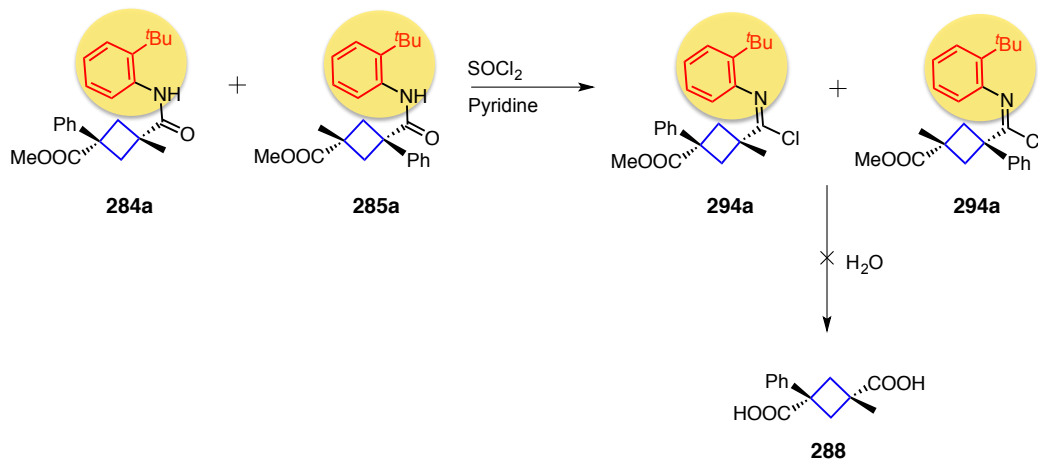
Scheme 5.29: Hydrolysis of 1,3-disubstituted cyclobutane derivative with thionyl chloride and pyridine.

5.3.8. X-Ray crystal structure data for atropisomeric acrylimide and its photoproducts

Structure determination: Single crystal XRD data of optically pure acrylimide **279a** was collected on a Bruker Apex Duo diffractometer with a Apex 2 CCD area detector at T = 100 K. Cu radiation was used for all the single crystal XRD analysis. All structures were processed with Apex 2 v2010.9-1 software package (SAINT v. 7.68A, XSHELL v. 6.3.1). Direct method was used for solving the structures after multi-scan absorption corrections.
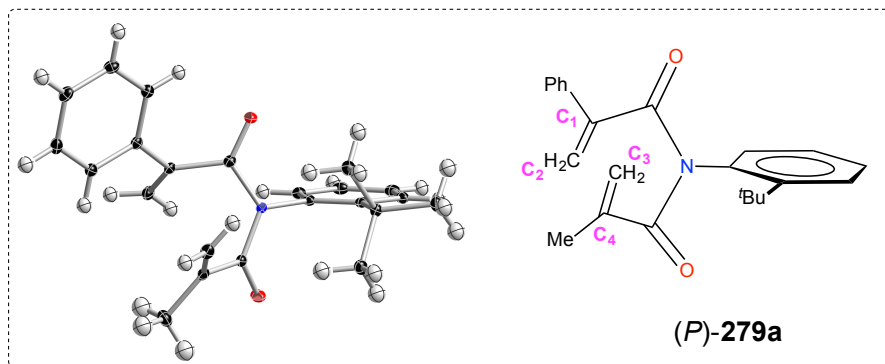
Figure 5.19: Acrylimide (*P*) – **279a** (crystallized from hexanes/chloroform).
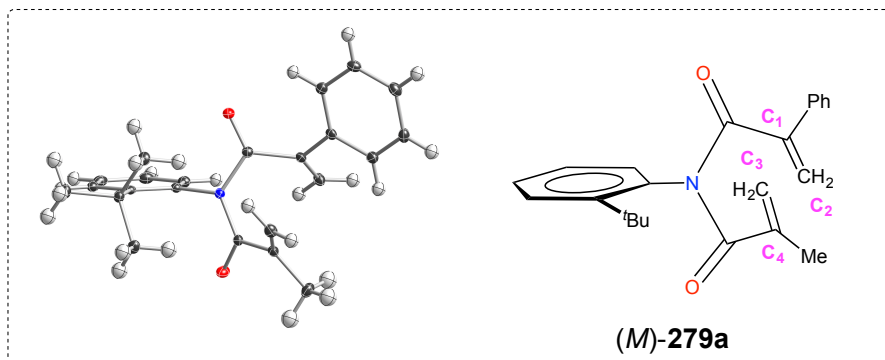
Figure 5.20: Acrylimide (*M*) – **279a** (crystallized from hexanes/chloroform).
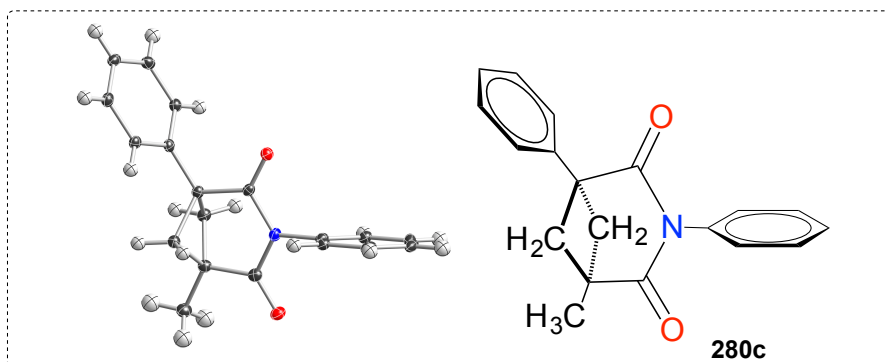
Figure 5.21: Photoproduct **280c** (crystallized from hexanes/ethylacetate).

473

Table 5.9: Structural parameters table for atropisomeric acrylimides $(P) - $ **279a**, $(M) - $ **279a** and achiral photoproduct **280c**.

Crystals	(P)- 279a	(M)- 279a	280c
Formula	$C_{23}H_{25}NO_2$	$C_{23}H_{25}NO_2$	$C_{19}H_{17}NO_2$
Formula Weight	347.44	347.44	291.33
Crystal size[mm^3]	0.232 × 0.095 × 0.035	0.3 × 0.14 × 0.065	0.189 × 0.102 × 0.049
Space Group, Z	$P2_1$, 2	$P2_1$, 2	$P2_12_12_1$, 4
a/Å	9.9249(4)	9.9205(4)	5.6485(2)
b/Å	8.8190(3)	8.8195(3)	11.8378(3)
c/Å	11.1611(4)	11.1609(4)	21.6295(6)
α /°	90	90	90
β/°	105.551(2)	105.611(2)	90
γ /°	90	90	90
V (Å^3)	941.14(6)	940.49(6)	1446.27(7)
ρ_{calc} [mg/mm^3]	1.226	1.227	1.338
μ [mm^{-1}]	0.609	0.0609	0.691
Radiation type	CuKα (λ = 1.54178)	CuKα (λ = 1.54178)	CuKα (λ = 1.54178)
F(000)	372.0	372.0	616.0
No. of measured reflections	10608	10630	10051
No. of independent reflections	3288	3303	2564
Final R indexes (I ≥ 2 s)	R_1 = 0.0315, wR_2 = 0.0765	R_1 = 0.0260, wR_2 = 0.0647	R_1 = 0.0307, wR_2 =
R1/wR2 (I ≥ 2 s) [%]	0.0315/0.0765	0.0260/0.0647	0.0307/0.0778
R1/wR2 (all data) [%]	0.0331/0.0776	0.0263/0.0648	0.0320/0.0786

5.3.9. Summary and outlook

The present study has illustrated the use of a non-biaryl axially chiral photochromophore for a facile [2+2] photocycloaddition in acrylimides. The photocycloaddition of atropisomeric acrylimides proceeded smoothly to afford the exclusive formation of cross photocycloaddition product. Results from laser flash photolysis have shown that atropisomeric imides can react efficiently from both singlet (direct irradiation) and triplet (sensitized irradiation) excited states. The restricted *N*-C(aryl) bond rotations not only controls the regioselectivity that leads to the formation of the less studied cross [2+2]-photocyclized product but also influences the enantioselectivity in the photoproduct. The acrylimides possess triplet energy ~63 kcal/mol and thus are amenable to visible light irradiations highlighting a clean and efficient strategy for performing photochemical transformations. As the bicyclic photoproducts have structural skeleton similar to the compounds that have been shown to be effective as aromatase inhibitors,[60] our strategy can be extended to synthesize pharmaceutically relevant and useful scaffolds.

5.3.10. Experimental section for [2+2] photocycloaddition of atropisomeric acrylimide

5.3.10.1. General methods for experiments

All commercially obtained reagents/solvents were used as received; chemicals were purchased from Alfa Aesar®, Sigma-Aldrich®, Acros®, TCI America®, Mallinckrodt®, and Oakwood Products®, and were used as received without further purification. Unless otherwise stated, reactions were conducted in oven-dried glassware under nitrogen atmosphere. Unless otherwise stated dichloromethane and acetone were freshly distilled from CaH_2 and potassium carbonate before employing in a reaction. Unless otherwise state deionized water (DI water) was used for work up procedures. ^{1}H-NMR and ^{13}C-NMR spectra were recorded on Varian 400 MHz (100 MHz for ^{13}C) and on 500 MHz (125 MHz for ^{13}C) spectrometers. Data from the ^{1}H-NMR spectroscopy are reported as chemical shift (δ ppm) with the corresponding integration values. Coupling constants (J) are reported in hertz (Hz). Standard abbreviations indicating multiplicity are used as follows: s (singlet), b (broad), d (doublet), t (triplet), q (quartet), m (multiplet) and virt (virtual). Data for ^{13}C NMR spectra are reported in terms of chemical shift (δ ppm).

High-resolution mass spectrum data in Electrospray Ionization mode were recorded on a Bruker – Daltronics® BioTof mass spectrometer in positive (ESI+) ion mode. HPLC analyses were performed on Waters® HPLC equipped with 2525 pump or on Dionex® Ultimate 3000 HPLC. Waters® 2767 sample manager was used for automated sample injection on Waters® HPLC or Ultimate 3000 sample injector was used for injection on Dionex® HPLC. All HPLC injections on Waters® HPLC were monitored using a Waters® 2487 dual wavelength absorbance detector at 254 and 270 nm or on Dionex®. HPLC were monitored using a diode array detector (DAD3000125). Analytical and semi-preparative injections were performed on chiral stationary phase using various columns as indicated below.

i) Regis® PIRKLE COVALENT (*R,R*) WHELK–01

a) 25 cm x 4.6 mm column for analytical injections.

b) 25 cm x 10 mm column for semi-preparative injections.

ii) CHIRACEL® OD-H

a) 0.46 cm x 25 cm column for analytical injections.

b) 10 mm x 25 cm column for semi-preparative injections.

iii) CHIRALPAK® IC

a) 0.46 cm x 25 cm column for analytical injections.

b) 10 mm x 25 cm column for semi-preparative injections

iv) CHIRALPAK® AD-H

a) 0.46 cm x 15 cm column for analytical injections.

b) 10 mm x 25 cm column for semi-preparative injections.

v) CHIRALCEL – OD-3

a) 0.46 cm x 15 cm column for analytical injections.

vi) CHIRAPAK – AD-3

a) 0.46 cm x 15 cm column for analytical injections.

Masslynx software version 4.1 was used to monitor/analyze the HPLC injections on Waters® and to process HPLC traces. Chromeleon 7 software was used to monitor and process HPLC injections on Dionex® HPLC. Igor Pro® Software version 6.0 was used to process the HPLC graphics. When necessary, the compounds were purified by combiflash equipped with dual wavelength UV-Vis absorbance detector (Teledyne ISCO) using hexanes:ethyl acetate as the mobile phase and Redisep® cartridge filled with silica (Teledyne ISCO) as stationary phase. In some cases, compounds were purified by column chromatography on silica gel (Sorbent Technologies®, silica gel standard grade: porosity 60 Å, particle size: 230 x 400 mesh, surface area: 500 – 600 m^2/g, bulk density: 0.4 g/mL, pH range: 6.5 – 7.5). Unless indicated, the Retardation Factor (R_f) values were recorded using hexanes:ethyl acetate as mobile phase and on Sorbent Technologies®, silica Gel TLC plates (200 mm thickness w/UV$_{254}$).

5.3.10.2. Photophysical methods

Spectrophotometric solvents were used unless otherwise mentioned. UV-Vis spectra were recorded using Shimadzu 2501PC UV-Vis spectrometer equipped with UV quality fluorimeter cells (with range until 190 nm) were purchased from Luzchem®. Absorbance measurements were performed using a Shimadzu® UV-2501PC UV-Vis spectrophotometer. Laser flash photolysis experiments employed the pulses from a Spectra Physics GCR-150-30 Nd:YAG laser (355 nm, *ca.* 5 mJ/pulse, 7 ns pulse length or 266 nm, ca 5 mJ/pulse, 5 ns pulse length) and a computer controlled system that has been described elsewhere. Singlet oxygen phosphorescence measurements were performed on a modified Fluorolog-3 spectrometer (HORIBA Jobin Yvon) in conjunction with a NIR sensitive photomultiplier tube (H10330A-45, Hamamatsu). A 450-W Xe was use for steady-state excitation to record singlet oxygen phosphorescence spectra and a Spectra Physics GCR-150-30 Nd:YAG laser (266 nm, *ca.* 2 mJ/pulse, 5 ns) was used for pulsed excitation to collect $^1O_2$ phosphorescence decay traces at 1270 nm which were stored on a digital oscilloscope (TDS 360 from Tektronics).

5.3.11. General procedure for synthesis of acrylimide derivative 279a-c and intermediates

5.3.11.1. Synthesis of phenylglyoxalyl chloride 278
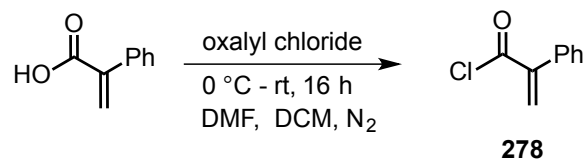
Scheme 5.30: Synthesis of phenylglyoxalyl chloride **278**.

To a solution of phenylglyoxylic acid (1.00 g, 6.74 mmol, 1 equiv) in dichoromethane (10 mL) at 0 °C oxalyl chloride (2.5 equiv) was slowly added with stirring. After complete addition, two drops of DMF was added during which effervescence was observed. After stirring for 15 min, the mixture was brought to room temperature and stirred for 3 h. The solvent and excess oxalyl chloride was then removed under reduced pressure while the temperature was maintained at 25 °C. After vacuum was released under N_2 atmosphere and the crude was taken to the next step without further purification.

5.3.11.2. General procedure for the synthesis of anilides 277a-c
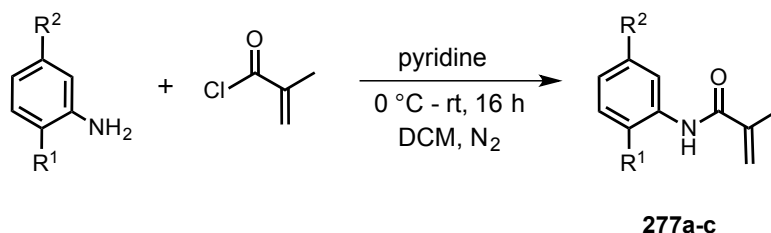
Scheme 5.31: Synthesis of anilides **277a-c**.

Following the modified procedure reported by Curran et al., 2,5-di-*tert*-butylaniline (1 equiv) was dissolved in anhydrous dichloromethane under N_2 atmosphere.[79] To this solution, 1.5 equiv of pyridine was added and the reaction mixture was then cooled to 0 °C, followed by the dropwise addition of methacryloyl chloride (1.2 equiv). After stirring for 15 min, the mixture was brought to room temperature and stirred for 16 h. The reaction was quenched with 10 mL of DI water, stirred and the layers were separated. The organic layer was sequentially washed with DI water (2 × 10 mL), saturated $NaHCO_3$ (2 × 10 mL) and finally with brine. The organic layer was dried over anhyd Na_2SO_4, filtered and the solvent was removed under reduced pressure to yield crude product. The crude product was purified by combiflash using hexanes and ethyl acetate mixture to get the desired amide. The product was characterized by NMR spectroscopy and mass spectrometry.

277a, TLC condition - R_f = 0.3 (80% hexanes:20% ethyl acetate) Yield = 90%

277b, TLC condition - R_f = 0.3 (85% hexanes:15% ethyl acetate) Yield = 70%

277c, TLC condition - R_f = 0.3 (80% hexanes:20% ethyl acetate) Yield = 70%

¹H-NMR (400 MHz, CDCl₃, δ ppm): 1.40 (s, 9H), 2.08 (s, 3H), 5.46 (s, 1H), 5.82 (s, 1H), 7.11-7.15 (m, 1H), 7.20-7.23 (m, 1H), 7.36-7.38 (m, 1H), 7.55 (bs, 1H) and 7.66-7.68 (m, 1H).
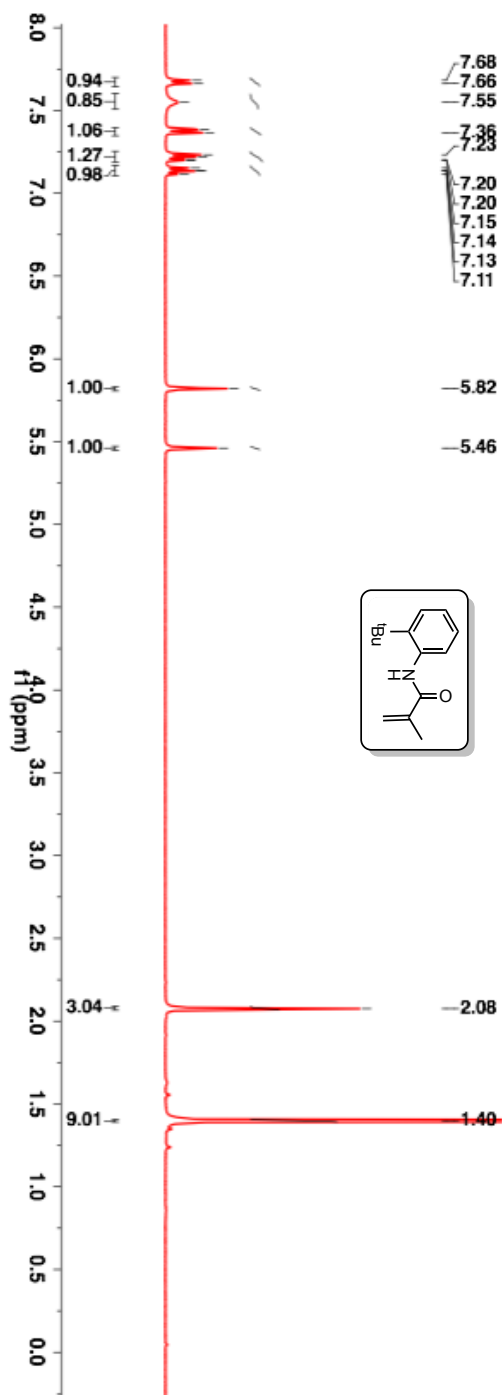
Figure 5.22: ¹H-NMR (400 MHz, CDCl₃, δ ppm) spectrum 2-*tert*-butylphenyl anilide **277a**.

^{13}C-NMR (100 MHz, CDCl$_3$, δ ppm): 19.1, 30.8, 34.7, 120.0, 126.2, 126.7, 127.0, 127.6, 135.3, 141.1, 149.3 and 166.6.
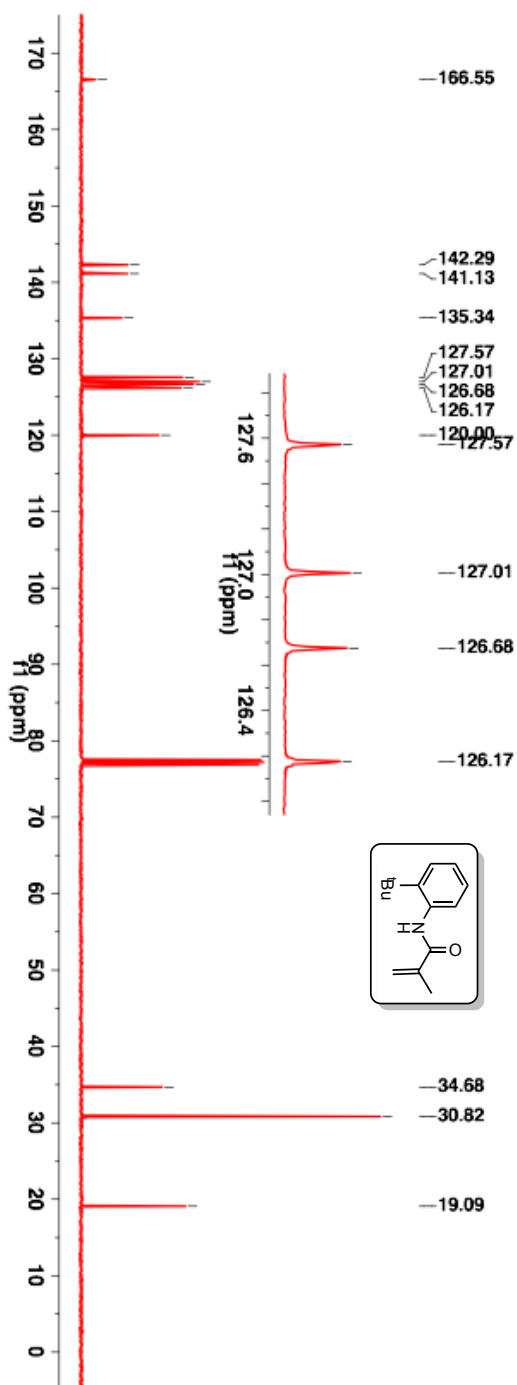
Figure 5.23: ^{13}C-NMR (100 MHz, CDCl$_3$, δ ppm) spectrum 2-*tert*-butylphenyl anilide **277a**.

HRMS-ESI (m/z) ([M + Na]$^+$):

Calculated   : 240.1359

Observed   : 240.1363

|Δm| : 1.7 ppm
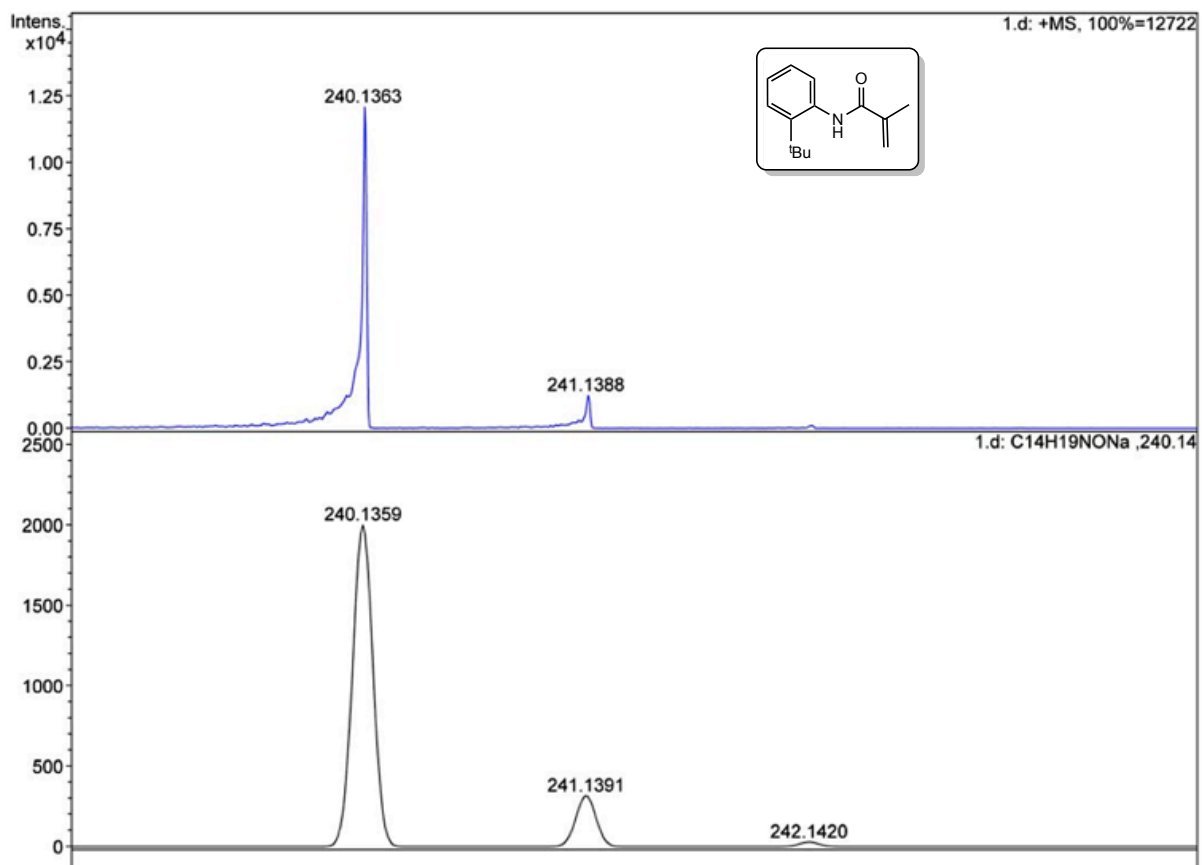
Figure 5.24: HRMS of 2-*tert*-butylphenyl anilide **277a**.

^{1}H-NMR (400 MHz, CDCl$_3$, δ ppm): 1.32 (s, 9H), 1.41 (s, 9H), 2.11 (s, 3H), 5.49 (s, 1H), 5.85 (s, 1H), 7.16-7.18 (m, 1H), 7.31-7.33 (m, 1H), 7.59 (bs, 1H) and 7.78 (s, 1H).
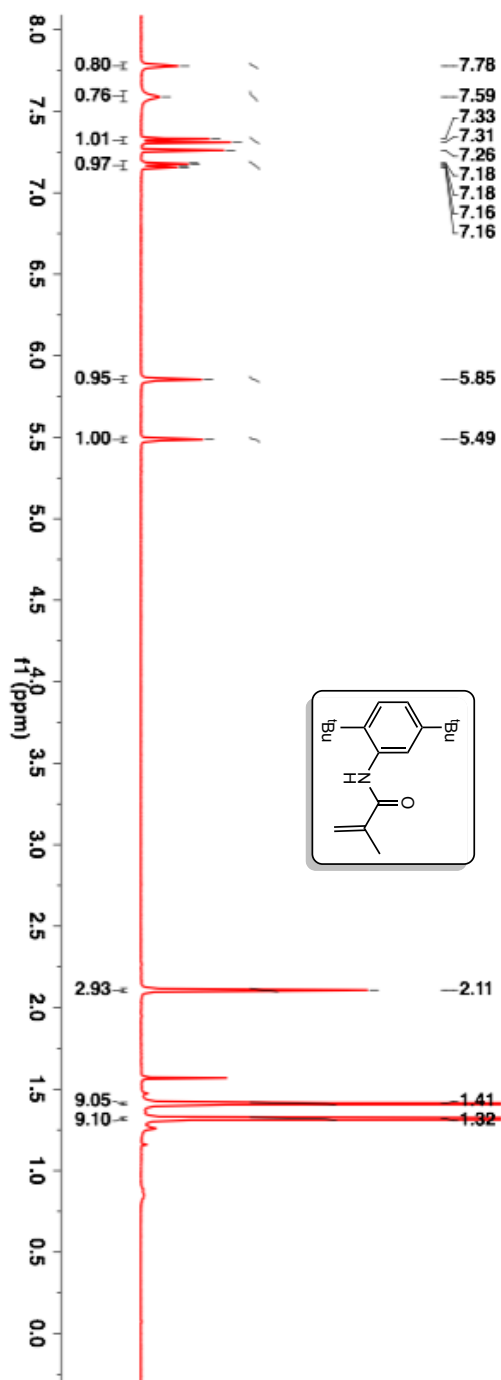
Figure 5.25: ^{1}H-NMR (400 MHz, CDCl$_3$, δ ppm) spectrum 2,5-di-*tert*-butylphenyl acrylanilide **277b**.

^{13}C-NMR (100 MHz, CDCl$_3$, δ ppm): 19.2, 30.9, 31.4, 34.3, 34.5, 119.9, 122.9, 124.4, 126.4, 135.0, 138.9, 141.3, 149.9 and 166.5.
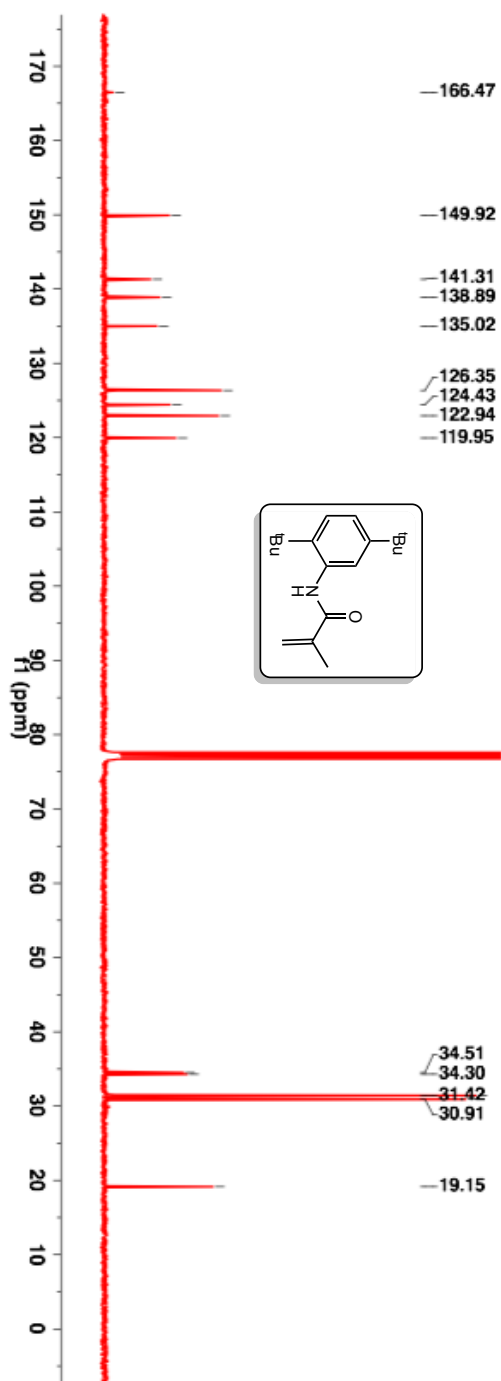
Figure 5.26: ^{13}C-NMR (100 MHz, CDCl$_3$, δ ppm) spectrum 2,5-di-*tert*-butylphenyl anilide **277b**.

HRMS-ESI (m/z) ([M + Na]$^+$):

Calculated   : 296.1985

Observed   : 296.1988

|Δm| : 1.0 ppm
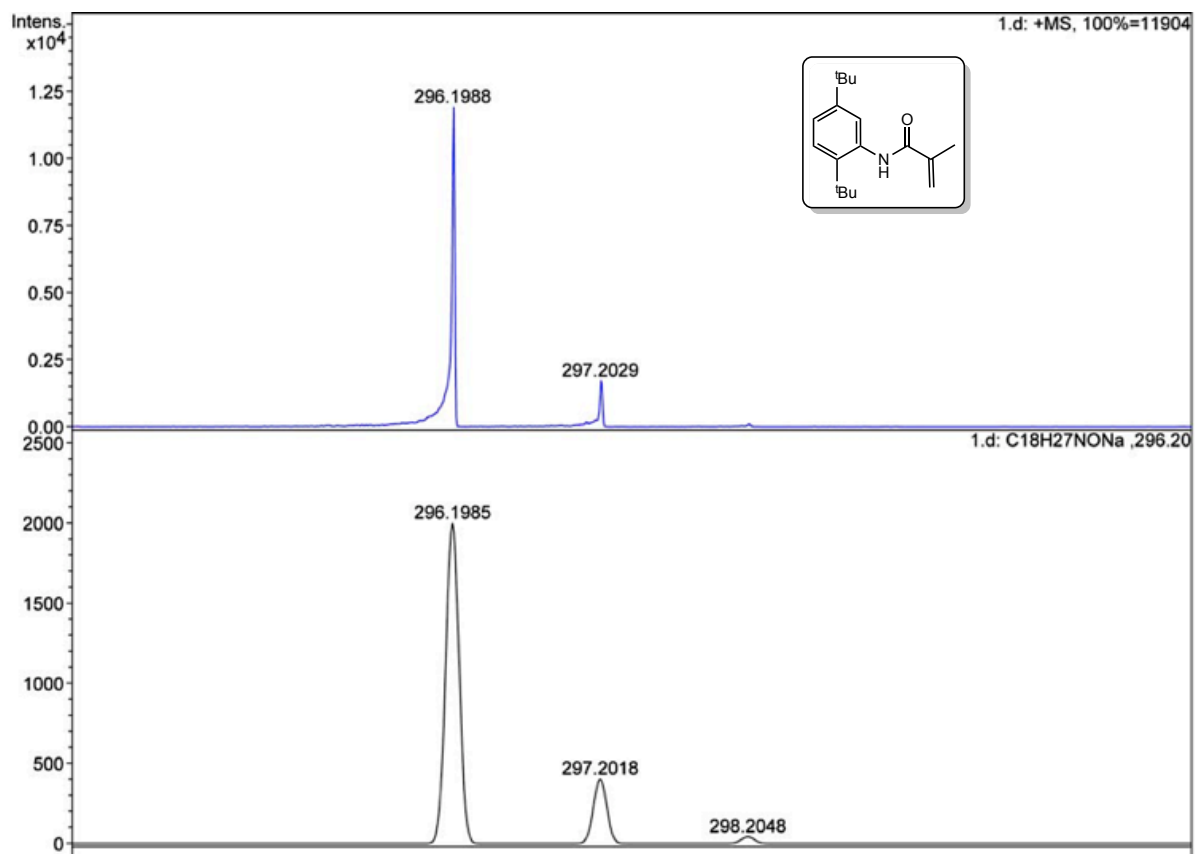
Figure 5.27: HRMS of 2,5-di-*tert*-butylphenyl acrylanilide **277b**.

^{1}H-NMR (400 MHz, CDCl$_3$, δ ppm): 2.05 (s, 3H), 5.44 (s, 1H) 5.78 (s, 1H), 7.09-7.13 (m, 1H), 7.30-7.34 (m, 1H), 7.55-7.57 (m, 1H) and 7.67 (bs, 1H).
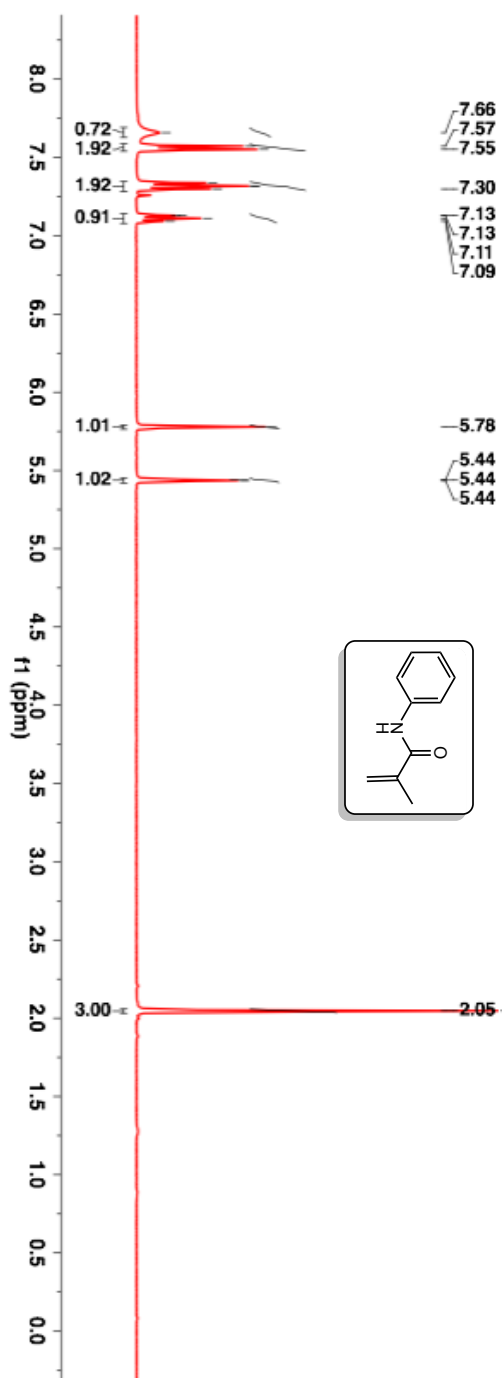
Figure 5.28: ^{1}H-NMR (400 MHz, CDCl$_3$, δ ppm) spectrum anilide **277c**.

¹³C-NMR (100 MHz, CDCl₃, δ ppm): 18.9, 119.9 120.2, 125.5, 129.1, 137.9, 141.1 and 166.8.
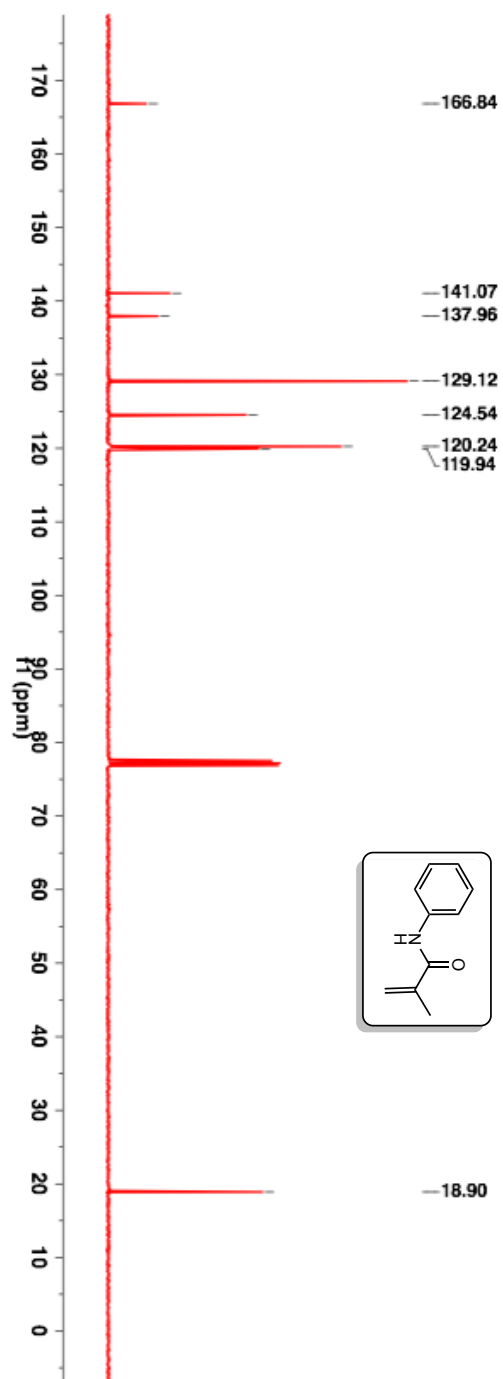
Figure 5.29: ¹³C-NMR (100 MHz, CDCl₃, δ ppm) spectrum anilide **277c.**

HRMS-ESI (m/z) ([M + Na]$^+$):

Calculated : 184.0733

Observed : 184.0744

|Δm| : 5.9 ppm
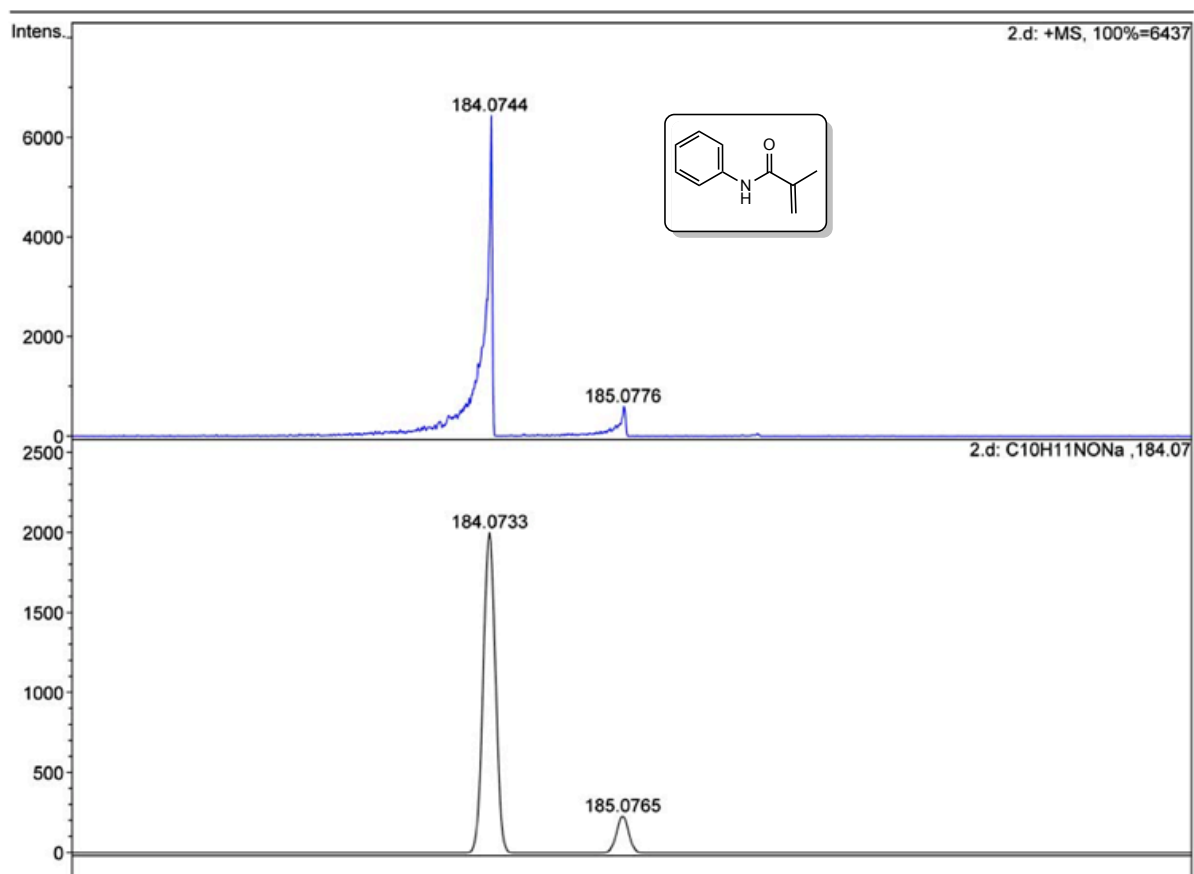
Figure 5.30: HRMS of anilide **277c**.

5.3.12. General procedure for the synthesis of acrylimides 279a-c
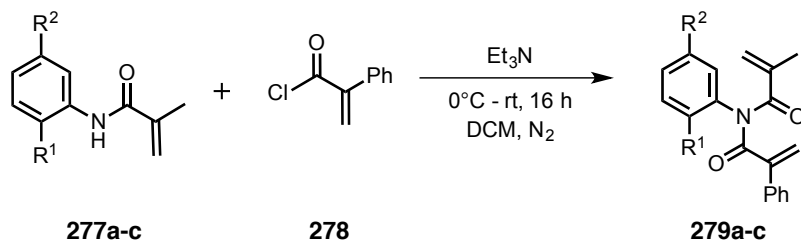
Scheme 5.32: Synthesis of acrylimides **279a-c**.

The appropriate anilide (1 equiv) was dissolved in anhydrous dichloromethane. To this solution, triethylamine (1.5 equiv) was added. The reaction mixture was then cooled to -10 $^{\circ}$C. To this 2-phenylprop-2-enoyl chloride (1.5 equiv) was added dropwise. After stirring for 15-20 min at this temperature, the mixture was brought to room temperature and stirred for 16 h. The reaction was quenched with 10 mL of DI water, stirred and the layers were separated. The organic layer was fractioned and concentrated. The organic layer was washed in sequence with DI water (2 × 10 mL), 1 N NaOH (1 × 15 mL) and finally with brine. The organic layer was dried over anhyd Na_2SO_4, filtered and the solvent was removed under reduced pressure to yield crude product. The crude product was purified by combiflash using hexanes and ethyl acetate mixture to get the desired amide. The product was characterized by NMR spectroscopy and mass spectrometry.

279a, TLC condition - R_f = 0.5 (50% hexanes:50% ethyl acetate) Yield = 73 %

**279b**, TLC condition - R_f = 0.5 (90% hexanes:10% ethyl acetate) Yield = 64 %

279c, TLC condition - R_f = 0.5 (80% hexanes:20% ethyl acetate) Yield = 60 %

^{1}H-NMR (400 MHz, CDCl$_3$, δ ppm): 1.38 (s, 9H), 1.91 (s, 3H), 5.19 (m, 1H), 5.40 (s, 1H), 5.64 (s, 1H), 5.80 (s, 1H), 6.91-6.93 (m, 1H), 7.19-7.23 (m ,1H), 7.30-7.33 (m, 4H), 7.45-7.47 (m, 1H) and 7.54-7.57 (m, 1H).
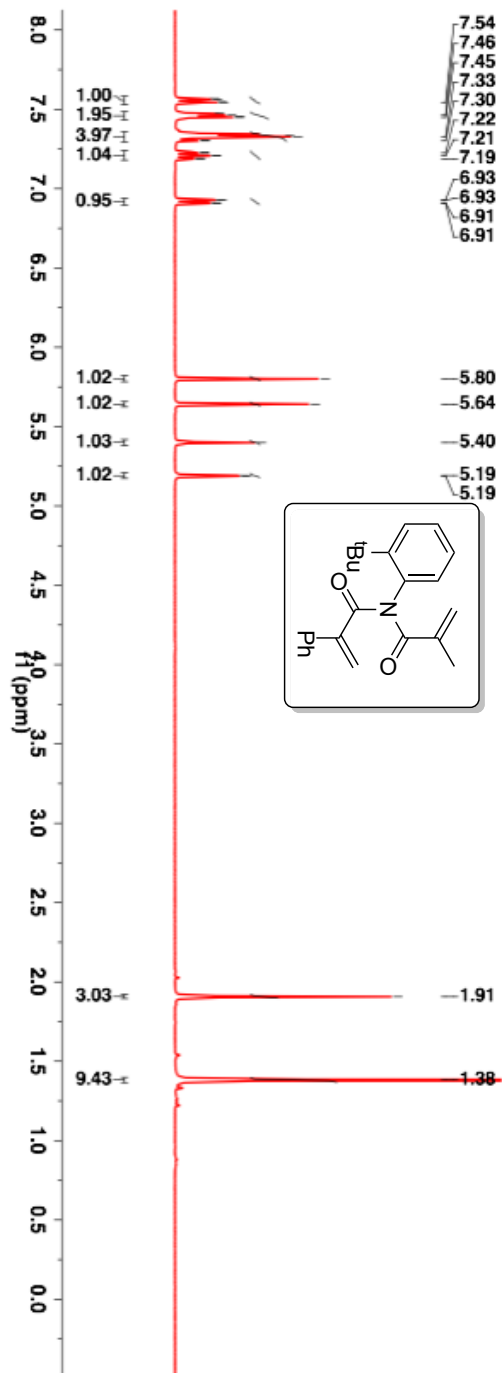
Figure 5.31: ^{1}H-NMR (400 MHz, CDCl$_3$, δ ppm) spectrum of acrylimide **279a**.

¹³C-NMR (100 MHz, CDCl₃, δ ppm): 19.7, 31.8, 36.0, 118.6, 121.5, 126.8, 127.4, 128.7, 128.9 129.1, 129.3, 131.4, 136.3, 136.9, 147.6, 147.9, 172.7 and 174.5.

Figure 5.32: ¹³C-NMR (100 MHz, CDCl₃, δ ppm) spectrum of acrylimide **279a**.

^{13}C-NMR (100 MHz, CDCl$_3$, δ ppm): 19.7, 31.8, 36.0, 118.6, 121.5, 126.8, 127.4, 128.7, 128.9 129.1, 129.3, 131.4, 136.3, 136.9, 147.6, 147.9, 172.7 and 174.5.
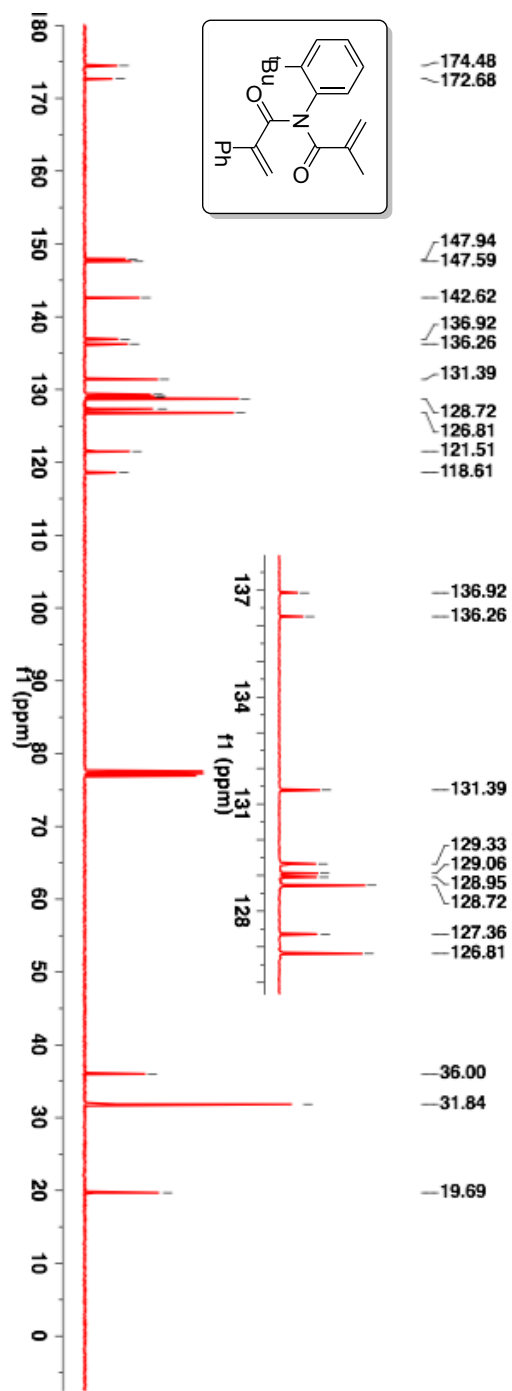
Figure 5.32: ^{13}C-NMR (100 MHz, CDCl$_3$, δ ppm) spectrum of acrylimide **279a**.

HRMS-ESI (m/z) ([M + Na]$^+$):

Calculated   : 370.1778

Observed   : 370.1762

|Δm| : 4.3 ppm
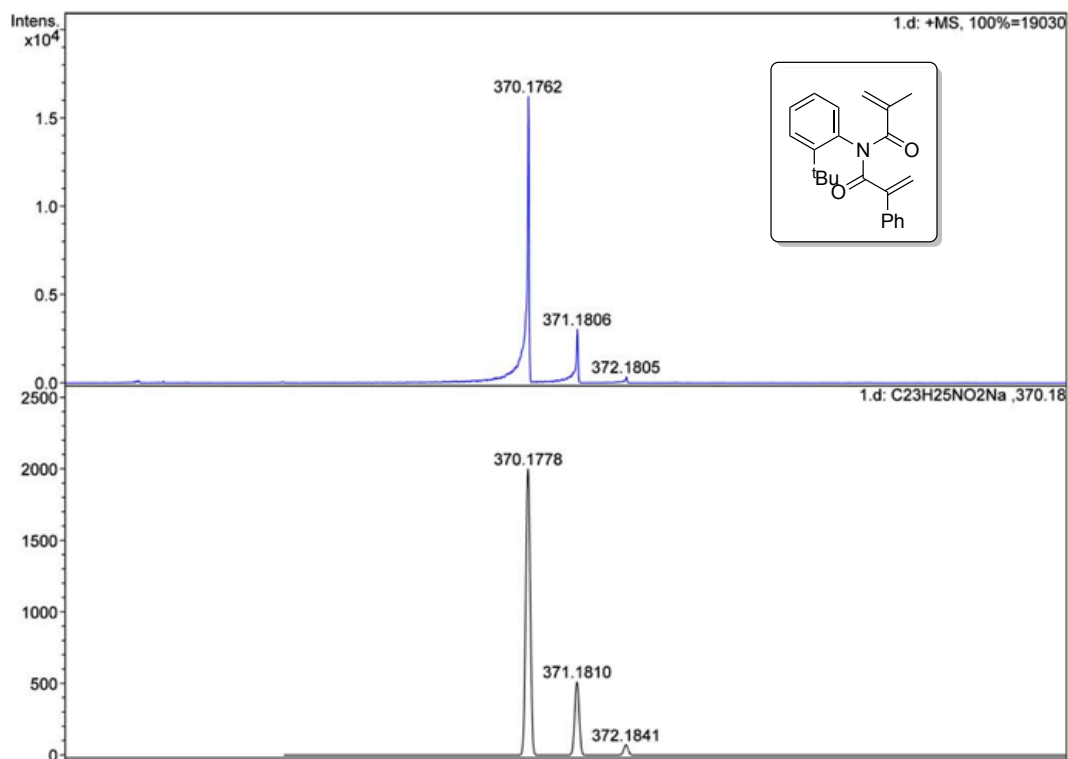
Figure 5.33: HRMS of acrylimide **279a**.

5.3.13. Conditions for HPLC analysis of 279a

For analytical conditions,

Column : CHIRALPAK® IC

Abs. detector wavelength : 254 nm and 270 nm

Mobile phase : Hexanes:2-propanol = 95:5

Flow rate : 1.0 mL/min

Retention times (min) : ~ 8.7 and 12.6

For preparative conditions,

Column : CHIRALPAK® IC

Abs. detector wavelength : 254 nm and 270 nm

Mobile phase : Hexanes:2-propanol = 93:7

Flow rate : 2.0 mL/min

Retention times (min) : ~ 18.8 and 26.5

^{1}H-NMR (400 MHz, CDCl$_3$, δ ppm): 1.29 (s, 9H), 1.41 (s, 9H), 1.95 (s, 3H), 5.23 (m, 1H), 5.44 (s, 1H), 5.69 (s, 1H), 5.80 (s, 1H), 6.90 (s, 1H), 7.36-7.38 (m, 4H) and 7.49-7.52 (m. 3H).
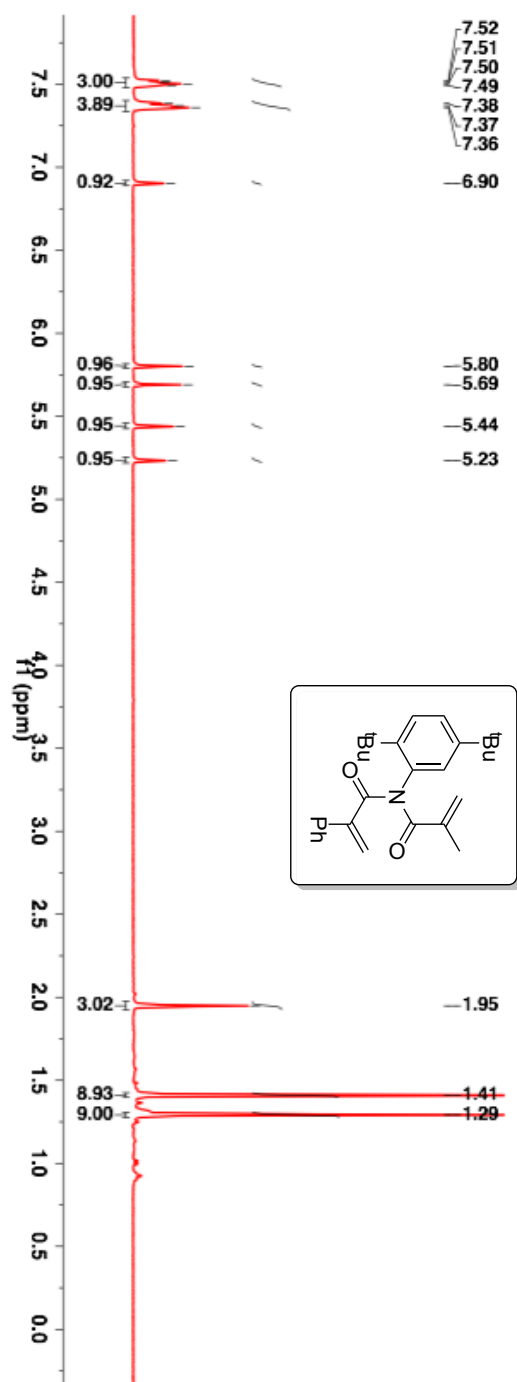
Figure 5.34: ^{1}H-NMR (400 MHz, CDCl$_3$, δ ppm) spectrum of acrylimide **279b**.

^{13}C-NMR (100 MHz, CDCl$_3$, δ ppm): 19.6, 31.2, 31.8, 34.1, 35.5, 118.5, 121.1, 126.1, 126.7, 127.9, 128.6, 128.8, 128.9, 136.1, 136.3, 142.6, 144.6, 147.5, 149.8, 172.6 and 174.4.
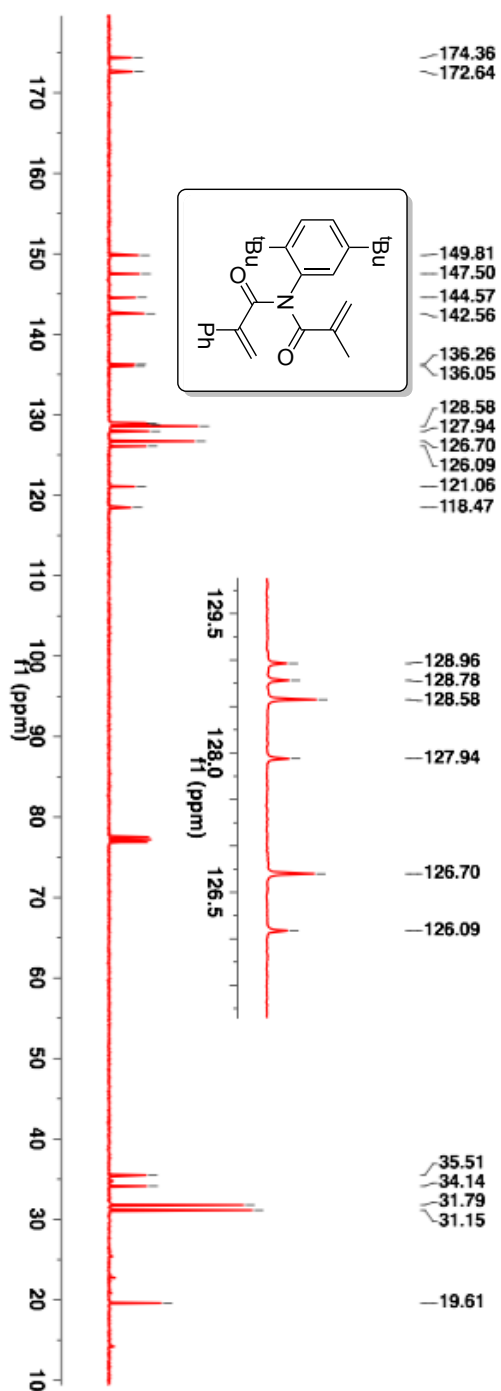
Figure 5.35: ^{13}C-NMR (100 MHz, CDCl$_3$, δ ppm) spectrum of acrylimide **279b**.

HRMS-ESI (m/z) ([M + Na]$^+$):

Calculated   : 426.2404

Observed   : 426.2416

|Δm| : 2.8 ppm
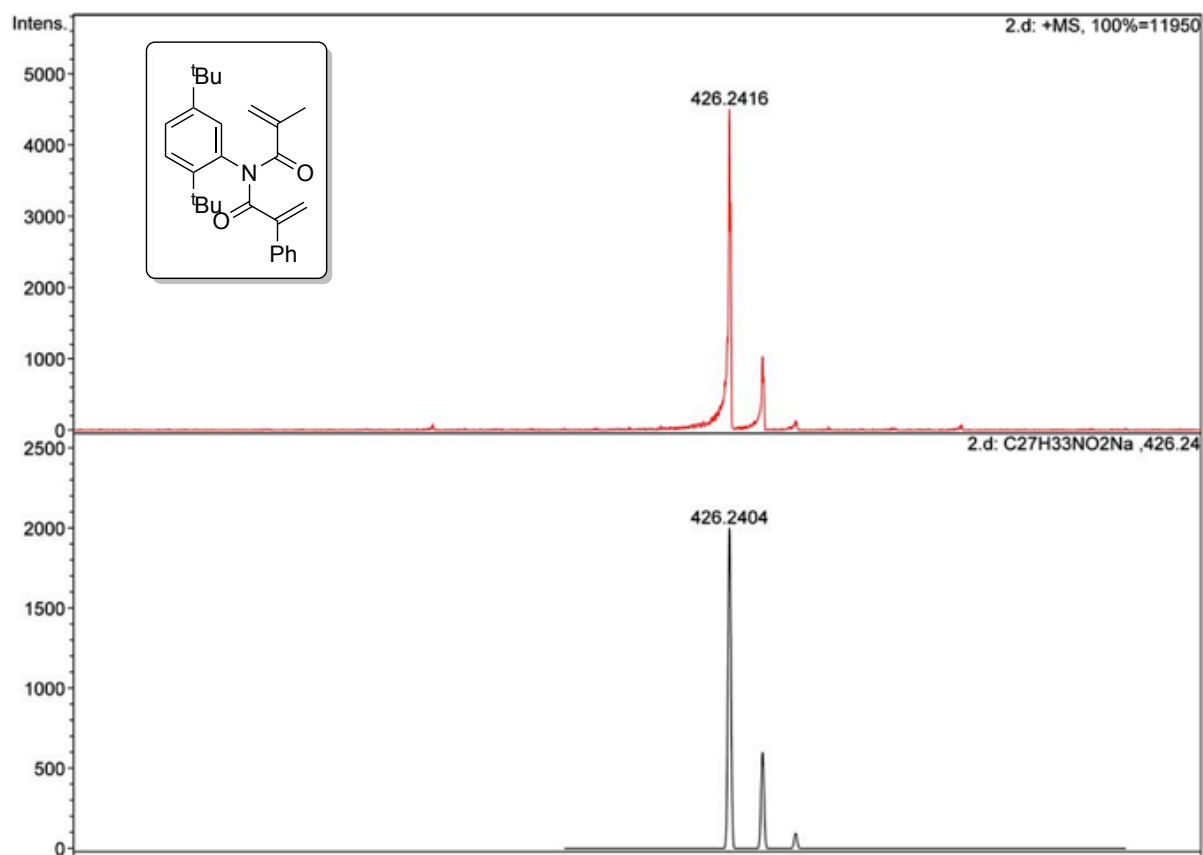
Figure 5.36: ^{1}HRMS of acrylimide **279b**.

5.3.14. Conditions for HPLC analysis of 279b

For analytical conditions,

Column	: CHIRALPAK® IC
Abs. detector wavelength	: 254 nm and 270 nm
Mobile phase	: Hexanes:2-propanol = 98:2
Flow rate	: 1.0 mL/min
Retention times (min)	: ~ 6.3 and 8.0

For preparative conditions,

Column	: CHIRALPAK® IC
Abs. detector wavelength	: 254 nm and 270 nm
Mobile phase	: Hexanes:2-propanol = 98:2
Flow rate	: 2.0 mL/min
Retention times (min)	: ~ 13.4 and 16.1

¹H-NMR (400 MHz, CDCl₃, δ ppm): 1.82 (s, 3H), 5.25 (s, 1H), 5.35 (s, 1H), 5.73 (s, 1H), 5.76 (s, 1H), 7.06-7.08 (m, 2H), 7.20-7.30 (m, 6H) and 7.40-7.41 (m, 2H).
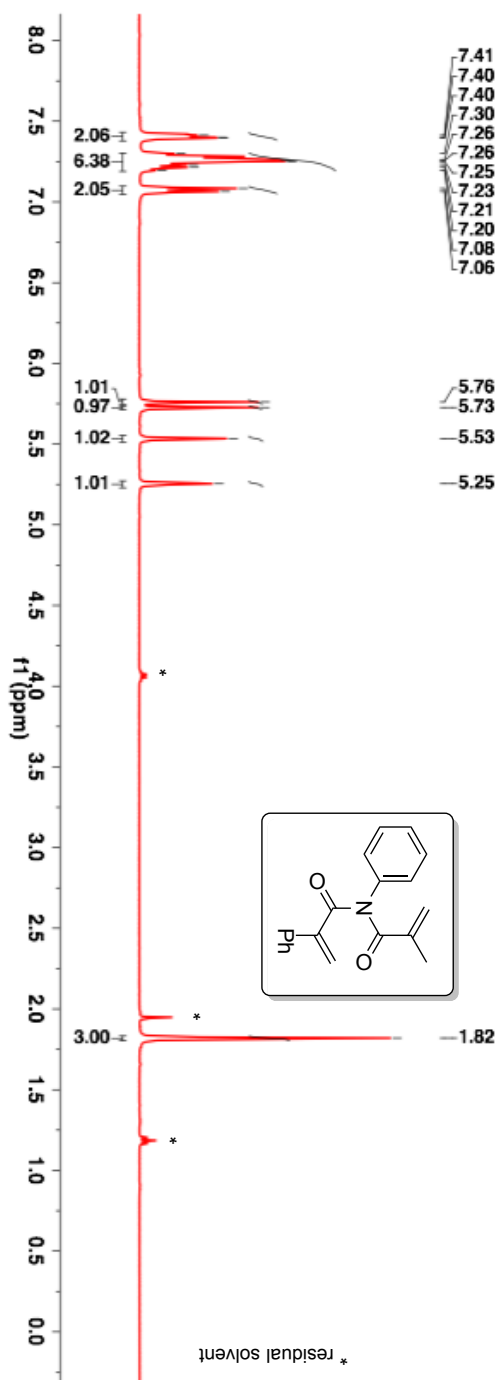
Figure 5.37: ¹H-NMR (400 MHz, CDCl₃, δ ppm) spectrum of acrylimide **279c**.

^{13}C-NMR (100 MHz, CDCl$_3$, δ ppm): 18.4, 120.6, 122.6, 126.7, 127.4, 127.5, 128.1, 128.2, 128.9, 135.7, 138.5, 141.4, 146.2, 172.2 and 173.8.
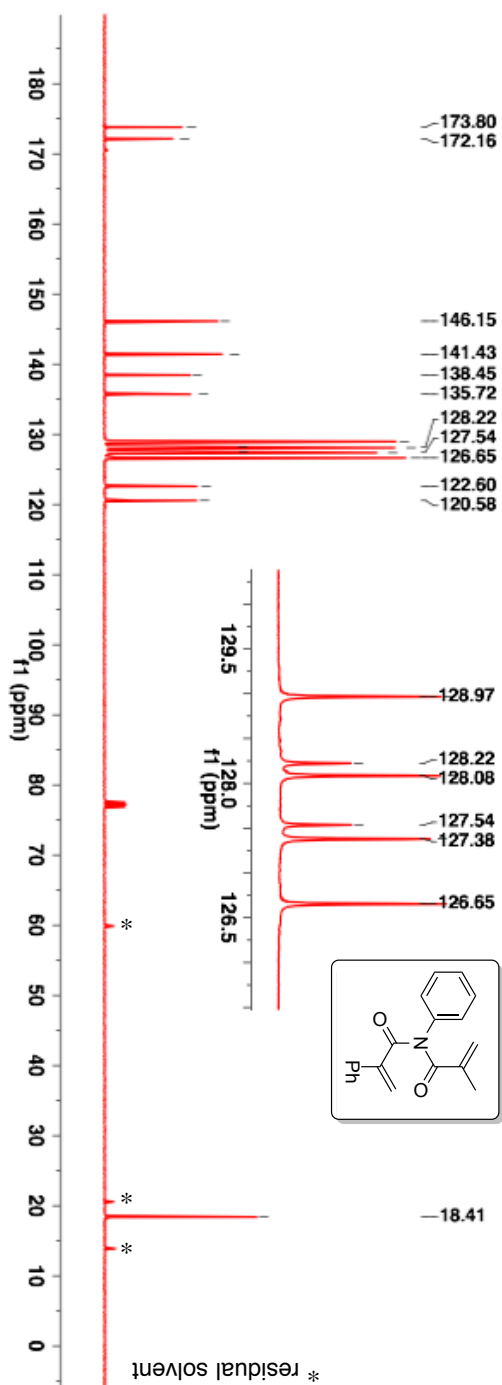
Figure 5.38: ^{13}C-NMR (100 MHz, CDCl$_3$, δ ppm) spectrum of acrylimide **279c**.

HRMS-ESI (m/z) ([M + Na]$^+$):

Calculated   : 314.1149

Observed   : 314.1151

|Δm| : 0.6 ppm
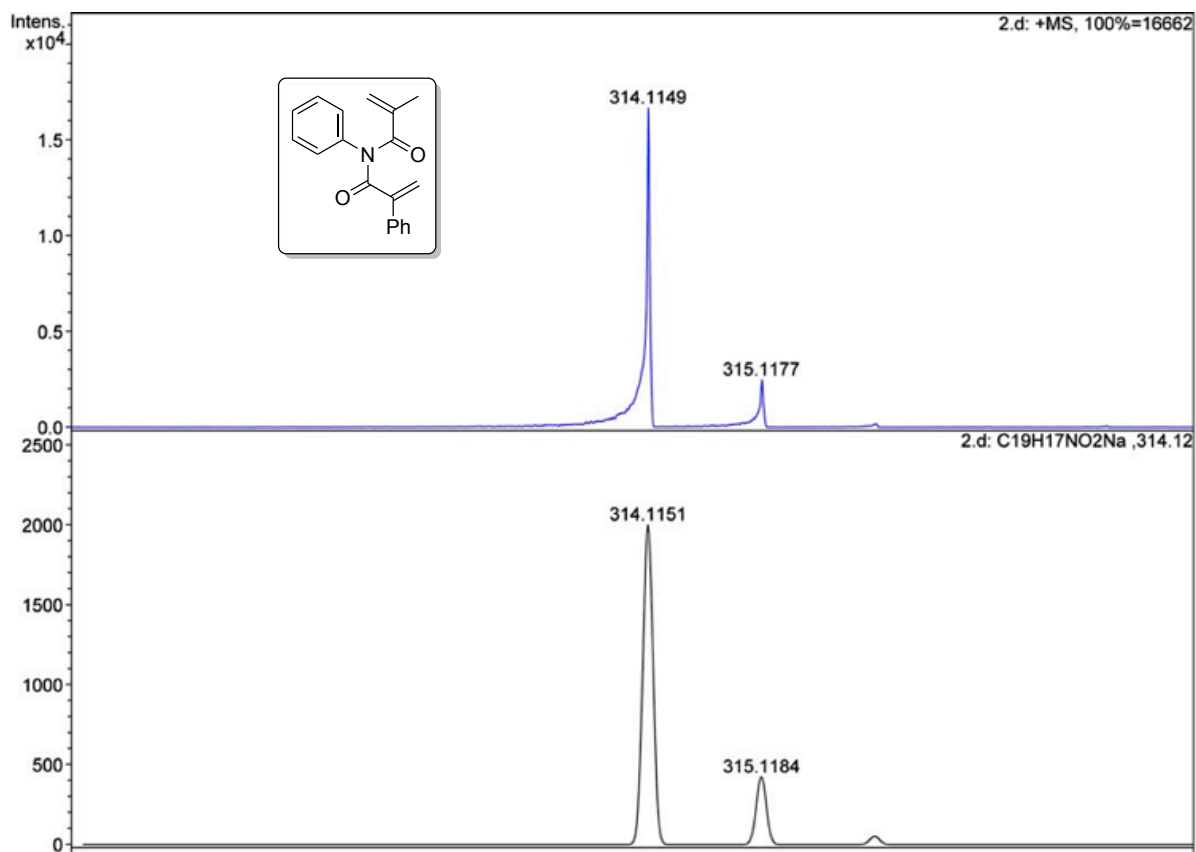
Figure 5.39: HRMS of acrylimide **279c**.

5.3.15 Racemization kinetics of acrylimides 279a-b

MeOH, 45 °C
k_{rac} (s^{-1}) = 4.30 x 10^{-6}
$\tau_{1/2}$ (h) = 1.9
$\Delta G^{\ddagger}_{rac}$($k$cal.mol^{-1}) = 26.5

MeCN, 45 °C
k_{rac} (s^{-1}) = 4.10 x 10^{-6}
$\tau_{1/2}$ (h) = 2.0
$\Delta G^{\ddagger}_{rac}$($k$cal.mol^{-1}) = 26.5
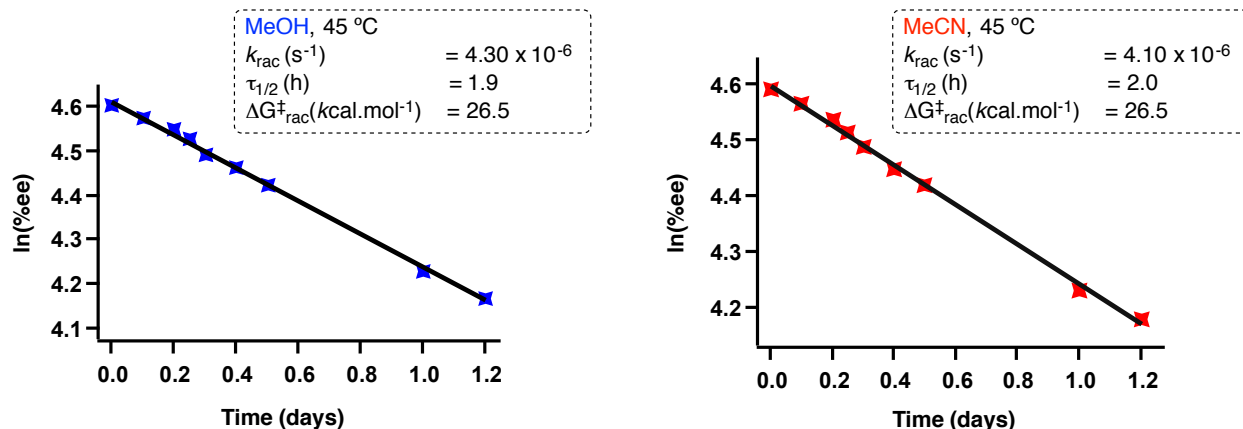
Figure 5.40: Racemization kinetics of acrylimide **279a** recorded in methanol and acetonitrile at 45 °C.

MeOH, 45 °C
k_{rac} (s^{-1}) = 8.56 x 10^{-6}
$\tau_{1/2}$ (h) = 0.9
$\Delta G^{\ddagger}_{rac}$($k$cal.mol^{-1}) = 26.0

MeCN, 45 °C
k_{rac} (s^{-1}) = 4.05 x 10^{-6}
$\tau_{1/2}$ (h) = 2.0
$\Delta G^{\ddagger}_{rac}$($k$cal.mol^{-1}) = 26.5
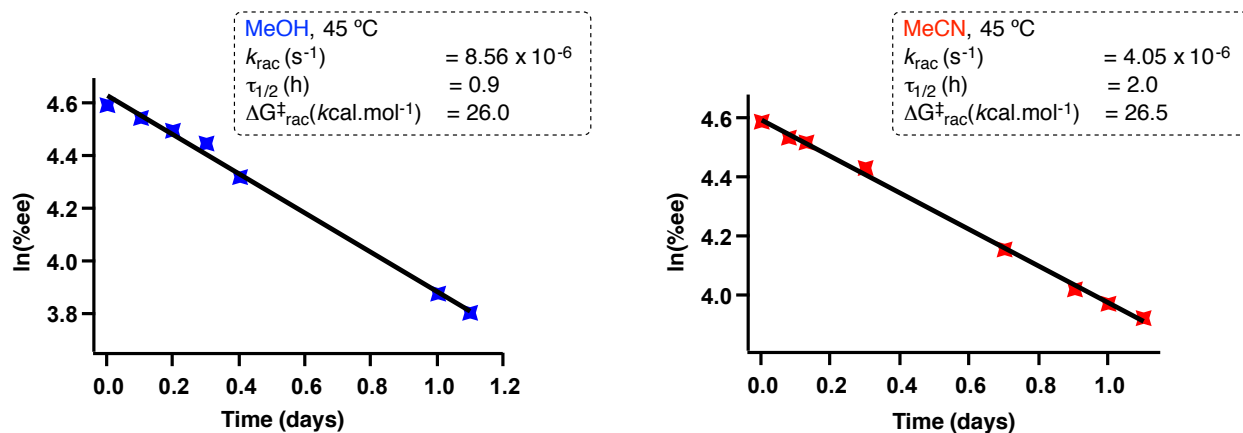
Figure 5.41: Racemization kinetics of acrylimide **279b** recorded in methanol and acetonitrile at 45 °C.

5.3.16 Photoreactions of acrylimides 279a-c

279a-c

a. $R^1 = {}^tBu$, $R^2 = H$;
b. $R^1 = {}^tBu$, $R^2 = {}^tBu$
c. $R^1 = H$, $R^2 = H$

cross addition (**280a-b**)   parallel addition (**281**)
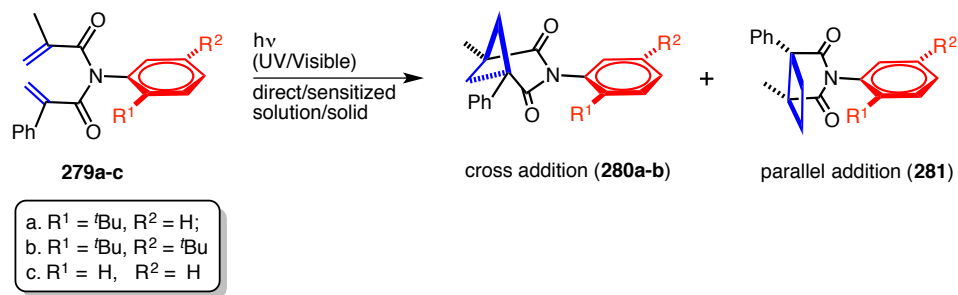
Scheme 5.33: [2+2] Photocycloaddition of acrylimides **279a-c**.

5.3.17 General procedure followed for direct irradiation of acrylimides and characterization of photoproducts

Solution of acrylimides **279a-c** in methanol or acetonitrile ([**279a**] = 2.88 mM, [**279b**] = 2.48 mM and [**279c**] = 3.43 mM) was irradiated at ambient conditions using quartz tubes in a Rayonet reactor equipped with 254 nm tubes (16 tubes x 35 Watt). For broadband irradiation, the solution of substrates **279a-c** in appropriate solvent was irradiated in Pyrex tubes with a 450 W medium pressure mercury lamp placed inside water-cooled quartz well. After irradiation, Ph_3CH was added as internal standard and the solvent was evaporated under reduced pressure. Conversion and mass balance was determined using the following equation by NMR spectroscopy:

$$mol_a = mol_i \times \left(\frac{Integral\ of\ analyte}{Integral\ of\ internal\ standard} \right) \times \frac{N_a}{N_i}$$

Where, N_a and N_i are the number of nuclei giving rise to the relevant analyte and internal standard peaks respectively. Similarly, mol_a and mol_i are the number of moles of analyte and the internal standard respectively.

5.3.18 General procedure followed for sensitized irradiation of acrylimides and characterization of photoproducts

Solution of acrylimide **279a-c** in methanol or acetonitrile acetonitrile ([**279a**] = 2.88 mM, [**279b**] = 2.48 mM and [**279c**] = 3.43 mM) along with 10 mol% triplet sensitizer was irradiated at ambient conditions using Pyrex tubes in a Rayonet reactor. For acetone sensitization, acetone was used as both solvent and sensitizer and irradiated with a 450 W medium pressure mercury lamp with Pyrex cut off filter under a constant flow of nitrogen. The Rayonet reactor was equipped with ~350 nm (16 tubes × 14 Watt) for xanthone and ~420 nm tubes (16 tubes × 14 Watt) for triplet sensitization with thioxanthone. After irradiation, Ph$_3$CH was added as internal standard and the solvent was evaporated under reduced pressure. Conversion and mass balance was determined by ^{1}H NMR spectroscopy. For irradiation of optically pure isomers, the ee values were determined by HPLC analysis on a chiral stationary phase.

5.3.19 General procedure followed for gram scale photoreaction of acrylimides and characterization of photoproducts

Photoreactions with sample (>1g scale) were carried out in a round bottom flask under nitrogen atmosphere on racemic acrylimide using compact fluorescent lamp (CFL, 13 W) under triplet sensitization with thioxanthone (Figure 5.42). After the irradiation the solutions was evaporated under reduced pressure. The residue was purified by combiflash using a hexanes:ethyl acetate mixture as mobile phase.

Figure 5.42: Typical photoreaction set-up for large-scale photoreaction of acrylimides.

Table 5.10: Large-scale [2+2] photocycloaddition of atropisomeric acrylimides **279a**. [a]

Entry	Compound	Solvent	Irradiation Conditions	% Yield (**280a**)[b]
1	**279a**	MeCN	TX (10 mol%), CFL/ 4 h / N$_2$	90
2		MeOH	TX (10 mol%), CFL/ 4 h / N$_2$	80

[a] Irradiation at room temperature for using compact fluorescent lamp (CFL), 13W using 10 mol% of thioxanthone (TX) as the triplet sensitizer [**279a**] = 12 mM. [b] Yield refers to isolated yield.

5.3.20 General procedure followed for large scale photoreaction of acrylimides and characterization of photoproducts

In certain cases N_2 saturated solutions of acrylimides were irradiated in batches using pyrex/quartz tubes in a Rayonet reactor placed in a merry-go-round (8 x 20 mL test tubes) for given time period. After the irradiation, the solutions were combined and the solvent was evaporated under reduced pressure. The residue was purified by combiflash using a hexanes:ethyl acetate mixture as mobile phase.

280a, TLC condition - R_f = 0.30 (80% hexanes:20% ethyl acetate)

280b, TLC condition - R_f = 0.40 (90% hexanes:10% ethyl acetate)

280c, TLC condition - R_f = 0.30 (80% hexanes:20% ethyl acetate)

¹H-NMR (400 MHz, CDCl₃, δ ppm): 1.35 (s, 9H), 1.45 (s, 3H), 2.56 (d, *J* = 9.6 Hz, 1H), 2.65 (d, *J* = 9.2 Hz, 1H), 2.97-3.01 (dd, *J* = 9.2 Hz, 8 Hz, 1H), 3.16-3.21 (dd, *J* = 9.6 Hz, 8 Hz, 1H), 6.88-6.90 (m, 1H), 7.14-7.16 (m, 2H), 7.27-7.40 (m, 5H) and 7.55-7.57 (m, 1H).
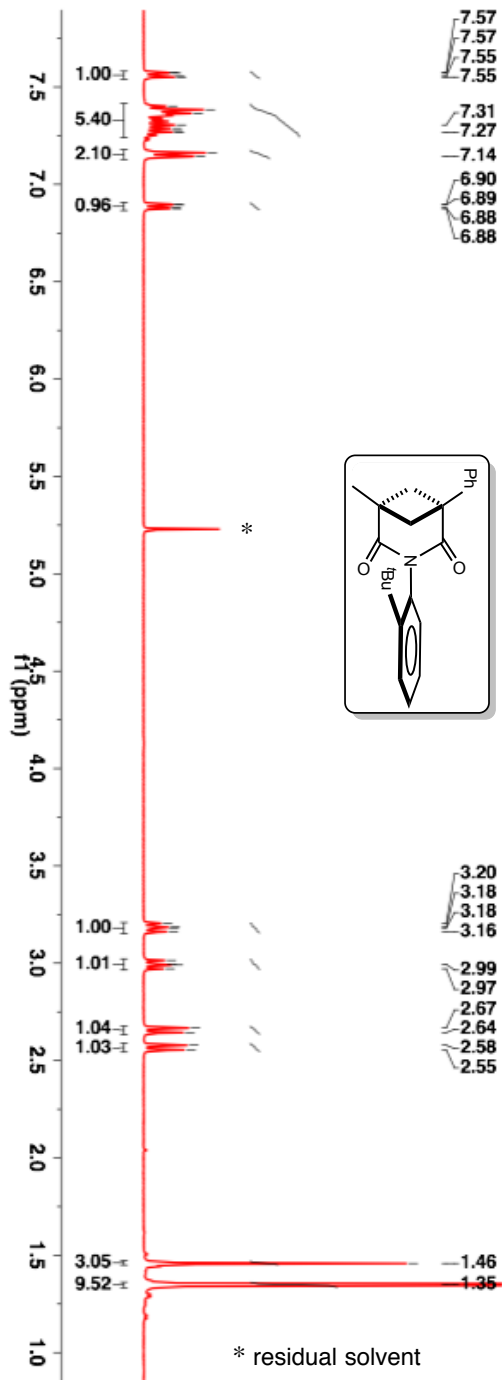
Figure 5.43: ¹H-NMR (400 MHz, CDCl₃, δ ppm) spectrum of photoproduct **280a**.

^{13}C-NMR (100 MHz, CDCl$_3$, δ ppm): 19.8, 31.7, 35.7, 42.1, 43.1, 45.3, 50.8, 126.6, 127.4, 127.6, 128.5, 128.6, 129.1, 131.0, 130.9, 139.3, 147.9, 176.4 and 177.7.
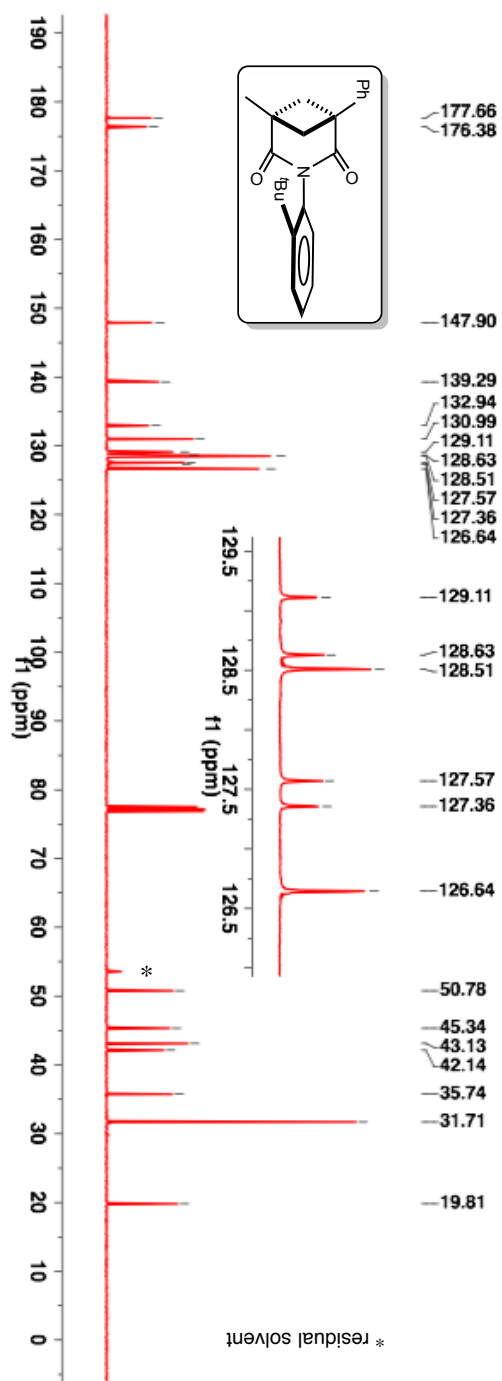
Figure 5.44: ^{13}C-NMR (100 MHz, CDCl$_3$, δ ppm) spectrum of photoproduct **280a**.

HRMS-ESI (m/z) ([M + Na]$^+$):

Calculated   : 370.1778

Observed   : 370.1772

|Δm| : 1.6 ppm
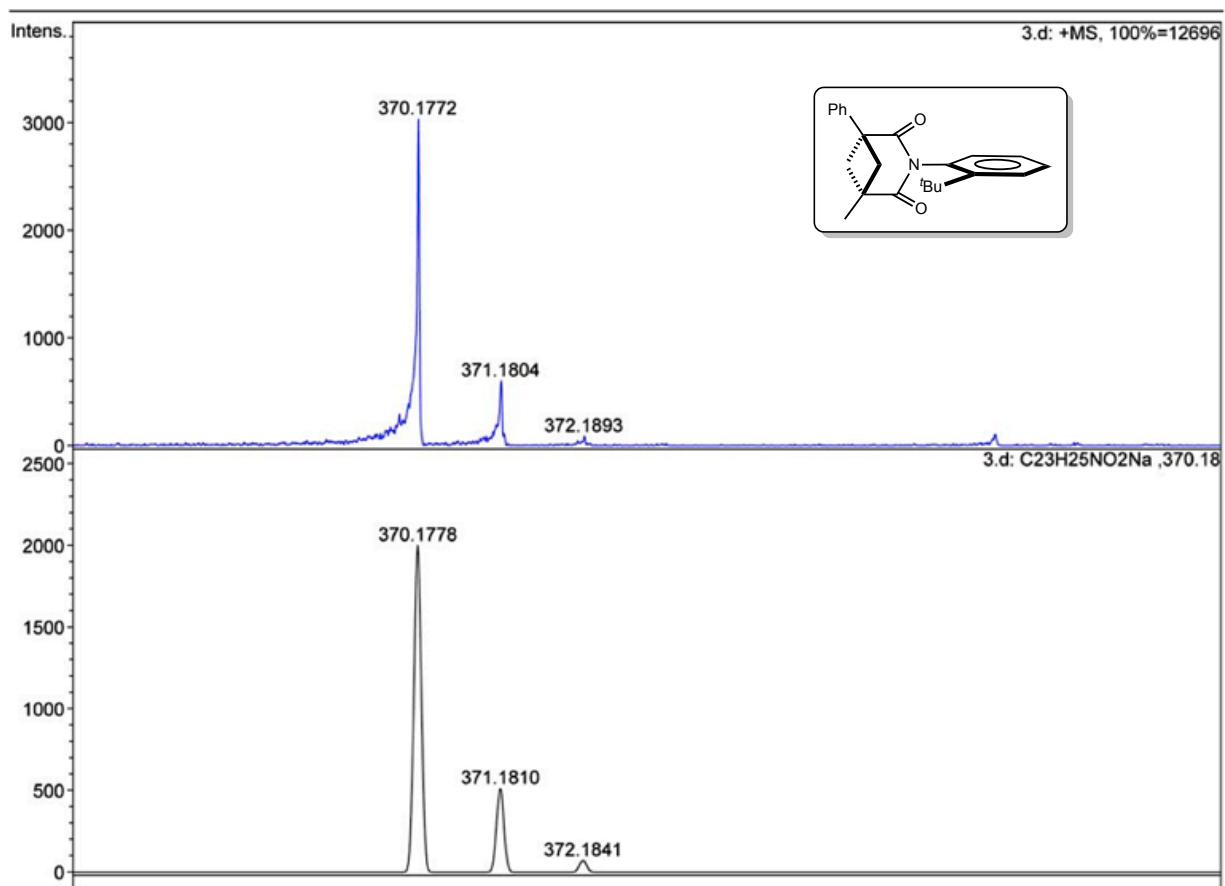
Figure 5.45: HRMS of photoproduct **280a**.

^{1}H-NMR (400 MHz, CDCl$_3$, δ ppm): 1.29 (s, 9H), 1.32 (s, 9H), 1.46 (s, 3H), 2.52 (d, J = 9.6 Hz, 1H),

2.69 (d, J = 9.6 Hz, 1H), 2.99-3.03 (dd, J = 9.6 Hz, 8 Hz, 1H), 3.16-3.21 (dd, J = 9.6 Hz, 8 Hz, 1H),

6.67-6.77 (m, 1H), 7.15-7.17 (m, 2H), 7.29-7.31 (m, 1H), 7.34-7.40 (m, 3H) and 7.45-7.47 (m, 1H).
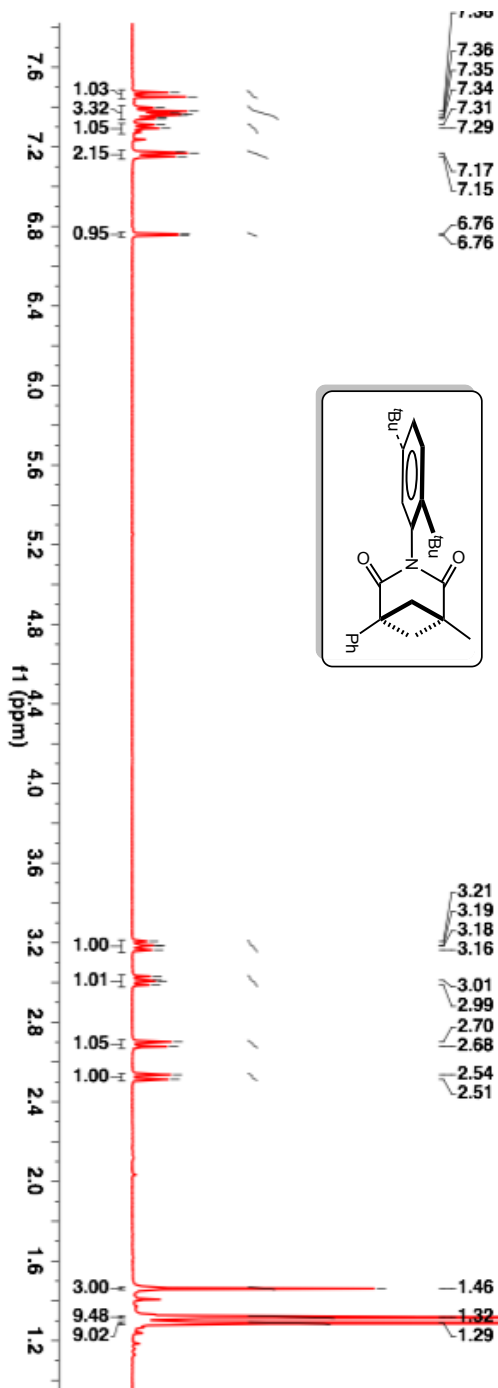
Figure 5.46: ^{1}H-NMR (400 MHz, CDCl$_3$, δ ppm) spectrum photoproduct **280b**.

^{13}C-NMR (100 MHz, CDCl$_3$, δ ppm): 19.9, 31.3, 31.8, 34.3, 35.3, 42.7, 43.2, 45.1, 50.9, 126.3, 126.7, 127.5, 127.6, 128.3, 128.6, 132.4, 139.5, 144.6, 150.1, 176.3 and 177.7.
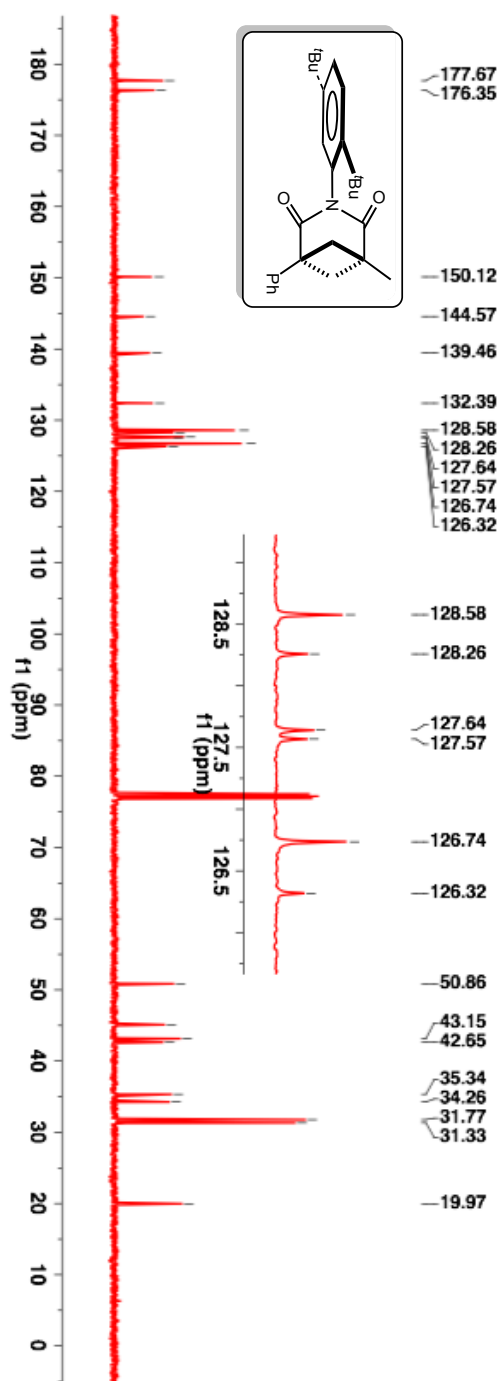
Figure 5.47: ^{13}C-NMR (100 MHz, CDCl$_3$, δ ppm) spectrum of photoproduct **280b**.

HRMS-ESI (m/z) ([M + Na]$^+$):

Calculated   : 426.2404

Observed   : 426.2409

|Δm| : 1.2 ppm
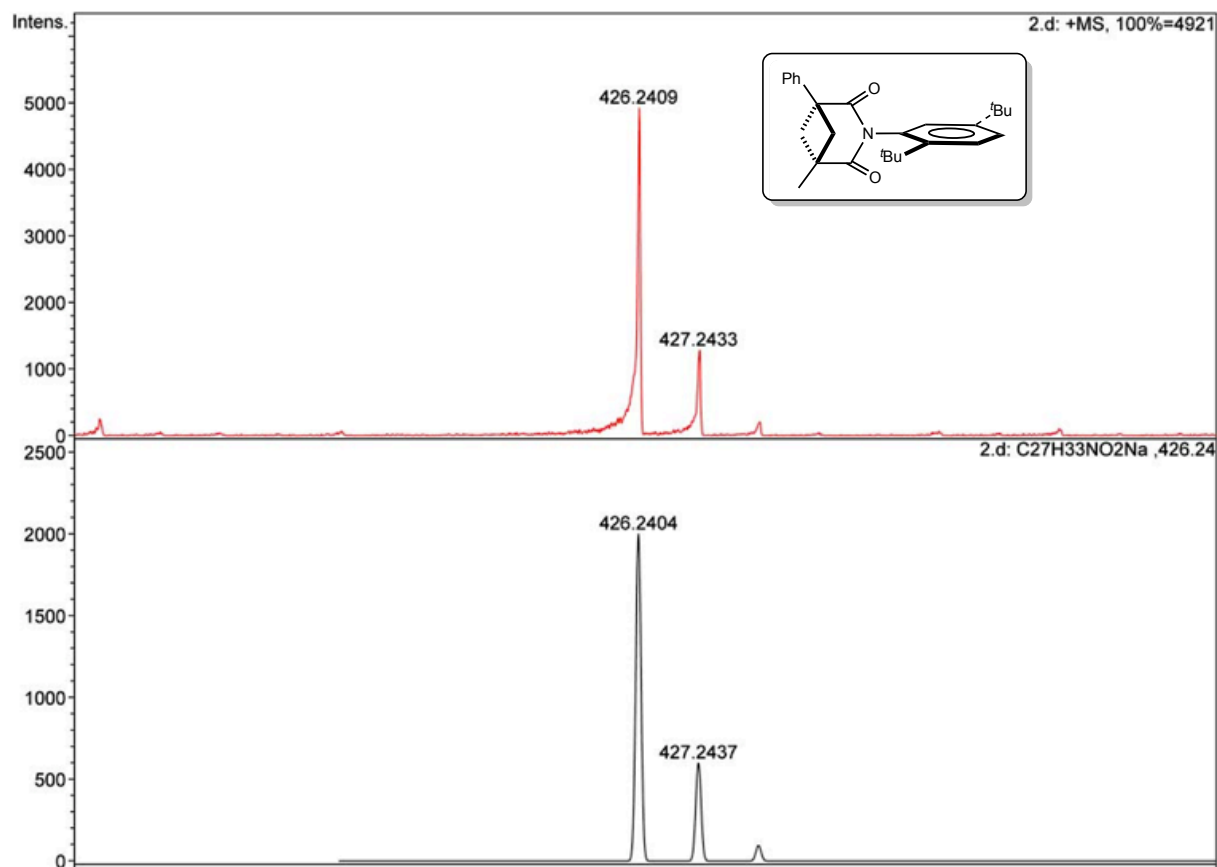
Figure 5.48: HRMS of photoproduct **280b**.

Major regioisomer ^{1}H-NMR (400 MHz, CDCl$_3$, δ ppm): 1.45 (s, CH$_3$), 2.59-2.62 (m, CH$_2$), 3.01-3.04 (m, CH$_2$) and 7.27-7.49 (m, Aromatic) Minor regioisomer: and 1.16 (s, CH$_3$), 2.18-2.25 (m, CH$_2$), 2.47-2.57 (m, CH$_2$), 7.13-7.27 (m, Aromatic).
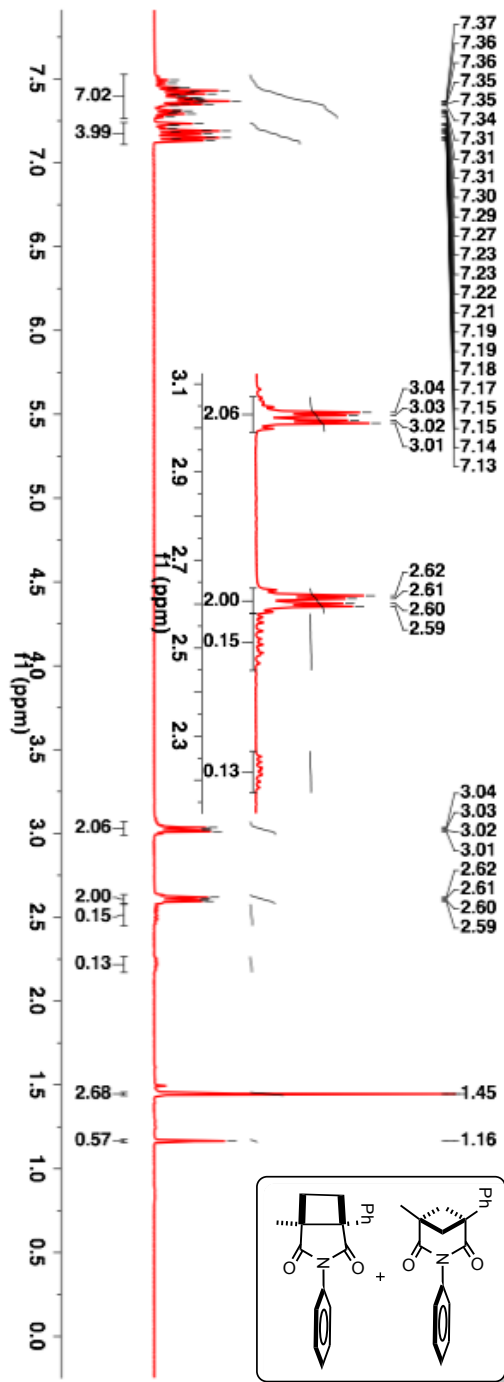
Figure 5.49: ^{1}H-NMR (400 MHz, CDCl$_3$, δ ppm) spectrum of photoproduct **280c**.

Note: Several peaks for the regioisomers overlap;

^{13}C-NMR (100 MHz, CDCl$_3$, δ ppm): 16.5, 19.9, 24.9, 29.7, 43.2, 44.7, 49.2, 50.8, 55.1, 126.6, 126.7, 127.2, 127.7, 128.1, 128.6, 128.6, 128.7, 128.8, 129.1, 129.2, 129.4, 132.5, 133.9, 135.8, 139.3, 176.3, 177.5.

Figure 5.50: ^{13}C-NMR (100 MHz, CDCl$_3$, δ ppm) spectrum of photoproduct **280c**.

HRMS-ESI (m/z) ([M + Na]$^{+}$):

Calculated   : 314.1136

Observed   : 314.1151

|Δm| : 4.7 ppm
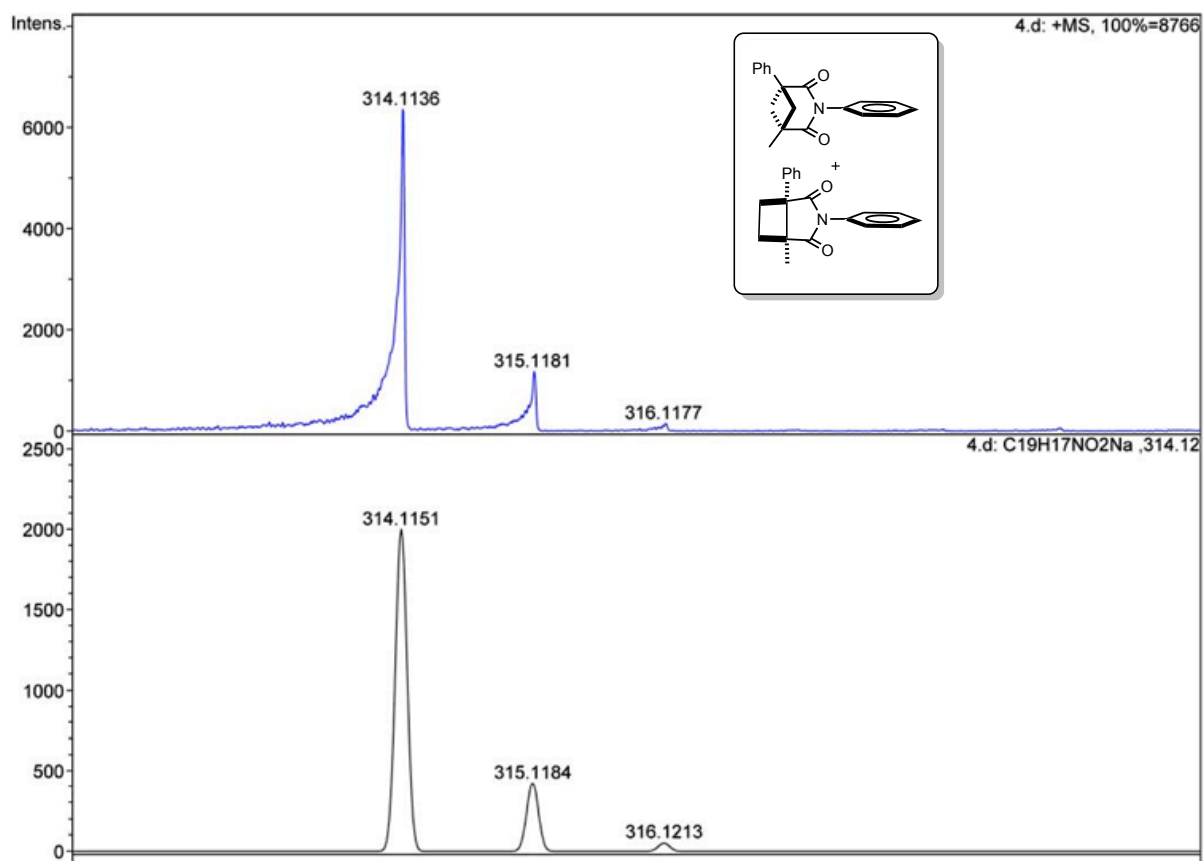
Figure 5.51: HRMS of photoproduct **280c**.

5.3.21 Procedure for hydrolysis of the photoproduct
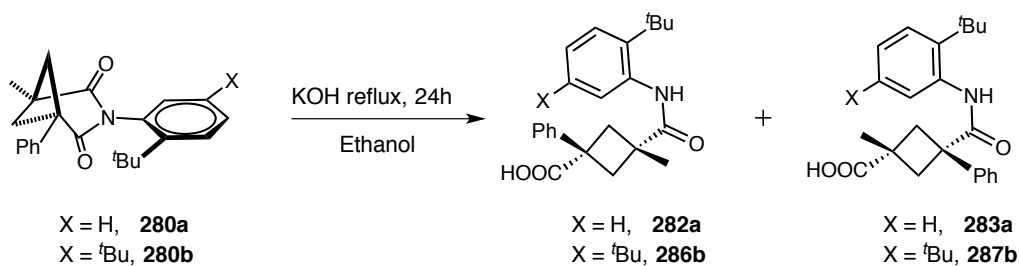
Scheme 5.34: Base hydrolysis of photoproduct **280a/280b**.

Photoproduct **280a/280b** (1 equiv) was taken in a round bottom flask and absolute ethanol was added. This was followed by addition of 5 equiv of 4.5N KOH. The solution was stirred at room temperature for 15 minutes and then refluxed for 24 h. The solution was cooled and excess base was neutralized with conc. HCl. The precipitate was dissolved in diethyl ether and the organic fraction was dried over anhyd Na_2SO_4. The solution was then concentrated under reduced pressure affording the product mixture as a white solid.

282a+283a,   Solid (taken to next step without any other purification)

286b+287b,   Solid (taken to next step without any other purification)

Yield = 68%

Several peaks overlap, both the products are reported together.

^{1}H-NMR (400 MHz, CDCl$_3$, δ ppm): 1.46 (s), 1.84 (s), 1.88 (s), 1.89 (s), 2.95–3.11 (m), 3.93–4.1 (m), 7.37 (bs), 7.54–7.60 (m), 7.63 (m), 7.63–7.99 (m), 8.09–8.10 (m) and 11.00 (bs).

Figure 5.52: ^{1}H-NMR (400 MHz, CDCl$_3$, δ ppm) spectrum of photoproduct **282a+283a**.

Several peaks overlap, both the products are reported together

^{13}C-NMR (100 MHz, CDCl$_3$, δ ppm): 26.3, 26.4, 30.2, 30.9, 34.2, 34.8, 38.5, 39.9, 41.8, 45.8, 47.1, 126.4, 126.5, 126.6, 126.7, 126.9, 126.9, 127.1, 127.2, 127.2, 127.3, 128.1, 128.3, 128.7, 129.7, 134.9, 135.5, 142.2, 142.8, 142.9, 143.0, 174.9, 175.6, 180.3 and 180.7.
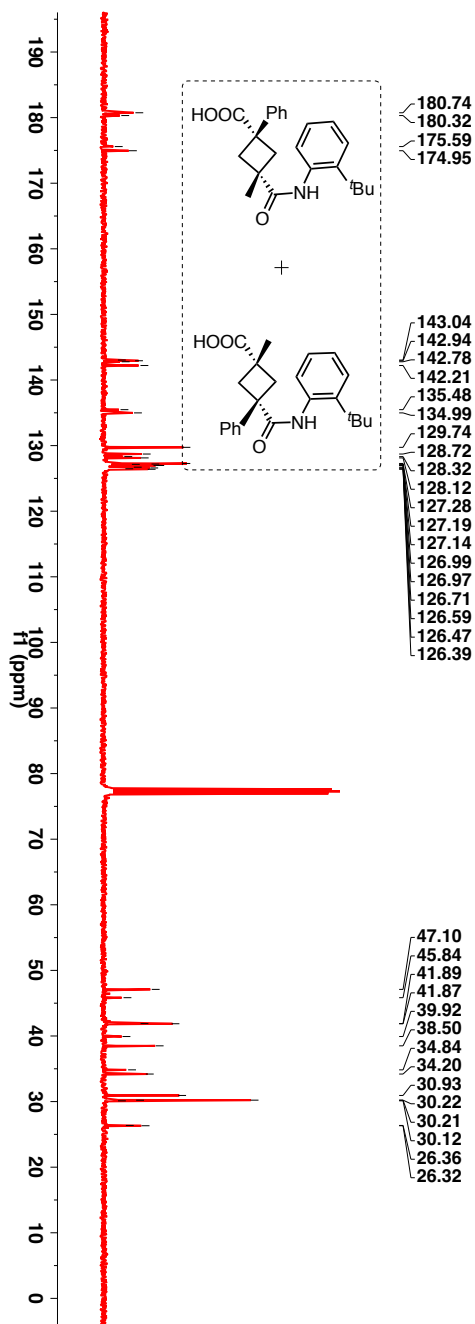
Figure 5.53: ^{13}C-NMR (100 MHz, CDCl$_3$, δ ppm) spectrum of photoproduct **282a+283a**.

HRMS-ESI (m/z) ([M + Na]⁺):

Calculated   : 388.1883

Observed   : 388.1900

|Δm| : 4.4 ppm
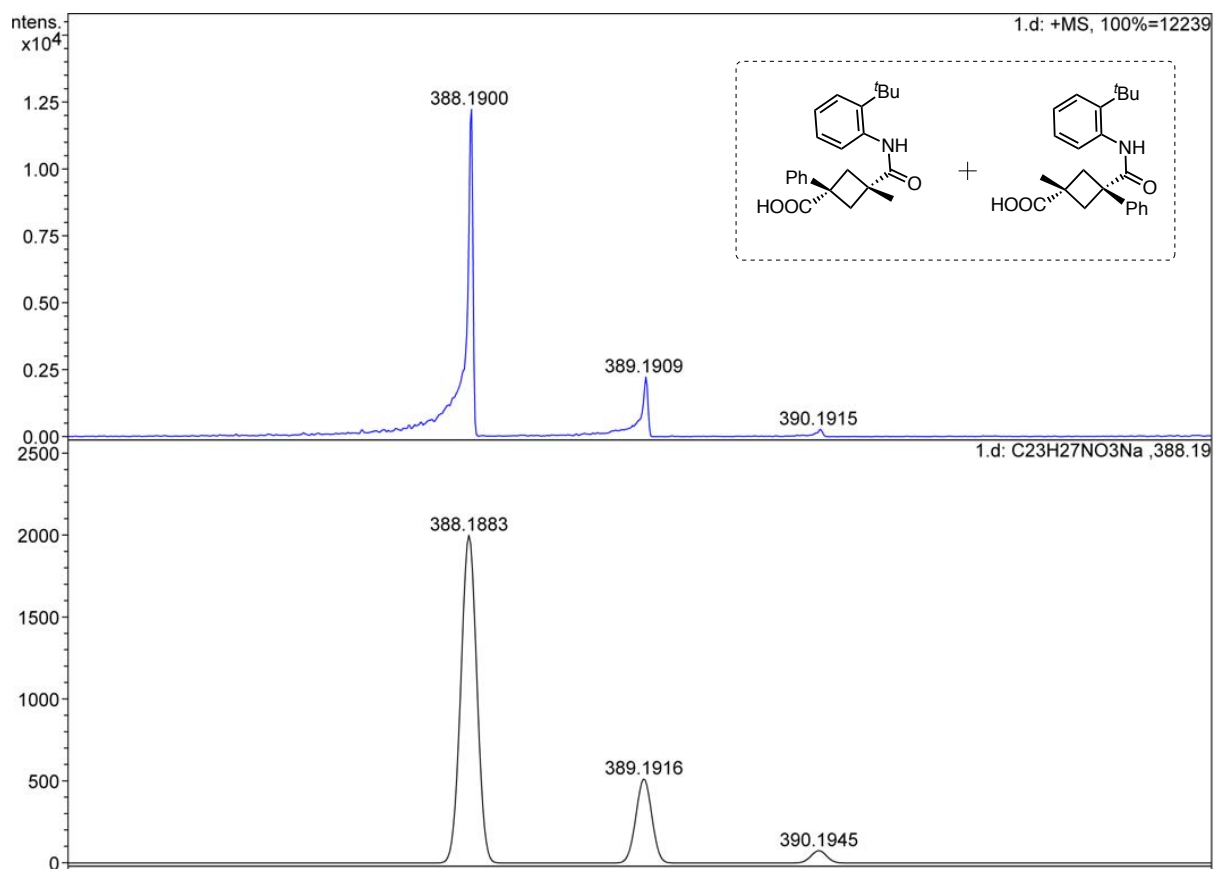
Figure 5.54: HRMS of photoproduct **282a+283a**.

Several peaks overlap, both the products are reported together.

^{1}H-NMR (400 MHz, CDCl$_3$, δ ppm): 1.01 (s), 1.31 (s), 1.34 (s), 1.38 (s), 1.43 (s), 1.45 (s), 2.61 – 2.66 (m), 3.60 – 3.67 (m), 6.93 (bs), 7.13 – 7.53 (m), 7.70 – 7.72 (m) and 10.9 (bs)
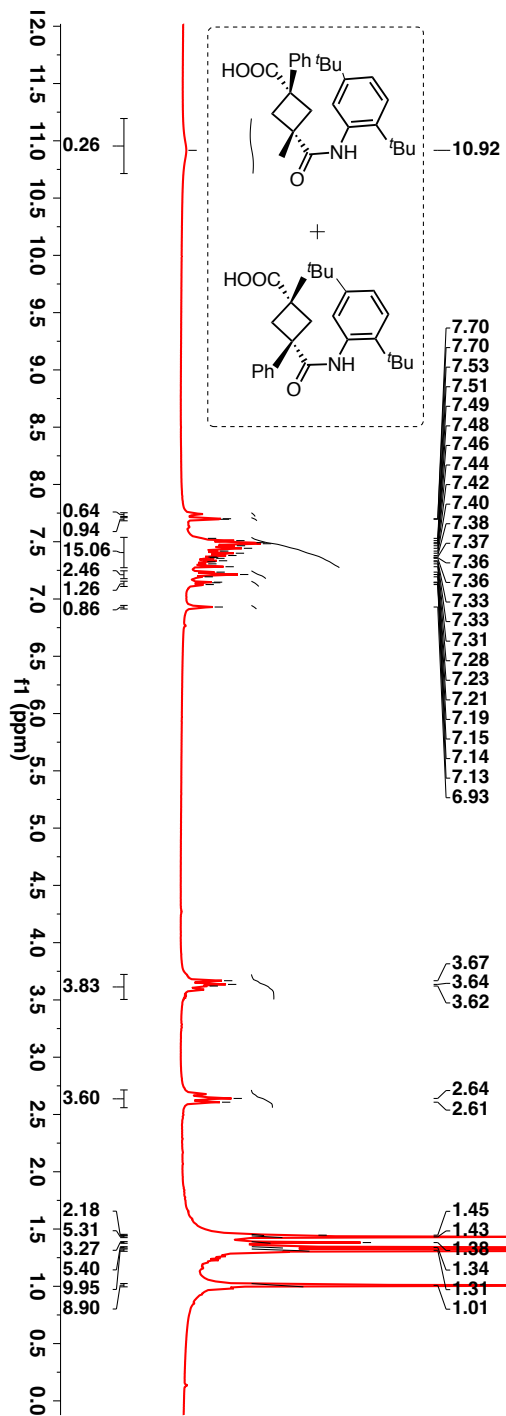
Figure 5.55: ^{1}H-NMR (400 MHz, CDCl$_3$, δ ppm) spectrum of photoproduct **286b+287b**.

Several peaks overlap, both the products are reported together

^{13}C-NMR (100 MHz, CDCl$_3$, δ ppm): 26.4, 26.7, 30.3, 30.9, 31.4, 31.8, 31.8, 34.2, 34.8, 34.9, 38.8, 40.1, 42.0, 46.0, 47.6, 123.5, 124.4, 125.2, 126.6, 126.7, 127.5, 127.6, 127.7, 128.4, 129.1, 130.1, 135.1, 135.5, 139.3, 139.8, 143.2, 143.4, 150.2, 150.3, 175.0, 175.8, 180.5 and 181.1.
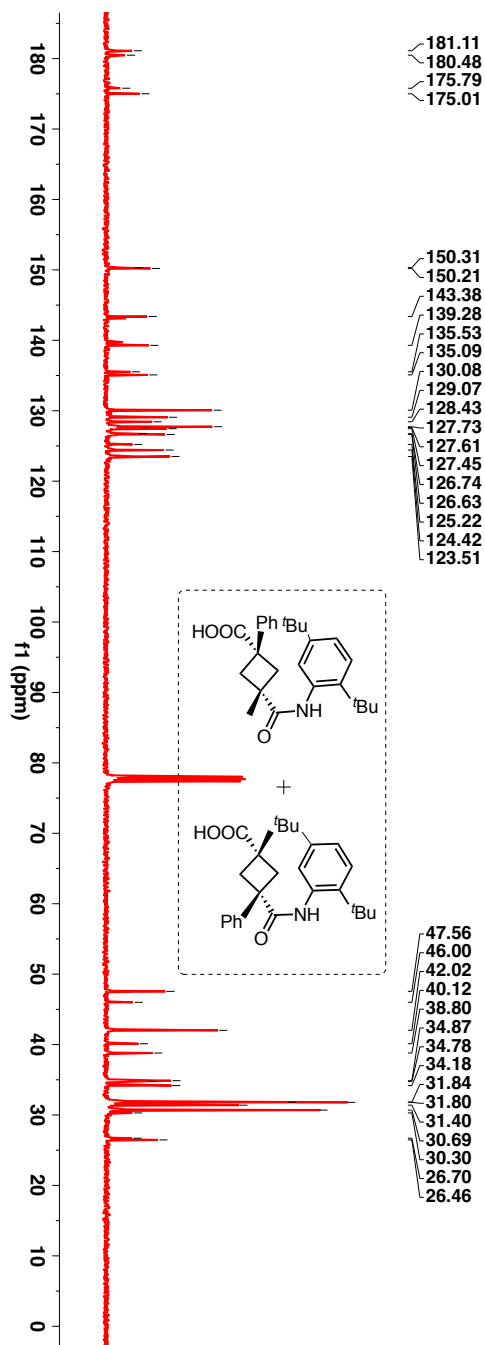
Figure 5.56: ^{13}C-NMR (100 MHz, CDCl$_3$, δ ppm) spectrum of photoproduct **286b+287b**.

HRMS-ESI (m/z) ([M + Na]$^+$):

Calculated   : 444.2509

Observed   : 444.2601

|Δm| : 2.0 ppm
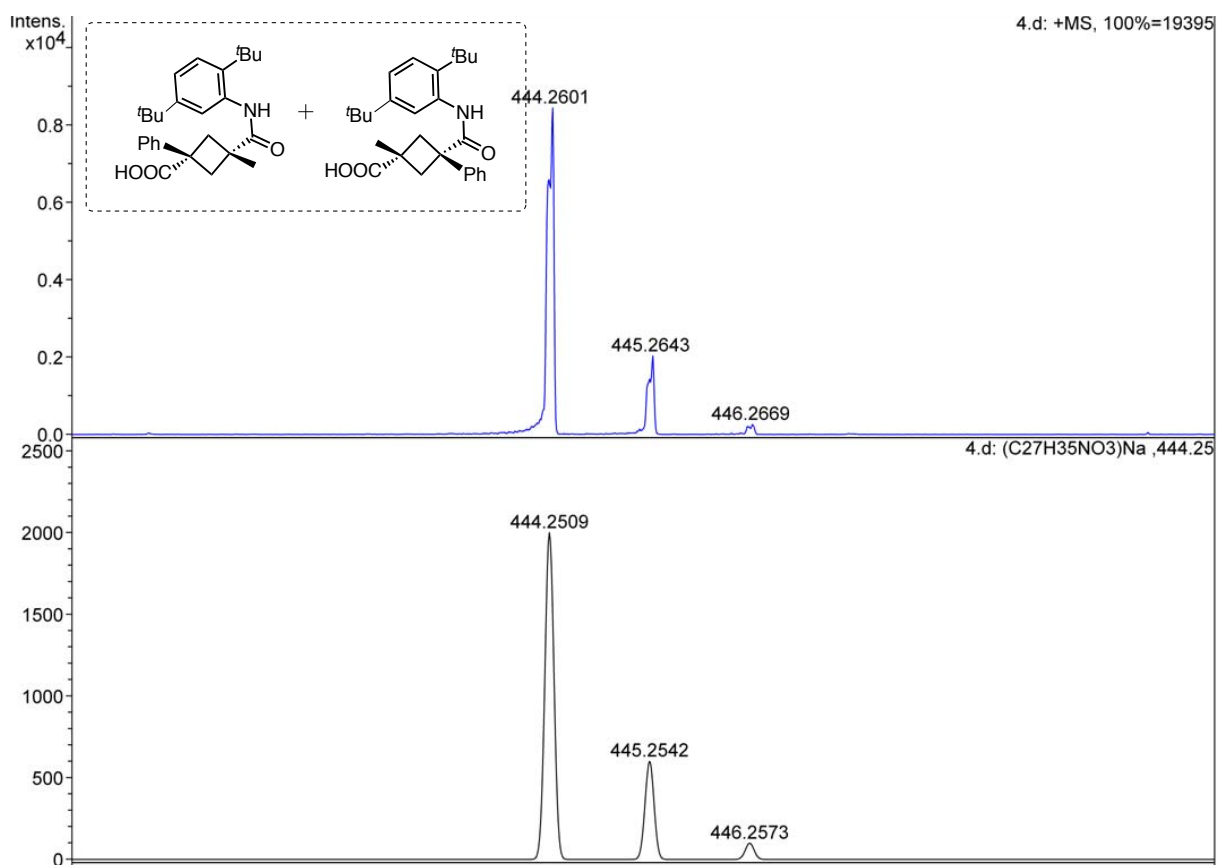
Figure 5.57: HRMS of photoproduct **286b**+**287b**.

5.3.22 Esterification of the hydrolyzed product
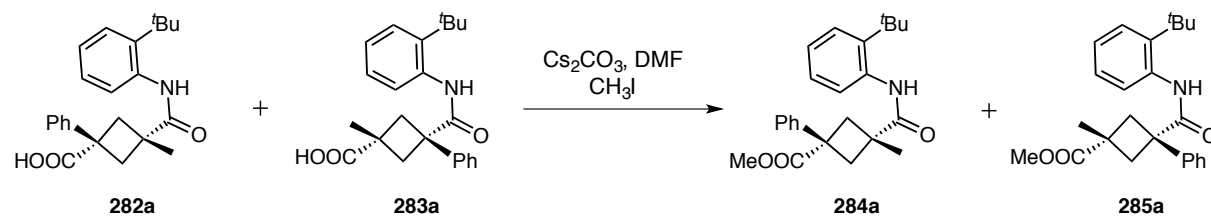
Scheme 5.35: Esterification of cyclobutane based product mixture (**284a+285a**).

The 1,3 diacid mixture (**282a+283a**) (1 equiv) was dissolved in anhyd DMF. To this solution cesium carbonate (1.5 equiv) was added. The solution was stirred at room temperature for 15 minutes and then iodomethane (1 equiv) was added dropwise. The stirring was continued at room temperature for 20 h. The reaction was quenched with water and then with water and the organic layer was extracted with ethyl ether. The organic fraction was dried over anhyd $MgSO_4$. The solution was then concentrated under reduced pressure affording the product mixture as yellow oil.

284a+285a, Yellow oil. Yield = 58%

Several peaks overlap, both the products are reported together.

^{1}H-NMR (400 MHz, CDCl$_3$, δ ppm): 0.97 (s), 1.30 (s), 1.41 (s), 2.48–2.59 (m), 3.48–3.56 (m), 3.59 (s), 3.74 (s), 6.80 (bs), 7.01–7.03 (m), 7.13–7.43 (m) and 7.59–7.65 (m).
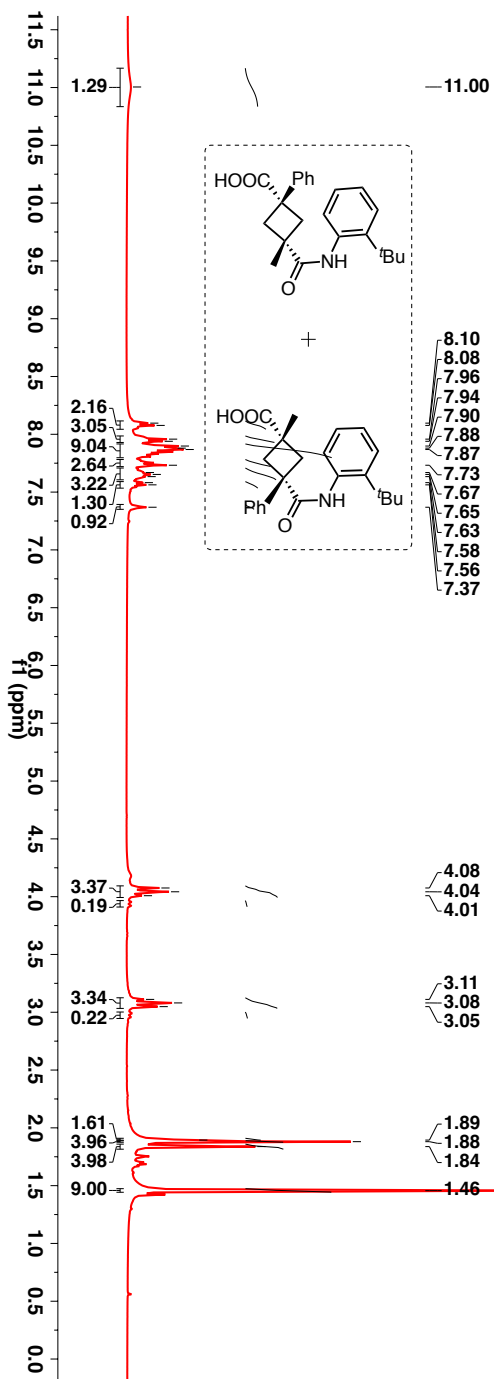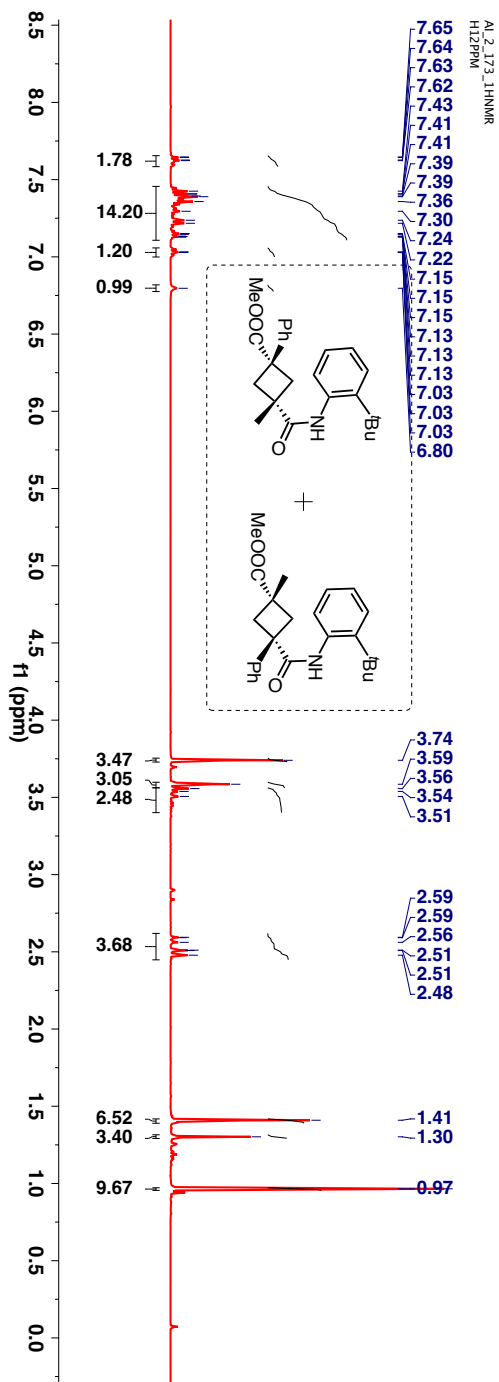

Figure 5.58: ^{1}H-NMR (400 MHz, CDCl$_3$, δ ppm) spectrum of photoproduct **284a+285a**.

Several peaks overlap, both the products are reported together.

^{13}C-NMR (100 MHz, CDCl$_3$, δ ppm): 26.3, 26.5, 30.2, 30.9, 34.2, 34.8, 39.1, 40.2, 41.7, 42.1, 46.2, 47.7, 52.4, 52.8, 125.8, 126.3, 126. 4, 126.7, 126.8, 126.9, 127.1, 127.1, 127.1, 127.7, 128.1, 128.7, 129.6, 135.7, 135.8, 141.8, 142.9, 143.6, 173.1, 175.2, 175.9 and 177.8.
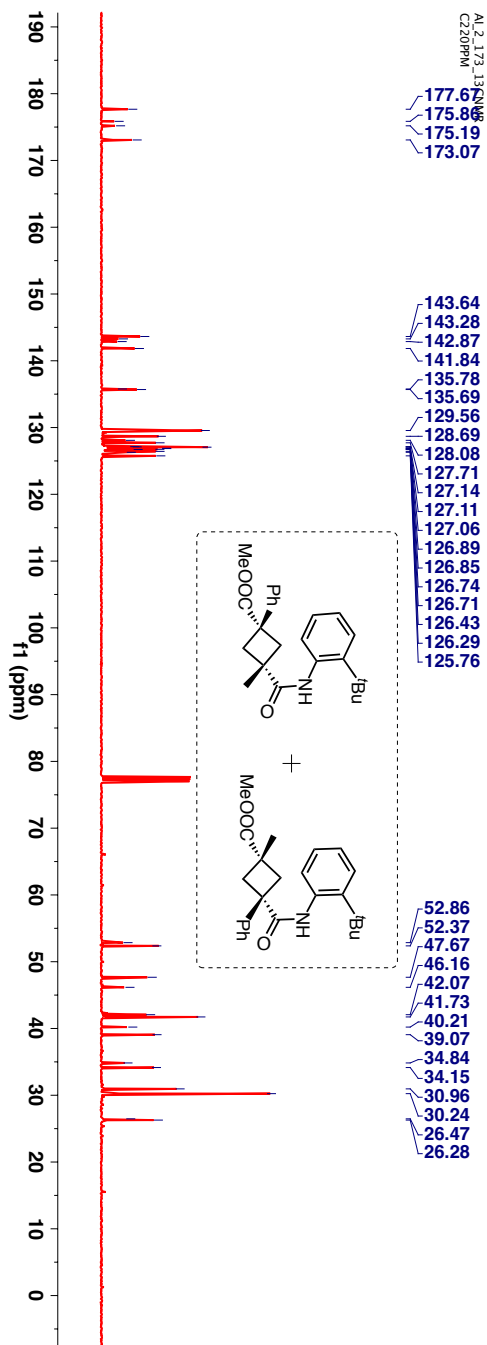
Figure 5.59: ^{13}C-NMR (100 MHz, CDCl$_3$, δ ppm) spectrum of photoproduct **284a**+**285a**.

HRMS-ESI (m/z) ([M + Na]$^+$):

Calculated   : 402.2040

Observed   : 402.2030

|Δm| : 2.5 ppm
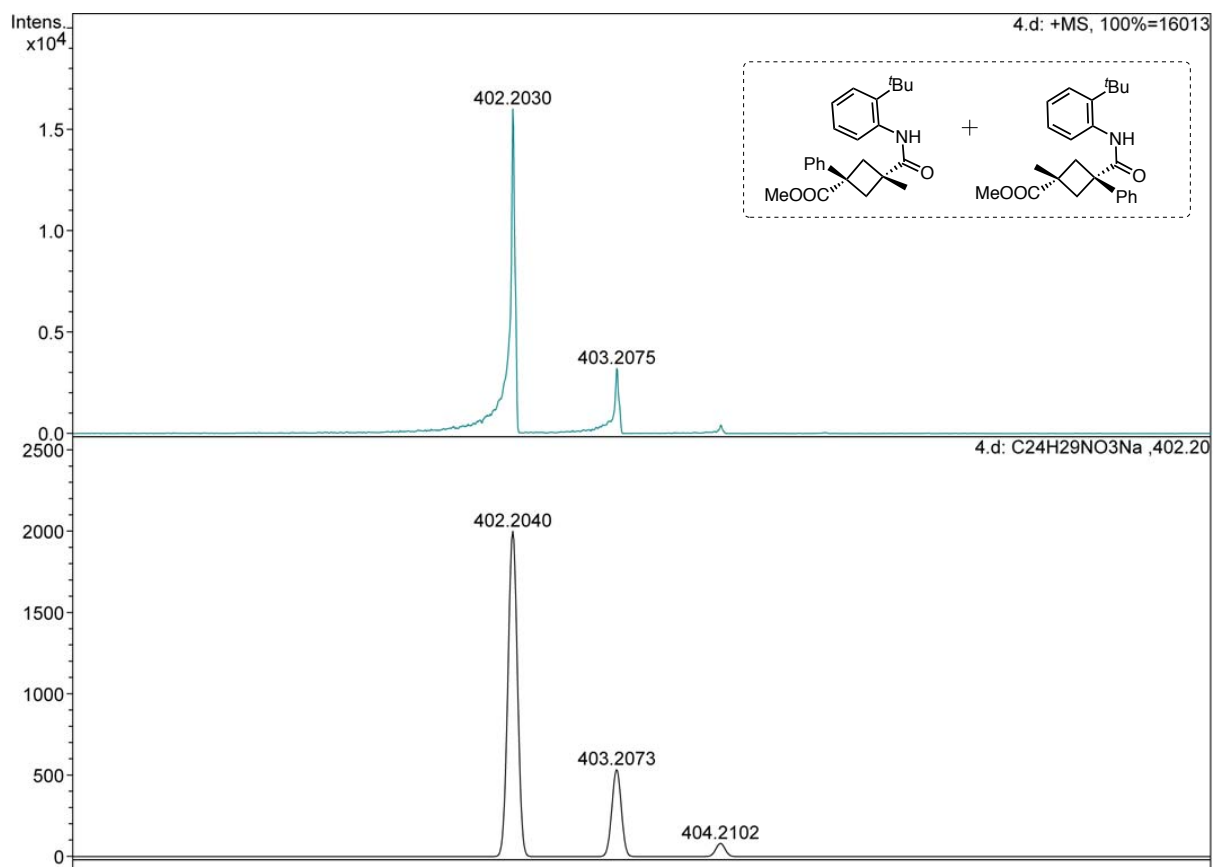
Figure 5.60: HRMS of photoproduct **284a**+**285a**.

5.3.23 UV-Vis spectrum of acrylimides 279a-c
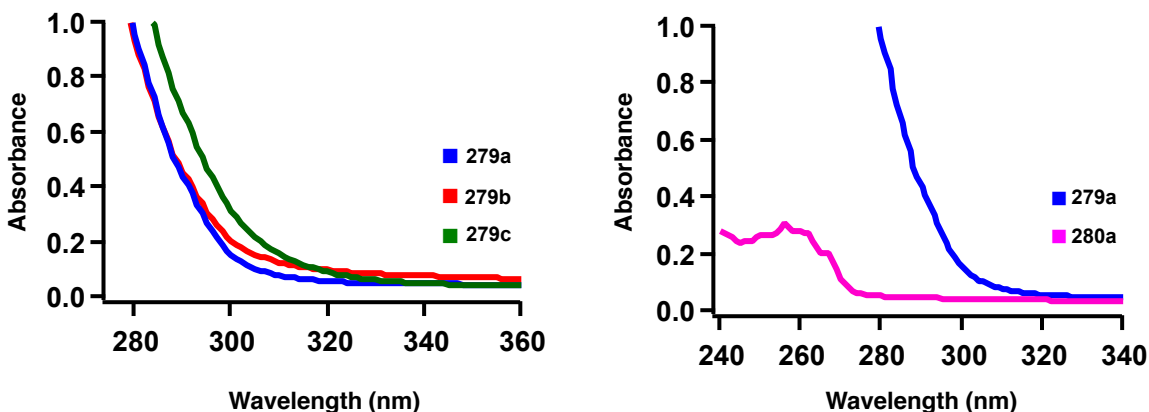
Figure 5.61: (left) UV-Vis spectra of acrylimides recorded at a concentration of 0.5 mM in acetonitrile at room temperature. (right) UV-Vis spectra of atropisomeric acrylimide **279a** and its corresponding photoproduct **280a** recorded at a concentration of 0.5 mM and 0.4 mM respectively.

5.3.24 Photophysical data
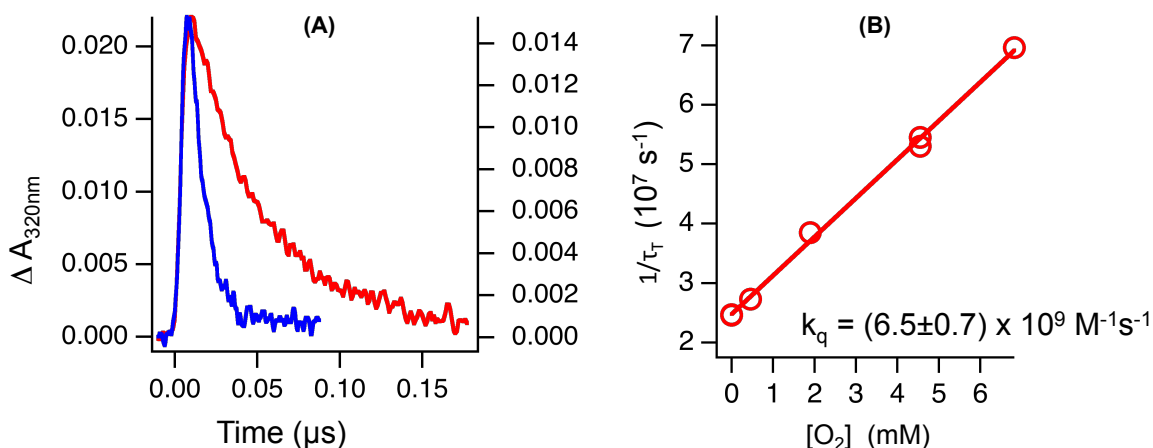
Figure 5.62: (A) Absorbance decay traces of **279a** triplet states in argon (red) or oxygen (blue) saturated acetonitrile solutions using laser flash photolysis (λ_{ex} = 266 nm, 5 ns pulse width) monitored at 320 nm. (B) Determination of the bimolecular quenching rate constant k_q of **279a** triplet states by O_2 from the slope of the plot of the inverse triplet lifetime vs. the [O_2].
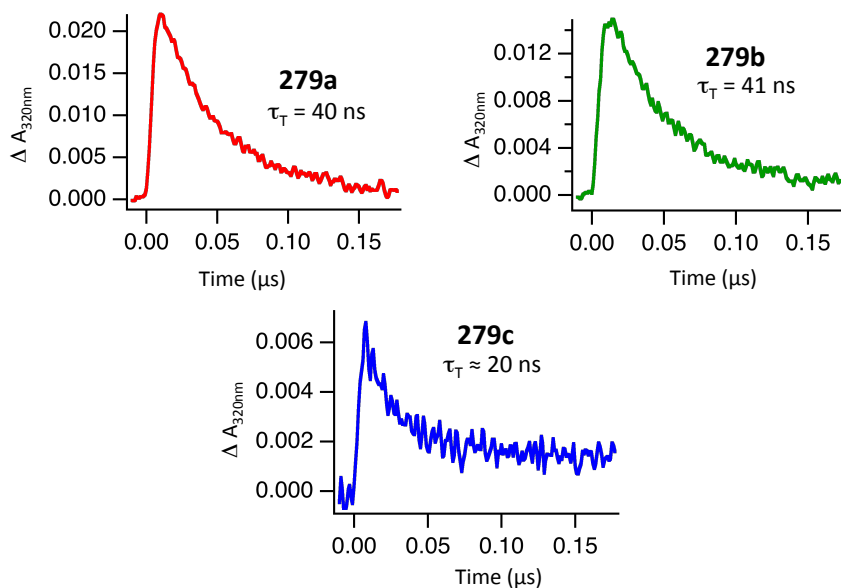
Figure 5.63: Absorbance decay traces of **279a-c** triplet states in argon saturated acetonitrile solutions using laser flash photolysis (λ_{ex} = 266 nm, 5 ns pulse width) monitored at 320 nm.

k_q = (7.3±0.2) x 10^9 $M^{-1}s^{-1}$ k_q = (4.0±0.1) x 10^9 $M^{-1}s^{-1}$ k_q = (8.6±0.2) x 10^7 $M^{-1}s^{-1}$
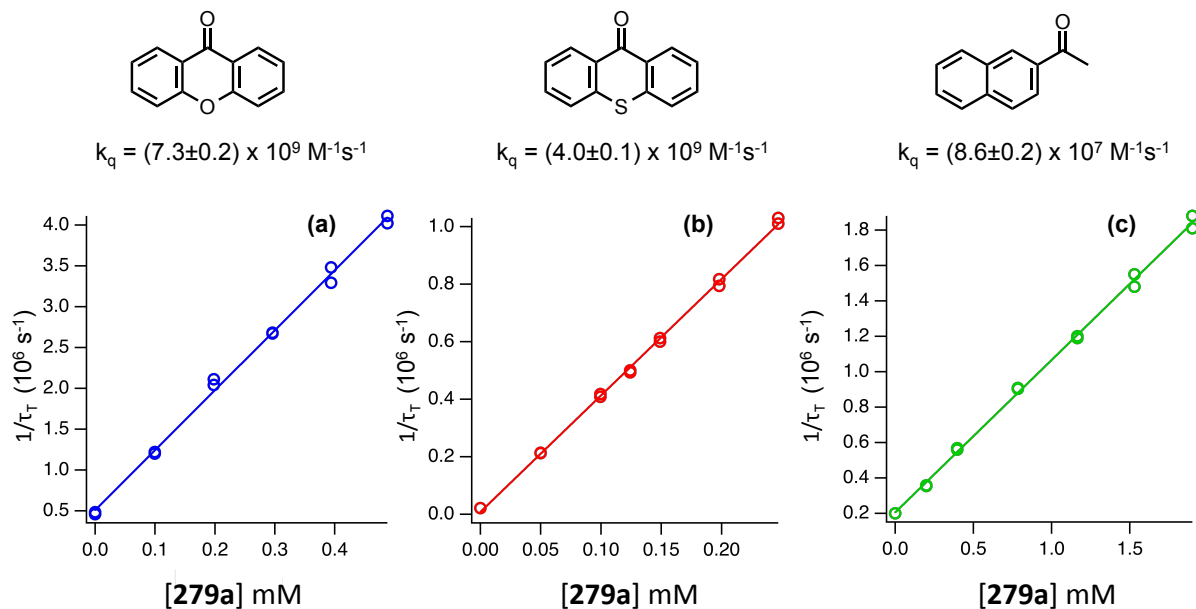
Figure 5.64: Determination of the bimolecular quenching rate constants k_q of quenching of sensitizer triplet states by **279a** using laser flash photolysis (λ_{ex} = 355 nm, 7 ns pulse width). Inverse triplet lifetime determined from triplet absorption decay traces monitored at 620 nm for xanthone (a) and thioxanthone (b) and 425 nm for 2-acetonaphthone (c) with varying concentration of **279a** in argon saturated acetonitrile solutions.

5.4 **References**

(1)   Bergbreiter, D. E. *ACS Macro Lett.* **2014**, *3*, 260-65.

(2)   Maitz, M. F. *Biosurface and Biotribology* **2015**, *1*, 161-76.

(3)   Reichmanis, E.; Thompson, L. F. *Chem. Rev.* **1989**, *89*, 1273-89.

(4)   Habault, D.; Zhang, H.; Zhao, Y. *Chem. Soc. Rev.* **2013**, *42*, 7244-56.

(5)   Odian, G. *Principles of Polymerization*; Wiley, 2004.

(6)   Havelka, K. O.; McCormick, C. L. *Specialty Monomers and Polymers*; American Chemical

        Society, 2000; Vol. 755.

(7)   Havelka, K. O. In *Specialty Monomers and Polymers*; American Chemical Society: 2000; Vol.

        755, p 2-10.

(8)   Hastings, G. W. *Polymer* **1985**, *26*, 1331-35.

(9)   Bowden, M. J.; Turner, S. R. *Electronic and Photonic Applications of Polymers*; American

        Chemical Society, 1988; Vol. 218.

(10)   Ghosh, P.; 21 Sept 2006 ed. 2006.

(11)   Theriot, J. C.; Lim, C.-H.; Yang, H.; Ryan, M. D.; Musgrave, C. B.; Miyake, G. M. *Science*

        2016, 10.1126/science.aaf3935.

(12)   Miyake, G. M.; Theriot, J. C. *Macromolecules* **2014**, *47*, 8255-61.

(13)   Mahmoud, E.; Watson, D. A.; Lobo, R. F. *Green Chem.* **2014**, *16*, 167-75.

(14)   Klán, P.; Wirz, J. *Photochemistry of Organic Compounds: From Concepts to Practice*; Wiley-

        Blackwell, 2009.

(15)   Dadashi-Silab, S.; Aydogan, C.; Yagci, Y. *Polymer Chem.* **2015**, *6*, 6595-615.

(16)   Rodrigues, J. F.; Silva, F. d. A. d.; Netto-Ferreira, J. C. *J. Braz. Chem. Soc.* **2010**, *21*, 960-65.

(17)   Thompson, L. G.; Webber, S. E. *J. Phys. Chem.* **1972**, *76*, 221-24.

(18)   Ruud, K.; Schimmelpfennig, B.; Ãgren, H. *Chem. Phys. Lett.* **1999**, *310*, 215-21.

(19)   Bolton, O.; Lee, K.; Kim, H.-J.; Lin, K. Y.; Kim, J. *Nat Chem* **2011**, *3*, 205-10.

(20)   Lin, S. H.; Tweed, D. *Int. J. Quantum Chem* **1969**, *3*, 315-24.

(21)   Turro, N. J.; Ramamurthy, V.; Scaiano, J. C. *Modern Molecular Photochemistry of Organic*

        Molecules; University Science Books: Sausalito, CA, 2010.

(22)   Wang, H.; Meng, L.; Shen, X.; Wei, X.; Zheng, X.; Lv, X.; Yi, Y.; Wang, Y.; Wang, P. *Adv. Mater.* **2015**, *27*, 4041-47.

(23)   Lalevée, J.; Tehfe, M.-A.; Dumur, F.; Gigmes, D.; Graff, B.; Morlet-Savary, F.; Fouassier, J.-P. *Macromol. Rapid Commun.* **2013**, *34*, 239-45.

(24)   Kärkäs, M. D.; Porco, J. A.; Stephenson, C. R. J. *Chem. Rev.* **2016**, 10.1021/acs.chemrev.5b00760.

(25)   Wagner, P. J. *Acc. Chem. Res.* **2001**, *34*, 1-8.

(26)   Dauben, W. G.; Salem, L.; Turro, N. J. *Acc. Chem. Res.* **1975**, *8*, 41-54.

(27)   Roth, H. D. *Angewandte Chemie International Edition in English* **1989**, *28*, 1193-207.

(28)   Fritzsche *Journal für Praktische Chemie* **1867**, *101*, 333-43.

(29)   Schönberg, A. *Photodimerizations involving formation of eight-membered rings*; Springer Berlin Heidelberg: Berlin, Heidelberg, 1968, 10.1007/978-3-642-87918-0_9.

(30)   Ehrenberg, M. *Acta Crystallographica* **1966**, *20*, 177-82.

(31)   Garcia-Garibay, M. A. *Photochem. Photobiol. Sci.* **2010**, *9*, 1574-88.

(32)   Bach, T. *Synthesis* **1998**, *1998*, 683-703.

(33)   Poplata, S.; Tröster, A.; Zou, Y.-Q.; Bach, T. *Chem. Rev.* **2016**, 10.1021/acs.chemrev.5b00723.

(34)   Subrata, G. In *CRC Handbookof Organic Photochemistry and Photobiology, Volumes 1 & 2, Second Edition*; CRC Press: 2003, doi:10.1201/9780203495902.ch18 10.1201/9780203495902.ch18.

(35)   Crimmins, M. T.; Reinhold, T. L. In *Organic Reactions*; John Wiley & Sons, Inc.: 2004, 10.1002/0471264180.or044.02.

(36)   Dexter, D. L. *The Journal of Chemical Physics* **1953**, *21*, 836-50.

(37)   Whitten, D. G.; Zarnegar, P. P. *J. Am. Chem. Soc.* **1971**, *93*, 3776-77.

(38)   Bock, C. R.; Connor, J. A.; Gutierrez, A. R.; Meyer, T. J.; Whitten, D. G.; Sullivan, B. P.; Nagle, J. K. *J. Am. Chem. Soc.* **1979**, *101*, 4815-24.

(39)   Whitten, D. G. *Acc. Chem. Res.* **1980**, *13*, 83-90.

(40)   Fagnoni, M.; Dondi, D.; Ravelli, D.; Albini, A. *Chem. Rev.* **2007**, *107*, 2725-56.

(41)   Hari, D. P.; Schroll, P.; König, B. *J. Am. Chem. Soc.* **2012**, *134*, 2958-61.

(42)   Du, J.; Skubi, K. L.; Schultz, D. M.; Yoon, T. P. *Science* **2014**, *344*, 392-96.

(43)   Hari, D. P.; Konig, B. *Chem. Commun.* **2014**, *50*, 6688-99.

(44)   Schultz, D. M.; Yoon, T. P. *Science* **2014**, *343*.

(45)   Jin, J.; MacMillan, D. W. C. *Nature* **2015**, *525*, 87-90.

(46)   Chen, J.-R.; Hu, X.-Q.; Lu, L.-Q.; Xiao, W.-J. *Chem. Soc. Rev.* **2016**, *45*, 2044-56.

(47)   Prier, C. K.; Rankic, D. A.; MacMillan, D. W. C. *Chem. Rev.* **2013**, *113*, 5322-63.

(48)   Ramamurthy, V.; Sivaguru, J. *Chem. Rev.* **2016**, 10.1021/acs.chemrev.6b00040.

(49)   Brimioulle, R.; Lenhart, D.; Maturi, M. M.; Bach, T. *Angew. Chem. Int. Ed.* **2015**, *54*, 3872-90.

(50)   Vallavoju, N.; Selvakumar, S.; Pemberton, B. C.; Jockusch, S.; Sibi, M. P.; Sivaguru, J. *Angew. Chem. Int. Ed* **2016**, *55*, 5446-51.

(51)   Vallavoju, N.; Selvakumar, S.; Jockusch, S.; Sibi, M. P.; Sivaguru, J. *Angew. Chem. Int. Ed.* **2014**, *53*, 5604-08.

(52)   Vallavoju, N.; Selvakumar, S.; Jockusch, S.; Prabhakaran, M. T.; Sibi, M. P.; Sivaguru, J. *Adv. Synth. Catal.* **2014**, *356*, 2763-68.

(53)   Bach, T.; Bergmann, H.; Harms, K. *Angew. Chem. Int. Ed.* **2000**, *39*, 2302-04.

(54)   Bach, T.; Hehn, J. P. *Angew. Chem. Int. Ed.* **2011**, *50*, 1000-45.

(55)   Selig, P.; Bach, T. *J. Org. Chem.* **2006**, *71*, 5662-73.

(56)   Kumarasamy, E.; Sivaguru, J. *Chem. Commun.* **2013**, *49*, 4346-48.

(57)   Raghunathan, R.; Kumarasamy, E.; Iyer, A.; Ugrinov, A.; Sivaguru, J. *Chem. Commun.* **2013**, *49*, 8713-15.

(58)   Dalton, J. C.; Wriede, P. A.; Turro, N. J. *J. Am. Chem. Soc.* **1970**, *92*, 1318-26.

(59)   Barltrop, J. A.; Carless, H. A. J. *J. Am. Chem. Soc.* **1972**, *94*, 1951-59.

(60)   Stanek, J.; Alder, A.; Bellus, D.; Bhatnagar, A. S.; Haeusler, A.; Schieweck, K. *J. Med. Chem.* **1991**, *34*, 1329-34.

(61)   LaLonde, R. T.; Aksentijevich, R. I. *Tetrahedron Lett.* **1965**, *6*, 23-27.

(62)   Maruyama, K.; Ishitoku, T. *Chemistry Lett.* **1980**, *9*, 359-60.

(63)   Alder, A.; Bühler, N.; Bellus, D. *Helv. Chim. Acta* **1982**, *65*, 2405-12.

(64)   Srinivasan, R.; Carlough, K. H. *J. Am. Chem. Soc.* **1967**, *89*, 4932-36.

(65)   Liu, R. S. H.; Hammond, G. S. *J. Am. Chem. Soc.* **1967**, *89*, 4936-44.

(66)   Christian, W. *Dynamic Stereochemistry of Chiral Compounds. Principles and Applications*, *RSC publishing: Cambridge, UK., 2008*.

(67)   Inoue, Y. *Chem. Rev.* **1992**, *92*, 741-70.

(68)   Frisch, M. J.; Trucks, G. W.; Schlegel, H. B.; Scuseria, G. E.; Robb, M. A.; Cheeseman, J. R.; Scalmani, G.; Barone, V.; Mennucci, B.; Petersson, G. A.; Nakatsuji, H.; Caricato, M.; Li, X.; Hratchian, H. P.; Izmaylov, A. F.; Bloino, J.; Zheng, G.; Sonnenberg, J. L.; Hada, M.; Ehara, M.; Toyota, K.; Fukuda, R.; Hasegawa, J.; Ishida, M.; Nakajima, T.; Honda, Y.; Kitao, O.; Nakai, H.; Vreven, T.; Montgomery Jr., J. A.; Peralta, J. E.; Ogliaro, F.; Bearpark, M. J.; Heyd, J.; Brothers, E. N.; Kudin, K. N.; Staroverov, V. N.; Kobayashi, R.; Normand, J.; Raghavachari, K.; Rendell, A. P.; Burant, J. C.; Iyengar, S. S.; Tomasi, J.; Cossi, M.; Rega, N.; Millam, N. J.; Klene, M.; Knox, J. E.; Cross, J. B.; Bakken, V.; Adamo, C.; Jaramillo, J.; Gomperts, R.; Stratmann, R. E.; Yazyev, O.; Austin, A. J.; Cammi, R.; Pomelli, C.; Ochterski, J. W.; Martin, R. L.; Morokuma, K.; Zakrzewski, V. G.; Voth, G. A.; Salvador, P.; Dannenberg, J. J.; Dapprich, S.; Daniels, A. D.; Farkas, Ö.; Foresman, J. B.; Ortiz, J. V.; Cioslowski, J.; Fox, D. J.; Gaussian, Inc.: Wallingford, CT, USA, 2009.

(69)   Heldt, W. *Justus Liebigs Annalen der Chemie* **1847**, *63*, 10-83.

(70)   Brede, O.; David, F.; Steenken, S. *J. Photochem. Photobiol A* **1996**, *97*, 127-31.

(71)   Swiderek, P.; Fraser, M. J.; Michaud, M.; Sanche, L. *The Journal of Chemical Physics* **1994**, *100*, 70-77.

(72)   Schmidt, R.; Tanielian, C.; Dunsbach, R.; Wolff, C. *Journal of Photochemistry and Photobiology A: Chemistry* **1994**, *79*, 11-17.

(73)   Bucholtz, K. M.; Gareiss, P. C.; Tajc, S. G.; Miller, B. L. *Org. Biomol. Chem.* **2006**, *4*, 3973-79.

(74)   Gutekunst, W. R.; Baran, P. S. *J. Am. Chem. Soc.* **2011**, *133*, 19076-79.

(75)   Gutekunst, W. R.; Gianatassio, R.; Baran, P. S. *Angew. Chem. Int. Ed.* **2012**, *51*, 7507-10.

(76)   Parella, R.; Gopalakrishnan, B.; Babu, S. A. *J. Org. Chem.* **2013**, *78*, 11911-34.

(77)   Yuqing, C.; Dingxiang, D.; Xiaojun, Y.; Xiangtao, X.; Fangrui, S.; LiYa, X. *Agri. Sci. Tech.* **2012**, *13*, 1-3.

(78)   Yagci, Y.; Jockusch, S.; Turro, N. J. *Macromolecules* **2007**, *40*, 4481-85.

(79)   Curran, D. P.; Hale, G. R.; Geib, S. J.; Balog, A.; Cass, Q. B.; Degani, A. L. G.; Hernandes, M. Z.; Freitas, L. C. G. *Tetrahedron: Asymmetry* **1997**, *8*, 3955-75.